Analytical CHEMISTRY

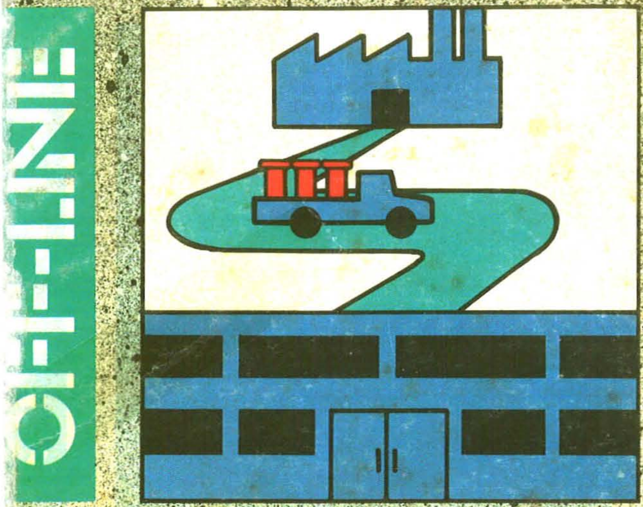

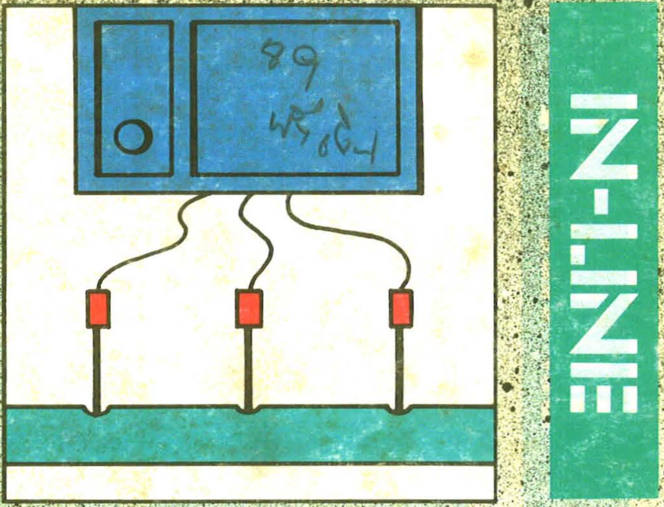

89

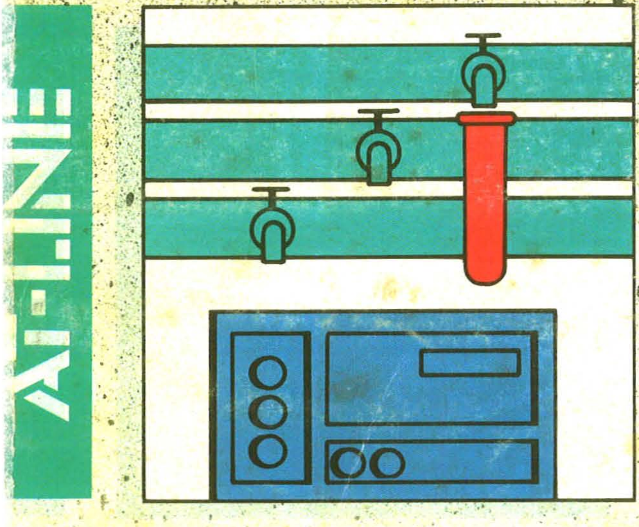

PROCESS ANALYTICAL CHEMISTRY

624 A

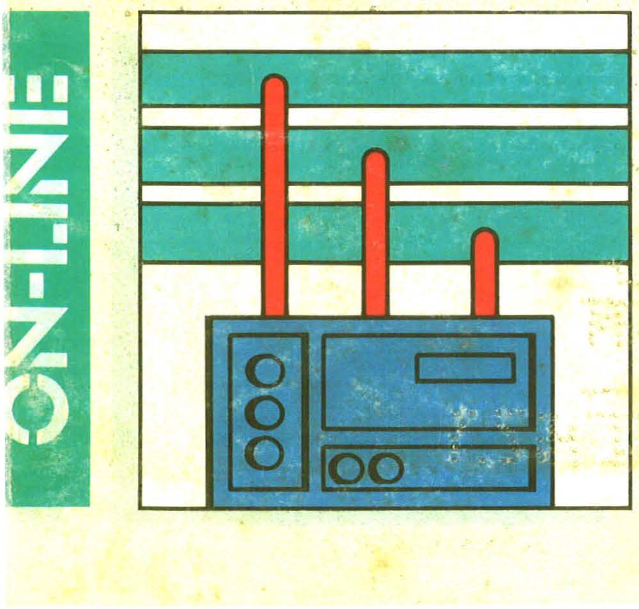

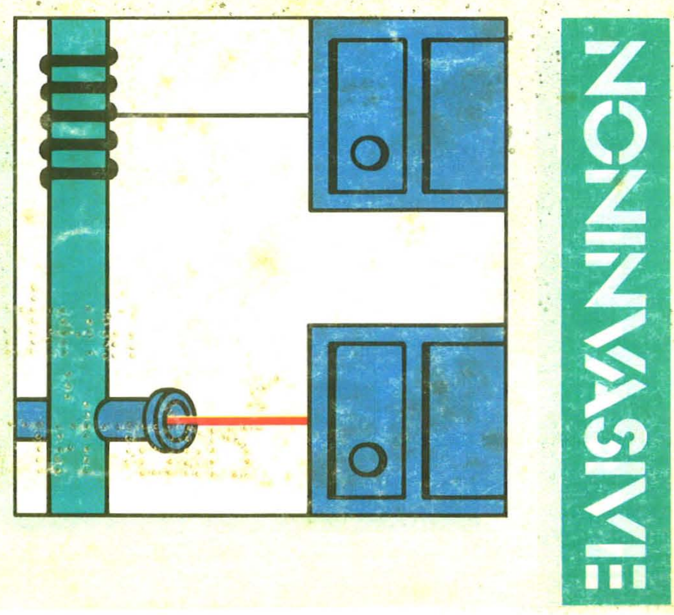
NONINVASIVE

Which SepTech Prep HPLC Instrument Meets Your Needs?

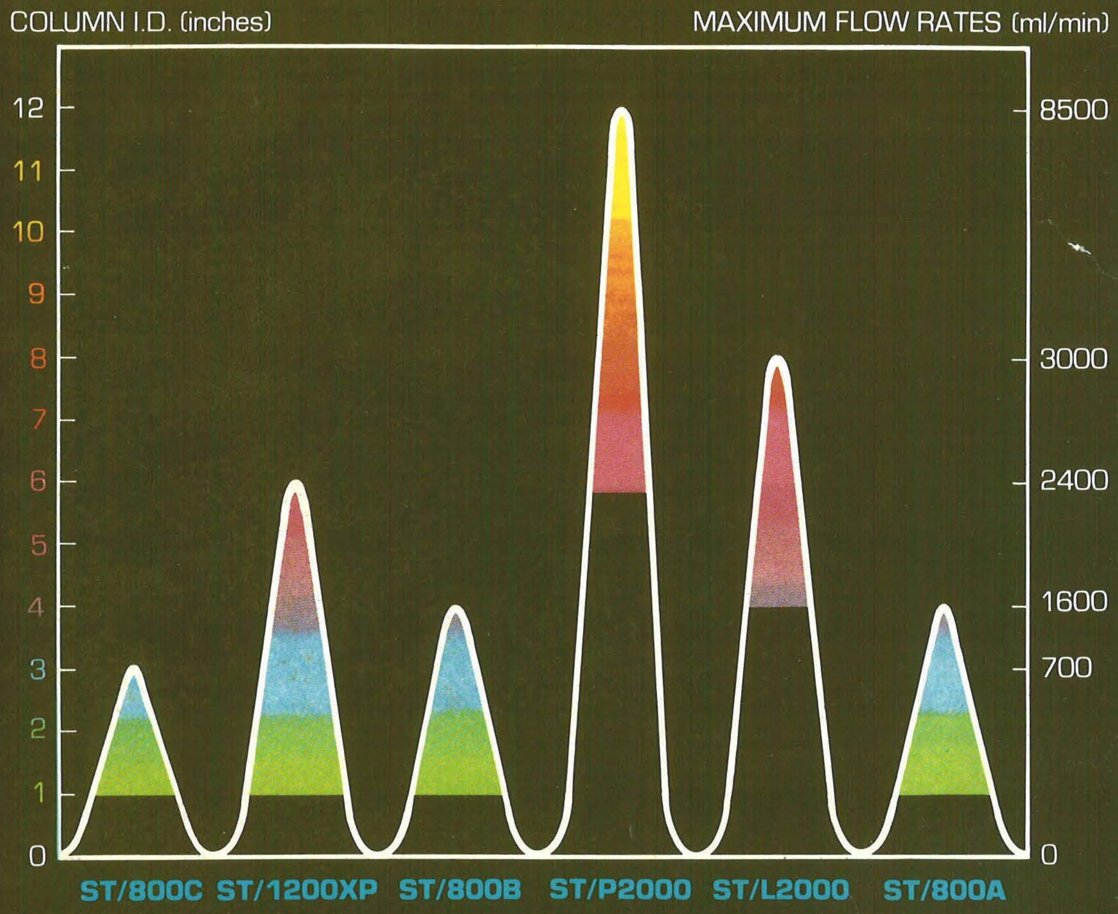

R&D SCALE

MG TO MULTIGRAM SAMPLE LOADS

ST/800A
- EXCELLENT SCALE-UP VERSATILITY
- ISOCRATIC OR GRADIENT MODELS
- 1800 PSI CAPABILITY

ST/800B
- PERFORMANCE SPECIFICATION IDENTICAL TO ST/800A
- GENESIS™ AUTOMATION MODULE (COMPUTER CONTROLLED)
- CONTINUOUS GRADIENT FORMATION

ST/800C
- HIGH EFFICIENCY PACKING MEDIA CAPABILITY (4000 PSI)
- WELL-SUITED FOR PEPTIDE/PROTEIN APPLICATIONS
- CONTINUOUS GRADIENT FORMATION
- GENESIS™ AUTOMATION MODULE (COMPUTER CONTROLLED)

CIRCLE 153 ON READER SERVICE CARD

PILOT PLANT SCALE

GRAM TO KILOGRAM SAMPLE LOADS

ST/1200XP
- MULTI-PURPOSE R&D/PILOT PLANT CAPABILITY
- SUPERIOR SCALE-UP VERSATILITY
- EXPLOSION PROOF
- GENESIS™ AUTOMATION SYSTEM (COMPUTER CONTROLLED)
- 1800 PSI CAPABILITY
- CONTINUOUS GRADIENT FORMATION

ST/Lab 2000
- BEST-SUITED FOR Kg SAMPLE LOAD CONDITIONS
- EXPLOSION PROOF
- GENESIS™ AUTOMATION MODULE (COMPUTER CONTROLLED)

CIRCLE 154 ON READER SERVICE CARD

PROCESS SCALE

MULTI KILOGRAM SAMPLE LOADS

ST/Process 2000
- SUPERIOR THROUGHPUT
- EXPLOSION PROOF
- EXCELLENT RELIABILITY
- 2000 PSI CAPABILITY
- GENESIS™ AUTOMATION MODULE (COMPUTER CONTROLLED)

FACILITIES PLANNING
- CONTRACT METHODS DEVELOPMENT
- CUSTOM SYSTEMS DESIGN
- PROCESS PLANT DESIGN

CIRCLE 155 ON READER SERVICE CARD

SepTech
SEPARATIONS TECHNOLOGY
P.O. BOX 63, 2 COLUMBIA ST., WAKEFIELD, R.I. 02879
(401) 789-5660

In minutes, we'll show you how to save HPLC hours with our free demo diskette.

GILSON
INTERNATIONAL
714 V1.1
HPLC SYSTEM CONTROL
© GILSON INTERNATIONAL, 1986

Don't waste a second!

Save time, reduce frustration and get the HPLC results you need faster than ever before. Just take a moment now and send for our free demo diskette.

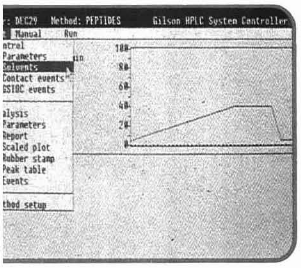
r: DEC29 Method: PEPTIDES Gilson HPLC System Controller
Manual
Run
ntrol
Parameters
Solvents
Contact events
GSIOC events
alysis
Parameters
Report
Scaled plot
Rubber stamp
Peak table
Events
thod setup
100
80
60
40
20
0

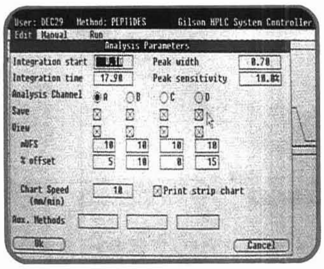
User: DEC29 Method: PEPTIDES Gilson HPLC System Controller
Edit
Manual
Run
Analysis Parameters
Ok
Cancel

Integration start [illegible]
Peak width 0.70
Integration time 17.90
Peak sensitivity 10.0%
Analysis Channel ● A ○ B ○ C ○ D
Save ☒ ☒ ☒ ☒
View ☒ ☒ ☒ ☒
mUFS 10 10 10 10
% offset 5 10 0 15
Chart Speed (mm/min) 10
☒ Print strip chart
Aux. Methods

You'll only need 15 minutes to learn how Gilson HPLC systems put you in total control with minimum effort.

Our new 714 HPLC System Controller software runs on an IBM PC AT™, using MS DOS™ and Microsoft Windows.™ This windows format gives you fast, easy access to all parameters for method development and data analysis.

The 714 controls up to four Gilson pumps, in addition to major peripherals like our 231/401 Auto-Injector and 116 UV Detector. And it doesn't stop there. Other application programs, like word processing and graphics, are supplied with our software, so you can use your computer for everything it was built to do.

Data analysis that's sophisticated, yet simple.

Our data analysis functions offer the sophistication you need with a simplicity you'll enjoy. Save, analyze and plot up to four channels, applying different parameters to each channel for optimal analysis. Get real-time, on-screen chromatography display in addition to hard copy printouts of all methods, plots and reports.

Re-analyze one or a hundred files, all automatically. The high-capacity memory is ideal for the multi-user, multi-application lab.

Gilson systems. Built to grow. Built to last.

Our systems are modular, so you can combine components to best suit your needs—from microbore to prep, at up to 100 ml/min. As your needs change, you can easily add components to meet those needs.

And every Gilson system is built to keep on running, day after day. So it stays on your lab bench. Not on a workbench.

We've done everything we can to simplify HPLC... the rest is up to you.

For immediate response, call toll-free 800-445-7667 for your free demo diskette. Or, circle the reader service numbers below for more information.

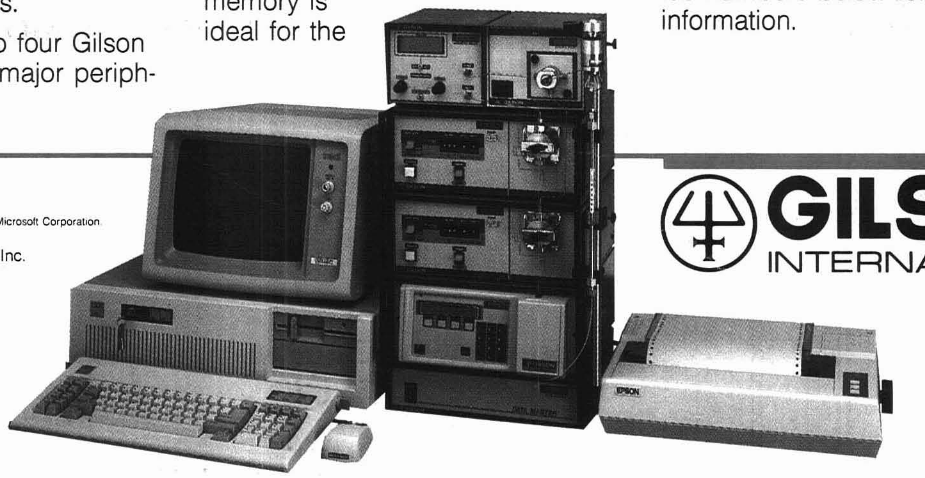

IBM PC AT is a registered trademark of International Business Machines Corporation.
MS DOS and Windows are registered trademarks of Microsoft Corporation.

© 1987 Gilson Medical Electronics, Inc.

GILSON
INTERNATIONAL

GILSON MEDICAL ELECTRONICS, INC., BOX 27, 3000 W. BELTLINE HWY., MIDDLETON, WI 53562 USA, TEL.: (608) 836-1551 TELEX: 26-5478
IN EUROPE: GILSON MEDICAL ELECTRONICS (FRANCE) S.A., 72 RUE GAMBETTA, B.P. NO. 45,95400, VILLIERS-LE-BEL, FRANCE, TEL.: (1) 39.90.54.41 TELEX: 696682

Circle (61) for literature. Circle (62) to have a representative call.

"B&J (is) much better in purity than competitors."

Paul L. Richard

Paul Richard
Monsanto Company
Luling, LA

"B&J was first and is the best. Trace impurities in other brands are greater."

Hugh Waldrum
Spectrum Labs
Dallas, TX

"Haven't used other brands...totally satisfied with B&J."

Dana Svedberg

Dana Svedberg
Witco Corporation
Bakersfield, CA

"Only use B&J."

John Alonzo

John Alonzo
Union Carbide
Bound Brook, NJ

"Exact specifications and competitive prices make B&J #1 on my list."

Angelita de Leone
Applied Biosystems
Foster City, CA

"Excellent product/good service."

Gregory R. Johnson
Schnee Morehead
Irving, TX

"B&J solvents are the only solvents that are used at Enviropact Laboratories."

Larry Korn
Enviropact, Inc.
Miami, FL

True Confessions

When professionals like these send fan mail, you know there must be something special about B&J Brand solvents. Find out why...by requesting our new 1987 HPLC brochure, write: Burdick & Jackson, 1953 South Harvey Street, Muskegon, MI 49442. For technical assistance, please call us toll free at 1 800 368-0050.

Burdick & Jackson
HIGH PURITY SOLVENTS

Manufactured by
Burdick & Jackson
A Division of Travenol Laboratories, Inc.
1953 South Harvey Street
Muskegon, MI USA 49442
Telephone 616 726 3171
800 368 0050

Distributed Exclusively in USA by
American Scientific Products
A Division of Travenol Laboratories, Inc.
1430 Waukegan Rd.
McGaw Park, IL USA 60085
Telephone 312 689 8410

CIRCLE 14 ON READER SERVICE CARD

MAY 1, 1987
VOLUME 59
NUMBER 9

ANCHAM
59(9) 603A–658A/1249–1376 (1987)
ISSN 0003 2700

Registered in U.S. Patent and Trademark Office; Copyright 1987 by the American Chemical Society

ANALYTICAL CHEMISTRY (ISSN 0003-2700) is published semimonthly by the American Chemical Society at 1155 16th St., N.W., Washington, D.C. 20036. Editorial offices are located at the same ACS address (202-872-4600; TDD 202-872-8733). Second-class postage paid at Washington, D.C., and additional mailing offices. Postmaster: Send address changes to ANALYTICAL CHEMISTRY Membership & Subscription Services, P.O. Box 3337, Columbus, Ohio 43210.

Claims for missing numbers will not be allowed if loss was due to failure of notice of change of address to be received in the time specified; if claim is dated (a) North America: more than 90 days beyond issue date, (b) all other foreign: more than one year beyond issue date, or if the reason given is "missing from files."

Copyright Permission: An individual may make a single reprographic copy of an article in this publication for personal use. Reprographic copying beyond that permitted by Section 107 or 108 of the U.S. Copyright Law is allowed, provided that the appropriate per-copy fee is paid through the Copyright Clearance Center, Inc., 27 Congress St., Salem, Mass. 01970. For reprint permission, write Copyright Administrator, B&J Division, ACS, 1155 16th St., N.W., Washington, D.C. 20036.

Registered names and trademarks, etc., used in this publication, even without specific indication thereof, are not to be considered unprotected by law.

Advertising Management: Centcom, Ltd., 500 Post Rd. East, Westport, Conn. 06880 (203-226-7131)

1987 subscription rates include air delivery outside the U.S., Canada, and Mexico

	1 yr	2 yr
Members		
Domestic	$ 25	$ 42
Canada and Mexico	50	92
Europe	77	146
All Other Countries	104	200
Nonmembers		
Domestic	37	62
Canada and Mexico	62	112
Europe	127	231
All Other Countries	154	285

Three-year and other rates contact: Membership & Subscription Services, ACS, P.O. Box 3337, Columbus, Ohio 43210 (614-421-3776).

Subscription orders by phone may be charged to Visa, MasterCard, Barclay card, Access, or American Express. Call toll free at (800) ACS-5558 from anywhere in the continental United States; from Washington, D.C., call 872-8065. Mail orders for new and renewal subscriptions should be sent with payment to the Business Management Division, ACS, P.O. Box 57136, West End Station, Washington, D.C. 20037.

Subscription service inquiries and changes of address (Include both old and new addresses with ZIP code and *recent mailing label*) should be directed to the ACS Columbus address noted above. Please allow six weeks for change of address to become effective.

ACS membership information: Bebe Olsen, Washington address.

Single issues, current year, $5.00 except review issue and LabGuide, $10.00; **back issues and volumes and microform editions** available by single volume or back issue collection. For information or to order, call (800) ACS-5558 or write the Sales Department at the Washington address.

Nonmembers rates in Japan: Rates above do not apply to nonmember subscribers in Japan, who must enter subscription orders with Maruzen Company Ltd., 3-10 Nihonbashi 2-chome, Chuo-ku, Tokyo, 103, Japan. Tel: (03) 272-7211.

Analytical CHEMISTRY

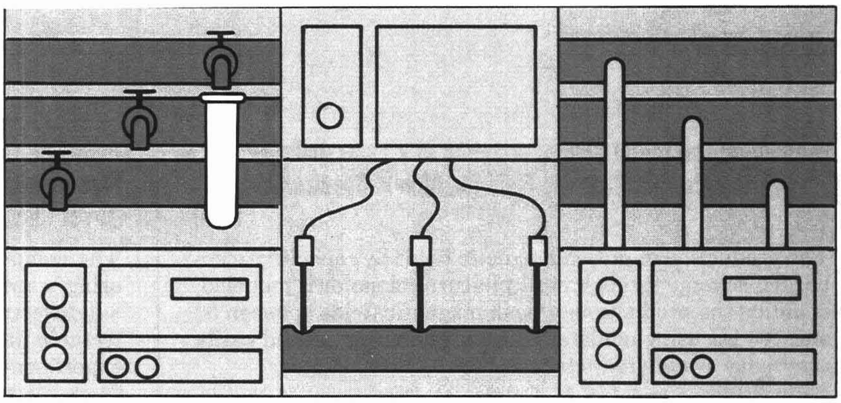

REPORT 624 A

***On the cover.* Process analytical chemistry.** The practice of process analytical chemistry involves much more than improved chemical sensing. James B. Callis, Deborah L. Illman, and Bruce R. Kowalski of the University of Washington discuss the technological, methodological, and chemometric advances that make a revolution in this field possible

BRIEFS 608 A

EDITORIAL 617 A

Postdoctoral associateships. The National Research Council, through its Postdoctoral Associate Program, provides opportunities for scientists in more than 28 government laboratories

NEWS 619 A

Capillary SFC patent validated: a victory for Lee Scientific and Brigham Young University. ▶ **Georges Guiochon** receives a joint appointment at the University of Tennessee and Oak Ridge National Laboratory

MEETINGS 638 A

Gordon Conference. This year's sessions of particular interest to the analytical community are on analytical chemistry, analytical pyrolysis, magnetic resonance, and separation and purification

BOOKS 642 A

Critical reviews. Books on computer-supported spectroscopic databases and air pollution analysis are reviewed by Charles Wilkins and Roger Jenkins

FOCUS 647 A

Pittsburgh Conference. Attendance at this year's conference and exhibition, held March 9–13 in Atlantic City, N.J., reached an all-time high of 31,555. A record 2040 booths were manned by 790 exhibitors, and 1145 technical papers were presented

NEW PRODUCTS & MANUFACTURERS' LITERATURE 652 A

AUTHOR INDEX 1249

ห้องสมุดกรมวิทยาศาสตร์บริการ

BRIEFS

Production and Initial Characterization of a Laser-Induced Plasma in a Pulsed Magnetic Field for Atomic Spectrometry 1250

The production of pulsed magnetic fields by capacitive electrical discharge through multiple-turn solenoids is modeled, enabling the production of peak magnetic fields between 50 and 100 kG using moderate discharge conditions and easily attainable system inductances.

Kelly J. Mason and Joel M. Goldberg*, Department of Chemistry, University of Vermont, Burlington, Vt. 05405
Anal. Chem., *59* (*1987*)

Removing Artifacts in Supercritical Fluid and Gas Chromatograms Generated from Fourier Transform Infrared Data 1255

Sloping baselines caused by density programming (SFC) or purge fluctuation (GC) are removed from chromatograms calculated from FT–IR data. The detection of weak signals is enhanced.

Richard C. Wieboldt* and D. Alan Hanna, Nicolet Instrument Corporation, 5225 Verona Road, Madison, Wis. 53711
Anal. Chem., *59* (*1987*)

Curve Resolution and Figures of Merit Estimation for Determination of Trace Elements in Geological Materials by Inductively Coupled Plasma Atomic Emission Spectrometry 1260

The method is used to evaluate the correction procedure, test the statistical significance of the determined concentration, and establish limits of detection for each sample.

Avraham Lorber*, Alon Harel, and Zvi Goldbart, Nuclear Research Centre—Negev, P.O. Box 9001, Beer-Sheva 84190, Israel, and **I. B. Brenner,** Geological Survey of Israel, 30 Malkhe-Israel Street, Jerusalem 95501, Israel *Anal. Chem.*, *59* (*1987*)

Continuous Infrared Spectroscopic Analysis of Isocratic and Gradient Elution Reversed-Phase Liquid Chromatography Separations 1266

The solvent from a microbore HPLC is evaporated with a heated gas nebulizer positioned just above a rotating reflective disk. Reflectance–absorbance IR spectra of the solution deposited on the disk are then recorded. Closely eluting components can be resolved; the sensitivity is in the low nanogram range.

John J. Gagel and Klaus Biemann*, Department of Chemistry, Massachusetts Institute of Technology, Cambridge, Mass. 02139 *Anal. Chem.*, *59* (*1987*)

Detection and Quantification of Picogram Amounts of Macrocyclic Trichothecenes in Brazilian *Baccharis* Plants by Direct Chemical Ionization Tandem Mass Spectrometry 1272

The compounds detected in these samples are quantified using a synthetically modified macrocyclic trichothecene, 8-ketoverrucarin A, as the internal standard. Minimum detectable limits of roridins and baccharinoids under various experimental conditions are 10–100 pg.

Thaiya Krishnamurthy* and Emory W. Sarver, Research Directorate, Chemical Research, Development, and Engineering Center, Aberdeen Proving Ground, Md. 21010-5423
Anal. Chem., *59* (*1987*)

Chemical Ionization in an Ion Trap Mass Spectrometer 1278

Chemical ionization can be performed by applying an appropriate sequence of rf voltages to an ion trap operated in the mass-selective instability mode.

Jennifer S. Brodbelt, John N. Louris, and R. Graham Cooks*, Department of Chemistry, Purdue University, West Lafayette, Ind. 47907 *Anal. Chem.*, *59* (*1987*)

Theoretical Description of Nonlinear Chromatography, with Applications to Physicochemical Measurements in Affinity Chromatography and Implications for Preparative-Scale Separations 1286

A theoretical model of nonlinear chromatography is derived, characterized by extensive computations of peak moments, and used to make physicochemical measurements in affinity chromatography.

James L. Wade, Alan F. Bergold, and Peter W. Carr*, Department of Chemistry, University of Minnesota, 207 Pleasant Street, Minneapolis, Minn. 55455 *Anal. Chem.*, *59* (*1987*)

Determination of Atmospheric Carbonyl Sulfide by Isotope Dilution Gas Chromatography/Mass Spectrometry 1296

Tenax, Molecular Sieve 5A, Carbosieve B, and Carbosieve S are evaluated for collecting atmospheric carbonyl sulfide. A precision of 2% is achieved at 500 parts per trillion by volume.

Ella E. Lewin, Rebecca L. Taggart, Marija Lalevic, and Alan R. Bandy*, Department of Chemistry, Drexel University, Philadelphia, Pa. 19104 *Anal. Chem.*, *59* (*1987*)

Gas Chromatographic and Mass Spectrometric Determination of Chlorophenoxy Acids and Related Herbicides as Their (Cyanoethyl)dimethylsilyl Derivatives 1302

Response–concentration plots show that detection is linear over several decades. Limits of detection are in the low picogram range for all compounds studied.

Michel J. Bertrand*, A. W. Ahmed, Benoit Sarrasin, and Victorin N. Mallet, Department of Chemistry, University of Montreal, P.O. Box 6128, Station A, Montreal, Quebec, Canada H3C 3J7
Anal. Chem., *59* (*1987*)

---

*Corresponding author

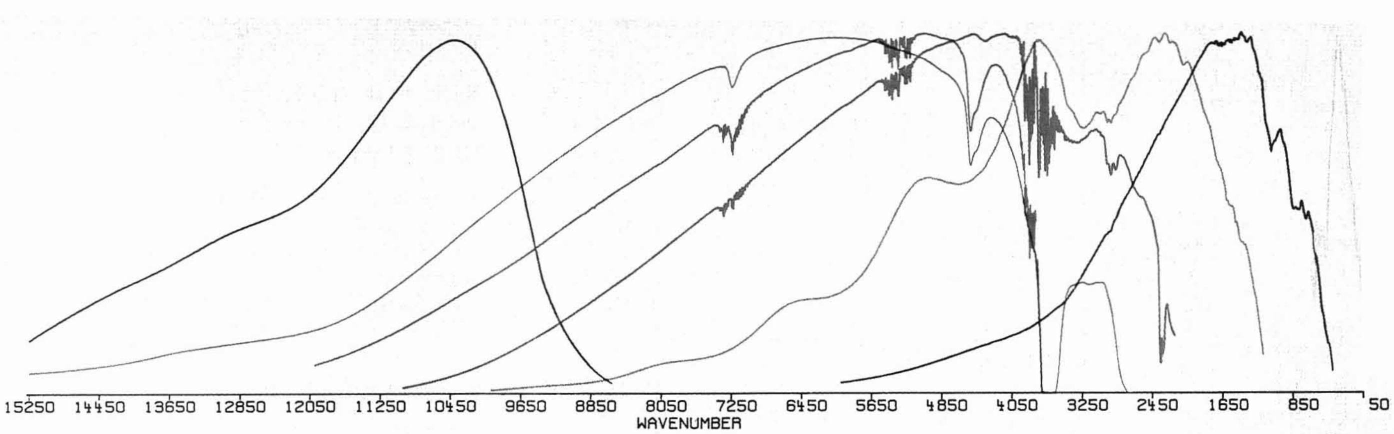

System 740 FT-IR provides routine spectral coverage from 15,000 - 50 cm⁻¹.

Nicolet's new System 740 FT-IR obsoletes the traditional notion of massive, complicated, expensive research spectrometers. The 740 is the first true bench-top spectrometer to combine 15,000 to 50 cm⁻¹ spectral coverage, research performance, versatile application capabilities and ease-of-operation in a system that is ideal for novice users and expert spectroscopists alike . . . at a system cost comparable to exclusively mid-IR systems.

System features include proprietary technology beamsplitters and detectors which are designed for "no hassle" interchange in one minute or less, without tools or loss of purge. Optimal alignment is performed quickly, accurately and *automatically* by advanced chemometric techniques. Exceptional signal-to-noise from the Near-IR to the Far-IR is enhanced by the industry's most advanced signal processing electronics.

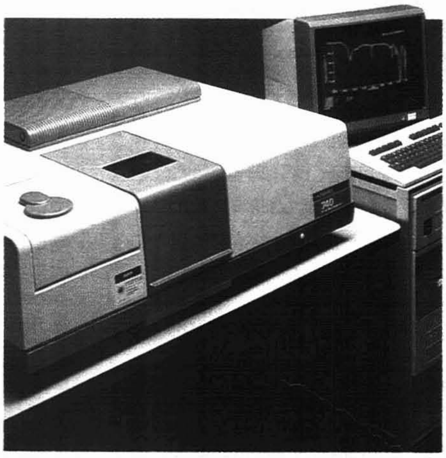

Expand your infrared spectral horizons into the near- and far-IR without going beyond your budget.

The System 740 has the versatility to accommodate all your applications including advanced hyphenated techniques such as GC-IR, TGA-IR and SFC-IR. Priced comparably with many mid-IR range spectrometers, the full spectral coverage System 740 is the best value in FT-IR today.

Nicolet

INSTRUMENTS OF DISCOVERY

Nicolet Analytical Instruments 5225-1 Verona Rd. / P.O. Box 4508 / Madison, WI 53711 / 608/271-3333 / Telex: 910-286-2736

CIRCLE 110 ON READER SERVICE CARD

Swagelok®
TUBE FITTINGS
...a tradition of Excellence

SWAGELOK
Patented
CRAWFORD PAT'D SWAGELOK

Unique Swaging Action

• Provides a seal between ferrule and body at a point different from where the heavy work is performed • Supports tube ahead of seal to resist vibration • Does not create torque or leave residual strain on tubing • Does not significantly reduce flow area.

Inspection Gage Assures Sufficient Pull-Up

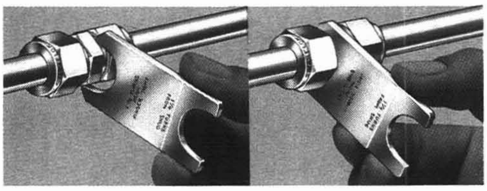

• Useful for both the installer and inspector
• If the gage will not fully enter the gap between the nut and body shoulder, fitting pull-up is sufficient • If the gage enters the gap, you'll know pull-up is incomplete.

Effective Metal-to-Metal Seal

• Interaction of precision parts — body, front ferrule, back ferrule and nut — produces a leak-free seal with simple 1-1/4 turn pull-up • Works on thick or thin wall tubing • Seals repeatedly under make-and-break conditions • Seals consistently over a wide range of pressures, temperatures and temperature cycling.

Only SWAGELOK Tube Fittings offer gageability of straight fittings, and forged shaped elbows and tees in stainless steel and steel. Gages are available for 1/8" through 1" sizes. Torque-free swaging action, effective sealing and gageability are just three of the many elements of excellence for which SWAGELOK Tube Fittings are known and respected...a tradition of Excellence.

Swagelok®
TUBE FITTINGS

SWAGELOK Co., Solon, Ohio 44139
SWAGELOK Canada, Ltd., Ontario

© 1986 SWAGELOK Co. / all rights reserved C-36f

CIRCLE 30 ON READER SERVICE CARD

BRIEFS

Microgram Scale Determination of Total Lipid Carbon in Valuable Sediments Using a Thin-Layer Chromatography/Flame Ionization Detector Analyzer 1306

A minimum of 60 samples of total lipid carbon can be analyzed in 10 min. The sample size averages 2.5 μg of lipid carbon with a standard deviation of ± 10%.

Kazuko Ogura*, Masako Ishimura, and Junko Hisatake, Department of Chemistry, Faculty of Science, Tokyo Metropolitan University, Setagaya, Tokyo, Japan 158 *Anal. Chem., 59 (1987)*

Supercritical Fluid Chromatography/Fourier Transform Mass Spectrometry 1309

The feasibility of on-line SFC/FT–MS is demonstrated by continuous introduction of supercritical CO_2 via a 50-μm i.d. 5-m bonded fused-silica capillary column maintained at 100 °C.

Edgar D. Lee and Jack D. Henion*, Drug Testing and Toxicology, New York State College of Veterinary Medicine, Cornell University, 925 Warren Drive, Ithaca, N.Y. 14850, and **Robert B. Cody* and James A. Kinsinger,** Nicolet Analytical Instruments, 5225-1 Verona Road, Madison, Wis. 53711 *Anal. Chem., 59 (1987)*

Isolation of Nonvolatile, Organic Solutes from Natural Waters by Zeotrophic Distillation of Water from *N,N*-Dimethylformamide 1313

Recoveries of hydrophilic organic standards from aqueous salt solutions and of natural organic solutes from water samples vary from 60 to 100%. Losses of organic solutes are related to the number of salt- and precipitate-washing cycles in the isolation procedure.

Jerry A. Leenheer*, Patricia A. Brown, and Eric A. Stiles, U.S. Geological Survey, P.O. Box 25046, Mail Stop 407, Denver Federal Center, Lakewood, Colo. 80225 *Anal. Chem., 59 (1987)*

Synthesis of Dabsylhydrazine and Its Use in the Chromatographic Determination of Monosaccharides by Thin-Layer and High-Performance Liquid Chromatography 1320

The limits of detection are in the 10-pmol (2-ng) range, and the optimum pH for the formation of monosaccharide dabsylhydrazones is ~2–3. The method is used to determine glucose concentrations in human serum and various fruit juices.

Jen-Kun Lin* and Shan-Shou Wu, Institute of Biochemistry, College of Medicine, National Taiwan University, Taipei, Taiwan, Republic of China *Anal. Chem., 59 (1987)*

Comparison of Extraction Techniques for Munitions Residues in Soil 1326

The abilities of four extraction techniques (Soxhlet, ultrasonic bath, mechanical shaker, and homogenizer–sonicator) and two solvents (acetonitrile and methanol) to remove munitions residues from two field-contaminated soils are compared.

Thomas F. Jenkins*, U.S. Army Cold Regions Research and Engineering Laboratory, 72 Lyme Road, Hanover, N.H. 03755-1290, and **Clarence L. Grant,** Department of Chemistry, University of New Hampshire, Durham, N.H. 03824 *Anal. Chem., 59 (1987)*

VICI

Valco Instruments Co. Inc.
P.O. Box 55603 Houston, Texas 77255
(713) 688-9345
TWX 910-881-5550 Telex 79-0033.

Valco Switzerland
Tannenberg P.O. Box 13 CH-6214 Schenkon
(045) 216868
Telex 72609 vici ch

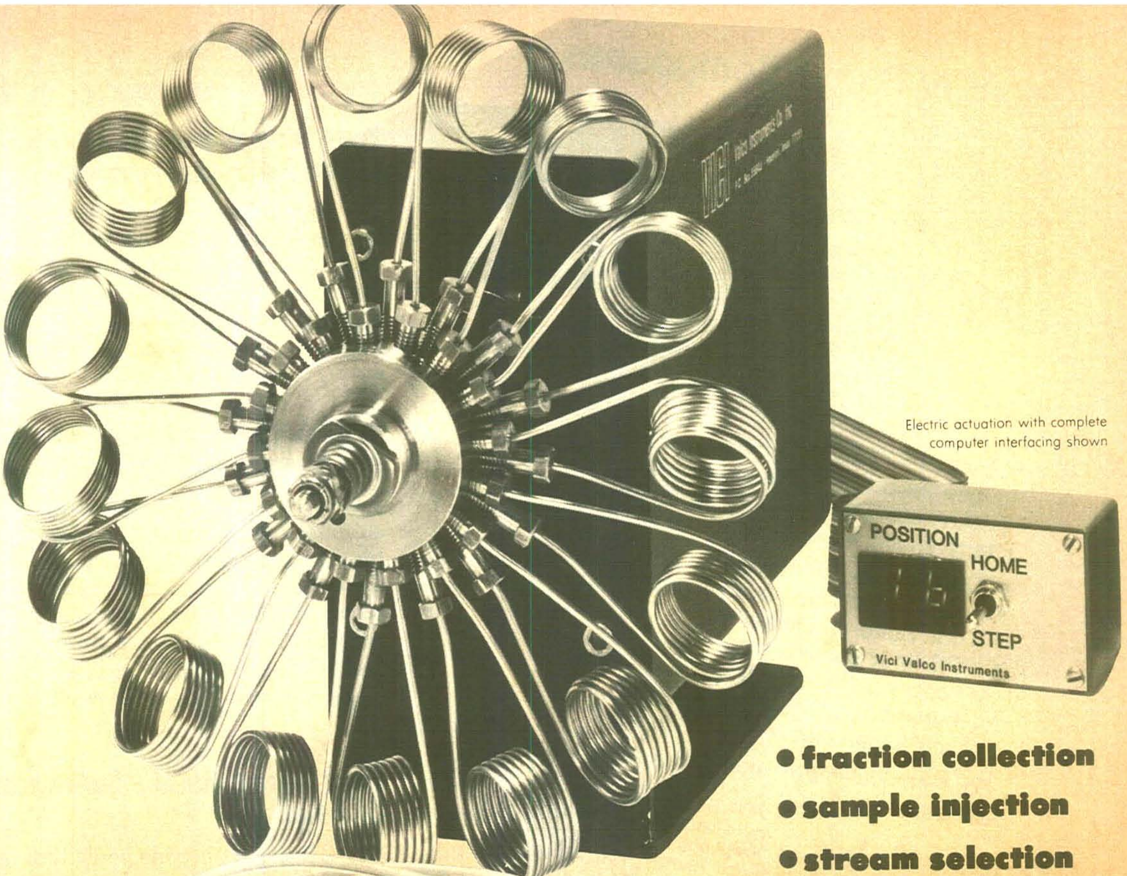
POSITION
HOME
STEP
Vici Valco Instruments

Electric actuation with complete computer interfacing shown

- **fraction collection**
- **sample injection**
- **stream selection**
- **reactor selection**
- **column selection**

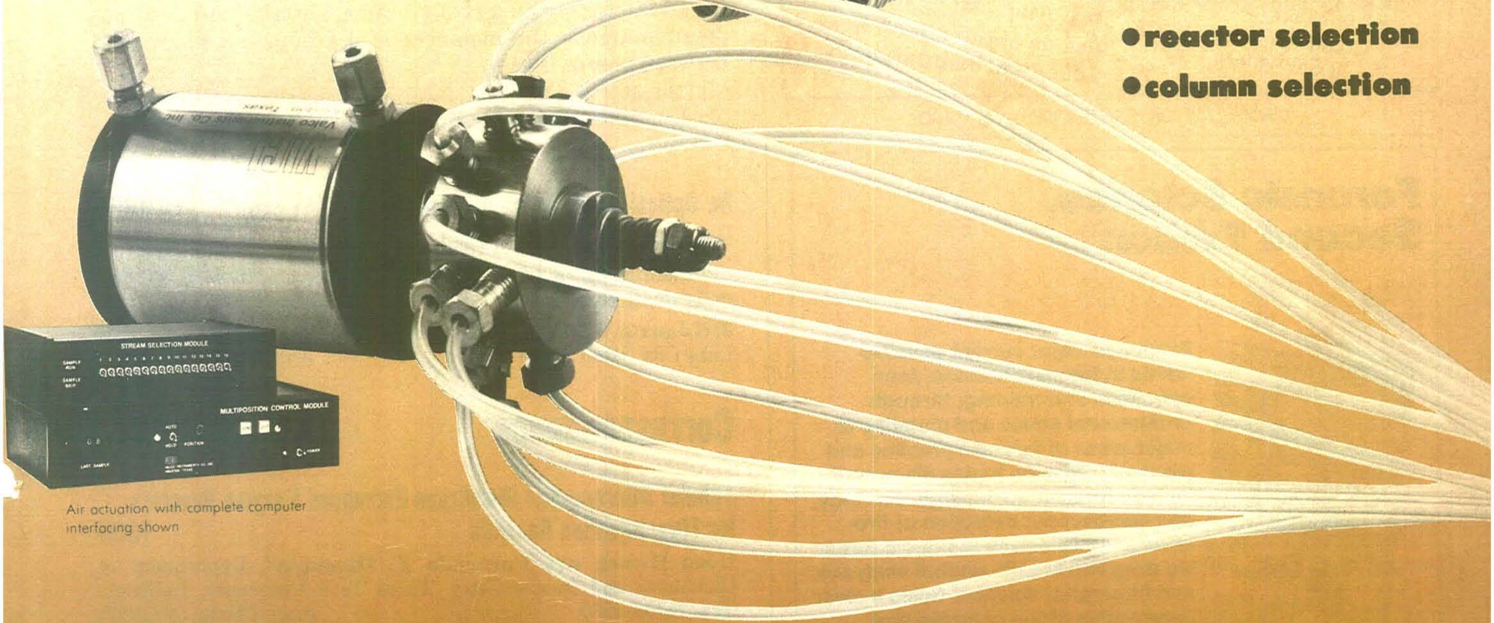
STREAM SELECTION MODULE
MULTIPOSITION CONTROL MODULE

Air actuation with complete computer interfacing shown

POWERFUL NEW TOOLS

FOR RESEARCH AND PROCESS CONTROL

Valco multiposition switching / sampling valves present a world of possibilities.

SD Type Flowpath
Inputs dead-ended, flow when selected, or input to multiple selected outputs.

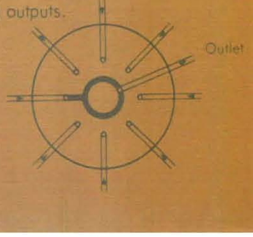

SC Type Flowpath
All inputs to a common outlet except selected one.

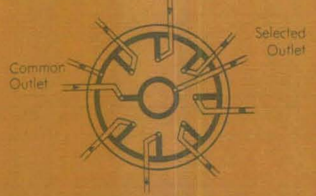
Selected Outlet
Common Outlet

SF Type Flowpath
Each input flows to individual outlet except selected one which is diverted.

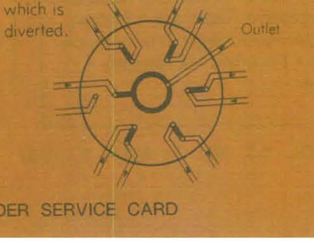

ST Type Flowpath
Used for multi-column, multi-sampling, or multi trap selection.

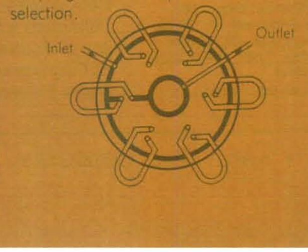
Inlet
Outlet

CIRCLE 170 ON READER SERVICE CARD

Separate and Identify Sulfur Compounds in Gases and Liquids

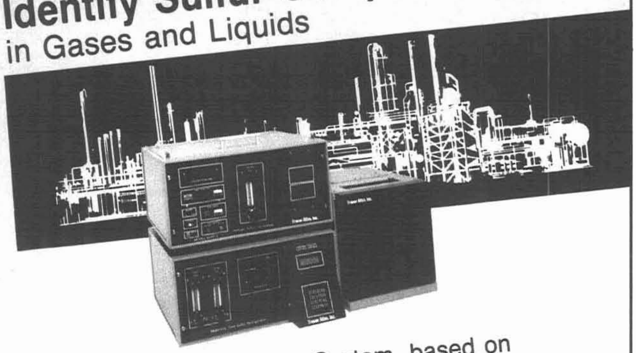

TRACOR ATLAS Sulfur System, based on unique patented and approved ASTM methods, quickly, economically and accurately provides interference-free analysis of sulfur compounds.

- Odorant Levels in Natural Gas
- Naphtha reformer catalyst protection
- Total Sulfur in olefins
- PPB level catalyst protection
- Product purity specifications
- Methanol synthesis catalyst protection
- Natural gas pipeline specifications

For technical information and application assistance contact:

Tracor Atlas
"Experience Keeps Us a Step Ahead"

9441 Baythorne Drive
Houston, Texas 77041-7709
Telephone: 713/462-6116
Telex: 75-0197 TRATLAS HOU UD
FAX: 713/462-1831

Ask us about our on-line analytical instrumentation

CIRCLE 156 ON READER SERVICE CARD

Forensic Science, Second Edition

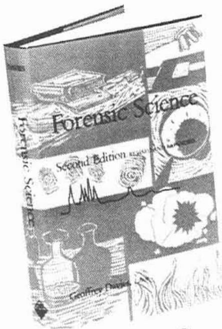

New!

Examines major current developments in forensic science, from education and training, through professional ethics and morality, to major areas of forensic practice and research. Specific topics discussed include forensic toxicology, serology, and microscopy; detection of firearms and explosives residues; forensic drug and breath-alcohol analyses; and fingerprint science. Gives a clear perspective of the potential and limitations of physical evidence in the administration of justice.

Geoffrey Davies, *Editor*
Northeastern University

388 pages (1986)
LC 85-28688
Clothbound
ISBN 0-8412-0918-9
US & Canada **$64.95**
Export **$77.95**
Paperbound
ISBN 0-8412-0919-7
US & Canada **$39.95**
Export **$47.95**

Order from:
American Chemical Society
Distribution Dept. 14
1155 Sixteenth St., N.W.
Washington, DC 20036
or CALL TOLL FREE 800-424-6747
and use your credit card!

CONTENTS

Forensic Science Education • On Being an Expert • Ethical and Moral Dimensions • Ethical Issues • Forensic Science in a Liberal Arts Curriculum • Forensic Science Courses • In-Service Training • Training and Research in the FBI • Practice and Training in Canada • Graduate Education • Forensic Science Research • Forensic Toxicology • Drug Analysis by HPLC • Breath-Alcohol Analysis • Genetic-Marker Systems • Firearms Residue Detection • Explosive Residues • Recovery of Accelerant Residues • The Science of Fingerprints • Forensic Microscopy • Trace Evidence

BRIEFS

Properties of an Asymmetrical Flow Field-Flow Fractionation Channel Having One Permeable Wall 1332

An asymmetrical flow FFF channel is developed, and its properties are examined both theoretically and experimentally. A mixture of proteins is fractionated to illustrate the potential for macromolecular separations.

Karl-Gustav Wahlund and J. Calvin Giddings*, Department of Chemistry, University of Utah, Salt Lake City, Utah 84112

Anal. Chem., *59 (1987)*

Retention by Electrical Field-Flow Fractionation of Anions in a New Apparatus with Annular Porous Glass Channels 1339

Polystyrenesulfonate and chromium phthalocyaninetetrasulfonate are retained in porous Vycor glass channels using high- and low-conductivity aqueous carrier. Retention ratios differ considerably from theoretical expectation, but measured and theoretical plate heights agree when the necessary parameters are estimated from experimental data.

Joe M. Davis, F.-R. F. Fan, and A. J. Bard*, Department of Chemistry, University of Texas at Austin, Austin, Tex. 78712

Anal. Chem., *59 (1987)*

Direct Determination of β-Lactam Antibiotics by Circular Dichroism 1349

The CD spectra of nine penicillins and three cephalosporins are characterized in pH 5.4 buffer. Discrimination is not possible among the members of a group, but distinction between groups is easy.

Neil Purdie* and Kathy A. Swallows, Department of Chemistry, Oklahoma State University, Stillwater, Okla. 74078-0447

Anal. Chem., *59 (1987)*

Do Optical Sensors Really Measure pH? 1351

The performance of optical and electrochemical sensors for determination of hydrogen and other ion activities is critically evaluated.

Jiří Janata, Center for Sensor Technology, University of Utah, Salt Lake City, Utah 84112 *Anal. Chem.*, *59 (1987)*

Correspondence

Tubular Microporous Membrane Entrapped Enzyme Reactors for Flow Injection Analysis 1356

Hoon Hwang and Purnendu K. Dasgupta*, Department of Chemistry and Biochemistry, Texas Tech University, Lubbock, Tex. 79409-4260 *Anal. Chem.*, *59 (1987)*

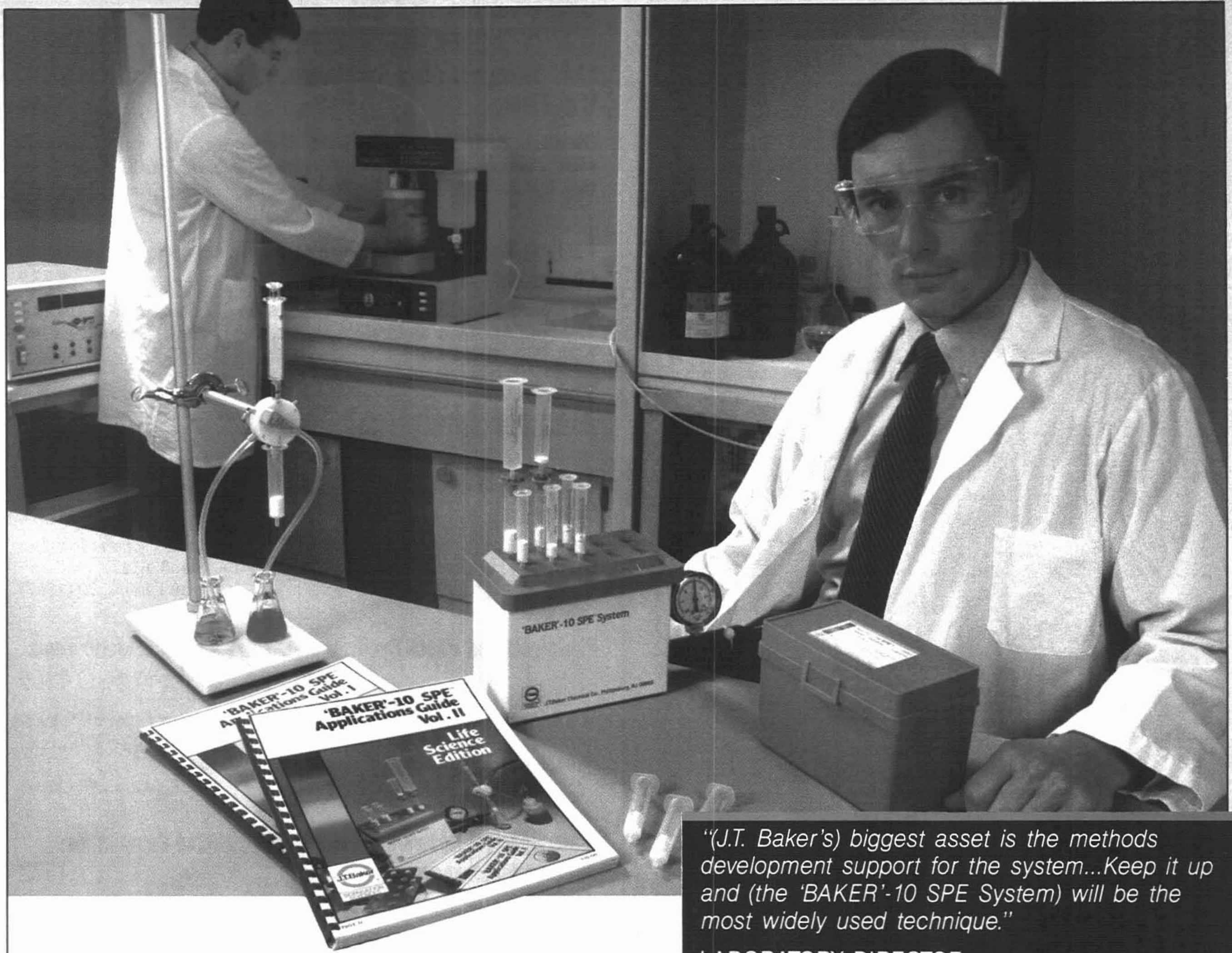

"(J.T. Baker's) biggest asset is the methods development support for the system...Keep it up and (the 'BAKER'-10 SPE System) will be the most widely used technique."

LABORATORY DIRECTOR

'BAKER'-10 SPE™

The Sample Preparation System That Comes With Built-In Applications Support.

Almost anyone can sell you a Solid Phase Extraction system to dramatically reduce the time you spend on sample preparation. Only J.T. Baker offers the applications support you need to make the technique work in your laboratory.

We developed the 'BAKER'-10 SPE™ family of products as alternatives to costly, time-consuming liquid/liquid extractions. With 'BAKER'-10, you can prepare samples 6 to 9 times faster. In minutes, your sample is ready for GC, HPLC, AA, UV, IR or RIA analysis.

But that's only part of the 'BAKER'-10 advantage. Through our knowledge of the chemistry and chromatographic principles behind the technique, we developed over 90 detailed procedures for preparing environmental, pharmaceutical, biological, food and cosmetic samples. You'll find these step-by-step procedures—and more—in Volumes I and II of the 'BAKER'-10 SPE Applications Guides. Plus, we offer courses in sample preparation, a Methods Development Kit, and a toll-free number you can call for solutions to specific sample preparation problems.

So if your application includes:

- Pesticides
- Herbicides
- PCB's
- PAH's
- PCB's in Transformer Oil
- Crude Oil
- Trace Metals
- Aflatoxins
- Caffeine
- Preservatives
- Nitrosamines
- Drugs and Metabolites
- Antibiotics
- Steroids
- Vitamins
- Catecholamines
- Nucleotides
- Carbohydrates
- Proteins
- Peptides

...and more...you can count on J.T. Baker to make Solid Phase Extraction work for you. Call us now for complete information.

CIRCLE 17 ON READER SERVICE CARD

J.T.Baker®

J.T. Baker Chemical Company
Research Products Division • 222 Red School Lane • Phillipsburg, NJ 08865 U.S.A.
Call Toll-Free: (800)582-2537 • In New Jersey or Canada: (201)859-2151 • FAX 201-859-2865 • Telex 299514 BAKR UR

Gross Gerau, West Germany • Deventer, Holland • Singapore • Mexico City, Mexico

ENVIRONMENTAL SCIENCE & TECHNOLOGY

ES&T

The premiere research publication in the environmental field.

Environmental science continues to be one of the fastest growing fields. And ES&T has grown right along with it!

ES&T continues to give you the practical, hard facts you need on this science . . . covering research, techniques, feasibility, products and services.

Essential reading for environmental scientists both in the business and academic world . . . ES&T has increased its emphasis on peer-reviewed research dealing with water, air, and waste chemistry in addition to adding critical reviews of important environmental science issues—all relevant to understanding the management of our natural environment.

Also included are discussions on environmental analyses, governmental regulations, current environmental lab activities, and much more!

For rate information, and to subscribe, call toll free:

(800) 424-6747

BRIEFS

Field Desorption Mass Spectrometry with Suppression of the High Field 1360

Stephen C. Davis, Gregory M. Neumann, and Peter J. Derrick*, School of Chemistry, University of New South Wales, P.O. Box 1, Kensington, 2033 NSW, Australia *Anal. Chem.*, *59* (*1987*)

Positive-Signal Indirect Fluorometric Detection in Ion Chromatography 1362

Kazimierz Jurkiewicz and Purnendu K. Dasgupta*, Department of Chemistry and Biochemistry, Texas Tech University, Lubbock, Tex. 79409-4260 *Anal. Chem.*, *59* (*1987*)

Aids for Analytical Chemists

Generation of Excess Low Frequency Noise on an Optical Source 1364

Edward Voigtman and James D. Winefordner*, Chemistry Department, University of Florida, Gainesville, Fla. 32611 *Anal. Chem.*, *59* (*1987*)

Photolysis and Photo Cyclic Voltammetry as Mechanistic Tools 1366

William R. LaCourse, Carl M. Selavka, and Ira S. Krull*, Barnett Institute and Department of Chemistry, 341 Mugar Building, Northeastern University, Boston, Mass. 02115 *Anal. Chem.*, *59* (*1987*)

Mass Spectral Analysis of Isotopically Labeled Compounds: Average Mass Approach 1372

Karl Blom, Cecil Dybowski, and Burnaby Munson*, Department of Chemistry, University of Delaware, Newark, Del. 19716, and **Bruce Gates and Lori Hasselbring,** Department of Chemical Engineering, University of Delaware, Newark, Del. 19716 *Anal. Chem.*, *59* (*1987*)

Microdetermination of Chlorine in Noble Metal Organic Compounds and Determination of Palladium by Atomic Absorption Spectrometry 1375

Virendra G. Shah and Suresh Y. Kulkarni*, Division of Organic Chemistry, National Chemical Laboratory, Pune 411008, India *Anal. Chem.*, *59* (*1987*)

Correction. Automated Sample Deoxygenation for Improved Luminescence Measurements 1376

M. E. Rollie, Gabor Patonay, and I. M. Warner*, Department of Chemistry, Emory University, Atlanta, Ga. 30322 *Anal. Chem.*, *59* (*1987*)

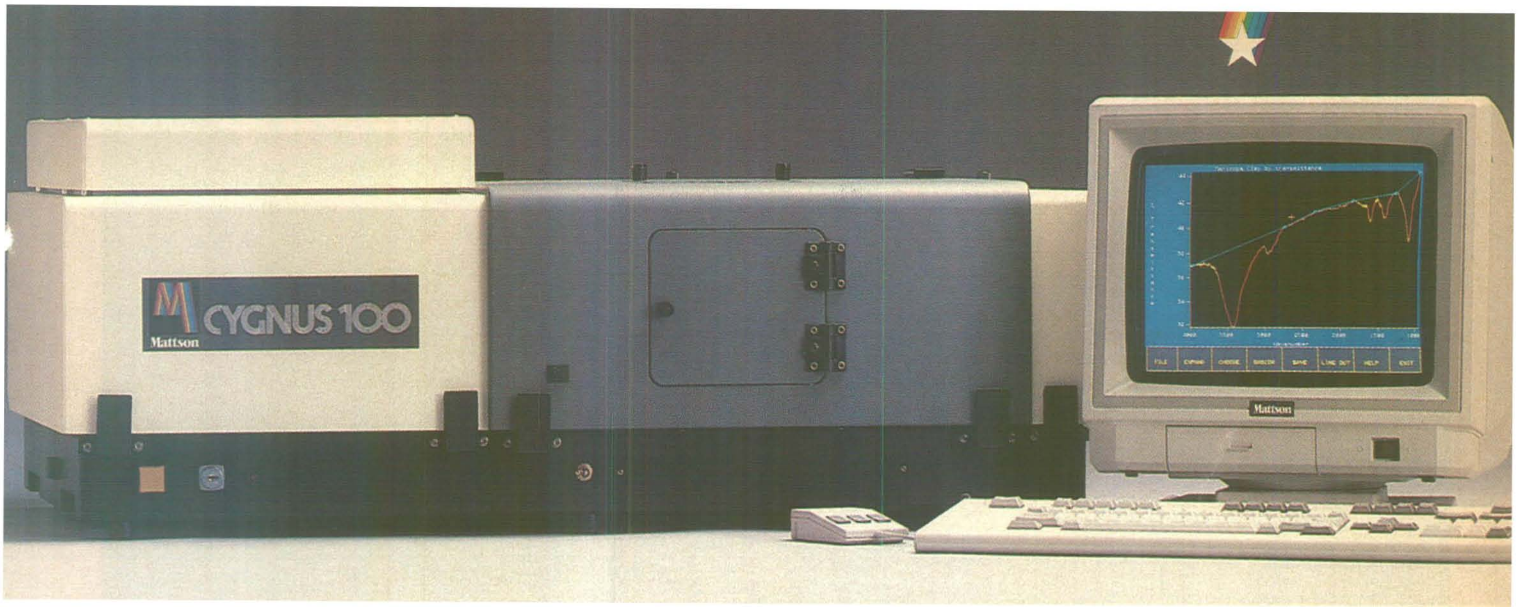

Cygnus® 100 FT-IR — 68020 Series Speed; EXPERT-IR™ Smarts

The Cygnus 100 FT-IR — powered by the most advanced 32-bit microprocessor on the market and backed by the only expert, knowledge-based FT-IR software package in the business.

That gives you fast access to the problem-solving expertise of hundreds of spectroscopists, educators, and senior analytical chemists — and features you won't find anywhere else. Multi-component quantitative analysis. Spectral deconvolution. Elegant search capability supported by an extensive library of commercial spectra and Mattson's exclusive relationship with Fluka Chemicals. Even MOM™ (Mattson Owner Maintenance) modem service.

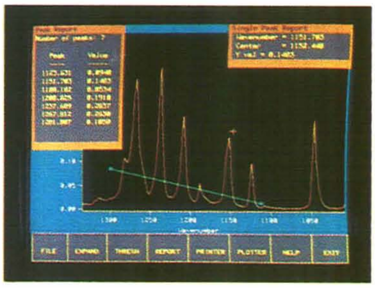

Cygnus 100 hardware redefines what a research-grade FT-IR is all about, too. Just compare the Cygnus 100 to what Digilab's FTS-40 offers and you'll see that only Mattson gives you these *standard* features. Like 0.125 cm^{-1} resolution for the stability that long, repeatable experiments demand. Stand-alone capability that lets you keep running spectra even when the computer is down or borrowed. Mouse control so you can do chemistry, not keypunching. Full expandability that means the Cygnus 100 can grow to meet your demands. Add to all that the best optics in the business, and it's easy to see that Cygnus 100 offers *far* more for the price.

Find out for yourself why the Cygnus 100 makes more analytical and financial sense in your lab. Send for technical literature today.

Cygnus 100 — the speed and smarts that leave the others behind.

Mattson Instruments, Inc.
1001 Fourier Court
Madison WI 53717 U.S.A.
Tel. (608) 831-5515
Telex: 262006
Fax: (608) 831-2093

Mattson Instruments, Ltd.
Linford Forum
Rockingham Drive
Linford Wood
Milton Keynes MK14 6LY
England
Tel. (0908) 679961
Telex: 82304 Forum G
Fax: (0908) 668974

Mattson Instruments Pty. Ltd.
88 Station Street
Nunawading, 3131 Victoria
Australia
Tel. (03) 873 2177
Telex: 151823
Fax: (03) 874 4215

Mattson

Cygnus™, EXPERT-IR™ and MOM™ are trademarks of Mattson Instruments, Inc.

CIRCLE 95 ON READER SERVICE CARD

Analyze your food and beverage samples in *minutes.*

When it comes to chromatographic analysis of food and beverage products, it makes more sense than ever before to contact Bio-Rad first. Because in addition to our experience and expertise, we've added a new dimension — HRLC™: The New Generation in HPLC. It combines speed, performance, and remarkable ease of operation.

Specific for your application

Our food analysis packages are geared to satisfying your specific analysis needs. For example, suppose you want to monitor preservative levels in soft drinks. That calls for our HRLC Isocratic UV Analyzer and Fast Preservative Analysis Kit. It's a complete package, with step-by-step protocols that guide you every step of the way. "Food and Beverage Analysis by HPLC," Bio-Rad's new applications book, is included.

In addition to our fast preservative kit, we offer applications kits for the following analyses:

- ***Fish spoilage analysis*** •
- ***Fermentation monitoring*** •
- ***Fruit quality* • *Ions in food*** •
- ***Corn sweeteners*** •
- ***Non-nutritive sweeteners*** •
- ***Organic acids* • *Carbohydrates*** •

With four different high resolution HRLC analyzers and an unparalleled selection of application kits and columns, we cover the entire analysis range from carbohydrates to alcohols to organic acids to aflatoxins. HRLC analyzers are available with your choice of UV, refractive index, fluorescence, or conductivity detection.

Pre-assembled and ready to go

When your HRLC analyzer arrives, it's pre-assembled, pre-calibrated, pre-plumbed, and extensively pre-tested. It'll be working in a matter of minutes.

To find out more how Bio-Rad can meet your specific analysis requirements, we invite you to contact us today.

BIO-RAD
ISOCRATIC UV ANALYZER
BIO-RAD
UV MONITOR MODEL 1306

BIO-RAD

Chemical Division

1414 Harbour Way South
Richmond, CA 94804
(415) 232-7000
800-843-1412

Also in Rockville Centre, NY; Hornsby, Australia; Vienna, Austria; Mississauga, Canada; Watford, England; Munich, Germany; Milan, Italy; Tokyo, Japan; Utrecht, The Netherlands; and Glattbrugg, Switzerland.

It's the Chemistry that Counts.™

CIRCLE 22 ON READER SERVICE CARD

Postdoctoral Associateships

Upon completion of graduate study, it is most advisable for anyone with a Ph.D. in the sciences to embark on a one- or two-year postdoctoral fellowship to prepare for a productive career in independent research. In addition to broadening one's expertise, the fellowship provides an excellent opportunity to work with leaders in respective fields. For those choosing an academic career, a postdoctoral fellowship is almost mandatory; however, it also can be very beneficial to those interested in careers in industry. Later in one's career a senior postdoctoral fellowship provides an excellent opportunity for faculty on sabbatical leave to gain expertise in a new area of research or to explore more deeply other aspects of his or her research.

Although one usually associates postdoctoral assignments with academic institutions, there are many excellent opportunities in government laboratories. The National Research Council (NRC), through its Postdoctoral Associates Program, provides fellowships on behalf of more than 28 federal laboratories at some 60 locations. Two important objectives of the program are to provide superior postdoctoral scientists and engineers with opportunities to research problems, largely of their own choice, that are compatible with the research interests and facilities of the sponsoring laboratories; and to contribute thereby to the general research efforts of the sponsoring laboratories.

For recent doctoral graduates, the research opportunities provided by the programs are a rewarding finale of formal career preparation. For senior investigators, the programs afford opportunities for full-time research without the interruption and distraction of other duties. The programs also provide an infusion of new ideas into the federal laboratories and stimulation for their permanent staff. At the same time, some of the unique research facilities in federal laboratories are made more readily available to the scientific and engineering communities.

These NRC fellowships are provided in a broad spectrum of disciplines including the chemical sciences, earth and atmospheric sciences, engineering and applied science, life sciences, mathematics, space sciences, and physics. A number of programs of particular interest to analytical chemists include those of the Environmental Protection Agency, the National Aeronautics and Space Administration, the National Bureau of Standards, the National Institutes of Health, and the Naval Research Laboratory. Several of my former students and colleagues have taken advantage of these opportunities and found them to be very rewarding. I encourage more analytical chemists to explore the possibilities available. Further information can be obtained from the National Research Council, Washington, D.C. 20418.

G. H. Morrison

SGE
MADE IN AUSTRALIA

how do you improve automated g.c. reliability

simply

Using SGE precision state of the art syringe systems.
Domed tip needles for extended septum life and reduced loading on autosampler mechanisms. SGE's predrilled PTFE coated triple layer septum provide system inertness and eliminates septum coring.
Replaceable needles in case of mechanical failure.
Sizes from 0.5 ul to 10 ul.
Contact your nearest SGE Office for details.

SGE

OFFICES: SGE AUSTRALIA - 7 Argent Place, Ringwood, Victoria, 3134. Telex: 33930. Telephone: (03) 874 6333.
SGE USA - 2007 Kramer Lane, Austin, Texas 78758. U.S.A. Telex: 9108741358. Telephone (512) 837 7190.
SGE UNITED KINGDOM - 1 Potters Lane, Kiln Farm, Milton Keynes, MK11 3LA. Telex: 825017. Telephone: (0908) 56 8844.
SGE FRANCE - 10 Rue Henri Janin, F94190, Villeneuve St. Georges, France. Telex: F201901 SGE. Telephone: 1/382 29 43.
SGE GERMANY - Fichtenweg 15, D-1608 Weiterstadt 1, Germany. Telex: 419518. Telephone: (6150) 40662.

CIRCLE 150 ON READER SERVICE CARD

AD.DAM 86129

Capillary SFC Patent Validated

The U.S. Patent and Trademark Office (PTO) has upheld the fundamental patent for capillary supercritical fluid chromatography (SFC), which is held by Brigham Young University (BYU) and licensed exclusively to Lee Scientific of Salt Lake City, Utah. Patent 4,479,380 had been under review since December 1985 as a result of contentions in the industry that the patent's claims had been fully anticipated by "prior art," that is, work published before the patent was granted.

On December 31, 1986, PTO preliminarily rejected the claims of the patent, and BYU was given the opportunity to respond to this interim decision. According to Lee Scientific president Hal Rosen, "The process of initially rejecting claims is a route the patent office tends to use. It's kind of a devil's advocate point of view, if you will, to put the burden back on the patent owner to really justify why those claims should be valid."

In its response to the patent challenge, BYU advised PTO to cancel one of the patent's 24 claims and to amend the wording of two other claims. On March 9, the first day of the Pittsburgh Conference exhibit, PTO made a final decision to confirm 21 of the original claims. The two amended claims were also accepted, and the 24th claim was cancelled as BYU had requested. Rosen had earlier predicted, "We expect that we will probably hear back from the [patent] examiner . . . by the time of the Pittsburgh Conference. We're quite confident that . . . the patent will be upheld." Although BYU did not learn of the ruling until just after the conference, this turned out to be a remarkably accurate prediction.

Did amendment of two claims and cancellation of another mitigate the power of the original patent? "In our opinion, no," Rosen responded. "The amendment of the two claims clarified what was the intent all along, that we were talking about a chromatographic process in capillary SFC. In our opinion, this does nothing to minimize the effect of the patent. As a result of these changes, the claim that was cancelled became redundant and was no longer needed."

"Some critics asserted the methods described in the patent were obvious to any chromatographer," Rosen continued. "After the fact, it is easy to claim that the invention would be obvious to someone skilled in the field, but it wasn't so obvious at the time. In fact, the practical application of SFC had eluded all those who had tried it prior to 1981, when Milton Lee and Milos Novotny published the first paper on capillary SFC in ANALYTICAL CHEMISTRY."

What effect do these decisions have on the competing manufacturers? "I think they are obviously disappointed," said Rosen. "It puts a real restriction on what they have to sell in SFC instrumentation. They can still sell packed-column instruments. In fact, a couple of manufacturers have been pushing very hard in that direction in the last few months. Packed-column SFC has its place. In fact, we have customers who are using our instruments for packed-column SFC. But it's not nearly as widely applicable as capillary SFC is. If somebody can get an instrument that can do both, they have a definite advantage."

Ray Houck of Suprex Corporation, a Lee Scientific competitor, contended that the patent "doesn't affect a lot of what we are doing and the approaches we are taking to SFC, so it's pretty much business as usual. But we are somewhat dismayed that the decision came out as it did because I think there were issues that could not legally be analyzed by PTO."

"I don't think anybody has done more than BYU and Lee Scientific to try to expand this technology," Rosen said, "and we're not going to try to bar the advancement of capillary SFC now. But I think people also have to realize that BYU has a tremendous investment in the development of capillary SFC, and it's only fair that it enjoy the benefits of that."

Rosen contends that sublicensing agreements are a possibility: "At this point I'm sure we'd be more than happy to listen to a good faith inquiry."

Guiochon Appointed Distinguished Scientist

Georges Guiochon, a leading authority on separations and an associate editor of ANALYTICAL CHEMISTRY, has accepted a joint appointment as distinguished scientist at the University of Tennessee—Knoxville and Oak Ridge National Laboratory. Guiochon is currently a professor of chemistry at Georgetown University, Washington, D.C. His tenure in the new position will begin this summer.

A native of Nantes, France, Guiochon completed graduate studies at Ecole Polytechnique in 1954 and doctoral work at the University of Paris in 1958. For the next 10 years he taught at Ecole Polytechnique and headed an analytical chemistry group that performed contract research for French chemical and petroleum companies and government agencies. He then served as director of the Ecole Polytechnique's Laboratoire de Chimie Analytique Physique (1968–84). He was appointed full professor at Ecole Polytechnique and the University of Paris (Université Pierre et Marie Curie) in 1974. Guiochon came to the United States in 1984 to accept the position at Georgetown.

For Your Information

Kratos Group PLC has signed an agreement to acquire Cambridge Mass Spectrometry Ltd. (CMS) of Cambridge, England. CMS markets and manufactures LIMA, a laser ionization mass analyzer for the microanalysis of organic and inorganic surface contaminants. CMS will operate as a subsidiary of Kratos.

Varian Associates has acquired all of the outstanding stock of Analytichem International for an undisclosed amount of cash. In 1984 Varian purchased a 20% interest in Analytichem, a supplier of bonded-phase sample preparation products. With completion of the acquisition, Analytichem becomes a subsidiary operating within Varian's Instrument Group, which had sales of $168 million in 1986.

ENVIRONMENTAL ANALYSIS

with Tekmar® Purge & Trap Concentrators

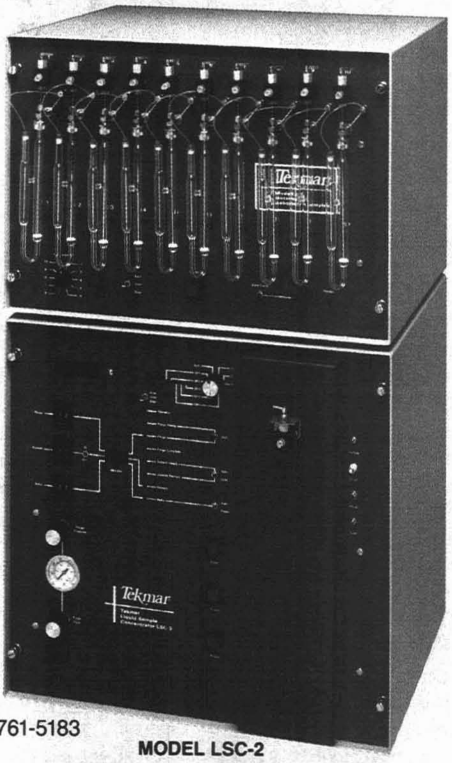

- Is in strict compliance with EPA protocols.
- Operates with wide bore capillary columns. An optional cryofocusing unit is available for narrow bore columns.
- Includes a "no compromise" automatic sampler with ten discrete samplers which provide true minimum carry-over.
- Is able to run any type of purge and trap sample: water, soils, sludge, slurries and air samples.

Since 1975 Tekmar *Purge and Trap Concentrators* have been used for the trace analysis of volatile organic compounds in environmental samples. Over the years Tekmar Concentrators have become the industry standard for their reliability and for providing the best reproducibility available. Most importantly, our products are supported by an integrated network of technical salespeople, application specialists, service engineers, and product managers with a level of experience greater than all of our competitors combined! ***Call us today for answers to your environmental analysis needs!***

Tekmar® ***The world's leader in Purge & Trap Technology.***

Tekmar Company, P.O. Box 371856, Cincinnati, Ohio 45222-1856
Call (800) 543-4461 / In Ohio (800) 344-8569 / Telex No. 21-4221 / Telefax (513) 761-5183
In Canada, call Technical Marketing Associates (416) 826-7752

CIRCLE 157 ON READER SERVICE CARD

PURGE AND TRAP

Introducing the new Model 4460 sample concentrator:

- Wide bore capillary capability at no extra cost.
- Full compliance with EPA protocols for standard methods.
- Microprocessor for easy, automated operation. Fully programmable.
- Times and temperatures for standard methods (including EPA 502.1/601 and 524.1) are default programmed.
- Autosampler optional. Up to 76 vials, auto rinse.

Write or call for details. Phone (409) 690-1711.
P. O. Box 2980, College Station, TX 77841.

O·I·CORPORATION

CIRCLE 120 ON READER SERVICE CARD

MOST USED

....because it's the most useful.

Published since 1955, the annual *LabGuide* leads all others in advertising pages and in reader usage (22,000 references daily). It's the true one-stop buying source where most manufacturers say with their ads, "Here we are. Compare our products with those of our competitors." That's why in more than six out of ten purchases by the 277,000 users it serves, the *LabGuide* is consulted before the purchase is made.

+159.93255 g
0.0000g
0.00000g
CAL
ON
OFF
PRINT

SARTORIUS.
The future is in the balance.

The most advanced analytical balance: a toploader with 160 g capacity, full-range precise readability, and ultra-fast LCD readout.

The new Sartorius R160P gives you features so advanced, they outweigh those of any other balance. Features that add up to toploader convenience and stability with semi-micro accuracy.

New advanced-generation LCD readout.
Larger, easier to read, crisper, with no distracting flicker. And ultra-fast update speed so you'll never again over-shoot target weight during formulation or fill weighing.

Comprehensive data displays.
In plain language—like POWER OFF, STANDBY, BUSY, CAL (calibration), or *g* (stable weight). And internal programs to let you select from a wide range of mass unit conversions.

New extra-accessible weighing chamber.
The sides and top of the R160P slide completely back to give you unrestricted access. Now, weigh bulky objects easily and pipette directly into large vessels on the weighing pan.

Poly-Range: readability matched to weighing range.
It's the broadest, most adaptable weighing range available: automatically activated, predetermined readability levels. Get the most sensitive level any time simply by taring.

R160P
L420P
L2200P
U3600P
E8100P

New Sartorius Poly-Range Balances

Single-touch front-panel operating ease.
Control all functions from the front panel. Switch on, program over 38 operational parameters, tare to zero, switch off. With one touch, calibrate to semi-micro accuracy over the full 160 g weighing range. The R160P returns to weighing mode automatically.

Sartorius leads the weigh.
Take advantage of the ultimate in electronic balance performance with the new Sartorius R160P—and a whole family of electronic Poly-Range Balances that cover every need, every application. Capacities up to 8 kg, readabilities down to 10 µg. Fast, comprehensive LCD readouts, compact design, complete single-touch front-panel control, optional computer/printer/keyboard interface (RS232C)–and economical prices. Now, as always, Sartorius leads the weigh. For more information or a demonstration: call 800-645-3050; in New York, 516-334-7500. Or write Brinkmann Instruments, Inc., Cantiague Road, Westbury, NY 11590.

Sartorius

Shaping the future. **Brinkmann**
INSTRUMENTS, INC.

BRK-5463

CIRCLE 18 ON READER SERVICE CARD

Process Analytical

James B. Callis
Deborah L. Illman
Bruce R. Kowalski
Center for Process Analytical Chemistry
Department of Chemistry, BG-10
University of Washington
Seattle, Wash. 98195

The goal of process analytical chemistry is to supply quantitative and qualitative information about a chemical process. Such information can be used not only to monitor and control a process, but also to optimize its efficient use of energy, time, and raw materials.

In addition, it is possible to simultaneously minimize plant effluent release and improve product quality and consistency. Although process analytical chemistry has long been an important endeavor in industry (*1*), it is now receiving increased attention because of the opportunities presented by technological and methodological advances, as well as changing needs within the chemical and allied products industries.

As an example, consider the potential impact of process analytical chemistry on the traditional production of basic chemicals. The emphasis is shifting from adding capacity to making existing plants more efficient to meet the demands of increasing international competition. This competition involves not only pricing; in many cases the issues of product quality and consistency are equally important. Greater emphasis has been placed on lowering the "quality cost" of production—the loss suffered when a batch of product fails to meet specifications and has to be reprocessed, sold at reduced cost, or discarded.

But more important are the possibilities posed by a decade of advances in materials science (*2*). With improved theoretical understanding of the relationship of molecular and supramolecular structure to material properties and with new synthetic methodologies and analytical instrumentation, materials scientists are producing advanced engineering plastics, ceramics, and composites of widespread applicability. It is frequently stated that those countries capable of manufacturing the new materials in quantity and at a competitive price will prosper in the next decade.

At the same time, we should not fail to mention two other recently emphasized areas of the chemical industry. The first is the use of living organisms to produce materials. Bioprocessing will continue to grow exponentially for at least the next two decades. The second is the production of specialty materials for the electronics industry. In some cases this might involve traditional chemicals that are of higher quality than those currently available (i.e., ultrapure solvents with low particulate counts). In other cases, new materials will be required for integrated optoelectronic semiconductor structures, ultramicrolithography, and ceramic substrates, to name a few examples.

The key element underlying all of these endeavors is improved process monitoring and control. Advances in electronic hardware, especially microcomputers, and improved algorithms for feedback control have led to the rapid implementation of distributed, intelligent control systems. Such networks already have vastly improved process optimization, materials accounting, resource utilization, and inplant management.

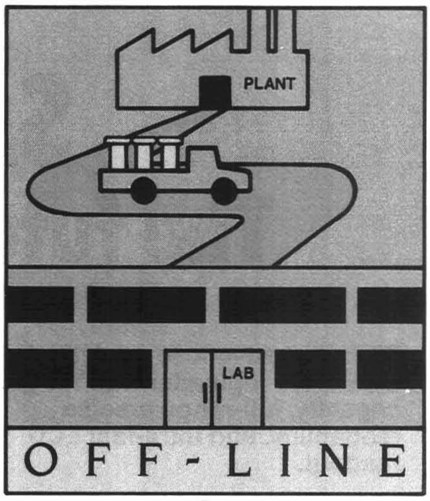

Although process engineers will continue to be preoccupied by process control intelligence issues, they will readily admit that the current process controllers are literally starved for information, and that the continuing lack of sensors, especially chemical sensors, has become a major bottleneck. Indeed, it is now widely appreciated that the same tools that have revolutionized the electronics industry have the potential to further the scope of chemical sensing, and a flurry of activity in this

Table I. Five eras of process analytical chemistry

Era	Current example	Future example
Off-line	GC/MS	Capillary electrophoresis with tandem MS detection
At-line	Colorimeter	Flow injection analyzer
On-line (intermittent)	Capillary GC	Microbore LC
On-line (continuous)	Correlation IR	FT-IR using circle cell
In-line	Conductivity sensor	Micro UV-vis with fiber optic probe
Noninvasive	Diffuse reflectance near-IR	Multifrequency microwave radar

0003-2700/87/0359-624A/$01.50/0
© 1987 American Chemical Society

Chemistry

REPORT

area has begun (3, 4).

However, one must realize that the practice of process analytical chemistry involves much more than improved chemical sensing (5). The issues of sampling (6), extraction of information from the sensor data, integration of the information into process control, and the sociological difficulties of gaining process engineers' and plant operators' confidence in the new measurement tools must all be given equal consideration. Clearly, process analytical chemistry should be considered a worthy subdiscipline of analytical chemistry, and it requires an interdisciplinary systems approach so that progress can be made. Our purpose is to acquaint the reader with the important technological, methodological, and chemometric advances that are making possible a major revolution in this field. We particularly recommend that our academic colleagues make a closer study of this field, not only for the employment opportunities it creates for students, but also for the intellectual challenges it offers creative scientists.

Five eras of process analytical chemistry

As a conceptual framework, we find it useful to identify five eras of process analytical chemistry: off-line, at-line, on-line, in-line, and noninvasive (see Table I). Historically, there has been no systematic progression of the eras, and it is not uncommon to find examples from all stages simultaneously functioning in a single modern chemical processing plant.

Off-line and at-line eras. The first two eras of process analytical chemistry are distinguished by the requirement of manual removal of the sample and transport to the measuring instrument. In off-line process analysis, the sample is analyzed in a centralized facility with sophisticated, and perhaps even automated, instrumentation. The advantages of this approach include the economy and efficiency of time-sharing use of expensive instruments and the availability of an expert staff for consultation, methods development, and maintenance. The disadvantages, which include the delay between submission of sample and reporting of results, the additional administrative costs, and the competition among users for the resources, have led to a second era: at-line process analysis. In this type of analysis a dedicated instrument is installed in close proximity to the process line. The advantages include faster sample processing, closer control of the analysis by the process personnel, and employment of a simpler instrument with less cost and maintenance and greater ease of use. The above eras of process analytical chemistry are so close to the usual practice of analysis that we will not discuss them further.

On-line era. In the on-line era of process analytical chemistry the subdiscipline becomes distinct from its parent. An automated sampling system is used to extract the sample, condition it, and present it to an analytical instrument for measurement (6). Yet another difference between process analyzers and their laboratory counterparts is the end point of the analysis. For the laboratory counterparts, one is generally trying to elucidate the chemical composition of a mixture (less frequently, to understand molecular structure and interactions). For the process analyzers, the end point might be much closer to quality parameters, such as octane number or elongation index. We will have more to say on this topic later.

It is possible to subdivide the on-line era into two categories: intermittent methods that require injection of a portion of the sample stream into the instrument and continuous methods that permit the sample to flow continuously through the instrument.

The classic example of an intermittent on-line process analyzer is the gas chromatograph. Until recently, packed columns held at a fixed temperature

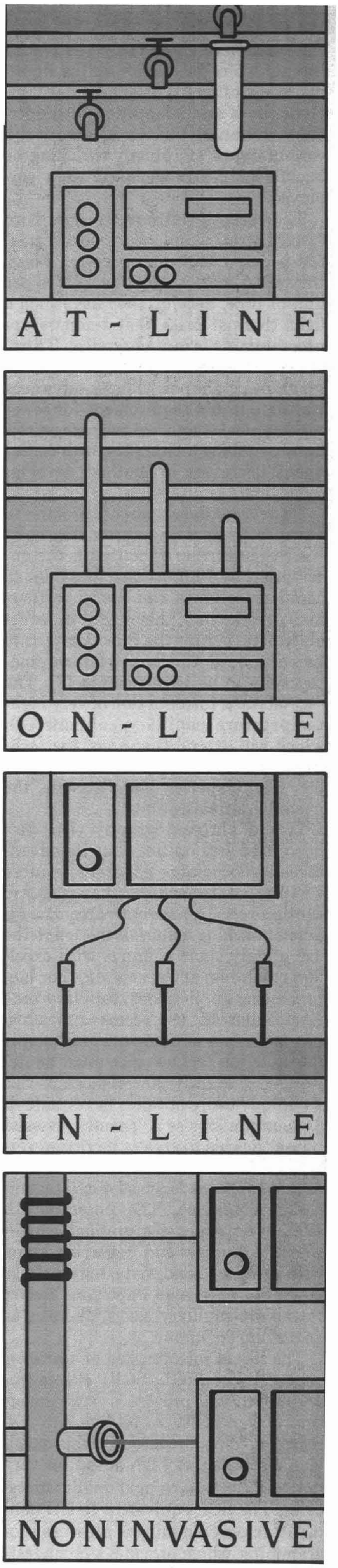

generally were employed. This placed the burden of selectivity on the liquid phase and often led to lengthy development times and adaptation of proprietary stationary phases. Alternatively, various types of column switching or backflushing arrangements were employed.

The recently introduced wide-bore fused quartz columns seem nearly ideal for process chromatography. First, they yield more theoretical plates per unit of time. Second, they have such a light thermal mass that temperature programming is quite practical. Third, the columns are inert and yield almost ideal peak shapes. These advances translate into a requirement for fewer types of phases and less reliance on column-switching techniques, with consequent decreases in method development time.

Two recent developments promise to advance process gas chromatography (GC) even further. The first is the observation by Phillips that the inlet to capillary columns can easily be thermally modulated; this might, in favorable cases, permit the injection port to be eliminated and multiplex chromatography to be implemented (*7*). The second is the introduction of very high-temperature capillary columns (*8*), which will extend the use of the technique to ever more polar, high molecular weight species and decrease the need for derivatization.

Liquid chromatography (LC) has been used less on-line, but its advantages are becoming apparent as more complex, water-soluble materials are synthesized. The advent of smaller diameter packing materials has led to the use of very short columns with excellent resolution and sensitivity. For bioprocessing applications, capillary zone electrophoresis (*9*) seems appealing, but new types of detectors and sample introduction technologies must be developed. Recently, an offshoot of this technique using micelles or tetraalkylammonium ions as a "pseudo reversed phase" has led to greatly increased versatility for the technique and should provide impetus for accelerated technical development. The potential for eliminating expensive, unreliable high-pressure pumps and replacing them with compact, solid-state, high-voltage power supplies is an important reason to explore capillary electrophoresis as an on-line technique.

The recent introduction of a process supercritical fluid (SCF) chromatograph (*10*) will provide a new dimension of versatility to on-line chromatography. This technique yields excellent resolution at high speed on very nonvolatile polar, heat-labile molecules. The SCF equivalent to GC temperature programming is pressure programming, which provides a much faster recycle time. Compared to an LC, the SCF system does not need expensive solvents and is much faster, especially from the standpoint of recycling, when a solvent programmed run is employed.

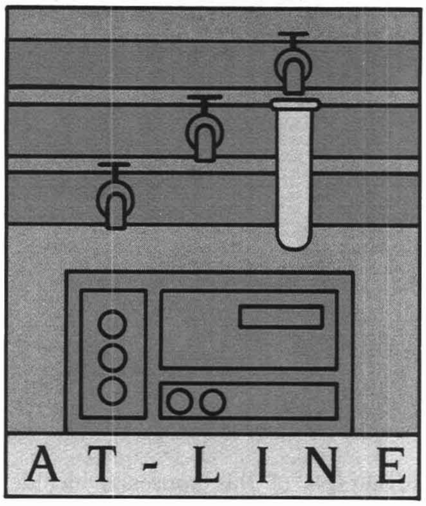

The final intermittent technique to consider is flow injection analysis (FIA), a technique that may be thought of as an on-line alternative to manual wet chemical analysis (*11*). The major advantages of FIA are high throughput, reliability, and precision. However, an even greater range for FIA will be forthcoming as new technologies are added. First is the capability to perform on-stream liquid–liquid extractions. Second is the incorporation of a chromatographic step. Third is the inclusion of sophisticated multichannel, rapid-scan spectroscopic detectors to provide a more robust single-component analysis or simultaneous multicomponent analysis. As these capabilities are added to FIA, it will become more apparent that this technology is an appealing paradigm for developing an automated universal microlaboratory that integrates the functions of sample acquisition, clean-up, concentration, separation, sensing, and identification. Process engineers will find the approach particularly attractive because it so closely resembles the flow-stream concept used in automated chemical-processing lines.

Continuous on-line process analysis is the first era to offer true real-time capability. The instrumentation is largely spectroscopic in nature. Until recently, spectroscopic devices were limited by the technological constraints imposed by extreme reliability requirements, the hostile nature of the plant environment, and the necessity to remain accurate through long periods of inattention. In the past, such constraints led to the development and use of dedicated process analyzers that achieved ruggedness and reliability at the expense of analytical power. As an example, consider infrared (IR) spectroscopy. Process IR analyzers previously were based on nondispersive, dual-cell correlation devices with microphone detectors. The state of the art in laboratory analysis is, of course, the Fourier transform infrared spectrometer (FT–IR), an instrument that in the past would hardly have been thought suitable for use on the factory floor. Thanks to innovative design, the reliability of laboratory instruments has so greatly increased that the FT–IR is being used on-line. At least two commercial manufacturers have begun to offer instruments that were developed specifically for on-line process analysis. Another trend that has enhanced the versatility of FT–IR use on-line is the development of improved methods for continuous sampling. For liquid streams, attenuated total reflectance (*12*) offers a way to eliminate ultra-narrow path-length cells and their attendant difficulties with blockage from particle matter in the sample and interference fringes. In addition, this approach is well suited to analysis of multiphase processes such as emulsions. The cylindrical geometry cell provides a simple method for implementing attenuated total reflectance technology in a form well suited to high-pressure, high-temperature, mixed-phase process applications (*13*).

In the ultraviolet–visible (UV–vis) arena, technological developments have made scanning versions of these instruments far more rugged and reliable. Three key concepts are the adaptation of single-beam techniques that use stored baselines rather than mechanically sampled reference and sample compartments; the use of concave holographic gratings that yield acceptable stray light rejection in a single monochromator and eliminate the need for collimating mirrors; and the introduction of photodiode arrays that eliminate mechanical scanning of the grating (*14*). The current generation of low-end UV–vis spectrometers based on these principles is almost cost-competitive with filter wheel photometers and is certainly more cost-effective and just as reliable.

In-line era. The major disadvantage of on-line analysis is the need to construct a separate analytical line that properly samples the main stream and presents it to the instrument at a suitable temperature and pressure. This has led to the fourth era: in-line process analytical chemistry. Here, chemical analysis is done in situ, directly inside the process line, using a probe that is chemically sensitive. In its ideal form, the device might resemble a typical industrial temperature probe. Such an implementation obviously would be attractive to process engineers.

It is widely believed that the key to scaling down chemical sensors is to fab-

In LC sample injection, "just right" is all wrong.

Rheodyne explains why.

Why not load a 20-μL sample into a 20-μL sample loop? Seems just right. But it's all wrong.

It's wrong because loading a volume of sample equal to the volume of the loop produces the worst accuracy and precision. Much more sample—or much less—is better.

This is one of several important facts about LC sample injection not immediately apparent to those who use liquid chromatographs. All are explained in our one-page bulletin, "Tips on LC Injection." It clears up many common misconceptions. And helps you get better quantitative results.

For a copy contact Rheodyne, Inc., P.O. Box 996, Cotati, California, 94928, U.S.A. Phone (707) 664-9050.

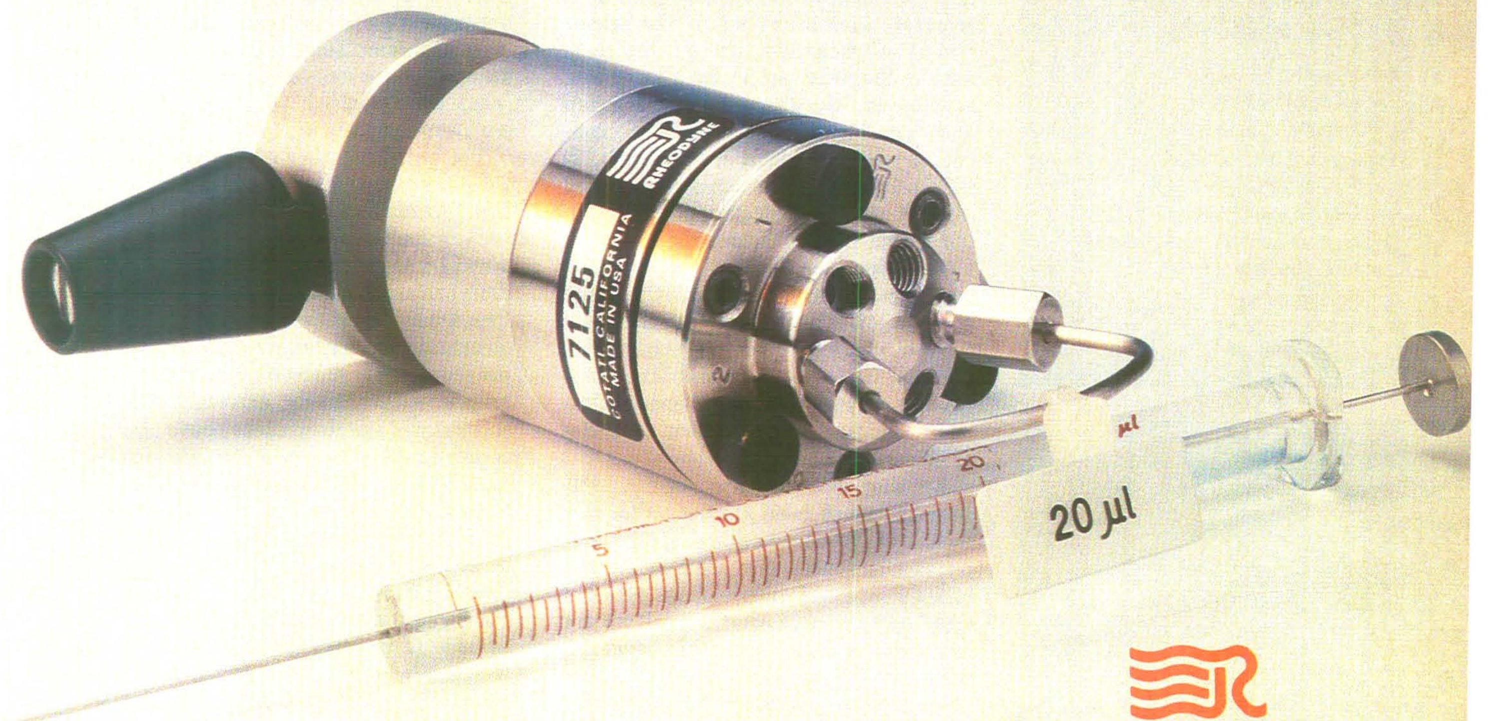

RHEODYNE
THE LC CONNECTION COMPANY

CIRCLE 140 ON READER SERVICE CARD

ricate them with tools that originate in the microelectronics revolution: microlithography and micromachining (*3*). Virtually all of the microsensors fabricated to date use a two-stage detection scheme. In the first stage, chemical selectivity is obtained by a chemical transformation or by physisorption or chemisorption to a chemically selective surface. Table II lists various schemes that have been used to obtain chemical selectivity for microsensing. In the second stage, some physical consequence of the chemically selective stage, such as release of heat or change of optical absorption, is converted to an electrical signal by a suitable microtransducer. Table III lists the various physical properties that can be sensed and the types of transducers that have been employed. Together Tables II and III form a matrix of possibilities for chemical sensing. Virtually all entries in the tables have been explored.

The most noted of the microsensors are the CHEMFET and the ISFET (*15*). The ISFET, which was first reported by Bergveld some 15 years ago, arose from a desire to scale down common pH or ion-specific electrode technology. It is therefore important to note that such devices share all of the advantages and disadvantages of potentiometric electrochemical detectors. It is now widely appreciated that the development of long-lived, reliable versions of these devices will require considerable progress in encapsulation and packaging.

Table II. Chemical/physical transformations employed in microsensors to obtain chemical selectivity

Chemical transformations
- Electrochemical
- Enzyme catalyzed

Physisorption to a surface
- From gas phase
- From liquid phase

Binding to an immobilized receptor
- Immunoadsorption
- Ion exchange

Membrane transport
- Electrolyte separation

ble III. Techniques for detection and nsduction employed by chemical icrosensors

hysical property	Transducer(s)
hemical potential	Field effect transistor
ptical	Photodiode
eat	Thermistor, pyroelectric
ass	Piezoelectric balance
ass	Surface acoustic wave
onduction	Dielectrometer
urface resistance	Chemiresistor, Taguchi
urrent flow	Ampometer

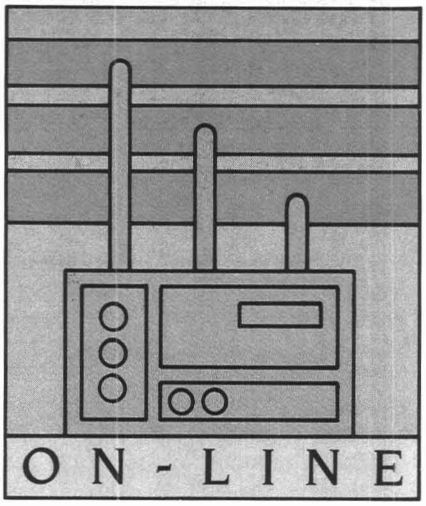

In the CHEMFET, the ion-selective membrane is replaced by a chemically selective layer. For example, a palladium-gate FET has been developed for detection of hydrogen at the parts-per-million level. Janata pioneered the use of this approach for biochemical detection by developing enzyme-based (ENFET) and antibody-based (IMMUNOFET) sensors. One of the major issues in the design of these microsensors is the optimization of their responses. (See the paper by Janata and co-workers that shows the multitude of considerations involved [*16*].)

A second class of microsensors takes advantage of the electrooptical revolution: fiber optic sensors (*4*). With these microsensors, probe light is generated remotely and conveyed to the sensor end by a light guide, where it interacts with a chemical probe by absorption, scattering, fluorescence, or Raman emission. The light, which has been encoded with chemical information, is then returned by the same or a second light guide to an electrooptical transducer that creates the desired electrical signal. Such an optical technique is very versatile. One has the entire range of chemistries developed over the years as spot tests to provide inspiration. Many of these can be immobilized onto glass or polymer beads and encapsulated into microcuvettes to form optrodes of all sorts.

Another use of fiber optics may prove to be of even greater value as a means of elevating optical spectroscopy to the fourth era. This is accomplished by developing various types of fiber optic probes that substitute for the conventional sampling streams. Still another advantage of this approach, as pointed out by Hirschfeld (*17*), is the ability to employ fiber optic multiplexing schemes so that a single expensive instrument can be placed in a safe, convenient location to sense multiple points in a process line. At present, fiber optic sensing is limited to the UV–vis–near-IR, but new types of IR transparent glasses are rapidly being developed.

Thus far, we have confined our thinking about chemical microsensors to the one-sensor/one-analyte concept. These microsensors, however, offer many other possible applications, and we find it useful to think in terms of a hierarchical complexity of devices that the microelectronics paradigm provides. Simple single sensors are at the first level.

The second level in the hierarchy is the sensor array. Here, the ability to use microlithography to fabricate multiple sensors on one chip is an obvious way to avoid having multiple probes for multiple analytes. The straightforward approach to implement a multifunction sensor is to devote one sensor to each analyte of interest. This method, however, does not address the well-known problem of interferences in the chemical selectivity step. An alternative strategy is to use a set of relatively unselective sensors, each of which has a different response profile to all the analytes of interest. In this case, the array generates a response pattern that may be analyzed by various powerful methods of multivariate statistics and pattern recognition. The combination of sensor array and data processing constitutes a robust analytical system that can yield simultaneous multicomponent analyses with the capability of recognizing and correcting for interferences and drift (*18, 19*). The same multivariate methods also may be used to optimize specific multicomponent analyses problems, selecting the minimum number of sensors or sensing channels (e.g., wavelengths) to yield optimal performance (*20*).

The third member of the microsensor hierarchy is the ultraminiature optical spectrometer. One possible approach employs the highly successful optical imaging device, which is a microfabricated array of photosensors. Previously these devices were used as electronic photographic plates in conjunction with conventional spectrographs. Alternatively, extremely small solid-state spectrometers have been constructed using tiny diffraction gratings and graded index of refraction lenses as collimators (*21*). Unfortunately, diffraction gratings do not scale down very small, because fewer and fewer grating lines are sampled and lower resolution results. A different approach is multibeam interferometry, which is widely known as the basis of interference filters. Here, wavelength analysis takes place over the dimensions of microns rather than centimeters. One suitable implementation of this concept is the linear interference

The new Brownlee SFC System Two:
Because SFC shouldn't be a mystery.

Now there's a supercritical fluid chromatography (SFC) system that impresses you with results, not theory. The new Brownlee SFC System Two goes from sample injection through peak integration with just a few simple commands. Its fully integrated system incorporates the state-of-the-art in pump technology, a capillary GC and an IBM® compatible microcomputer.

Second generation pump design, based on the successful Brownlee MicroFeed™ Pump, gives you uninterrupted fluid delivery. There is no stopping to refill, ever. Unlike the oversized pumps of the competition, the Brownlee SFC System Two does not require refrigeration for filling nor temperature control of the pumps to maintain accurate delivery.

SFC System Two's built-in microcomputer comes complete with SFC software for GC, pump control and data collection. Choose from density or pressure programming, even options for peak integration and specialized applications such as simulated distillation.

Getting started with SFC couldn't be simpler with the Brownlee SFC System Two. We'll install your system and train your staff, right in your lab. To meet your ongoing SFC requirements, we stock a complete family of accessories and supplies. Got a tough analytical problem you want to discuss? Our application scientists will be happy to share their experience.

Contact Brownlee today for some straight answers that take the mystery out of SFC. And let Brownlee put SFC to work for you.

IBM is a registered trademark of International Business Machines Corporation.

ABI Analytical
Brownlee Division
SFC System Two

Brownlee Labs
A division of Applied Biosystems, Inc.
2045 Martin Avenue Santa Clara, CA 95050 408/727-1346 800/231-4038

CIRCLE 20 ON READER SERVICE CARD

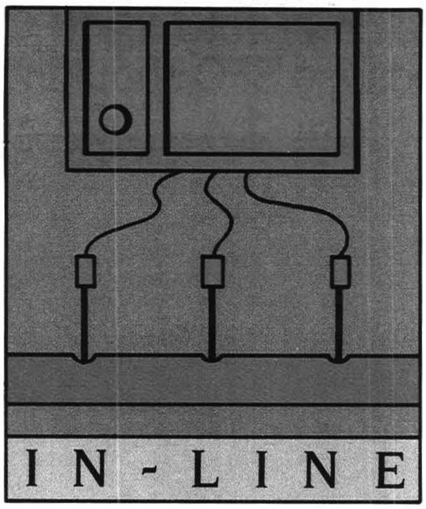

wedge filter in which the wavelength of maximum transmission varies continuously along one axis. A prototype compact planar spectrometer using a wedge filter and linear array detector gives acceptable results (*22*).

The remaining member of the hierarchy is the chemical microlaboratory. The goal is to integrate all functions of a chemical analysis laboratory into a unit no larger than a credit card. The key to this development is the integration of microconduits, microvalves, and microsensors by various types of hybrid circuit fabrication techniques (*23*). Although this device is really a third era concept, it provides a pathway to the implementation of chemical microsensors. These devices should last much longer when incorporated into a microlaboratory because of extensive sample conditioning and intermittent use.

Noninvasive era. The final era of process analytical chemistry, the noninvasive era, represents the ultimate in desirability. Because the probe does not physically contact the sample, the sampling problem is greatly alleviated. This era obviously has a great deal in common with remote sensing and nondestructive evaluation.

Near-IR spectroscopy from 700–1100 nm has much to offer (*24*) in this regard. First, the extinction coefficients in this region are very small and allow path lengths of 0.5–20 cm for clear solutions. Generally, absorptions in this region arise from the second and third overtones of CH, OH, and NH stretches together with combination bands from other vibrations. Because these are highly forbidden transitions, most materials are very transparent (exceptions are metals and graphite containing composites). At these optical distances, a thin layer of adsorbed material in the windows does not fatally degrade the results. Also, quantitative measurements of highly scattering materials can be made because scattering coefficients are much greater than absorption coefficients. Consequently, diffuse log inverse reflectance and diffuse absorbance measurements show good linear correlation with composition variation. Diffuse reflectance is particularly useful, because only a single window into the process need be established. In addition, the high degree of light scattering results in the sampling of a large volume. The hardware is inexpensive and employs widely available fiber optic components, conventional monochromators, tungsten lamps, and silicon detectors. Finally, the spectra are characterized by an extremely high signal-to-noise ratio. Thus subtle shifts in the spectra, which might go undetected by the unaided eye, can become the basis for highly successful analytical procedures developed by computer learning methods.

A second remote analysis technology is IR emission spectroscopy. This approach starts from the observation that all bodies at a temperature higher than their surroundings will emit radiation. For simple black bodies the spectral distribution of radiation is very smooth and is given by Planck's law. For real substances, however, discrete lines are observed on top of the Planck emission. These lines correspond well with those observed in the normal IR absorption spectrum of the emitting substance. Thus it is certainly possible to obtain qualitative information. But obtaining quantitative information is more difficult because most of the emission originates at the surface, severe reabsorption effects are evident, and the lines are present on a large background. Nevertheless, the potential advantages of a truly remote in situ technique justify further effort to understand the quantitative aspects.

At lower energies, in the microwave and radiofrequency bands, objects become rather more transparent, and therefore information can be obtained from deep within. Whereas the microwave absorption spectroscopy of gas-phase molecules is characterized by high-resolution unique spectra, condensed phases exhibit a much broader "dielectric" behavior. Nevertheless, different materials do exhibit different enough spectral characteristics to obtain compositional analysis, and even to form the basis for imaging (*24*). Other advantages of microwave technology for condensed phases include the ability to perform spectroscopy directly in the frequency domain with high-speed GaAs integrated circuitry and the ability to sample large, well-defined volumes with near-field resonators.

Yet another noninvasive technology involves X-rays. Most analytical chemists will immediately think of X-ray fluorescence, which has been adapted

Laser Light Scattering Systems

for particle size analysis, molecular weight measurement and other applications

The Malvern SYSTEM 4700c is an advanced modular system designed for research and development applications. It features the 8-bit Malvern 7032 Multi-8 correlator with Variable Time Expansion (VTE) allowing up to eight sampling times per measurement. Fixed and expandable configurations ranging from 72 up to 264 data channels are available.

A 16-bit IBM compatible processor plus full range of software for photon correlation spectroscopy and total intensity light scattering ensure optimum utilisation of the top quality manual or computer controlled goniometer.

Optical units are also available for use with SYSTEM 4700c for fixed angle PCS and electrophoretic zeta potential measurements.

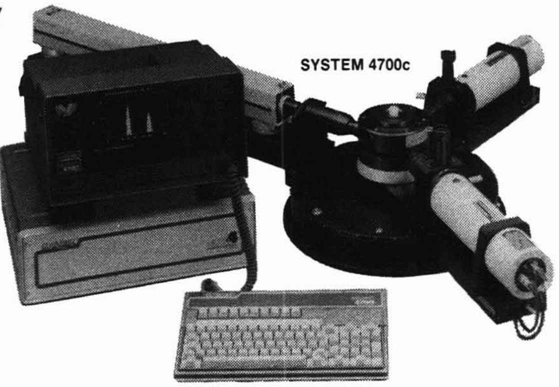

MALVERN

Malvern Instruments Inc
200 Turnpike Road, Southborough, MA 01772, USA
Tel. (617) 480 0200

CIRCLE 94 ON READER SERVICE CARD

Kevex Celebrating its 3rd Decade in Materials Analysis with Exciting New Products.

NEW Delta Class Analyzer—The first microanalysis system to fully integrate high performance elemental and image analysis into a family of completely upgradable systems. (Circle #80 on Reader Service Card)

NEW Kevex Surface Science System—Adds surface analysis capabilities to your SEM. (#81)

NEW Quantum Light Element Detector—World's only failsafe one-atmosphere ultrathin window (UTW) detector for all elements boron and heavier. (#82)

NEW Fast X-ray Mapping—Produces digital X-ray maps up to 100 times faster than conventional systems. (#83)

NEW No-LN X-ray Detector—Provides a rugged, convenient, reliable alternative to liquid nitrogen-cooled detectors. (#84)

NEW Light Element XRF—Permits analysis of C,N,O, and F by energy dispersive X-ray fluorescence. (#85)

Ask about these and other new products by Kevex—the innovator in materials analysis instrumentation and services. Call us at 1-800-227-0277.

The Delta Class Analyst: extends the power and convenience of energy dispersive XRF to include the elements carbon, nitrogen, oxygen and fluorine!

kevex®

KEVEX CORPORATION
1101 Chess Drive, Foster City, CA 94404
415-573-5866 Toll Free: 1-800-227-0277

Kevex Affiliate (Getac GmbH) Tel 49-6131-40091
Kevex Canada, Ltd. Tel 416-731-2161
Kevex France (Fondis, S.A.) Tel 33-1-34810024
Kevex UK Tel 44-582-400596

to both on-line and in situ use to yield high-speed elemental analysis. At the same time, it has been shown that differential X-ray absorption can be used to give compositional selectivity. Formerly, tunable X-ray sources were extremely rare, but major advances in X-ray optical coatings, materials, and sources will remedy this difficulty (*25*).

The final, fifth era of technology to consider is ultrasound. The major use of ultrasound has been for out-line imaging of flaws, employing reflections from index of refraction boundaries. However, a recent paper makes a strong case for further research on the mechanisms for ultrasound absorption, which is based at least in part on chemical composition (*26*).

In reviewing the remote era, we can see how much commonality the field has with nondestructive evaluation and noninvasive medical diagnosis. As an example of the use of the process analytical chemistry paradigm, consider the current practice of clinical chemistry. For the most part, its status is similar to the first and second eras of process analytical chemistry. Blood is drawn from the patient and is either sent to a remote central laboratory (off-line) or analyzed by a simpler doctor's office instrument (at-line). At the University of Washington, we are developing the fifth era of clinical analysis (real-time, noninvasive) by exploiting new concepts in spectroscopy and data reduction. A new role is sure to emerge for the clinical chemist who becomes a full partner in supplying critical data to the doctor and, with multivariate statistics, interprets it in terms of the patient's current physiological status and prognosis.

Role of chemometrics

We have completed an outline of some of the possibilities for chemical sensing in process analysis. How does one analyze the data from the array of instruments and sensors that have been placed on-line? At this point, a major cultural gap becomes evident between the analytical chemist and the process engineer. Most analytical chemists regard their function as supplying chemical composition information, which is, after all, what they have been trained to do. Unfortunately, this does not always meet the needs of the process engineer, whose job is to provide a product that meets quality specifications. In some cases, especially for chemicals production, composition data suffices. In many situations, however, and especially for consumer products, the specifications are not obviously chemical in nature. An example of this is gasoline testing. Here, the most important consumer quality parameter is the antiknock property as expressed by the octane number. Presently, this parameter is measured by a knock engine that is extremely expensive, requires a subjective judgment (listening for pinging) to make the measurement, and must be exactingly maintained (*1*). Even worse, the measurement takes 20 min to perform and consumes a full pint of gasoline. Finally, the poor precision and large interinstrument variability cost the refiner a lot of money, because the quality specifications must be set high enough to allow for octane measurement uncertainty, and they cause a lot of irritation, because the regulatory agency's octane determinations may not agree with the company's.

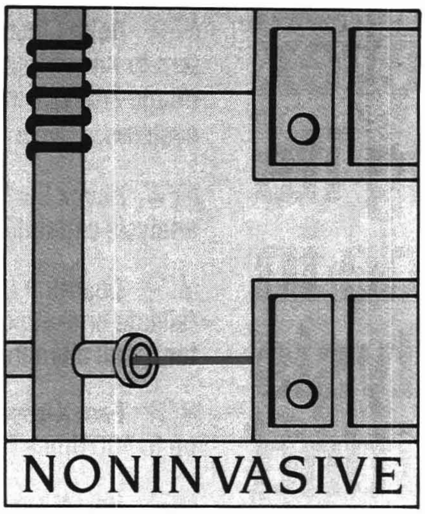

At the Center for Process Analytical Chemistry, we have been exploring a new approach to on-line quality evaluation. We begin with the observation that vibrational absorption spectroscopy can yield information about functional groups, molecular structure, and conformation, as well as intermolecular interactions. In principle, one should be able to obtain chemical and physical material properties from the spectrum. Unfortunately, such information often is present in subtle variations in the spectrum and might not be recognized by the naked eye, or it might be dependent upon an unknown relationship among several spectral features. Accordingly, to obtain the structure–property relationship, one must either develop a first principles theory, which is generally impossible, or use an empirical method such as multivariate statistical calibration (*27*). In the latter approach, the computer is provided with a training set consisting of the spectrum of each of the samples and the property, measured by an independent reference method. It is important that the training set consist of representative samples with variations spanning that of the set of all samples that might reasonably be encountered by the method. Once the data set is acquired, the computer searches for correlations between the spectra and the sought-for property. Eventually a transformation vector is produced that, when multiplied by the spectral vector, yields an estimate for the property. Once the derived transformation vector has been validated with a double-blind study of a second set of samples for which spectra and property have been measured, the method is ready for use.

In the case of gasoline, a study of 43 samples of unleaded gasoline of known octane number was made using near-IR spectroscopy over fiber optics. By simple step-forward multilinear regression, a linear equation involving only the absorption intensities at three wavelengths was found that correlated to the reference octane number with a standard error of 0.3 octane, the known precision of the octane engine (*28*). Further studies involving more samples clearly will be required to verify the method and to assure its robustness. But the effort is justified because the spectroscopic test takes only 20 s to perform, and the instrumentation costs far less and requires considerably less maintenance than that used in other methods.

Another major advantage of on-line spectroscopy is that a number of chemical and physical properties can be measured simultaneously from one spectrum. For gasoline, we have been able to correlate the spectrum to both research and motor octane, API density, Reid vapor pressure, distillation points, and total aromatics, olefins and aliphatics—eight tests in 20 seconds!

One of the most intriguing aspects of multivariate calibration is the capability to generate the correlation spectrum that is associated with a paticular property (*29*). This may prove to be an extremely valuable tool in materials research. For example, the correlation spectrum of tensile strength might reveal the presence of specific supramolecular structures or unique intermolecular bonds that determine the specific property. Such knowledge could lead to new materials with significantly improved performance.

Thus far, no algorithms have been formulated that use multiwavelength spectroscopy in real-time process control. A study by Wise (*30*), however, shows how multiple physical measurements (temperature at various points, applied power, substrate resistance) together with multivariate statistics can be employed to prevent runaway foaming during the operation of a liquid-fed ceramic melter.

Another potential use for multivariate calibration is to qualify incoming raw materials. Many types of processes are bedeviled by batch-to-batch variations in the raw materials. A recent study (*31*) showed that multiblock partial least-squares regression could be used to form a model with which one

OUR FIVE-YEAR MISSION:

TO EXPLORE NEW FRONTIERS, TO BOLDLY GO WHERE NO CHROMATOGRAPH HAS GONE BEFORE.

The first and only truly *distributed system* of process gas and liquid chromatography that now also allows you to use temperatured programmed methods to analyze high-boiling materials in on-line applications. Optichrom® Advance.

NOW AVAILABLE – Programmed Temperature Process Gas Chromatography used in the Advance System incorporates a separate temperature-controlled zone into the existing oven. PTPGC allows the user to further expand gas chromatography analysis to a wider boiling range of materials - for example, simulated distillation.

TRULY DISTRIBUTED – An Advance System follows the true *distributed system* concept. Each analyzer operates *independently* of other analyzers in the system and needs no central operator station or master controller to function.

CONFIGURED FLEXIBILITY – Advance systems allow you the option of tying into a central operating station for efficient data management, yet no analyzer is dependent on it for daily operation.

Or you can eliminate expensive and complex central peripheral equipment. And more analyzers can be added at any time without costly hardware or program modifications.

OPTIONAL APC – An optional IBM Application Personal Computer can provide mass data storage and off-line number crunching, application program modification with up and down loading of analyzer software, plus chromatogram display.

DATA HIWAY – System communications travel along a high speed network of up to eight data hiways. Even though 200 analyzers can be tied into one network, no one analyzer failure will affect communications via the data hiway. Twin cable sets with both signal paths active provide system redundancy and create a communications network with *no single point of failure.*

USER FRIENDLY – English language readouts and application programs written in BASIC language, table oriented and menu driven, encourage familiarity and facilitate day to day operation.

Optichrom Advance. The most cost-effective, user friendly, reliable, flexible and only truly distributed system now with PTPGC capabilities available.

For more information write to Applied Automation, Inc., Pawhuska Road, Bartlesville, Oklahoma 74004, or call 918/661-0660.

A NEW DIRECTION IN CHROMATOGRAPHY.

APPLIED AUTOMATION, INC.

A subsidiary of Phillips Petroleum Company. © MCMLXXXVII Phillips Petroleum Company.

CIRCLE 3 ON READER SERVICE CARD

SIEMENS

The Siemens x-ray Diffraction Concept —

Modular, Affordable, Versatile, Reliable

Every aspect of the Siemens concept — its design, its price, and its application potential — allows you to start small and build big, assured each step of the way of Siemens' first-rate performance and complete support.

Modular
Siemens' modular design lets you begin with the basic manual diffraction system, expand it with our DACO microcomputer, then take it to the limits of complete computer control with DIFFRAC, one of the largest and most versatile XRD user-oriented software systems.

Affordable
At Siemens, affordable means value. Because the cost of purchasing, upgrading and operating a Siemens system is so surprisingly low, you can expect your x-ray diffraction system to more than justify its initial investment.

Versatile
Through a full complement of Siemens accessories — all enhanced with Siemens extensive modular DIFFRAC software — you can extend the capabilities of your basic system and adapt it to almost any application.

Reliable
Siemens instrumentation is backed by a worldwide installation base of over 600 D 500 satisfied users, all more than willing to verify our system's superior performance.

We'd like to show you how our x-ray diffraction concept can make the most of your analyses and your money. Find out why we earned our reputation as the choice you can believe in.

Siemens AG, Analytical Systems, E689, D-7500 Karlsruhe 21, P.O. Box 21 1262, Federal Republic of Germany. Tel: (0721) 595-2425, Telex: 78255-69

Siemens Energy & Automation, Inc., Analytical Systems, One Computer Drive, P.O. Box 5477, Cherry Hill, New Jersey 08034, Tel: (609) 424-9210

Siemens . . . The company you can believe in.

CIRCLE 152 ON READER SERVICE CARD

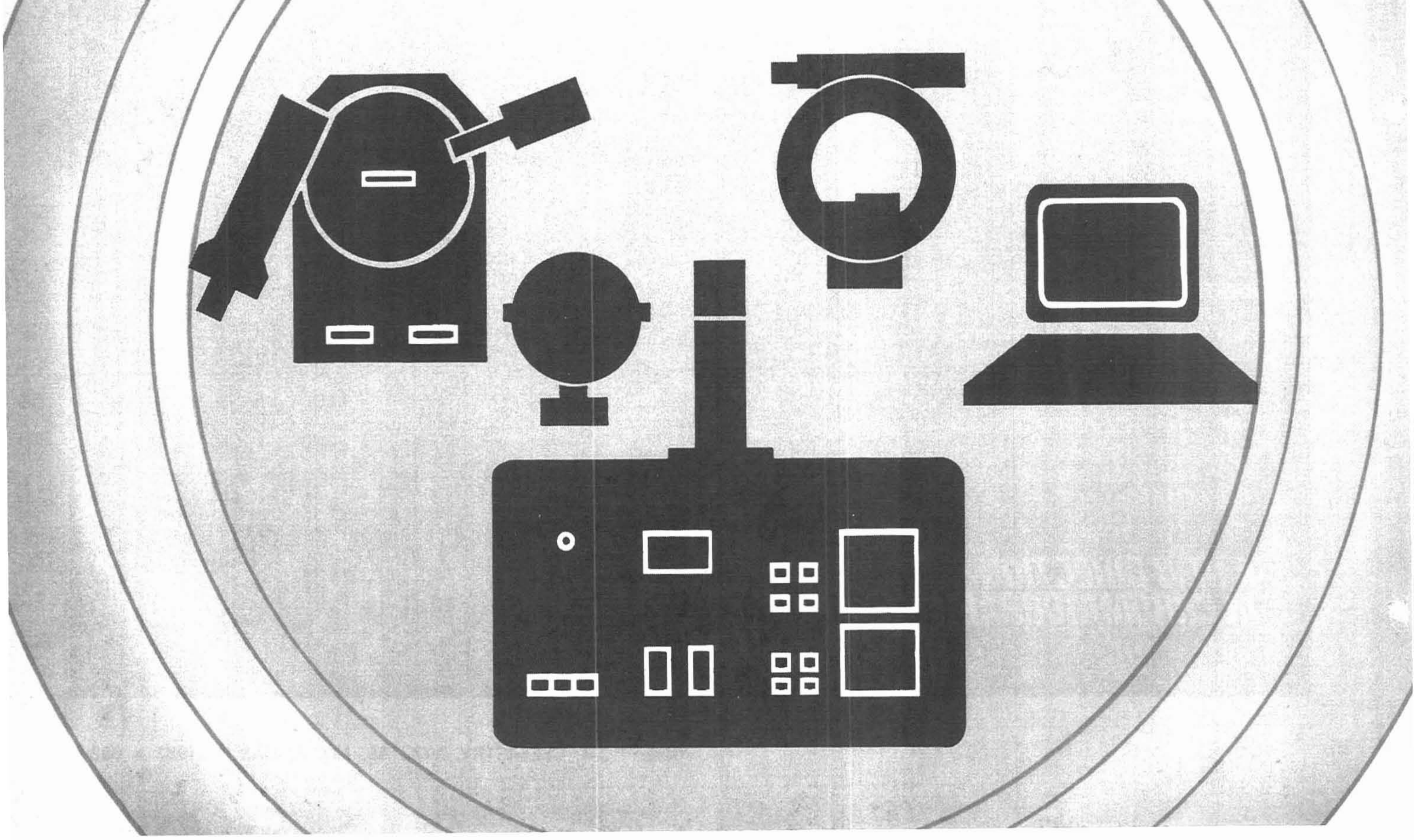

could use the quality control data—in this case, IR spectra and sonic spectra—to predict the outcome of the process in terms of the performance of the final product. In the future it should be possible to combine information about the properties of incoming raw materials with a process model to adjust conditions and accommodate variations in raw materials, thereby producing a product of more consistent quality.

Implementing process analytical chemistry

In industry, process engineers and analytical chemists all too often are separate groups, each with its own goals and distinct culture. Thus it is not uncommon for the analytical group to convince managers to install a sophisticated process analyzer but to avoid the issues of maintenance and calibration. Frequently the shiny new instrument becomes rusty while the two groups argue over responsibility. We have observed that companies that are most successful in implementing process analytical chemistry have formed interdisciplinary working groups of engineers and scientists devoted solely to that task.

Another difficulty in implementation arises from barriers created by horizontal integration in a company. Seldom does the bench chemist who develops a new synthetic method participate actively in scale-up operations. Even pilot plant personnel seldom migrate to the full-scale operation. This communication gap should be eliminated by encouraging vertical movement within a company. The benefits of this strategy are well known in a few instrument companies, where a research engineer or scientist might actually move through the design process to developmental engineering, to manufacturing, to marketing, and, finally, to participating in selling the product.

The vertical concept can be readily applied to process analytical chemistry. The process analytical chemist should become involved with a new synthetic project at its earliest stages of development. The on-line tools supplied to the bench chemist will greatly aid the process of converging to a useful synthetic strategy. When the new process is worked out, ideally the synthetic chemist and process analytical chemist alike will move vertically to the pilot plant level. The bridge between these levels will be the analytical instruments, which should greatly decrease the pilot plant time. In the final step, the on-line instrumentation will migrate onto the plant floor.

The above scenario has embedded within it a means whereby academic analytical chemists may also become involved in on-line analysis. The time is right for analytical chemists to approach their colleagues involved in synthesis concerning a collaborative effort with a goal of optimizing new synthetic approaches, using analytical instruments to give real-time information about how a given reaction is proceeding. A recent contribution from academia describes a simple mass spectrometer interface to reaction mixtures that uses semipermeable capillary tubing and illustrates its use in reaction monitoring (*32*).

The future

Process analytical chemistry is a discipline poised to have a major impact both on industrial processing and on the parent discipline. The savings to be obtained from installation of the present generation of process analyzers has been quantified (*33*), and it can be enormous. The new generation of online spectroscopic instruments and the accompanying multivariate analysis promise even more capabilities, with the possibility of developing new processing methods that previously could not be considered because of the lack of adequate control. Perhaps the most exciting promise of process analytical chemistry is to make process lines so efficient and so well controlled that effluent release is decreased or even eliminated altogether. Imagine the good will such efficient plants might generate in the community.

The changing practice of process analytical chemistry is sure to influence the discipline as a whole. It is a leading force behind the migration of analytical instruments from the protected laboratory into the real world. The use of the micro- and optoelectronics paradigms is leading to a new generation of personal, portable instruments and sensors that can be used as tools even by those who are inexperienced. The parallel with the impact of personal computers should be obvious and should be welcomed by analytical managers who see the trend as a way to free their personnel from the drudgery of routine analysis.

References

(1) Clevett, K. J. *Process Analyzer Technology;* John Wiley: New York, 1986.
(2) *Sci Am.* **1986,** *255*(4), 1–212.
(3) Wohltjen, H. *Anal. Chem.* **1984,** *56,* 87 A–103 A.
(4) Seitz, R. *Anal. Chem.* **1984,** *56,* 16 A–34 A.
(5) Hirschfeld, T.; Callis, J. B.; Kowalski, B. R. *Science* **1984,** *226,* 312–18.
(6) Cornish, D. C.; Jepson, G.; Smurthwaite, M. J. *Sampling Systems for Process Analyzers*; Butterworths: London, 1981.
(7) Phillips, J. B.; Luu, D.; Pawliszyn, J. B.; Carle, G. C. *Anal. Chem.* **1985,** *57,* 2779–2787.
(8) Lipsky, S. R.; Duffy, M. L. *LC-GC* **1986,** *4*(9), 898–907.
(9) Jorgenson, J. W. *Anal. Chem.* **1986,** *58,* 743 A–760 A.
(10) Levy, G. B. *Am. Lab.* **1986,** *18*(12), 62–71.

HPLC Systems

For superior HPLC analyses, ESA provides a complete line of HPLC components and systems–pumps, injectors, detectors, and automatic sampling equipment.

Use these modular components to design an HPLC system to meet your exact applications and budget needs. Or add high-performance components to your existing HPLC for analysis results you can trust.

For example, our systems–

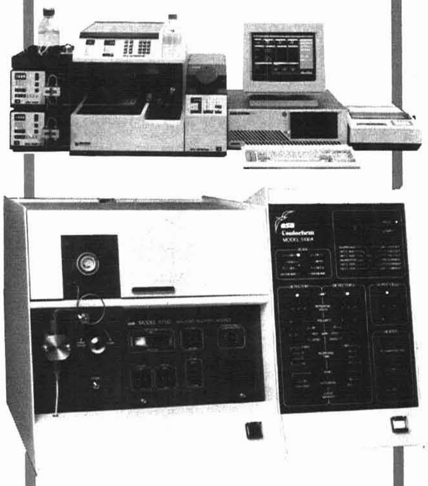

- **Advanced Modular HPLC System** includes random access variable volume injection autosampler with most sensitive dual wavelength UV/Vis detector available and completely automatic dual-channel data acquisition and control system.
- **The World Standard Coulochem® Electrochemical Detector and Solvent Delivery System** makes electrochemical detection at the picogram level as easy as UV detection at the microgram level.

Send today for our complete HPLC products catalog.

esa

ESA, Inc.
45 Wiggins Avenue
Bedford, Massachusetts 01730
(617)275-0100

CIRCLE 41 ON READER SERVICE CARD

Your chance in '87! Don't miss these popular

HANDS-ON COURSES!

ACS Short Courses to be held at VPI, Blacksburg, Virginia

LIQUID CHROMATOGRAPHY

THEORY AND PRACTICE

Monday–Thursday, June 8–11, 1987
Monday–Thursday, December 14–17, 1987

This state-of-the-art, hands-on course provides the training you need to effectively and efficiently work with this important analytical method. Through lectures and the do-it-yourself learning experience, you will

☞ learn important fundamentals of high-speed, high-efficiency liquid chromatography

☞ cover theory, instrumentation, and applications

☞ focus on BPC (partition), LSC (adsorption), reverse phase, and gel permeation

☞ work with commercially available equipment as well as several modular systems

☞ have free lab time to use or experiment with equipment

Faculty
Dr. Harold McNair (Course Director), Professor of Analytical Chemistry, Virginia Polytechnic Institute and State University, Blacksburg, VA. Guest lecturers from industry, instrument companies, and universities will participate.

Fee
ACS Members: $815.00; Nonmembers: $895.00 (Includes tuition, lecture and laboratory materials, and all lunches.)

THE COMPUTER-INTEGRATED LABORATORY

A HANDS-ON EXPERIENCE IN LAB AUTOMATION

Sunday–Friday, June 7–12, 1987
Sunday–Friday, September 20–25, 1987

Essential for all scientists who need or want to learn how computers operate at the machine/assembler level. This highly-rated course gives you hands-on, problem-solving experience that will enable you to

☞ find the right lab information management system for your needs

☞ integrate your old analog instruments with your new intelligent ones into a network environment

☞ help your management and computing center understand the problems of the scientific lab and show them how the electronic lab is fiscally and legally essential

Faculty
Dr. Raymond E. Dessy, Professor of Chemistry, Virginia Polytechnic Institute and State University, Blacksburg, VA, and the VPI and SU Chemistry Department Computer-Aided Research Group.

Fee
ACS Members: $845.00; Nonmembers: $925.00 (Includes tuition, lecture and laboratory materials, and all lunches.)

MODERN NMR SPECTROMETRY

PRINCIPLES AND PRACTICE

Monday–Friday, June 8–12, 1987

Of benefit to anyone wanting an operational knowledge of NMR spectrometers and state-of-the-art techniques, this course offers basic FT-NMR theory. Develop an understanding of this method and be able to

☞ run basic and state-of-the-art ^{13}C and ^{1}H NMR experiments

☞ prepare NMR samples for data collection at the consoles

☞ choose "special" experiments to aid in structure elucidation

Faculty
Dr. Harry C. Dorn, Professor of Chemistry at VPI, will be joined by Drs. Gennard Iannaccone, Tom Glass, William Bebout, and Cecil Dybowski in teaching this popular course.

Fee
ACS Members: $795.00; Nonmembers: $875.00 (Includes tuition, lecture and laboratory materials, and all lunches.)

The Site
All three courses will be held at Virginia Polytechnic Institute and State University (VPI) in Blacksburg, VA. Further specifics, including information on accommodations, will accompany confirmation of registration.

American Chemical Society • Education Division • 1155 Sixteenth Street, N.W. • Washington, DC 20036

Please register me in the following ACS Short Course at VPI:

Liquid Chromatography: Theory and Practice
☐ June 8–11, 1987 ☐ December 14–17, 1987
☐ ACS Member $815.00 ☐ Nonmember $895.00

The Computer-Integrated Laboratory:
A Hands-On Experience in Lab Automation
☐ June 7–12, 1987 ☐ September 20–25, 1987
☐ ACS Member $845.00 ☐ Nonmember $925.00

Modern NMR Spectrometry: Principles and Practice
☐ June 8–12, 1987
☐ ACS Member $795.00 ☐ Nonmember $875.00

NOTE: PREPAYMENT REQUIRED FOR CONFIRMATION.

DO NOT MAIL this form if less than two weeks remain before course starting date. Call (202) 872-4508 to confirm that space is available.

Name ______________________
Title ______________________
Organization ______________________
City, State, ZIP ______________________
Home Phone ______________________
Business Phone ______________________

(11) Ruzicka, J.; Hansen, E.H.H. *Flow Injection Analysis*; John Wiley: New York, 1981.
(12) Harrick, N. J. *Internal Reflection Spectroscopy*; Harrick Scientific Corp.: Ossining, N.Y., 1979.
(13) Rein, A. J.; Wilks, P. *Am. Lab.* **1982,** *14*(10), 152–55.
(14) Miller, J. C.; George, S. A.; Willis, B. G. *Science* **1982,** *57*, 1917–20.
(15) *Solid State Chemical Sensors;* Janata, J.; Huber, R. J., Eds.; Academic: New York, 1985.
(16) Caras, S. D.; Janata, J.; Saupe, D.; Schmidt, K. *Anal. Chem.* **1985,** *57*, 1917–20.
(17) Hirschfeld, T. *Adv. Instrum.* **1985,** *40*, 305–18.
(18) Kalivas, J. H.; Kowalski, B. R. *Anal. Chem.* **1981,** *53*, 2207.
(19) Kalivas, J. J.; Kowalski, B. R. *Anal. Chem.* **1982,** *54*, 560.
(20) Carey, W. P.; Beebe, K. R.; Kowalski, B. R.; Illman, D. L.; Hirschfeld, T. *Anal. Chem.* **1986,** *58*, 149–53.
(21) Fuh, M. S.; Burgess, L. *Anal. Chem.*, in press.
(22) Pfeffer, J. C.; Skoropinski, D. B.; Callis, J. B. *Anal. Chem.* **1984,** *56*, 2973–74.
(23) Ruzicka, J. *Anal. Chem.* **1983,** *55*, 1040 A–1053 A.
(24) Rao, P. S.; Santosh, K.; Gregg, E. C. *Radiology* **1980,** *135*, 769–70.
(25) *Low-Energy X-Ray Diagnostics*; Attwood, D. T.; Henke, B. L., Eds.; American Institute of Physics: New York, 1981.
(26) Slutsky, L. J. *IEEE Trans. Ultrason. Eng.* **1986,** *UFFC-33*, 156–61.
(27) Martens, H.; Naes, T. *NATO Adv. Study Inst. Ser. C.* **1984,** *138*, 147–56.
(28) Kelly, J. J.; Barlow, C. H.; Jinguji, T. M.; Callis, J. B., unpublished results.
(29) Honigs, D. E.; Hieftje, G. M.; Hirschfeld, T. *Appl. Spectrosc.* **1984,** *38*, 317–22.
(30) Wise, B. M.; McMakin, A. H., submitted for publication in *Glass Industry Journal.*
(31) Frank, I. E.; Feikema, J.; Constantine, N.; Kowalski, B. R. *J. Chem. Inf. Comput. Sci.* **1984,** *24*, 20–24.
(32) Brodbelt, J. S.; Cooks, R. G. *Anal. Chem.* **1985,** *57*, 1155–57.
(33) Reeves, P. *Proceedings of the ANATECH '86 International Conference;* Norwijkerhout, The Netherlands, April 1986.

Suggested reading

Huskins, D. J. *Quality Measuring Instruments in On-Line Process Analysis;* Halstead Press: New York, 1982.
Mix, Paul E. *The Design and Application of Process Analyzer Systems;* Wiley Interscience: New York, 1984.

This work was supported by the Center for Process Analytical Chemistry from grants provided by the National Science Foundation (#ISI-8415075), the 30 sponsors, and the University of Washington.

James B. Callis (right) is co-director of the Center for Process Analytical Chemistry (CPAC) and professor of chemistry and adjunct professor of bioengineering at the University of Washington. He received his B.S. in chemistry from the University of California at Davis and his Ph.D. in physical chemistry from the University of Washington. Callis's major research interest is instrumentation for optical spectroscopy. He is developing ultraminiature spectrometers based on novel transform principles, laser-based chromatography detectors, and noninvasive diagnostic devices.

Deborah L. Illman (center) is associate director of CPAC. She received her B.S. in chemistry (1976) from the University of Washington and her Ph.D. in chemistry (1982) from the State University of Campinas, Brazil. She then accepted a lectureship and postdoctoral position at the University of Washington, where her research interests focus on chemometrics: multivariate methods of pattern recognition and statistics applied to analyzing chemical data. Illman manages the operations, industrial relations, and policy development at CPAC and contributes to its research program.

Bruce R. Kowalski (left) is professor of chemistry and co-director of CPAC. He received his B.S. with majors in chemistry and mathematics (1965) from Millikin University and his Ph.D. in chemistry (1969) from the University of Washington, Seattle. His research interests include the application of methods of multivariate analysis to the resolution and calibration steps in analytical instrumentation in order to develop new analytical methods and improve existing ones. Kowalski is editor-in-chief of the Journal of Chemometrics. *In 1974 he cofounded the Chemometrics Society.*

HPLC

Autosamplers

For superior HPLC analyses, ESA provides a complete line of HPLC components and systems–pumps, injectors, detectors, and automatic sampling equipment.

Use intelligent components to design an HPLC system to meet your exact applications and budget needs. Or add these high-performance components to your existing HPLC system for analysis results you can trust.

For example, our autosamplers–

- **Model 460**–110 position random access, variable volume autosampler for maximum chromatographic versatility. Requires only 5 µL more than injection volume to preserve valuable samples.
- **Model 660**–60 position, fixed-loop autosampler for reliable, routine processing of samples at a reasonable cost.

Send today for our complete HPLC products catalog.

esa

ESA, Inc.
45 Wiggins Avenue
Bedford, Massachusetts 01730
(617)275-0100

CIRCLE 42 ON READER SERVICE CARD

1987 Gordon Research Conferences

The aim of the Gordon Research Conferences is to extend the frontiers of science by fostering a free and informal exchange of ideas among those actively involved in research in particular fields. At each conference, meetings are held in the morning and evening, Monday through Friday, except Friday evening. The afternoons are available for recreation, reading, or participation in discussion groups.

To promote discussion and to protect individual rights, it is the established requirement of each conference that no information be used without specific authorization of the individual making the contribution. Recording of lectures and photographing of slides also are prohibited.

The unique concept of the Conferences was established by Neil Gordon of Johns Hopkins University in 1931. Gordon foresaw the importance of establishing good, direct communication between scientists while removing the distractions prevalent at larger scientific meetings.

This year, four conferences are of particular interest to analytical chemists: analytical chemistry, analytical pyrolysis, magnetic resonance, and separation and purification. Technical programs for these conferences follow. Other conferences of interest to analytical chemists include corrosion; drug metabolism; environmental sciences (air); physics and chemistry of laser diagnostics in combustion; molten salts and liquid metals, nonlinear optics and lasers; polymers; proteins; reactive polymers, ion exchangers, and adsorbents; reverse osmosis, ultrafiltration, and gas separation; spectroscopy of matrix-isolated species; statistics in chemistry and chemical engineering; and three-dimensional electron microscopy of macromolecules.

Interested individuals should submit an application form (available from the Office of the Director). Each application will be evaluated to determine the eligibility of the prospective conferee. Attendance at each conference is limited to approximately 100 conferees. A registration card will be mailed to those selected.

The conference fee for resident participants is $310, which covers registration, room (double occupancy), and meals. The fee is $270 for nonresident conferees, which covers registration and meals but does not include a room. Guests are required to pay $220, which covers only the cost of a room and meals.

Requests for registration forms or for additional information should be directed to Alexander Cruickshank, Gordon Research Center, University of Rhode Island, Kingston, R.I. 02881-0801 (401-783-4011 or -3372). From June 15 to August 21, Cruickshank can be reached at Colby-Sawyer College, New London, N.H. 03257 (603-526-2870).

Analytical Chemistry

August 10–14
New Hampton School
New Hampton, N.H.
Bruce Chase, *Chairman*
William Heineman, *Vice Chairman*

AUGUST 10

B. Chase, *discussion leader*

F. Lytle, Two-Photon Spectroscopy of Molecules in Fluid Solution
D. Lubman, Laser-Induced Ionization of Biological Compounds in Supersonic Beam Mass Spectroscopy

M. Wirth, *discussion leader*

L. Carreira, CARS, An Analytical Technique?
T. Gustafson, Time-Resolved Optical Characterization of Thin Film Materials

AUGUST 11

W. Heineman, *discussion leader*

J. Kirkland, Recent Developments in the High-Resolution Separation of Very High Molecular Weight Components
T. Chester, Supercritical Fluid Chromatography: Progress and Applications
E. Yeung, Combining Spectroscopy and Chromatography in Chemical Analysis
I. Krull, Recently Detected Detection Approaches in Liquid Chromatography

AUGUST 12

B. Fateley, *discussion leader*

G. Richmond, Probing the Solid–Liquid Interface with Nonlinear Optics
H. Abruna, X-Rays as In-Situ Probes of Electrochemical Interfaces

G. Hieftje, *discussion leader*

S. Chiang, Scanning Tunneling Microscopy of Metals on Semiconductors
A. Wieckowski, Application of Nuclear Properties in the Analysis of Electrode Surfaces

AUGUST 13

I. Levin, *discussion leader*

R. Salemme, Applications of X-Ray Crystallography in Protein Engineering and Rational Drug Design

L. Faulkner, *discussion leader*

R. Mathies, Determination of Retinal Chromophore Structure in Rhodopsins with Resonance Raman Spectroscopy
S. Carr, Structural Analysis of Proteins by Tandem Mass Spectrometry

AUGUST 14

J. Robinson, *discussion leader*

A. Marshall, Data Reduction in Fourier Transform Spectrometry: Advantages and Artifacts
J. Bettridge, Pattern Recognition from Different Perspectives

Analytical Pyrolysis

July 6–10
Holderness School
Plymouth, N.H.
R. P. Lattimer, *Chairman*
J. W. de Leeuw, *Vice Chairman*

JULY 6

S. A. Liebman, *discussion leader*

I. Ericsson, Pyrolysis–Gas Chromatography: A Powerful Technique for Identification of Synthetic Polymers
D. O. Hummel, Three Decades of Analytical Spectroscopy of Polymer Pyrolyzates

T. Szekely, *discussion leader*

R. S. Lehrle, Individual Activation Energies for Concurrent Scission and End Initiation of Polymer Depropagation, Evaluated by Py-GC
J. R. MacCallum, Thermal Decomposition of Polymers: Theoretical and Practical Problems

JULY 7

S. C. Israel, *discussion leader*

J.C.W. Chien, Analytical Pyrolysis of Polyolefins, Polydienes, Polyacetylenes, and Polyacetals, and Their Degradation Mechanisms
I. C. McNeill, Pyrolysis Studies of Polymer Systems Based on Methyl Methacrylate

M. A. Grayson, *discussion leader*

S. Tsuge, Characterization of Thermosetting Polymers by Pyrolysis–Gas Chromatography
I. V. Bletsos and D. M. Hercules, Time-of-Flight Secondary Ion Mass Spectrometry of Polymers

JULY 8

G. Montaudo, *discussion leader*

M. M. O'Mara, Combustibility of Polymers
T. Kashiwagi, Polymer Gasification Process

K. J. Voorhees, *discussion leader*

G. Camino, Thermal Degradation and Fire Retardant Mechanisms of Polymeric Materials
W. H. Starnes, Jr., Poly(vinyl chloride) Smoke Suppression by Metals Salts: Current Status

JULY 9

K. Kawaoka, *discussion leader*

H.L.C. Meuzelaar, Learning More from Pyrolyzing Less
H.-R. Schulten, Soft Ionization Mass Spectrometry of Technical and Biological Polymers

R. Saferstein, *discussion leader*

C. G. Smith, Industrial Applications of Analytical Pyrolysis Techniques
T. O. Munson, Applications of Analytical Pyrolysis to Forensic Samples

JULY 10

J. W. de Leeuw, *discussion leader*

Selected poster presentations.

Magnetic Resonance

June 15–19
Brewster Academy
Wolfeboro, N.H.
Constantino S. Yannoni, *Chairman*
W. Gilbert Clark, *Vice Chairman*

JUNE 15

M. Mehring, Sublevel Coherence Spectroscopy
H. M. Vieth, Dynamics of Photoprocesses in Molecular Crystals by Nanosecond Time-Resolved Optical Nuclear Polarization
K. Zilm, Solid-State NMR Methods for Studying Matrix Isolation Photochemistry
R. M. Shelby, Generation of Squeezed Light and Quantum Nondemolition Detection in Optical Fibers
E. L. Hahn, Nuclear Electric Quadrupole Induction of Atomic Polarization

JUNE 16

A. Schweiger, New Techniques in Pulsed ESR Spectroscopy
K. P. Dinse, Ultimate Time Resolution in ESR with Stochastic Excitation
J. H. Freed, J. Gorcester, Two-Dimensional ESR and Molecular Dynamics
E. Lippmaa, High Resolution MAS-NMR of Quadrupolar Nuclei
A. Pines, Berry's Phase in Magnetic Resonance

JUNE 17

D. L. VanderHart, Natural Abundance ^{13}C–^{13}C Spin Exchange in Solids
H. W. Spiess, 2D-NMR Methods for Studying Structure and Dynamics of Solid Polymers
T. Terao, One- and Two-Dimensional Powder Patterns in Rotating Solids
R. F. Haglund, Jr., Probing Surface Structure and Dynamics with Nuclear-Spin-Polarized Atomic Beams
W. S. Warren, Effects of Crafted Pulse Shapes in Laser and NMR Spectroscopies

JUNE 18

F. Noack, Relaxation Dispersion and Zero Field Spectroscopy in Liquid Crystals by Electronic Field Cycling
C. P. Slichter, The Structure and Motion of Charge Density Waves in $NbSe_3$
H. Thomann, Transport Models in Polyacetylene: Insights from New Magnetic Resonance Experiments
M. Bloom, The Complete Proton NMR Spectrum of Whole Cells
D. Weitekamp, Nuclear Spin Statistics: A New Handle on NMR Sensitivity

JUNE 19

J. S. Waugh, A Chemist's View of NMR Spectra and Relaxation Below 1 K
G. Bodenhausen, Some Implications of Relaxation on Coherence Transfer
A. Bax, Homonuclear Hartman-Hahn Effects Among Protons in Isotropic Liquids

HPLC Data Station

For superior HPLC analyses, ESA provides a complete line of HPLC components and systems–pumps, injectors, detectors, automatic sampling equipment, and data stations.

Use these modular components to design an HPLC system to meet your exact applications and budget needs. Or add these high-performance components to your existing HPLC for analysis results you can trust.

For example, our Model 450 HPLC Data Station–

DATA SYSTEM

■ **Automates virtually any HPLC system–** Operates up to 8 HPLC modules and 16 relays to provide the ultimate in system control.

■ **Two channels of data acquisition–** Intelligent default parameters and autoranging make the Data Station versatile as well as simple to use.

■ **Raw Data Storage–**Stores raw data from two channels permitting sample reintegration and recalibration at any time.

Send today for our complete HPLC products catalog.

esa

ESA, Inc.
45 Wiggins Avenue
Bedford, Massachusetts 01730
(617)275-0100

CIRCLE 43 ON READER SERVICE CARD

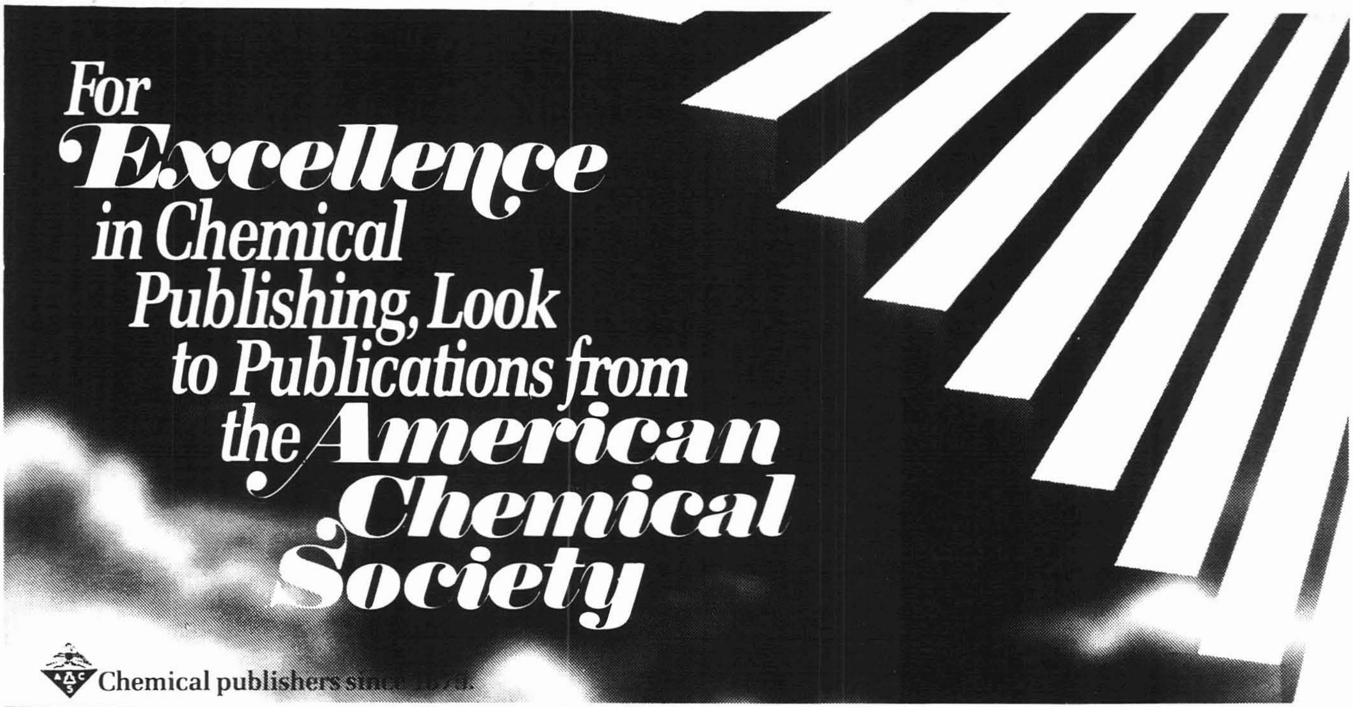
For Excellence in Chemical Publishing, Look to Publications from the American Chemical Society
Chemical publishers since 1879.

☐ **ACCOUNTS OF CHEMICAL RESEARCH**
Editor, F.W. McLafferty
Cornell University
12 issues a year. ISSN 0001-4842
Member $23 Nonmember $99

☐ **ANALYTICAL CHEMISTRY**
Editor, George H. Morrison
Cornell University
24 issues a year. ISSN 0003-2700
Member $25 Nonmember $37

☐ **BIOCHEMISTRY**
Editor, Hans Neurath
University of Washington
26 issues a year. ISSN 0006-2960
Member $75 Nonmember $386

☐ **CHEMICAL & ENGINEERING NEWS**
Editor, Michael Heylin
51 issues a year. ISSN 0009-2347
Nonmember $44

☐ **CHEMICAL REVIEWS**
Editor, Josef Michl
University of Texas
6 issues a year. ISSN 0009-2665
Member $22 Nonmember $99

☐ **CHEMTECH**
Editor, Benjamin J. Luberoff
12 issues a year. ISSN 0009-2703
Member $34 Nonmember (Pers.) **$44**
Nonmember (Inst.) **$244**

☐ **ENERGY & FUELS**
Editor, John W. Larsen
Lehigh University
6 issues a year. ISSN 0887-0624
Member $46 Nonmember $269

☐ **ENVIRONMENTAL SCIENCE & TECHNOLOGY**
Editor, Russell F. Christman
University of North Carolina, Chapel Hill
12 issues a year. ISSN 0013-936X
Member $30 Nonmember (Pers.) **$45**
Nonmember (Inst.) **$176**

☐ **INDUSTRIAL & ENGINEERING CHEMISTRY RESEARCH**
Editor, Donald R. Paul
University of Texas, Austin
12 issues a year. ISSN 0888-5885
Member $52 Nonmember $286

☐ **INORGANIC CHEMISTRY**
Editor, M. Frederick Hawthorne
University of California, Los Angeles
26 issues a year. ISSN 0020-1669
Member $79 Nonmember $422

☐ **JOURNAL OF AGRICULTURAL AND FOOD CHEMISTRY**
Editor, Irvin E. Liener
University of Minnesota
6 issues a year. ISSN 0021-8561
Member $24 Nonmember $126

☐ **JOURNAL OF THE AMERICAN CHEMICAL SOCIETY**
Editor, Allen J. Bard
University of Texas
26 issues a year. ISSN 0002-7863
Member $70 Nonmember $350

☐ **JOURNAL OF CHEMICAL AND ENGINEERING DATA**
Editor, Bruno J. Zwolinski
Texas A&M University
4 issues a year. ISSN 0021-9568
Member $29 Nonmember $160

Call Toll Free (U.S.)

800-424-6747

Telex: 440159 ACSP UI or
892582 ACSPUBS
Cable Address: JIECHEM
Telecopier (SANYO Group 1,2,3): 202-872-4615

American Chemical Society
Marketing Communications
Department
1155 Sixteenth St., N.W.
Washington, D.C. 20036
U.S.A.

☐ **JOURNAL OF CHEMICAL INFORMATION AND COMPUTER SCIENCES**
Editor, Thomas L. Isenhour
Utah State University
4 issues a year. ISSN 0095-2338
Member $17 Nonmember $90

☐ **JOURNAL OF MEDICINAL CHEMISTRY**
Editor, Philip S. Portoghese
University of Minnesota
12 issues a year. ISSN 0022-2623
Member $40 Nonmember $208

☐ **THE JOURNAL OF ORGANIC CHEMISTRY**
Editor, Frederick D. Greene
Massachusetts Institute of Technology
26 issues a year. ISSN 0022-3263
Member $53 Nonmember $276

☐ **JOURNAL OF PHYSICAL AND CHEMICAL REFERENCE DATA**
Editor, David R. Lide, Jr.
National Bureau of Standards
4 issues a year. ISSN 0047-2689
Member $55 Nonmember $240

☐ **THE JOURNAL OF PHYSICAL CHEMISTRY**
Editor, Mostafa A. El-Sayed
University of California, Los Angeles
26 issues a year. ISSN 0022-3654
Member $65 Nonmember $387

☐ **LANGMUIR**
Editor, Arthur W. Adamson
University of Southern California
6 issues a year. ISSN 0743-7463
Member $55 Nonmember $329

☐ **MACROMOLECULES**
Editor, Field H. Winslow
AT&T Bell Laboratories
12 issues a year. ISSN 0024-9297
Member $53 Nonmember $306

☐ **ORGANOMETALLICS**
Editor, Dietmar Seyferth
Massachusetts Institute of Technology
12 issues a year. ISSN 0276-7333
Member $55 Nonmember $330

☐ **SINGLE ARTICLE ANNOUNCEMENT**
24 issues a year. ISSN 0044-7587
Member $63 Nonmember $126

Rates listed are for 1987 U.S. subscriptions. For subscription rates outside the U.S., contact American Chemical Society or your subscription agency. Member rates are for personal use only. For nonmember subscriptions in Japan, write Maruzen Co., Ltd.

MEETINGS

Separation and Purification

August 10–14
Colby-Sawyer College
New London, N.H.
Richard D. Noble, *Chairman*
Edward L. Cussler, *Vice Chairman*

AUGUST 10

R. A. Bartsch, *discussion leader*

D. H. Busch, Longevity, the Critical Factor in Oxygen Carrier Design
W.S.W. Ho, Olefin Separations via Complexation with Cuprous Diketonate

A. L. Bunge, *discussion leader*

S. D. Alexandratos, Design and Development of Metal–Ion Separations with Dual Mechanism Ion Exchange-Redox/Coordination/Precipitation Resins
M. M. Sharma, New Strategies in Separation of Close Boiling Substances

AUGUST 11

E. L. Cussler, *discussion leader*

J. D. Way, Facilitated Transport Membranes for Hydrogen Production
C.J.D. Fell, Solvent Swollen/Filled Membranes for Recovery of Heavy Molecular Weight Components from Gas Streams

E. L. Cussler, *discussion leader*

D. W. Deetz, Stabilized Liquid Membranes for Gas Separations
J. Draxler, Industrial Scale Process for Zinc Removal Using Emulsion Liquid Membranes

AUGUST 12

T. A. Hatton, *discussion leader*

P.-A. Albertsson, Separation of Biopolymers and Cell Particles by Partition in Aqueous–Aqueous Two-Phase Systems
C. J. van Oss, Aqueous-Phase Partitioning Mechanism and Its Implications

J. Shaeiwitz, *discussion leader*

C. Fabiani, Physicochemical Aspects of Transport in an Implantable Bioartificial Pancreas.
E. Drioli, Enzyme Membranes and Enzyme Membrane Reactors in Biotechnological Processes

AUGUST 13

M. L. Heinitz, *discussion leader*

P. K. Dasgupta, Trace and Ultratrace Analysis of Ionic Species
W. Nitsch, The Importance of Surfactants for the Kinetics in Liquid–Liquid Systems

G. Pez, *discussion leader*

L. A. Robbins, Industrial Scale Separation of Parts per Quadrillion Dioxin from Water
W. F. Prouty, Large-scale Purification of Recombinant Human Insulin

AUGUST 14

M. L. Heinitz, *discussion leader*

H. A. Chase, Optimization of Fixed Bed Adsorption Separation of Proteins
M. V. Novotny, Microcolumn Separation Methods

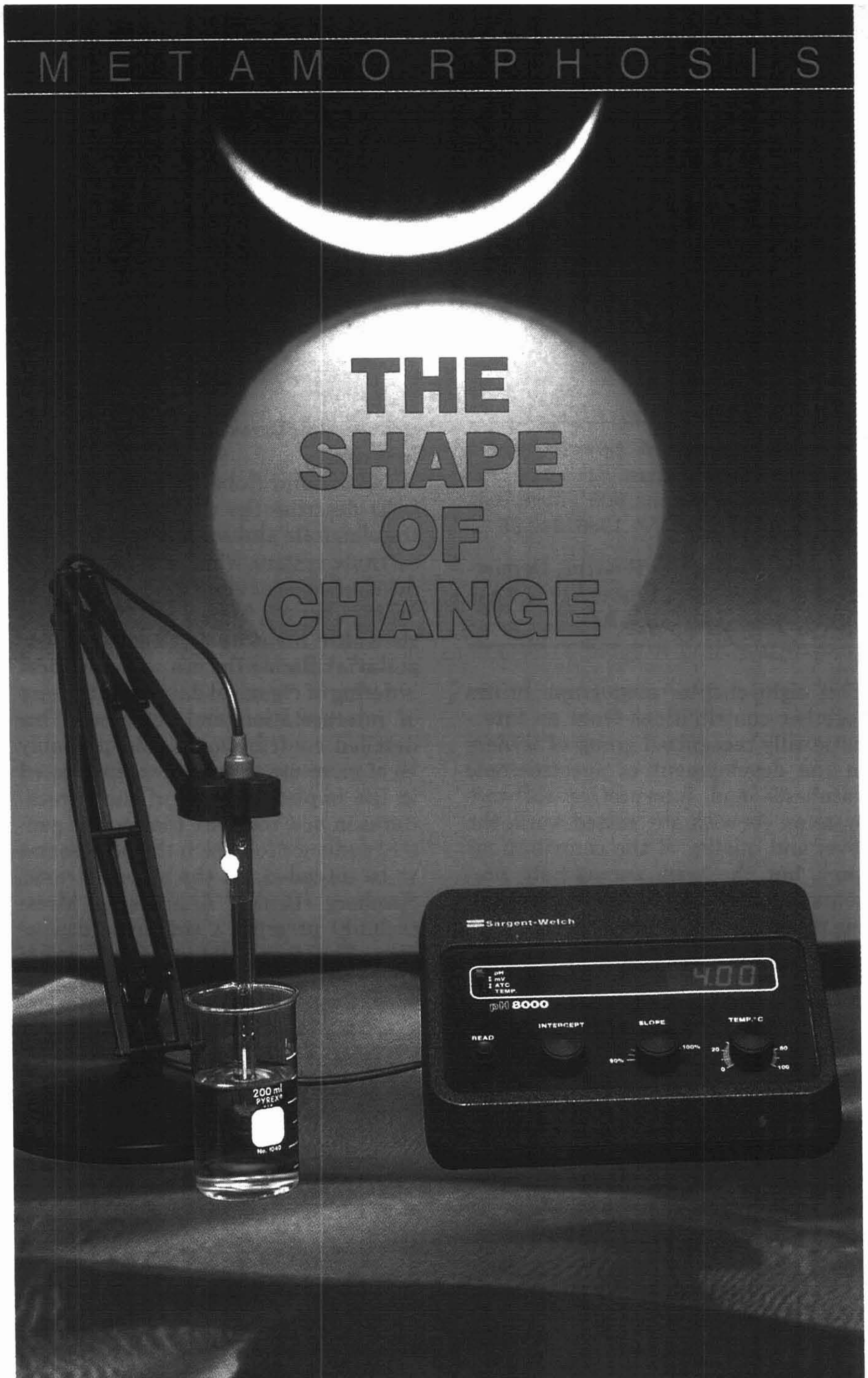

Introducing the new 8000 Digital pH Meter:

It's economical, superior electronics are designed for fast, accurate and reliable performance, in school, industry and hospital use.

The Shape of Change:
Performance-priced to fit your budget, from . . .

Sargent-Welch Scientific Company
7300 North Linder Avenue • PO Box 1026, Skokie, IL 60077 • (312) 677-0600

CIRCLE 145 ON READER SERVICE CARD

The Status of Spectroscopic Databases

Computer-Supported Spectroscopic Databases. Jure Zupan, Ed. viii + 165 pp. John Wiley & Sons, 605 Third Ave., New York, N.Y. 10158. 1986. $49.95

Reviewed by Charles Wilkins, Department of Chemistry, University of California, Riverside, Calif. 92521

This eight-chapter monograph brings together contributions from an internationally recognized group of leaders in the development of spectroscopic databases and interpretive software systems. As with any edited work, the level and quality of the contributions vary, but the book successfully presents the current status of this developing research area.

In an engaging introduction, Zupan does an outstanding job of setting the theme for what is to follow. He cautions that databases, like icebergs, have unseen parts that can be dangerous. It is encouraging that this book opens with cautionary statements regarding the potential pitfalls of spectroscopic data collections. Such admonitions are especially needed because the numerous commercial purveyors of these types of collections generally have placed quantity before quality (the former being more profitable than the latter when sold to the unwary).

> “. . . databases, like icebergs, have unseen parts that can be dangerous.”

The first chapter, by Craig Shelley (Eastman Kodak), provides a useful discussion of the problems involved in computer-assisted spectral interpretation. Shelley makes several important points regarding the need for high-quality databases and then describes the intended features of a multispectral structure elucidation software system being developed at Eastman Kodak. This chapter is a good introduction for anyone considering the use of spectral databases and software for the first time.

Dubois and Sobel (Université Paris 7) describe the philosophy behind the elaborate and sophisticated DARC software system, which has been under development for many years. In the following chapter, Zupan and Novic (Boris Kidric Institute of Chemistry, Yugoslavia) discuss the use of hierarchical ordering of chemical databases for ease of interpretation and retrieval. This detailed contribution would probably be of more use to specialists interested in the implementation of such procedures in new software than to the general audience for which the book seems to be intended. At the other extreme, Somberg (Bruker Analytische Messtechnik) presents a simplistic discussion of infrared databases in somewhat strained English. Somberg's chapter ranges from the general and obvious to a detailed discussion of internal chemical structure storage in the Bruker software. The value of this chapter is that it reveals the philosophy behind one instrument manufacturer's approach to an essential database and the software to manipulate it.

In several succeeding chapters Passlack and Bremser (BASF), Heller (U.S. Department of Agriculture), and Sasaki and coauthors (Toyohashi University of Technology, Japan) discuss infrared, mass spectral, and nuclear magnetic resonance databases, respectively. Particularly valuable aspects of these discussions are the quality control procedures, which all of the authors consider central to spectral database development. In these chapters the reader encounters the recurring theme of the book: the essentiality of well-defined and usable means of ensuring the high quality of spectral data before they are entered into data banks and the equal need for reliable data error detection and correction methods for spectroscopic databases. In that regard, Heller notes the increasing difficulty of obtaining complete raw data from the scientific literature, along with the trend of reporting partial spectroscopic data selectively.

The final chapter, by Hippe (Technical University, Rzeszow, Poland) gives a brief overview of the general challenge of multispectroscopy computer-aided structure elucidation systems and concludes with a discussion of the author's approach to such a software system.

In summary, this book is very readable, and it provides a generally realistic assessment of the current status of spectroscopic databases, including the remaining problems with their development, maintenance, and use. The few typographical errors found in the book are generally minor (e.g., on p. 5, $_{13}$C for ^{13}C; on p. 49, “specta” for “spectra”; and on p. 59, “reprsentation” for “representation”). In view of its overall quality, *Computer-Supported Spectroscopic Databases* is highly recommended for anyone interested in this increasingly important topic.

Handbook of Air Pollution Analysis. Second Edition. Roy Harrison, Roger Perry, Eds. xxii + 634 pp. Chapman & Hall, 29 West 35th St., New York, N.Y. 10001. 1986. $79.95

Reviewed by Roger Jenkins, Analytical Chemistry Division, Oak Ridge National Laboratory, P.O. Box X, MS-120, Oak Ridge, Tenn. 37831

This book was first published in 1977 as a comprehensive manual on the theory and practice of air pollution analysis. The second edition updates the various topics in light of technological advances and expands the scope of the book to reflect increasing interest in other areas. In many cases, the editors have succeeded; in others, they have missed the target.

Chapter 1 is a good overview of general sampling techniques, particularly the discussion of particle size determination and isokinetic effects. However, I was surprised that there was no discussion of the use of Tenax-GC or XAD-2 as organic vapor trapping media. The number of references dated 1980 or later was minimal, and the discussion of modern collection media was lacking. Chapter 2 appears to be designed to acquaint the novice with meteorological situations that could alter sampling strategy and to encourage seeking the counsel of a qualified meteorologist. Chapter 3 consists of a good, basic overview of air pollution chemistry and includes many up-to-date references.

The discussion of particle analysis (Chapter 4) was disappointing. It appears that little effort was expended to update this section, and relatively old references are cited. For example, in the discussion of portable sampling pumps, a 1963 reference is cited. In contrast, the chapters on the analysis of metals and sulfur and nitrogen compounds are quite good. The critical review of techniques can be very helpful to investigators new to the field. The experimental sections are rich in detail. Although I would not recommend performing the analysis without consulting the original manuscript, I believe it is helpful for the novice to be exposed to the complexity (or lack thereof) in a particular approach. The discussion on the analysis of oxides of nitrogen could have been better updated. For example, many commercially available NO_x analyzers no longer use stainless steel-based NO_2 converters. The discussion of secondary pollutants (Chapter 7) is also good. It explains the generalities and specifics of analyses of ozone, HNO_3, PAN, aldehydes, and so on. I was baffled that there was no description of analysis of aldehydes via dinitrophenylhydrazine derivatization and subsequent HPLC analysis, an approach that is widely used.

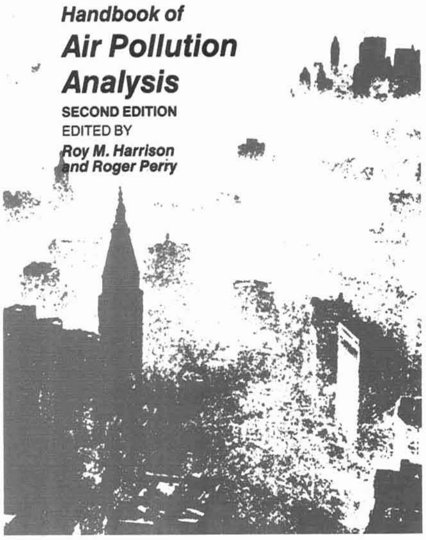
Handbook of
Air Pollution
Analysis
SECOND EDITION
EDITED BY
Roy M. Harrison
and Roger Perry

Chapter 8 describes the determination of organics and carbon monoxide. The discussion generally is up to date, although most of the citations are pre-1980. Interestingly, this chapter describes certain advanced instrumental

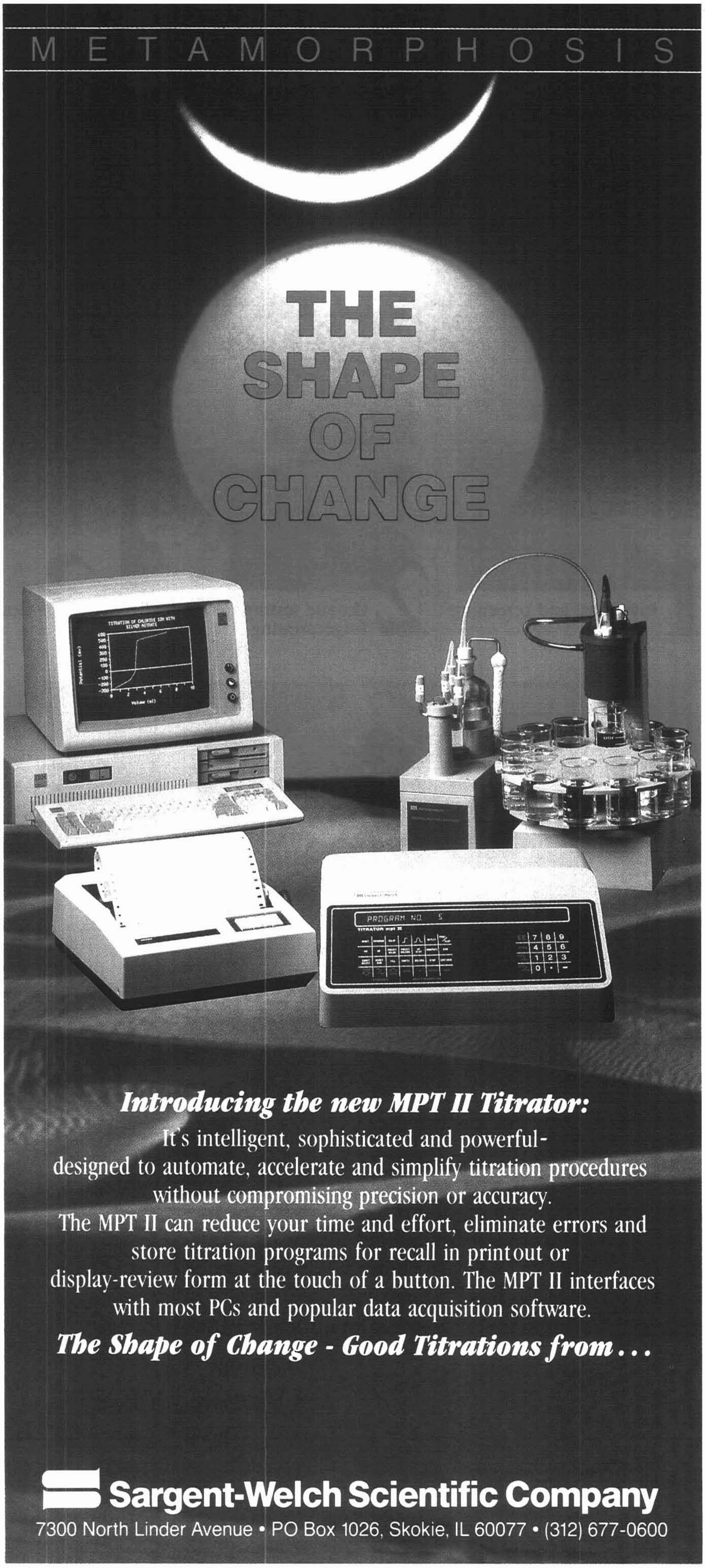

Introducing the new MPT II Titrator:

It's intelligent, sophisticated and powerful-
designed to automate, accelerate and simplify titration procedures
without compromising precision or accuracy.
The MPT II can reduce your time and effort, eliminate errors and
store titration programs for recall in printout or
display-review form at the touch of a button. The MPT II interfaces
with most PCs and popular data acquisition software.

The Shape of Change - Good Titrations from...

Sargent-Welch Scientific Company
7300 North Linder Avenue • PO Box 1026, Skokie, IL 60077 • (312) 677-0600

CIRCLE 146 ON READER SERVICE CARD

Laboratory Chemical Clean-Up, Packaging & Disposal

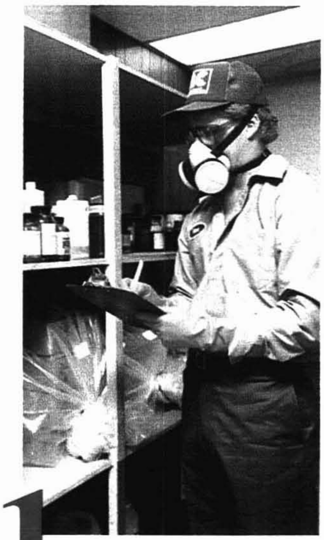

1 Inventory and screening

2 On-site testing and fingerprinting

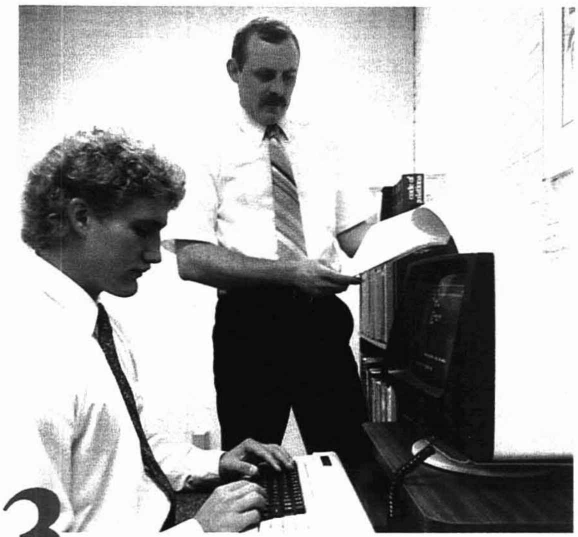

3 Computerized identification - classification

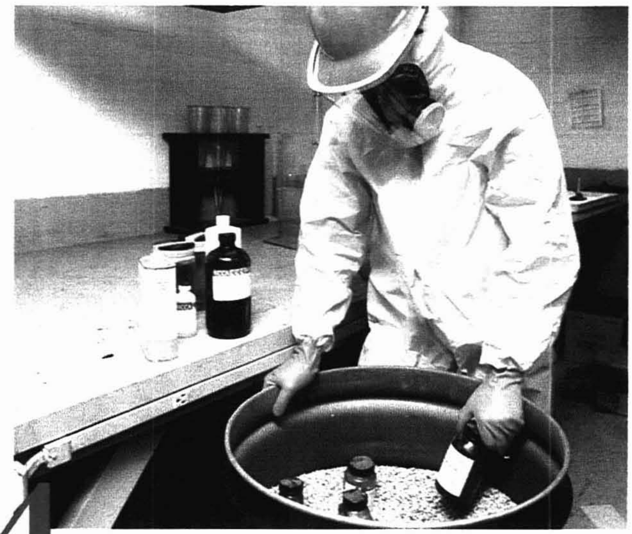

4 D.O.T "Lab-Pack" packaging of compatible materials

5 Environmentally secure packaging and transportation

This exclusive system is a self-designed and constantly updated computerized turnkey program. Experienced environmental chemists are fully equipped for on-site chemical inventory, fingerprinting and classification. Packaging and transport of chemicals to disposal facilities are in compliance with all EPA and DOT regulations.

A wide assortment of laboratory and small quantity chemicals are efficiently identified, packaged and disposed of within one safe full service program.

great lakes environmental services, inc.

a subsidiary of environmental systems company

22077 Mound Rd., P.O. Box 1208, Warren, Michigan 48091 • (313) 758-0400 • MI 1-800-482-4484 • US 1-800-482-4482
Chicago Sales Office: 15 Spinning Wheel Rd., Suite 327, Hinsdale, Illinois 60521 • (312) 323-0410

CIRCLE 60 ON READER SERVICE CARD

techniques, such as automated thermal desorption, and ignores others, such as sequential or multidimensional chromatography, that might be particularly pertinent to the analysis of complex mixtures. Halogen-containing compounds are addressed in Chapter 9. The discussions of sampling and analytical aspects are very thorough, and the chapter has one of the more recent sets of references. Chapter 10 is an interesting discussion of remote monitoring techniques, mostly related to plume measurement. It was fun to read, in contrast to the chapter on speciation techniques for atmospheric particles. The chapter on precipitation measurement also required considerable energy and concentration.

The inclusion of a chapter on low-cost methods of air pollution analysis was a novel idea, but it might have been more appropriate to call it "Basic Considerations in Air Sampling" and to have moved it to the beginning of this edition. Coverage of individual topics in the chapters on planning and executing an air pollution study and quality assurance is so brief that it is of little value other than to remind the reader to consider certain related aspects.

My overall impression is that this is a good book for someone new to the field of air pollution measurement or for someone moving into a new area within the field. I would have preferred to have article titles in the references because the book appears to have been designed for collaboration with particular references. This is a book that I would want to have on my bookshelf, but I would not want it to be my only reference source on air pollution.

Books Received

Ion Chromatography. James Tarter, Ed. 448 pp. John Wiley & Sons, 605 Third Ave., New York, N.Y. 10158. 1987. $79.75

Development of Drugs and Modern Medicines. J. Gorrod, G. Gibson, M. Mitchard, Eds. 669 pp. VCH Publishers, 303 N.W. 12th Ave., Deerfield Beach, Fla. 33442. 1986. $163

Secondary Ion Mass Spectrometry. Basic Concepts, Instrumental Aspects, Applications, and Trends. A. Benninghoven, F. Rudenauer, H. Werner. 1227 pp. John Wiley & Sons, 605 Third Ave., New York, N.Y. 10158. 1987. $150

Organic Pollutants in Water. I. Suffet, Ed. xv + 797 pp. American Chemical Society, 1155 16th St., N.W., Washington, D.C. 20036. 1987. $109.95

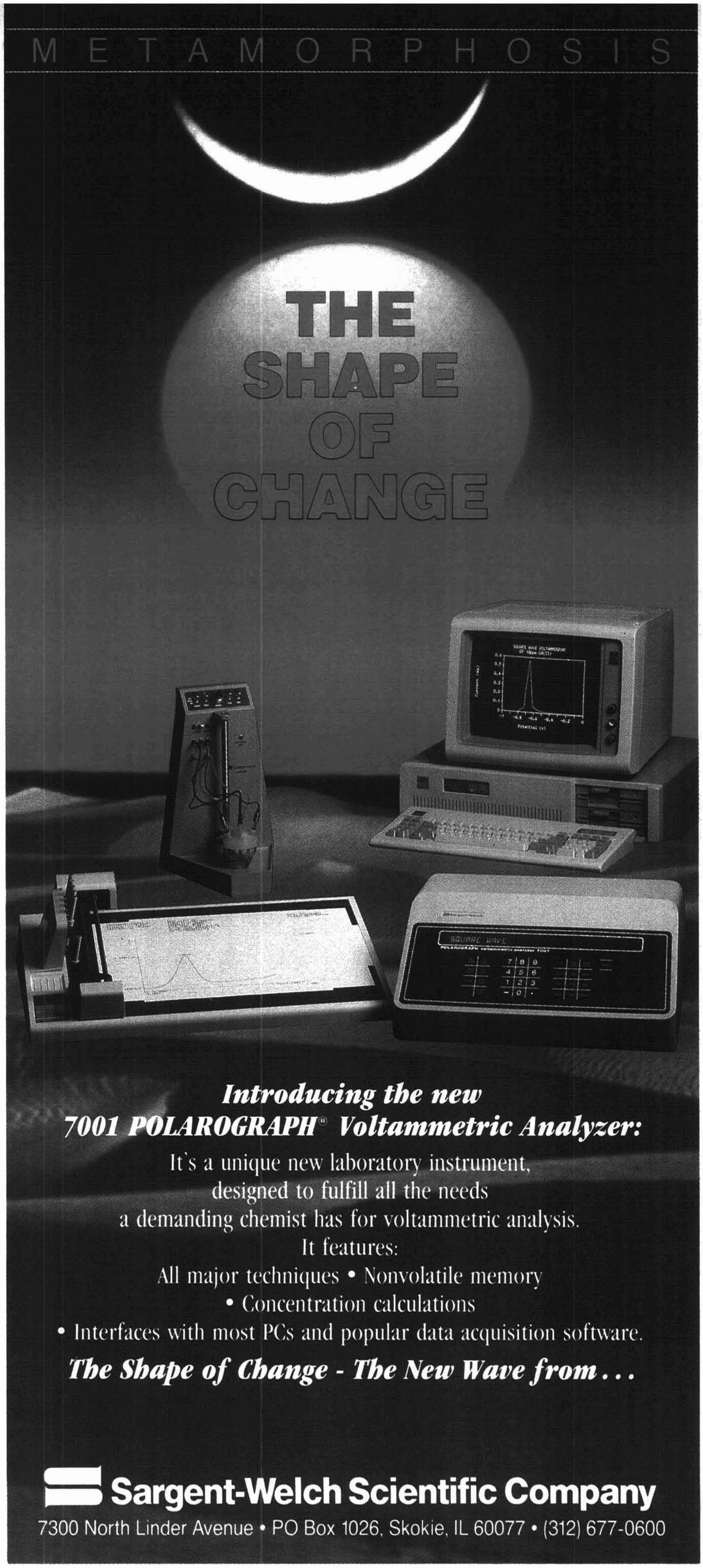

Introducing the new
7001 POLAROGRAPH® Voltammetric Analyzer:

It's a unique new laboratory instrument,
designed to fulfill all the needs
a demanding chemist has for voltammetric analysis.
It features:
All major techniques • Nonvolatile memory
• Concentration calculations
• Interfaces with most PCs and popular data acquisition software.

The Shape of Change - The New Wave from . . .

Sargent-Welch Scientific Company
7300 North Linder Avenue • PO Box 1026, Skokie, IL 60077 • (312) 677-0600

CIRCLE 147 ON READER SERVICE CARD

The VG TS-250...
Not just a new mass spectrometer but a new technology

TS-250 triple-sector technology starts at the magnet. Its unique, fast, hysteresis-free design gives the extremely rapid scanning usually associated with quadrupoles. In addition, the high scanning accuracy eliminates the need for magnet calibration in all ionization modes.

Other VG advances that make the TS-250 a whole new concept in mass spectrometry are electronically selectable mass resolution directly programmable from the microprocessor keyboard and a unique source changeover system that goes from EI to FAB in under 30 seconds!

And... we've made it a simple push-button operation.

Put an entirely new MS technology at your command. Contact VG Instruments for more details on the TS-250.

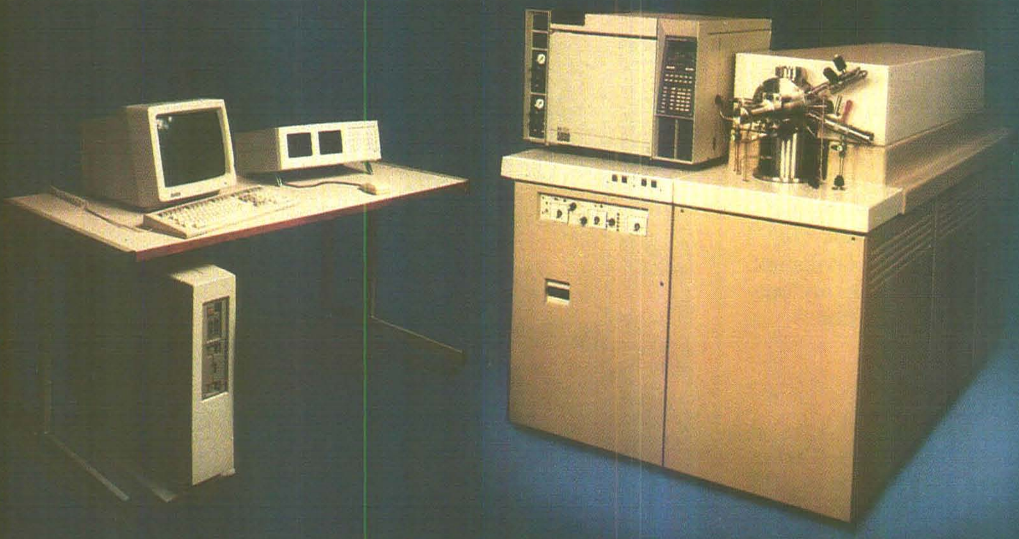

VG INSTRUMENTS
The third technology

A VG INSTRUMENTS GROUP COMPANY

USA. VG Instruments Inc., 32 Commerce Center, Cherry Hill Drive, Danvers, MA 01923. Tel. (617) 777-8034.
VG Tritech, Crewe Rd., Wythenshawe M23 9LE, England. Tel. (61)9982500.
WEST GERMANY. VG Instruments GmbH, Gustav-Nachtigal-Strasse 4, 6200, Wiesbaden. Tel. (6121) 713030.
FRANCE. VG Instruments, 3 Rue du Marechal de Lattre de Tassigny, 78150 Le Chesnay. Tel. (1) 3955 5120.
ITALY. VG Instruments Limited, Viale Dell'Assunta 101, 20063 Cernusco Sul Naviglio, Milano. Tel. (2) 924 8808.
THE NETHERLANDS. VG Instruments bv, PO Box 171, 1380 AD, Weesp. Tel. (2940) 80484.
CHINA. VG Instruments, Room 7059, Xi Yuan Hotel, Erligou, Xijiao, Beijing. Tel. 890721 Ext 759.
HONG KONG. VG Instruments Asia Limited, GPO Box 217, Hong Kong. Tel. (5) 8613651.
JAPAN. Jasco International Co. Ltd. 2-4-21, Sennin-Cho, Hachioji City, Tokyo 193. Tel. (426) 661321.

Circle 172 for literature. Circle 173 to have a representative call.

Pittsburgh Conference

March 9–13, 1987

FOCUS

The Pittsburgh Conference and Exposition returned to Atlantic City this year for one last time at the New Jersey shore before moving on to New Orleans in 1988 and Atlanta in 1989. Although the weather was unusually bad (even for Atlantic City in March), the mood in the convention center was upbeat. Attendance reached an all-time high of 31,555, and 790 exhibitors occupied 2040 booths. The number of technical papers presented (1145) was also up from 1986 (see Table I for comparison with previous years).

Table I. Pittsburgh Conference attendance statistics, 1984–1987

Category	1984	1985	1986	1987
Total no. of conferees	24,648	20,733	29,146	31,555
No. of technical papers	962	1,213	1,094	1,145
No. of exhibitors	~610	730	730	790
No. of booth spaces	1,607	1,830	2,012	2,039

The number of job candidates registering with the employment bureau increased slightly this year (939 vs. 909 in 1986), but the number of job openings was far less than last year's figure (700 vs. 884 in 1986). Decreases in job openings occurred in government (28 vs. 64 in 1986), industrial labs (413 vs. 543 in 1986), and industrial sales (143 vs. 198 in 1986). (See Tables II and III for comparison with previous years.)

Centcom, Ltd., advertising management for American Chemical Society publications, held its annual Pittsburgh Conference breakfast on Tuesday, March 10. This year's discussion, "Marketing Directions for the Nineties," was aimed at instrument industry executives and moderated by Richard A. Dreher, president of RAD Associates. The three panelists were John Nelson, senior vice president of marketing for Waters Chromatography Division of Millipore; Jeff Freeman, marketing manager of J. Freeman; and Don Schoeny, group marketing manager for the analytical instrument products division of Hewlett-Packard. Panelists discussed strategies for sales, service, and marketing in the coming decade with an eye toward using evolving technology and maintaining good customer relations.

In addition to the presentation of awards announced previously (see the February 1 issue of ANALYTICAL CHEMISTRY, p. 136 A), the first Tomas Hirschfeld Award in Near Infrared Analysis was presented to Don Pivonka, a fourth-year graduate student at Kansas State University, Manhattan, Kan. The award, sponsored by Technicon, recognizes Pivonka for demonstrating expertise in many different areas of spectrometry and for implementing many of his own ideas in the laboratory.

Another new feature of this year's conference was the User–Manufacturer Information Exchange (UMIX) symposium program organized by Robin Garrell and Stephen Weber. Pharmaceutical analysis, polymer analysis, and surface analysis were the topics of this year's UMIX symposia held on

Table II. No. of job candidates, 1984–1987

Degree	1984	1985	1986	1987
Ph.D.	333	272	380	535
M.S.	174	105	168	72
B.A. or B.S.	276	182	322	314
Other	8	11	39	18
Total	788	570	909	939

Table III. Comparison of job openings, 1984–1987

Description	1984	1985	1986	1987
Academic	11	22	15	19
Government	8	18	64	28
Industrial labs	520	392	543	413
Industrial sales	140	116	198	143
Industrial management	20	16	*	*
Research institutions	*	12	3	26
Employment agencies	*	*	61	71
Total	~700	576	884	700

* Comparable breakdown not available.

Friday, March 13. Aimed at industrial analytical chemists, each UMIX symposium featured an overview of the subject by an expert in the field, brief presentations by technical representatives of instrument manufacturers, and a discussion between an expert panel and the audience.

In keeping with the theme of this year's conference, "A Blueprint for Excellence!", all three exhibit halls were filled with instruments, many of which incorporate new technological advances, as well as laboratory equipment designed to help scientists simplify and plan their work. Whereas only a few years ago computers were a rarity in the analytical laboratory (and on the exhibition floor), this year they were everywhere. Not only was the convention floor full of computer-controlled instruments, but many exhibitors were demonstrating ways in which networking hardware and software, compact disk (CD-ROM) technology, and software packages for data collection, database management, and technical word processing can be used to facilitate information collection, handling, and transfer.

Many of the instruments introduced at this year's show are hyphenated systems. For example, both Hewlett-Packard (HP) and Mattson Instruments showed new gas chromatography–Fourier transform infrared spectrometry–mass spectrometry (GC/FT–IR/MS) systems, which can provide both infrared and mass spectral information in addition to gas chromatographic retention times. The HP system uses lightpipe GC/FT–IR technology and can also be used as either a GC/MS or GC/FT–IR instrument alone, whereas the Mattson instrument, which includes an HP gas chromatograph and mass selective detector, uses matrix isolation rather than lightpipe technology to achieve greater sensitivity.

Several instruments coupling supercritical fluid chromatography (SFC), thin-layer chromatography (TLC), thermogravimetric analysis (TGA), and thermal analysis (TA) with FT–IR and MS were also introduced at this year's show. The first commercial capillary SFC instruments were introduced only last year, but the field is moving ahead rapidly and SFC instruments were shown this year both alone and interfaced with infrared or mass spectrometers. Lee Scientific, Suprex, Computer Chemical Systems, and Brownlee Labs introduced new versions of their capillary SFC instruments, and all four companies indicated that their instruments could be readily coupled to FT–IR or mass spectrometers. For example, Lee Scientific's new system was also shown at the Nicolet booth interfaced to an FT–IR spectrometer, and a Suprex SFC was coupled to a triple quadrupole MS system at the Extrel booth.

TLC has been combined with FT–IR by Analect Instruments, whose Chromalect system uses a conventional TLC plate for separation followed by elution of the analyte spots into 64 sample cups containing diffuse reflectance media. After evaporation of the solvent, the sample cups are placed into an optical system and diffuse reflectance FT–IR spectra of the analyte

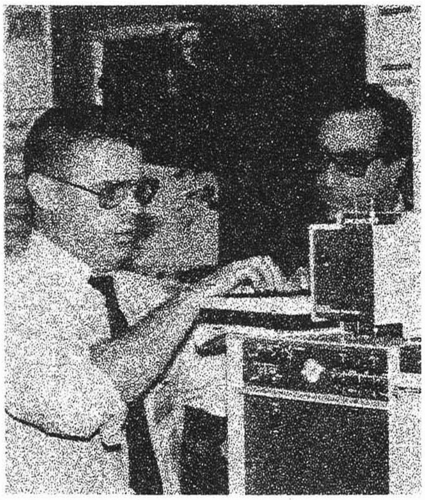

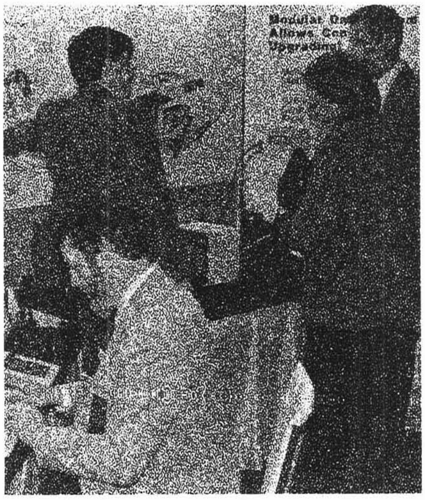

Modular Design Allows Con Upgrading

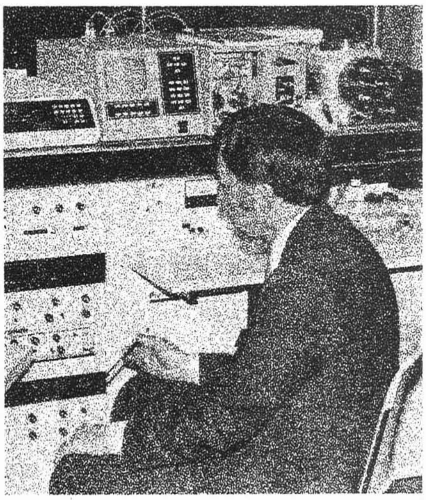

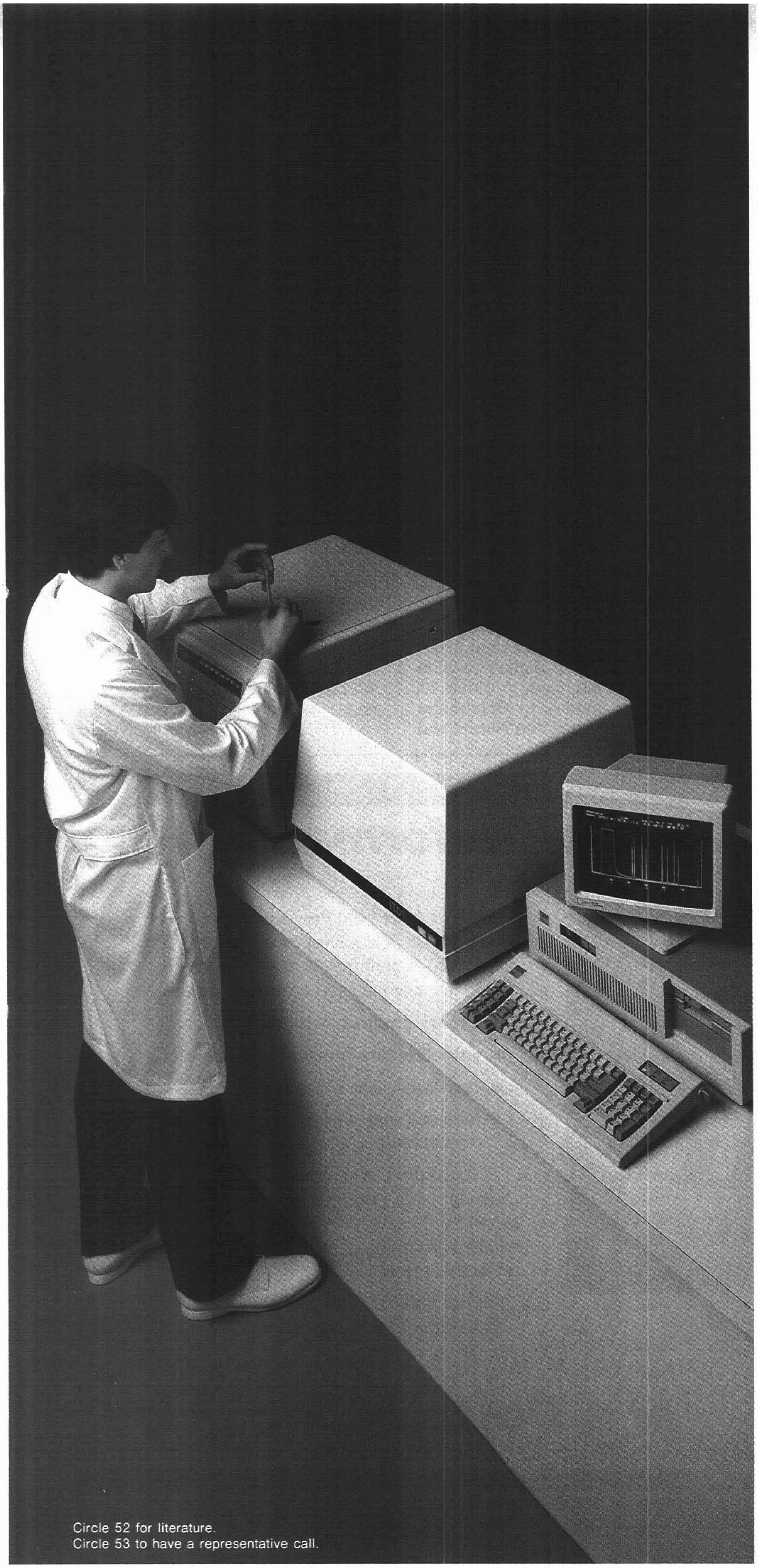

Circle 52 for literature.
Circle 53 to have a representative call.

Don't sacrifice GC/MS specificity for sensitivity.

Reach for a new level of sensitivity while scanning the full mass range throughout your GC run. All with a linear dynamic range of over five decades, and the use of internal standards for the highest quantitative precision.

The new Finnigan MAT Model 800 Ion Trap Detector™ gives you positive identification at sample levels as low as 10 picograms, with the confidence level only a full mass scan can offer. To attain equivalent sensitivity, competitive detectors depend on the measurement of a few selected ions, sacrificing specificity for sensitivity.

For molecular weight confirmation, the ITD™ 800 offers chemical ionization (CI) capabilities, a feature previously available only on mass spectrometers costing twice as much as the ITD 800.

As always, the ITD's powerful library search program can match an unknown spectrum in seconds.

Richard A. Yost (University of Florida), William McClennen and Henk L.C. Meuzelaar (University of Utah) put the ITD to the test. Their findings are documented in our Technical Report #209, "Enhanced full scan sensitivity and dynamic range in the Ion Trap Detector." Ask your Finnigan MAT representative for a copy today, and demand to see results like these from *your* next mass spec detector.

Mass spectrometry:
We make the difference.

Finnigan
MAT

U.S.A., 355 River Oaks Parkway, San Jose, CA 95134. (408) 433-4800
Germany, Postfach 14 40 62, D-2800 Bremen 14. (0421) 54 93-0
U.K., Paradise, Hemel Hempstead, Herts HP2 4TG. (0442) 233555
France, 69, rue de Paris, F-91400 Orsay. (1) 69 28 52 53
Sweden, Årstaänsvagen 1C, 117 43 Stockholm. (08) 190480
Benelux, Landjuweel 7, 3905 PE Veenendaal. 08385 27266
Italy, Via Valadier, 37B, 00193 Rome. (06) 316000
Japan, Shiozaki Bldg., 2-7-1 Hirakawa-cho, Chiyoda-ku, Tokyo 102. (03) 221-1

spots are collected. The system can achieve detection limits of 300 ng for a barbiturate mixture, although the company claims that lower detection limits are possible.

In the MS arena, several new hyphenated products were introduced. Two of these were liquid chromatography–mass spectrometry (LC/MS) instruments designed to provide more fragmentation, and thus more structural information, than thermospray LC/MS. Extrel introduced the ThermaBeam interface, which uses a particle beam to remove LC solvent prior to the sample entering the mass spectrometer. The analyte molecules can then be ionized using a variety of techniques, including electron impact and chemical ionization. Finnigan's new TSP 46 dedicated thermospray LC/MS system, on the other hand, uses variable repeller voltage to increase the amount of fragmentation that can be induced.

Two interfaces that allow continuous introduction of a sample into a standard fast atom bombardment (FAB) source also were introduced at the exhibition. One of these, VG Instruments' Dynamic-FAB LC/MS technique, is an option available with the company's new Trio 3 triple quadrupole tandem MS system. The other, Kratos Analytical's continuous-flow FAB probe, is available for use with the MS50 and MS890 mass spectrometers. Both companies indicate that continuous-flow FAB methods improve signal-to-noise ratios and thus provide lower detection limits than conventional FAB.

Two hyphenated techniques, TGA/FT–IR and TA–MS, made their debut this year. Bio-Rad's Digilab division has developed interfaces to couple its FT–IR spectrometers to Omnitherm Corp.'s TGA systems, and Nicolet and Du Pont together have developed an interface for connecting a Du Pont Model 9900 TGA system to Nicolet's FT–IR systems. TGA, which measures sample weight loss as a function of time and temperature, is a standard technique in the polymer, fuel, and catalyst industries, and its combination with FT–IR will increase the usefulness of TGA experiments by allowing determination of the identity of the gases that evolve as the sample is heated. Stanton-Redcroft's TA–MS system, shown by Omnitherm, provides simultaneous thermogravimetric analysis, differential thermal analysis, and mass spectrometry. This system also will increase the amount of information that can be obtained from thermal analysis experiments. (For a more detailed description of instrumentation introduced at this year's Pittsburgh Conference, see the March 23 issue of *Chemical & Engineering News.*)

Next year the Pittsburgh Conference and Exhibition will return to the site of the 1985 conference in New Orleans. The New Orleans and Rivergate Convention Centers both will be used for the 1988 conference, which organizers expect to be bigger and better than ever.

Mary Warner

Get Top-of-the-Line Performance . . .

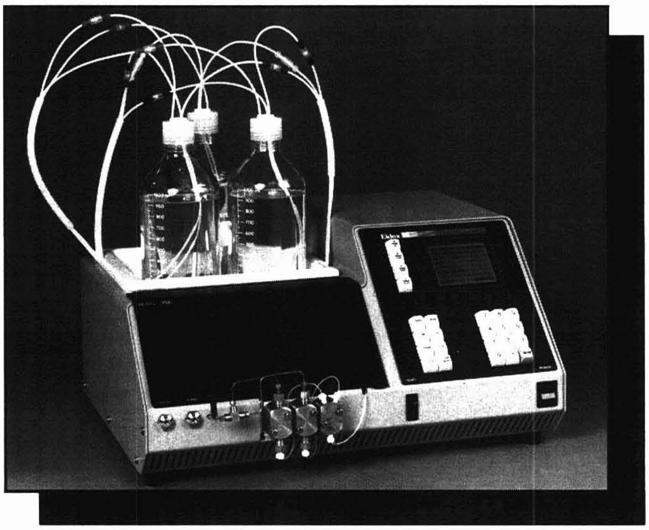

Eldex's Model 9600 Programmable Solvent Delivery System is a breakthrough in the HPLC pump price-to-performance ratio. For the cost of a simple isocratic pump, you can now have:

- **ternary gradient** capabilities.
- **pulse-free flow** rates from 0.01 to 10.0 mL/min.
- **easy-to-use** menus for programming.
- **fully automated** analyses and methods development.

Eldex is known in the industry for durable precision metering pumps – nearly 10,000 are in the field. The Model 9600 continues our tradition of providing reliable, quality equipment for chromatography at reasonable prices.

Call us today at **(415) 592-9270.**
You owe it to your bottom line.

Eldex
831 Bransten Road
San Carlos, CA 94070
(415) 592-9270
Telex: 171596

at a Bottom-Line Price.

CIRCLE 45 ON READER SERVICE CARD

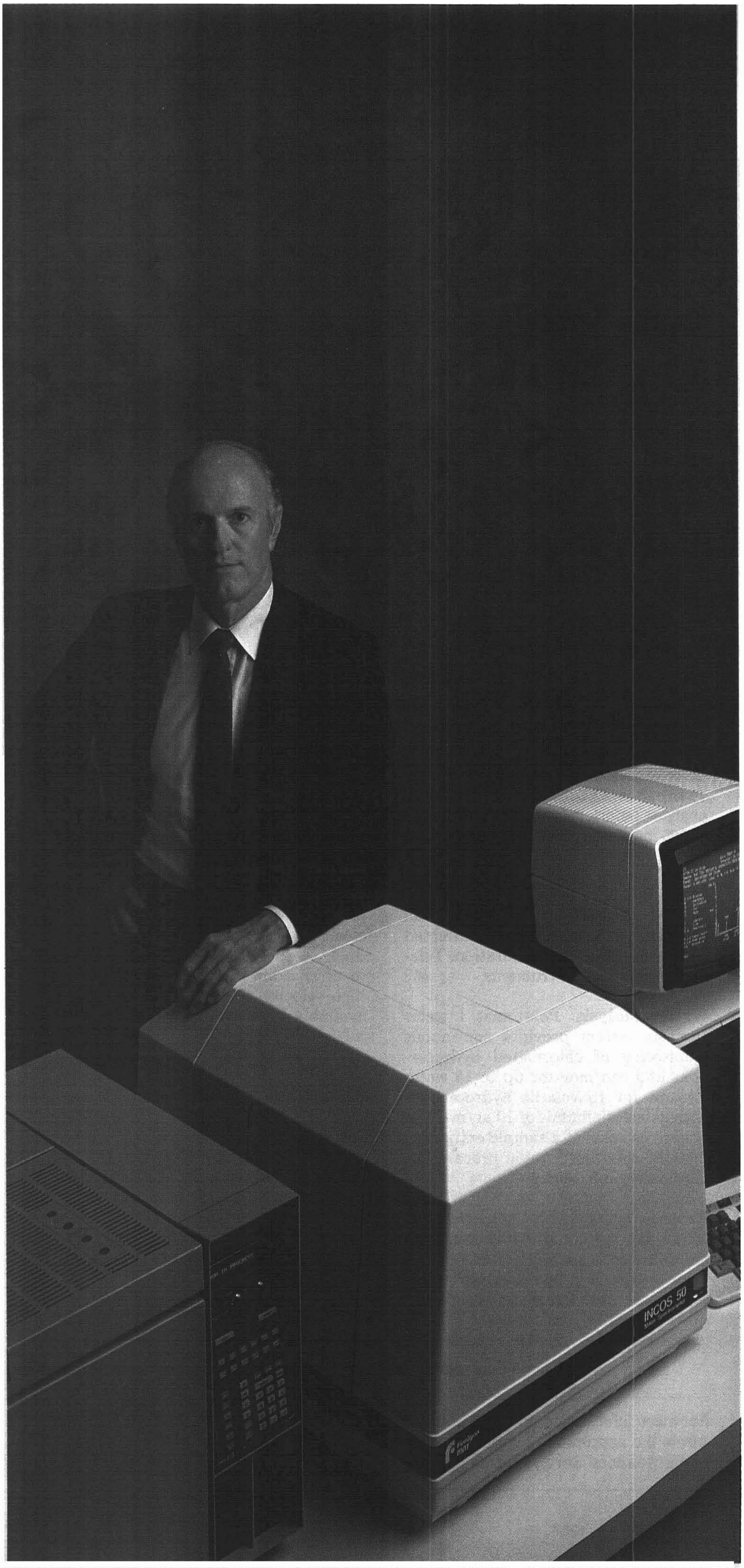

The INCOS™ 50 GC/MS means business.

Whether you run a commercial lab or an analytical department, you can't afford to be without the INCOS 50 quadrupole mass spectrometer. It's a small investment in big performance.

The INCOS 50 gives you EI or CI with positive or negative ion detection. We've made it compatible with capillary, wide-bore and packed column GCs. You can also use it with desorption or other solids probes. The advanced controls guarantee easy, stable and reproducible tuning. The result: highest analytical flexibility, highest data quality, highest throughput... every day.

Multiply your productivity with the 4th generation data system. True foreground/background. Large internal memory. Print spooling. Communications with the whole world... PCs, LIMS, mainframes. You name it.

Of course the INCOS 50 incorporates the industry-standard Incos™ software and is compatible with EPA protocols. Bob Finnigan wouldn't have it any other way.

Your investment? Minimal bench space and a remarkably low price. Contact your Finnigan MAT representative today, and let's talk business.

Mass spectrometry:
We make the difference.

Finnigan MAT

U.S.A., 355 River Oaks Parkway, San Jose, CA 95134. (408) 433-4800
Germany, Postfach 14 40 62, D-2800 Bremen 14. (0421) 54 93-0
U.K., Paradise, Hemel Hempstead, Herts HP2 4TG. (0442) 233555
France, 69, rue de Paris, F-91400 Orsay. (1) 69 28 52 53
Sweden, Årstaänsvagen 1C, 117 43 Stockholm. (08) 190480
Benelux, Landjuweel 7, 3905 PE Veenendaal. 08385 27266
Italy, Via Valadier, 37B, 00193 Rome. (06) 316000
Japan, Shiozaki Bldg., 2-7-1 Hirakawa-cho, Chiyoda-ku, Tokyo 102. (03) 221-100

Circle 54 for literature.
Circle 55 to have a representative call.

NEW PRODUCTS

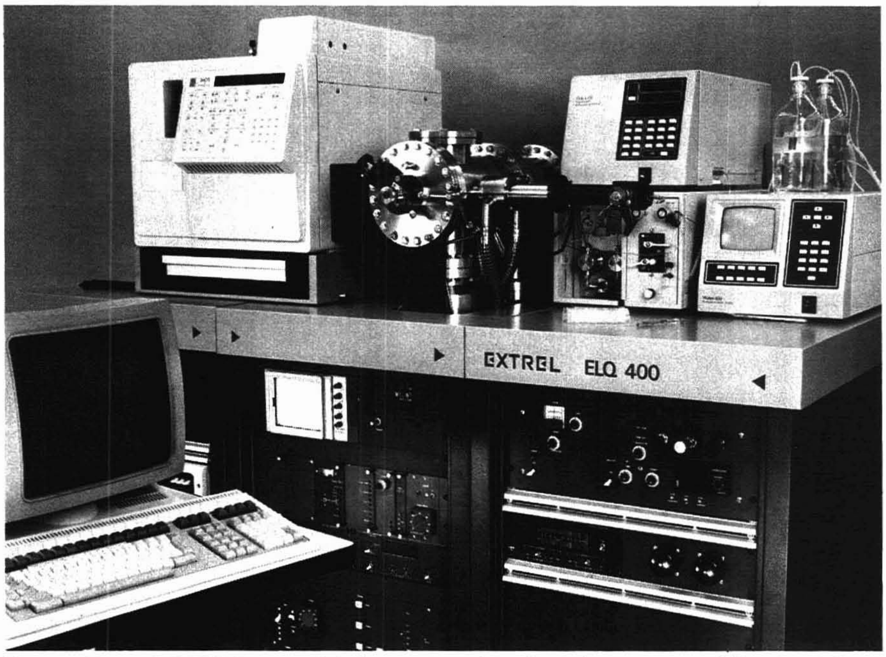

ThermaBeam LC/MS is a particle beam-type interface that removes LC solvent from analytes before they enter the mass spectrometer. Various LC separation conditions or MS ionization modes are possible. Extrel **401**

GC/IR/MS. The GC/IRD/MSD system is a customized combination of three standard HP instruments: 5890A GC, 5965A IRD, and 5970B MSD. From a single injection, retention times and infrared and mass spectra are produced for compound identification and confirmation. Hewlett-Packard **403**

Peptide synthesizer. Coupler 2100 produces peptides on scales of 0.5 or 2 mmol. Integrated synthesis logic controls the system and allows operator interaction through a keyboard designed for specific synthesis input. The synthesizer is compatible with protocols using fluorenyl–methoxycarbonyl reagents. Du Pont **404**

Spectrometer. PC spectrometer is an integrated, optical multichannel system that provides high-speed spectral acquisition and analysis in the 200–900-nm region. The system incorporates a UV photodiode array detector, an Ebert spectrograph, and an IBM PC. SC Technology **405**

LC. HPLC solvent recycling system is a completely automatic spinning band distillation system that recycles high-purity LC solvents such as acetonitrile, methanol, hexane, ethyl acetate, and THF. B/R Instrument Corp. **406**

Peak area quantitation. MC-503 distributed-control chromatograph system determines the true areas of merged peaks through the automatic application of the Gaussian orthogonal node separation algorithm. The system is compatible with the IBM PC-XT and is capable of sampling up to 100 streams and 100 components while simultaneously controlling the analyzer functions and manipulating data for printout. Analytical Instruments **407**

LC detector. Model 7510 refractive index detector has a built-in temperature controller and is sensitive down to 1.5×10^{-7} RIU. The cell capacity is 6.8 μl and the RI range is 1.00–1.75. HPLC Technology **408**

Oxygen analyzer. Model 316R trace oxygen analyzer features four standard analysis ranges: 0–10, 0–100, 0–1000, and 0–10,000 ppm. Optional ranges as low as 0–1 ppm are available for specialized applications. The microfuel cell used in the analyzer is unaffected by motion, position, or vibration. Teledyne Analytical Instruments **409**

Water analysis. Polutomat I water analysis system provides continuous monitoring of chlorinated hydrocarbons and can monitor up to 15 water streams for 15 volatile hydrocarbons with a detection limit of 10 $\mu g/m^3$. The system consists of a sample extraction module interfaced to a process gas chromatograph. Siemens **410**

Freeze-drying. Lyph-Lock bench-top freeze-dry system provides complete lyophilization capabilities and fits on a table or cart. A ⅓-hp refrigeration system cools the freeze-dry condenser down to −54 °C, and up to 4.5 L of ice can be loaded in the condenser. Labconco **411**

For more information on listed items, circle the appropriate numbers on one of our Readers' Service Cards

---

pH Electrode. Quartz combination pH electrode incorporates a reference electrode junction consisting of hundreds of micron-size quartz capillaries to offer a low-volume flow rate with high-velocity flow. The electrode is available in standard and semimicro models. Iotron **412**

Software

Reprocessing and storage. VAX reprocess software allows computer-based chromatography data stations and detectors to interface with DEC VAX computers. Data are transferred by direct connection to DECnet/Ethernet local area networks or via telecommunication. Waters **414**

Data management. LAB60 is designed for production and quality control applications and provides sample data management for multi-instrument laboratories. The software is compatible with DEC computers and can be used with any equipment capable of delivering suitable ASCII output. Philips **415**

THE LATEST GREATEST PLATE IS OURS

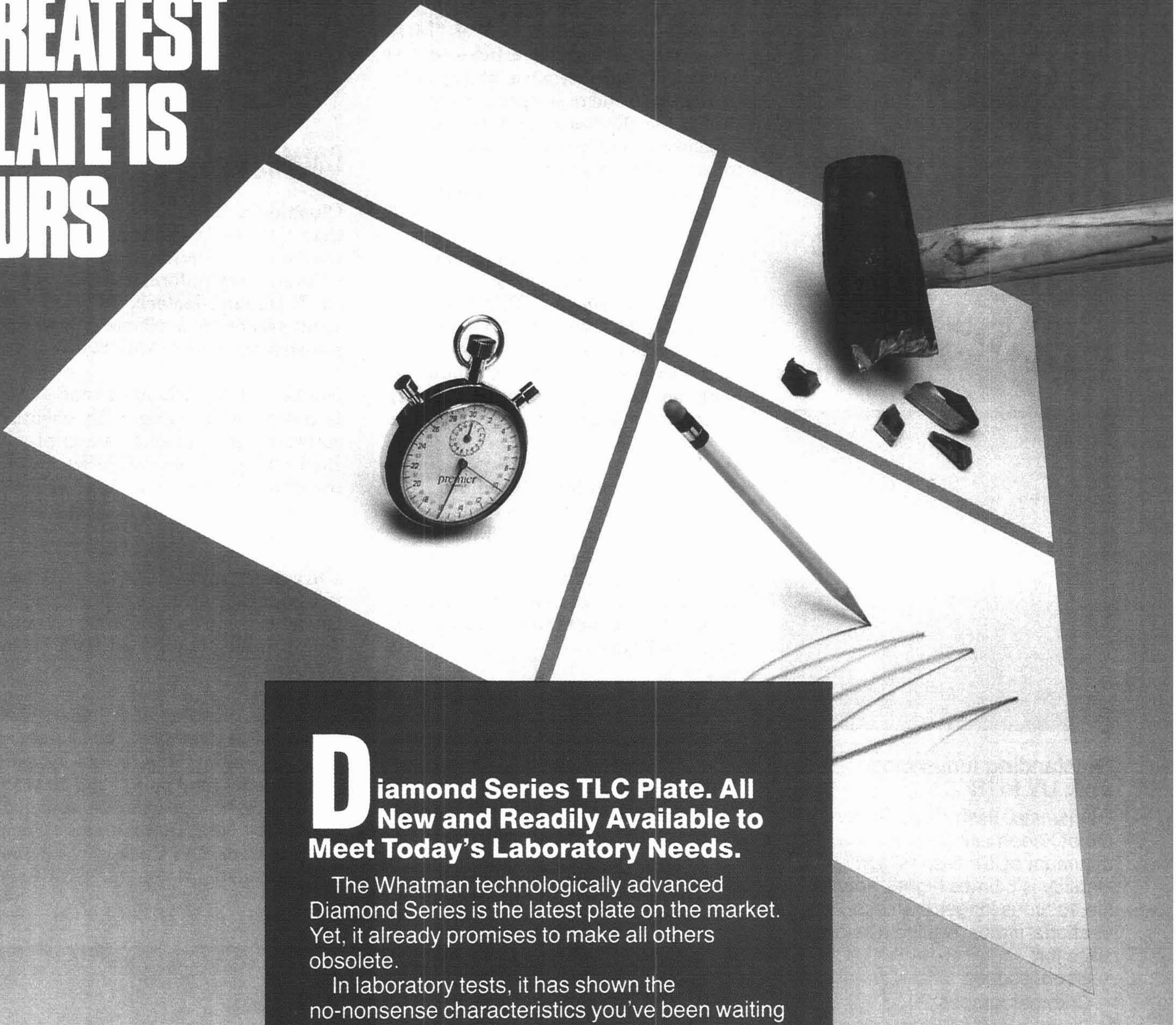

Diamond Series TLC Plate. All New and Readily Available to Meet Today's Laboratory Needs.

The Whatman technologically advanced Diamond Series is the latest plate on the market. Yet, it already promises to make all others obsolete.

In laboratory tests, it has shown the no-nonsense characteristics you've been waiting for . . . like a superior hard and reflective surface, a quality organic binder, and uniform particle size and distribution.

So what you end up with, of course, is a great plate. One that doesn't flake, can be easily written on, gives off less background noise, isn't reactive towards reagents, is highly efficient and offers fast development time.

And, just as great, a plate that can be delivered in the quantities you want . . . where you want them . . . when you want them.

Why not put our "latest and greatest" claim to the test today. Contact your nearest Whatman chromatography distributor or call our special Diamond Series line. We'll give you a plate you can depend on and service to match. (800) 922-0361 or in N.J. (201) 773-5800, Ext. 219.

Whatman®

CIRCLE 176 ON READER SERVICE CARD

SUPER-QUIET XENON LAMPS FOR PHOTOMETRIC INSTRUMENTS

Outstanding luminance from UV to IR

Hamamatsu flash mode Super-Quiet Xenon Lamps provide a minimum of 10^9 flashes! Arc stability is 5 times higher, service life 10 times longer than conventional lamps. Available in three sizes for:

- Stroboscopes
- Chromatographs
- Photoacoustic Spectroscopes
- Strobe Cameras
- Photomasking Devices
- Fluorospectrophotometers
- Color and SO_2 Analyzers
- Other light-sensitive instruments

For Application Information, Call 1-800-524-0504
1-201-231-0960 in New Jersey

HAMAMATSU

HAMAMATSU CORPORATION
360 FOOTHILL ROAD
P. O. BOX 6910
BRIDGEWATER, NJ 08807
PHONE: 201/231-0960
International Offices in
Major Countries of
Europe and Asia.

© Hamamatsu Photonics, 1986

CIRCLE 63 ON READER SERVICE CARD

NEW PRODUCTS

Manufacturers' Literature

Newsletter. Vol. X, No. 1 of "Mass Spec Source" features articles on the service and maintenance of gas chromatographs and mass spectrometers. A list of MS discussion groups, used instruments and parts for sale, and a question-and-answer section also are included. Scientific Instrument Services 417

Pesticide analysis. Application note demonstrates the use of GC with photoionization detection (PID) for pesticide analysis. Using a 9.5-eV lamp, the PID can detect specific compounds in complex matrices. When combined with an ECD, an extended linearity range of 10^8 is possible. HNU Systems 418

Chromatography. Brochure describes the ChromStation multichannel chromatography workstation. Diagrams are included to illustrate the features of the system, in which as many as eight single-channel or four dual-channel integrators can be used. 8 pp. Spectra-Physics 419

Rental guide. Complete directory of instrument rental inventory features gas, ion, and liquid chromatographs, GC–MS systems, and IR, UV–vis, fluorescence, FT–IR, and AA spectrophotometers. 4 pp. U.S. Analytical Instruments 420

Newsletter. The second issue of "The Dry Lab" provides information on HPLC method development with the aid of a personal computer. Also described is the DryLab series of software products for optimization of gradient and isocratic HPLC methods. 8 pp. LC Resources 421

Catalogs

Chemicals. 1987 catalog lists more than 300 specialty chemicals for biotechnologists. Performance characteristics and assay information are provided. Ultrapure, biotech, ACS, and reagent grades are available in bulk and research quantities. AMRESCO 425

Books. Catalog lists more than 10,000 technical books along with scientific software and complete descriptions. Books in 16 subject categories including the sciences, computer science, mathematics, and engineering are listed. Omega Press. 426

Chromatography. LC and GC supplies catalogs include chromatographs, columns, syringes, standards, reagents, data-handling equipment, and books. Varian 427

Software. Catalog lists educational programs in chemistry, biochemistry, physics, engineering, statistics, and mathematics for Apple II and IBM PC computers. New program titles include NMR Simulator, IR Simulator, Chemical Reactions, and Chemistry Laboratory Simulations. 36 pp. COMPress 428

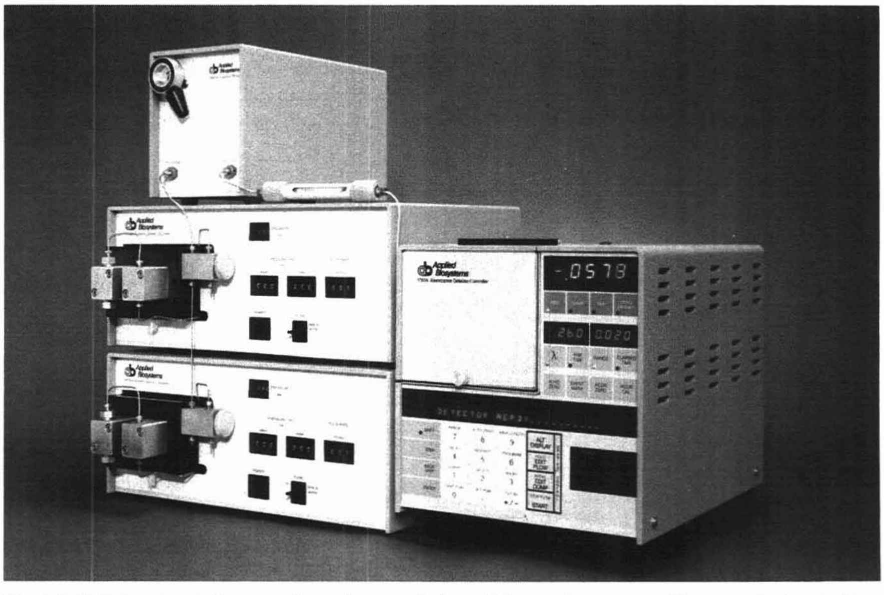

Model 152A separation system for nucleic acids analyzes, purifies, and characterizes synthetic polynucleotides. The system can isolate plasmid DNA and DNA restriction fragments and determine base compositions of synthetic or natural products. Applied Biosystems **402**

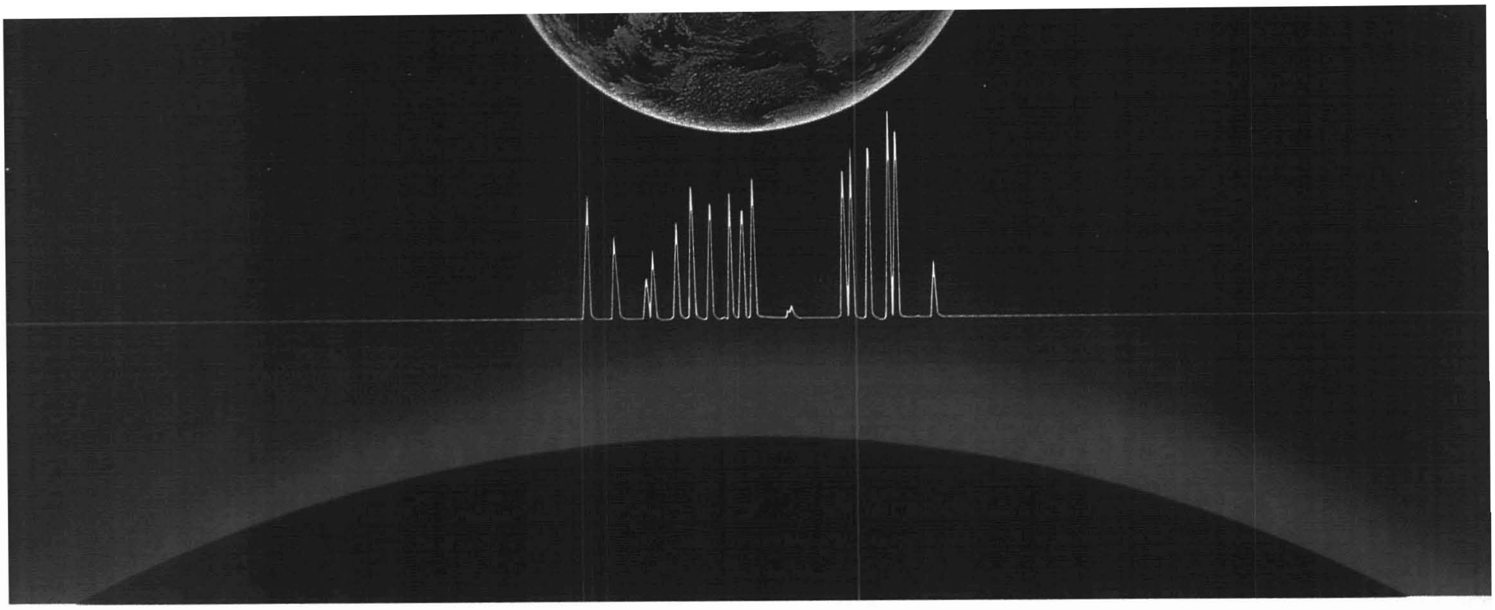

HPLC: 2002.

OMARS Project, 2002. Ten years in planning and 28 months under construction, the second Orbital Manufacturing and Research Station (OMARS) went on line with little public fanfare. Its purpose: zero-G manufacture of enzymes, and continuing study of the long-term effects of life in space.

Without HPLC, OMARS wouldn't have gotten off the ground. The space-tough, high tensile strength polymer composites used to construct the station were engineered using specialized GPC characterization methods. HPLC analysis of amino acids and other nutritional elements led to the development of super-efficient hydroponic produce that helps keep the project self-sufficient. On-line HPLC streamlines the genetic manufacturing process for maximum yield, and robotized Q.C. sampling saves precious man-hours. Automated monitoring of the artificial environment measures and identifies trace contaminants down to the parts per quadrillion level, to guarantee the safety of the orbital scientists. And instantaneous two-way data transmission links the HPLC power in space with the best minds on Earth.

Milford, Massachusetts, 1987. Waters is already meeting tomorrow's HPLC challenges. We're putting our technology to work in new ways, in new applications. From GPC characterization of space-age polymers to fast purification of bioactive proteins; from sensitive ion analysis of acid rain to metabolic mapping of therapeutic drugs. No one can predict exactly where HPLC will be fifteen years from now. But we plan to be there with you.

Whether you need an analytical result or a purified product, we can offer a range of solutions tailored to your needs and budget. And a guarantee you can't get anywhere else: whatever your application—simple, complex or "out of this world"—we'll keep working with you until you're successful. We've proven it thousands of times, in the lab, in the field, and on the production floor.

If you're putting HPLC to work, take your best shot at success and work with Waters. For immediate applications information, call toll-free (800) 252-HPLC; in Massachusetts, (617) 478-2000. Waters Chromatography Division, Millipore Corporation, 34 Maple St., Milford, MA 01757.

For a free poster of this illustration, circle Reader Service Card.

© 1987 Millipore Corporation

Waters
Division of MILLIPORE

CIRCLE 178 ON READER SERVICE CARD

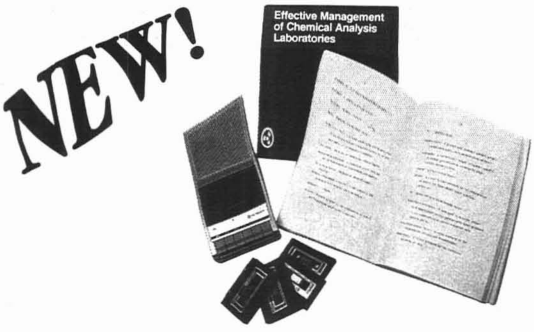

Learn how to increase productivity and decrease costs— the twin goals of a well-run laboratory

Effective Management of Chemical Analysis Laboratories

An Audio Course Produced by the American Chemical Society

Designed with analytical laboratories in mind, this unique and valuable course draws on the extensive experiences of the instructors to give you an in-depth understanding of the problems and solutions involved in laboratory management.

Beginning with a comparison of different types of analytical laboratories, you examine the organizational structure, the methods of analysis, and other laboratory operations. Several examples are given in each area to aid in understanding the system that best fits your needs.

Throughout this unique course, you are made aware of what is expected of you as a manager. At the same time, you learn how to

- improve communication at all levels in the lab
- increase lab efficiency and balance workloads
- assess work performance and productivity
- motivate personnel and operate with technical proficiency

This course is a genuine asset to anyone involved in managing service or research laboratories. No matter what the level, everyone will benefit from this valuable course.

Course Highlights

Introduction
Charter & Image
Operations
- Organization Structure
- Standard Operating Procedures
- Sample Control Center
- Document Control
- Safety
- Laboratory Information Management
- Statusing Work in Process
- Workload Balancing
- Reports

Communications
Productivity
The Laboratory Manager
The Employee
Delegation
Financial Analysis
- Measuring Financial Peformance
- Projecting the Cost of a Job
- Financial Indicators
- How to Really Make Money

Your Instructors

John H. Taylor, Jr., Vice President-General Manager, Analytical Technologies, Inc., has responsibility for a multimillion dollar chemical services laboratory. He has many publications/presentations in lab and project management.

Dr. Mary M. Routson, Bechtel Corporation, has directed analytical labs in two contract research institutes. She is experienced in management of organic and inorganic analytical efforts for both industrial and government clients.

Unit (Catalog No. 94)
Four cassettes (3.8 hours playing time) and 120-page manual: U.S. and Canada, $345.00; Export $416.00. Additional manuals: U.S. and Canada, $19.00 each; Export, $23.00 each.

No-Risk Guarantee
All ACS Audio Courses come to you with a money-back guarantee. If you are not completely satisfied, return the course within ten days for a full refund or cancellation of invoice.

Use the coupon below to place your order or CALL TOLL FREE 800-424-6747 and use your credit card or purchase order number. To help us serve you better, please mention Department 80 and Catalog No. 94 when ordering.

American Chemical Society
Distribution Office, Dept. 80
1155 Sixteenth Street, N.W.
Washington, DC 20036

Yes! Please send me the following:

Qty.		Total
____	Complete course(s), *Effective Management of Chemical Analysis Laboratories,* at $345.00 each (US & Canada) or $416.00 each (export).	$________
____	Additional manuals at $19.00 each (US & Canada) or $23.00 each (export).	$________
	TOTAL	$________

☐ Payment enclosed (make checks payable to ACS).
☐ Purchase order enclosed. PO #________
☐ Charge my ☐ MasterCard ☐ VISA ☐ American Express ☐ ACCESS ☐ Barclaycard ☐ Diners Club/ Carte Blanche

Account # ________
Expires ________ Interbank #________ (MC and ACCESS only)
Name of cardholder ________
Signature ________
Ship to:
Name ________
Title ________
Organization ________
Address ________
City, State, ZIP ________

INDEX TO ADVERTISERS IN THIS ISSUE

CIRCLE INQUIRY NO.	ADVERTISERS	PAGE NO.
3	**Applied Automation, Inc.** Tracy-Locke	633A
17	**J. T. Baker Chemical Company** Stiegler, Wells & Brunswick, Inc.	613A
22	***Bio-Rad Chemical Division** Pan & Associates	616A
18	***Brinkmann Instruments, Inc.** Lavey/Wolff/Swift, Inc.	623A
20	***Brownlee Labs, Inc.** Lena Chow, Inc.	629A
14	**Burdick & Jackson** Nordstrom/Cox Marketing	606A
30	***Crawford Fitting Company/ A Swagelok Company** Falls Advertising Company	610A
45	***Eldex Laboratories, Inc.**	650A
41–43	**ESA, Inc.** James F. Balderson & Associates	635A, 637A, 639A
52–55	**Finnigan MAT Corporation** Lena Chow, Inc.	649A, 651A
61–62	***Gilson Medical Electronics, Inc.**	605A
60	**Great Lakes Environmental Services** Alden Design Associates	644A
63	**Hamamatsu Corporation** Mandabach & Simms, Inc.	654A
80–85	***Kevex Corporation** Technical Marketing Programs	631A
78	****Kontron Instruments AG** Promotion Kontron AG	622B
90	***Leco Corporation**	OBC
94	**Malvern Instruments, Inc.**	630A
95	**Mattson Instruments, Inc.** Bjork, Cunningham & Welch	615A
110	***Nicolet Instrument Corporation** Nicolet Advertising	609A
120	***O.I. Corporation**	620A
125	***PolyScience Corporation**	603A
140	***Rheodyne, Inc.** Bonfield Associates	627A
145–147	**Sargent-Welch Scientific Company** Polytech Advertising	641A, 643A, 645A
150	***Scientific Glass Engineering, Inc.** Arden Advertising Agency	618A
153–155	**Separations Technology, Inc.** Scott Laboratories Inc.	IFC
152	**Siemens AG** Barbeau-Hutchings Advertising, Inc.	634A
157	**Tekmar** Kenyon Hoag Associates	620A
156	**Tracor Atlas**	612A
170	***Valco Instruments Company, Inc.** Technical Advertising Associates	611A
172–173	**VG Instruments** Barbeau-Hutchings Advertising, Inc.	646A
178	**Waters Chromatography/Division of Millipore** Millicom, Inc.	655A
176	**Whatman, Inc.** Northeast Communications Associates	653A

* *See ad in ACS Laboratory Guide.*

** *Company so marked has advertisement in Foreign Regional edition only.*

Advertising Management for the American Chemical Society Publications

CENTCOM, LTD

President
Thomas N. J. Koerwer

Executive Vice President **James A. Byrne**
Senior Vice President **Benjamin W. Jones**
Alfred L. Gregory, *Vice President*
Clay S. Holden, *Vice President*
Robert L. Voepel, *Vice President*
Joseph P. Stenza, *Production Director*

500 Post Road East
P.O. Box 231
Westport, Connecticut 06880
(Area Code 203) 226-7131
Telex No. 643310

ADVERTISING SALES MANAGER
James A. Byrne, VP

ASSISTANT ADVERTISING SALES MANAGER
Bruce E. Poorman

ADVERTISING PRODUCTION MANAGER
Jane F. Gatenby

SALES REPRESENTATIVES

Philadelphia, PA . . . Patricia O'Donnell, CENTCOM, LTD., GSB Building, Suite 725, 1 Belmont Avenue, Bala Cynwyd, Pa. 19004. Telephone: 215-667-9666

New York, NY . . . Dean A. Baldwin, CENTCOM, LTD., 60 East 42nd St., New York, N.Y. 10165. Telephone: 212-972-9660

Westport, CT . . . Edward M. Black, CENTCOM, LTD., 500 Post Road East, P.O. Box 231, Westport, Ct. 06880. Telephone: 203-226-7131, Telex 643310

Cleveland, OH . . . Bruce E. Poorman, John C. Guyot, CENTCOM, LTD., 325 Front St., Suite 2, Berea, Ohio 44017. Telephone: 216-234-1333

Chicago, IL . . . Michael J. Pak, CENTCOM, LTD., 540 Frontage Rd., Northfield, Ill. 60093. Telephone: 312-441-6383

Houston, TX . . . Michael J. Pak, CENTCOM, LTD., Telephone: 312-441-6383

San Francisco, CA . . . Paul M. Butts, CENTCOM, LTD., Suite 1070, 2672 Bayshore Frontage Road, Mountain View, CA 94043. Telephone: 415-969-4604

Los Angeles, CA . . . Clay S. Holden, CENTCOM, LTD., Newton Pacific Center, 3142 Pacific Coast Highway, Suite 200, Torrance, CA 90505. Telephone: 213-325-1903

Boston, MA . . . Edward M. Black, CENTCOM, LTD., Telephone: 203-226-7131

Atlanta, GA . . . Edward M. Black, CENTCOM, LTD., Telephone: 203-226-7131

Denver, CO . . . Paul M. Butts, CENTCOM, LTD., Telephone: 415-969-4604

United Kingdom

- **Reading, England . . . Malcolm Thiele, Technomedia Ltd., Wood Cottage, Shurlock Row, Reading RG10 OQE, Berkshire, England. Telephone: 073-434-3302, Telex #848800**
- **Lancashire, England . . . Technomedia Ltd., c/o Meconomics Ltd., Meconomics House, 31 Old Street, Ashton Under Lyne, Lancashire, England. Telephone: 061-308-3025**

Continental Europe . . . Andre Jamar, International Communications, Inc., Rue Mallar 1, 4800 Verviers, Belgium. Telephone: (087) 22-53-85, Telex #49263

Tokyo, Japan . . . Shuji Tanaka, International Media Representatives Ltd., 2-29 Toranomon, 1-Chome Minato-ku Tokyo 105 Japan. Telephone: 502-0656, Telex #22633

Liquid Chromatograph
Liquefied Coal
Bill,
Could you
have a PAH
analysis by
4 pm? GW

Chemists—
How can you quickly find an analytical procedure to solve this problem?

Search CHEMICAL JOURNALS ONLINE.

CHEMICAL JOURNALS ONLINE is the new powerful information search system that permits you to quickly search over 45,000 journal articles and display:

Experimental Procedures • Experimental Data • Preparation Techniques • New Chemical Names • Synthesis Information

• PLUS CROSSOVER CAPABILITIES WITH CAS ONLINE

As part of STN, International, CHEMICAL JOURNALS ONLINE provides you with the unique ability to instantaneously cross over from CAS ONLINE to the full-text of appropriate journals.

CHEMICAL JOURNALS ONLINE is not only precise in its searching but also cost effective. In minutes you can save yourself days of tedious work.

CHEMICAL JOURNALS ONLINE contains:

- The American Chemical society's 18 primary journals with over 45,000 articles dating back to 1982.
- A learning file for training and teaching purposes for one low connect hour charge.
- John Wiley & Son's Polymer Journals Online dating back to 1984. (Available Summer 1987)
- Other publisher's journals in the future.

To put CHEMICAL JOURNALS ONLINE to work for you, call an American Chemical Society sales representative today at **800-424-6747**. The call is free.

Or write, Sales Office, American Chemical Society, 1155 Sixteenth Street, N.W., Washington, D.C. 20036.

CHEMICAL JOURNALS ONLINE

Your Research Is Not Complete Until You Search

Analytical
CHEMISTRY

EDITOR: **GEORGE H. MORRISON**

ASSOCIATE EDITORS: **Klaus Biemann, Georges Guiochon, Fred Lytle, Robert Osteryoung**

Editorial Headquarters
1155 Sixteenth St., N.W.
Washington, D.C. 20036
Phone: 202-872-4570
Teletype: 710-8220 151

Managing Editor: Sharon G. Boots
Associate Editors: Stuart A. Borman, Rani A. George, Louise Voress
Assistant Editors: Mary D. Warner, Grace K. Lee
Production Manager: Leroy L. Corcoran
Art Director: Alan Kahan
Designer: Sharon Harris Wolfgang
Production Editor: Elizabeth E. Wood
Circulation: Cynthia G. Smith
Editorial Assistant, LabGuide: Joanne Mullican

Journals Dept., Columbus, Ohio
Associate Head: Marianne Brogan
Associate Editor: Rodney L. Temos

Advisory Board: Shier S. Berman, Brian S. Bidlingmeyer, Henry N. Blount, Gary D. Christian, Harry V. Drushel, Larry R. Faulkner, Peter R. Griffiths, Gary M. Hieftje, Nobuhiko Ishibashi, Mary A. Kaiser, David L. Nelson, Erno Pungor, Dennis Schuetzle, Nicholas Winograd, Edward S. Yeung, Andrew T. Zander

Instrumentation Advisory Panel: Howard G. Barth, Richard F. Browner, James B. Callis, Richard S. Danchik, Thomas C. Farrar, Joel M. Harris, John F. Holland, Ronald E. Majors, Linda B. McGown

The Analytical Approach Advisory Panel: Edward C. Dunlop, Robert A. Hofstader, Wilbur D. Shults

Published by the
AMERICAN CHEMICAL SOCIETY
1155 16th Street, N.W.
Washington, D.C. 20036

Books and Journals Division
Director: D. H. Michael Bowen
Journals: Charles R. Bertsch
Research and Development: Lorrin R. Garson

Manuscript requirements are published in the January 1, 1987 issue, page 219. Manuscripts for publication (4 copies) should be submitted to ANALYTICAL CHEMISTRY at the ACS Washington address.

The American Chemical Society and its editors assume no responsibility for the statements and opinions advanced by contributors. Views expressed in the editorials are those of the editors and do not necessarily represent the official position of the American Chemical Society.

AUTHOR INDEX

Ahmed, A. W., 1302

Bandy, A. R., 1296
Bard, A. J., 1339
Bergold, A. F., 1286
Bertrand, M. J., 1302
Biemann, K., 1266
Blom, K., 1372
Brenner, I. B., 1260
Brodbelt, J. S., 1278
Brown, P. A., 1313

Carr, P. W., 1286
Cody, R. B., 1309
Cooks, R. G., 1278

Dasgupta, P. K., 1356, 1362
Davis, J. M., 1339
Davis, S. C., 1360
Derrick, P. J., 1360
Dybowski, C., 1372

Fan, F.-R. F., 1339

Gagel, J. J., 1266
Gates, B., 1372
Giddings, J. C., 1332
Goldbart, Z., 1260
Goldberg, J. M., 1250
Grant, C. L., 1326

Hanna, D. A., 1255
Harel, A., 1260
Hasselbring, L., 1372
Henion, J. D., 1309
Hisatake, J., 1306
Hwang, H., 1356

Ishimura, M., 1306

Janata, J., 1351
Jenkins, T. F., 1326
Jurkiewicz, K., 1362

Kinsinger, J. A., 1309
Krishnamurthy, T., 1272
Krull, I. S., 1366
Kulkarni, S. Y., 1375

LaCourse, W. R., 1366
Lalevic, M., 1296
Lee, E. D., 1309
Leenheer, J. A., 1313
Lewin, E. E., 1296
Lin, J.-K., 1320
Lorber, A., 1260
Louris, J. N., 1278

Mallet, V. N., 1302
Mason, K. J., 1250
Munson, B., 1372

Neumann, G. M., 1360

Ogura, K., 1306

Patonay, G., 1376
Purdie, N., 1349

Rollie, M. E., 1376

Sarrasin, B., 1302
Sarver, E. W., 1272
Selavka, C. M., 1366
Shah, V. G., 1375
Stiles, E. A., 1313
Swallows, K. A., 1349

Taggart, R. L., 1296

Voigtman, E., 1364

Wade, J. L., 1286
Wahlund, K.-G., 1332
Warner, I. M., 1376
Wieboldt, R. C., 1255
Winefordner, J. D., 1364
Wu, S.-S., 1320

Production and Initial Characterization of a Laser-Induced Plasma in a Pulsed Magnetic Field for Atomic Spectrometry

Kelly J. Mason and Joel M. Goldberg*

Department of Chemistry, University of Vermont, Burlington, Vermont 05405

Electromagnetic compression techniques were evaluated as a means of enhancing the atomization characteristics of atmospheric pressure laser-induced plasmas. The production of pulsed magnetic fields by capacitive electrical discharge through multiple-turn solenoids was modeled enabling the production of peak magnetic fields between 50 and 100 kG using moderate discharge conditions (9.5 kV, 24 μF) and easily attainable system inductances (1.5 μH). The effects of a 69-kG pulsed magnetic field oriented perpendicular to the laser axis of a laser-induced plasma formed using an Al alloy sample were investigated using spatially resolved but temporally integrated spectrographic methods. Increases in line-broadening, neutral atom self-reversal, and minor constituent emission intensities were observed with the magnetic field. Both ion and neutral atom emission were confined close to the sample surface by the magnetic field indicating compression of the laser-induced plasma.

Laser-induced plasmas have been investigated as atom cells for the direct spectrochemical analysis of solid samples ever since the laser was first introduced over 20 years ago (*1*, *2*). The ability of these plasmas to directly microsample both conducting and nonconducting materials has stimulated numerous studies of their use as atom/ion cells for optical emission (*3*) as well as mass spectrometric measurements (*4*). Nevertheless, laser-induced plasma sources have not attained the wide-spread popularity expected of an atom cell seemingly well-suited for direct solid sampling. This is partly due to both the limited sensitivity of commercial laser microprobes as well as the inability of laser-induced plasmas to effectively atomize and excite sampled material (*2*).

Ironically, the properties of the laser-induced plasma which make it such an attractive solid sampling source also are responsible, in part, for its limited sensitivity. Although the very high power-densities operative in laser-induced plasmas are responsible for their ability to rapidly microsample solid materials, the shock waves generated from the sampling process result in an extremely rapid expansion of the plasma—thus, the plasma is diluted after the initial sampling process. The relatively low energy per pulse delivered by the laser (typically much less than 1 J) is insufficient to completely atomize the material sampled during the initial high power-density laser pulse; as a result, much of the sampled material never contributes to an analytical signal (*1*, *2*, *5*).

The use of spark cross-excitation techniques produces a dramatic improvement in both the atomization and excitation characteristics of laser-induced plasmas through the direct injection of upward of 50 J of energy to the expanding plasma. While this results in approximately an order of magnitude improvement in analytical sensitivity, analytical precision is degraded (*3*, *5*). Additionally, the cross-excitation electrodes are sampled heavily and can introduce contaminants as well as contribute to dilution of the laser-induced plasma (*2*, *3*).

More recently, laser-induced plasmas have been coupled successfully with high-frequency excitation sources such as the inductively coupled plasma (ICP) (*6–8*). Here again the reexcitation source serves both to atomize and excite the material sampled by the laser-induced plasma. Difficulties due to electrode contamination are eliminated with this technique, but dilution of the laser-sampled material is significant, resulting in limits of detection comparable to those obtained with spark cross-excitation.

Some researchers have recognized that the atomization characteristics of laser-induced plasmas may be enhanced by confining the plasma to a relatively small volume—this is especially important for sensitive analyte quantitation using atomic absorption techniques. To date this has primarily been accomplished by generating laser-induced plasmas within a heated graphite furnace (*9*).

Physicists have successfully investigated electromagnetic compression techniques for confinement and heating of laser-induced plasmas (*10–15*). This approach seems especially attractive for spectrochemical analysis as it requires no direct electrode contact with the plasma; in addition, compression/confinement of the plasma results in an increase in the plasma power-density which should enhance atomization efficiencies.

Recent studies of the interaction of pulsed magnetic fields on spectrochemical plasmas indicate that electromagnetic confinement and/or compression can have profound effects on the analytical characteristics of these plasmas. Sacks and co-workers have demonstrated the utility of a variety of pulsed magnetic field orientations for the confinement of exploding thin film plasmas (*16*, *17*). Scheeline and co-workers have reported on the use of a theta-pinch device for the compression and heating of low-pressure spark and glow discharge plasmas (*18*, *19*), while Goode and Pipes used a theta-pinch discharge for the compression of a microwave-induced plasma (*20*). In all of these studies, the major impact of the electromagnetic compression scheme was to enhance the vaporization/atomization characteristics of the plasmas. This report, describes our initial investigations of the utility of electromagnetic compression as a means of enhancing the atomization characteristics of laser-induced plasmas.

EXPERIMENTAL SECTION

A block diagram of the overall experimental setup is shown in Figure 1.

Laser Atomizer. A Jarrell-Ash Mark II laser microprobe was used in all experiments. This system is based on a flashlamp-pumped Nd:glass laser which is semi-Q-switched by a rotating prism. The laser delivers approximately 1 J of energy per shot. The laser was focused onto the sample through microscope optics using a 32-mm focal length objective lens. The laser and optics were removed from the original microscope stage assembly and mounted on an adjustable stage on an optical rail oriented parallel to the optical rail of the spectrographic optical system. The spark cross-excitation capability of the laser microprobe was not used in any of the studies presented in this report.

Discharge Circuit. The high-voltage capacitive discharge source used for the generation of the pulsed magnetic field has been described previously (*21*). For this work, two modifications were made to the source: (1) leads to the capacitor bank were shortened considerably in order to reduce the residual circuit

0003-2700/87/0359-1250$01.50/0 © 1987 American Chemical Society

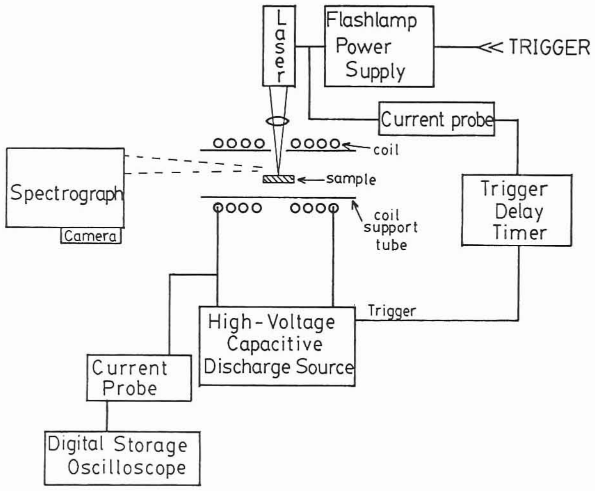

Figure 1. Instrument block diagram.

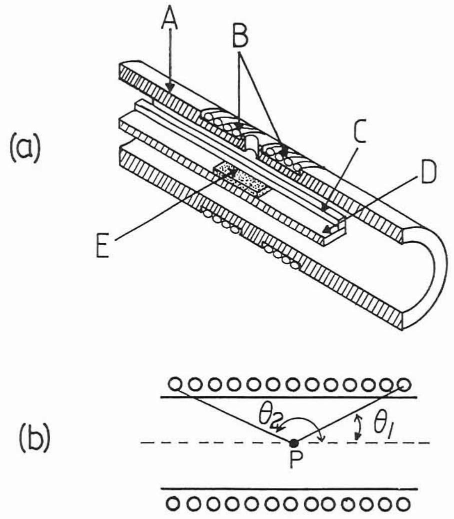

Figure 2. (a) Coil and sample support: (A) coil support tube; (B) coil; (C) sample anchor; (D) sample platform; (E) sample. (b) Solenoid geometry.

inductance and (2) a triggerable spark-gap switch (*22*) was used to initiate the discharge.

Coil/Sample Support. A cross-sectional view of the coil and sample support is shown in Figure 2a. The eight-turn coil was wound on a 1-in.-o.d. polycarbonate tube using 14-gauge insulated magnet wire; a $^1/_4$-in.-diameter hole was located between the fourth and fifth turns in order to allow the focused laser to impinge on the sample supported inside the tube. The surface of the sample was located approximately 1 mm below the central axis of the coil. The entire coil assembly was clamped inside a 2-in.-o.d. PVC tube for additional structural support. This assembly was then secured in a suitable mount for positioning on the optical rail of the spectrographic system.

Optical and Electrical Monitoring. A schematic of the overall timing sequence for the experiment is presented in Figure 3. The laser was modified so that a toroid could monitor the discharge current of the flashlamp (Figure 3a). The signal from the toroid was then used to trigger a timing/trigger network (circuit schematic is available from the authors upon request). The timing circuit consists of three 555 timers used to generate buffer, delay, and trigger pulses. The 10-ms buffer timer pulse (Figure 3b) serves to prevent multiple triggering of the timer chain. The delay timer pulse (Figure 3c) is used to temporally orient the final trigger pulse with respect to the firing of the laser—the length of this pulse is variable and is controlled by two 10-turn potentiometers for coarse and fine adjustments. The trigger timer pulse (Figure 3d) activates a trigger pulse circuit (*22*) which fires the spark gap switch, initiating current flow through the main discharge circuit (Figure 3e) and producing the pulsed magnetic field. Since the laser fires at a known delay with respect to the initiation of the flashlamp discharge (Figure 3f), the temporal orientation of the pulsed magnetic field with respect to firing of the laser is easily controlled.

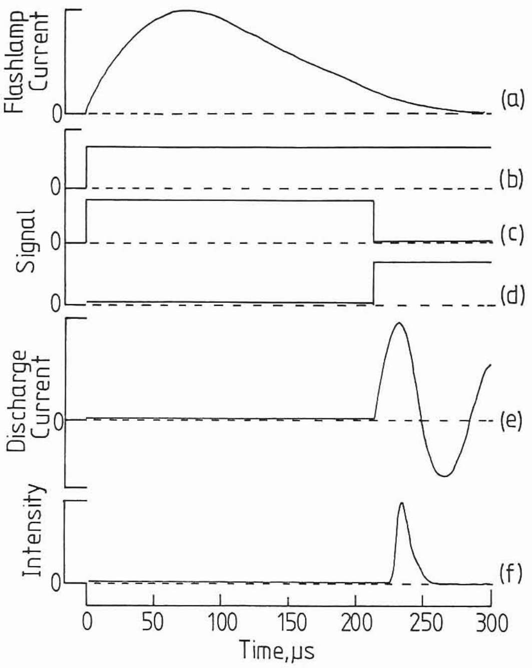

Figure 3. Timing schematic: (a) flashlamp current waveform, (b) buffer timer output, (c) delay timer output, (d) trigger timer output, (e) capacitive discharge current waveform, (f) laser-induced plasma emission waveform.

All electrical waveforms were recorded by use of a digital storage oscilloscope (Nicolet Model 4094-2). The main discharge current waveform was monitored by use of a Rogowski coil (Pearson Model 1025). The derivative of the magnetic field intensity waveform was measured with a laboratory-constructed probe (*23*) and integrated on the Nicolet oscilloscope.

Optical emission spectra were obtained by using the spatially resolved but temporally integrated spectrographic system available in our laboratory (see ref 24 for details) and recorded on Kodak SA-1 plates. Microphotometer traces were obtained by using the system described previously (*21*).

Experimental Procedures. All experiments were performed in air at atmospheric pressure. Due to the limited sensitivity of the SA-1 emulsion, all spectra were obtained by integration over five replicate laser shots. In order to increase the reproducibility of laser plasma formation, the laser was fired at a maximum rate of once every 5 min (*5*, *25*). Each firing of the laser impinged on a new location on the sample.

Materials and Reagents. Reynolds no. 2024 aluminum stock ($^1/_{16}$ in. thick) was cut into $^1/_2$ in. square pieces and used as a sample for all experiments. The aluminum stock was polished chemically before use via the following procedure (*26*): samples were placed in a bath containing 1.3% (w/w) KOH at 60–70 °C for 3 min, producing a uniform coating of Al_2O_3; the Al_2O_3 was then removed by placing the samples into a 1 M solution of H_2SO_4; the samples were then dried and stored in a desiccator. The nominal elemental composition (*27*) of the sample is as follows: Al, 93.5%; Cu, 4.4%; Mg, 1.5%; Mn, 0.6%.

RESULTS AND DISCUSSION

Coil Design: Theoretical Design. While a detailed treatment of pulsed magnetic field production via capacitive electrical discharge through a solenoid may be found in the physics literature (*28*), it is not immediately obvious how the electrical and physical characteristics of such systems affect the magnetic fields produced. In previous work by analytical spectroscopists, little attention was paid to these relationships: Goode and Pipes reported that the number of turns of their theta-pinch coil had very little impact on the magnitude of the pinch observed (*20*), while Kamla and Scheeline observed profound differences between the two coil designs utilized in their studies of theta-pinched spark and glow discharge plasmas (*18*). Before our studies were initiated, a mathematical model of the pulsed magnetic field generation circuit was developed so that the discharge system available in our laboratory could be used most efficiently for the production of pulsed magnetic fields.

The magnetic field intensity, B_z, produced in the center of a solenoid (point P in Figure 2b) may be calculated from

$$B_z = (6.28 \times 10^{-7})(nI/l)(\cos\theta_1 - \cos\theta_2) \qquad (1)$$

where B_z is in tesla, n is the number of turns of the coil, l is the length of the coil in meters, I is the current through the coil in amperes, and θ_1 and θ_2 are angles as shown in Figure 2b (*29*). The current flowing through the coil at any point in time may be obtained by using equations derived for underdamped RCL tank circuits; maximum B_z, however, will be obtained at the first current peak of the discharge. The peak current may be approximated by

$$I_p = V_0(C/L_{\text{total}})^{1/2} \qquad (2)$$

where V_0 is the initial capacitor bank voltage in volts, C is the capacitance of the capacitor bank in microfarads, and L_{total} is the inductance of the entire discharge circuit in microhenrys (*30*).

The total inductance of the system is due to both the residual inductance of the discharge circuit (L_{sys}) and the inductance of the solenoid itself (L_{coil}). While L_{sys} must be measured for the system, L_{coil} may be calculated from

$$L_{\text{coil}} = 39.97[(r^2n^2)/(9r + 10l)] \qquad (3)$$

where r is the radius of the solenoid in meters and n and l are as defined previously (*31*).

Optimization of some of the discharge circuit parameters is straightforward: the highest possible values of capacitance and charging voltage will maximize B_z. Furthermore, the turn-density (n/l) for the load coil should be as great as possible in order to maximize B_z. Optimum values for the total circuit inductance (L_{total}) and the radius of the coil (r) are not as easily determined however, as they are related to the discharge current as well as the coil turn-density.

The effect of coil radius on B_z was modeled by using typical discharge conditions (V_0 = 9.5 kV; C = 24 μF; L_{sys} = 1.5 μH; wire diameter, 1.7 mm; 10-turn coil). B_z was found to increase quite rapidly with decreasing coil radius for coil radii below about 18 mm while decreasing very gradually with increasing coil radius at higher coil radii. Clearly, then, maximum B_z will be attained with a coil designed with as small a radius as possible.

Optimization of L_{total} is not as straightforward. For a fixed (minimum) radius and a constant (maximum) turn-density, B_z will vary with the number of turns, n, of the coil as well as with the value of L_{sys}. The effect of n on B_z for values of L_{sys} between 10 nH and 10 μH is shown in Figure 4a. Three important trends are apparent: (1) B_z increases as L_{sys} decreases, (2) there is an optimum value of n where B_z reaches a maximum value, and (3) this optimum value of n increases with increasing L_{sys}. The optimum number of turns of the coil, then, should be calculated based on the value of L_{sys} measured for the discharge system.

For a theta-pinch experiment, the rate of change of the magnetic field with respect to time (dB/dt) should be optimized (*18*). An accurate model of dB/dt, however, would require differentiation of a calculated B_z waveform with respect to time—this was judged to be well beyond the scope of our simple parametric investigation. Instead, an estimate of the dB/dt during the first quarter-cycle was calculated based on the peak value of B_z. For a simple RCL circuit, the time to reach the first current maximum (t) may be estimated by

$$t = \pi/[2(1/L_{\text{total}}C)^{1/2}] \qquad (4)$$

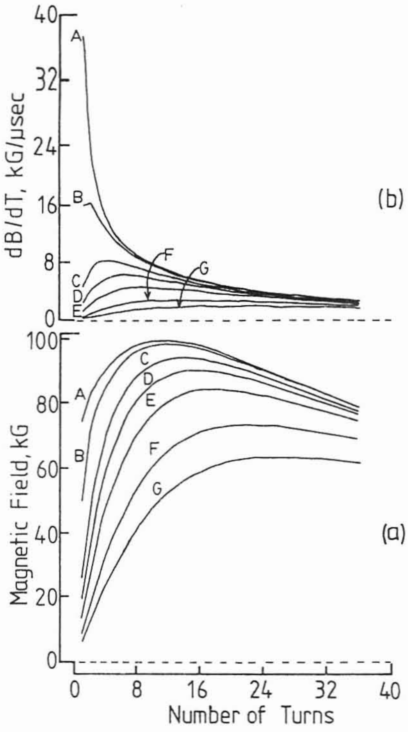

Figure 4. Effect of number of turns on (a) peak magnetic field and (b) dB/dt. Model system parameters are as follows: V_0 = 9.5 kV; C = 24 μF; L_{sys} = (A) 0.010, (B) 0.100, (C) 0.500, (D) 1.00, (E) 2.00, (F) 5.00, (G) 10.00 μH; wire diameter, 1.7 mm; coil radius, 15 mm.

An estimate of dB/dt, then, may be calculated by dividing B_z by t. Figure 4b shows how dB/dt varies with n for the same values of L_{sys} investigated in Figure 4a. L_{sys} has a profound effect on dB/dt, so much so that single-turn coils are most efficient for systems having a residual circuit inductance less than about 100 nH. This explains why single-turn coils are used almost exclusively in theta-pinch experiments reported in the physics literature where the megajoule discharge sources used typically have very low system inductances (*32*). For values of L_{sys} of 500 nH to 10 μH, however, single-turn coils are not the most efficient; these curves reach a maximum value of dB/dt at values of n between about 4 and 16. It is important to note that the coil configuration for optimum dB/dt is different than the configuration for optimum B_z (see Figure 4). Note also that maximum dB/dt drops off quite rapidly as L_{sys} increases.

Coil Design: Practical Application. For the initial experiments described in this paper, a coil design that would result in both a rapidly changing magnetic field as well as a high peak magnetic field intensity was desired. In order to maximize both B_z and dB/dt, the maximum charging voltage and capacitance combination available with our discharge system (9.5 kV with a 24-μF capacitance) was chosen and the discharge system modified so that the residual system inductance, L_{sys}, was reduced to about 1.5 μH (further reduction in L_{sys} would have required redesign of the discharge apparatus). In order to maximize the peak magnetic field intensity, the coil radius was kept as small as possible and the coil turn-density was maximized by using the smallest gauge magnet wire judged to be able to withstand the pulsed magnetic fields to be generated in these experiments (*28*). Based on these discharge circuit parameters, the number of turns used in the coil was determined by using theoretical calculations similar to the ones described in the previous section for maximizing dB/dt—all discharge and coil parameters are presented in Table I.

Electrical Characteristics. The important characteristics of the discharge current and magnetic field waveforms for the system used in this study are presented in Table I. Since laser

Table I. Coil and Discharge Conditions

coil parameters	
coil radius, mm	15
wire radius, mm	0.9
coil length, mm	20.8
coil inductance, μH	1.4[a]
discharge conditions	
charging voltage, kV	9.5
capacitance, μF	24.0
system inductance, μH	1.5[b]
total inductance, μH	3.9[b]
ringing frequency, kHz	16.3
time to current peak, μs	15
peak current, kA	23.6
peak magnetic field, kG	69

[a] Calculated (excluding leads). [b] Measured.

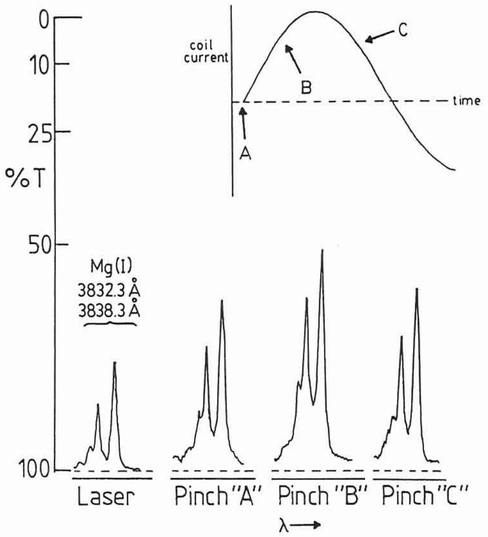

Figure 5. Effect of temporal orientation of laser-induced plasma in varying magnetic field on Mg(I) emission. Temporal positions A, B, and C correspond to laser plasma formation 0, 12, and 25 μs after initiation of current flow through the magnetic field coil (see inset).

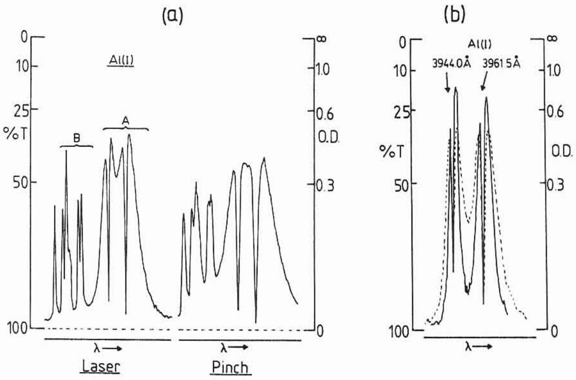

Figure 6. Effects of a pulsed magnetic field on Al(I) emission: (a) A, 308.22 nm, 309.27 nm; B, 305.01 nm, 305.47 nm, 305.71 nm, 306.43 nm, 306.62 nm; (b) solid lines, laser; dashed lines, pinch.

plasma formation was initiated only at times during the first current half-cycle of the capacitive discharge, only the properties of the magnetic field produced during the first cycle of the discharge are of interest.

Our initial studies of temporally resolved emission from the laser plasma showed that the laser fired approximately 240 μs after initiation of the flashlamp discharge; thus, the pulsed magnetic field discharge was triggered off of a signal generated by the flashlamp discharge current. Since the repeatability of the timing circuitry is within the 0.5-μs resolution of our digital storage oscilloscope, the reproducibility of the temporal placement of the laser discharge with respect to the magnetic field is limited primarily by the reproducibility of the laser firing with respect to the flashlamp current. Generally, the laser firing delay was reproducible to within ±1 μs.

Initial Emission Spectroscopic Studies. All spectra obtained were integrated over time but were spatially resolved. For all experiments, only emission from a vertical slice oriented in the center of the laser plasma was observed—the high fidelity imaging system provided vertical resolution along the vertical axis of the slit-image on the exit focal plane of the spectrograph.

For these experiments, three different temporal relationships between laser plasma formation and magnetic field production were investigated. Emission from laser-induced plasmas produced coincident with magnetic field initiation, during a rising magnetic field and during a falling magnetic field, were recorded—these temporal configurations are represented by points A, B, and C (respectively) on the coil current waveform shown in Figure 5 (inset). Qualitative observation of the spatially resolved spectra showed that the greatest change in emission characteristics was obtained when laser initiation occurred during the rising portion of the magnetic field (point B). Figure 5 shows spatially integrated microphotometer traces of Mg(I) emission obtained with the three magnetic field temporal configurations as well as with only the laser. All three configurations show an increase in emission intensity as well as increased continuum background and line width over the laser-only configuration. These effects are greatest when temporal magnetic field configuration B is utilized; similar trends are observed for emission from all other analyte species. All further discussion will relate only to spectra obtained with this configuration.

Spatially integrated microphotometer traces of emission from Al(I) species for configurations without a magnetic field (denoted "Laser") and with a magnetic field (denoted "Pinch") are presented in Figure 6a. This spectral region contains two neutral resonance lines (marked A) which are strongly self-reversed as well as a number of closely spaced lines of lesser intensity (marked B). The magnetic field is observed to have a profound effect on the characteristics of these lines. All lines are broadened significantly by the magnetic field; the closely spaced lines (B) in the laser-only spectrum are no longer resolved in the pinch spectrum, and the two neutral resonance lines (A) are broadened in the pinch so that there is a peak in emission in the region between them. In addition, the degree of self-reversal in the pinch spectrum is increased not only with respect to intensity but also with respect to the absorbance line width. Similar effects are also observed with the two Al(I) neutral resonance lines shown in Figure 6b. Here, the pinch and laser spectra are superimposed so that a more direct comparison may be made. Again, these lines are observed to be broadened significantly by the magnetic field interaction.

Direct quantitative comparisons of emission intensities for these spectra are difficult due to the spatially resolved nature of the spectra themselves as well as the nonlinear relationship between the %T microphotometer scale and the actual plasma emission intensity. Qualitatively, however, significant changes are evident upon comparison of spatially resolved spectra obtained with and without the pulsed magnetic field. Figure 7 shows the spatially resolved spectral features of the Al(I) emission lines discussed above. Clearly, the magnetic field has a significant impact on the spatial distribution of these species—the pinch spectra show much more spatially homogeneous spectral features as well as a significantly smaller plasma height.

Studies of emission from ionic species show very similar effects of the magnetic field on the laser-induced plasma.

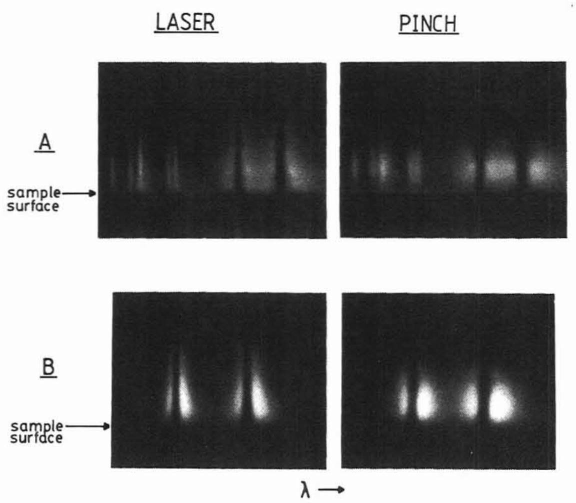

Figure 7. Spatially resolved Al(I) emission spectra: (A) 305.01 nm, 305.47 nm, 305.71 nm, 306.43 nm, 306.62 nm, 308.22 nm, 309.27 nm; (B) 394.40 nm, 396.15 nm.

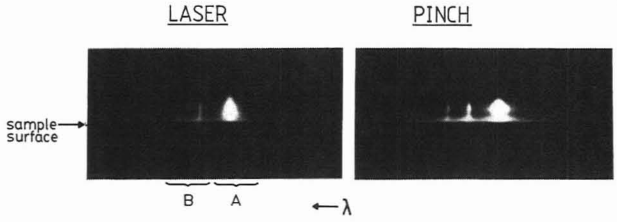

Figure 8. Spatially resolved Al(II) and Al(III) emission spectra: (A) Al(II) 358.66 nm, 358.71 nm, 358.75 nm; (B) Al(III) 360.16 nm, 360.19 nm, 361.24 nm.

Figure 8 shows spatially resolved emission spectra recorded for both Al(II) (marked "A") and Al(III) (marked "B") species. The pinch spectrum, again, shows a "squashed" plasma with significantly broadened lines and an increased continuum background. Figure 9 shows microphotometer traces of these lines which have been integrated in three successive 0.7 mm wide zones. Increased continuum background emission and line broadening in the pinch spectrum are quite apparent in the lower two zones (A and B). Emission from the uppermost zone (C), however, is almost nonexistent for the pinch case while it is still quite significant for the laser-only case. Emission from Al ions, then, is confined to an approximately 1.5 mm region above the sample surface in the magnetic field while this region extends up to 2.1 mm or more for an unperturbed laser-induced plasma.

Spatial profiles of neutral and ionic species in the plasma are shown in Figure 10 for pinch and laser configurations. In regions close to the sample surface, emission intensities are generally greater for the pinch configuration, while at heights further from the sample surface the laser configuration shows a greater emission intensity. The spatial distributions of the ionic versus the neutral species show significant differences. In general, the ions are confined to regions much closer to the sample surface than are neutral atoms for both pinch and laser configurations.

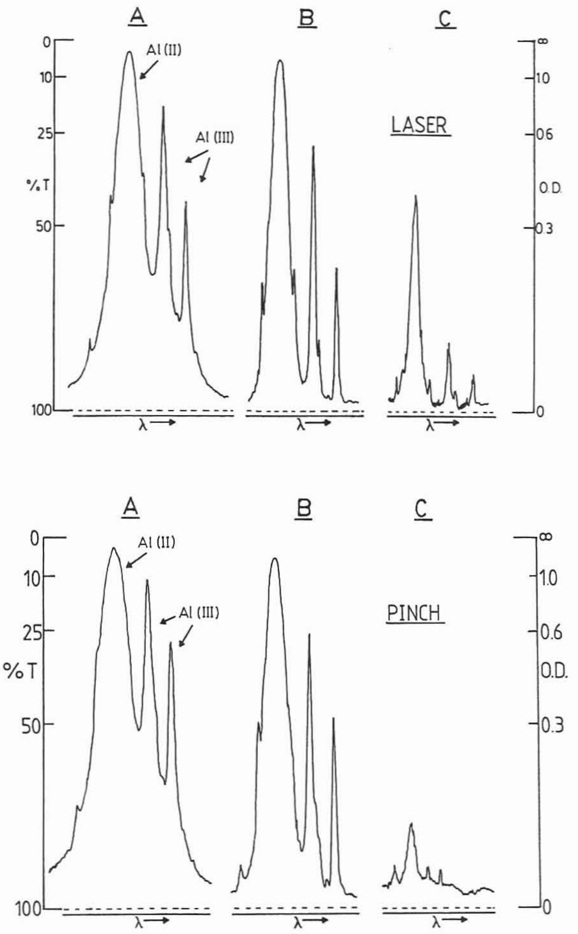

Figure 9. Microphotometer traces of Al(II) and Al(III) emission spectra spatially integrated in three 0.7 mm wide regions: (A) 0–0.7 mm, (B) 0.7–1.4 mm, (C) 1.4–2.1 mm above the sample surface.

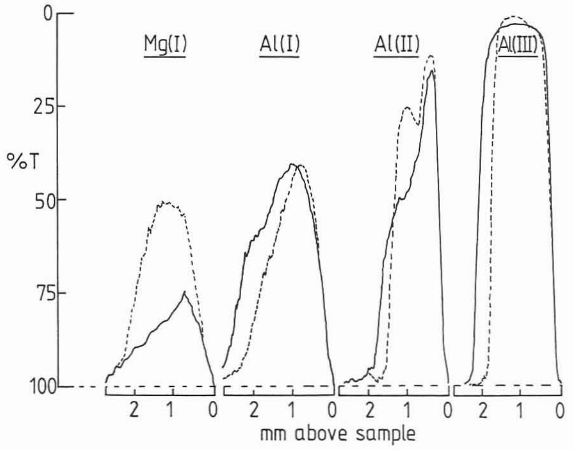

Figure 10. Spatially resolved microphotometer traces for laser (solid lines) and pinch (dashed lines) configurations. Emission is integrated over approximately 0.4 nm wide spectral regions centered around the emission line(s) of interest: Mg(I), 383.83 nm; Al(I), 396.15 nm—self-reversed; Al(II), 358.66 nm, 358.71 nm; Al(III), 360.16 nm, 360.19 nm.

CONCLUSIONS

Overall, the pulsed magnetic field is observed to have a significant impact on both the physical and spectral characteristics of the laser-induced plasma. Our initial spatially resolved spectrographic studies demonstrated that it is possible to confine and compress a laser-induced plasma at atmospheric pressure using a pulsed magnetic field. With the plasma confined, the emission lines are broadened significantly; this is most probably due to an increase in pressure/collisional broadening processes. More importantly, a pronounced increase in both self-reversal (for resonance lines of major constituents) and line emission intensity for analyte was observed, possibly indicating more efficient atomization of the sample.

The possible mechanisms of interaction of the magnetic field with the plasma are not clear at this time. Since the greatest effect was observed when the plasma was formed at the maximum magnetic field strength and not under conditions of maximum dB/dt (see Figure 5), it is doubtful that we are observing a significant theta-pinch interaction. There are, however, significant electric fields generated in laser-induced plasmas as well as a relatively high expansion velocity—thus, $E \times B$ and $v \times B$ interactions could be quite significant (*33–36*). Emission spectroscopic studies utilizing both spatial and temporal resolution are currently under way in order to better understand the nature of these interactions.

While these initial studies have not resulted in a significantly improved analytical laser-induced plasma source, we have demonstrated the possibility of electromagnetic control of a small plasma at atmospheric pressure. Confinement of the plasma improves the plasma characteristics desired for more complete sample atomization—atomic absorption studies are planned so that ground-state atom populations may be studied. Furthermore, electromagnetic control of laser-induced plasmas may allow more precise control of sample–plasma interactions.

ACKNOWLEDGMENT

We thank Walter Weir, Harry Preston, and Norman Rosberg for their help with the design and construction of the apparatus.

LITERATURE CITED

(1) Laqua, K. In *Analytical Laser Spectroscopy*; Omenetto, N., Ed.; Wiley: New York, 1979.
(2) Dittrich, K; Wennrich, R. *Prog. Anal. At. Spectrosc.* **1984**, *7*, 139–198.
(3) van Deijck, W.; Balke, J.; Maessen, F.J.M.J. *Spectrochim. Acta, Part B* **1979**, *34B*, 359–369.
(4) Jansen, J. A. J.; Witmer, A. W. *Spectrochim. Acta, Part B* **1982**, *37B*, 483–491.
(5) Allemand, C.D. *Spectrochim. Acta, Part B* **1972**, *27B*, 185–204.
(6) Thompson, M.; Goulter, J. E.; Sieper, F. *Analyst* (*London*) **1981**, *106*, 32–39.
(7) Carr, J. W.; Horlick, G. *Spectrochim. Acta, Part B* **1982**, *37B*, 1–15.
(8) Ishizuka, T.; Uwamino, Y. *Spectrochim. Acta, Part B* **1983**, *38B*, 519–527.
(9) Matousek, J. P.; Orr, B. J. *Spectrochim. Acta, Part B* **1976**, *31B*, 475–481.
(10) Haught, A. F.; Polk, D. H.; Fader, W. J. *Phys. Fluids* **1970**, *13*, 2842–2857.
(11) Chan, P. W.; DeMichekis, C.; Kronast, B. *Appl. Phys. Lett.* **1968**, *13*, 202–203.
(12) Vardzigulova, L. E.; Kaitmazov, S. D.; Prokhorov, A. M. *JETP Lett.* **1967**, *6*, 253–255.
(13) Kaitmazov, S. D.; Shklovskii, E. I. *Sov. Phys. JETP* **1976**, *44*, 1098–1103.
(14) Crawford, E. A.; Hoffman, A. L.; Milroy, R. D.; Quimby, D. C. In *Laser Techniques for Extreme Ultraviolet Spectroscopy*; McIlrath, T. J., Freeman, R. R., Eds; American Institute of Physics: New York, 1982.
(15) Loter, N. G.; Halverson, W; Lax, B. *J. Appl. Phys.* **1981**, *52*, 5014–5023.
(16) Albers, D.; Johnson, E.; Tisack, M.; Sacks, R. *Appl. Spectrosc.* **1986**, *40*, 60–70.
(17) Albers, D.; Sacks, R. *Spectrochim. Acta, Part B* **1986**, *41B*, 391–402.
(18) Kamla, G. J.; Scheeline, A. *Anal. Chem.* **1986**, *58*, 923–932.
(19) Kamla, G. J.; Scheeline, A. *Anal. Chem.* **1986**, *58*, 932–939.
(20) Goode, S. R.; Pipes, D. T. *Spectrochim. Acta, Part B* **1981**, *36B*, 925–929.
(21) Carney, K. P.; Goldberg, J. M. *Anal. Chem.* **1986**, *58*, 3108–3115.
(22) Suh, S. Y.; Collins, R. J.; Sacks, R. D. *Appl. Spectrosc.* **1981**, *35*, 42–52.
(23) Huddlestone, R. H.; Leonard, S. L. *Plasma Diagnostic Techniques*; Academic: New York, 1965.
(24) Carney, K. P.; Goldberg, J. M. *Anal. Chem.* **1986**, *58*, 3115–3121.
(25) Piepmeier, E. H.; Osten, D. E. *Appl. Spectrosc.* **1971**, *25*, 642–652.
(26) Nutt, Merle C. *Metallurgy and Plastics for Engineers*; Associated Lithographers: Phoenix, AZ, 1976.
(27) *Aluminum Standards and Data*, 1st ed.; The Aluminum Association: New York, 1968.
(28) Herlach, F. *Rep. Prog. Phys.* **1968**, *31*, 341–417.
(29) Richards, J. A.; Sears, F. W.; Wehr, M. R.; Zemansky, M. W. *Modern University Physics*; Addison-Wesley: Reading, MA, 1964.
(30) Sacks, R. D.; Goldberg, J. M.; Collins, R. J.; Suh, S. Y. *Prog. Anal. At. Spectrosc.* **1982**, *5*, 111–154.
(31) *The Radio Amateur's Handbook*; The American Radio Relay League, Inc.: Newington, CT, 1979.
(32) Kachilla, D.; Herlach, F.; Erber, T. *Rev. Sci. Instrum.* **1970**, *41*, 1–7.
(33) Hughes, T. P. *Plasmas and Laser Light*; Wiley: New York, 1975.
(34) Chen, F. *Introduction to Plasma Physics*; Plenum: New York, 1974.
(35) Matoba, T.; Ariga, S. *J. Phys. Soc. Jpn.* **1971**, *30*, 1477–1487.
(36) Okada, S.; Sato, K.; Sekiguchi, T. *Jpn. J. Appl. Phys.* **1981**, *20*, 157–165.

RECEIVED for review November 19, 1986. Accepted January 7, 1987. We gratefully acknowledge financial support from a Research Corporation Cottrell Research Grant, the donors of the Petroleum Research Fund, administered by the American Chemical Society, and the University of Vermont Committee on Research and Scholarship. We also are grateful to BASF Wyandotte Corporation for donation of the microphotometer and to IBM for donation of the spectrograph and laser microprobe.

Removing Artifacts in Supercritical Fluid and Gas Chromatograms Generated from Fourier Transform Infrared Data

Richard C. Wieboldt* and D. Alan Hanna

Nicolet Instrument Corporation, 5225 Verona Road, Madison, Wisconsin 53711

A method is presented for removing undesirable features in chromatograms generated from Fourier transform infrared data by using Gram–Schmidt orthogonalization. The procedure involves adding vectors containing the undesired information to the basis set and recalculating the chromatogram with the augmented basis set. The resulting reconstructed chromatograms suppress the undesired feature and exhibit stronger signal intensity with respect to the base line. Detection of small chromatographic peaks is enhanced. The technique is applied to base-line drift and solvent tail removal in gas chromatography/Fourier transform infrared spectrometry and to density programming in supercritical fluid chromatography/Fourier transform infrared spectrometry.

The calculation of chromatograms based on infrared absorbance (often referred to as reconstructed chromatograms or reconstructions) using the Gram–Schmidt algorithm was first reported by de Haseth and Isenhour in 1977 (*1*). In a comparison of reconstruction methods, Hanna et al. (*2*) determined that the Gram–Schmidt method offers the best compromise between computational efficiency and sensitivity. Since that time, the method has gained widespread acceptance and has been applied to both liquid chromatography/Fourier transform infrared (LC/FTIR) (*3*) and supercritical fluid chromatography/Fourier transform infrared (SFC/FTIR) spectrometry (*4*, *5*). It is now the standard method for locating chromatographic peaks in a collection of infrared spectra recorded during a chromatographic separation with Fourier transform infrared (FTIR) detection.

The Gram–Schmidt algorithm is a vector orthogonalization technique commonly used in linear algebra (*6*). The technique

0003-2700/87/0359-1255$01.50/0 © 1987 American Chemical Society

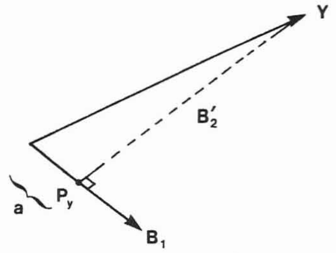

Figure 1. Projection of second reference vector, **Y**, on the first basis vector, $\mathbf{B}_1$.

is capable of removing redundant information from a set of vectors. As applied to gas chromatography/Fourier transform infrared (GC/FTIR) spectrometry, these vectors are formed by selecting a portion of the interferogram signal collected by the FTIR spectrometer during the course of a GC separation. The parameters used to select this interferogram segment, i.e., offset from the centerburst and number of points, have been discussed in the literature (*1*, *7*). The parameters are instrument dependent (*8*) and are presumably selected by instrument manufacturers for optimum performance with their systems. These interferogram segments are the vectors described in the following discussion of Gram–Schmidt orthogonalization.

The principle involved in Gram–Schmidt reconstruction can be extended to improve detection of peaks in a reconstructed chromatogram. In the application described here, reference vectors taken from undesired features in the reconstructed chromatogram are added to the basis set. Recalculating the Gram–Schmidt projection using this augmented basis set produces a result that effectively suppresses the undesired feature. In doing so, the signal intensity of minor components is enhanced making it easier to detect these components. This approach has also been applied to the removal of overlapping peaks in a homologous series (*9*).

THEORY

Gram–Schmidt Orthogonalization. Although the Gram–Schmidt algorithm has been described previously (*1*, *2*), it is helpful to restate it here so the technique described in this paper can be clearly understood.

Gram–Schmidt orthogonalization is a technique for removing redundant information from a set of vectors (**X**, **Y**, **Z**, ...) This is a sequential process of subtracting those portions of the vectors that lie in the same direction in a multidimensional space. The result is a set of linearly independent, orthogonal vectors which we call a basis set. In other words, each vector in the basis set contains only unique information—information not already contained in the other vectors in the basis set.

The first vector, $\mathbf{B}_1'$, can be chosen to lie in any direction; all that needs to be done is to normalize this vector to unit length. Normalization is carried out by dividing each element in a vector by its length. The length of a vector is given by the square root of its dot product:

$$\|\mathbf{X}\| = \left(\sum_{i=1}^{k} \mathbf{x}_i \mathbf{x}_i\right)^{1/2} \tag{1}$$

The first basis vector is defined as

$$\mathbf{B}_1 = \mathbf{X}/\|\mathbf{X}\| \tag{2}$$

The unnormalized basis vector $\mathbf{B}_2'$ which will be orthogonal to $\mathbf{B}_1$ is found by subtracting that component of the second vector, **Y**, lying in the same direction as $\mathbf{B}_1$ (Figure 1). This is denoted as $\mathbf{P}_y$

$$\mathbf{B}_2' = \mathbf{Y} - \mathbf{P}_y \tag{3}$$

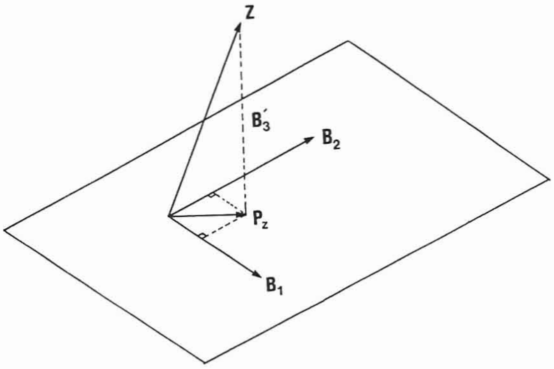

Figure 2. Projection of third reference vector, **Z**, on the plane (or subspace) defined by the first two basis vectors, $\mathbf{B}_1$ and $\mathbf{B}_2$.

The quantity $\mathbf{P}_y$ is simply the projection of vector **Y** onto the unit vector $\mathbf{B}_1$ as shown in Figure 1. Because $\mathbf{P}_y$ lies on the vector $\mathbf{B}_1$, one may express $\mathbf{P}_y$ as some fraction, a, of the unit vector $\mathbf{B}_1$

$$\mathbf{P}_y = a\mathbf{B}_1 \tag{4}$$

and therefore

$$\mathbf{B}_2' = \mathbf{Y} - a\mathbf{B}_1 \tag{5}$$

In order to solve for a, one of the properties of orthogonal vectors is employed: the dot product of two orthogonal vectors is equal to zero. This means the dot product of $\mathbf{B}_2'$ and $\mathbf{B}_1$ must equal zero. Using the expression of $\mathbf{B}_2'$ given in eq 5, we have

$$(\mathbf{Y} - a\mathbf{B}_1)\cdot\mathbf{B}_1 = 0 \tag{6}$$

The dot product is distributive allowing us to solve for the factor a as

$$\mathbf{Y}\cdot\mathbf{B}_1 - a\mathbf{B}_1\cdot\mathbf{B}_1 = 0 \tag{7}$$

$$a = (\mathbf{Y}\cdot\mathbf{B}_1)/(\mathbf{B}_1\cdot\mathbf{B}_1) \tag{8}$$

By use of the property that the dot product of a unit vector with itself, $\mathbf{B}_1\cdot\mathbf{B}_1$, is equal to one, eq 8 reduces to

$$a = \mathbf{Y}\cdot\mathbf{B}_1 \tag{9}$$

Substituting for a in eq 4 gives a definition of the projection, $\mathbf{P}_y$, in terms of the first basis vector

$$\mathbf{P}_y = (\mathbf{Y}\cdot\mathbf{B}_1)\mathbf{B}_1 \tag{10}$$

From eq 5 the unnormalized second basis vector $\mathbf{B}_2'$ follows as

$$\mathbf{B}_2' = \mathbf{Y} - (\mathbf{Y}\cdot\mathbf{B}_1)\mathbf{B}_1 \tag{11}$$

All that remains is to normalize $\mathbf{B}_2'$ to produce the second orthonormal basis vector, $\mathbf{B}_2$

$$\mathbf{B}_2 = \frac{\mathbf{Y} - (\mathbf{Y}\cdot\mathbf{B}_1)\mathbf{B}_1}{\|\mathbf{B}_2'\|} \tag{12}$$

These two basis vectors now define a subspace of a higher dimensional space as shown in Figure 2. In order to form a third basis vector $\mathbf{B}_3'$ the same procedure is followed

$$\mathbf{B}_3' = \mathbf{Z} - \mathbf{P}_z \tag{13}$$

The difference being that the projection of vector **Z** is onto a subspace rather than onto a single vector as was the case in eq 2. Because vectors $\mathbf{B}_1$ and $\mathbf{B}_2$ are orthogonal to one another, the expression for $\mathbf{P}_z$ may be simply expressed as the projection of **Z** onto each of the previous basis vectors. By use of the definition for projection derived in eq 10, this gives

$$\mathbf{P}_z = (\mathbf{Z}\cdot\mathbf{B}_1)\mathbf{B}_1 + (\mathbf{Z}\cdot\mathbf{B}_2)\mathbf{B}_2 \tag{14}$$

Substituting for $\mathbf{P}_z$ in eq 13

$$\mathbf{B}_3' = \mathbf{Z} - (\mathbf{Z}\cdot\mathbf{B}_1)\mathbf{B}_1 - (\mathbf{Z}\cdot\mathbf{B}_2)\mathbf{B}_2 \tag{15}$$

Normalization gives the third basis vector, $\mathbf{B}_3$

$$\mathbf{B}_3 = \frac{\mathbf{Z} - (\mathbf{Z}\cdot\mathbf{B}_1)\mathbf{B}_1 - (\mathbf{Z}\cdot\mathbf{B}_2)\mathbf{B}_2}{\|\mathbf{B}_3'\|} \tag{16}$$

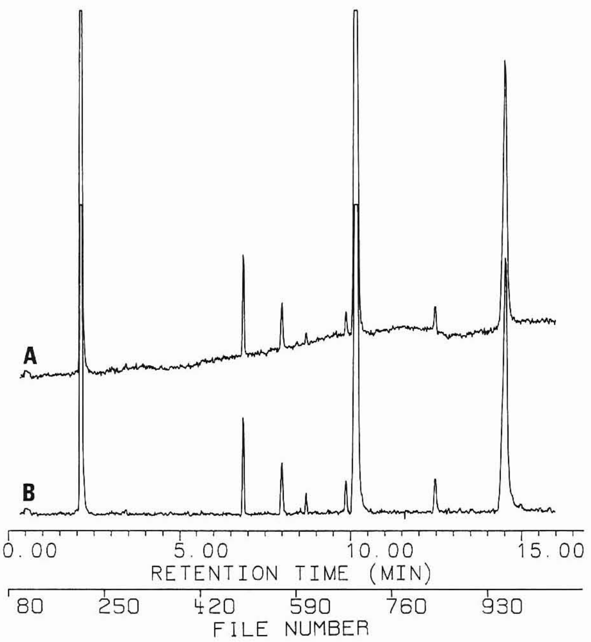

Figure 3. Removal of base-line drift in GC/FTIR: (A) Gram–Schmidt reconstructed chromatogram using 10 basis vectors from start of run; (B) same data with an additional basis vector taken from file 783 (11.58 min) added to the basis set.

This procedure can be extended to any number of basis vectors. Given a set of n vectors in the general case, the nth basis vector may be formed by sequentially subtracting the projection of vector $\mathbf{X}_n$ onto each of the previous $n-1$ basis vectors, followed by normalization

$$\mathbf{B}_n = \frac{\mathbf{X}_n - (\mathbf{X}_n\cdot\mathbf{B}_1)\mathbf{B}_1 - (\mathbf{X}_n\cdot\mathbf{B}_2)\mathbf{B}_2 - \ldots - (\mathbf{X}_n\cdot\mathbf{B}_{n-1})\mathbf{B}_{n-1}}{\|\mathbf{B}_n'\|} \tag{17}$$

Gram–Schmidt Reconstruction. Equation 17 is the mathematical calculation used in forming the basis set for a chromatographic reconstruction based on infrared data. Each vector in the basis set, $\mathbf{B}_1$, $\mathbf{B}_2$, ..., contains unique information because the vectors are orthogonal to one another. When a new vector (i.e., interferogram segment) is compared with the basis set, any information common to both will be removed upon orthogonalization. By use of the three-dimensional case as an example, the result of projecting vector $\mathbf{Z}$ onto the basis set ($\mathbf{B}_1 + \mathbf{B}_2$) is the vector $\mathbf{B}_3'$ in Figure 2. Vector $\mathbf{B}_3'$ contains only that information that is different from the basis set. The length of this projection, $\|\mathbf{B}_3'\|$, is the Gram–Schmidt response or signal intensity plotted in a reconstructed chromatogram. Each point in the Gram–Schmidt reconstruction is calculated in the same manner

$$\|\mathbf{B}_n'\| = \left(\sum_{i=1}^{k}\mathbf{B}_{n_i}'\mathbf{B}_{n_i}'\right)^{1/2} \tag{18}$$

where

$$\mathbf{B}_n' = \mathbf{X}_n - (\mathbf{X}_n\cdot\mathbf{B}_1)\mathbf{B}_1 - (\mathbf{X}_n\cdot\mathbf{B}_2)\mathbf{B}_2 - \ldots - (\mathbf{X}_n\cdot\mathbf{B}_{n-1})\mathbf{B}_{n-1} \tag{19}$$

EXPERIMENTAL SECTION

Apparatus. The GC/FTIR data were collected with a Nicolet 20SXB/GC GC/FTIR system (Nicolet Instrument Corp., Madison, WI). The SFC/FTIR data were collected with a Nicolet 5SXC spectrometer equipped with a prototype 1 mm i.d. × 5 mm pathlength high-pressure flow-through cell. All data analysis and reconstructed chromatograms were produced by use of the standard GC/FTIR software supplied with the systems.

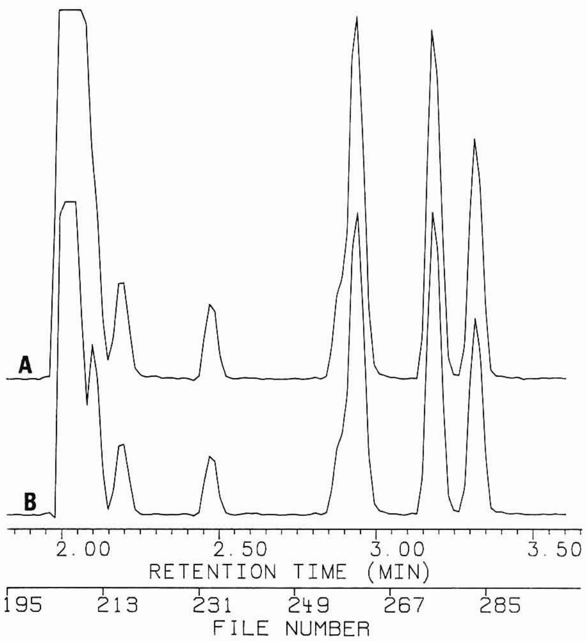

Figure 4. Suppression of solvent tailing in GC/FTIR: (A) Gram–Schmidt reconstructed chromatogram using 10 basis vectors taken from start of run; (B) same data with an additional basis vector taken from file 204 (1.98 min) added to the basis set.

GC/FTIR Examples. The GC/FTIR data were collected by coadding seven scans at 8-cm^{-1} resolution and storing the transformed data to disk. Time resolution between files stored to disk was 1.0 s. The sample in Figure 3 is a 1.0-μL injection split 40:1 of a polymer extract. It was separated on a 30-m 0.25 mm i.d. 0.25 μm film DB-1 capillary column (J&W Scientific, Folsom, CA). The data for this example were obtained after the FTIR optical bench was opened for several hours. The bench was closed and a dry air purge was turned on immediately before the run began. The data therefore represent a changing purge condition. The sample in Figure 4 is a 2.0-μL injection split 40:1 of a mixture of solvents prepared in dichloromethane. It was separated by use of a 30-m 0.32 mm i.d. 1.0 μm film bonded methyl silicone capillary column (Alltech Associates, Deerfield, IL). An HP5890A gas chromatograph (Hewlett-Packard, Avondale, PA) was used for both GC/FTIR samples.

SFC/FTIR Example. The SFC/FTIR data were collected by coadding 10 scans at 8-cm^{-1} resolution as described above. Time resolution between files stored to disk was 2.0 s. The sample, a paraffin wax mixture, was separated with a 10.2 m 100 μm i.d. 1.0 μm film SB Methyl capillary column (Lee Scientific, Salt Lake City, UT) and a Lee Scientific Model 501 supercritical fluid chromatograph. The carrier was carbon dioxide density programmed from an initial density of 0.30 g/mL with a 6.0 min hold to 0.35 g/mL at a rate of 0.10 (g/mL)/min. This was immediately followed by a second ramp of 0.010 (g/mL)/min to a final density of 0.70 g/mL. The column and connection to the flow-through cell were maintained at 100 °C. The flow-through cell was at 31 °C.

RESULTS AND DISCUSSION

The Gram–Schmidt reconstructed chromatogram is heavily dependent on the selection of vectors included in the basis set. Normally the basis vectors are taken at the start of the FTIR experiment. The basis set then describes the initial conditions when only carrier gas (GC/FTIR) or mobile phase (SFC/FTIR) is flowing through the chromatograph/FTIR interface.

When interferogram segments from each of the interferograms in the run are projected on the basis set using eq 19, there is a difference value, $\|\mathbf{B}_n'\|$. Generally this difference will be small during those portions of the run when no peaks are eluting and a base line is achieved. When a sample peak elutes through the interface, infrared absorption occurs and the resulting interferogram segment is considerably different from the basis set. A large signal response or peak results. An important aspect of the Gram–Schmidt reconstruction technique is that it responds to changes in all regions of the infrared spectrum. You cannot limit detection to a specific region as you can with integrated absorbance type reconstructions. While nonspecific detection is generally desirable, it can produce problems when the spectral changes are caused by undesired events.

It is possible to profoundly change the Gram–Schmidt response by adding one or more vectors to the basis set from other portions of the experiment. The procedure involves selecting an interferogram which is collected during the undesired event. A segment (i.e., vector) from this interferogram is made orthonormal to the existing basis set using eq 17. The resultant orthonormal vector is then added to the basis set. This augmented basis set now contains both the information describing the initial experimental conditions and the characteristics of the added basis vector.

Selection of the additional basis vector is completely subjective. Any interferogram segment from the original experimenal data may be added to the existing basis set. In fact, the cause of the undesired feature does not need to be known in order to remove it from the reconstructed chromatogram. As a result, this technique can be a useful tool in analyzing chromatographic results by using the additional basis vectors as probes to locate related species (*9*).

By recalculation of the Gram–Schmidt reconstruction with this new basis set, any features in the chromatogram caused by circumstances similar to those described by the added basis vector are also removed. This is because the subspace defined by the basis set now includes the undesired feature. Therefore, the length of the resultant Gram–Schmidt projection vector, $||\mathbf{B}_n'||$, is now very small.

In some chromatography applications, there may be an experimental parameter which is slowly changing during the course of a run. Often it is desirable to compensate for such drifts because they are irrelevant to the experiment at hand. Accordingly, many modern chromatographs provide some type of detector compensation which subtract either a constant artifact or a previously recorded background chromatogram from the chromatographic data. The procedure presented here achieves the same effect for chromatograms generated from FTIR data.

Application to GC/FTIR. A good example of a slowly changing experimental parameter is a fluctuating instrument purge during the course of a GC/FTIR experiment. Spectra collected during a run are referenced to a background spectrum collected at the beginning of the experiment. Toward the end of a GC/FTIR experiment this time difference between collections may be an hour or more. It is certainly possible to see some type of instrumental drift over this period of time. The data shown in Figure 3 are an example of such an experiment. In this case the purge was intentionally upset to produce the effect shown.

Figure 3A is a Gram–Schmidt reconstruction using 10 basis vectors formed from the first 10 data files collected after injection (retention time 0.0–10.0 s). The reconstruction shows a sloping base line which fluctuates as the level of carbon dioxide and water vapor in the instrument change. On other words, the standard Gram–Schmidt reconstruction gives a faithful representation of what is occurring during the experiment.

To remove the effects of the purge fluctuation, a basis vector is formed from the interferogram data stored in file 785 which was collected at a retention time of 11.58 min. At this point in the experiment, the level of carbon dioxide and water vapor in the bench is considerably reduced. Accordingly, the infrared spectra show negative absorption bands in these regions. The actual difference in water vapor absorbance at this point in the run compared to the beginning of the experiment is 0.002 absorbance unit.

This additional vector is added to the basis set and the Gram–Schmidt reconstruction (Gram–Schmidt plus additional basis vector or GSP) is recalculated. The effect of the purge fluctuation is suppressed in the resulting GSP chromatogram.

The GSP result is more than just cosmetic—it actually enhances the detection of small peaks. This can be seen in the improved signal to noise ratio for the peaks at 8.7 and 12.5 min in Figure 3B. An even more dramatic enhancement is shown by the example in Figure 4.

Figure 4A is a standard Gram–Schmidt reconstructed chromatogram of GC/FTIR data from a mixture prepared in dichloromethane. As in the last example, this basis set is formed from the first 10 data files collected after injection. The injection is 2.0 μL split 40:1. The solvent peak (dichloromethane) tails slightly due to the severe column overload conditions at this point in the run. The figure shows an expansion of the region around the solvent peak.

To remove this solvent tailing, a vector is formed from an interferogram collected on the leading edge of the solvent peak, file 204 (1.98 min). This vector is added to the basis set and the GSP reconstruction is calculated. The resulting chromatogram is shown in Figure 4B. As you can see, the effect of the solvent tail is suppressed revealing the presence of a small peak at 2.10 min. This corresponds to a minor component of the sample which is an impurity. By suppression of the undesirable features of the solvent tailing, the intensity of the small peak is enhanced making it easier to detect.

Application to SFC/FTIR. Probably the most exciting application of the GSP technique is in the area of density programmed supercritical fluid chromatography with FTIR detection. With SFC, it is advantageous to be able to change the density of the mobile phase. Changing the density of the fluid alters its solvating characteristics. This results in better control over the chromatographic separation. Density programming is particularly advantageous in capillary SFC applications.

Carbon dioxide is a good mobile phase when using FTIR detection because its infrared spectrum in the supercritical state is transparent over a wide region. In the past few years, several researchers have presented results obtained by using FTIR detection and a variety of flow-through cells (*4*, *5*, *10*, *11*). Work has been largely limited to carbon dioxide under isoconfertic (constant density) conditions. As long as the temperature and pressure in the cell remain constant, the carbon dioxide absorption spectrum does not change. This enables the use of standard reconstruction techniques and data analysis routines which are already in use for GC/FTIR applications.

The infrared absorption spectrum of carbon dioxide in the supercritical state is quite sensitive to changes in pressure and temperature. This is particularly noticeable in the region from 1475 to 1225 cm^{-1} where absorption due to Fermi resonance occurs (*4*, *10*). Morin et al. (*11*) report a 2-fold increase in the absorbance of the 1387-cm^{-1} band in changing the density from 0.5 to 0.7 g/mL.

The Gram–Schmidt response to changing carbon dioxide absorbance in the FTIR data is very strong. Olesik, French, and Novotny (*5*) have shown that the magnitude of this change can be the dominant feature in the reconstructed chromatogram. While the GSR is very useful in monitoring the density program during the run, it is clearly undesirable when trying to detect chromatographic peaks.

Figure 5A is a GSR from a density programmed SFC/FTIR separation. The basis set is formed from the first ten interferogram segments collected at the beginning of the experi-

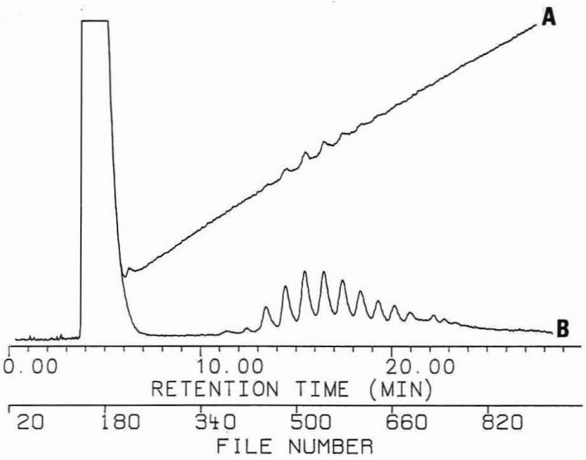

Figure 5. Compensation for carbon dioxide density gradient in SFC/FTIR: (A) Gram–Schmidt reconstructed chromatogram using 10 basis vectors from start of run; (B) same data with an additional basis vector taken from file 900 (29.12 min) added to the basis set.

ment under isoconfertic conditions (0.30 g/mL). The system is programmed to a final density of 0.70 g/mL. The chromatographic peaks are difficult to detect in the presence of the response caused by the density gradient. Figure 5B is a GSP reconstructed chromatogram generated from the same set of data. In this case, one additional basis vector was added to the original basis set. This vector was formed from the interferogram data stored in file 900 (29.12 min). Because these data were collected at a density of 0.70 g/mL, the added vector describes the spectral characteristics of supercritical CO_2 at higher densities. The recalculated GSP chromatogram completely suppresses the density ramp and enhances detection of the chromatographic peaks.

The small peak at 6.6 min in the GSR (Figure 5A) also disappears in the GSP reconstructed chromatogram. Since this time coincides with the end of the first density gradient (0.30–0.35 g/mL at 0.10 (g/mL)/min), we originally thought this peak was caused by a density overshoot. However, examination of the spectra through this region shows a steady increase in the CO_2 absorption indicating an increasing density. This is inconsistent with the overshoot hypothesis. To obtain a better look at the first density gradient, a different GSP chromatogram was generated by using the original 10 basis vectors plus one from the leading edge of the solvent peak. Figure 6A is the resulting GSP chromatogram. With the solvent tail suppressed, the initial density gradient is very clear. The small peak at 6.6 min also disappears. This confirms that the peak is not due to a density overshoot. In fact, the actual density gradient follows the density program perfectly. The only explanation for the peak is a combined response caused by the decreasing solvent tail and increasing density gradient. Compensating for either of these factors removes the peak as seen by Figure 6, parts A and B. When these two curves are added, the small peak at 6.6 min appears (Figure 6C) and is virtually identical with that in the original Gram–Schmidt reconstruction. The peak is actually just an artifact.

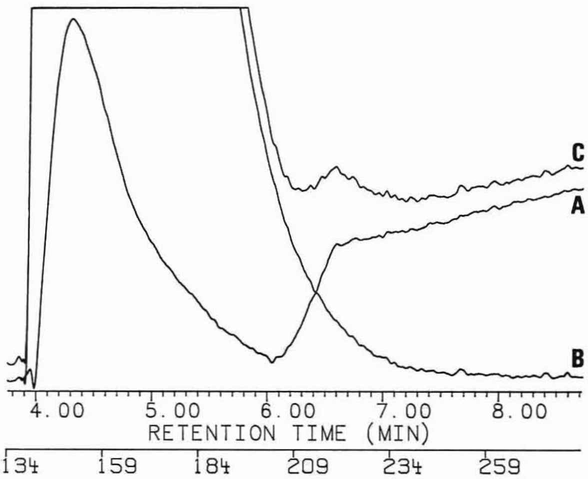

Figure 6. (A) GSP chromatogram with solvent suppression revealing initial density ramp. (B) GSP chromatogram with density program suppressed (expansion of Figure 5B). (C) Summation of curves A and B revealing peak at 6.6 min.

These applications demonstrate the power of the GSP technique in coping with chromatogram artifacts. Clearly the more pronounced the artifact, such as density gradients in SFC/FTIR, the more valuable the technique. It is important to realize that the GSP technique does not alter the original FTIR spectral data in any way. The spectra still contain the infrared features characteristic of the changing experimental parameter. The only change is in the chromatogram generated from the stored FTIR data.

ACKNOWLEDGMENT

The authors thank K. Kempfert of the Nicolet applications laboratory for the GC/FTIR data used in these examples and D. W. Later of Lee Scientific for assistance in obtaining the SFC/FTIR data.

LITERATURE CITED

(1) de Haseth, J. A.; Isenhour, T. L. *Anal. Chem.* **1977**, *49*, 1977–1981.
(2) Hanna, D. A.; Hangac, G.; Hohne, B. A.; Small, G. W.; Wieboldt, R. C.; Isenhour, T. L. *J. Chromatogr. Sci.* **1979**, *17*, 423–427.
(3) Wang, C. P.; Sparks, D. T.; Williams, S. S.; Isenhour, T. L. *Anal. Chem.* **1984**, *56*, 1268–1272.
(4) Johnson, C. C.; Jordan, J. W.; Taylor, L. T.; Vidrine, D. W. *Chromatographia* **1985**, *20*, 717–723.
(5) Olesik, S. V.; French, S. B.; Novotny, M. *Chromatographia* **1984**, *18*, 489–495.
(6) Strang, G. *Linear Algebra and Its Applications*; Academic: New York, 1976; Chapter 3.
(7) White, R. L.; Giss, G. N.; Brissey, G. M.; Wilkins, C. L. *Anal. Chem.* **1981**, *53*, 1778–1782.
(8) Brissey, G. M.; Henry, D. E.; Giss, G. N.; Yang, P. W.; Wilkins, C. L. *Anal. Chem.* **1984**, *56*, 2002–2006.
(9) Hanna, D. A.; Azzaraga, L. V. Presented at the VI Annual Meeting of the Federation of Analytical Chemistry and Spectroscopy Societies, Philadelphia, PA, Sept 1979; Paper No. 393.
(10) Shafer, K. H.; Griffiths, P. R. *Anal. Chem.* **1983**, *55*, 1939–1942.
(11) Morin, P.; Caude, M.; Richard, H.; Rosset, R. *Chromatographia* **1986**, *21*, 523–530.

RECEIVED for review November 20, 1986. Accepted January 12, 1987.

Anal. Chem. 1987, 59, 1260–1266

Curve Resolution and Figures of Merit Estimation for Determination of Trace Elements in Geological Materials by Inductively Coupled Plasma Atomic Emission Spectrometry

Avraham Lorber,*[1] **Alon Harel, and Zvi Goldbart**

Nuclear Research Centre—Negev, P.O. Box 9001, Beer-Sheva 84190, Israel

I. B. Brenner

Geological Survey of Israel, 30 Malkhe-Israel Street, Jerusalem 95501, Israel

In geochemical analysis using inductively coupled plasma atomic emission spectrometry (ICP-AES), spectral interferences and background enhancement in response to sample concomitants are the main cause of deterioration of the limit of detection (LOD) and inaccuracy of the determination at the trace and minor element levels. In this account, we describe the chemometric procedure of curve resolution for compensating for these sources of error. A newly developed method for calculating figures of merit is used to evaluate the correction procedure, test the statistical significance of the determined concentration, and determine LODs for each sample. The technique involves scanning the vicinity of the spectral line of the analyte. With prior knowledge of potential spectral interferences, deconvolution of the overlapped response is possible. Analytical data for a wide range of geological standard reference materials demonstrate the effectiveness of the chemometric techniques. Separation of 0.002 nm spectral coincidence, employing a 0.02 nm resolution spectrometer, is demonstrated.

The claim that atomic emission spectrometry (AES) is a *fully selective* analytical procedure (*1*) can be generally accepted for the determination of major and minor elements. However, in trace element analytical geochemistry using AES, the principal sources of inaccuracy and degradation of the limit of detection (LOD) are spectral coincidences and variation in background emission intensity due to complex spectra from sample concomitants (*2*). At this level of determination, the AES cannot be regarded as a *nonspecific* procedure. The extent of spectral overlap is reflected in a number of recently published ICP–AES wavelength tables (*3–7*).

Multivariate information obtained from several detectors in polychromators or from sequential monochromators is the base for different approaches for mathematical compensation of spectral interferences in ICP-AES. This type of multivariate information is first-order data, whereas a single point measurement is zeroth-order data. (Higher order data are obtained by independently varying more than one parameter.) The intrinsic advantage of first-order data over a single-point measurement is the possibility of quantitation from nonspecific responses, and numerous methods for accomplishing it may be used (*8*).

Boumans (*9*) suggested the application of matrix inversion to the matrix of partial sensitivities (response of the *i*th detector to the concentration of the *j*th element; i.e., slope of the calibration curve). A commonly used procedure is to divide all partial sensitivities of the interferents by the partial sensitivity of the analytes (i.e., divide all *i,j*th elements by the *j,j*th element). The dimensionless coefficients obtained by this division are the so-called *interference coefficients* used by Botto (*10–13*) in multielement analysis employing polychromators. Kalivas and Kowalski (*14*) demonstrated the applicability of the generalized standard addition method (GSAM) to counter interference problems in ICP-AES. Lorber et al. (*15*) and Wirsz and Blades (*16*) utilized spectral profile data and applied a curve resolution method to compensate for both spectral interferences and background variations. Taylor and Schutyser (*17*) also utilized profile data and applied methods of peak searching and curve fitting for the same purpose.

Recently (*18*), a procedure for calculating various figures of merit for characterizing the curve resolution performance and the analytical results obtained from first-order data was developed. In the present investigation we will examine the adequacy of those figures of merit for the determination of trace elements in the presence of high concentrations of sample concomitants (Fe, Ti) exhibiting various degrees of coincidence.

THEORY

First-Order Calibration and Quantitation. Quantitating the concentration, $c_{\mathrm{un},k}$, of the kth constituent ($k = 1, ..., K$, where K is the number of constituents) for a sample from first-order data involves measuring the vector, $\mathbf{r}_{\mathrm{un}}$, which consists of J ($j = 1, ..., J$) responses at J wavelength positions. The relation between measured responses and concentration is performed according to the linear additive model. Hence the response measured at each wavelength may be described as

$$r_{\mathrm{un},j} = \sum_{k=1}^{K} c_{\mathrm{un},k} s_{j,k} + b_j \tag{1}$$

here $s_{j,k}$ designates the partial-sensitivities (*1*) which are the sensitivity (slope of the analytical calibration function) of the kth analyte at the jth wavelength position and b_j is the background contribution at this wavelength. In matrix notation, eq 1 is written as

$$\mathbf{r}_{\mathrm{un}} = \mathbf{c}_{\mathrm{un}}^{\mathrm{T}}\mathbf{S} + \mathbf{b} \tag{2}$$

here $\mathbf{c}_{\mathrm{un}}$ is the vector of the concentration in the unknown sample and the superscript T denotes the operation of matrix or vector transposition, $\mathbf{S}$ is an $K \times J$ matrix of sensitivities, and $\mathbf{b}$ is the vector of backgrounds.

To quantify from the model in eq 2, a calibration set is required that will supply data to calculate a matrix of sensitivities. The measured responses of I ($i = 1, ..., I$) calibration samples at J wavelengths is the matrix $\mathbf{R}$ which is a $I \times J$ matrix. From this matrix and from the concentrations of all constituents in all calibration samples, the matrix of sensi-

---

[1] Present address: Center for Process Analytical Chemistry and Laboratory for Chemometrics, Department of Chemistry, BG-10, University of Washington, Seattle, WA 98195.

0003-2700/87/0359-1260$01.50/0 © 1987 American Chemical Society

tivities can be derived, which is then substituted in eq 2 to solve for the concentrations of the unknown constituents. For the sake of simplicity we will not present here the so-called *direct* or *total calibration* approach but rather the *indirect* or *partial calibration* approach (*19*). The *total calibration* differs from the *partial calibration* by that in the former comprehensive information on the concentrations of all constituents in all calibration samples or the spectra of the pure components is required while in the *partial* case only the concentration of one analyte in all the calibration set suffices. The *partial calibration* automatically solves for background variation (provided that the sources for background variations in the unknown sample are the same as in the calibration set).

In the *partial calibration* approach we determine the concentration of the kth constituent by

$$c_{\mathrm{un},k} = \mathbf{r}_{\mathrm{un}}^{\mathrm{T}}\mathbf{R}^{+}\mathbf{c}_k \qquad (3)$$

where $\mathbf{c}_k$ is the vector of concentrations of the kth analyte in the calibration set. $\mathbf{R}^{+}$ is the pseudoinverse of the matrix $\mathbf{R}$ and the superscript + denotes the operation of pseudoinverse. The pseudoinverse (*20*) is used to solve a system of linear equations and differs from the regular inverse by permitting the direct solution of nonsquare and singular matrices. The derivation of this equation is presented elsewhere (*19*). In the simple case where the matrix $\mathbf{R}$ is measured for K pure samples, eq 3 becomes

$$c_{\mathrm{un},k}/c_{0,k} = \mathbf{r}_{\mathrm{un}}^{\mathrm{T}}\mathbf{R}^{+} \qquad (4)$$

where $c_{0,k}$ is the concentration of the kth constituent in the calibration.

Figures of Merit for First-Order Quantitation. The availability of first-order data provides us a means of overcoming spectral interferences. However, determination of the concentration is only one step in the quantitation process. One can hardly speak on quantitative results without furnishing each determination with its precision and accuracy. The figures of merit used to characterize the analytical determination are (a) signal-to-noise ratio (S/N), (b) precision or relative precision which is expressed as the percent relative standard deviation (RSD) of the determined concentration, (c) accuracy which is the sum of precision and bias from true chemical quantities, and (d) limit of determination (LOD). In addition to these specifications there are also other figures which characterize the analytical procedure: (a) limit of detection which is based on the calibration data and usually is lower than limit of determination in true samples, (b) sensitivity, and (c) selectivity (*1*). Recently a mathematical formulation for calculating all the above-mentioned figures of merit for the first-order case was presented (*18*). The essential equations will be presented here; the reader is referred to another article for complete mathematical derivation (*18*).

The principal concept in calculating figures of merit is the "*net analyte signal*" of the kth constituent in the unknown sample, $r_k^{(\mathrm{net})}$. The importance of the net signal is obvious since S/N of the concentration and thus precision is dependent on the net signal contribution from the analyte rather than the measured gross signal which is the sum of several contributions. The "*net analyte signal*" of the kth constituent for first-order data was defined as the "*part of the kth constituent spectrum which is orthogonal to the spectra of the other constituents taken into calibration*". This definition is a consequence of solving a set of equations in which only the orthogonal part contributes to information on the kth constituent. The computation is according to

$$r_k^{(\mathrm{net})} = \mathbf{r}_{\mathrm{un}}^{\mathrm{T}}\mathbf{R}^{+}\mathbf{c}_k/\|\mathbf{R}^{+}\mathbf{c}_k\| \qquad (5)$$

here $\|\cdot\|$ designates the Euclidian norm of a vector, defined as the square root of the sum of squared elements of the vector. By comparison of eq 5 to eq 3 and 4 it is obvious that eq 5 may also be written as

$$r_k^{(\mathrm{net})} = c_{\mathrm{un},k}/\|\mathbf{R}^{+}\mathbf{c}_k\| \qquad (5a)$$

The sensitivity for zeroth-order data is equal to the net analyte signal divided by the concentration. Applying this relation to eq 5a results in the following value for the sensitivity in the first-order case

$$S_k = 1/\|\mathbf{R}^{+}\mathbf{c}_k\| \qquad (6)$$

The S/N of the kth constituent in the unknown sample, $(\mathrm{S/N})_k$, is given by

$$(\mathrm{S/N})_k = r_k^{(\mathrm{net})}/\epsilon_{\mathrm{un}} = c_{\mathrm{un},k}/(\|\mathbf{R}^{+}\mathbf{c}_k\|\epsilon_{\mathrm{un}}) \qquad (7)$$

where ϵ_k is the error in the measured responses of the unknown sample and calculated as the residuals between the measured and fitted values. The relative precision in determining the concentration of the kth constituent, $(\delta c/c)_k$, is equal to the inverse of $(\mathrm{S/N})_k$

$$(\delta c/c)_k = \|\mathbf{R}^{+}\mathbf{c}_k\|\epsilon_{\mathrm{un}}/c_{\mathrm{un},k} = (\|\mathbf{R}^{+}\mathbf{c}_k\|\ \|\mathbf{r}_{\mathrm{un}}\|/c_{\mathrm{un},k}/\|\mathbf{r}_{\mathrm{un}}\|) \qquad (8)$$

The "*error propagation*", κ_k, which is the ratio of the relative error in the measured response data in the unknown sample to the relative error in the determined concentration of the kth constituent, is directly represented in eq 8 to equal

$$\kappa_k = \|\mathbf{R}^{+}\mathbf{c}_k\|\ \|\mathbf{r}_{\mathrm{un}}\|/c_{\mathrm{un},k} \qquad (9)$$

The "*selectivity*", ζ_k, of the kth constituent was redefined in ref 18 to measure the degree of overlap of the kth constituent with the other constituents taken into the calibration. Selectivity was defined to equal the ratio of *the k'th constituent pure spectra*, $\mathbf{r}_k^{(\mathrm{pure})}$, *which is orthogonal to the spectra of the others to its total value*. The part which is orthogonal to the others is the net analyte signal given in eq 5a. For the pure kth constituent it will equal $c_{0,k}/(\|\mathbf{R}^{+}\mathbf{c}_k\|)$ and thus the selectivity is computed as

$$\zeta_k = c_{0,k}/(\|\mathbf{R}^{+}\mathbf{c}_k\|\ \|\mathbf{r}_k^{(\mathrm{pure})}\|) \qquad (10)$$

The range of the selectivity is between one (fully selective or specific (*1*)), for the case that the spectra of the kth constituent is completely free from overlap, and zero, in the case that the spectra is the same as the other constituent's spectra or may be described as a linear combination of them.

When the kth constituent is the only component in the unknown sample, we obtain that the error propagation (eq 9) for this case is equal to

$$\kappa_k = 1/\zeta_k \qquad (11)$$

This equation is derived by inserting in the appropriate values from eq 4 and 10 in eq 9. Inserting this value of the condition number into eq 8, we obtain the relative precision

$$(\delta c/c)_k = (1/\zeta_k)(\epsilon_{\mathrm{un}}/\|\mathbf{r}_{\mathrm{un}}\|) \qquad (12)$$

If the concentration is equal to the concentration in the calibration, this is simplified to

$$(\delta c/c)_k = (1/\zeta_k)(\epsilon_{\mathrm{cal}}/\|\mathbf{r}_k^{(\mathrm{pure})}\|) \qquad (13)$$

here ϵ_{cal} designates the error in the calibration. This specific case of the error propagation is directly connected to the limit of detection of the kth constituent, $(\mathrm{LO\text{-}DTC})_k$. In the first-order case we suggest the use of $(\mathrm{LO\text{-}DTC})_k$ to characterize the case when only the kth constituent is present in the sample. This is completely different than the limit of determination of the kth constituent, $(\mathrm{LO\text{-}DTR})_k$, that is affected by the concentration of the other sample constituents. By using the conventional definition of LOD which is the amount of analyte equal to three times the precision of the concentration, we directly obtain from eq 13

$$(\text{LO-DTC})_k = (3c_{0,k}/\zeta_k)(\epsilon_{\text{cal}}/\|\mathbf{r}_k^{(\text{pure})}\|) \qquad (14)$$

This equation stresses the importance of "selectivity" for characterizing the analytical procedure. The relative error in the measured signal, $\epsilon_{\text{un}}/\|\mathbf{r}_{\text{un}}\|$, is a characteristic of the analytical instrument. Thus, the inverse of selectivity is the only term which accounts for the mathematical difficulty to resolve an overlapped spectrum.

The relative accuracy, $(\delta c(\text{acc})/c)_k$, is the sum of the relative precision in the determined concentration of the unknown sample (eq 8) and the error in the calibration itself (eq 14). Consequently we can write

$$(\delta c(\text{acc})/c)_k = \kappa_k(\epsilon_{\text{un}}/\|\mathbf{r}_{\text{un}}\|) + (1/\zeta_k)(\epsilon_{\text{un}}/\|\mathbf{r}_k^{(\text{pure})}\|) \quad (15)$$

In a low power argon ICP-AES it was found that for most spectral lines the relative error is almost constant and equal to 1% RSD (*3*). Thus we can write $\epsilon_{\text{un}}/\|\mathbf{r}_{\text{un}}\| = \epsilon_{\text{un}}/\|\mathbf{r}_{\text{k}}^{(\text{pure})}\|$ and simplify eq 15 to

$$(\delta c(\text{acc})/c)_k = (\kappa_k + 1/\zeta_k)(\epsilon_{\text{un}}/\|\mathbf{r}_{\text{un}}\|) \qquad (16)$$

From this equation it is possible to calculate $(\text{LO-DTR})_k$ by using the definition of κ_k given in eq 9 to obtain

$$(\text{LO-DTR})_k = 3\ \|\mathbf{R}^{+}\mathbf{c}_k\|\ \|\mathbf{r}_{\text{un}}\|/(\|\mathbf{r}_{\text{un}}\|/\epsilon_{\text{un}} - 3/\zeta_k) \qquad (17)$$

If we subtract from this formula the effect of the error in calibration we obtain

$$(\text{LO-DTR})_k = 3\ \|\mathbf{R}^{+}\mathbf{c}_k\|\epsilon_{\text{un}} \qquad (18)$$

In zeroth-order data, LOD is computed as three times the error divided by the sensitivity (*21*). The sensitivity was identified in eq 6 to equal the inverse of $\|\mathbf{R}^{+}\mathbf{c}_k\|$. Thus, without including the effect of error in the calibration, the LOD obtained for first-order data is the same as for zeroth-order data. This observation applies also for eq 14.

Equation 17 assures that $(\text{LO-DTR})_k$ will always be greater than $(\text{LO-DTC})_k$. However, negative results in the denominator may also appear for samples below $(\text{LO-DTR})_k$. This is a logical result since $(\text{LO-DTR})_k$ cannot be estimated from concentrations below $(\text{LO-DTR})_k$.

EXPERIMENTAL SECTION

Experimental facilities and operating conditions were described previously (*15, 22*). In this study, the Jobin-Yvon JY48 direct reading spectrometer was operated as a scanning monochromator. A multielement scan was achieved by moving the computer-controlled entrance slit to scan a spectral region of ±0.05 nm across the analytes' spectral lines. The spectral region was characterized by 11 data points, each data point was integrated for 3 s and the total measurement time for each sample was 40 s. The current software is capable of simultaneously processing data from 20 detectors and deals with eight interferents for each detector.

Sample Decomposition and Calibration Samples Preparation. One gram of standard reference material was weighed into a Teflon dish and moistened with water. Five milliliters of nitric acid (1:1 (v/v)) was added. The contents of the dishes were heated on a sand bath at 200 °C until dryness. After this step was repeated, 10 mL of $HClO_4$ (1:1 (v/v)) were added and the mixture was heated until formation of white perchloric fumes. The Teflon dishes were then removed from the bath; hot water and 5 mL of nitric acid (1:1 (v/v)) were added to the solution. After cooling, the volume was made up to 100 mL.

Stock solutions of analytes and interferents were prepared by dissolving pure metals or reagents (Specpure grade, Johnson-Matthey) in dilute acids (Suprapur grade, Merck) and deionized, distilled water.

Calibration Procedure. The background data vector was determined by nebulizing deionized water; the background profile was determined from the mean of three successive scans. Background contribution was removed from all calibration and unknonw samples as described previously (*15*). The accurate determination of the background profile is important to minimize the bias in quantitation near LOD. The RSD within the three measured values is computed and printed. If the RSD is too high, there is an option to repeat the measurements of the background.

Subsequent to background determination, the profiles of the interferents and the calibration samples were determined. Each interferent was determined separately by aspirating a solution that contained only the interferent. The standard solutions, contained low concentrations of the determined elements to avoid mutual interferences from the elements in the same calibration solution. All interferents and background data are stored on hard disk.

Evaluation of Interferences. Selectivity values for each channel are computed for all interferents and the analyte. For an interferent having a selectivity value less than 0.03, no interference occurs and the data from this interferent should not be taken into account to minimize bias near the LOD. If both the analyte and an interferent have selectivity values less than 0.03, complete coincidence occurs and quantitation is impossible employing the examined spectral line. Intermediate selectivity values ($0.03 < \xi > 1.0$) of the analytes represent the expected error propagation as discussed in the theoretical section.

Analysis of Unknown Samples. After calibration and evaluation of interferences, it is not necessary to repeat these procedures at the beginning of each analytical run. Only the standard calibration solution should be measured prior to analysis. In order to ensure that the detectors always observe the same spectral region, it is essential to be able to move to the same spectral position. An option to run a subroutine that will move the spectrometer to a fixed position is optional at the beginning of every instrument operation. After more than 1 year of experience we found no difficulty in accomplishing this with our instrument.

Concentration, S/N, and, in cases where S/N is less than 3, the LOD are printed for each analyte in the unknown sample. Computation of the concentration of the unknown sample is according to eq 3. The number of mathematical operations needed for quantitation is one addition and one multiplication for each data point. This is a very modest requirement and allows a real-time computation.

Software. Subroutines were written in FORTRAN IV and incorporated in the original software that operates the JY48 spectrometer. Several modifications in the original program that allow for real time calculations were also incorporated. The pseudoinverse was computed by the singular value decomposition (SVD) (*20*). The SVDRS subroutine of Lawson and Hanson (*20*) served to compute the SVD. All computations were performed on a Digital Equipment Co. PDP 11/23 minicomputer.

RESULTS AND DISCUSSION

The currently used approaches to overcome the problem of spectral interferences involve the use of high-resolution spectrometers (*2, 11, 23–26*), generalized standard addition method (*14*), matrix matching (*27*), application of predetermined interference coefficients with on-line background compensation (*9–13*), application of peak identification and curve fitting to profile data (*17*), and curve resolution (*15, 16*). These techniques are limited in use for the following reasons: (a) Due to physical line broadening, even a high-resolution spectrometer cannot usually separate spectral lines located 0.01 nm apart (*26, 28*). (b) Correction for interferences by standard additions is tedious and relies heavily on accurate background subtraction and therefore is unsuitable for trace element determinations. (c) For samples with diverse chemical composition such as geological materials, matrix matching is very restricted in application. (d) Use of interference coefficients requires a quality assurance procedure for maintaining long-term stability. Botto (*10, 12*) found a mean value of 10–15% RSD for the coefficients when he applied a procedure that assures reproducibility of plasma parameters. An additional restriction in applying the interference coefficients technique for simultaneous multielement analysis is the

Table I. Printout of Analytical Results for Various Uranyl Mixtures[a]

				0 mg/L U					
				Concentrations (mg/L)					
Al	******	B	0.0177	Ca	−0.0412	Cd	******	Cr	******
Cu	******	Fe	******	Mg	−0.00268	MN	******	Mo	******
Ni	******	P	******	S	******	Sr	******	Ti	******
V	******	Zn	******	Zr	******	U	−0.235		
				S/N or LOD					
Al	0.32	B	3.64	Ca	3.07	Cd	0.013	Cr	0.023
Cu	0.022	Fe	0.012	Mg	7.225	MN	0.0033	Mo	0.023
Ni	0.024	P	0.38	S	0.031	Sr	0.0011	Ti	0.012
V	0.019	Zn	0.0055	Zr	0.032	U	3.88		
				1 g/L U					
				Concentrations (mg/L)					
Al	******	B	0.0675	Ca	******	Cd	******	Cr	******
Cu	******	Fe	−0.0161	Mg	******	MN	******	Mo	******
Ni	−0.0227	P	******	S	0.0641	Sr	******	Ti	******
V	******	Zn	0.0055	Zr	******	U	980		
				S/N or LOD					
Al	0.35	B	5.14	Ca	0.0086	Cd	0.013	Cr	0.020
Cu	0.068	Fe	4.39	Mg	0.0069	MN	0.012	Mo	0.012
Ni	4.69	P	0.46	S	3.78	Sr	0.0019	Ti	0.026
V	0.15	Zn	4.21	Zr	0.047	U	52.2		
				5 g/L U					
				Concentrations (mg/L)					
Al	******	B	0.235	Ca	−0.483	Cd	******	Cr	******
Cu	******	Fe	−0.333	Mg	******	MN	******	Mo	******
Ni	******	P	******	S	******	Sr	******	Ti	******
V	******	Zn	******	Zr	******	U	5070		
				S/N or LOD					
Al	1.56	B	4.55	Ca	3.77	Cd	0.090	Cr	0.075
Cu	0.23	Fe	12.8	Mg	0.066	MN	0.033	Mo	0.092
Ni	0.073	P	1.01	S	0.69	Sr	0.0095	Ti	0.091
V	0.98	Zn	0.041	Zr	0.18	U	47.1		

[a] Normally the S/N's are printed. When asterisks are printed, the concentration is below the LOD, and the LOD is printed for the corresponding element.

difficulty of selecting the appropriate background positions. In practice the use of several background positions for multielement analysis results in a decrease of the analytical throughput. Selection of the optimal S/N position is also not trivial in the case of spectral overlap and may differ from the peak position (*24*). (e) The method of using peak search and curve fitting is very interesting because it does not require any preliminary knowledge of the interferents. However, in the absence of a valley between the spectral lines it is impossible to deconvolute the peaks, and if the background is very structured, appropriate background positions may not be found. Furthermore, the period for acquisition of a large spectral region reduces sample throughput.

The proposed technique, although free from the abovementioned flaws, suffers from the inherent limitation of error propagation. For example, the inclusion of an interferent will result in lower selectivity and sensitivity of the analyte, hence inherent deterioration of the LOD as expressed in eq 17. If the amount of the interferent in the sample is low, no correction is needed but the inclusion of this interferent already caused degradation in precision and LOD. This disadvantage may be avoided by first taking into account all potential interferents and then solving only for those that are present in the sample. However, such a procedure will require matrix inversion for each determined element in every sample which may exceed normal laboratory computing facilities.

The most important achievement of the technique is the confidence in the reported analytical values which include computation of LOD, S/N, and accuracy for each sample (Table I). This table is the printout of the computer and represents the dependence of LOD on interferent level. The values in the table as well as other tables are not average values and are results of a single determination. Therefore, the LOD and the determined concentrations are not expected to represent their true values. The S/N values are an estimate for the precision of these values. Data for pure aqueous solution and two levels of uranium are represented. The complex spectra of uranium results in numerous spectral interferences which degrade LODs. For example, V II 310.230 nm is subject to interference from U 310.261, 310.239, and 309.905 nm spectral lines. The LOD for V in pure aqueous solution in this particular run is 19 μg/L but degrades to 0.98 mg/L in the presence of 5 g/L uranium. The provision of the LOD and S/N for each sample allows a critical evaluation of the analytical significance of each result. This is a unique feature of first-order data (profile) not provided by zero-order data (single point).

Other benefits of the method are as follows: (a) elimination of the time-consuming process of determining optimal background and peak positions, hence method development is simple; (b) the measured spectral region is very narrow and there is no need to measure directly the background, hence sample throughput is similar to quantitation from the peak position; (c) sample throughput is enhanced due to the fact that precision data are obtained from a single scan and there is no need for repeated measurements; (d) once the inter-

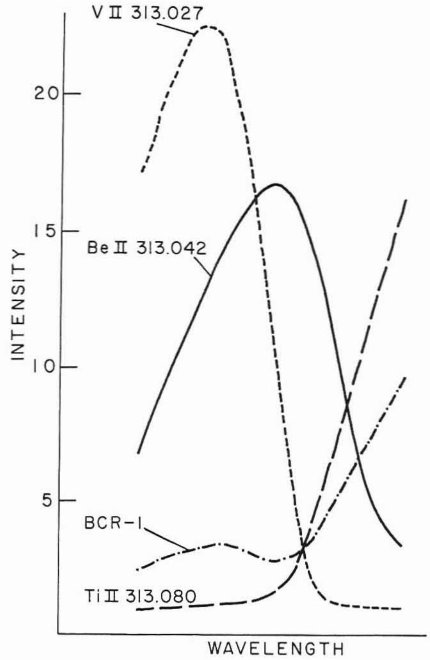

Figure 1. Spectral region (0.05 nm) in the close vicinity of Be II 313.042 nm. The concentrations are as follows: V, 50 mg/L; Ti, 200 mg/L; Be, 0.27 mg/L; BCR-1, 1:100.

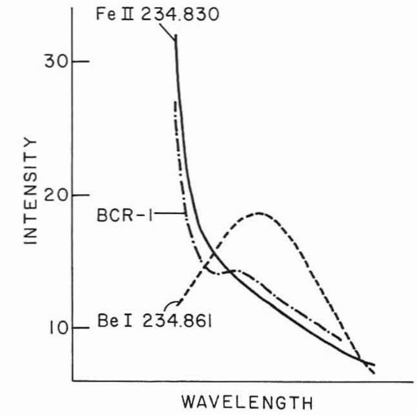

Figure 2. Spectral region (0.05 nm) in the close vicinity of Be II 234.861 nm. The concentrations are as follows: Fe, 1000 mg/L; Cu, 1000 mg/L; Be, 0.04 mg/L.

ferents and background are known, there is no need to measure them again and only the spectrum of the analytes are measured prior to analysis.

The benefits and limitations of the technique are exemplified by the determination of beryllium and cobalt in various geological and environmental certified reference materials by ICP-AES.

Determination of Beryllium. The two most prominent spectral lines for the determination of beryllium are Be II 313.042 and Be I 234.861 nm (*3, 4*). The limit of detection in aqueous solution in our system is 0.5 μg/L for both spectral lines. The main spectral interferences on Be II 313.042 nm in geological materials are Ti II 313.080 and V II 313.027 nm which are 0.038 and 0.015 nm, respectively, away from the beryllium spectral line. The profiles of these spectral lines are presented in Figure 1. It is evident that these spectral lines are incompletely resolved. The profile of Be I 234.861 nm in the presence of a high concentration of iron clearly shows that the wing of Fe II 234.820 nm causes a substantial interference (Figure 2). This interference causes a background enhancement at this position and results in degradation of the LOD (1 g/L iron causes a 10-fold background enhancement).

Table II. Results (mg/kg) of Determining Be in Geological Materials

		Be II 313.042 nm		Be I 234.861 nm	
	quoted	found	S/N	found	S/N
NBS1633a	12	13.5	74	14	120
NIM-D	0.5	0.06	1.5	−0.1	1
NIM-N	1	0.4	14	0.37	8
NIM-L	20	27	50	30	140
AGV-1	2	2.0	40	1.9	30
BCR-1	1.7	1.5	20	1.0	17
SO-1	0.6, 1.4	2.0	40	1.9	30
SO-2	1.7	2.1	40	1.9	30
SO-4	1.7, 1.5	1.2	40	1.1	20
SY-3	22	23	50	25	170
MRG-1	0.6	0.6	7	−1.0	3
FER-2	3	3.5	70	−0.8	3
FER-4	1	1.1	44	−0.5	1
selectivity		0.21		0.4	

The selectivities of Be I 234.861 nm and Be II 313.042 nm, 0.4 and 0.21, respectively, reflect the actual degree of interference on the spectral lines. Because in ICP-AES there is always an appreciable amount of background emission, the highest selectivity that is obtainable is for a flat background without interferences. For this case the selectivity is approximately 0.7. Therefore, it is predicted, from the values of selectivities, that a 40% and 70% degradation of the LOD and a 2- and 3-fold degradation in precision will occur for Be I 234.861 nm and Be II 313.042 nm, respectively (compared to aqueous solution).

Analytical data for beryllium and the S/N associated with each determination are presented in Table II. The recomended values are from ref 29. The LODs for each determination are not listed since the S/N values clearly indicate the level of determination (S/N values less than 3 are below LOD). Taking into account that most of the quoted values are proposed and not recommended (except for SY-3) (*29*), the determined values are in satisfactory agreement (values for NIM-D and NIM-N are quoted as an order of magnitude estimate). The fact that correct results are obtained for MRG-1 and BCR-1 (V 520 and 420 ppm; TiO_2 3.3 and 2.2%, respectively) employing Be II 313.042 nm demonstrates the effectiveness of the proposed technique. By use of Be I 234.861 nm, MRG-1, FER-2, and FER-4 could not be analyzed due to the very high iron content (17.8, 39.2, 39.9% T Fe_2O_3) which enhances the background at the analyte peak position. This fact is reflected in the S/N ratios for these samples and their values are below the LOD.

Botto (*12*) applied a method of correction by using interference coefficients for Be I 234.861 nm. Using an instrument with 0.03 nm resolution, he was unable to obtain analytical data for the coal-ash NBS1633a SRM, although the content of beryllium is relatively high in this sample. Meaningful analytical results were obtained only with a high resolution echelle spectrometer (*12*). For this lab, with the JY48 ($\sim$0.02 nm resolution) a concentration of beryllium lower by an order of magnitude (and iron content comparable to NBS1633a) was determined. This improved detection power is mainly attributed to the superior resolution capability of the method used here over the interference coefficients procedure.

Comparison of S/N ratios for samples with high beryllium content shows that predicted degradation in precision for the two spectral lines (from the selectivities) agrees with the actual measured values.

Determination of Cobalt. The determination of cobalt in geological materials is hindered by severe spectral interferences (*30*). The most prominent line, Co II 238.892 nm, is interfered by Fe II 238.862 nm to such an extent that it is

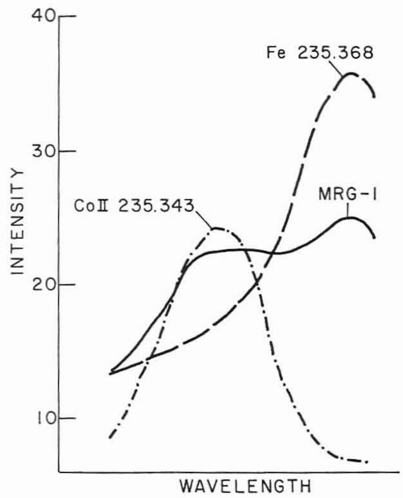

Figure 3. Spectral region (0.05 nm) in the close vicinity of Co II 235.343 nm. The concentrations are as follows: Fe, 3000 mg/L; Co, 2 mg/L; MRG-1, 1:100.

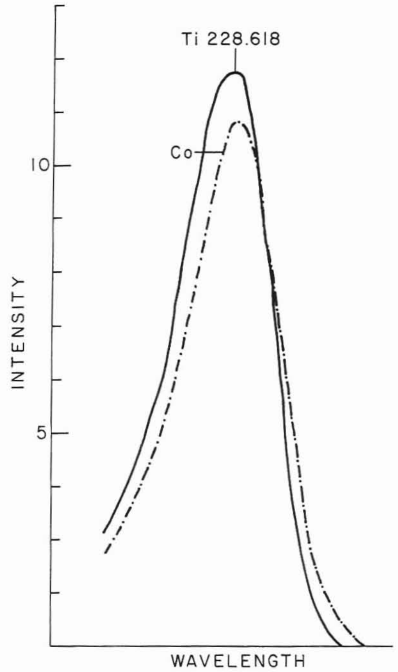

Figure 4. Spectral region (0.05 nm) in the close vicinity of Co II 228.616 nm. The concentrations are as follows: Ti, 1000 mg/L; Co, 2 mg/L.

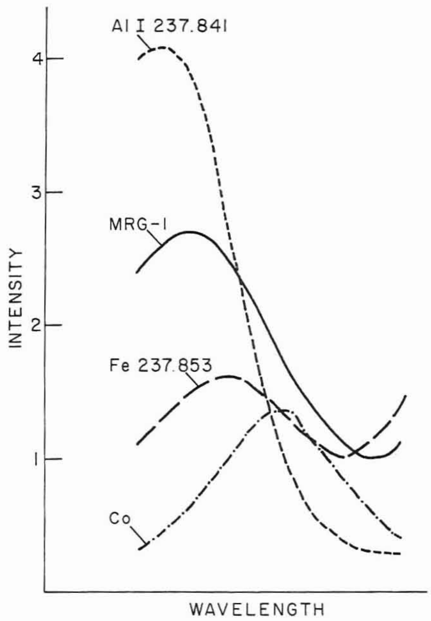

Figure 5. Spectral region (0.05 nm) in the close vicinity of 237.862 nm. The concentrations are as follows: Al, 1000 mg/L; Fe, 3000 mg/L; Co, 2 mg/L; MRG-1, 1:100.

Table III. Results (mg/kg) of Determining Co in Geological Materials

		235.342 nm		228.616 nm		237.862 nm	
	quoted	found	S/N	found	S/N	found	S/N
NBS1633a	46	45	40	43	12	57	6
NIM-D	210	200	115	192	25	180	58
NIM-L	8	−82	3	−1	1	9	2.5
NIM-N	58	55	46	53	16	60	10
AGV-1	15	18	10	21	10	29	6
BCR-1	36	34	22	41	6	37	10
SO-1	32	33	21	30	22	45	6
SO-2	13	12	6	15	7	20	4
SO-4	15	14	9	14	4	19	7
SY-3	12	12	6	11	4	35	6
MRG-1	86	82	42	83	23	80	40
FeR-2	7	10	6	6	3	8	4
FeR-4	2	5	2	1	1	8	3
GH	1.5	1	1	−1	1	15	3
selectivity		0.33		0.120		0.33	

inapplicable for the analysis of most geological materials. Three other spectral lines were inspected: Co II 235.343 nm (Figure 3), Co II 228.616 nm (Figure 4), and Co II 237.862 nm (Figure 5). It should be noted that the iron interference on Co II 235.343 nm is not cited in the literature. In aqueous solution the LOD for the three spectral lines are 10, 8, and 20 μg/L and the selectivities are 0.33, 0.11, and 0.33 respectively.

Analytical data obtained by using these lines are presented in Table III. The values obtained by using Co II 235.343 nm are in good agreement with reported values (most of which are recommended (*29*)). The actual LOD is 6 ppm which is in good agreement with that predicted from the selectivity value. The values obtained by using this line show that analytical data close to LOD is reliable when the determination is coupled with the figures of merit for the analyzed sample. The negative cobalt content found for NIM-L is a result of the spectral interference from Zr II 235.320 nm. The content of zirconium in this sample is relatively large (1.1%). We did not add this interferent to the calibration data matrix to demonstrate the effectiveness of S/N value in detecting unexpected interferences. The low S/N ratio indicates that this result is spurious. The accuracy of the results employing Co II 237.862 nm is strongly dependent on the aluminum content. For example, the NBS1633a contains 13% Al which corresponds to an apparent concentration of 300 ppm cobalt.

The severe overlap of Ti II 228.618 nm which is 0.002 nm away from Co II 228.616 nm can be handled by the proposed technique as demonstrated by the data in Table III. However, the accuracy of the results is approximately 10% caused by the similarity of the spectral line profiles as indicated by the low selectivity value (0.11). This error propagation is inherent in the mathematical treatment and is not dependent on the titanium concentration. This spectral line thus demonstrates the major pitfall of the proposed technique. Nevertheless, since the method is furnished with diagnostic tools (figures of merit) such an ill-conditioned case is readily detected and the analyst should choose an alternate spectral line or other methods of correction.

Registry No. Al, 7429-90-5; B, 7440-42-8; Ca, 7440-70-2; Cd, 7440-43-9; Cr, 7440-47-3; Cu, 7440-50-8; Fe, 7439-89-6; Mg, 7439-95-4; Mn, 7439-96-5; Mo, 7439-98-7; Ni, 7440-02-0; P, 7723-14-0; S, 7704-34-9; Sr, 7440-24-6; Ti, 7440-32-6; V, 7440-62-2;

Zn, 7440-66-6; Zr, 7440-67-7; U, 7440-61-1; Be, 7440-41-7; Co, 7440-48-4.

LITERATURE CITED

(1) Kaiser, H. *Spectrochim. Acta, Part B* **1978**, *33B*, 551.
(2) Boumans, P. W. J. M.; Vrakking, J. J. A. M. *Spectrochim. Acta, Part B* **1985**, *40B*, 1085.
(3) Boumans, P. W. J. M. *Line Coincidence Tables for ICP-OES*, 2nd ed.; Pergamon: Oxford, 1984.
(4) Winge, R. K.; Fassel, V. A.; Peterson, V. J.; Floyd, M. A. *ICP-AES, An Atlas of Spectral Information*; Elsevier: Amsterdam, 1985.
(5) Parsons, M. L.; Forster, A.; Anderson, D. *An Atlas of Spectral Interferences in ICP Spectrometry*; Plenum: London, 1980.
(6) Brenner, I. B.; Eldad, H. *ICP Inf. Newsl.* **1984**, *10*, 451.
(7) Wohlers, C. C. *ICP Inf. Newsl.* **1985**, *10*, 601.
(8) Ramos, L. S.; Beebe, K. R.; Carey, W. P.; Sanchez, E.; Erickson, B. C.; Wilson, B. E.; Wangen, L. E.; Kowalski, B. R. *Anal. Chem.* **1986**, *58*, 294R.
(9) Boumans, P. W. J. M. *Spectrochim. Acta, Part B* **1976**, *31B*, 147.
(10) Botto, R. I. *Anal. Chem.* **1982**, *54*, 1654.
(11) Botto, R. I. *Spectrochim. Acta, Part B* **1983**, *38B*, 129.
(12) Botto, R. I. *Spectrochim. Acta, Part B* **1984**, *39B*, 95.
(13) Botto, R. I. In *Development in Atomic Plasma Spectrochemical Analysis*; Barnes, R. M., Ed.; Heyden: Philadelphia, PA, 1981; p 141.
(14) Kalivas, J. H.; Kowalski, B. R. *Anal. Chem.* **1982**, *54*, 560.
(15) Lorber, A.; Goldbart, Z.; Harel, A. *Anal. Chem.* **1985**, *57*, 2537.
(16) Wirsz, D. F.; Blades, M. W. *Anal. Chem.* **1986**, *58*, 51.
(17) Taylor, P.; Schutyser, P. *Spectrochim. Acta, Part B* **1986**, *41B*, 81.
(18) Lorber, A. *Anal. Chem.* **1986**, *58*, 1167.
(19) Lorber, A.; Wangen, L. E.; Kowalski, B. R. *J. Chemometrics* **1987**, *1*, 19.
(20) Lawson, C. L.; Hanson, R. J. *Solving Least Squares Problems*; Prentice-Hall: Englewood, NJ, 1974.
(21) Long, G. L.; Winefordner, J. D. *Anal. Chem.* **1983**, *55*, 712A.
(22) Lorber, A.; Eldan, M.; Goldbart, Z. *Anal. Chem.* **1985**, *57*, 851.
(23) Boumans, P. W. J. M.; Vrakking, J. J. A. M. *Spectrochim. Acta, Part B* **1984**, *39B*, 1239.
(24) Boumans, P. W. J. M.; Vrakking, J. J. A. M. *Spectrochim. Acta, Part B* **1984**, *39B*, 1261.
(25) Boumans, P. W. J. M.; Vrakking, J. J. A. M. *Spectrochim. Acta, Part B* **1984**, *39B*, 1291.
(26) McLaren, J. W.; Mermet, J. M. *Spectrochim. Acta, Part B* **1984**, *39B*, 1307.
(27) Thomson, M.; Ramsey, M. H.; Coles, B. J. *Analyst (London)* **1982**, *107*, 1286.
(28) Batal, A.; Mermet, J. M. *Spectrochim. Acta, Part B* **1981**, *36B*, 993.
(29) Govindaraju, K. *Geostand. Newsl.* **1984**, *8* (Special Issue), 1.
(30) McLaren, J. W.; Berman, S. S. *Spectrochim. Acta, Part B* **1985**, *40B*, 217.

RECEIVED for review June 12, 1986. Resubmitted January 16, 1987. Accepted January 16, 1987.

Continuous Infrared Spectroscopic Analysis of Isocratic and Gradient Elution Reversed-Phase Liquid Chromatography Separations

John J. Gagel and Klaus Biemann*

Department of Chemistry, Massachusetts Institute of Technology, Cambridge, Massachusetts 02139

A method is described for the continuous recording of infrared spectra of the components of mixtures separated by reversed-phase high-performance liquid chromatography (HPLC) operated in the isocratic or gradient mode. The solvent from a microbore HPLC is continuously sprayed onto and evaporated from a rotating reflective surface by a heated gas nebulizer. The deposited solute provides a continuous record of the chromatographic separation, which is then analyzed by reflectance–absorbance spectroscopy while the reflective disk is again rotated in the sample compartment of a Fourier transform infrared spectrometer. The analysis of closely eluting isomers and a spectrum of a 31-ng injection of phenanthrenequinone obtained by using this method are shown. Since the solvent evaporation rate is dependent on the nebulizer gas temperature, less volatile solvents require higher temperatures and gradient elution separations require adjustment of the temperature during the run. Therefore, the gas heater temperature is programmed by a microprocessor for the deposition of mixtures separated by gradient elution.

The continuous recording of infrared spectra of components eluting from a high-performance liquid chromatograph (HPLC) requires the removal of the contributions of the mobile phase either by spectral subtraction or by evaporation of the solvent before analysis of the solute. The design of an interface for use with organic solvents common to normal-phase HPLC has been possible since these may be judiciously chosen to provide regions of IR transparency when used with flow cells (*1, 2*) or can be evaporated during or after deposition on conventional infrared sampling media such as KBr (*3, 4*). The use of aqueous solvents in the commonly employed reversed-phase mode of HPLC, however, further complicates either design because water absorbs strongly over broad regions of the infrared, is of comparatively low volatility, and readily dissolves KBr. To extend methods originally developed with normal-phase solvents, an additional step of solute transfer from aqueous to IR-compatible solvents may be incorporated after separation but before spectroscopic analysis. Griffiths et al. (*5*) reported the on-line extraction of reversed-phase solvents with dichloromethane similar to that developed for moving-belt HPLC–mass spectrometry (*6*) before deposition onto KBr in a train of diffuse–reflectance (D–R) sample cups. Taylor et al. (*7*) used a similar process before analysis by flow cell. Kalasinsky et al. (*8*) prefer a postcolumn conversion of water to methanol and acetone by reaction with 2,2-dimethoxypropane before deposition and analysis by D–R, while Wilcox et al. (*9*) used a solid-phase extraction method for discretely collected HPLC fractions to obtain the solute in IR-compatible solvents before D–R. All these methods not only added complexity but also reduced sensitivity when compared to operation with normal-phase solvents.

More recent work has been directed toward eliminating the solvent-transfer step by evaporating aqueous solvents and directly depositing the sample onto a compatible sampling media. Jinno et al. (*10*) developed a method by which the effluent from a capillary HPLC column is flowed onto a stainless steel wire net (SSWN) from which the solvent is eliminated by a heated gas flow. This technique relies on

0003-2700/87/0359-1266$01.50/0 © 1987 American Chemical Society

material being suspended between the metal meshing, and the deposits are analyzed in the transmission mode. Azarraga et al. (*11*) have reported preliminary experiments using an ultrasonic nebulizer, which facilitates desolvation of HPLC effluent before being deposited onto diamond powder and analyzed by D–R.

Recently we have reported (*12*) the development of another method of HPLC–IR in which effluent from a microbore HPLC is continuously sprayed onto a rotating reflective surface. After elimination of the solvent, the solute remains on the disk as a record of the chromatographic separation and can be analyzed by reflectance–absorbance (R–A) infrared spectroscopy. The objectives of this design are to provide a continuous analysis of the chromatographic separation with good sensitivity on a sampling medium impervious to normal or reversed-phase solvents. The work below reports the use of this method with aqueous solvents employing a new nebulizer capable of depositing and quickly eliminating the mobile phase.

EXPERIMENTAL SECTION

I. Chromatography. A Brownlee (Santa Clara, CA) Model MPLC dual-syringe micro HPLC pump capable of isocratic flow rates as low as 1 μL/min and gradients down to 10 μL/min was used at a flow rate of 30 μL/min for all the separations discussed below. The system is equipped with a Rheodyne (Cotati, CA) Model 7410 internal loop injector with a 1-μL loop volume. Ultraviolet absorbance detection is accomplished with a Jasco (Easton, MD) Model Uvidec-100-V detector with a 1-μL volume, 5-mm path length flow cell set to 254 nm. All separations were performed on an Alltech (Deerfield, IL) 1-mm i.d., 25-cm-long microbore HPLC column with 5-μm C_{18} packing. Water used in the mobile phase was purified by using a Milli-Q (Waters Associates, Milford, MA) purification system. Methanol and dichloromethane were HPLC or UV grade from various manufacturers.

II. Spectroscopy. Infrared data were obtained by using a Digilab (Digilab division of Bio-Rad Inc., Cambridge, MA) Model FTS-15/90E Fourier transform infrared spectrometer (FTIR). Continuously collected data were obtained with software intended for gas chromatography (GC)–FTIR which coadded eight scans at 8 cm^{-1} resolution before transforming to give a time resolution of 1.5 s and the R–A spectra shown below are a result of this analysis with the disk in motion. Gram–Schmidt chromatograms were generated by using reference vectors from a blank spot on the disk's surface ahead of or during the deposition. Wavelength chromatograms are produced by software that monitors absorbance at a user-specified frequency throughout the chromatogram or any portion thereof. Spectra of HPLC deposits may be background subtracted by using spectra of blank spots on the disk adjacent to the deposit. Base line correction software used successive linear least-square regessions to find the base line slope (*13*) and then subtracted this best fit line from the spectrum.

In the earlier part of this work (e.g., naphthalenediol experiments), a wide-band mercury/cadmium/telluride (MCT) detector was used. In order to reduce stray light arising from a beam size larger than the sample deposit, an iris aperture that could be closed to narrow the beam was placed in the sample compartment before the reflectance accessory and a more sensitive, narrow-band MCT detector was installed. At the same time, the 1-mm-thick by 60-mm-diameter aluminum front surface mirrors used for the deposition surface were replaced by 3-mm × 64-mm-diameter mirrors (Edmund Scientific, Barrington, NJ) to avoid the slight warping present in some of the thinner mirrors, which manifests itself as a gradual roll in Gram–Schmidt base lines or as an offset in spectral base lines. The sensitivity evaluation using phenanthrenequinone was carried out in this configuration.

Comparison spectra in KBr were measured after thoroughly grinding small amounts of the sample in KBr and pressing a pellet with a two-bolt minipress (Foxboro Co., South Norwalk, CT).

III. Continuous Collection/Detection Device. The collection device, motor drive system, and modified 3× beam condensing reflectance accessory were the same as described previously for the normal-phase experiments (*12*). The mirrors were cleaned before use by peeling the surface with Scotch tape to remove a protective overcoat as was recommended by the manufacturer and then by washing with lens cleaner. Background absorbance due to occasional incomplete removal of overcoat material could be compensated for by spectral subtraction.

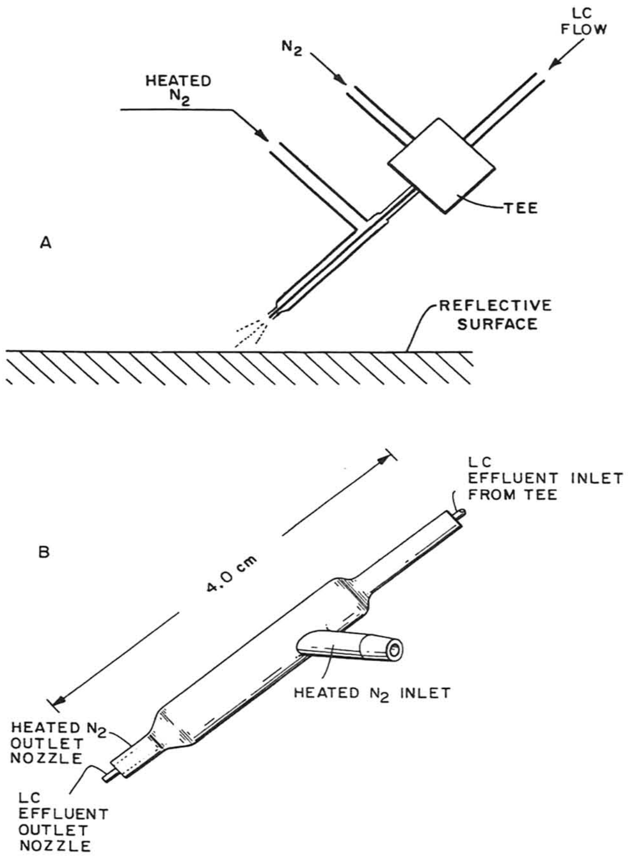
LC FLOW
N_2
HEATED N_2
TEE
A
REFLECTIVE SURFACE
B
4.0 cm
LC EFFLUENT INLET FROM TEE
HEATED N_2 INLET
HEATED N_2 OUTLET NOZZLE
LC EFFLUENT OUTLET NOZZLE

Figure 1. Schematic diagrams of the nebulizer: (A) during operation and (B) detailed view of the glass nebulizer design.

IV. Nebulizer Design. Since the deposition surface of the collection device is impervious to water, the direct deposition of reversed-phase HPLC effluent is possible if these less-volatile solvent mixtures can be adequately eliminated. Thus an improved nebulizer with capability for aqueous solvent elimination was built. In this design (Figure 1) the HPLC effluent is mixed with and pressurized by nitrogen gas in a high-pressure tee and directed to the deposition surface through a syringe needle fitted to one of the tee ports. The syringe needle is itself placed inside another nozzle through which heated nitrogen gas is flowed. This configuration allows the heated gas to warm both the HPLC effluent as it passes through the inner nozzle and the disk surface as it moves under the nebulizer and then finally to envelope the nebulized liquid as it emerges and is deposited. The high-pressure tee used to mix the internal nitrogen flow with the effluent was the same as that used for the normal-phase experiments (*12*). The syringe needle (SGE, Austin, TX) fitted to the tee port had a 0.64-mm o.d., 0.15-mm i.d., and was cut to extend about 4.5-cm beyond the tee. For the external heated nitrogen, flow nozzles were formed from 18-gauge Teflon shrink tubing or were made of glass. The Teflon nozzles were made by shrinking the last 5 mm of the tubing to a diameter of about 1 mm with a heat gun. The inner nozzle was placed inside the tube catheter-style by piercing the Teflon. The other end of the tubing was connected to the gas heater. The glass nozzles used (Figure 1B) were tee shaped with one neck designed to fit snugly over the inner nozzle where it was held in place by epoxy and the parallel neck serving as the nozzle outlet with an inside diameter of about 1 mm. The final neck of the tee was connected to the gas heater via Teflon tubing. Rates for both internal and external flows were controlled with Allborg (Monsey, NY) flow tubes and metering valves. Typical rates for the internal flow were about 40 mL/min and the external flow was much higher, about 2400 mL/min. The inner nozzle extended several millimeters beyond the end of the external nozzle and the nebulizer unit was mounted such that the effluent would be sprayed at an angle of 45° off normal and about 3 mm above the disk surface. For these experiments the outer nozzle rested upon the top of the inner. This created a flow pattern which caused effluent to form a small jet and be sprayed into a narrow (0.5–1.5 mm) region on the disk.

The gas heater consisted of $^{1}/_{8}$-in. copper tubing coiled around a 70-W block heater (Hewlett-Packard, Palo Alto, CA). For the isocratic separations, the block heater power was controlled with a variable transformer and adjusted to raise the temperature of the gas to the level sufficient to eliminate the solvent rapidly as it contacted the disk. This rapid elimination is required to prevent pools of solvent from forming, which could either be blown about by the force of the external nitrogen flow or cause mixing of separated components. The gas temperature was kept below the point where all the solvent was eliminated before reaching the disk to avoid formation of dry particles, which might not adhere to the surface. Too much heat could also cause premature evaporation of the solvent in the needle, which would clog.

V. Gradient Elution. From the isocratic experiments it was evident that less volatile solvent mixtures required higher gas temperatures and for a continuously varying composition in a gradient elution separation the gas temperature would have to be varied during the chromatogram. This automated control was achieved by connecting the block heater to the auxiliary heater terminals of a Hewlett-Packard Model 5880 gas chromatograph. The thermocouple feedback for the temperature controller circuit was placed between the copper coils of the gas heater the temperature of which could then be automatically controlled by the programmed settings of the GC data station.

In this experiment the mobile phase was pumped at its initial composition while the gas temperature was brought to its initial temperature. When the starting conditions were reached, the sample was injected and both the solvent and temperature programs were initiated. The solvent composition was linearly varied from 55% to 5% water in methanol in 30 min and, after a delay corresponding to the chromatographic void volume, the temperature of the coils was reduced such that the gas temperature varied from about 80 to 40 °C (as was measured in a separate experiment at the exit end of the external nozzle) over the same time period. Although useful in these preliminary experiments this mode of operation was not ideal because the heater relied on convectional cooling of the coils to lower the temperature and the temperature controller utilized on an on/off circuit, which causes the gas temperature to swing about the setpoint. The response and accuracy of the gas temperature could also be improved with a heater in which the gas flows directly over a resistive heating element.

VI. Test Mixtures. A solution of a mixture of naphthalenediols (Aldrich Chemical Co., Milwaukee, WI) was prepared in methanol at the following concentrations: 2,6-dihydroxynaphthalene, 0.51 mg/mL; 1,5-dihydroxynaphthalene, 0.50 mg/mL; 2,7-dihydroxynaphthalene, 0.49 mg/mL; 1,3-dihydroxynaphthalene, 0.52 mg/mL; and 2,3-dihydroxynaphthalene, 0.56 mg/mL. One microliter of the solution was injected to generate the data shown in Figures 2–6.

For the sensitivity experiment a stock solution of phenanthrenequinone (Aldrich) was prepared in methanol/dichloromethane (1:1) at 0.990 mg/mL, diluted to 0.248 mg/mL with methanol, and then serially diluted to produce solutions of 0.124, 0.062, 0.031, and 0.016 mg/mL. Starting with the most dilute solution, 1 μL of each of the five dilutions was injected at 3-min intervals.

The mixture used for the gradient elution experiment contained the following: caffeine (Aldrich), 0.525 mg/mL; 2,7-dihydroxynaphthalene (Aldrich), 0.550 mg/mL; carbazole (Chem Service, West Chester, PA), 0.430 mg/mL; phenanthrenequinone (Aldrich), 0.500 mg/mL; anthrone (Aldrich), 0.485 mg/mL; 9-nitroanthracene (Aldrich), 0.490 mg/mL; and anthracene (Chem Service) 0.555 mg/mL in methanol/dichloromethane (1:1). One microliter of this solution was injected to produce the data in Figures 9–12.

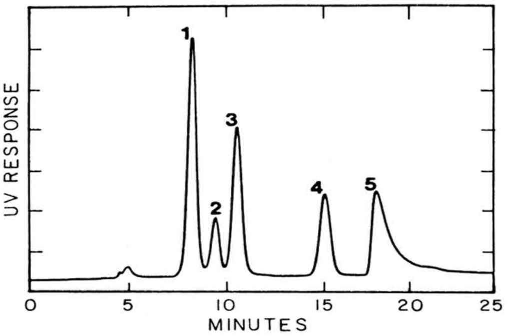

Figure 2. Chromatogram recorded at 254 nm of the microbore HPLC separation of a five component mixture of naphthalenediols with 55% water in methanol as the mobile phase. Peak identities are given in Table I.

Table I. Composition of the Naphthalenediol Mixture (Figures 2 and 3)

peak no.	compound	amt injected, ng
1	2,6-dihydroxynaphthalene	510
2	1,5-dihydroxynaphthalene	500
3	2,7-dihydroxynaphthalene	490
4	1,3-dihydroxynaphthalene	520
5	2,3-dihydroxynaphthalene	560

RESULTS AND DISCUSSION

The new nebulizer configuration was tested with a mixture of naphthalenediol isomers. This mixture was selected because it represented a challenging separation from the standpoint of chromatographic resolution—the first and third peak are separated by only 2.5 min—and because a fairly nonvolatile reversed-phase solvent composition of 55% water in methanol was employed as the mobile phase. Furthermore, the ability to differentiate positional isomers on aromatic rings is an important feature of infrared spectroscopy. In Figure 2 the UV chromatogram of this mixture is shown to be compared with Figure 3, the Gram–Schmidt infrared chromatogram taken after deposition. The ability of the system to maintain the chromatographic resolution and detect the deposits in the infrared analysis relies on the rapid elimination of solvent by the nebulizer, which prevents mixing of the components in solvent pools on the disk and leaves the solute in neat narrow packets. The infrared resolution is also influenced by the speed at which the deposition surface rotates and by the diameter of the infrared beam. A narrower beam would have a number of advantages: the components could be more closely spaced, allowing lower disk speeds and therefore longer chromatograms; the components could be deposited over a smaller area resulting in increased sensitivity.

Figures 4–6 compare the R–A spectra of the first three components of the naphthalenediol separation with the spectra of the same compound in a KBr pellet. The O–H stretching region of the R–A spectra show a broadening, which could be attributed to intermolecular hydrogen bonding, and Figure 6 shows a free O–H stretching band not present in the KBr spectrum. Factors that could contribute to spectral differences between R–A and the standard KBr data include interactions between the sample and the deposition surface, retention of residual traces of water by polar compounds, frequency and intensity shifts dependent on the variables of reflectance spectroscopy, light scattering, and the polymorphic nature of the solid sample. However, inspection of Figures 4–6 shows that, for these polar compounds, good qualitative comparison is still possible despite some relative intensity differences and

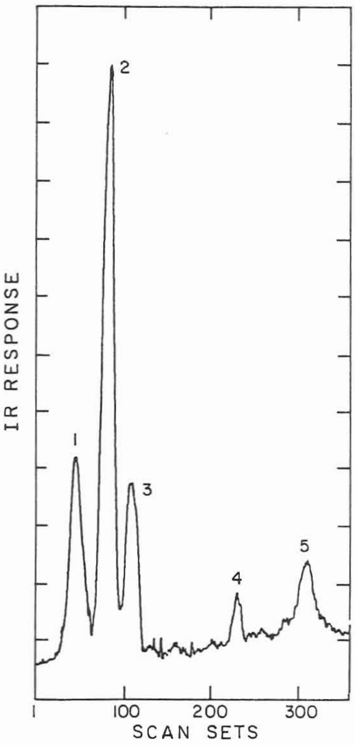

Figure 3. Gram–Schmidt infrared chromatogram of the five-component mixture in Figure 2 after depostion onto the reflective surface at a speed of 7 mm/min. The peak identities and amounts injected are given in Table I.

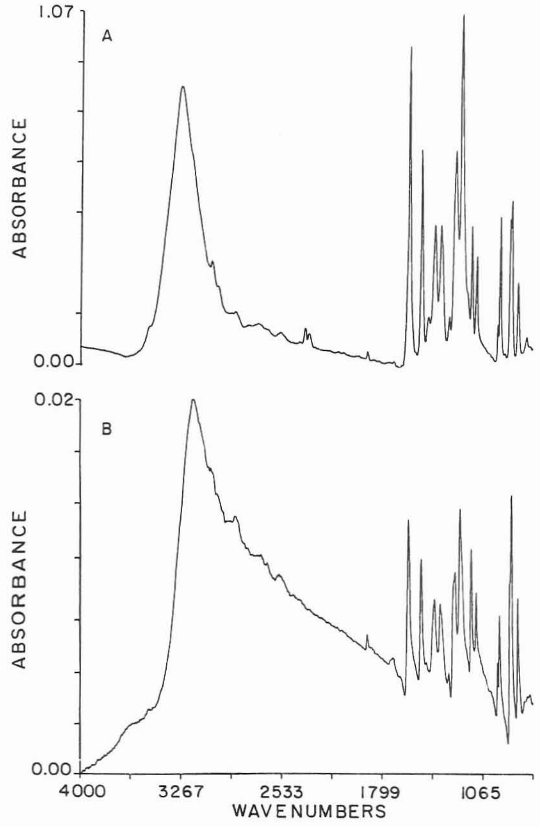

Figure 4. Infrared spectra of 2,6-dihydroxynaphthalene: (A) transmission spectrum taken in a KBr pellet and (B) R–A spectrum from peak 1 in Figure 3.

base line curvature. Furthermore, the out-of-plane bending region below 1000 cm^{-1} compares sufficiently well with the KBr data to be used for isomer differentiation.

To determine the sensitivity of this method, increasing amounts of phenanthrenequinone were injected and deposited. Figure 7 shows the wavelength chromatogram monitoring absorbance due to the C=O stretching frequency at 1678 cm^{-1}. It demonstrates that the deposit from a 16-ng injection can be detected. However, to obtain a complete spectrum exhibiting useful characteristic absorbances of the compound, 31 ng has to be injected (Figure 8). This sensitivity represents

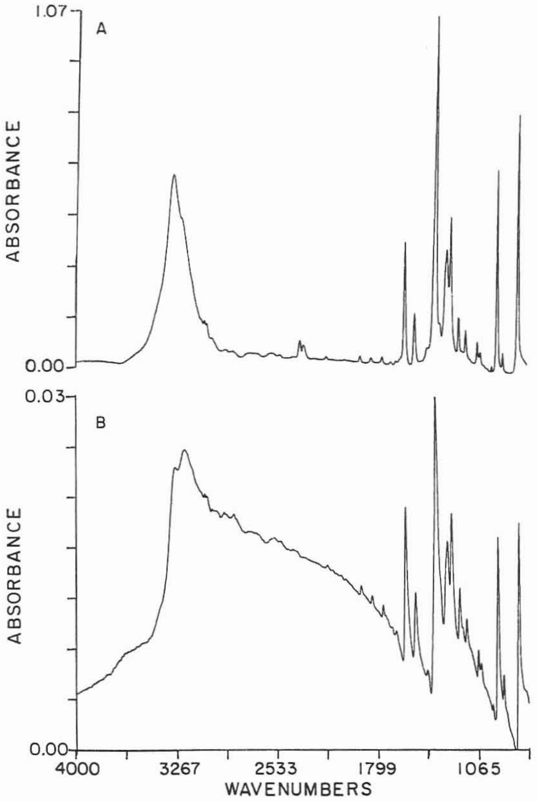

Figure 5. Infrared spectra of 1,5-dihydroxynaphthalene: (A) transmission spectrum taken in a KBr pellet and (B) R–A spectrum from peak 2 in Figure 3.

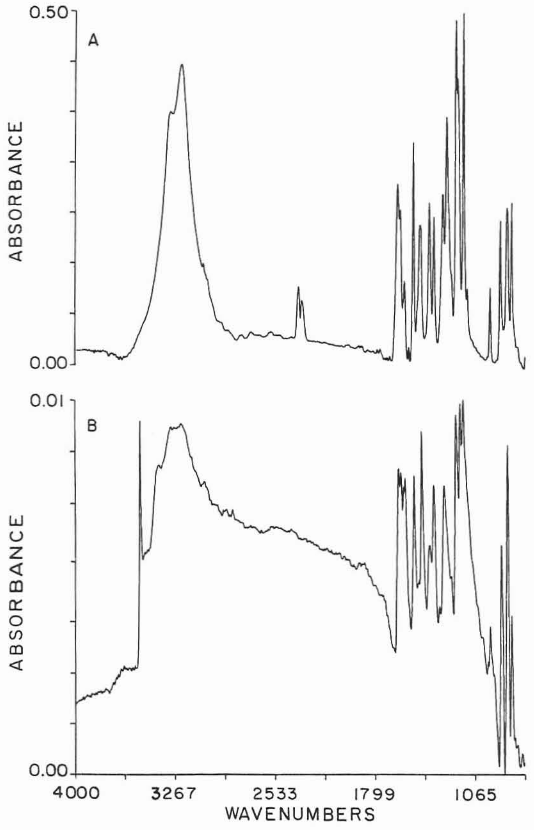

Figure 6. Infrared spectra of 2,7-dihydroxynaphthalene: (A) transmission spectrum taken in a KBr pellet and (B) R–A spectrum from peak 3 in Figure 3.

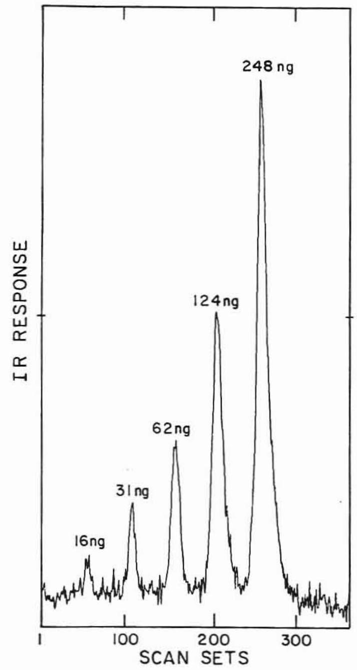

Figure 7. Wavelength chromatogram at 1678 cm^{-1} from five successive injections of phenanthrenequinone deposited from 29% water in methanol at a disk speed of 4 mm/min. Weights shown are the amounts injected.

Table II. Composition of the Gradient Elution Test Mixture (Figures 9 and 10)

peak no.	compound	amt injected, ng
1	caffeine	525
2	2,7-dihydroxynaphthalene	550
3	phenanthriquinone	500
4	carbazole	430
5	anthrone	485
6	9-nitroanthracene	490
7	anthracene	555

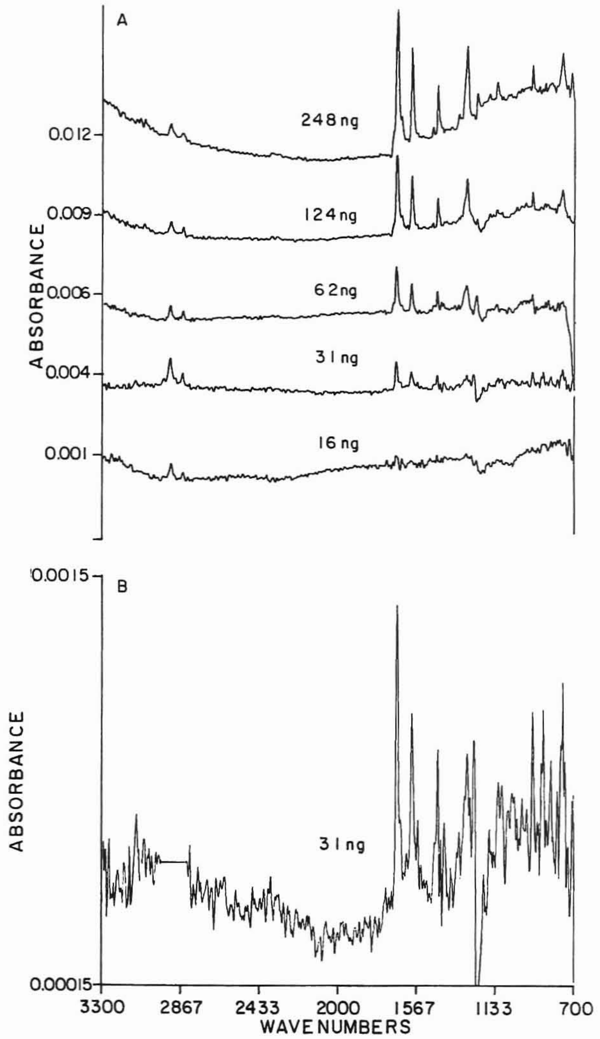

Figure 8. Infrared spectra of phenanthrenequinone: (A) spectra obtained for the five deposits detected (Figure 7) and (B) expanded view of the 31-ng deposit. Note that aliphatic C–H stretching bands in (A) arise from an impurity and have been omitted from (B) for clarity.

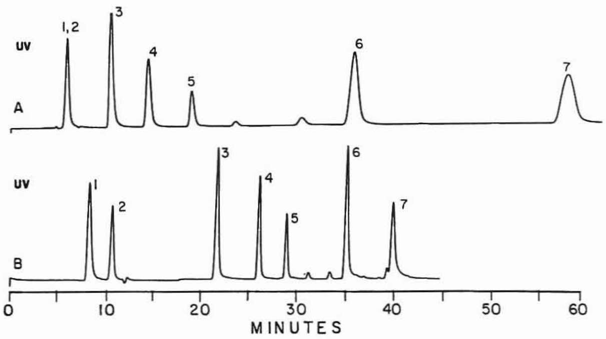

Figure 9. Separation of a seven-component mixture recorded at 254 nm: (A) isocratic elution with 29% water in methanol as the mobile phase; (B) linear gradient elution from 55% water to 5% water in methanol over 30 min. Peak identities and amounts injected are listed in Table II.

a considerable improvement over previous reversed-phase HPLC/IR methods. Griffiths et al. (*5*) obtained a spectrum of a 250-ng injection of butter yellow and sudan red by using the on-line extraction interface and Kalasinsky (*8*) reported the spectrum of a 1-μg injection of caffeine with the on-line reaction of water and 2,2-dimethoxypropane. Both of these systems used the noncontinuous D–R collection station. Jinno (*10*) reported a spectrum of 500 ng of carbaryl obtained by using the stainless steel wire net interface, and the preliminary experiments of Azarraga (*11*) produced spectra of 3 μg of *m*-nitroaniline and 2-methyl-3-nitrophenol after desolvation with the ultrasonic nebulizer and D–R analysis on diamond powder. For flow cells the sensitivity is lower than the sample deposition systems.

Taylor (*7*) required on the order of 300 μg/component for flow cell analysis after solvent extraction and results from an ATR interface, which flows aqueous solvent around the internal reflectance crystal, reported spectra from milligram injections (*14*). Jinno et al. (*2, 15*) achieved submicrogram detection limits by using D_2O and deuteriated acetonitrile as the mobile phase and a short path length Teflon flow cell. However, large portions of the spectrum still remained opaque due to absorbance of the solvent and the flow cell material. As mentioned earlier, the sensitivity of the method reported here could be enhanced by depositing the sample in a smaller spot, slowing collection speeds, and more powerful beam condensing. Griffiths (*16, 17*), using an IR microscope for beam condensing, has recently obtained good spectra of narrow deposits from GC, normal-phase HPLC, and supercritical fluid chromatography (SFC) onto KBr for transmission or metal surfaces for reflectance.

An important requirement for any practical HPLC–IR system is the ability to analyze mixtures that need gradient elution for efficient separation. To test our method for the capability to analyze gradient separations, a mixture of compounds with varying functionality and polarity was prepared. The peak identities and amounts injected are given in Table

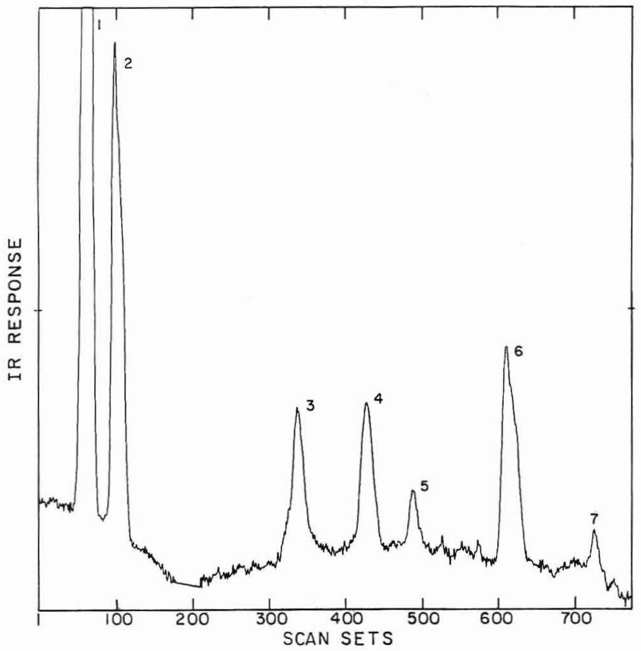

Figure 10. Gram–Schmidt infrared chromatogram recorded after the deposition of the gradient elution separation of the seven-component mixture (Figure 9B).

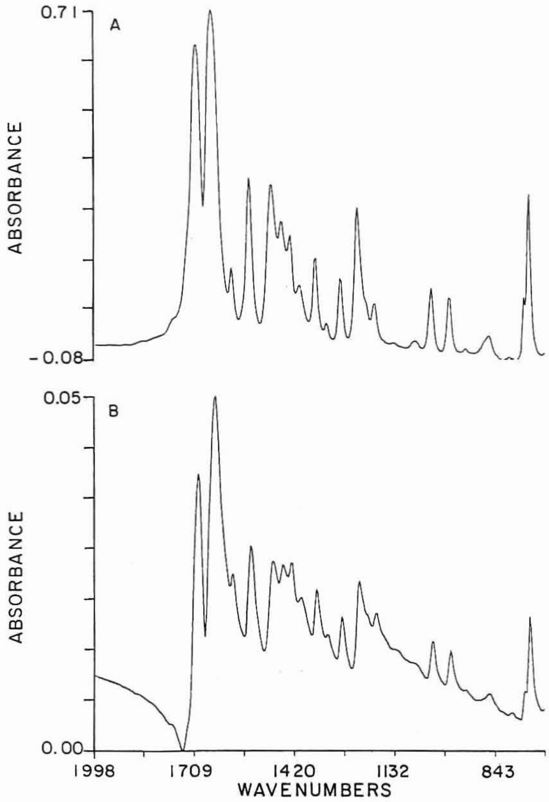

Figure 11. Infrared spectra of caffeine in the region from 1998 to 698 cm^{-1}: (A) transmission spectrum taken in a KBr pellet and (B) R–A spectrum from peak 1 in Figure 10.

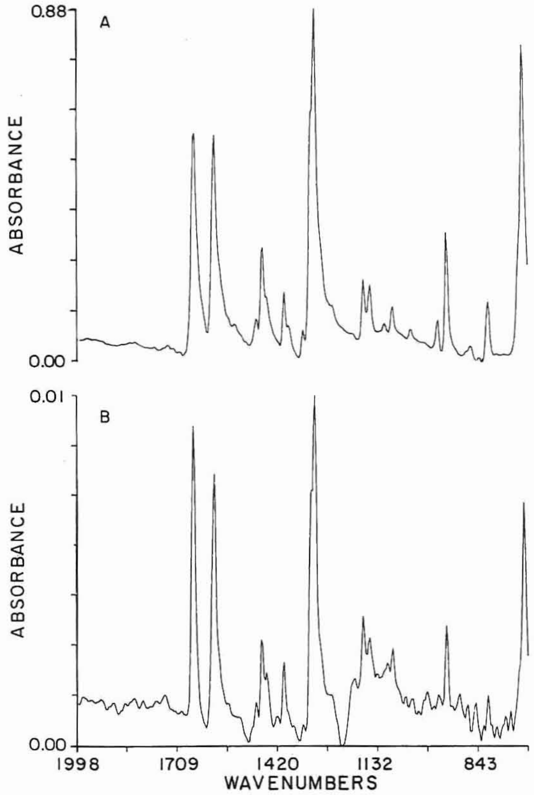

Figure 12. Infrared spectra of anthrone in the region from 1998 to 698 cm^{-1}: (A) transmission spectrum taken in a KBr pellet and (B) R–A spectrum from peak 5 in Figure 10.

II. Figure 9 shows the chromatogram of this mixture recorded with a UV detector, separated under isocratic conditions (9A) and with a linear gradient from 55% to 5% water in methanol in 30 min (9B). The isocratic separation with 29% water in methanol is inefficient because components 1 and 2 are not resolved and the last component elutes only after 1 h and as a broad peak. The gradient separation, however, completely resolves all seven components, reduces the analysis time, and elutes the last component as a well-shaped peak. The effluent of the gradient separation was deposited on the reflective surface by elimination of the continuously changing solvent mixture made possible by programming the gas temperature, which is under computer control during the chromatogram. In Figure 10 the Gram–Schmidt chromatogram of the gradient deposit is shown and it compares well with the UV chromatogram in Figure 9B. Figures 11 and 12 represent the R–A spectra from the first component, caffeine, and the fifth component, anthrone, respectively, compared to the spectrum of the same compound in KBr.

CONCLUSION

The use of a rotating reflective surface as a deposition and sampling medium with a heated gas nebulizer has been demonstrated with isocratic and gradient reversed-phase separations. The ability to rapidly eliminate the less volatile aqueous solvents allows the resolution of closely eluting components and leaves the solute in narrow packets that provide good sensitivity for IR analysis by R–A.

ACKNOWLEDGMENT

The authors thank K. Krishnan of the Digilab division of Bio-Rad for the loan of the reflectance accessory used in these experiments.

LITERATURE CITED

(1) Brown, R. S.; Taylor, L. T. *Anal. Chem.* **1981**, *53*, 197.
(2) Taylor, L. T. *J. Chromatogr. Sci.* **1985**, *23*, 265.
(3) Kuehl, P.; Griffiths, P. R. *J. Chromatogr. Sci.* **1979**, *17*, 471.
(4) Jinno, K.; Fujimoto, C.; Hirata, Y. *Appl. Spectrosc.* **1982**, *36*, 67.
(5) Conroy, C. M.; Griffths, P. R.; Duff, P. J.; Azarraga, L. V. *Anal. Chem.* **1984**, *56*, 2636.
(6) Karger, B. L.; Kirby, D. P.; Vourous, P.; Foltz, R. L.; Hidy, B. *Anal. Chem.* **1979**, *51*, 24.
(7) Johnson, C. C.; Hellgeth, J. W.; Taylor, L. T. *Anal. Chem.* **1985**, *57*, 610.
(8) Kalasinsky, K. S.; Smith, J. A. S.; Kalasinsky, V. F. *Anal. Chem.* **1985**, *57*, 1969.
(9) Wilcox, C. D.; Phelan, R. M. *J. Chromatogr. Sci.* **1986**, *24*, 130.
(10) Fujimoto, C.; Oosoka, T.; Jinno, K. *Anal. Chim. Acta* **1985**, *178*, 159.
(11) Castles, M. A.; Azarraga, L. V.; Carreira, L. A. *Appl. Spectrosc.* **1986**, *40*, 673.
(12) Gagel, J. J.; Biemann, K. *Anal. Chem.* **1986**, *58*, 2184.

(13) Goehner, R. P. *Anal. Chem.* **1978**, *50*, 1223.
(14) Sabo, M.; Gross, J.; Wang, J. S.; Rosenberg, I. E. *Anal. Chem.* **1985**, *57*, 1822.
(15) Jinno, K.; Fujimoto, C. *Chromatographia* **1983**, *17*, 259.
(16) Griffiths, P. R. Presented at the Digilab users meeting, Cambridge, MA, June 1986.
(17) Pentoney S. L., Jr.; Shafer, K. H.; Griffiths, P. R. *J. Chromatogr. Sci.* **1986**, *24*, 230.

RECEIVED for review October 27, 1986. Accepted January 20, 1987. The work reported here was supported by grants from the National Institutes of Health (ESO-1640 and ESO-2109).

Detection and Quantification of Picogram Amounts of Macrocyclic Trichothecenes in Brazilian *Baccharis* Plants by Direct Chemical Ionization Tandem Mass Spectrometry

Thaiya Krishnamurthy* and Emory W. Sarver

Research Directorate, Chemical Research, Development, and Engineering Center,
Aberdeen Proving Ground, Maryland 21010-5423

Roridins and baccharinoids are macrocyclic trichothecenes. They formed $(M + NH_4)^+$ adducts with ammonia effectively under chemical ionization conditions. The daughter spectra of these adducts were characteristic of the macrocyclic ester bridges and indicate several common neutral losses. Experiments designed for the simultaneous detection of these macrocyclic trichothecenes by sequentially monitoring their characteristic daughter ions and the corresponding parent spectra were found to be applicable for the analysis of Brazilian *Baccharis* plants. The compounds detected in these samples were accurately quantified by use of a synthetically modified macrocyclic trichothecene, 8-ketoverrucarin A, as the internal standard. The minimum detectable limits of roridins and baccharinoids under various experimental conditions used for their detection and quantification were measured to be 10–100 pg.

Macrocyclic trichothecenes are polar, toxic molecules originated from several species of fungi such as *Myrothecium*, *Stachybotrys*, etc. (*1–3*). They are di- and triesters of unsubstituted simple trichothecenes such as verrucarols or oxygenated verrucarols (*1–4*). The diesters are termed roridins, satratoxins, or baccharinoids depending on the structural features of the verrucarol and ester moieties (*4*). The triesters are known as verrucarins (*4*). In general, these molecules have been found to be the most toxic of all known trichothecenes (*1–6*). However, some of the macrocyclic trichothecenes (baccharinoids) with substituents at the A ring (Figure 1) possess strong antileukemic properties (*4*).

These toxic compounds are detected and isolated primarily from environmental and agricultural samples and fermentation broths. However, recently a few toxic roridins along with some biologically active baccharinoids have been isolated from *Baccharis megapotamica* plants in Brazil (*4, 7*). It is postulated that the former compounds are transformed into the latter under chemical or microbial conditions (*4, 5*). Similar results are observed with the verrucarins as well (*4, 5*). Presence of the toxic roridins in the *Baccharis* plants was originally recognized by the death of cattle feeding on the plants in Brazil (*4*). Extensive investigations by Jarvis et al. have led to the isolation of several roridins and baccharinoids from the *Baccharis megapotamica* plants and their characterization (*4*).

Loss of livestock due to the ingestion of fungi infested feed has been recognized and documented for decades (*1–12*). Recently several cases of human health problems have also been attributed to these macrocyclic trichothecenes (*12–15*). Development of rapid, specific, and sensitive methods for the analysis of toxic macrocyclic trichothecenes has become essential to prevent economic loss and health hazards. It is also required to check for the presence of toxic roridins in purified samples of baccharinoids. However, the methodologies for the analysis of any of these macrocyclic trichothecenes were virtually unknown until recently (*16, 17*).

Direct analysis of these trichothecenes by gas chromatography/mass spectrometry (GC/MS) is impossible because of the presence of polar, labile ester bridges in the molecules. Some macrocyclic trichothecenes have been converted into their trimethylsilyl derivatives, separated by capillary GC column, and analyzed by a mass spectrometric method (*16*). The detection limits of these molecules under the selected ion monitoring mode are reported to be 1–100 ng (*16*). A gas chromatography/negative ion chemical ionization mass spectrometry (GC/NICI-MS) method based on the alkaline hydrolysis of the molecules, followed by conversion of the hydrolysate (verrucarols) into their hepatafluorobutyryl (HFB) derivatives and GC/MS analysis of the HFB esters has been reported (*17*). This method, despite being useful in the simultaneous detection of several macrocyclic trichothecenes with excellent sensitivity, provides only the identities of the verrucarol moieties and not of the ester bridges.

We have reported earlier that several macrocyclic trichothecenes form negatively charged molecular ions (M^-) more effectively than the positively charged protonated molecules under chemical ionization (methane) conditions (*18*). When the M^- ions are subjected to collisionally activated dissociation, daughter ions characteristic of the ester brides are detected (*18*). A direct, negative chemical ionization MS/MS method developed for the analysis of satratoxins is applicable in the analysis of *Stachybotrys* atra fermentation samples (*19*).

We now report a direct, rapid, selective, and sensitive chemical ionization (DCI)-MS/MS method of analysis to detect baccharinoid-4 and baccharinoid-5 in the presence of

This article not subject to U.S. Copyright. Published 1987 by the American Chemical Society

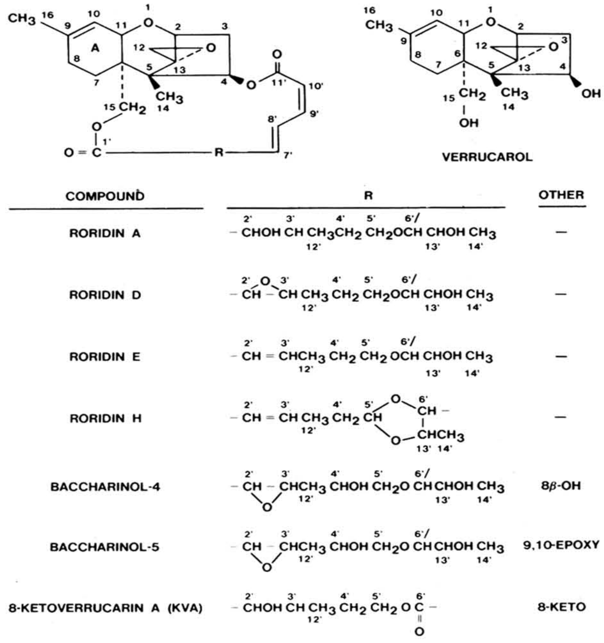

Figure 1. Macrocyclic trichothecenes.

four frequently observed toxic roridins. Mixtures of roridins and baccharinoids are subjected to chemical ionization in the presence of ammonia followed by the sequential collisionally activated dissociation of the specific $(M + NH_4)^+$ adducts using argon. Experimental conditions developed for the simultaneous analysis of these molecules, by detecting their specific daughter ions and their associated parent ions during a single analysis, are applicable for the analysis of several Brazilian *Baccharis* plant samples. A synthetically modified macrocyclic trichothecene (*7*), 8-ketoverrucarin A (KVA), was used as the internal standard for the accurate quantification of the detected compounds.

EXPERIMENTAL SECTION

All chemical ionization and collisionally activated dissociation (CAD) experiments were conducted with a Finnigan-MAT TSQ triple quadrupole mass spectrometer. Pure standards of roridins and baccharinoids and *Baccharis* plant extracts were generously donated by Bruce B. Jarvis, Department of Chemistry, University of Maryland, CollegePark, MD. Standard solutions were prepared by using glass-distilled methanol and stored at 0 °C in Reacti-vials fitted with Mininert valves (Supelco, Inc.).

Analysis of Standards and *Baccharis* Plant Samples. One microliter of standard mixture (solution) was loaded on the direct exposure probe (DEP) filament and evaporated. The DEP was introduced into the mass spectrometer and the sample was subjected to CI using ammonia with a source temperature and pressure of 100 °C and 0.45 torr, respectively. The probe was heated from the initial temperature of 140 to 270 °C at a rate of 200 °C/s. The $(M + NH_4)^+$ adducts were dissociated in the collision chamber using argon at a pressure of 2.0–2.3 and 1.0 mtorr for the daughter spectra and parent spectra experiments, respectively. The collision energies were maintained at 15 eV. The *Baccharis* plant samples along with the internal standard (KVA) were also analyzed under identical conditions.

RESULTS AND DISCUSSION

Roridins and baccharinoids under CI conditions produced the M^- ions preferably (at least 1 order of magnitude more) over the positively charged protonated molecules in the presence of all common CI reagent gases except ammonia. However, these molecules produced both M^- and $(M + NH_4)^+$ ions with almost equal efficiency, when ammonia was used as the reagent gas. The relative abundances of the M^- and the $(M + NH_4)^+$ with respect to their corresponding total ion intensities were also similar. Optimum conditions for heating the sample in the source were determined by introducing the individual standards (50 ng) into the source via a direct exposure probe and heating the probe at a rate of 10 °C/s in the presence of ammonia (CI) and recording their positive ion chemical ionization (PICI) spectra. Careful analysis of the reconstructed ion chromatogram (RIC) and the spectral data was performed to determine the ideal temperature range in which the rate of ionization of the molecules exceeded their rate of thermal decomposition. Then each standard was introduced and analyzed under the same conditions, except the probe was heated rapidly at a rate of 100 °C/s over the temperature range characteristic of each compound, to increase the sensitivity. Later, when the mixture of all the compounds was analyzed, the initial (140 °C) and final (270 °C) temperatures of the probe and the rate of heating (200 °C/s) were adjusted to produce narrow, sharp peaks to increase sensitivity of detection with negligible decomposition of all the analytes. The optimum temperature ranges thus determined for individual molecules are listed in Table I.

Table I. Optimum CI and CAD Conditions[a]

compound	temp,[b] °C min	max	collision energy, eV $(M + NH_4)^+$	M^-
roridin A	135	230	15.0	18.0
roridin D	150	220	14.0	24.0
roridin E	140	200	14.0	19.0
roridin H	140	280	14.0	18.0
baccharinoid-4	175	270	14.0	21.0
baccharinoid-5	175	270	14.0	20.0

[a] Collision gas pressure, 2.30 mtorr. [b] Rate of heating, 100 °C/s.

The ammonium adduct ions thus produced were subjected to CAD in the presence of argon. Daughter spectra of individual compounds (50 ng) were recorded, at constant collision gas pressure of 2.3 mtorr, increasing the collision energy (12–30 eV) stepwise by 1 eV. The optimum collision energy for the compound was determined based on the relative abundances of the $(M + NH_4)^+$, $(M + H)^+$, and other most characteristic daughter ions. The optimum collision gas pressures for individual molecules were determined at the corresponding optimum collision energy measured earlier. The collision gas pressure was increased stepwise (0.2 mtorr) from 1.2 to 3.0 mtorr. The CAD conditions at which the measured ion intensity of the most abundant daughter ion was maximum and the relative abundance of the adduct ion was less than 50%, were determined. The experimentally determined optimum CAD conditions for obtaining the daughter spectra of $(M + NH_4)^+$ and M^- ions of all compounds are also listed in Table I. The positive CAD spectra of roridins and baccharinoid-4 and baccharinoid-5 are shown in Figures 2–5. The daughter spectra of the M^- ions are listed in Table II.

The mode of fragmentation of negatively charged molecular ions of some of the macrocyclic trichothecenes under CAD conditions has been described elsewhere in detail (*18*). The CAD spectra of the positively charged ammonium adducts and negative molecular ions of four toxic roridins and baccharinoid-4 and baccharinoid-5 were characteristic of the ester bridges. Most of the daughter ions seemed to be formed by the cleavages between C1′–O, C5′–O, O–C6′, C11′–O, or C10′–C11′ bonds. The positive and negative daughter spectra of the $(M + NH_4)^+$ and M^- ions of KVA, the intended internal standard, under the same conditions were recorded and the mode of fragmentation was found to be similar to that of the analytes. The daughter spectrum of the $(M + NH_4)^+$ ions of

Table II. Daughter Spectra of the M⁻ Ions of Roridins and Baccharinoids

compound	mol wt	m/z (% rel abundance)
roridin A	532	402 (35.8), 401 (100.0), 153 (19.6), 145 (69.8)
roridin D	530	530 (1.7), 417 (1.3), 401 (100.0), 359 (2.3), 349 (1.0), 193 (2.5), 175 (1.1), 153 (7.1), 151 (1.2), 149 (2.5), 145 (3.1), 135 (13.1), 127 (1.2)
roridin E	514	514 (14.9), 484 (7.0), 470 (2.1), 403 (71.4), 386 (3.4), 385 (17.2), 359 (100.0), 154 (6.2), 153 (20.3), 136 (10.7), 134 (3.8), 111 (8.1)
roridin H	512	512 (1.1), 468 (1.4), 403 (5.8), 401 (2.2), 387 (10.1), 385 (6.5), 359 (24.3), 219 (1.3), 175 (1.8), 153 (4.0), 137 (11.1), 125 (100.0), 109 (25.8)
baccharinoid-4	562	562 (3.8), 501 (10.1), 417 (100.0), 375 (2.4), 365 (29.9), 161 (1.4), 153 (19.9), 143 (12.8), 141 (1.2), 135 (12.9), 125 (12.2)
baccharinoid-5	562	562 (2.5), 501 (6.0), 417 (100.0), 375 (1.0), 365 (17.6), 279 (1.5), 161 (1.5), 153 (9.0), 135 (4.7), 125 (1.8)

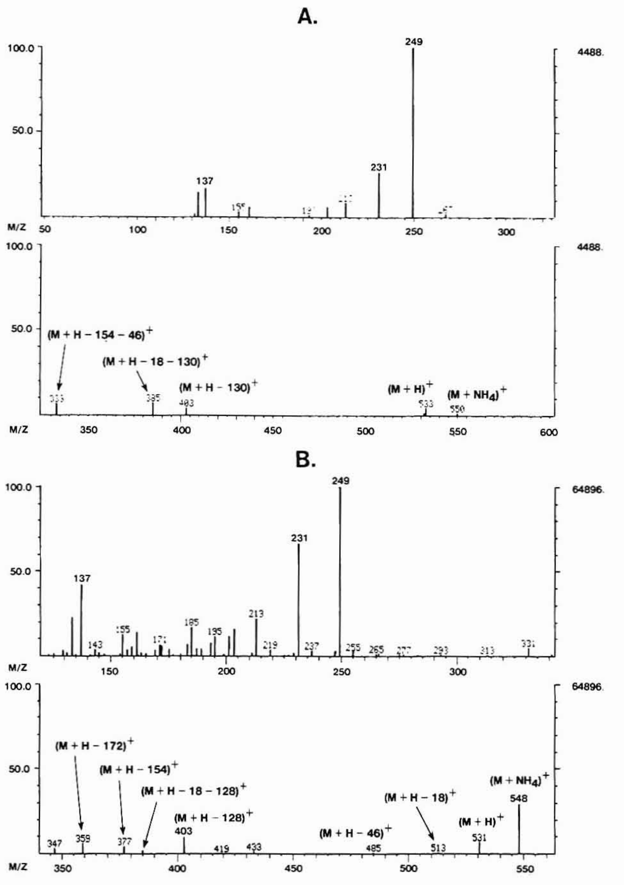

Figure 2. (A) Daughter spectrum of $(M + NH_4)^+$ ion of roridin A (m/z 550). (B) Daughter spectrum of $(M + NH_4)^+$ ion of roridin D (m/z 548).

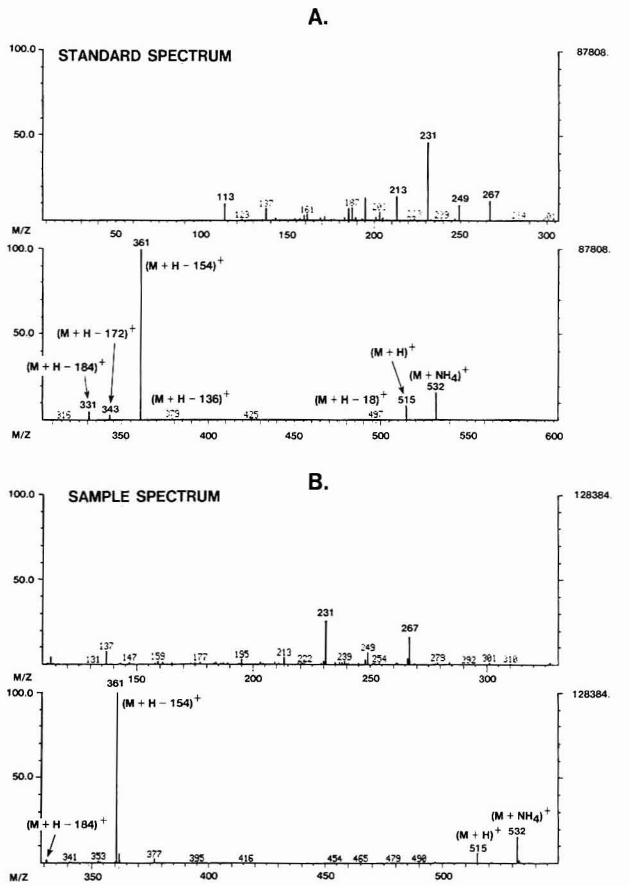

Figure 3. (A) Daughter spectrum of $(M + NH_4)^+$ ion of roridin E (m/z 532). (B) Daughter spectrum of m/z 532 in *Baccharis coridifolia* plant sample 15.

KVA is shown in Figure 6. Analysis of the positive ion daughter spectra of roridins and baccharinoids indicated some common daughter ions that could be used for the analysis of these compounds by daughter and parent mass spectral modes.

The three most intense daughter ions were chosen from both positive and negative ion CAD spectra of roridins and baccharinoids samples. Experiments (programs) listed in Table III were designed for the direct analysis and simultaneous confirmation of roridins and baccharinoids present in *Baccharis* plant sample extracts under both positive and negative CAD conditions. Initially, the standard mixture (1 μL) containing 25 ng of each standard was introduced into the source via direct exposure probe and subjected to chemical ionization in the presence of ammonia. The ammonium adducts of each compound were introduced into the collision chamber sequentially and dissociated with argon. Only three characteristic daughter ions of three compounds were sequentially monitored during a single analysis to improve the sensitivity. The plant extracts (1 μL) were also analyzed under the same conditions. The whole process was computer-controlled. The measured relative abundances and the sample

Table III. Screening Conditions for Roridins and Baccharinoids

expt	ions	compound	collision energy, eV	m/z setting	
				Q1[a]	Q3[b]
RS	positive	roridin A	15	550	137, 231, **249**
	positive	roridin D	14	548	137, 231, **249**
	positive	roridin E	14	532	231, 267, **361**
RB	positive	roridin H	14	530	137, 231, **359**
	positive	baccharinoid-4	14	580	137, 157, **247**
	positive	baccharinoid-5	14	580	201, 219, **247**
RN	negative	roridin A	18	532	135, 153, **401**
	negative	roridin D	24	530	135, 153, **401**
	negative	roridin E	19	514	385, 403, **359**
BN	negative	roridin H	18	512	109, 137, **125**
	negative	baccharinoid-4	19	562	135, 153, **417**
	negative	baccharinoid-5	20	562	153, 365, **417**

[a] Q1, quadrupole 1. [b] Q3, quadrupole 3.

Table IV. Sample (*Baccharis* Plants) Analysis Results

% RELATIVE ABUNDANCES OF DAUGHTER IONS (m/z)

SAMPLE	RORIDIN A			RORIDIN D			RORIDIN E			RORIDIN H			BACCHARINOID 4			BACCHARINOID 5		
	249	231	137	249	231	137	361	231	267	137	231	359	247	137	157	247	201	219
STANDARD	100	33.4	11.8	100	57.8	63.5	100	57.6	5.0	100	74.7	48.7	100	94.7	6.4	100	15.2	9.0
PLANT 1	100	40.9	25.9 *	43.6	100	81.4	100	7.1	3.8 d	100	21.4	—	—	100	—	13.9	27.3	100
PLANT 3	100	33.5	17.7 *	46.5	64.0	100	100	21.9	4.0 d	100	23.7	—	—	100	—	100	70.0	70.6 d
PLANT 4	100	29.6	16.8 *	72.2	70.3	100	100	23.8	23.0 d	100	0.6	—	100	22.4	8.5	100	23.9	15.1 *
PLANT 6	100	26.4	19.7 *	56.9	68.2	100	100	18.6	4.1 d	100	63.2	—	—	100	3.5	100	55.2	77.3
PLANT 10	82.3	50.5	100	100	10.7	55.4 d	100	39.5	42.9 d	100	0.1	—	100	14.0	11.4	100	26.0	7.2 *
PLANT 13	100	35.7	22.9 *	66.9	77.2	100	100	21.9	16.1 d	100	82.2	15.1	22.6	100	—	13.8	60.5	100
PLANT 15	100	29.6	16.9 *	72.6	70.8	100	100	24.2	23.1 *	69.7	100	—	55.0	100	—	9.6	61.8	100

* PRESENCE

d DOUBTFUL

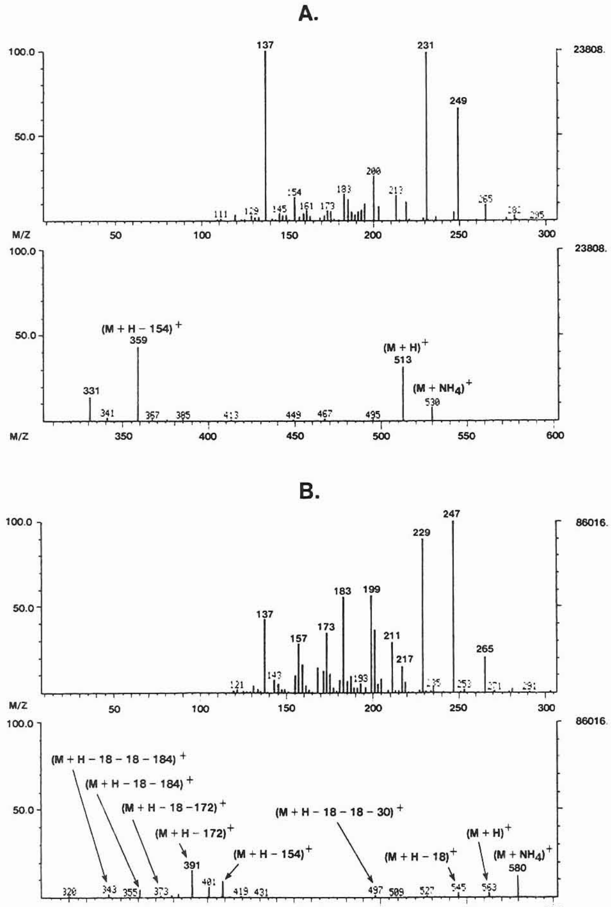

Figure 4. (A) Daughter spectrum of $(M + NH_4)^+$ ion of roridin H (*m/z* 530). (B) Daughter spectrum of $(M + NH_4)^+$ ion of baccharinoid-4 (*m/z* 580).

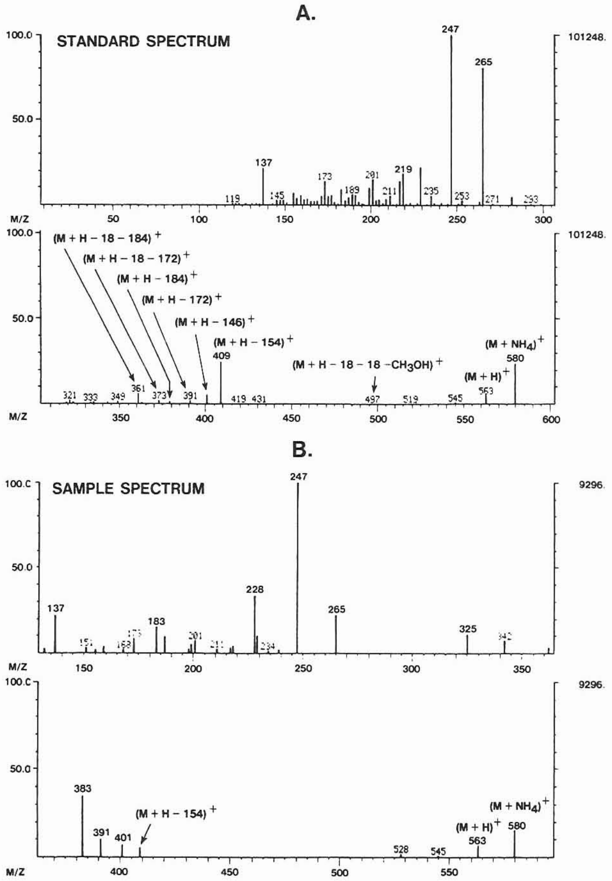

Figure 5. (A) Daughter spectrum of $(M + NH_4)^+$ ion of baccharinoid-5 (*m/z* 580). (B) Daughter spectrum of *m/z* 580 in *Baccharis megapotamica* plant sample 10.

analyses results are listed in Table IV.

The criteria for the identification of macrocyclic trichothecenes in samples were set as follows: (1) The appropriate most abundant daughter ion must be present. (2) The relative abundances of the other two daughter ions must be similar to that of the standard (±15%). The sample analysis data listed in Table IV were analyzed based on these criteria. The compounds that were identified definitively are marked by an asterisk in the Table IV. When the identities were doubtful, they are marked as "d" in the table. Roridin A was identified in all the plant samples except plant 10. Baccharinoid-5 was detected in plant samples 4 and 10 and roridin E was found in plant 15. However, the presence of roridin D in plant 10 and roridin E in all but plant 15 was doubtful. Baccharinoid-5 in plant 3 remained uncertain based on the observed ratios as well.

We investigated the possibility of using daughter ions of M^- and $(M + NH_4)^+$ ions, as specified in the experiments in Table III, to detect roridins and baccharinoids more conclusively even during the initial screening process. The ratios of intensities the daughter ions of M^- ions for baccharinoids standards could not be reproduced over a period of even a few hours. The cause for this is unknown at this point. This is in contradiction with the observed results when methane was used as the CI reagent gas (*18, 19*). The ion intensities of the negative daughter ions and their relative abundances varied even more dramatically during the analysis of samples, and

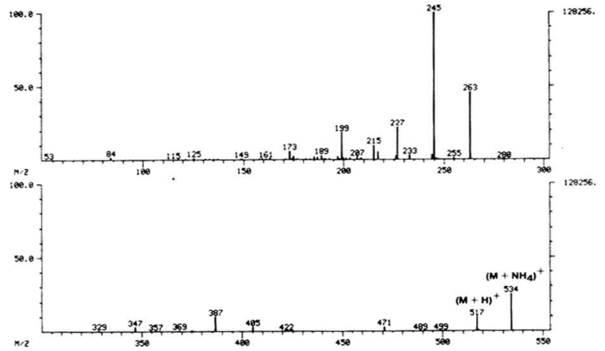

Figure 6. Daughter spectrum of (M + NH$_4$)$^+$ ion of 8-ketoverrucarin A (m/z 534).

Table V. Analytical Conditions[a]

expt	compound	mass setting (m/z) quadrupole 1	quadrupole 2
X1	roridin A	550	137, 231, 249
	roridin D	548	137, 231, 249
	roridin E	532	231, 267, 361
	roridin H	530	137, 231, 359
	KVA[b]	534	199, 231, 359
	roridins A, D, H	500–600	249
	roridin E	500–600	361
X2	baccharinoid-4	580	137, 157, 247
	baccharinoid-5	580	201
	KVA[b]	534	199, 245, 263
	baccharinoids-4 and -5	500–600	247

[a] Parent spectral tuning; collision energy, 14.0 eV; collision gas pressure, 1.0 mtorr; time spent for monitoring each ion, 0.08 s. [b] Internal standard.

the ion source needed cleaning after a few analyses. Similar observations were also made while monitoring the parent ions of negative ions, m/z 401, 359, and 417. Hence this attempt to use negative CAD ions during the screening was not pursued any further.

An alternate mode of screening of these molecules, shown in Table V, was devised. The KVA was also analyzed along with the macrocyclic trichothecenes to check its possible use as the internal standard. The trichothecenes were grouped separately to improve the sensitivity during analysis.

Quadrupole 1 (Q1) and 3 (Q3) were tuned specifically for obtaining the parent spectra in the positive ion mode. Perfluoro-*tert*-butylamine (PFTBA) was used as calibration compound and the instrument was tuned to obtain the parent spectrum of m/z 219 with maximum intensity, maintaining the collision gas pressure and collision energy at 1 mtorr and 14 eV, respectively. Under these conditions, the mixture containing roridins, baccharinoids, and KVA standards (1 μL containing 25 ng of each compound) was analyzed separately under the experimental conditions as specified in Table V. The ratios of the characteristic daughter ions for all compounds under these conditions were calculated. One microliter of the sample solutions along with 25 ng of KVA was also analyzed under these experimental conditions. The daughter ion intensities and their ratios were measured and compared with the values observed for the standard. The combined information obtained from the daughter and parent spectral data was used in the detection of roridins and baccharinoids in the samples.

The compounds whose identities were doubtful from the results of experiments (RB and RS) shown in Table III were also detected and confirmed under these conditions (X_1 and X_2). Thus, the presence of roridin E in plant samples 1, 3, 10, 13, and 15 and its absence in samples 4 and 6 were confirmed. The absence of roridin D and baccharinoid-5 in sample 10 and 3, respectively, was also deduced. On the basis of the sample analysis results, it was concluded that the conditions described in Table V should be used for the routine sample analyses.

The compounds detected were also confirmed by obtaining full scan daughter spectra of the samples. The daughter spectra of m/z 532 (roridin E) in sample 15 and m/z 580 (baccharinoid-5) in sample 10 are shown in Figures 3B and 5B, respectively. The standard and sample spectra were recorded under identical CAD conditions but were recorded on consecutive days. Despite this, the sample spectra were comparable with that of the standards. Most of the daughter ions and their relative abundances in the sample daughter spectra are comparable with that of the standards. The daughter spectrum of m/z 580 for sample 10 contained daughter ions at m/z 325, 342, and 528, which were not present in the standard spectrum, and were probably due to the impurities present in the sample extract that was not subjected to any cleanup processes. The results were in agreement with the observations of Jarvis et al., who have isolated, purified, and characterized these trichothecenes from several kilogram quantities of the corresponding plant samples (*20*). It should be pointed out at this point that distinction between baccharinoid-4 and baccharinoid-5 cannot be made with certainty by this procedure since the same daughter ions arising from the same parent ion are monitored for both compounds. The relative abundances (RA) of three characteristic daughter ions of KVA were measured from all sample runs. The RA of m/z 199 (14.5 ± 2.3) and m/z 263 (47.6 ± 5.2) with respect to the most abundant daughter ion (m/z 245) remained reasonably constant even in sample matrices.

The following series of experiments were designed and conducted to quantify the detected analytes. A mixture containing 100 pg of the roridins, baccharinoid-4 and baccharinoid-5, and KVA were analyzed at 1.0, 1.5, and 2.3 mtorr using a collision energy of 14 eV. Three daughter ions as specified in Table IV were monitored for each compound. The optimum CAD conditions for the production of the most abundant daughter ion in most instances were found to be 14 eV and 2.3 mtorr. Hence, all the quantification measurements were made under these conditions, using tuning conditions adequate for obtaining daughter spectra.

An experiment was designed to sequentially monitor the most abundant daughter ion only for each compound to increase the sensitivity during quantification measurements. The daughter ions specified in bold letters in Table III were chosen for this. The collision gas pressure and the collision energy were maintained at 2.3 mtorr and 14 eV, respectively. Varied amounts (5–30000 pg) of roridins and baccharinoids along with KVA (100 pg) were analyzed under these conditions. The daughter ion intensities of analytes and the internal standard were measured. The ion intensities of a compound relative to that of the internal standard (m/z 534 → m/z 245) were plotted against their relative amounts. Linear relationships were observed over a range of 3 orders of magnitude. The linear response ranges of the roridins and baccharinoids are shown in Table VI along with their linear regression constants. Response factors of all the analytes with respect to KVA were also calculated and are listed in the same table. The standard deviation values for the response factors and the correlation coefficients showed that the quantification of these macrocyclic trichothecenes in standard solutions could be performed with excellent precision. This information along with the relative abundances of the daughter ions observed in sample matrices proved that these analytes could be ac-

Table VI. Calibration Data

compound	mass/charge		response factor[c]	linear response range, pg	corr coeff	slope	intercept
	Q1[a]	Q3[b]					
roridin A	550	249	0.15 ± 0.02	5–5000	0.993	0.110	0.147
roridin D	548	249	0.17 ± 0.03	5–5000	0.998	0.127	0.054
roridin E	532	361	0.04 ± 0.01	5–10000	0.985	0.048	−0.088
roridin H	530	137	0.16 ± 0.02	5–10000	0.990	0.160	−0.010
baccharinoids	580	247	0.02 ± 0.003	10–20000	0.997	0.023	−0.07
KVA (int std)	534	245	1.000				

[a] Q1, quadrupole 1. [b] Q3, quadrupole 3. [c] Value from 10 measurements or more.

Table VII. Quantification of *Baccharis* Plant Samples

sample extract no.	analyzed fraction	identified compound	amt in total sample,[a] μg
10	1/10000	roridin E	1.8
		baccharinoid-5	387
	1/100000	baccharinoid-5	780 (880)
13	1/1000	roridin A	28.9
		roridin E	68.5
	1/10000	roridin A	26
		roridin E	63
15	1/10000	roridin A	72
		roridin E	114
	1/100000	roridin A	55 (50)
		roridin E	100 (95)

[a] Values mentioned in the parentheses were obtained by standard addition method.

curately quantified in samples. The detected compounds in plant samples 10, 13, and 15 were quantified by analyzing an aliquot (1 μL) of the extract in methanol along with KVA (100 pg) by the same procedure. When the measured quantities of the analytes exceeded the linear response range, the sample was further diluted and analyzed again. The quantification results are shown in Table VII.

Six spiked solutions of plant extract 10, containing 50 pg/μL to 5 ng/μL of baccharinoid-5 were also prepared and analyzed to quantify baccharinoid-5 present in the sample by the standard addition method. The measured ion intensity ratios were plotted against the amount of the spiked standard. The intercept provided the ion intensity ratio of baccharinoid-5 in the sample. The measured quantities of the compound, by the standard addition method, in the analyzed aliquot and the total sample, in parentheses, are listed in Table VII. The quantification of baccharinoid-5 in sample 10 by direct analysis agreed with the value obtained by the standard addition procedure. Similar results were observed for sample 15 as well, when spiked with roridin A and E. The measured concentrations of roridin A and E in sample 15 by both processes are also shown in Table VII. The matrix effect seemed to be insignificant during these quantification procedures. The internal standard (KVA), which was used earlier for the quantification of satratoxins by the NICI-MS/MS procedure (*18*), was observed to be an adequate internal standard for the quantification of roridins and baccharinoids by the positive ion chemical ionization (PICI)-MS/MS technique as well.

Several experiments were carried out to measure the minimum detectable levels of these compounds under various experimental conditions used for the detection and quantification of these compounds. Initially the three most abundant positive daughter ions of a compound, as specified in Table III, were monitored by use of corresponding standard solutions. The criterion was that all ions should be observed with the specific relative abundances (within ±15%) with a signal-to-noise (S/N) ratio of at least 10/1. The minimum detectable levels for roridins and baccharinoids were determined to be 10 and 20 pg, respectively. The detection limits of roridins and baccharinoids were measured to be 100 and 150 pg, respectively, under the conditions used initially for screening the samples, shown in Table III. Under the conditions mentioned in Table VI, the roridins and the baccharinoids were detected in 150- and 100-pg levels, respectively. Similarly, 50 pg of all the analytes and the internal standards could be detected under the conditions used for quantifying the analytes. These results indicated that, under the various experimental conditions used for the detection and quantification of the roridins and baccharinoids, 50–150 pg of the analytes and 50 pg of the internal standard could be detected with the S/N ratio of at least 10/1.

Thus, it is demonstrated that the four roridins and two baccharinoids could be identified and accurately analyzed by the DCI-MS/MS technique. Monitoring three characteristic positive daughter ions of each compound and the parent ion of the corresponding most abundant daughter ions was determined to be suitable for the unambiguous detection of the analytes in a single screening step. The detected analytes were accurately quantified by using a semisynthetic macrocyclic trichothecene, 8-ketoverrucarin A, as the internal standard. All the developed procedures were applicable for the detection and quantification in *Baccharis* plant extracts. The minimum detectable quantities for all compounds under the various adopted experimental conditions were determined to be in the range of 10–150 pg.

ACKNOWLEDGMENT

The authors gratefully acknowledge Bruce Jarvis of University of Maryland, College Park, MD, for the macrocyclic trichothecene standards and the Brazilian plant samples and Marguerite E. Brooks of US Army CRDEC, Aberdeen Proving Ground, MD, for her continued interest and valuable suggestions rendered during this investigation.

Registry No. Roridin A, 14729-29-4; roridin D, 14682-29-2; roridin E, 16891-85-3; roridin H, 29953-50-2; baccharinoid-4, 61251-97-6; baccharinoid-5, 63783-94-8.

LITERATURE CITED

(1) *Trichothecenes—Chemical, Biological, and Toxicological Aspects*; Ueno, Y., Ed.; Elsevier: New York, 1983.

(2) *Toxigenic Fungi—Their Toxins and Health Hazards*; Kurata, H., Ueno, Y., Eds.; Elsevier: New York, 1984.

(3) *Mycotoxins in Human and Animal Health*; Rodricks, J. V., Hesseltine, C. W., Mehlman, M. A., Eds.; Pathtox: Park Forest, IL, 1977.

(4) Jarvis, B. B. In *Trichothecenes—Chemical, Biological, and Toxicological Aspects*; Ueno, Y., Ed.; Elsevier: New York, 1983; pp 20–38.

(5) Jarvis, B. B.; Stahly, G. P.; Pavanasasivam, G. *J. Med. Chem.* **1980**, *23*, 1054–1058.

(6) Eppley, R. M.; Mazzola, E. P.; Slack, M. E.; Dreifuss, P. A. *J. Org. Chem.* **1980**, *45*, 2522–2523.

(7) Pavanasasivam, G.; Jarvis, B. B. *Environ. Microbiol.* **1983**, *46*, 480–483.

(8) Harrach, B.; Bata, A.; Daljmozy, E.; Benko, M. *Environ. Microbiol.* **1983**, *45*, 1419–1422.

(9) Rajendran, M. P.; Hussian, J. J.; Ramani, K. *Indian Vet. J.* **1975**, *52*, 234–235.

(10) Schneider, D. J.; Morasas, W. F. O.; Dale Kuys, J. C.; Kriek, N. P. J.; Van Schalkwyk, G. C. *J. S. Afr. Vet. Assoc.* **1979**, *50*, 73–81.

Anal. Chem. **1987**, *59*, 1278–1285

(11) Le Bars, J.; Gerard, J. P.; Michel, C. H. *Ann. Nutr. Aliment.* **1977**, *31*, 509–517.
(12) Drobotko, V. G. In *Fungus Disease of Horses and People*, Ukranian Academy of Sciences Ed: Kiev, USSR, 1949.
(13) Andrassy, K.; Horvath, I.; Lakos, T.; Toke, S. *Mycosen* **1980**, *23*, 130–133.
(14) Szabo, I.; Ratz, F.; Aldasy, P.; Syabo, P.; Goal, L. *I. Magy, Allatorv. Lapja.* **1970**, *25*, 21–26.
(15) Croft, W. A.; Jarvis, B. B.; Yatawasa, C. S., personal communication, 1985.
(16) Rosen, J. D.; Rosen, R. T.; Hartman, T. G. *J. Chromatogr.* **1986**, *355*, 241–251.
(17) Krishnamurthy, T.; Sarver, E. W.; Greene, S. L.; Jarvis, B. B. *J. Assoc. Off. Anal. Chem.*, in press.
(18) Krishnamurthy, T.; Sarver, E. W. *Biomed. Environ. Mass Spectrom.*, in press.
(19) Krishnamurthy, T.; Sarver, E. W., submitted for publication in *Biomed. Environ. Mass Spectrom. J.*
(20) Jarvis, B. B.; et al., University of Maryland, College Park, MD, personal communication, 1984.

RECEIVED for review June 4, 1986. Resubmitted December 4, 1986. Accepted January 15, 1987.

Chemical Ionization in an Ion Trap Mass Spectrometer

Jennifer S. Brodbelt, John N. Louris, and R. Graham Cooks*
Department of Chemistry, Purdue University, West Lafayette, Indiana 47907

Chemical ionization (CI) mass spectra are obtained by using the mass-selective instability mode of mass analysis in a quadrupole ion trap. The spectra of a variety of compounds are reported for both proton transfer and charge exchange reagents, and comparisons are made with CI spectra recorded by using other types of mass spectrometers. Instrumental parameters that affect the spectra (temperature, buffer gas pressure, trapping times) are characterized. Detection limits for CI (methane and isobutane) are comparable to or lower than they are for EI in the ion trap. When appropriate radio frequency voltage sequences are used, mass-selected reagent ions can be stored for reaction with sample molecules. Ion/molecule reactions demonstrated include methyne addition to phenol (addition of CH_2Cl^+ and subsequent loss of HCl).

With the recent introduction of the quadrupole ion trap as a commercial gas chromatographic detector (*1, 2*), there is interest in the potential of this device as a general-purpose mass spectrometer. For example, its capabilities as a tandem mass spectrometer have been noted (*3, 4*). The trap also enjoys features that make it a promising device for the study of ion/molecule reactions, namely the ability to hold ions for relatively long periods, so that gas-phase reactions can be followed in a time-resolved fashion, and the capability for mass-selective storage of ions.

The ion trap discussed in this paper is a three-dimensional quadrupole device of the type originally described by Paul (*5*). The trap is operated by using the mass-selective instability mode (*6, 7*) in which only radio frequency (rf) voltages are applied to the ring electrode. At a fixed frequency, the operating voltage determines the range of mass-to-charge ratios of ions which can be trapped in the field (*8*). As the rf voltage is raised, ions of increasing mass escape from the device and may be detected by using an external detector. For best performance in this mode, the motion of the ions stored within the trap is damped by a high background pressure of helium (*6, 7*). With the development of the mass-selective instability mode for trap operation, the capability of the device for storing and analyzing ions has been greatly improved in terms of scan speed, width of stored mass range, mass resolution, sensitivity, and even simplicity of operation.

In the commercial ion trap, EI was until very recently the only type of ionization method available. Although adequate for many purposes, including the recording of spectra comparable to those found in published spectral libraries, electron impact is not always the ionization method of choice. Molecular weight determinations are often more appropriately based on chemical ionization, which has the advantage of allowing better control (through choice of the reagent gas) of the internal energies of the protonated molecules or radical cations formed, respectively, from proton transfer or charge exchange processes. These features allow one to enhance either the protonated molecule or the fragment ions, as desired (*9–13*).

An early indication that ion/molecule reactions might be studied in an ion trap operated in the mass-selective instability mode is found in the anomalously abundant $(M + H)^+$ ions occasionally observed in EI mass spectra. This is especially the case for more basic compounds, which can undergo self-protonation at the relatively large sample pressures associated with elution of peaks from gas chromatographs. Preliminary results on chemical ionization in the ion trap obtained by using the mass-selective instability mode have been communicated (*14, 15*). In this paper we discuss reagent ion selection and the optimization of conditions for performing CI in the ion trap. We also compare CI spectra recorded by using the ion trap with those obtained by using other types of mass spectrometers, provide some performance characteristics for ion trap CI, and demonstrate the value of the ion trap operated in the mass-selective instability mode as a device for studying ion/molecule reactions.

Ion/molecule reactions (*16–19*), and in particular chemical ionization processes (*20–23*) have previously been studied in the ion trap operated in the earlier scan modes. Todd and co-workers (*21*) employed a quadrupole ion storage trap as a low-pressure chemical ionization source in conjunction with a conventional quadrupole mass spectrometer used for mass analysis and its characteristics were compared (*23*) to both chemical ionization in an ion cyclotron resonance (ICR) spectrometer and in a conventional mass spectrometer. Reagent and sample pressures intermediate between those employed in an ICR and a conventional source were used in the trap, and ion residence times were 3 orders of magnitude longer than in a conventional source. This instrument was also used to examine the products and kinetics of some simple ion/molecule reactions (*23*). In 1978, the trap was utilized as an ion source for a magnetic sector mass spectrometer (*20*), and it was noted that in this instrument ions underwent fewer collisions and thus did not experience the collisional stabilization that occurred in conventional chemical ionization sources at higher pressures. Cluster ions and association products were not observed for similar reasons.

In contrast to the limited data taken by using ion traps, there is a wealth of published information on ion/molecule reactions studied by using ICR techniques (*24–29*). Although

0003-2700/87/0359-1278$01.50/0 © 1987 American Chemical Society

the principles by which ions are stored and analyzed in the ICR spectrometer are different from those applicable to ion traps, in both cases ions may be stored for long times (1 ms to 1 s) and reactions may occur at low pressures (10^{-8} to 10^{-4} torr). Many of the problems, advantages, and applications of low-pressure chemical ionization in ICR have been discussed (*25, 29*), and some will be seen to be analogous to those observed in this work.

An initial comparison of chemical ionization in a conventional mass spectrometer, an ICR spectrometer, and an ion trap is instructive for understanding the basic series of chemical processes occurring in each. Unlike chemical ionization carried out in a conventional mass spectrometer source, CI in an ion trap is effected by using only 10^{-6} to 10^{-4} torr of reagent gas. In a conventional mass spectrometer source, where the sample molecules have a residence time of less than 100 μs, the reagent gas pressure may be from 0.1 to 0.8 torr to ensure sufficient ion/molecule collisions for adequate ionization efficiency. Furthermore, the reagent gas is generally 100–1000 times in excess of the sample, effectively precluding significant electron ionization of the sample.

What is accomplished in conventional CI by using high reagent gas pressure is achieved by using long reaction times in the ICR cell and in the ion trap. In each case, both the sample and reagent pressures are low, so ample conversion of sample molecules to ions necessitates a long (millisecond) reaction period. In these experiments, the electron beam for ionization is only on for a short period at the start of the reaction sequence during which time both reagent and sample molecules undergo electron ionization. The sample to reagent gas ratio may even be 1:10 because the total ion population is limited by space charge effects. Thus, EI fragments from the sample can contribute significantly to the resulting CI mass spectrum. In the conventional ICR technique, these EI interferences can be diminished by using extremely long reaction times so that more CI-related ions accumulate relative to the EI-related ions (*29*). These EI interferences are not eliminated by any form of mass-selective ejection, although this problem can be solved by using MS/MS techniques, which afford elegant ejection capabilities with the Fourier transform ion cyclotron resonance (FTICR) instrument (*30*).

In the ion trap, mass-selective storage capabilities may be used to eliminate the problem of EI interferences in the resulting CI spectra (vide infra). That is, the rf voltages applied to the ring electrode may be set during specified reaction periods so that all ions above a certain mass-to-charge are not efficiently trapped. In this way reagent ions may collect and react without the accumulation of sample ions. As will be shown, this mass-selective capability is an important feature of chemical ionization in an ion trap.

EXPERIMENTAL SECTION

The trap used was a Finnigan 700 ion trap detector (ITD) with several minor modifications. The software used to implement the modified rf voltage sequences was a special version of the standard ITD software supplied by the manufacturer. The trap vacuum manifold was modified for CI by equipping it with an ionization gauge that allowed gas pressures (reagent gases, helium buffer gas, and sample) in the trap to be measured. All pressures were read directly from the ionization gauge without correction. The gas chromatograph (GC) transfer line was removed from the trap for many of the experiments described herein, and the helium flow was routed through the GC transfer line inlet via a solenoid-operated needle valve. This was done as a convenience to allow more precise adjustment of pressures. Reagent gases and samples were introduced through the calibration compound inlet and metered with Granville–Phillips valves. In the detection limit experiments and the quantitative analyses, samples were introduced via the GC line.

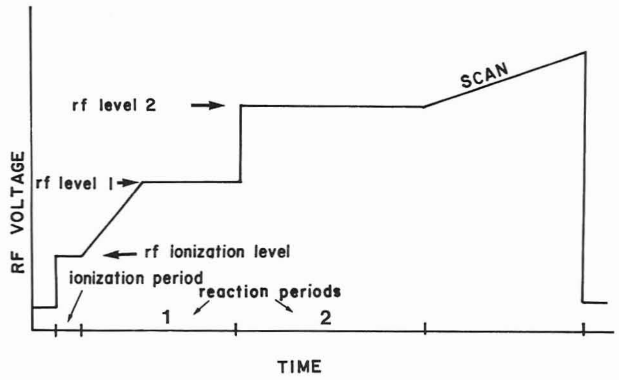

Figure 1. Timing diagram for CI using an ion trap operated in the mass-selective instability mode. The trap is first cleared by applying a low rf voltage and then the voltage is raised and set at the rf ionization voltage during the ionization period. Reaction period 1 is the reagent ion reaction period; reaction period 2 is the sample reaction period.

Table I. Selected Reagent Ions for CI of Cyclohexanone

reagent ions stored[a]	PA's[b]	ratio *m/z* 99 to *m/z* 81[c]
17^+, 19^+, 29^+	125, 159, 165	4.3
19^+, 29^+	159, 165	4.8
29^+	165	6.1

[a] $17^+ = CH_5^+$, $19^+ = H_3O^+$, $29^+ = C_2H_5^+$. [b] Proton affinities (av) from ref 33, in kcal/mol. [c] $(M + H)^+:(MH - H_2O)^+$.

Unless otherwise stated, helium buffer gas was introduced at an uncorrected gauge pressure of about 2.5×10^{-5} torr. Typical optimized reagent gas pressures were 1.0×10^{-5} torr methane, 6.0×10^{-6} torr isobutane, 3.5×10^{-6} torr ammonia, 8.0×10^{-6} torr methyl chloride, and 1.0×10^{-5} torr argon. Standard conditions (see Figure 1) for recording CI spectra were as follows: ionization time, 2 ms; reagent gas reaction period, 8.5 ms (up to 100 ms for isobutane); sample reaction period, 100 ms. A typical scan was accumulated in ca. 1 s. Five to ten scans were generally averaged to produce the CI spectra discussed in this paper. The trap was operated at an rf frequency of 1.1 MHz.

Conventional chemical ionization mass spectra were recorded by using a standard Finnigan 4500 series CI source on a Finnigan 4500 triple quadrupole instrument operated in the mass spectrum scan mode with the first quadrupole being used for mass analysis. Methane was used as the reagent gas at a pressure of 0.3 torr.

A Varian 3700 gas chromatograph was used to introduce samples for the quantitative studies. A 10-m SE-30 capillary column (0.32 mm i.d.) was used. All samples were diluted with hexane and injected in the splitless mode. The injector was held at 220 °C, and the column temperature was programmed from 50 to 170 °C. Helium was used as the carrier gas at a flow rate of 1 mL/min.

A Finnigan MAT 8200 mass spectrometer was used for acquisition of the methane CI spectra shown in Table I. The indicated pressure in the source manifold was 4.2×10^{-4} torr.

RESULTS AND DISCUSSION

Implementation of the CI Experiment. When low rf voltages are applied to the ring electrode of the trap, ions of high mass are not efficiently stored, while ions below a well-defined mass-to-charge cut-off value are ejected from the trap. The result is mass-selective storage of ions in the specified range of interest. In particular, the rf voltage level can be adjusted to set this range so as to store only the CI reagent ion(s) of interest while excluding other undesired ions of higher molecular weight.

The software-controlled selection of a sequence of radio frequency voltages and time intervals, used to carry out a chemical ionization experiment, is shown in Figure 1. Parameters of particular interest include the ionization time and ionization rf voltage, the two reaction periods, and the rf potentials applied during each. In a typical CI scan, the trap

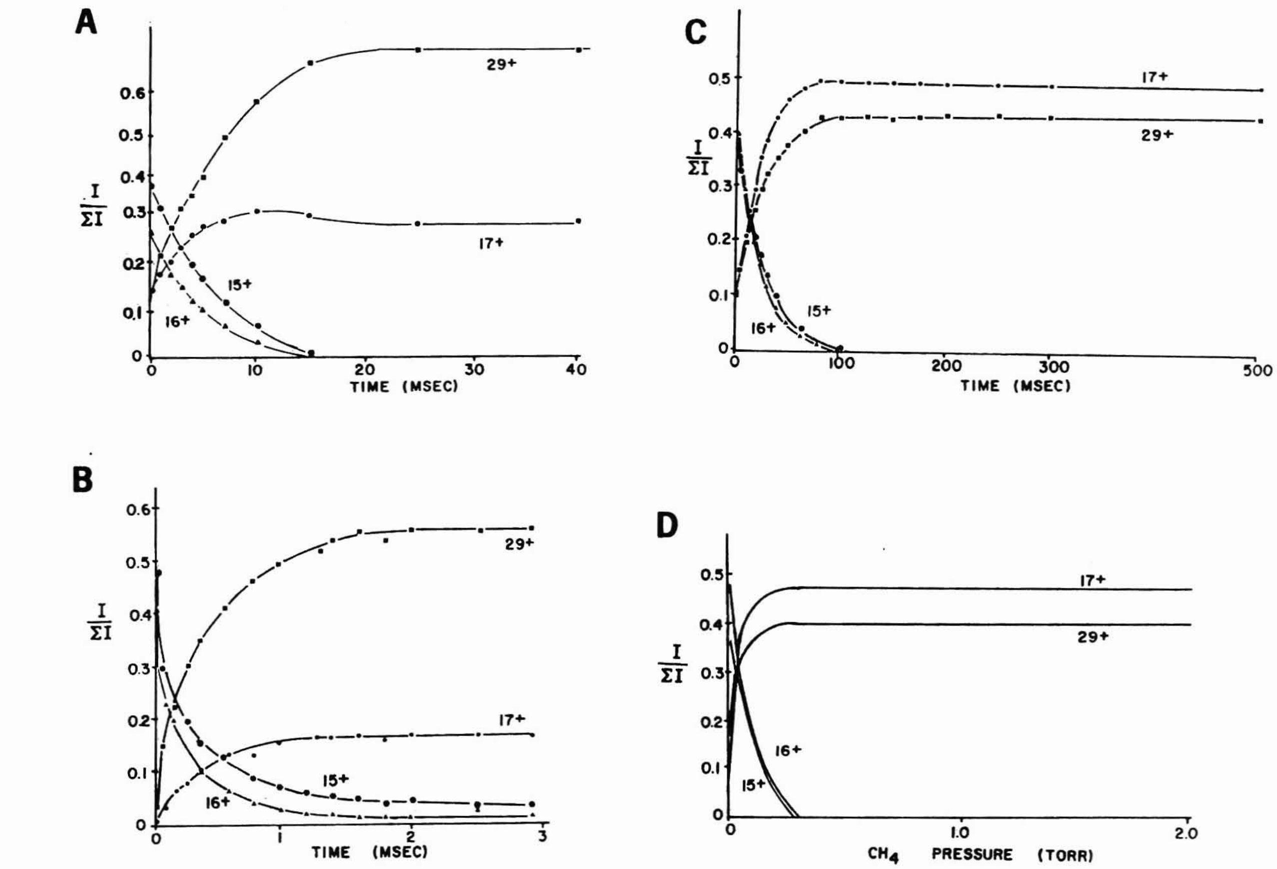

Figure 2. Establishment of methane reagent ion population followed directly as a function of time or indirectly as a function of pressure in four different types of mass spectrometers: (A) ion trap operated in the mass-selective instability mode, methane pressure 1.0×10^{-5} torr (this work); (B) ion trap/quadrupole mass filter, methane pressure 2.0×10^{-4} torr (*16*); (C) FTICR spectrometer, methane pressure 2.0×10^{-6} torr (*29*); (D) magnetic sector mass spectrometer, methane pressure, 0–2.0 torr (*31*).

is first held at a low rf voltage to clear it of residual ions. The ionization rf voltage governs ion stability and is selected to store ions throughout the mass range of interest. The ionization time is established by a lens system operating as an electron gate that controls access of the ionizing electron beam to the trap. At the termination of the ionization period, the rf potential is raised in ca. 4.5 ms to rf level 1, a value chosen so that only ions in the low mass range corresponding to reagent ions are stored. At the chosen rf amplitude, lower mass ions are inherently unstable, while higher mass ions are not efficiently trapped. Shorter ramp times have been investigated but they result in a less satisfactory reagent ion population.

The first reaction period is used to establish a population of reagent ions through ion/molecule reactions. A period of 8.5 ms is typically used, during which the initially formed reagent ions are presumably stabilized both internally and translationally. As a result of the low rf voltages used during reaction period 1, any sample molecules that may be ionized through interactions with the reagent ions and those created directly by electron ionization are not efficiently stored. This permits control over the ongoing ion/molecule reactions and eliminates EI interferences. The length of the first reaction period determines the nature of the reagent ion population that will be available to react with the sample during the second reaction period. In methane CI, for example, if period 1 is shortened, CH_5^+ increases at the expense of $C_2H_5^+$.

The desired reagent ion population is subjected to a fast rf voltage ramp to achieve level 2. The rate of increase of the rf voltage does not appear to have large effects on the spectra, so the voltage is raised rapidly as indicated in Figure 1. Ion/molecule reactions between the sample molecules and reagent ions occur during the second reaction interval in which the rf level is appropriate to store the resulting product ions. The number of sample ions that accumulate depends upon the length of this period. After a typical reaction time of 50–100 ms, the rf voltage is scanned for mass analysis. The entire sequence is then repeated and the spectra added. Note that the rf voltage and timing scheme are tailored for each reagent gas to achieve optimum performance.

Reagent Ion Selection and Scan Parameters. Three reagent gases were of particular interest: methane, isobutane, and ammonia. Methane is one of the most widely used ionizing agents because of the moderately low proton affinities of the conjugate bases of $C_2H_5^+$ and CH_5^+, the dominant reagent ions. Thus methane often induces considerable sample fragmentation while also producing a recognizable ion due to the protonated molecule. Isobutane is the reagent gas of choice when an abundant pseudo molecular ion is desired with minimal fragmentation. If selectivity for nitrogen-containing compounds is desirable, ammonia is often the optimum ionizing agent.

Since methane is widely used, it will serve as the reagent gas for many of the results presented in this paper. The pressure of the reagent gas in the trap was set to optimize sensitivity. At the optimum pressure of methane, nominally 1.0×10^{-5} torr, a steady-state population of CH_5^+ and $C_2H_5^+$ ions was reached after a reaction period of about 15 ms. Figure 2 displays on a time axis the fall in abundance of CH_3^+ and $CH_4^{\bullet+}$ and the increase in $C_2H_5^+$ and CH_5^+. These trends are familiar from experiments done as a function of methane pressure in conventional chemical ionization sources (*31*). Comparison (Figure 2) of the present data and that obtained by Gross et al. using FTICR spectrometry (*29*), by Munson and Field using conventional CI in a magnetic sector instrument (*31*), and by Bonner et al. with a trap/quadrupole mass filter instrument (*16*) is an excellent indication that appropriate conditions for chemical ionization can be obtained within the trap. Note that there is no loss of total ion current apparent during the period used to establish the reagent ion population.

Calculation from the data of Figure 2A of the bimolecular rate constants for removal of the ions of m/z 15 and 16 yields values of 7.4×10^{-10} cm^3/(molecule s) and 8.3×10^{-10} cm^3/(molecule s), respectively. These values are some 20–25% lower than the literature values (*32*), presumably because the pressure in the trap is systematically underestimated because of the method of measurement. The ratio of these rate constants, about 1.1 for removal of $CH_4^{\bullet +}$ to removal of CH_3^+, agrees with literature values which range from 1.1 to 1.3 (*32*). Note, in comparing the reagent ion spectra shown in Figure 2, at long times or high pressure, that both ion trap experiments show a $[17^+]/[29^+]$ ratio which is small relative to the ratio observed in the other devices. This appears to be intrinsic to the ion trap operating conditions.

Experimental variables are critical in obtaining reproducible CI spectra with any instrument. In the case of CI in the ion trap, improper selection of rf voltages, time intervals, or pressures can yield anomalous results. The rf potentials must be selected so that there is not undue discrimination in either the lower or upper mass range of interest. When ions are stored during the reaction periods, too high an rf value will not trap lower mass ions while too low an rf level can cause poor efficiency or failure to trap higher mass ions. But this feature makes possible one of the trap's primary advantages—selective storage of ions. For instance, the reagent ion population formed from the methane ion/molecule reactions can be trapped without trapping any sample ions of higher mass (generated directly by EI or indirectly by CI). The capability for mass-selective ion storage allows a particular subset of reagent ions to be chosen to cause sample ionization. As an example, if a softer ionization process is desired, $C_2H_5^+$ may be stored for reaction with the sample by setting a higher rf level during the second reaction period. By contrast, in the usual CI mode, both CH_5^+ (m/z 17) and $C_2H_5^+$ (m/z 29) act as ionizing agents while a small amount of water present in the system can also yield a significant quantity of H_3O^+ (m/z 19) as a protonating agent.

The effects of reagent ion selection can be seen in Table I, which indicates the relative amounts of fragmentation of cyclohexanone upon protonation by methane reagent ions. Reagent ions formed from conjugate bases with higher proton affinities deposit, on the average, less internal energy during ionization due to the lower exothermicity of the proton transfer reaction. With the rf ionization voltage set to store ions of 17^+, 19^+, and 29^+, or alternatively those of 19^+ and 29^+, or just 29^+, the average amount of internal energy deposited during ionization is expected to decrease as the average of the proton affinities for the conjugate bases of the corresponding CI reagents increases. At the lowest rf level (trapping all methane-derived ions as well as protonated water), the most extensive fragmentation of cyclohexanone is seen, the ratio of the protonated molecule (m/z 99) to its dehydration product (m/z 81) being about 4:1. As the rf voltage is raised, this ratio increases until it exceeds 6:1 when only $C_2H_5^+$ (29^+), the reagent ion whose conjugate base has the highest proton affinity, is stored. For many experiments using chemical ionization, it is convenient to trap all reagent ions to enhance ionization efficiency and signal intensity.

Table II. CI Mass Spectra Recorded in Ion Trap and Other Instruments

compound	m/z	% rel abundance ion trap	% rel abundance quadrupole	% rel abundance sector
cyclohexanone (M = 84)	43	14	10	9
	45	2	0	0
	55	3	3	1
	57	9	6	7
	69	1	1	1
	83	100	100	100
	84	12	13	19
	85	3	3	17
	113	0	0	1
cyclohexanone (M = 98)	55	1	4	1
	59	2	0	0
	69	<1	1	0
	71	3	2	7
	79	0	3	2
	81	23	22	9
	98	3	3	13
	99	100	100	100
	127	0	0	20
acetic anhydride (M = 102)	43	100	100	100
	61	2	5	19
	89	3	2	6
	101	0	0	2
	102	0	0	0
	103	0	8	19
	131	0	<1	1
	145	0	4	6
2-pentanol (M = 88)	42	3	2	1
	45	9	9	5
	46	12	3	0
	47	7	3	5
	61	<1	<1	<1
	71	100	100	100
	72	12	5	8
	87	4	2	3
	115	0	0	1
fluorobenzene (M = 96)	77	1	5	1
	96	10	29	10
	97	100	100	100
	125	0	1	0
butyraldehyde (M = 72)	55	100	100	56
	56	5	3	3
	57	5	6	6
	73	49	48	100
	89	0	6	2
	101	0	10	3
o-nitrotoluene (M = 137)	47	8	1	19
	91	5	6	1
	92	68	33	5
	93	65	21	2
	94	24	05	<1
	107	7	2	<1
	108	42	4	1
	109	5	0	1
	120	8	12	6
	121	3	3	3
	138	100	100	100
	166	0	0	10

CI Mass Spectra Obtained with Various Reagent Gases. Standard operating conditions were used, including a fixed rf voltage and timing sequence (see Experimental Section), to record the methane CI spectra of several simple compounds. For comparison, these compounds were also analyzed in a quadrupole mass spectrometer using 0.3 torr of methane and in a magnetic sector instrument using comparable methane pressure. The results are tabulated in Table II. With few exceptions, the spectra show good overall agreement. The greatest differences are observed in the case of *o*-nitrotoluene, a molecule known for its proclivity to undergo rearrangement (*34*). For example, in the CI spectra of *o*-nitrotoluene recorded by using the ion trap and the quadrupole instrument, the base peak is the protonated molecule while the most abundant fragment is due to loss of NO_2. Yet in the ion trap there is a far greater relative abundance of the ions due to NO loss (m/z 108) than in the data taken by using the conventional CI ion sources. Small differences in internal

Table III. Ion Trap CI Mass Spectra Obtained with Methane and Isobutane

		% rel abundance	
compound	*m/z*	methane CI	isobutane CI
2,2,6-trimethylcyclohexanone (M = 140)	59	90	46
	71	4	0
	73	9	0
	81	3	0
	83	45	19
	111	1	0
	123	100	71
	141	8	100
butyraldehyde (M = 72)	55	100	24
	56	5	0
	57	5	0
	73	49	100

energy and large differences in the time scales of the two types of experiments probably lead to this result. Note, however, that the ion trap CI mass spectrum of *o*-nitrotoluene, as well as those of the other compounds, is reproducible (±10%) provided acquisition parameters are fixed. Methane CI spectra obtained by using an FTICR spectrometer have also been published for cyclohexane and cyclohexanone (*29*). For cyclohexane the recorded ion abundances were as follows: *m/z* 43, 8%; *m/z* 55, 4%; *m/z* 57, 5%; *m/z* 69, 4%; *m/z* 83, 100%; *m/z* 84, 17%; *m/z* 85, <1%. The two listed abundances for cyclohexanone were 23% for *m/z* 81 and 100% for *m/z* 99. These data are in good agreement with the ion trap data given in Table II.

The absence of adduct ions such as $(M + 29)^+$ and $(M + 41)^+$ in the ion trap CI spectra should be noted. These ions are apparent to a slight extent in the quadrupole mass spectral data and to a greater extent in the magnetic sector instrument CI data. These adduct ions require additional stabilizing collisions to remove internal energy, and this is only possible at the higher pressures used in conventional CI sources. The ion trap result is similar to that observed in ion cyclotron resonance spectrometers.

Other reagent gases give equally promising chemical ionization results with the ion trap. Isobutane, which has a much higher proton affinity (193 kcal/mol (*12*)) than methane, causes less fragmentation and enhances the abundance of ions in the molecular ion region of most organic compounds. A lower pressure of isobutane (6.0×10^{-6} torr) was found to optimize signal intensity in the ion trap, although absolute ion abundances remained smaller than those produced when using methane. Nevertheless, the expected advantages of isobutane are apparent when compounds such as 2,2,6-trimethylcyclohexanone and butyraldehyde are examined with both reagent gases (Table III). In these cases, the $(M + 1)^+$ peaks in the isobutane spectra are of much greater relative abundance than those in the methane CI spectra. Fragments are reduced in abundance due to the smaller difference in proton affinities between the sample molecules and the conjugate bases of the corresponding reagent ions. This feature is important if selected ion monitoring is to be used for the detection of trace components in a mixture. For example, butyraldehyde dissociates almost exclusively to ions of *m/z* 41, 43, and 44 by electron ionization in the trap and predominantly to *m/z* 55 upon methane CI. These ions are so commonly found in the spectra of organic compounds that they fail to serve as diagnostic ions for selected ion monitoring. Furthermore, in the EI spectrum the molecular ion region of butyraldehyde is virtually devoid of ions. When isobutane CI is used, the $(M + 1)^+$ ion is the base peak and easily monitored.

Table IV. Ion Trap CI Mass Spectra Obtained with Methane and Ammonia

compound	*m/z*	methane CI	ammonia CI	methane ICR[a]	ammonia ICR[a]
triethylamine (M = 101)	57	24	0	NR[b]	NR
	74	12	0	11	NR
	86	28	0	47	12
	100	80	0	100	NR
	101	40	0	71	10
	102	100	100	90	100
	103	4	7	8	8
2-ethylpyridine (M = 107)	108	100	100		
	109	10	7		
2-methoxypyridine (M = 109)	108	8	0		
	110	100	100		
	111	10	6		

[a] From ref 29. [b] Not reported.

Ammonia is another selective reagent gas, one with an extremely high proton affinity (201 kcal/mol (*12*)) that assures that proton transfer occurs only to very basic compounds. Comparison of the methane to ammonia CI spectra (along with published FTICR data) listed in Table IV demonstrates the complete absence of fragmentation in the ammonia CI spectra. When mixtures of compounds such as cyclohexanone with triethylamine are examined, the nonbasic compounds are not detected due to their inability to abstract a proton from the ammonium ion. This demonstrates the expected specificity of chemical ionization by NH_3. The FTICR results are similar but do not show quite the degree of contrast when using the two reagent gases as observed in the ion trap. This reflects the value of reagent ion selection in the ion trap.

Ionization based on reactions other than proton transfer has also been investigated. When proton transfer agents such as methane do not yield fragmentation which allow meaningful spectral interpretation, an alternative ionization method is charge exchange (*35–37*). The types of fragments observed are controlled by the fact that the radical cation is generated, and the degree of dissociation is determined, by the difference in energy between the recombination energy of the reagent and the ionization potential of the sample molecule. A variety of reagents with a range of recombination energies are available (*35*), so charge exchange spectra can be tailored to fit the objectives of the analysis scheme. Argon is often selected as a charge exchange agent because of its wide availability, low cost, and high recombination energy (15.8 eV (*35*)), making it useful for generating molecular radical cations of relatively high internal energies. For example, anisole produces no useful fragments upon ionization by methane CI (Table V). Upon charge exchange with $Ar^{\bullet +}$, the molecule shows extensive dissociation and yields fragment ions that are characteristic of the structure. The ion trap charge exchange spectra of some representative compounds, toluene, benzaldehyde, anisole, naphthalene, and phenol, and argon charge exchange spectra acquired by using a conventional mass spectrometer, are shown in Table V. For comparison, the EI and methane CI spectra produced in the trap are also presented. Note that the EI spectra do not agree entirely with those reported in standard spectral compilations; this is most likely due to the vastly different environments in which ionization occurs (i.e., consider the high helium pressure in the trap and the greater possibility of ion/molecule collisions).

Effects of Time, Temperature, and Pressure. The time allowed for reaction of the sample molecules with the chemical ionization reagents can alter the appearance of ion trap spectra, and this is probably the major reason for the dif-

Table V. Charge Exchange and Protonation in the Ion Trap and a Conventional CI Instrument

compound	m/z	charge exchange[a]	charge exchange[b]	methane CI[a]	EI[a]
toluene (M = 92)	50	0	0	0	25
	51	0	0	0	55
	63	0	0	0	13
	65	6	1	0	27
	66	1	2	0	2
	69	<1	0	0	1
	77	4	2	0	0
	91	100	100	4	100
	92	10	16	4	28
	93	1	4	100	0
benzaldehyde (M = 106)	50	0	0	0	47
	51	0	0	0	100
	52	5	12	0	29
	76	0	2	0	<1
	77	100	100	0	73
	78	7	14	0	15
	79	7	0	29	22
	105	0	10	0	48
	106	0	4	4	19
	107	1	3	100	4
	108	0	0	8	0
naphthalene (M = 128)	50	0	0	0	6
	51	0	1	0	14
	64	0	0	0	2
	78	27	6	0	0
	102	100	28	0	38
	127	62	17	0	14
	128	21	100	3	100
	129	0	23	100	11
	130	0	0	6	0
phenol (M = 94)	55	0	0	0	90
	61	0	5	0	0
	65	100	3	0	100
	66	10	0	0	86
	77	8	2	2	0
	78	0	3	0	0
	93	0	2	0	0
	94	14	100	0	65
	95	0	5	100	0
anisole (M = 108)	39	0	0	0	100
	50	0	0	0	3
	51	0	0	0	10
	52	<1	4	0	3
	54	0	4	0	0
	65	100	100	0	30
	66	0	4	0	1
	77	22	15	0	6
	78	7	8	0	12
	79	3	0	0	3
	108	<1	11	5	10
	109	0	6	100	1

[a] In ion trap. [b] In quadrupole.

ferences noted in the tables between quadrupole and ion trap CI mass spectra. For example, benzaldehyde produces primarily two fragments, m/z 79 and 107, as a result of protonation by methane CI. If the time allowed for the ion/molecule reactions to proceed is increased from 10 ms to 1 s, the percentage of the ion current due to 107^+ increases from 70% to 90% while that due to 79^+ drops from 30% to 10%. In this particular experiment only m/z 29 ($C_2H_5^+$) from methane was stored for reaction with benzaldehyde, so that a fluctuating ionizing agent population could not cause the change in the benzaldehyde ion fragmentation. Feasible explanations include the following: (1) Increasing numbers of collisions with helium buffer gas cause deactivation of protonated benzaldehyde ions and diminish the probability of their dissociation. (2) Protonation of benzaldehyde molecules by benzaldehyde fragments instead of by $C_2H_5^+$ ions causes reduced internal energy transfer. Both of these factors would be compounded at longer storage times.

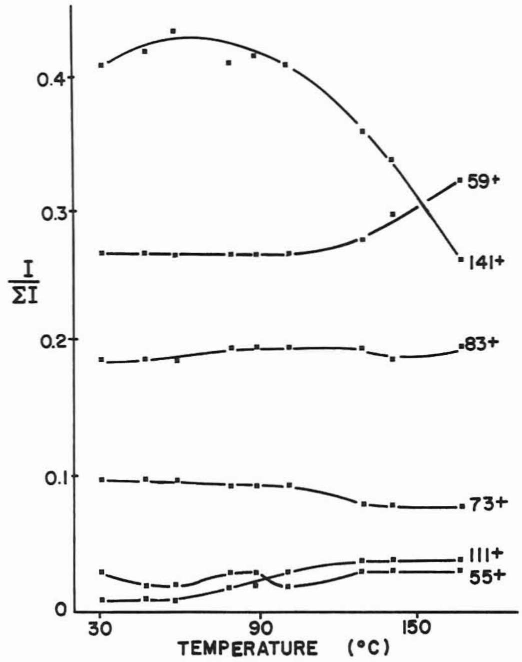

Figure 3. Effect of trap temperature on methane chemical ionization spectrum of 2,2,6-trimethylcyclohexanone (MW 140).

Note that when long reaction times are used and the rf voltage is set to store all possible reagent ions, there is significant accumulation of H_3O^+ (m/z 19), also a proton transfer agent. The conjugate base (H_2O) of this ion has a proton affinity of 159 kcal/mol (*33*), very similar to that of the conjugate base of $C_2H_5^+$ from methane (165 kcal/mol (*33*)).

Increasing the reaction time also increases the total accumulated number of ions related to the sample of interest. With a change in the storage time (reaction period 2) from 10 to 1000 ms, the sample ion population increases by a factor of 30 for benzaldehyde. This feature can be used to enhance weak signals within the confines of sampling time limitations. Studies of time dependences using FTICR (*29*) have established that the reaction time in the ICR cell controls the extent of proton transfer and thus ultimately affects the measurement sensitivity.

A noteworthy experimental parameter is the temperature of the trap. Previous studies using conventional CI sources have attributed the increasing amounts of fragmentation observed with increasing source temperature (*38–40*) to the additional thermal energy distributed among the degrees of freedom of the molecule and in some cases to isomerization in the neutral or ionic states (*41*, *42*). The fragment ion abundances for a typical organic molecule, 2,2,6-trimethylcyclohexanone, ionized by methane, are plotted as a function ion trap temperature in Figure 3. Marked changes are seen for ions of m/z 59 and 141 at temperatures exceeding 100 °C. The increased internal energy of the protonated molecule (m/z 141) due to the thermal energy transfer from the buffer gas is a possible explanation of these results.

Temperature effects are not as prominent for triethylamine (molecular weight 101). As the temperature of the trap is increased from 35 to 170 °C, the $M^{\bullet+}$ species decreases by about 8% while the ion formed by loss of methyl radical decreases by 10%. Concurrently, the species of m/z 74 increases by 5%. These changes of smaller magnitude are more usual for typical organic molecules in other types of mass spectrometers (*40*).

The helium buffer gas used as a damping agent in the trap also plays an important role in the CI process. Typically, the

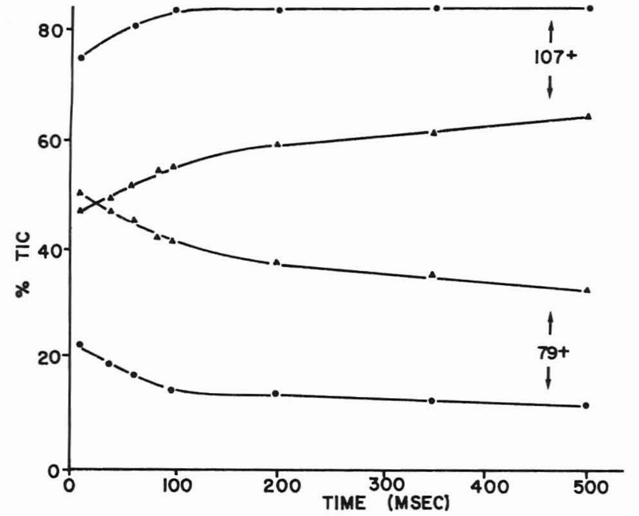

Figure 4. Effect of helium buffer gas on methane chemical ionization spectrum of benzaldehyde (MW 106): ▲, without helium; ●, with helium.

ratio of helium pressure to CI reagent pressure is 100 to 1. Methane CI spectra of benzaldehyde recorded with and without the use of helium are shown in Figure 4. Without helium present, the relative abundance of m/z 79 is almost 30% greater than when helium is used. This dramatic effect is tentatively attributed to collisional deactivation by helium, which stabilizes the protonated molecules so that subsequent dissociations do not occur as readily. Thus, the use of helium in the trap has a substantial influence on CI behavior.

Comparison of EI and CI Sensitivities. In many cases in which EI and CI have been compared in conventional mass spectrometers, results have indicated that the relative sensitivities are roughly comparable when instrumental conditions are optimized for each ionization method (*11*). A study of the relative sensitivities of CI and EI in the trap shows that chemical ionization can yield a factor of 10 lower detection limit than EI in some cases. Samples were introduced via a gas chromatograph so that a quantitative investigation of detection limits could be undertaken. For naphthalene, which does not dissociate significantly when ionized by EI, by isobutane CI, or by methane CI, the detection limit ($S/N = 2$, scan range 50–150 amu, total acquisition time of 2–3 s) was 1 ng in each case. (These data are taken under typical rather than best-performance instrument conditions.) For 3,5-dimethylphenol, on the other hand, the full spectrum detection limit was 0.1 ng when using either isobutane or methane CI but only 1 ng when employing EI conditions. This increased sensitivity can be attributed to two factors: (1) the ion current is distributed among many fragments for EI while it is divided among two or three structurally diagnostic ions for CI, and more importantly, (2) the long time available for ion/molecule reactions between the reagent ions and the sample molecules allows greater accumulation of sample ions for subsequent detection with improved S/N. Note that a new version of the software (*43*) has recently been developed which offers greatly improved sensitivity and quantitative dynamic range in the EI mode through automatic variation of the ionization time. This software is expected to further enhance the performance of the ion trap.

Analytical Applications of CI in the Ion Trap. The use of CI allows manipulation of the internal energy of ions for improved determination of compounds of analytical interest. What follows is a simple illustration of the analytical capabilities of the ion trap in the CI mode. Ephedrine, a mild stimulant of the central nervous system, does not produce a sufficient EI spectrum for unambiguous identification of the drug, since no molecular ion is observed and the diagnostic value of the single abundant fragment (m/z 58) is inadequate (Figure 5). Using methane CI, one can obtain a suitable spectrum for target drug analysis. The protonated molecule is evident, as are several interpretable fragments. The ion at m/z 148 results from dehydration of m/z 166, while m/z 135 is due to loss of methylamine and m/z 107 is most likely $C_7H_7O^+$. This example highlights the capabilities of the ion trap for CI.

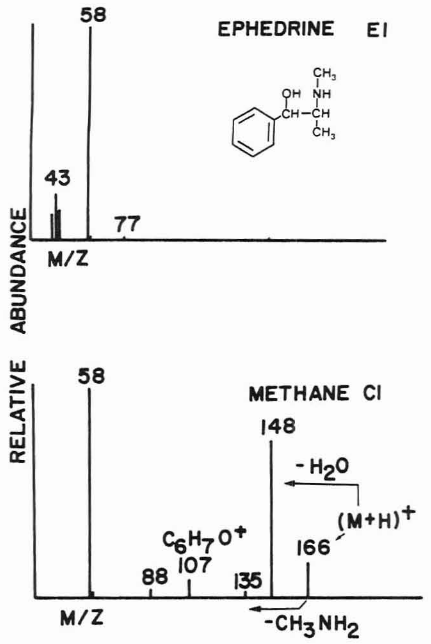

Figure 5. Comparison of electron ionization and methane chemical ionization spectra of ephedrine (MW 165).

Study of Ion/Molecule Reactions. It is often instructive to compare gas-phase ion/molecule reactions to solution chemistry (*44*), although the kinetics and thermodynamics associated with superficially analogous processes may differ greatly. Since solvation can affect both ion stability and accessible reaction mechanisms, gas-phase investigations can yield information about intrinsic reactivities of organic species. Moreover, reactive intermediates can occasionally be characterized. These well-known features of ion chemistry have prompted, inter alia, investigation of the gas-phase methylation and halomethylation of hydroxyaromatic compounds (*45, 46*).

Similar gas-phase alkylations may be performed by using the ion trap. With methyl chloride as the reagent, adduct species were produced from phenol. For the first experiments, the rf voltage was rapidly raised to rf level 2 to maximize the generation of m/z 49, CH_2Cl^+. Only small amounts (8% relative to m/z 49) of another reagent at m/z 65, $CH_3ClCH_3^+$, were observed, but two products, at m/z 95 and 107, were produced from phenol in equal abundance. Simple protonation of phenol by reagent ions derived from water, phenol, or methyl chloride yields the m/z 95 species, while 107^+ most likely corresponds to the product of halomethylation followed by dehydrohalogenation, viz. $C_6H_5OH + CH_2Cl^+ - HCl$. This reaction results in net *addition of methyne*. Under the same reaction conditions, methylated phenol is not observed. Increasing the first reaction interval to 85 ms allowed production of m/z 65 (dimethylchloronium ion) as the major reagent. In this case, a small amount of methylation (4% of total product ions) occurred with slightly less extensive halomethylation and protonation of phenol. The major products were still at m/z 95 and 107. The structures of the methylated phenol species have not been examined in detail. An appropriate method for studying the structures of such species would be the use of tandem mass spectrometry, which is possible with the

MS/MS version of the ion trap (*14*).

CONCLUSIONS

The ion trap has proved to be a useful device for chemical ionization. The spectra obtained by using a variety of reagent gases both for proton transfer reactions and charge exchange are consistent with expectations and comparable to those obtained by using conventional mass spectrometers. Those differences that are observed are accounted for by the variation in pressure and ion lifetimes. The problem of EI interferences is eliminated by using the selective mass storage feature. The trap's ability to store and accumulate ions facilitates study of ion/molecule reactions when using the mass-selective instability scanning method. Because of its capability for time resolution and selective storage of ions, the trap holds promise as a versatile instrument for operation in the CI mode and for detailed investigations of ion/molecule chemistry.

ACKNOWLEDGMENT

George Stafford, Michael Weber-Grabau, Paul Kelley, and John Syka, all of Finnigan MAT, and Jon Amy are thanked for valuable assistance.

Registry No. Cyclohexane, 110-82-7; cyclohexanone, 108-94-1; acetic anhydride, 108-24-7; 2-pentanol, 6032-29-7; fluorobenzene, 462-06-6; butyraldehyde, 123-72-8; *o*-nitrotoluene, 88-72-2; 2,2,6-trimethylcyclohexanone, 2408-37-9; triethylamine, 121-44-8; 2-ethylpyridine, 100-71-0; 2-methoxypyridine, 1628-89-3; toluene, 108-88-3; benzaldehyde, 100-52-7; naphthalene, 91-20-3; phenol, 108-95-2; anisole, 100-66-3; methane, 74-82-8; isobutane, 75-28-5; ammonia, 7664-41-7.

LITERATURE CITED

(1) Borman, S. *Anal. Chem.* **1983**, *55*, 726A.
(2) Stafford, G. C., Jr.; Kelley, P. E.; Bradford, D. C. *Am. Lab.* (*Fairfield, Conn.*) **1983**, *15* (June), 51.
(3) Kelley, P. E.; Stafford, G. C., Jr.; Syka, J. E. P.; Reynolds, W. E.; Louris, J. N.; Amy, J. W.; Todd, J. F. J. *33rd Annual Conference on Mass Spectrometry and Allied Topics*; San Diego, CA, 1985; p 707.
(4) Louris, J. N.; Brodbelt, J. S.; Cooks, R. G. *Int. J. Mass Spectrom. Ion Processes*, in press.
(5) Paul, W.; Steinwedel, H. U.S. Patent 2 939 952, 1960.
(6) Stafford, G. C., Jr.; Kelley, P. E.; Syka, J. E. P.; Reynolds, W. E.; Todd, J. F. J. *Int. J. Mass Spectrom. Ion Processes* **1984**, *60*, 85.
(7) Stafford, G. C., Jr.; Kelley, P. E.; Stephens, D. R. U.S. Patent 4 540 884, 1985.
(8) Todd, J. F. J.; Lawson, D. H.; Bonner, R. F. *Quadrupole Mass Spectrometry and its Applications*; Dawson, P. H., Ed.; Elsevier: Amsterdam, 1976; Chapter 8.
(9) Munson, B.; Field, F. M.; *J. Am. Chem. Soc.* **1965**, *87*, 3294.
(10) Munson, B. *Anal. Chem.* **1971**, *43*, 28A.
(11) Munson, B. *Anal. Chem.* **1977**, *49*, 9.
(12) Richter, W. J.; Schwarz, H. *Angew. Chem., Int. Ed. Engl.* **1979**, *17*, 424.
(13) Harrison, A. G. *Chemical Ionization Mass Spectrometry*; CRC Press: Boca Raton, FL, 1983.
(14) Louris, J. N.; Cooks, R. G., Syka, J. E. P.; Kelley, P. E.; Stafford, G. C., Jr.; Todd, J. F. I. *Anal. Chem.*, in press.
(15) Kelley, P. E.; Stafford, G. C., Jr.; Syka, J. E. P.; Reynolds, W. E.; Louris, J. N.; Todd, J. F. J. *Tenth International Mass Spectrometry Conference*; Swansea, United Kingdom, 1985.
(16) Bonner, R. F.; Lawson, G.; Todd, J. F. J. *Int. J. Mass Spectrom. Ion Phys.* **1972**, *10*, 197.
(17) Lawson, G.; Bonner, R. F.; Mather, R. E.; Todd, J. F. J.; March, R. E. *J. Chem. Soc., Faraday Trans. 1* **1976**, *2*, 545.
(18) Lawson, G.; Todd, J. F. J.; Bonner, R. F. *Dynamic Mass Spectrometry*; *Price*, D., Todd, J. F. J., Eds.; Heyden: London, 1975; Vol. 4, p 39.
(19) Todd, J. F. J. *Dynamic Mass Spectrometry*; Price, D., Todd, J. F. J., Eds.; Heyden: London, 1981; Vol. 6, p 44.
(20) Mather, R. E.; Lawson, G.; Todd, J. F. J.; Baker, J. M. B. *Int. J. Mass Spectrom. Ion Phys.* **1978**, *28*, 347.
(21) Bonner, R. F.; Lawson, G.; Todd, J. F. J. *J. Chem. Soc., Chem. Commun.* **1972**, 1179.
(22) Bonner, R. F.; Lawson, G.; Todd, J. F. J.; March, R. E. *Adv. Mass Spectrom.* **1974**, *6*, 377.
(23) Lawson, G.; Todd, J. F. J. *Anal. Chem.* **1977**, *49*, 1619.
(24) Baldeschweiler, J. D. *Science* **1968**, *159*, 263.
(25) Gross, M. L., Rempel, D. L. *Science* **1984**, *226*, 261.
(26) Clow, R. P.; Futrell, J. M.; *J. Am. Chem. Soc.* **1972**, *96*, 3748.
(27) Pesheck, C. V.; Buttrill, S. E., Jr. *J. Am. Chem. Soc.* **1974**, *96*, 6027.
(28) Hunter, R. L., McIver, R. T., Jr. *Anal. Chem.* **1979**, *51*, 699.
(29) Ghaderi, S.; Kulkarni, P. S.; Ledford, E. B., Jr.; Wilkens, C. L.; Gross, M. L. *Anal. Chem.* **1981**, *53*, 428.
(30) Freiser, B. S. *Talanta* **1985**, *32*, 697.
(31) Field, F. H., Munson, M. S. B. *J. Am. Chem. Soc.* **1965**, *87*, 3289.
(32) Huntress, W. T., Jr., Pinizzotto, R. F., Jr. *J. Chem. Phys.* **1973**, *59*, 4742.
(33) Walder, R.; Franklin, J. L. *Int. J. Mass Spectrom. Ion Phys.* **1980**, *636*, 85.
(34) Beynon, J. H. *Mass Spectrometry and its Applications to Organic Chemistry*; Elsevier: New York, 1960.
(35) Einolf, N.; Munson, B. *Int. J. Mass Spectrom. Ion Phys.* **1972**, *9*, 141.
(36) Hunt, D. F.; Gale, P. J. *Anal. Chem.* **1984**, *56*, 1111.
(37) Hsu, C. S.; Cooks, R. G. *Org. Mass Spectrom.* **1976**, *11*, 975.
(38) Munson, M. S. B.; Field, F. H. *J. Am. Chem. Soc.* **1966**, *88*, 4337.
(39) Field, F. H. *J. Am. Chem. Soc.* **1969**, *91*, 6334.
(40) Field, F. H. *J. Am. Chem. Soc.* **1969**, *91*, 2827.
(41) Wood, K. V.; McLuckey, S. A.; Cooks, R. G. *Org. Mass Spectrom.* **1986**, *21*, 11.
(42) McAdoo, D. J.; Hudson, C. E. *J. Am. Chem. Soc.* **1981**, *103*, 7710.
(43) *Automatic Gain Control*, *Option 660*; Finnigan MAT: San Jose, CA.
(44) Morton, T. H. *Tetrahedron* **1982**, *38*, 3195
(45) Lane, D. C., McGuire, J. M. *Org. Mass Spectrom.* **1983** *18*, 494.
(46) Isern-Flecha, I.; Cooks, R. G.; Wood, K. V. *Int. J. Mass Spectrom. Ion Processes* **1984**, *62*, 73.

RECEIVED for review October 16, 1986. Accepted December 19, 1986. This work was supported by the National Science Foundation CHE 84-08258.

Anal. Chem. **1987**, *59*, 1286–1295

Theoretical Description of Nonlinear Chromatography, with Applications to Physicochemical Measurements in Affinity Chromatography and Implications for Preparative-Scale Separations

James L. Wade, Alan F. Bergold, and Peter W. Carr*

Department of Chemistry, University of Minnesota, 207 Pleasant Street, Minneapolis, Minnesota 55455

The theory of nonlinear chromatography is developed further, and the behavior of chromatographic peaks obtained under nonlinear conditions is described by extensive computations of peak moment values. It is shown that when adsorption/desorption rates are slow, band broadening is insensitive to, or may actually be *decreased* by, a moderate degree of column overload. The linear model of Horvath and Lin and the nonlinear model developed here are used to characterize the retention behavior of *p*-nitrophenyl-α-D-mannopyranoside on silica-bound Concanavalin-A affinity columns. The two theories are compared in terms of their general applicability and the significance of the thermodynamic and kinetic constants derived from each. For heterogeneous affinity adsorbents such as Concanavalin-A (Con-A) more meaningful physical constants are derived by applying nonlinear theory to data obtained under the *most severe* nonlinear conditions. The analysis presented here yields adsorption/desorption rate constants and the binding site density for the more populous binding site in immobilized Con-A.

In this paper, we present the impulse input solution to the equations describing nonlinear chromatography, characterize its theoretical behavior, and use it to make physicochemical measurements in affinity chromatography. Efforts to derive a valid and workable theory of nonlinear chromatography grew out of earlier work in this laboratory (*1*, *2*), in which the Horvath and Lin model was used in measuring thermodynamic and kinetic quantities from chromatographic data. A serious practical difficulty of this approach is that it requires the experimental data be obtained under linear isotherm conditions, that is, at "infinite dilution". In affinity chromatography, this is difficult to achieve because of the low density of binding sites and, in the case of immobilized Concanavalin-A, the heterogeneity of these sites (*1*). Even when minute quantities of solute are injected, and linear conditions are approached, the signal-to-noise ratio of the resulting data is often so poor that precise measurement of the second moment becomes very difficult. The precision of this measurement is of critical importance in properly deconvolving the plate height contributions via the Horvath and Lin method (*3*, *4*). This paper describes the successful application of a new theoretical approach to the measurement of thermodynamic and kinetic parameters in affinity chromatography. The parameters obtained by fitting a nonlinear model to experimental chromatograms are compared to those obtained by the Horvath and Lin method.

The potential applications of a model for nonlinear chromatography, however, go beyond its use in physicochemical measurements. Preparative-scale chromatography, in which the column is overloaded to a significant extent, has long been in need of a more detailed theoretical description. Several treatments have relied upon the assumption of equilibrium conditions (infinitely fast adsorption/desorption kinetics) and a parabolic isotherm to approximate the Langmuir isotherm (*5–7*). While adequate for describing preparative gas chromatography, this approach is not valid for most liquid chromatography systems because interphase solute transfer cannot be considered infinitely fast. Moreover, the use of a parabolic isotherm limits the degree of column overload that may be simulated.

Although the equation for a finite chromatographic pulse under nonlinear, nonideal conditions was derived by Goldstein in 1953 (*8*), it has never been used to describe preparative-scale chromatography. There are two reasons for this: the solution is extremely difficult to evaluate, and there has been no precise, efficient way to evaluate the necessary Bessel function integrals (*9*). In the Appendix to this paper, we present an algorithm that is a significant improvement over the cumbersome and imprecise approximations that have been used in the past (*8–12*).

The impulse input solution, which is derived in the theoretical section of this paper, is simply an extension of the original solution for breakthrough curves obtained by Thomas in 1944 (*13*). It is also the easiest to evaluate, since it only contains one Bessel function integral; the breakthrough curve solution contains two, and the pulse solution contains four. The computer calculations described in the second part of the theoretical section provide a complete characterization, in terms of the first three peak moments, of chromatographic peaks obtained under nonlinear conditions. Understanding the behavior of these moments will be useful in optimizing preparative-scale separations.

THEORY

Derivation of the Impulse Input Solution. When axial dispersion (axial diffusion and "eddy diffusion") is negligible, the chromatographic mass balance and kinetic equations, along with the associated boundary and initial conditions, are given as follows:

$$u\frac{\partial C}{\partial x} + \frac{\partial C}{\partial t} + \epsilon\frac{\partial q}{\partial t} = 0 \qquad (1)$$

$$\frac{\partial q}{\partial t} = k_a(S_0 - q)C - k_d q \qquad (2)$$

$$C(0,t) = C_0\delta(t) \qquad (3)$$

$$q(x,0) = 0 \qquad (4)$$

where x is distance (cm) and t is time (s), C is the concentration of solute in the mobile phase (M), q is the concentration of solute in the stationary phase (M; moles of solute per liter of solid phase), S_0 is the concentration of binding sites (M; same units as q), k_a is the rate constant for solute adsorption (M^{-1} s^{-1}), k_d is the rate constant for solute desorption (s^{-1}), u is the chromatographic velocity (cm/s; the velocity of

0003-2700/87/0359-1286$01.50/0 © 1987 American Chemical Society

an unsorbed solute which explores the pores and elutes at t_0), ϵ is the porosity ratio which equals $(1 - \epsilon_T)/\epsilon_T$, where ϵ_T is the total porosity of the column (*4*), and C_0 is the concentration of solute injected (M) multiplied by the width of the injection pulse (as a fraction of column dead volume). We are thus assuming that the strength of an impulse function can be treated as the area of a very narrow pulse. We justify this assumption in the Discussion.

Slow mass transfer through the stagnant mobile phase may be treated as a contributing factor to k_a and k_d. Arnold has worked out the theoretical aspects of this (*14, 15*) and has applied her theory to measurements in affinity chromatography (*11*). We address this subject in more detail in the Discussion. After the independent variables, x and t, are rendered in dimensionless form, eq 1 and 2 become

$$\frac{\partial C}{\partial z} + \frac{\partial \tilde{q}}{\partial y} = 0 \tag{5}$$

$$\frac{\partial \tilde{q}}{\partial y} = \gamma[k'C - K\tilde{q}C - \tilde{q}] \tag{6}$$

where

$$\tilde{q} = \epsilon q$$

$$z = x/L$$

$$y = (t/t_0) - z$$

$$\gamma = k_d t_0$$

$$k' = (k_a/k_d)S_0\epsilon$$

$$KC_0 = (k_a/k_d)C_0$$

Application of the Thomas transformation (*12, 13*) to linearize eq 5 and 6 requires the following substitutions:

$$C(z,y) = \frac{\Psi_y(z,y)}{\gamma K \Psi(z,y)} - \frac{1}{K} \tag{7}$$

$$\tilde{q}(z,y) = \frac{k'}{K} - \frac{\Psi_z(z,y)}{\gamma K \Psi(z,y)} \tag{8}$$

$\Psi(z,y)$ is a yet-to-be obtained function of dimensionless distance and time, and the subscripts to Ψ denote its derivatives. Substitution of eq 7 and 8 into eq 5 and 6 leads to the linear equation:

$$\frac{\partial^2 \Psi(z,y)}{\partial z \partial y} = \gamma^2 k' \Psi(z,y) \tag{9}$$

In order to solve eq 9 and obtain an expression for $C(z,y)$, it is first necessary to develop expressions for the boundary and initial conditions. We are indebted to Rutherford Aris for his helpful comments on this subject. The relevant expressions are obtained by integrating eq 7 and 8

boundary condition:

$$H(y) = \Psi(0,y) = \Psi(0,0) \exp\left[\gamma K \int_0^y C(0,y')\,\mathrm{d}y' + \gamma y\right] \tag{10}$$

initial condition:

$$G(z) = \Psi(z,0) = \Psi(0,0) \exp\left[\gamma k'z - \gamma K \int_0^z \tilde{q}(z',0)\,\mathrm{d}z'\right] \tag{11}$$

Since Ψ occurs homogeneously in C and $\tilde{q}$, the value of $\Psi(0,0)$ must be the same in eq 10 and 11 (*16*); in accord with previous derivations (*8, 12, 17, 18*), we take it to be equal to unity. Substitution of eq 3 and 4 then leads to

$$H(y) = \exp[\gamma y] \exp\left[\gamma K C_0 \int_0^y \delta(y')\,\mathrm{d}y'\right] \tag{12}$$

$$G(z) = \exp[\gamma k'z] \tag{13}$$

The general solution to eq 9, which will be developed later, requires that an expression for $H(0)$ be obtained from eq 12. Because of the discontinuous nature of the delta function, however, this can only be derived by taking the limit of $H(y)$ as $y \rightarrow 0$, and the result is different depending on the direction of approach to the limit. Taking the limit as $y \rightarrow 0^+$ gives a value of $H(0)$ which leads to the correct expression for $C(z,y)$. Taking the limit as $y \rightarrow 0^-$ leads to an analogous expression for $\tilde{q}(z,y)$. We are only interested in the former case, and summarize here the resulting initial and boundary conditions, which will be required in the general solution

$$H(0^+) = \exp[\gamma K C_0] \tag{14a}$$

$$H'(0^+) = \gamma \exp[\gamma K C_0] \tag{14b}$$

$$H(y) = \exp[\gamma K C_0] \exp[\gamma y] \tag{14c}$$

$$H'(y) = \gamma \exp[\gamma K C_0] \exp[\gamma y] \tag{14d}$$

$$H''(y) = \gamma^2 \exp[\gamma K C_0] \exp[\gamma y] \tag{14e}$$

$$G(0) = 1 \tag{15a}$$

$$G(z) = \exp[\gamma k'z] \tag{15b}$$

$$G'(z) = \gamma k' \exp[\gamma k'z] \tag{15c}$$

The general solution to eq 9 is derived by using the two-dimensional Laplace transform (*19*), in which p is the Laplace variable for distance and q is the analogous time variable. After considerable algebraic manipulations, invertable Laplace-domain solutions for $\Psi(z,y)$ and $\Psi_y(z,y)$ are obtained as follows:

$$\mathcal{L}^2\{\Psi(z,y)\} = F(p,q) = \left[\frac{1}{pq - \gamma^2 k'}\right][pF(p,0) - G(0)] + \left[\frac{1}{pq - \gamma^2 k'}\right] \times [qF(0,q) - H(0)] + \left[\frac{1}{pq - \gamma^2 k'}\right][H(0) + G(0) - \Psi(0,0)] \tag{16}$$

$$\mathcal{L}^2\{\Psi_y(z,y)\} = (qF(p,q) - F(p,0)) = \gamma^2 k'\left[\frac{1}{pq - \gamma^2 k'}\right]F(p,0) + \left[\frac{1}{pq - \gamma^2 k'}\right]H'(0) + \left[\frac{1}{pq - \gamma^2 k'}\right][q^2F(0,q) - qH(0) - H'(0)] + \left[\frac{q}{pq - \gamma^2 k'} - 1 + 1\right][H(0) - \Psi(0,0)] \tag{17}$$

By application of the convolution theorem (*19*), general solutions are obtained

$$\Psi(z,y) = \int_0^z G'(z - z')I_0(2\gamma(k'z'y)^{1/2})\,\mathrm{d}z' + \int_0^y H'(y - y')I_0(2\gamma(k'zy')^{1/2})\,\mathrm{d}y' + [H(0) + G(0) - \Psi(0,0)]I_0(2\gamma(k'yz)^{1/2}) \tag{18}$$

$$\Psi_y(z,y) = \gamma^2 k' \int_0^z G(z - z')I_0(2\gamma(k'z'y)^{1/2})\,\mathrm{d}z' + \int_0^y H''(y - y')I_0(2\gamma(k'zy')^{1/2})\,\mathrm{d}y' + [H(0) - \Psi(0,0)][\gamma(k'z/y)^{1/2}I_1(2\gamma(k'yz)^{1/2}) + \delta(y)] + H'(0)I_0(2\gamma(k'yz)^{1/2}) \tag{19}$$

$I_0(x)$ and $I_1(x)$ denote the zeroth- and first-order modified

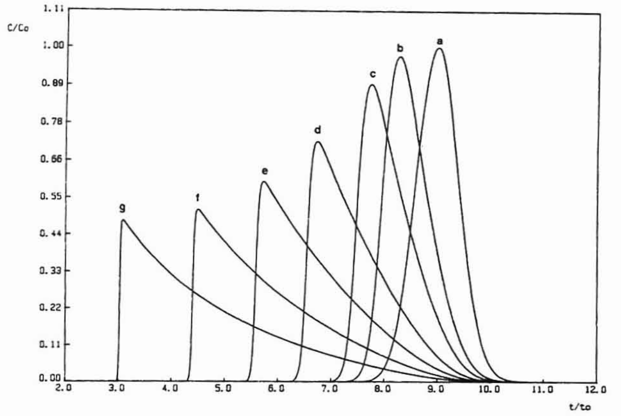

Figure 1. Theoretical peaks generated by eq 22: $k' = 8$; $\gamma = 100$; $KC_0 = 0$ (a), 0.05 (b), 0.10 (c), 0.25 (d), 0.50 (e), 1.0 (f), 2.0 (g).

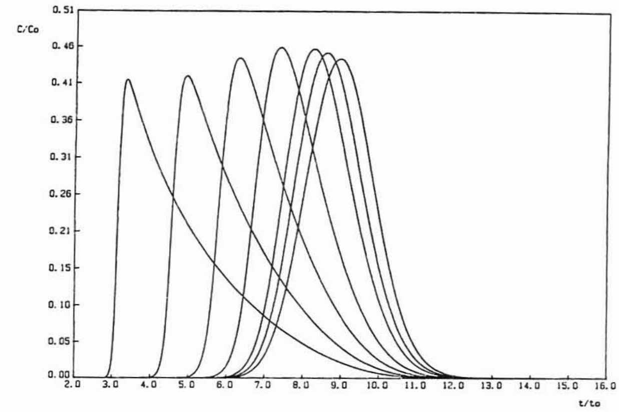

Figure 2. Same conditions as Figure 1, except with $\gamma = 20$.

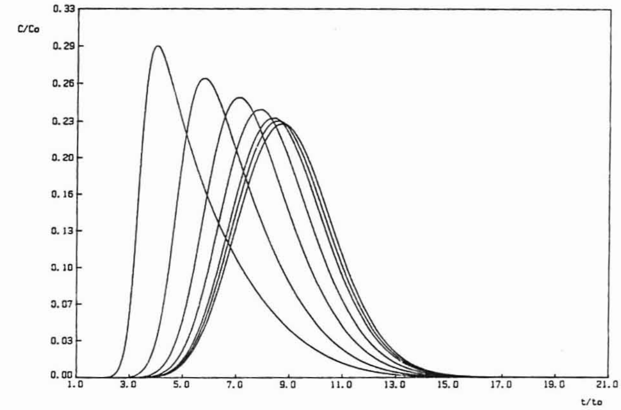

Figure 3. Same conditions as Figure 1, except with $\gamma = 5$.

Bessel functions (of the first kind), respectively.

It should also be noted that if delta functions are absent from the boundary and initial conditions, then $H(0) = G(0) = \Psi(0,0) = 1$, and the above equations reduce to those given by Amundson (*17*) and Aris and Amundson (*18*). The presence of a delta function in our boundary condition, however, requires that $H(0)$ be more carefully specified in the derivation of the general solution.

Upon substitution of eq 14a–e and 15a–c into the general solutions, it becomes clear that each of the integrals in eq 18 and 19 may be represented by a Thomas ϕ function (*12, 13*). The definition of this function is given in the Appendix. Thus

$$\Psi(z,y) = \phi(\gamma k'z,\gamma y) + \exp[\gamma KC_0]\phi(\gamma y,\gamma k'z) + \exp[\gamma KC_0]I_0(2\gamma(k'yz)^{1/2}) \quad (20)$$

$$\Psi_y(z,y) = \gamma\phi(\gamma k'z,\gamma y) + \gamma\exp[\gamma KC_0]\phi(\gamma y,\gamma k'z) + \gamma\exp[\gamma KC_0]I_0(2\gamma(k'yz)^{1/2}) + [\exp[\gamma KC_0] - 1][\gamma(k'z/y)^{1/2}I_1(2\gamma(k'yz)^{1/2}) + \delta(y)] \quad (21)$$

Equations 20 and 21 may now be substituted into eq 7 to develop an expression for $C(z,y)$. By application of some of the identities given in the Appendix and the fact that we are only concerned with the peak shape at the end of the column ($z = 1$), the final result may be obtained as

$$\frac{C}{C_0} = \left[\frac{1 - \exp[-\gamma KC_0]}{\gamma KC_0}\right] \times \left[\frac{(\gamma(k'/y)^{1/2}I_1(2\gamma(k'y)^{1/2}) + \delta(y))\exp[-\gamma y - \gamma k']}{1 - T(\gamma k',\gamma y)(1 - \exp[-\gamma KC_0])}\right] \quad (22)$$

where

$$\gamma = k_d t_0 \quad (22a)$$

$$k' = (k_a/k_d)S_0\epsilon \quad (22b)$$

$$KC_0 = (k_a/k_d)C_0 \quad (22c)$$

$$y = (t/t_0) - 1 \quad (22d)$$

The T function is defined in the Appendix. In the limit of a very high, very narrow pulse, the solution of Goldstein (*8*) becomes identical with eq 22. This is demonstrated in the Discussion.

Characterization of the Impulse Input Solution. To carry out a comprehensive and detailed analysis of nonlinear chromatography, eq 22 was used to generate theoretical chromatographic peaks under a wide variety of parameter conditions. With the noted exceptions, peaks were generated for all permutations of the following conditions: rate parameter, γ = 5, 10, 20, 40, 60, 80, 100; overload parameter, KC_0 = 0, 0.05, 0.10, 0.25, 0.50, 1.00, 2.00; thermodynamic k', k' = 1*, 2**, 4, 8, 12, 16, 20. (*No peaks were generated for KC_0 = 1.00 and KC_0 = 2.00. **No peaks were generated for KC_0 = 2.00.). A total of 322 peaks were thus obtained. Some of these are depicted in Figures 1–3. All calculations were performed on a Zenith-151 microcomputer equipped with an 8087 numeric coprocessor, and programs were written in double-precision Turbo-87 Pascal (Borland International). The Appendix describes the algorithm for evaluating Bessel function integrals.

The peaks were generated so that each would be represented by 50–75 points prior to the peak maximum, and 50–75 points after the peak maximum. This approach was adopted to adequately characterize extremely skewed peaks. The largest values for the column overload parameter (KC_0) often resulted in peaks that were, as expected, virtually right triangular; high point densities in the region of the discontinuity were thus required, while lower point densities were adequate for the long peak tail. The peak "beginning" and "end" were defined as the first points to fall below a threshhold level of 10^{-6} times the peak maximum. Each peak was integrated by Simpson's rule (*20*) to obtain the first three normalized, centralized moments (*1*). (For simplicity, we refer to these as just "moments".) The behavior of these moments under nonlinear conditions is summarized in Figures 4–6. In order to fully characterize the μ_1 curves, it was also necessary to obtain additional points at very low values of the column overload parameter. Hence, the curves in Figure 4 were completed by generating peaks with $KC_0 = 10^{-6}$, 10^{-4}, and 10^{-2}.

The first moment clearly demonstrates the characteristic decrease with increasing column overload. When the kinetics of adsorption/desorption are fast—i.e., approaching equilibrium—the decrease begins at a lower solute concentration (KC_0) and is more rapid. The decrease in the first moment is less pronounced when the kinetics are slow. This is due to the peak broadening, and hence concentration di-

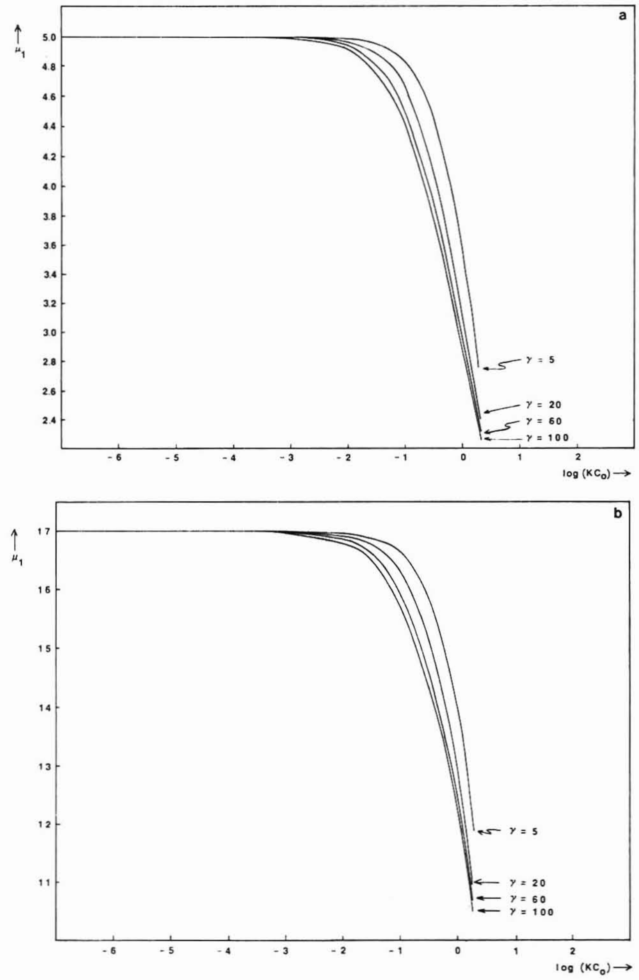

Figure 4. Behavior of the first normalized, centralized peak moment (μ_1) as a function of column overload: $k' = 4$ (a), and $k' = 16$ (b).

minishing, effect of slow kinetics. It should be noted that this general behavior is independent of the value of the thermodynamic k'. Figure 4 also indicates that in each case, the first moment begins to show a significant decrease at about $KC_0 = 0.01$. Indeed, the onset of the overload effect seems to occur at roughly this value of KC_0 for all the k' values investigated here.

The behavior of the second moment with increasing column overload is most interesting. Figure 5 indicates that when the kinetics of adsorption/desorption are slow, or the flow rate is fast, a moderate increase in column overload will actually *decrease* the second moment. The degree to which the column may be overloaded before the second moment begins to increase depends upon the kinetic parameter: the slower the kinetics, or the faster the flow rate, the more the column may be overloaded. Figure 5b also indicates that for solutes with a large thermodynamic k', the second moment is surprisingly insensitive to even moderate degrees of column overload, provided that the kinetics are sufficiently slow. Arnold's assertion that "the major effect of isotherm nonlinearity is zone spreading" (*21*) is thus strictly true only in the case of rapid interphase mass transfer.

This behavior has important implications for the applicability of the Horvath and Lin equations (*4*). It suggests that for well-retained solutes which exhibit slow rates of interphase mass transfer, the approach based on plate height equations—which is strictly valid only under linear conditions (*4, 11*)—may be useful under conditions of small to moderate column overload. We examine this hypothesis in the Discussion.

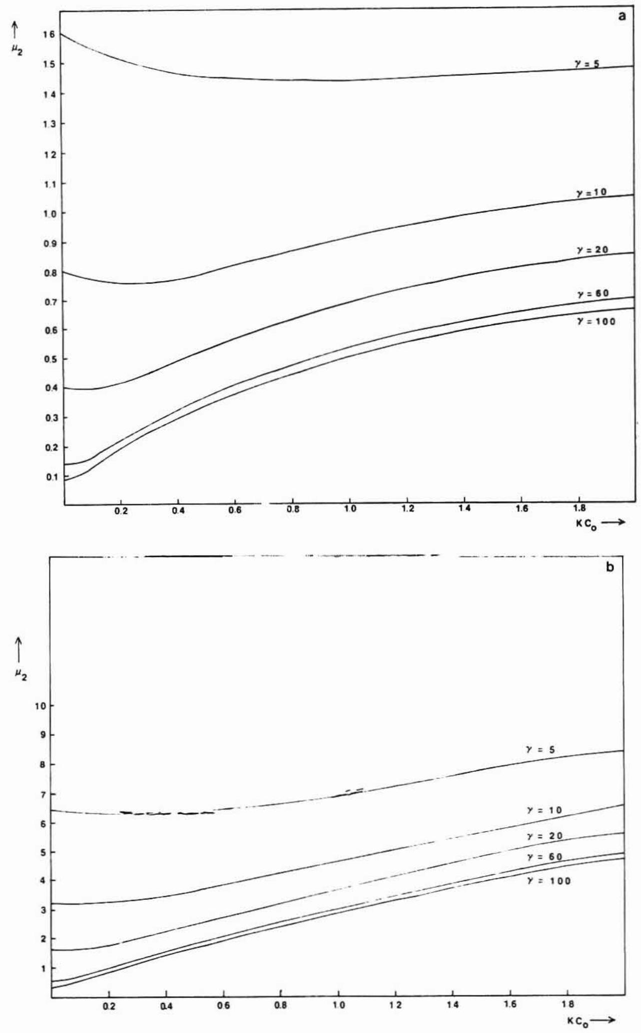

Figure 5. Behavior of the second normalized, centralized peak moment (μ_2) as a function of column overload: $k' = 4$ (a), and $k' = 16$ (b).

The behavior of the third moment, which reflects peak asymmetry, is shown in Figure 6. As expected, slow interphase mass transfer and column overload lead to more asymmetric peaks. The trends are monotonic and, in the case of well-retained solutes, virtually linear with KC_0.

It should also be noted that in some of our theoretically generated peaks, the "split peak" phenomenon (*22*) was observed. Split peaks occur when the kinetics of adsorption are so slow that a significant fraction of the solute does not adsorb even once, and elutes at the dead volume. The mathematical manifestation of this phenomenon is the δ function in eq 22. In the calculations carried out here, split peaks were observed only for the lowest values of k' and γ. In order to observe the effect with better-retained peaks, it would be necessary to carry out simulations using much smaller values of γ than those used here.

EXPERIMENTAL SECTION

Materials and Column Preparation. Concanavalin-A (Con-A, type IV), *p*-nitrophenyl-α-D-mannopyranoside (pNp-mannoside), uracil, and glutaraldehyde were purchased from Sigma Chemical Co. (St. Louis, MO). The Con-A was purified by the method of Cunningham (*23*). (γ-Aminopropyl)trimethoxysilane was purchased from Petrarch Systems, Inc. (Levittown, PA), and PSM-500 silica (lot no. 6; pore diameter, 500 Å; particle size, 8 μm) was obtained from Du Pont (Wilmington, DE). The Con-A was immobilized on the silica by the previously described method (*1*), except that sodium borate buffer (pH 8.5) was used in place of the phosphate buffer. The immobilization reaction was monitored spectrophotometrically (at 280 nm) to determine the amount of Con-A immobilized. The material was slurry packed, from HPLC grade water at 3000 psi, into a 2.1 mm × 5 cm column blank equipped with 2-μm screen end fittings.

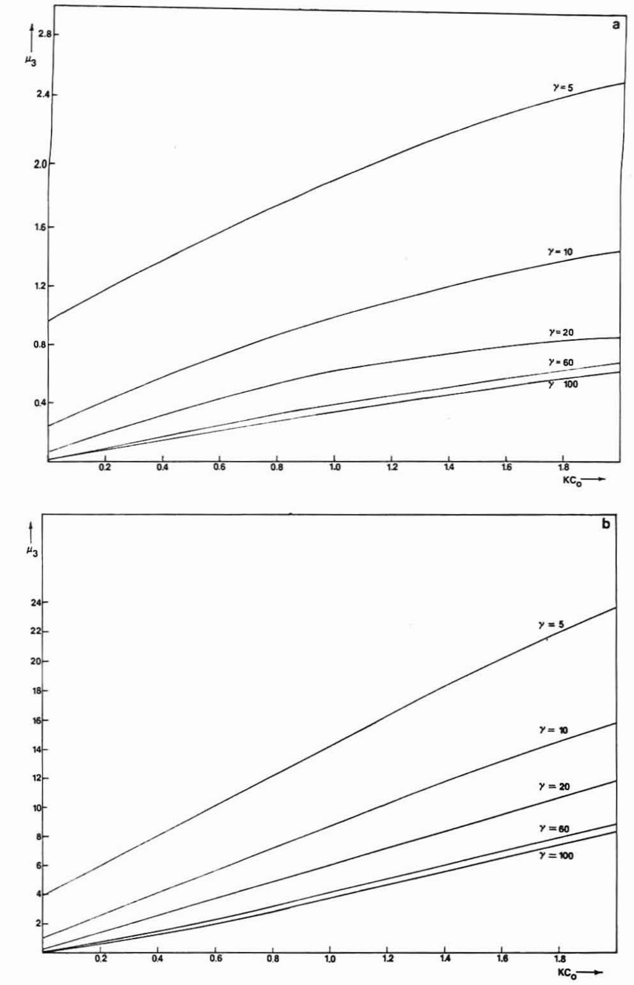

Figure 6. Behavior of the third normalized, centralized peak moment (μ_3) as a function of column overload: $k' = 4$ (a), and $k' = 16$ (b).

Equipment and Chromatographic Conditions. The chromatographic system consisted of a Hewlett-Packard 1084B liquid chromatograph, a Rheodyne 7120 injector fitted with a 10-μL loop, and a Perkin-Elmer LC-15 UV detector equipped with a 10-μL Max N flow cell, upgrade board, and 280-nm filter. The detector time constant was set to 0.2 s for uracil injections and 2 s for all others. The detector output was amplified by a Keithly 140 nV dc amplifier with a 99% rise time of 5 s (0.5 s for uracil injections). Data were digitized and stored in an Apple II+ microcomputer equipped with an Adalab analog-to-digital (A/D) converter (Interactive Microware, Inc., State College, PA). Data acquisition, which was controlled by Vidichart II software, was at a rate of 1 point/s for all injections except uracil (20 points/s).

The mobile phase used throughout this work was 0.02 M sodium phosphate buffer (pH 6.0) containing 0.5 M NaCl, 0.01 M $MgCl_2$, and 0.001 M $CaCl_2$. The temperature was maintained at 25 ± 0.2 °C by use of a Haake Model FE circulating thermostat. The dead time of the chromatographic system, as determined from uracil injections, was 9.53 ± 0.02 s at a flow rate of 1.0 mL/min.

Concentration Study. To obtain data suitable for analysis by nonlinear theory, pNp-mannoside was injected onto the Con-A column at six different concentrations: 35.95, 71.91, 143.8, 215.7, 359.6, and 719.2 μM. Four replicate injections were made at each concentration, and in all cases, the flow rate was 1.0 mL/min. Raw data files for each injection were then transferred to a Zenith-151 microcomputer (with 8087 coprocessor) for subsequent analysis and fitting to eq 22.

After subtracting the base line (which was determined by a least-squares procedure), the amplitude of each point in a data file was normalized to the sensitivity of the detector and the relative concentration of injected solute. The time at which each point was taken was normalized to the dead time of the system. Data pairs (normalized time, normalized concentration) were then stored on disk for later access by the data fitting program. Each peak stored was represented by at least 200 points.

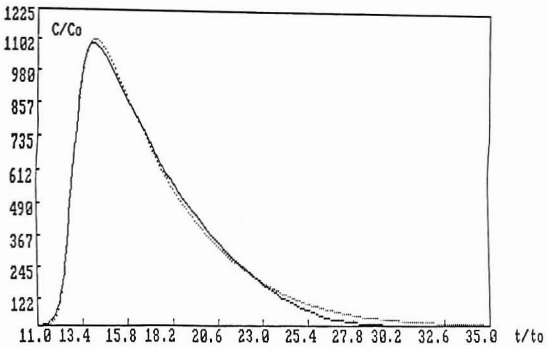

Figure 7. Experimental data fit using eq 22: concentration injected, 719.2 μM; "best fit" parameters, $\gamma = 8.203$, $k' = 22.37$, $KC_0 = 1.905$, $W = 6824$; the sum of residuals (defined in eq 23) was 5041; experiment (···), theory (——).

A simplex algorithm was used to fit eq 22 to the data. Four parameters were used in the fitting procedure: γ, k', KC_0, and W, a scaling factor. The scaling factor simply multiplies eq 22 so that the theoretical result is calibrated to the experimental point amplitude (in normalized A/D counts). Because of time constraints in the computation of eq 22, it was not possible to use all the data points (more than 200) in fitting experimental data. Hence, 25 points were chosen: 12 evenly spaced points before and after the peak maximum, as well as the peak maximum itself. The sum of residuals, defined in eq 23, was then minimized by the simplex algorithm. A typical data fit is shown in Figure 7.

$$R^2 = \sum_{i=1}^{25}[\bar{C}_i(\bar{t}_i) - \bar{C}(\gamma,KC_0,k',W,\bar{t}_i)]^2 \qquad (23)$$

where $\bar{C}_i$ is the experimental concentration (in normalized A/D counts) at the chosen value of normalized time, $\bar{t}_i$, and $\bar{C}$ is the theoretical concentration at $\bar{t}_i$, as calculated by eq 22 with the given set of parameters.

The fitting procedure was used several times on each peak, with different initial guesses, to assure that false minima were not obtained. It is also worth noting that the parameters obtained from the data fit in Figure 7 were not affected by the number of data points used in the fitting procedure. The number of points on the peak tail was doubled and then tripled; in each case, the same parameters were obtained. Typically, R^2 for the "best fit" was between 4000 and 6000, except for some injections at the lower concentrations, where poor signal-to-noise ratios caused R^2 to be somewhat higher (7000 or 8000). All of the data fits had the same general appearance as Figure 7; that is, the pattern of deviation between theory and experimental data was invariant.

Flow Rate Study. To obtain data suitable for analysis by the Horvath and Lin method, it is necessary to work under linear isotherm conditions and observe the effect of changing flow rates on the kinetic contribution to the plate height (*4*). Four flow rates were used in this study: 0.5, 1.0, 2.0, and 4.0 mL/min. Injections of pNp-mannoside were made at three concentrations: 71.91, 143.8, and 215.7 μM. Lower concentrations were not used because the signal-to-noise ratios of the resulting peaks were too poor to measure the second moments precisely. Base lines were calculated by a least-squares method consistent with the recommendations of Walters (*24*), and the peaks were integrated by Simpson's rule to yield normalized, centralized peak moments. From these, plate hieghts were calculated. Average relative standard deviations for the measured plate heights were as follows: 215 μM, 4.7%; 143 μM, 5.6%; 72 μM, 17.7%. Nonkinetic contributions to the total plate height were calculated by use of eq 16–18 in ref 4 and subtracted as shown below to yield kinetic plate height contributions

$$H_{\text{kin}} = H_{\text{measd}} - H_{\text{disp}} - H_{\text{i.diff}} - H_{\text{e.diff}} \qquad (24)$$

All of the nonkinetic terms were calculated using a particle diameter, d_p, of 8 μm and a solute diffusion coefficient, D_m, of 0.45 × 10^{-5} cm²/s (*1*). The H_{disp} term was calculated by use of structural parameters, λ and ω, of 7.5 and 2.7, respectively, and an interparticle obstruction factor, γ, of 0.6. The $H_{\text{i.diff}}$ and $H_{\text{e.diff}}$ terms were calculated by use of structural parameters, κ and k_0, of 1/15 and 0.6, respectively, and an intraparticle obstruction factor, θ,

Table I. Parameters Derived by Fitting Equation 22 to Experimental Data from Concentration Study[a]

sample	C_0[b] μM	rel concn	γ	k'	KC_0	$\overline{KC_0}$[c]	W
1	45.31	1.0	8.173 ± 0.129	22.40 ± 0.30	1.919 ± 0.052	1.919 ± 0.052	6847 ± 32
2	22.65	0.5	7.827 ± 0.093	23.71 ± 0.05	1.269 ± 0.013	2.537 ± 0.025	6867 ± 26
3	13.59	0.3	7.338 ± 0.037	24.31 ± 0.07	0.980 ± 0.018	3.265 ± 0.060	6882 ± 8
4	9.059	0.2	6.988 ± 0.047	24.84 ± 0.02	0.839 ± 0.007	4.195 ± 0.035	6839 ± 71
5	4.530	0.1	6.140 ± 0.096	25.40 ± 0.20	0.667 ± 0.043	6.670 ± 0.425	6854 ± 107
6	2.265	0.05	5.465 ± 0.282	25.87 ± 0.43	0.544 ± 0.090	10.87 ± 1.80	6894 ± 109

[a] Mobile phase: pH 6.0, 0.02 M sodium phosphate, 0.5 M sodium chloride, 0.01 M magnesium chloride, 0.001 M calcium chloride. Solute: 10 μL of pNp-mannoside. Flow Rate: 1.0 mL/min. System dead time: 9.53 s. [b] C_0 is the concentration of solute injected multiplied by 0.063, the width of the injection pulse as a fraction of column dead volume. [c] $\overline{KC_0}$ is defined as the actual value of KC_0 obtained in the data fit, divided by the relative amount injected.

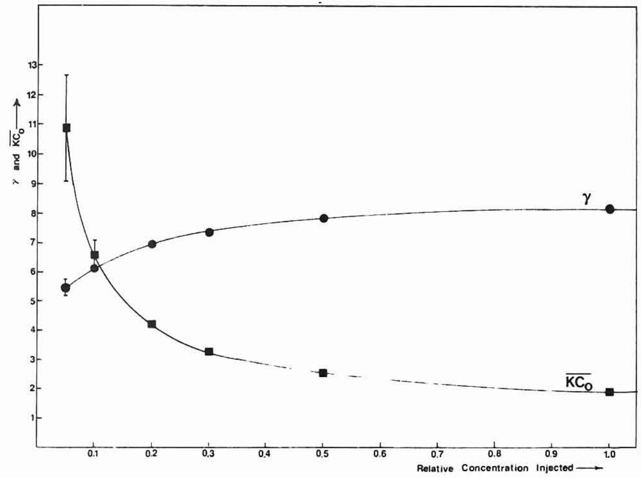

Figure 8. Plot of γ and $\overline{KC}_0$ (from Table I) as functions of the relative amount of solute injected.

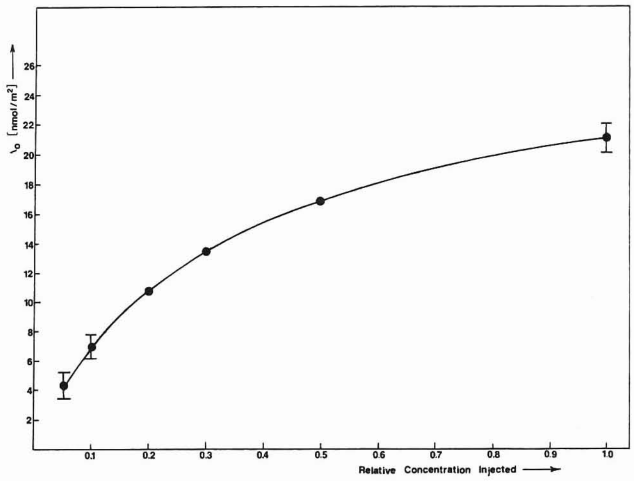

Figure 9. Plot of Λ_0 (in nmol/m²; determined from eq 25) as a function of the relative amount of solute injected.

of 2.0. H_{kin} values were then plotted as a function of interstitial flow velocity, U_e, so that by use of eq 19 in ref 4, desorption rate constants could be derived from the slopes of the plots.

RESULTS AND DISCUSSION

Application of Nonlinear Theory. The four parameters obtained by fitting eq 22 to experimental data are summarized in Table I. The scaling factor, which calibrates the amplitude of the theoretical peak to that of the experimental peak, is constant within the uncertainty of the individual fits, clearly indicating the precision and accuracy of the fitting procedure. $\overline{KC}_0$ is a normalized overload parameter, obtained by dividing the actual value of KC_0 (from the data fit) by the relative amount of solute injected (Table I, column 3).

If eq 22 is a valid description of the chromatographic system, then changes in the column overload parameter should be exactly accounted for by changes in the dilution factor of the sample injected; hence, $\overline{KC}_0$ should be constant. The rate parameter (γ) and the thermodynamic k' (from which binding site densities will be derived) should also be invariant with concentration. Figure 8 shows a plot of γ and $\overline{KC}_0$ as functions of the relative amount injected; Figure 9 shows a similar plot for the density of binding sites, Λ_0. Large error bars are the result of poor signal to noise (S/N) ratios at the lower concentrations. The values of Λ_0 were obtained from the "best fit" values of k' and KC_0 using the following relationship (*4*):

$$\Lambda_0 = \left(\frac{\epsilon_T}{\rho a_s}\right)\left(\frac{k'}{KC_0}C_0\right) \qquad (25)$$

where $\epsilon_T = \epsilon_e + \epsilon_i(1 - \epsilon_e)$. The interstitial and intraparticle porosities were both taken to be 0.4 (*25*); hence, $\epsilon_T = 0.64$. ρ is the density of adsorbent in the packed tube, which was taken to be 760 g/L (*25*). a_s is the specific surface area. The manufacturer's value of 20.9 m²/g was used, which is consistent with the literature value of 19 m²/g (*25*). C_0 is the concentration injected (in μM) times the fraction of the column dead volume represented by the 10-μL loop (0.063).

Before presenting an interpretation of the data in Table I and Figures 8 and 9, we first turn to a discussion of its robustness. During the course of testing our simplex optimizations for curve fitting, we observed that we could get false minima by fitting the majority of the peak exactly, and neglecting the extended peak tail. We could also get false minima by making better fits to the extended peak tail, and poorer fits to the rest of the peak. The fit pattern shown in Figure 7 is the least-squares compromise between these two. The rate parameter and the thermodynamic k' were both fairly insensitive to the false minima; they did not change much at all. The big differences came in the overload parameter (KC_0) and the calibration factor (W); both were significantly affected by the false minima. It is important to note that we could not consistently use one type of false minimum, and maintain the same calibration factor from one concentration to the next. Maintaining the same calibration factor, however, is absolutely vital to the reliability of the derived parameters. The values of W which we report in Table I for the least-squares fit maintain this consistency. We also point out that the least-squares criterion is really the only practical and fundamentally valid way to fit these peaks. The systematic lack of fit which we see in Figure 7 is consistent, we believe, with the interpretation we now present.

Figures 8 and 9 clearly indicate that after fitting the single site model (eq 22) to experimental data, all of the parameters obtained are concentration-dependent. This result is consistent with our earlier report that immobilized Con-A is heterogeneous with a small population of very strong sites and a large population of weaker sites (*1*). At lower concentrations of analyte, it would be expected that the small population of strong sites would play a relatively larger role in the retention process. This effect is clearly observed in Figures 8 and 9; the peak profile at lower concentrations is determined by a smaller number of binding sites and, hence, the relative column overload is increased.

The situation is quite different under conditions of high column loading; all of the parameters become constant. At high concentrations, the small population of strong sites is essentially saturated, and the large population of weaker sites then becomes the dominant factor in determining the shape, width, and position of the peak. Indeed, the effect of the small fraction of solute that saturates the strong sites is "drowned out" by the effect of the much larger fraction which interacts only with the weaker sites. The situation is analogous to the classic "flooding" experiments used in the study of reaction kinetics (*26*).

This has important implications for the general problem of characterizing heterogeneous affinity adsorbents. When physicochemical measurements are made at low concentrations ("infinite dilution"), the thermodynamic and kinetic parameters that are derived must inevitably reflect a complex convolution of different chemical processes. That is, they are "average" values. At higher concentrations, it is possible to "bury" some of these effects and measure physical parameters that better reflect one single, identifiable, chemical process. Although it would have been preferable to have data at somewhat higher concentrations, we nevertheless believe that the plateaus in Figures 8 and 9 are sufficiently well-established, particularly in the case of the dimensionless rate parameter, γ, to derive meaningful physical constants for the weaker binding site. Three questions must first be addressed, however: (1) To what extent does axial dispersion and extracolumn broadening affect the peak profile? (2) How valid is the impulse input approximation? (3) To what extent does the rate of mass transfer through the stagnant fluid affect the values of k_a and k_d which are obtained?

The effects of axial dispersion and extracolumn band broadening were examined by injecting uracil, which is taken to be unretained on Con-A columns. In all cases, the normalized, centralized second moment of the uracil peak was at least a factor of 500 less than that of the pNp-mannoside peaks. This confirms the expectation that in an affinity system, broadening due to extracolumn effects and dispersion is not significant.

In order to evaluate the validity of our use of the impulse input (which is also the basis of the Horvath and Lin theory (*3, 4*)), the parameters in Table I were used to generate theoretical peaks with both eq 22 and the finite (rectangular) pulse solution of Goldstein (*8*). The latter is given by

$$C/C_0 = [T(\beta,\alpha(y - y_0)) - T(\beta,\alpha y)]/[E_1 T(B,Ay) + T(\beta,\alpha(y - y_0)) - T(\beta,\alpha y) - E_2(T(B,A(y - y_0)) - 1)] \quad (26)$$

where

$$A = \gamma$$

$$B = \gamma k'$$

$$\alpha = \gamma(1 + KC_0)$$

$$\beta = \frac{\gamma k'}{1 + KC_0}$$

$$y = (t/t_0) - 1$$

C_0 = concentration of solute in the pulse

y_0 = pulse width as a fraction of column dead volume

$$E_1 = \exp[(A - \alpha)y - \beta + B]$$

$$E_2 = \exp[(A - \alpha)(y - y_0) - \beta + B]$$

Table II. First Three Moments of Theoretical Peaks Generated with the Pulse and Impulse Solutions[a]

	μ_1[b]		μ_2		μ_3	
sample	pulse	impulse	pulse	impulse	pulse	impulse
1	16.934	16.875	10.075	10.076	29.031	29.025
2	19.636	19.580	8.856	8.859	22.523	22.533
3	21.109	21.056	8.416	8.418	19.435	19.441
4	22.131	22.079	8.403	8.405	18.178	18.183
5	23.440	23.392	8.896	8.896	17.201	17.203
6	24.500	24.454	9.687	9.687	16.831	16.832

[a] Peaks were generated by use of the parameters given in Table I. The overload parameter for the pulse solution (KC_0) was taken to be the value of KC_0 for the impulse solution divided by 0.063, the width of the pulse. [b] All moments are in terms of dimensionless time units. The pulse and impulse values for μ_1 differ only by the pulse width (0.063).

Depending upon the arguments of the T functions, the evaluation of eq 26 requires a number of regroupings of exponential terms to avoid decimal overflow and underflow. This is the case even with the Turbo-87 Pascal compiler, which has a dynamic range of $1E \pm 308$. Theoretical peaks were generated and analyzed by the procedure described earlier; the first three moments are summarized in Table II. Given the precision of the integration procedure, it is clear that the impulse and pulse solutions yield identical results under all conditions used in this work. A more comprehensive comparison of the two equations is presently under way in this laboratory.

The contribution of mass transfer effects to the measured adsorption/desorption rate constants is given by (*11*)

$$k_d^* = \frac{k_d k_{mt}(1 + KC_0)}{k_{mt}(1 + KC_0) - k_d k'/\epsilon} \quad (27a)$$

$$k_a^* = \frac{k_a k_{mt}(1 + KC_0)}{k_{mt}(1 + KC_0) - k_d k'/\epsilon} \quad (27b)$$

where k_a and k_d are the measured (apparent) adsorption/desorption rate constants, k_a^* and k_d^* are the actual (chemical) adsorption/desorption rate constants, k_{mt} is the first order "rate constant" for stagnant fluid mass transfer, and KC_0 and k' are as defined for eq 5 and 6; ϵ is as defined for eq 1.

The necessary theory for a priori estimation of k_{mt} has been developed and applied by Arnold (*11, 14, 15*). k_{mt} can be calculated from fundamental parameters by using the following equation (*14*):

$$k_{mt} = \left[\frac{d_p^2}{60(1 - \epsilon_e)}\left(\frac{\theta}{\epsilon_i D_m} + \frac{10}{k_f d_p}\right)\right]^{-1} \quad (28)$$

where d_p is the particle diameter (8×10^{-4} cm), D_m is the solute diffusion coefficient (0.45×10^{-5} cm^2/s (*1*)), ϵ_e is the interstitial porosity (0.4), ϵ_i is the intraparticle porosity (0.4), θ is the intraparticle obstruction factor (2.0), and k_f is the fluid "film" mass transfer coefficient, as defined by Horvath and Lin (*3*). By use of a structural parameter, Ω, of 3.33 (*1*), this was computed to be 0.112 cm/s.

At the flow rate used in these experiments (1.0 mL/min), k_{mt} is then calculated to be 46.0 s^{-1}. The contribution of intraparticle diffusion (the D_m term in eq 28) to this value is about ten times as large as the contribution from fluid "film" mass transfer. Arnold has also derived an expression that allows k_{mt} to be measured empirically by using band broadening data from an unretained species (*14*). This latter method could not be used here for two reasons: First, the high flow rates and narrow columns used in this work prevented the precise measurement of extracolumn band broadening,

Table III. Lumped Rate Constants and Corrected Rate Constants Derived from the Data in Table I[a]

		lumped rate constants		chemical rate constants[c]		
sample	C_0,[b] μM	$10^4 k_a$, $M^{-1}\ s^{-1}$	k_d, s^{-1}	$10^4 k_a{}^*$, $M^{-1}\ s^{-1}$	$k_d{}^*$, s^{-1}	$10^4 K$, M^{-1}
1	45.31	3.63 ± 0.15	0.858 ± 0.015	4.87 ± 0.29	1.151 ± 0.041	4.24 ± 0.11
2	22.65	4.60 ± 0.11	0.821 ± 0.011	6.88 ± 0.24	1.228 ± 0.030	5.60 ± 0.06
3	13.59	5.55 ± 0.14	0.770 ± 0.005	8.75 ± 0.31	1.214 ± 0.021	7.21 ± 0.13
4	9.059	6.79 ± 0.11	0.733 ± 0.006	11.0 ± 0.3	1.187 ± 0.020	9.26 ± 0.08
5	4.530	9.48 ± 0.77	0.644 ± 0.011	15.3 ± 1.8	1.037 ± 0.053	14.7 ± 0.9
6	2.265	13.8 ± 3.0	0.573 ± 0.031	21.9 ± 7.1	0.911 ± 0.135	24.0 ± 4.0

[a] Temperature, 25.0 ± 0.2 °C; pH 6.0. [b] C_0 is the concentration of solute injected multiplied by 0.063, the width of the injection pulse as a fraction of column dead volume. [c] Lumped rate constants were obtained directly from the dimensionless parametes in Table I; chemical rate constants were computed from eq 27a and 27b using k_{mt} = 46.0 s^{-1}. Note that $k_a/k_d = k_a{}^*/k_d{}^* = K$.

which is necessary if various plate height contributions are to be properly accounted for. Second, the computed value of k_{mt} would give rise to a plate height contribution which is well within the precision of plate height measurements for unretained peaks.

Having computed a value for k_{mt}, we may now use eq 27a and 27b to derive chemical rate constants from the data in Table I. These values are summarized in Table III. It is interesting to compare the results in Table III with those recently reported by Anderson and Walters (*27*). The latter authors carried out similar studies with pNp-mannoside and Con-A immobilized by a CDI procedure (*28*). Using a frontal analysis method (*1*), they measured a thermodynamic binding constant of approximately 2.5 × 10^4 M^{-1}, and using the plate height equations of Scott (*29, 30*), they measured a desorption rate constant of 3.2 s^{-1}. They also suggested that some binding site heterogeneity was evident (a small population of binding sites with K ca. 2 × 10^5 M^{-1}), but that "the data were not conclusive".

It is quite likely that the immobilization method used by Anderson and Walters *does*, in fact, yield a less heterogeneous affinity adsorbent. It is carried out at a pH where the Con-A exists primarily as a dimer of subunits, while our glutaraldehyde procedure was carried out a pH where the Con-A exists primarily as a tetramer; the CDI reaction is milder and more easily controlled than the glutaraldehyde reaction, and it yields greater retention of Con-A activity (*27*). In this regard, it should be noted that the spectrophotometric protein assay results indicated we had immobilized 42 mg of Con-A/g of silica, or a concentration of about 74 nmol of binding sites/m^2. Experimentally, we found that our binding site density was 21.3 nmol/m^2 (top data point in Figue 9). It is highly unlikely that the harshness of the glutaraldehyde immobilization reaction can account for the entire discrepancy, but in any event, the protein assay results used to estimate the amount of Con-A in the column are clearly unreliable in this case; we would have observed the pNp-mannoside eluting at a k' well above 50. It should also be noted that our measured surface coverage of 21.3 nmol of binding sites/m^2 is comparable to that of the "high coverage" material (29 nmol/m^2) prepared by Anderson and Walters (*27*).

Our measured binding constant for the more populous binding site in Con-A (4.24 × 10^4 M^{-1}, from Table III) actually compares quite well with the value of 2.5 × 10^4 M^{-1} reported by Anderson and Walters (*27*). The latter authors worked at a pH of 5.0, whereas we worked at pH 6.0; from solution phase studies, it is known that the binding constant of 4-methylumbelliferylmannoside is about 50% higher at pH 6.0 than it is at pH 5.0 (*31*). The 5-fold increase in the binding constant at lower concentrations reflects the fact that a small population of very strong binding sites is dominating chromatographic behavior. That is, they are no longer "drowned out" by high solute concentrations.

The desorption rate constant for the more populous binding site in Con-A (1.2 s^{-1}, from Table III) is significantly higher than the k_d we reported previously (0.3 s^{-1}, from ref 1), but still significantly lower than the value reported by Anderson and Walters (3.2 s^{-1}, from ref 27). Our previous value is not particularly meaningful, for the reasons suggested earlier: it was measured under conditions approximating "infinite dilution" on a heterogeneous adsorbent, and hence, represents a complex set of chemical processes. It would be meaningful only for that particular column, and for the solute loading used. Further, it was measured by using the linear plate height equations of Horvath and Lin (*4*) under conditions that were almost certainly nonlinear. As we shall see in the next section, this can lead to serious errors in data interpretation. While it is unclear whether the measurements of Anderson and Walters (*27*) were carried out on a perfectly homogeneous column, we believe that their calculations of k_d are not correct. They calculated their k_d values from single data points, as we had previously done (*1*)—not from the slopes of H_{kin} vs. U_e plots. This procedure is only valid if a plot of H_{kin} vs. U_e has a zero intercept. If there was an imporper accounting of plate height contributions, however, or if nonlinear conditions were present, as was the case in this work, this procedure would yield incorrect values of k_d. They may also have overestimated the effect of stagnant fluid mass transfer by using plate height equations which were either incorrect or inapplicable for describing this process. The correct expression for the stagnant fluid contribution to the overall plate height was derived by Horvath and Lin (*3, 4*). It has since been confirmed by Arnold (*14*), who demonstrated that it was identical to expressions derived by other workers (*32, 33*). The Horvath and Lin equations have also been confirmed by the work of Weber (*34*), who derived them via a fundamentally different (random walk) approach. Recently, we have also confirmed their correctness in a third independent fashion, using a continuously stirred tank reactor model (unpublished results).

It should finally be noted that the data presented in Table III yield interesting mechanistic information regarding the nature of binding site heterogeneity in Con-A. The 5-fold increase in the binding constant is due almost entirely to a concomitant *increase* in the chemical adsorption rate constant. That is, the solute binds a great deal more quickly to the strong sites than it does to the weak sites, but it desorbs at roughly the same rate. Indeed, the rate constants for chemical desorption in Table III are almost invariant. This suggests that in a small portion of the immobilized Con-A, either the binding site has been made more accessible to the pNp-mannoside or, more likely, the conformation of the Con-A has been altered to what it normally would be *after* the binding takes place.

Application of the Horvath and Lin Theory. Although the results of the foregoing section clearly indicate that nonlinear conditions prevailed in all the experiments, Figure 5b suggests that the Horvath and Lin method may, in fact, be applicable under some of these conditions. This hypothesis was examined by carrying out the aforementioned measurements of the plate heights as a function of flow rate. After

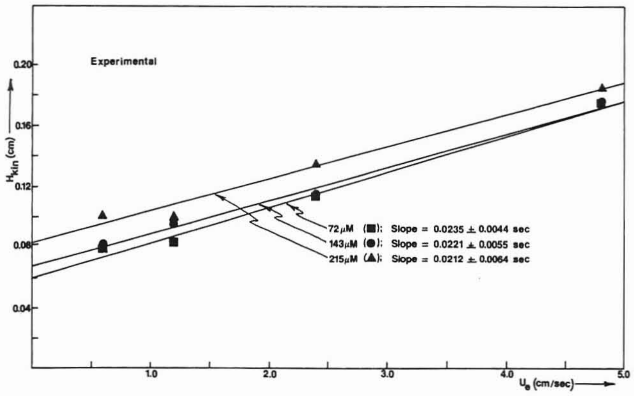

Figure 10. Kinetic plate height contributions (cm) from the experimental flow rate study as a function of interstitial flow velocity (cm/s). Slopes were obtained by linear regression; 90% confidence intervals calculated by the regression program are indicated.

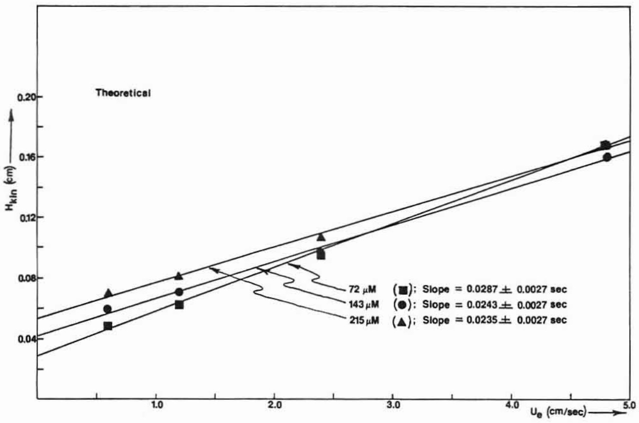

Figure 11. Theoretical plot of kinetic plate height contributions (cm) vs. the interstitial flow velocity (cm/s). Theoretical values of H_{kin} were generated from the nonlinear fit parameters as described in the text.

proper subtraction of the nonkinetic contributions to the plate height and calculation of kinetic plate height contributions as described in the Experimental Section, plots of H_{kin} vs. interstitial flow velocity were constructed for each of the three concentrations injected. These plots are shown in Figure 10. Theoretical plots of H_{kin} vs. U_e were also constructed; these are shown in Figure 11. The latter were obtained by generating a series of theoretical peaks by use of eq 22 and the parameters given in Tables I and III. The listed values for k' and KC_0 were used for each of the three concentrations; γ was computed by using the listed k_d* values and the appropriate values of the dead time (t_0). The theoretical peaks were integrated for their first two moments, from which theoretical values of H_{kin} were computed and plotted against U_e. It is important to emphasize that because the lumped rate parameters (k_d) were *not* used to generate theoretical peaks, the computed values of H can only result from slow *chemical* desorption (small k_d*)—not from mass transfer effects.

What is most striking about Figures 10 and 11 is that the theoretical and experimental slopes are the same (within experimental error) for each of the three concentrations. That is, the parameters derived by applying nonlinear theory in the concentration study can be used to predict the flow-rate dependence of H_{kin} observed in the flow-rate study. The difference in intercepts between theoretical and experimental plots can be explained by reference to Figure 7. The systematic lack of fit between theory and experiment was due to a small amount of additional peak tailing observed in all experimental peaks. This caused the second moment of experimental peaks to be systematically higher than what theory would predict. Earlier in the discussion, we postulated that the small amount of added peak tailing is due to the subpopulation of very strong binding sites in the immobilized Con-A.

Perhaps the most significant conclusion that can be drawn from Figures 10 and 11, however, is that rate constants derived from the slopes of these plots are erroneous. By use of eq 19 in ref 4, chemical rate constants, k_d*, can be computed from the slopes in Figure 10; these are found to be in the range 2.4–2.9 s^{-1}. It must be remembered, however, that the same slopes were predicted by nonlinear theory using a chemical rate constant, k_d*, of approximately 1.2 s^{-1}.

What this means is that our initial hypothesis—that the Horvath and Lin equations can be accurately applied under a restricted range of nonlinear conditions—is false for the conditions used in this experiment. The use of linear plate height equations under nonlinear conditions yields incorrect values for chemical rate constants.

CONCLUSIONS

In this paper, the impulse input solution to the equations describing nonlinear chromatography has been derived, fully characterized by a comprehensive set of peak moment calculations, and applied to an affinity chromatography system. Thermodynamic and kinetic constants were derived by use of a total curve-fitting procedure. This method of making physicochemical measurements has some significant advantages over the method of Horvath and Lin (*4*) and the methods of Arnold (*11, 14, 15, 21*) and Chase (*35, 36*). The latter two authors applied the original nonlinear theory of Thomas (*12, 13*) to derive physical parameters from the shape of breakthrough curves. Specifically, the advantages are as follows:

1. This method does not require that data be obtained under linear, or near-linear, isotherm conditions. Nonlinear chromatographic data with excellent S/N ratios may be used to extract valuable kinetic and thermodynamic information.
2. Binding site heterogeneity, which may not be evident in the behavior of breakthrough curves, may be more easily identified and characterized by its effect on peak shape.
3. Peak profiles are expected to be more sensitive than breakthrough curves to the accuracy of a theoretical data fit.
4. The impulse input solution is computationally much simpler, and more precisely evaluated, than either the breakthrough curve solution (*12*) or the finite pulse solution (*8*). Also, the new algorithm for computing Bessel function integrals (described in the Appendix) is a significant improvement over the cumbersome and imprecise approximations that have been used in the past (*8–12*).
5. It is experimentally more convenient and, if the solute is a precious protein, considerably less expensive to obtain chromatographic data in the form of peaks, rather than as breakthrough curves.

Finally, it should also be noted that the theoretical analyses outlined here have important implications for the design of preparative-scale separations. The design of efficient preparative-scale separations requires knowledge of the fundamental thermodynamic and kinetic parameters of the chromatographic system. The methodology used in this work allows these physicochemical measurements to be made by simple experimental techniques; it yields accurate values of important thermodynamic and kinetic constants, reveals the presence of binding site heterogeneity, and may be used to evaluate column activity over time. Further, the theoretical behavior of the peak moments under nonlinear conditions may be used to predict the proper flow rate and column loading for optimizing solute purity and yield. Exactly how this may be done is a subject of ongoing investigation.

Table IV. Number of Gaussian Quadrature Points Required to Achieve Seven-Digit Precision in the *T* Function

	R^b			
v^a	<1.05	1.05–1.10	1.1–1.25	*1.25
<30	8	8	8	8
30–100	12	12	12	8
100–300	16	16	12	12
300–600	20	16	12	12
600–800	20	16	16	16
800–6000	24	20	20	20
>6000	24	24	24	24

[a] v = larger argument in $T(u,v)$. [b] $R = (v/u)^{1/2}$.

ACKNOWLEDGMENT

The authors thank Gilberto Vazquez and Rutherford Aris, of the University of Minnesota Chemical Engineering Department, for their valuable mathematical insights, as well as Francis Arnold, of the University of California at Berkeley, for advance copies of her publications. The authors are also most grateful to Rod Walters for his helpful comments and suggestions.

APPENDIX

The following definitions and identities of Bessel function integrals (*8*, *12*) are important in this work:

$$\phi(u,v) = e^{u} \int_0^u e^{-t} I_0(2(vt)^{1/2})\, dt \qquad \text{(i)}$$

$$T(u,v) = e^{-v} \int_0^u e^{-t} I_0(2(vt)^{1/2})\, dt \qquad \text{(ii)}$$

$$J(u,v) = 1 - T(u,v) \qquad \text{(iii)}$$

$$T(u,v) = 1 - \exp[-u - v] I_0(2(uv)^{1/2}) - T(v,u) \qquad \text{(iv)}$$

$$T(u,u) = 0.5(1 - \exp[-2u] I_0(2u)) \qquad \text{(v)}$$

The values of both the T function and J function (*8*, *10*) are constrained to the interval zero to one. Gaussian quadrature is used to evaluate the T function (*37*). At each quadrature point, the exponential terms are combined with those of the rational approximation for $I_0(x)$ (*38*). The latter approximations are accurate to at least eight figures. The number of quadrature points is determined by Table IV, which is easily implemented using the Pascal "case" statement. Values of the T function obtained by this algorithm are accurate to at least seven figures, provided that the second argument of the T function is larger (i.e., $v > u$). If the first argument is larger ($u > v$), then eq iv may be used to determine $T(u,v)$ accurately.

Registry No. Con-A, 11028-71-0; *p*-nitrophenyl-α-D-mannopyranoside, 10357-27-4; uracil, 66-22-8; glutaraldehyde, 111-30-8.

LITERATURE CITED

(1) Muller, A. J.; Carr, P. W. *J. Chromatogr.* **1984**, *284*, 33–51.
(2) Muller, A. J.; Carr, P. W. *J. Chromatogr.* **1984**, *294*, 235–246.
(3) Horvath, C.; Lin, H.-J. *J. Chromatogr.* **1976**, *126*, 401–420.
(4) Horvath, C.; Lin, H.-J. *J. Chromatogr.* **1978**, *149*, 43–70.
(5) Houghton, G. *J. Phys. Chem.* **1963**, *67*, 84–88.
(6) Yamaoka, K.; Nakagawa, T. *J. Phys. Chem.* **1975**, *79*, 522–525.
(7) Jaulmes, A.; Vidal-Madjar, C.; Colin, H.; Guiochon, G. *J. Phys. Chem.* **1986**, *90*, 207–215.
(8) Goldstein, S. *Proc. R. Soc. London, A* **1953**, *219*, 151–171.
(9) Lassey, K. R. *Math. Comput.* **1982**, *39*, 625–637.
(10) Hiester, N. K.; Vermeulen, T. *Chem. Eng. Prog.* **1952**, *48*, 505–512.
(11) Arnold, F. H.; Blanch, H. W. *J. Chromatogr.* **1986**, *355*, 13–27.
(12) Thomas, H. C. *Ann. N.Y. Acad. Sci.* **1948**, *49*, 161–182.
(13) Thomas, H. C. *J. Am. Chem. Soc.* **1944**, *66*, 1664–1665.
(14) Arnold, F. H.; Blanch, H. W.; Wilke, C. R. *J. Chromatogr.* **1985**, *330*, 159–166.
(15) Arnold, F. H.; Blanch, H. W.; Wilke, C. R. *Chem. Eng. J.* **1985**, *30*, B9–B23.
(16) Aris, R., University of Minnesota, personal communication, Oct. 31, 1985.
(17) Amundson, N. R. *J. Phys. Colloid Chem.* **1950**, *54*, 812–820.
(18) Aris, R.; Amundson, N. R. *Mathematical Methods in Chemical Engineering*; Prentice-Hall: Englewood Cliffs, NJ, 1973; Vol 2, p 175.
(19) Hladik, J. *La Transformation de LaPlace à Plusieurs Variables*; Masson et Cie Éditeurs: Paris, 1969.
(20) Burden, R. L.; Faires, J. D.; Reynolds, A. C. *Numerical Analysis*; PWS Publishers: Boston, MA, 1981; p 142.
(21) Arnold, F. H.; Schofield, S. A.; Blanch, H. W. *J. Chromatogr.* **1986**, *355*, 1–12.
(22) DeLisi, C.; Hethcote, H. W.; Brettler, J. W. *J. Chromatogr.* **1982**, *240*, 283–285.
(23) Cunningham, B. A.; Wang, J. L.; Pflumm, M. N.; Edelman, G. M. *Biochemistry* **1972**, *11*, 3233–3239.
(24) Walters, R. R. *J. Chromatogr. Sci.* **1984**, *22*, 353–359.
(25) Unger, K. K.; Kinkel, J. N.; Anspach, B.; Giesche, H. *J. Chromatogr.* **1984**, *296*, 3–14.
(26) Adamson, A. W. *A Textbook of Physical Chemistry*; Academic: New York, 1979; p 549.
(27) Anderson, D. J.; Walters, R. W. *J. Chromatogr.* **1986**, *376*, 69–85.
(28) Anderson, D. J.; Walters, R. W. *J. Chromatogr.* **1985**, *331*, 1–10.
(29) Katz, E. D.; Scott, R. P. W. *J. Chromatogr.* **1983**, *270*, 29–50.
(30) Katz, E. D.; Ogan, K. L.; Scott, R. P. W. *J. Chromatogr.* **1983**, *270*, 51–75.
(31) Farina, R. D.; Wilkins, R. G. *Biochim. Biophys. Acta* **1980**, *631*, 428–438.
(32) Kucera, E. *J. Chromatogr.* **1965**, *19*, 237–248.
(33) Furusawa, T.; Suzuki, M.; Smith, J. M. *Catal. Rev.—Sci. Eng.* **1976**, *13*, 43–76.
(34) Chen, J.-C.; Weber, S. G. *Anal. Chem.* **1983**, *55*, 127–134.
(35) Chase, H. A. *J. Chromatogr.* **1984**, *297*, 179–202.
(36) Chase, H. A. *Chem. Eng. Sci.* **1984**, *39*, 1099–1125.
(37) *Handbook of Mathematical Functions*; Abramowitz, M., Stegun, I. A., Eds.; Dover Publications: New York, 1972; p 916.
(38) *Handbook of Mathematical Functions*; Abramowitz, M., Stegun, I. A., Eds.; Dover Publications: New York, 1972; p 378.

RECEIVED for review June 17, 1986. Accepted February 20, 1987. This work was supported in part by a grant from the National Science Foundation and by funds from the Bioprocess Technology Center of the University of Minnesota. J.W. also gratefully acknowledges his summer research grant from 3M.

1296 *Anal. Chem.* **1987**, *59*, 1296–1301

Determination of Atmospheric Carbonyl Sulfide by Isotope Dilution Gas Chromatography/Mass Spectrometry

Ella E. Lewin, Rebecca L. Taggart, Marija Lalevic, and Alan R. Bandy*

Department of Chemistry, Drexel University, Philadelphia, Pennsylvania 19104

A gas chromatography/mass spectrometry (GC/MS) method for determining atmospheric carbonyl sulfide (OCS) with a precision better than 2% is reported. High precision and insensitivity to sample loss and changes in detector response were achieved by using isotopically labeled OCS as an internal standard. Tenax, Molecular Sieve 5A, Carbosieve B, and Carbosieve S were evaluated for collecting atmospheric OCS. Molecular Sieve 5A provided the best trapping and recovery efficiencies.

The objective of this study was to develop a highly selective and precise method for determining atmospheric carbonyl sulfide (OCS). Carbonyl sulfide is the most abundant gaseous atmospheric sulfur species (*1*). It has an atmospheric residence time of at least 1 year (*1–3*); therefore, its global distribution is very uniform (±10%). The long tropospheric residence time of OCS, due in part to its low water solubility, allows most of it to escape to the stratosphere where it is converted to SO_2 and subsequently to H_2SO_4. The H_2SO_4 vapor quickly combines with available water to produce small particles that scatter the sun's radiation and absorb the Earth's radiation and thereby can have an important influence on the Earth's radiation budget and climate (*2, 4*).

Much of our knowledge of the atmospheric chemistry of OCS is obtained from measured temporal and spatial fluctuations of OCS. Since these fluctuations are ±10% or less, a measurement precision of 1% or better is desirable. The gas chromatographic method used by Maroulis et al. (*1*) and Torres et al. (*5*) for atmospheric OCS determinations has sufficient sensitivity but not the required precision. In this work high precision has been achieved by using isotopically labeled OCS, $^{16}O^{13}C^{32}S$ and $^{16}O^{12}C^{34}S$, as internal standards. A similar method for the determination of CS_2 has been reported by Bandy et al. (*6*).

The work described below shows that cryogenic preconcentration is a very effective means of increasing OCS concentrations to measurable levels. Unfortunately cryogenic preconcentrated samples usually require immediate analysis which in turn requires an on-site GC/MS. However, there are many applications, such as sample collections using small aircraft platforms, for which an on-site GC/MS is not feasible. Needed is another sampling method that does not require immediate sample analysis and thus direct access to the GC/MS.

One approach would be to collect samples on suitable solid adsorbents and return them to the laboratory for analysis. Several reports of successful preconcentration of sulfur gases on solid adsorbents have been published. Black et al. (*7*) used Molecular Sieve 5A for the collection and determination of H_2S and SO_2. Steudler and Kijowski (*8*) tested an adsorber based on molecular sieve 5A and Tenax for collecting OCS, H_2S, CS_2, dimethyl sulfide, dimethyl disulfide, and CH_3SH. Shalaby (*9*) has reported some preliminary work on the determination of atmospheric OCS by GC/MS using both cryogenic enrichment and preconcentration on Carbosieve B.

Based on this previous work, Molecular Sieve 5A, and Carbosieve B adsorbents were chosen for study. Consultations with various manufacturers and our previous experience (*6*) suggested that we should also evaluate Carbosieve S. Carbosieve S is spherical in shape and more dense than the granulated form of Carbosieve B. According to the manufacturer, type S should be the best for the more volatile sulfur gases, such as OCS.

EXPERIMENTAL SECTION

A Finnigan Model 4023 GC/MS (Finnigan Instruments, Sunnyvale, CA) was used for these studies. The sample was ionized with 30-eV electrons at a source pressure of about 0.04 torr. Higher energies degraded the signal-to-noise ratio while lower energies resulted in very short filament lifetimes. Carbonyl sulfide was separated from interfering compounds by use of a Teflon column, 4 m long, 0.125 in. (3.18 mm) o.d., and approximately 0.082 in. (2.08 mm) i.d., packed with 3% Carbowax 20M and 1% H_3PO_4 on Carbopack B (Supelco, Inc., Bellefonte, PA). The attributes of this column for atmospheric OCS determinations have been discussed by Maroulis et al. (*1*). The column was conditioned overnight at 100 °C while being purged with helium. The column was operated at 60 °C and a helium flow rate of 20 mL/min. The retention time of OCS was about 1 min. The sample was cryogenically preconcentrated and loaded onto the column by using the apparatus shown in Figures 1 and 2. The OCS was preconcentrated in an unpacked Teflon trap constructed from FEP Teflon tubing, 1 m long, 0.125 in. (3.18 mm) o.d., and 0.082 in. (2.08 mm) i.d. (*5, 6*).

The GC/MS operating conditions and calibration procedures were similar to those used by Bandy et al. (*6*). The instrument was carefully tuned before each series of measurements. The ion multiplier, quadrupole offset, and source lens voltages were adjusted to obtain the best compromise between sensitivity and peak shape (resolution). Changes in sensitivity were evaluated periodically by direct injection of a standard OCS sample (Scott Specialty Gases, Plumbsteadville, PA).

The data acquisition was carried out in the multiple ion detection mode of the INCOS data system (Finnigan Instruments, Inc., Sunnyvale, CA). The parent peak of OCS was monitored by using mass windows of 59.518–60.518 au for $^{16}O^{12}C^{32}S$, 60.518–61.518 au for $^{16}O^{13}C^{32}S$, and 61.518–62.518 au for $^{16}O^{12}C^{34}S$. Only two isotopomers were monitored in any given analysis. Each window was monitored for 0.2 s. The minimum fragment width and minimum peak area parameters of the INCOS data system were set to five. Chromatograms of $^{16}O^{12}C^{32}C$ and $^{16}O^{12}C^{34}S$ are shown in Figure 3.

Isotopically labeled OCS was purchased from U.S. Services (Summitt, NJ). Standard mixtures of both labeled and unlabeled OCS were prepared by Scott Specialty Gases (Plumbsteadville, PA). The standard having the terrestial isotopic abundance, OCS-60, had a concentration of 689 ppbv. The standard enriched in ^{13}C, OCS-61, had an overall OCS concentration of 169 ppbv, whereas the standard enriched in ^{34}S, OCS-62, had an overall OCS concentration of 106 ppbv. Mole fractions of OCS isotopomers in ambient air were calculated from known terrestrial abundances of O, C, and S (10). The percentage contents of the isotopomers in the standards were calculated from isotopic abundances provided by the manufacturer.

The total OCS concentration in the standard mixtures was determined by comparison to test atmospheres containing OCS prepared by use of permeation tubes (Metronics, Santa Clara,

0003-2700/87/0359-1296$01.50/0 © 1987 American Chemical Society

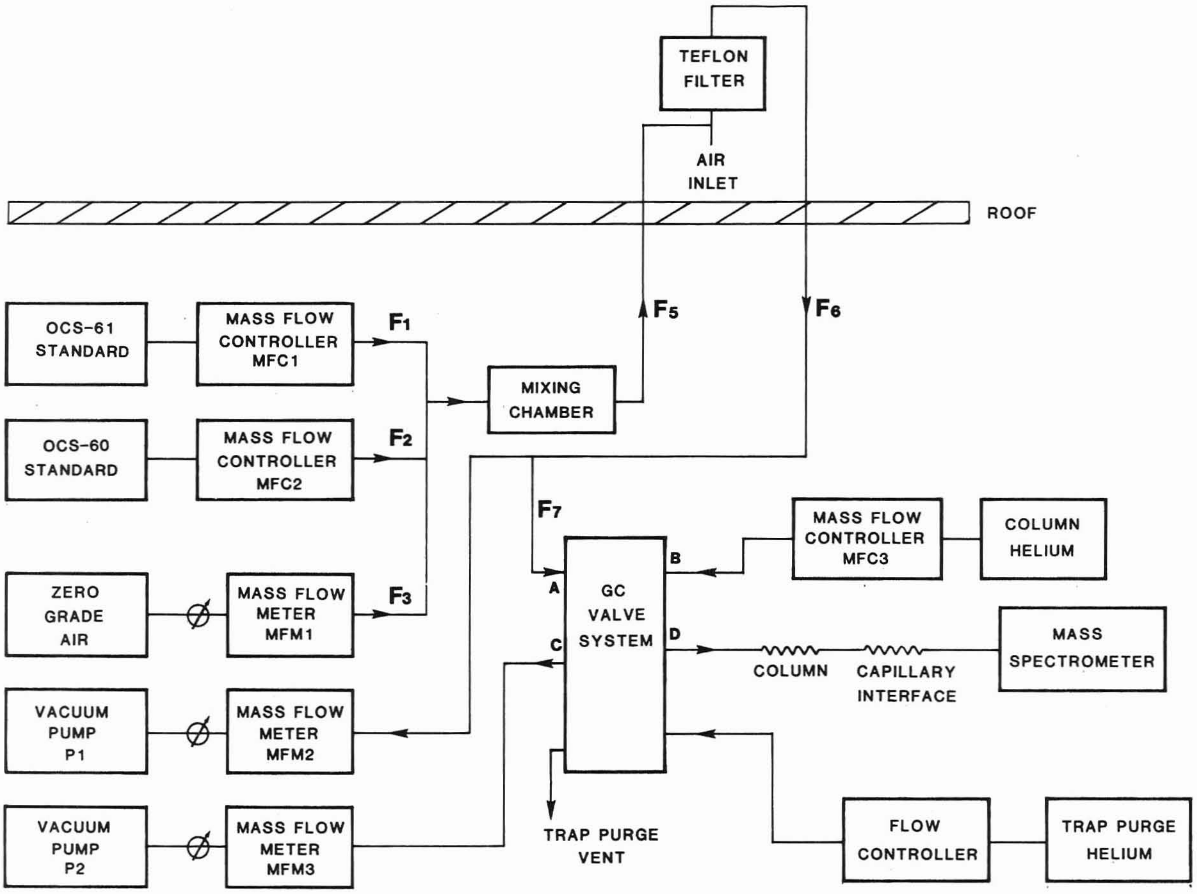
TEFLON FILTER
AIR INLET
ROOF
OCS-61 STANDARD
MASS FLOW CONTROLLER MFC1
F_1
OCS-60 STANDARD
MASS FLOW CONTROLLER MFC2
F_2
ZERO GRADE AIR
MASS FLOW METER MFM1
F_3
VACUUM PUMP P1
MASS FLOW METER MFM2
VACUUM PUMP P2
MASS FLOW METER MFM3
MIXING CHAMBER
F_5
F_6
F_7
A
B
C
D
GC VALVE SYSTEM
MASS FLOW CONTROLLER MFC3
COLUMN HELIUM
COLUMN
CAPILLARY INTERFACE
MASS SPECTROMETER
TRAP PURGE VENT
FLOW CONTROLLER
TRAP PURGE HELIUM

Figure 1. Block diagram of the calibration and collection system for in situ measurements of OCS in air.

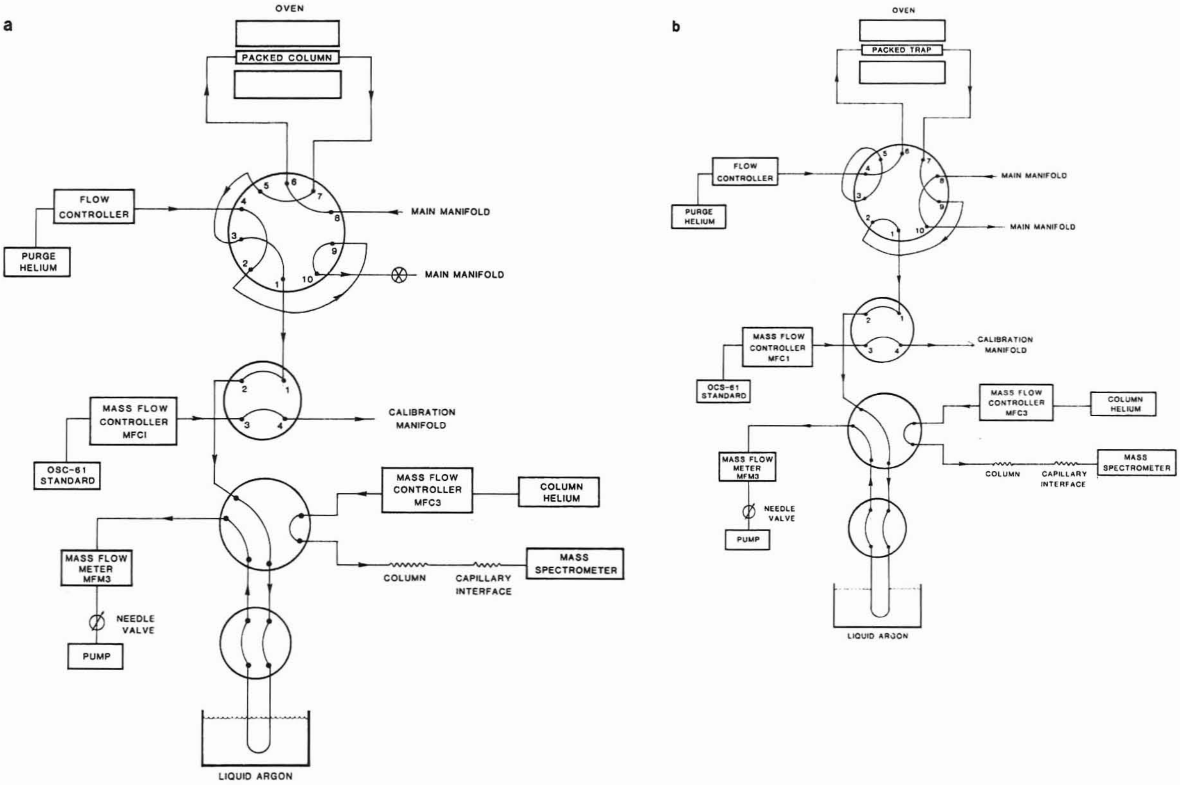
a
OVEN
PACKED COLUMN
FLOW CONTROLLER
PURGE HELIUM
1
2
3
4
5
6
7
8
9
10
MAIN MANIFOLD
MAIN MANIFOLD
MASS FLOW CONTROLLER MFCI
OSC-61 STANDARD
CALIBRATION MANIFOLD
MASS FLOW CONTROLLER MFC3
COLUMN HELIUM
MASS FLOW METER MFM3
NEEDLE VALVE
PUMP
COLUMN
CAPILLARY INTERFACE
MASS SPECTROMETER
LIQUID ARGON
b
OVEN
PACKED TRAP
FLOW CONTROLLER
PURGE HELIUM
MAIN MANIFOLD
MAIN MANIFOLD
MASS FLOW CONTROLLER MFC1
OCS-61 STANDARD
CALIBRATION MANIFOLD
MASS FLOW CONTROLLER MFC3
COLUMN HELIUM
MASS FLOW METER MFM3
NEEDLE VALVE
PUMP
COLUMN
CAPILLARY INTERFACE
MASS SPECTROMETER
LIQUID ARGON

Figure 2. Schematic diagram of the valving system used for collection (a) and desorption (b) of ambient air samples.

CA). The permeation tube calibration devices were calibrated by monitoring their weight loss for at least 3 months (after stabilization). The block diagram of the apparatus used for the preparation of test atmospheres is shown in Figure 1. All flowmeters were calibrated against either soap bubble flowmeters or wet gas meters. The standard mixtures were introduced into the mixing chamber at rates determined by mass flow controllers MFC1 and MFC2 where they were diluted with a zero air stream whose flow rate was monitored by flowmeter MFM1. The resulting gas mixture was then added to the main manifold near the ambient air inlet just upstream of the particle filter. The flow rate in the main manifold was measured with the mass flow meter

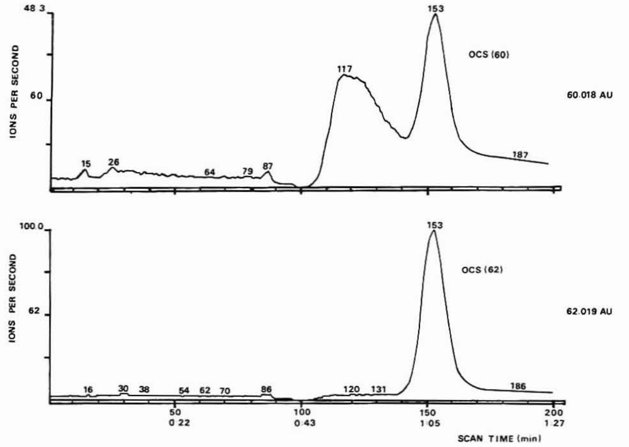

Figure 3. *m/z* 60 and *m/z* 62 chromatograms of ambient air with added OCS-62.

Table I. Background Loading in Picomoles per Centimeters of Packing

	OCS-60	OCS-61
Tenax	0.15	0.2
Carbosieve B	0.2	0.15
Carbosieve S	0.5	0.0
Molecular Sieve	0.5	0.22

MFM2. The test atmosphere produced was sampled at a rate of about 400–1000 mL/min.

For test atmospheres prepared in zero air, the flow rate of zero air/standard gas mixture (F5 = F1 + F2 + F3) was larger than the flow rate in the sample manifold (F6). Under these conditions zero air flowed out of the end of the manifold thus excluding ambient air from the manifold and the sample. For calibrations in zero air, the OCS-61 or OCS-62 concentration was maintained at about 500 pptrv, while the OCS-60 concentration was varied over the range 300–800 pptrv by varying F2. During ambient air measurements of OCS, F5 was maintained at a much lower flow rate than that of the main manifold, F6, to minimize the reduction of the $^{16}O^{12}C^{32}S$ signal by dilution. For these measurements, only isotopically labeled OCS was added to the sample air. A diagram of the valving system used for sample collection is shown in Figure 2.

The air inlet to the sample manifold was located on the roof of a four-story building on the Drexel University campus, near downtown Philadelphia. Atmospheric particles were removed at the manifold inlet system with an 0.5 μm pore Teflon filter. The standard mixture, enriched in ^{13}C or ^{34}S, was added to the main manifold between the manifold inlet and the particle filter, so that both the analyte and the internal standard were affected identically by the system. The sample manifold was constructed from 0.375 in (9.53 mm) o.d. FEP Teflon tubing and was approximately 6 m long. The sample was cryogenically preconcentrated in a FEP Teflon trap cooled with liquid argon (*1*). Samples were volatilized with warm water prior to injection onto the gas chromatographic column and were eluted into the MS with a 20 mL/min flow of high-purity helium (*6*).

Adsorbent Traps. Adsorbent traps were constructed from Pyrex tubes, 20 cm long and 4 mm i.d. The center section of each tube was filled with the adsorbent material. The packing length was 4 cm for Tenax and Carbosieve B and 2 cm for Carbosieve S and Molecular Sieve 5A. The packing was held in place with silanized glass wool plugs that had been treated with H_3PO_4. The tubes were sealed with a nylon nut, nylon ferrule, and brass caps. The pressure drop across the packed trap was about 50% at a sampling flow rate of 1 L/min. A diagram of the valving system used for collection and desorption of ambient air samples is shown in Figure 2. A photograph of the adsorption trap used in this work is shown in Figure 4.

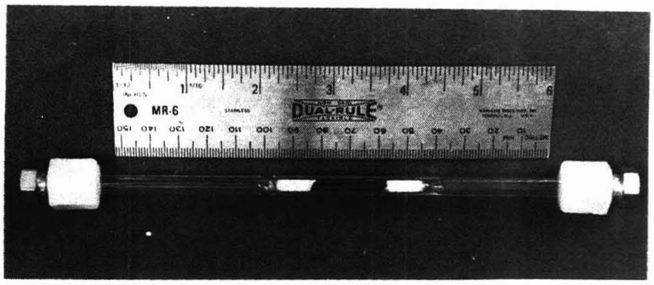

Figure 4. Adsorbent trap used for collection of ambient samples of OCS.

Prior to use, the traps were conditioned for at least 1 h at 300 °C while being continuously purged with helium. The traps were allowed to cool without interrupting the helium flow. When cool, they were sealed and stored at room temperature.

The traps were checked for background by desorbing them in exactly the same manner (temperature, time, helium flow, etc.) as was used for atmospheric sampling. The first desorption always yielded higher values than those for subsequent desorptions. The degree of contamination did not depend on storage time; thus contamination during storage apparently was negligible. Therefore, we concluded that the desorbed OCS probably arose from contamination introduced during cooling and sealing of the traps. Table I contains measured OCS background loadings for the adsorbents tested.

Carbonyl sulfide was desorbed by heating the trap in a small oven while purging the trap with helium at a flow rate of 200 mL/min. The OCS in the purge gas was cryogenically trapped and later volatilized and analyzed. Above 200 °C OCS recovery was complete after 3 min and depended little on the trap purge rate if the purge rate was greater than about 200 mL/min. As a precaution each trap was desorbed for an additional 3 min to verify that no residual OCS remained in the trap after the first desorption.

RESULTS AND DISCUSSION

The algorithm for converting GC/MS data to concentration data using an isotopically labeled standard has been derived by Bandy et al. (*6*)

$$C_a = \frac{K_2 - K_4 R}{K_3 R - K_1} C_s \tag{1}$$

Here C_a and C_s are the total OCS concentrations and H_a and H_s are the peak heights for ambient air and isotopically labeled standard, respectively, and R is the ratio of the peak heights, $R = H_a/H_s$. When the separation of the ions of the isotopomers of the analyte is complete, the constants in eq 1 are determined solely by the isotopic abundances of oxygen, carbon, and sulfur in the standard and ambient air (*6*). Under these conditions K_1 and K_3 are equal to the fractions of OCS, F_i, having masses 60 and 61 (or 62) in ambient air, respectively, and K_2 and K_4 are equal to the respective fractions, G_i, of these isotopomers in the standard mixture. By use of the isotopic

Table II. Sulfur Isotope Abundances for Ambient Air and Sulfur Gas Standards Enriched in ^{13}C or ^{34}S

	abundance, %						
	12 au	13 au	32 au	33 au	34 au	35 au	36 au
OCS-62 standard[a]	98.9	1.1	3.52	2.15	93.1	0.00	1.18
OCS-61 standard[a]	8.9	91.13	95.01	0.76	4.22	0.00	0.02
ambient air[b]	98.9	1.1	95.01	0.76	4.22	0.00	0.02

[a] Manufacturers analysis. [b] Reference 8.

Table III. Fraction of OCS Molecules in Ambient Air Having Mass m_i

	mole fraction					
	60 au	61 au	62 au	63 au	64 au	65 au
isotopomer						
34 13 18						0.0000
34 12 18					0.001	
34 13 17					0.0000	
34 12 17				0.0000		
34 13 16				0.0005		
34 12 16			0.0416			
32 13 18				0.0000		
32 12 18			0.0019			
32 13 17			0.0000			
32 12 17		0.0066				
32 13 16		0.0104				
32 12 16	0.9378					
F_i	0.9378	0.0170	0.0435	0.0005	0.0001	0.0000

Table IV. Fraction of OCS Molecules in Standard Gas Mixture Having Mass m_i

	mole fraction				
	60 au	61 au	62 au	63 au	64 au
	Enriched in ^{34}S				
isotopomer					
36 12 16					0.0116
34 13 16				0.0102	
34 12 16			0.9194		
33 13 16			0.0002		
33 12 16		0.0210			
32 13 16		0.0003			
32 12 16	0.0347				
G_i	0.0347	0.0213	0.9196	0.0102	0.0116
	Enriched in ^{13}C				
34 13 16				0.0384	
34 12 16			0.0373		
33 13 16			0.0069		
33 12 16		0.0007			
32 13 16		0.8641			
32 12 16	0.0841				
G_i	0.0841	0.8648	0.0442	0.0384	

abundances given in Table II, K_1 through K_4 were calculated and included in Tables III and IV. Substitution of these calculated values into eq 1 yields a theoretical data reduction formula. When the OCS-61 standard is used as an internal standard, the theoretical data reduction formula is

$$C_a = \frac{0.0841 - 0.8648R_{61}}{0.0170R_{61} - 0.9378}C_s \quad (2)$$

When OCS-62 is used as an internal standard, the theoretical data reduction formula is

$$C_a = \frac{0.0347 - 0.9196R_{62}}{0.0435R_{62} - 0.9378}C_s \quad (3)$$

Using the cryogenic preconcentration technique, we were able to verify the accuracy of these theoretical data reduction algorithms. In doing this it is convenient to rewrite eq 2 and 3

$$R_{61} = \frac{0.9378C_r + 0.0841}{0.0170C_r + 0.8648} \quad (4)$$

and

$$R_{62} = \frac{0.9378C_r + 0.0347}{0.0435C_r + 0.9196} \quad (5)$$

Here $C_r = C_a/C_s$. For $R_r < 1$, which is the range of interest in atmospheric studies, the term $0.0170C_r$ in eq 4 and the term $0.0435C_r$ in eq 5 are small relative to other terms; hence eq 4 and 5 can be simplified to

$$R_{61} = 1.084C_r + 0.097 \quad (6)$$

and

$$R_{62} = 1.020C_r + 0.038 \quad (7)$$

The accuracy of these algorithms was determined by conducting an experiment in which the isotopic standard concentration, C_s, was held constant at about 500 pptrv (parts per trillion by volume) while the concentration of the OCS-60 standard, C_a, was varied over a concentration range of 300–800 pptrv, which includes the range of OCS concentrations found in the atmosphere (450–550 pptrv (*1*)).

A linear regression analysis of the ratio of the accumulated ion counts for the 60 and 61 au channels as a function of the ratio of the concentrations of the OCS-60 and OCS-61 standards yielded a slope of 0.936 (±0.008) and an intercept of 0.207 (±0.012). The correlation coefficient was 0.997. These results are based on five calibration runs made on different days. Each point on the curve was determined at least three times for each run; the total number of measurements was 68. The high value of the correlation coefficient and the small standard deviations of the slope and intercept demonstrate the high precision of the technique; however, both the slope and the intercept of the experimental calibration curve are substantially different from that of the theoretical calibration curve. The major sources of these differences appear to result from errors in the isotopic abundances for the ^{13}C-labeled OCS supplied by the manufacturer and "cross-channeling" caused by inadequate resolution of the mass spectrometer (*6*). This experimental calibration curve, however, produced atmospheric OCS data in agreement with that obtained with the OCS-62 standard, for which, as described in detail below, much better agreement between the theoretical and experimental calibration curves was obtained.

A linear regression analysis of the ratio of the accumulated ion counts for the 60 and 62 au channels as a function of the ratio of the concentrations of the OCS-60 and OCS-62 standards yielded a slope of 0.990 (±0.006) and an intercept of 0.029 (±0.004). The correlation coefficient was 0.998. The intercept is within measurement precision of the background concentration of OCS in the zero air mixture used to prepare the test atmospheres. The slope of this experimental curve is statistically the same as the slope of the theoretical calibration curve. Therefore, we conclude that the calibration curve for ambient air is given by eq 7 within experimental error. A propagation of errors analysis indicates that the overall precision of this GC/MS determination of atmospheric OCS is about 2%.

Table V. Recovery of OCS Collected on Carbosieve S and Molecular Sieve 5A as a Function of Desorption Temperature[a]

material	temp, °C	amt collected, pmol	amt recovered, pmol	% recovery	mean, %
Carbosieve S	200	68.0	56.4	83	85 ± 2
		72.1	62.0	86	
		36.6	30.7	84	
		38.0	33.4	88	
	215	12.5	12.9	103	97 ± 6
		36.6	37.3	102	
		37.0	33.3	90	
		33.9	31.9	94	
		33.6	36.6	109[b]	
		33.6	46.4	138[b]	
		33.4	54.1	163[b]	
	235	36.9	36.9	100	95 ± 7
		38.4	33.0	86	
		38.4	36.1	94	
		61.9	62.5	101	
	275	39.6	20.6	52	48 ± 4
		40.7	19.5	48	
		40.8	17.9	44	
Molecular Sieve 5A	200	34.7	41.6	120	121 ± 7
		36.4	41.5	114	
		9.1	11.0	121	
		9.6	12.6	131	
	215	13.2	10.4	79	91 ± 10
		10.5	10.7	102	
		11.9	11.3	95	
		14.3	12.4	87	
	230	17.8	15.7	88	108 ± 30
		17.9	16.6	93	
		15.1	21.4	142	
	270	18.5	17.2	93	99 ± 15
		29.5	34.2	116	
		35.1	31.2	89	
		32.7	70.0	214[b]	

[a] The test was carried out for OCS-61 added to ambient air. [b] Consecutive collections on the same trap without regenerating; not included in computation of mean.

Evaluation of Adsorbent Traps. Trap capacity and recovery efficiencies were evaluated. The trapping process should be viewed as frontal elution chromatography. Therefore, breakthrough volumes were used as a measure of capacity. The breakthrough volume was defined as the volume of air sampled when 1% of the analyte loaded on the trap had penetrated the trap. These tests were conducted with test atmospheres prepared by adding a known amount of OCS-61 to ambient air. The trapping flow rate was about 500 mL/min. The trap was operated at room temperature. The concentration of the standard in the mixture entering the trap was about 500 pptrv; however, breakthrough was independent of the OCS-61 concentration for the range of concentrations used (100–200 pptrv).

Analyte, which had passed through the trap, was cryotrapped in increments of 1 to 3 L and analyzed for OCS content. The results of these investigations for the four adsorbents used are given in Figure 5. Here breakthrough is plotted as a function of the volume of air having passed through the trap. The shape of these breakthrough curves and their insensitivity to analyte concentration supports the validity of the frontal elution model for the trapping process.

Molecular Sieve 5A and Carbosieve S had breakthrough volumes greater than 2 and 3 L/cm of adsorbent, respectively. The breakthrough volume for Carbosieve B was less than 2 L/cm of packing while for Tenax the breakthrough occurred almost immediately. On the basis of these findings, further investigations were concentrated on Molecular Sieve 5A and Carbosieve S properties.

For recovery evaluation, zero air with added OCS-61 was collected on Carbosieve S and Molecular Sieve 5A traps. Immediately after collection, the traps were thermally desorbed and the amount of OCS-61 recovered was determined by GC/MS. The concentration of OCS-61 in the mixture entering the tube was about 500 pptrv. The flow rate through the trap was about 500 mL/min. The amount recovered was compared with the amount of OCS-61 collected in a similar experiment, in which the air was collected with an unpacked trap.

Desorption of the OCS was carried out at different temperatures, over the range 200–280 °C, to establish the optimum desorption temperatures. Prior to use, the background signal for each trap was determined. Only traps that showed a constant and acceptably low background level were used. After each use, the traps were desorbed again to obtain a correction for the trap background. Additional desorptions were carried out occasionally. These tests indicated that the trap background remained constant after the first desorption. All results reported were corrected for these blank values.

Background originating from OCS in the zero air was checked by collecting a few samples of test atmospheres to which no standard was added. No OCS in the zero air was detected in these samples.

Recovery results are given in Table V and in Figure 6. For Carbosieve S maximum recovery occurred at a desorption temperature of about 230 °C. Below 200 °C the recovery was less than 90%, and at temperatures above 270 °C recovery was less than 50%. For Molecular Sieve 5A the recovery was close to 100% over the entire range studied although the best temperature appeared to be close to 270 °C.

To test the stability of the collected samples during storage, samples of test atmospheres containing OCS-61 were collected

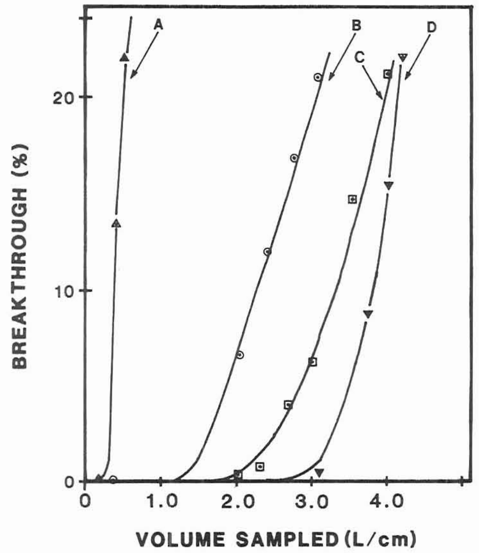

Figure 5. Breakthrough of OCS-61 in ambient air collected on (A) Tenax, (B) Carbosieve B, (C) Molecular Sieve 5A, and (D) Carbosieve S.

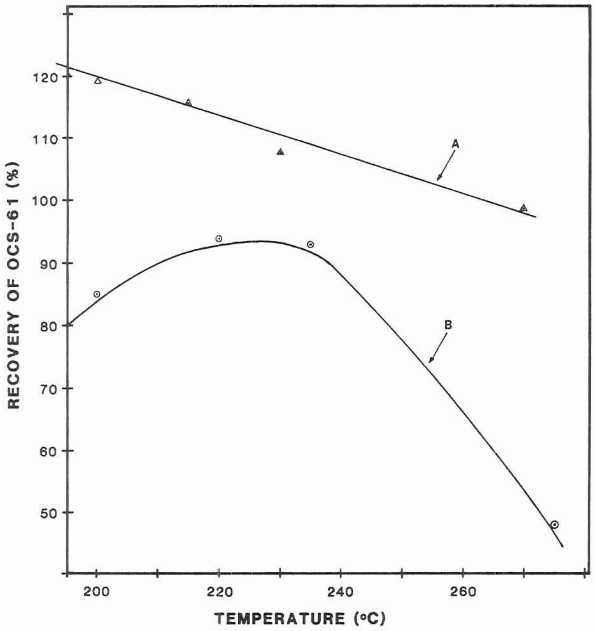

Figure 6. Recovery of OCS absorbed on (A) Molecular Sieve 5A and (B) Carbosieve S, as a function of temperature.

and stored at room temperature in sealed traps for 1–28 days. The amount of OCS that could be desorbed after this storage period was then determined. The desorption was carried out at the optimum temperature, for 3 min and with the zero grade helium flow of 200 mL/min. The results of these tests are shown in Table VI.

Table VI. Stability of OCS Samples Collected on Molecular Sieve 5A[a]

days stored	amt collected, pmol	amt recovered, pmol
1	16	20
	8	10
	15	12
	18	17
3	20	15
	16	13
	14	10
28	16	16
	15	11

[a] Samples stored in clean atmosphere at room temperature.

Almost no OCS could be recovered from Carbosieve S even for the shortest storage periods of only a few hours. Apparently the OCS becomes irreversibly bound during storage. We did not investigate procedures for limiting or preventing this loss, although refrigerating the samples would probably greatly slow this process (*8*). On the other hand, Molecular Sieve 5A appears to be a satisfactory adsorbent especially when isotopically labeled OCS is used as an internal standard to maintain precision in case of small amounts of OCS loss during the sampling and analysis.

CONCLUSIONS

Isotope dilution GC/MS is a highly sensitive, specific, and precise method for the determination of atmospheric OCS. It has the required precision to characterize the small fluctuations expected for such compounds having long atmospheric residence times. Collection of OCS on solid adsorbents followed by the determination of OCS by isotopic dilution GC/MS, should allow the global distribution of OCS to be studied using light-weight easily deployed samplers without sacrificing sensitivity or precision. Molecular Sieve 5A is the most suitable adsorption material because of its superior recovery properties and storage characteristics. Although Carbosieve S has even better breakthrough and recovery properties, large losses during storage negate these advantages.

Registry No. OCS, 463-58-1; Tenax, 24938-68-9; Carbosieve B, 74749-61-4.

LITERATURE CITED

(1) Maroulis, P. J.; Torres, A. L.; Bandy, A. R. *Geophys. Res. Lett.* **1977**, *4*, 510–512.
(2) Crutzen, P. J. *Geophys. Res. Lett.* **1976**, *3*, 73–76.
(3) Graedel, T. E. *Rev. Geophys. Space Phys.* **1977**, *15*, 421–428.
(4) Sze, Nien Dak; Ko, Malcolm K. W. *Atmos. Environ.* **1980**, *14*, 1223–1239.
(5) Torres, A. L.; Maroulis, P. J.; Goldberg, A. B.; Bandy, A. R. *J. Geophys. Res.* **1980**, *85*, 7357–7360.
(6) Bandy, A. R.; Tucker, B. J.; Maroulis, P. J. *Anal. Chem.* **1985**, *57*, 1310–1314.
(7) Black, M. S.; Herbst, R. P.; Hitchcock, D. R. *Anal. Chem.* **1978**, *50*, 848–851.
(8) Steudler, P. A.; Kijowski, W. *Anal. Chem.* **1984**, *56*, 1432–1436.
(9) Shalaby, L. Ph.D. Dissertation, Drexel University, 1982.
(10) Silverstein, R. M.; Bassler, G. C.; Morrill, T. C. *Spectrometric Identification of Organic Compounds*; Wiley: New York, 1974.

RECEIVED for review June 9, 1986. Accepted January 12, 1987. This research was supported by NSF Grant ATM 8515000.

1302 *Anal. Chem.* **1987**, *59*, 1302–1306

Gas Chromatographic and Mass Spectrometric Determination of Chlorophenoxy Acids and Related Herbicides as Their (Cyanoethyl)dimethylsilyl Derivatives

Michel J. Bertrand,* A. W. Ahmed, Benoit Sarrasin, and Victorin N. Mallet[1]

Department of Chemistry, University of Montreal, P.O. Box 6128, Station A, Montreal, Quebec, Canada H3C 3J7

A method using (2-cyanoethyl)dimethyl(diethylamino)silane to form derivatives with phenoxy acid herbicides and related compounds is presented. Results obtained with 18 compounds demonstrate that the reaction is quantitative and complete within minutes at room temperature. The derivatives formed can readily be analyzed by gas chromatography using a selective nitrogen–phosphorus detector which eliminates the need for rigourous cleanup of the sample required for detection by electron capture. Response–concentration plots show that detection is linear over several decades with limits of detection being in the low picogram range for all compounds studied. Mass spectral analysis of the derivatives of the 18 compounds studied indicates that the spectra are highly specific showing characteristic ions at (M – 54), (M – 82), or (M – 98) which are useful for structure confirmation or analysis at low levels by using selected ion monitoring. The analytical advantages of the approach for the analysis of acid herbicides are discussed.

Chlorophenoxy acids and related compounds are used worldwide as agricultural and forestry herbicides. Their main advantages are spray efficacy and biodegradability. They are considered to have low mammalian toxicity (*1*, *2*) but the presence of dioxin in the formulations may have serious health effects. There are still many requests for analysis of these compounds and particularly for samples originating from agricultural drainage, sanitary landfills, and industrial dumps.

Derivatization is an important aspect of acidic herbicide analysis when techniques such as gas chromatography and mass spectrometry are considered. Since these compounds include functional groups such as carboxyl, derivatization is used to enhance their volatility and stability prior to instrumental analysis. However, other reasons exist for derivatization such as increase in sensitivity, selectivity of detection, and improvement of the separation behavior. Many derivatization techniques such as esterification, alkylation, and silylation have been proposed for the analysis of herbicides and they have recently been reviewed by Cochrane (*3*, *4*). Methylation of the carboxylic acid group with diazomethane has been the traditional approach but the response of the electron capture detector to these derivatives is sometimes weak (*5*). In order to enhance the electron capture response in the gas chromatographic analysis of herbicides, other derivatives such as chloroethyl and pentafluorobenzyl esters have been suggested (*6–9*). Some of the problems associated with the latter approaches reside in the experimental conditions necessary for derivatization (up to 5 h for pentafluorobenzyl esters at room temperature (*10*)) and also in the rigourous cleanup procedures which are required for the use of the electron capture detector (*9*).

Recently, a new silylating reagent, (2-cyanoethyl)dimethyl(diethylamino)silane (CEDMSDEA) has been introduced (*11*). This reagent allows the introduction of a cyano group on the derivatives thus permitting the use of the nitrogen–phosphorus detector (*12*, *13*) for their sensitive and selective analysis. The reagent was found to react with carboxylic, phenolic, and hydroxyl groups but its reaction kinetics are especially suited for acidic groups with which the reaction is almost instantaneous at room temperature (*11*, *14*). Other advantages of the (cyanoethyl)dimethylsilyl derivatives are their uniform sensitivity (*14*) and good detection properties using the nitrogen–phosphorus detector or mass spectrometry in conjunction with gas chromatography.

Table I. List of the Pesticides Studied

no.	common name	chemical name	molecular wt	
			a	*b*
1	MCPP	2-(4-chloro-2-methylphenoxy)-propionic acid	214	325
2	dicamba	2-methoxy-3,6-dichlorobenzoic acid	220	231
3	MCPA	4-chloro-2-methylphenoxyacetic acid	224	335
4	2,3,6-TBA	2,3,6-trichlorobenzoic acid	200	311
5	2,4-DP	2-(2,4-dichlorophenoxy)propionic acid	234	345
6	2,6-D	(2,6-dichlorophenoxy)acetic acid	220	331
7	2,4-D	(2,4-dichlorophenoxy)acetic acid	220	331
8	2,5-D	(2,5-dichlorophenoxy)acetic acid	220	331
9	NAA	naphthaleneacetic acid	186	297
10	2,3-D	(2,3-dichlorophenoxy)acetic acid	220	331
11	3,4-D	(3,4-dichlorophenoxy)acetic acid	220	331
12	DCA	(4,6-dichloro-2-methylphenoxy)acetic acid	234	345
13	Silvex	2-(3,4,5-trichlorophenoxy)propionic acid	268	379
14	chloramben	3-amino-2,5-dichlorobenzoic acid	205	316
15	2,4,5-T	(2,4,5-trichlorophenoxy)acetic acid	254	365
16	MCPB	(4-chloro-2-methylphenoxy)butyric acid	228	339
17	benazolin	(4-chloro-2-oxobenzothiazolin-3-yl)-acetic acid	243	354
18	2,4-DB	(2,4-dichlorophenoxy)butyric acid	248	359

[a] Molecular weights of the herbicides. [b] Molecular weights of the (cyanoethyl)dimethylsilyl derivatives.

This study describes the evaluation of CEDMSDEA as a reagent for the determination of chlorophenoxy acids and related herbicides by gas chromatography using the selective nitrogen–phosphorus detector. The mass spectral properties of the herbicide derivatives are also discussed with regards to structure confirmation and specific detection at low levels by selected ion monitoring GC/MS.

EXPERIMENTAL SECTION

Chemicals and Reagents. Solvents used in this study were of pesticide grade and chemicals were purified by standard procedures before use. Chlorophenoxy acids and related herbicides were obtained as analytical standards from Agriculture Canada (Ottawa, Ontario). The authenticity of each compound was ascertained by mass spectrometry and a list is given in Table I. The silylating reagent, (2-cyanoethyl)dimethyl(diethylamino)silane (CEDMSDEA), was prepared in this laboratory according to a

---

[1] On leave from Université de Moncton, Moncton, NB, Canada.

0003-2700/87/0359-1302$01.50/0 © 1987 American Chemical Society

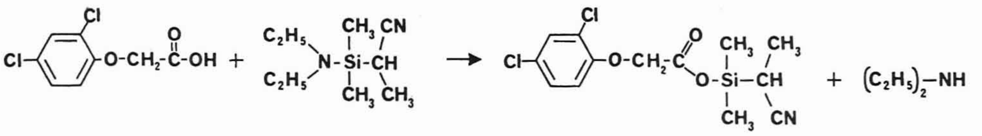

(I)

procedure published elsewhere (*11*).

Standard solutions of the herbicides (1 μg/μL) were prepared by dissolving appropriate amounts of each in ethyl acetate. Methanol was used for 2,3,6-TBA because it is slightly soluble in ethyl acetate.

Instrumentation. All chromatographic analyses were performed on a Perkin-Elmer Sigma 2B gas chromatograph equipped with a nitrogen–phosphorus detector. The fused-silica capillary column, 15 m × 0.23 mm i.d., was coated with a DB-1 poly(dimethylsiloxane) stationary phase (Chromatographic Specialties, Brockville, Ontario). The injector and detector temperatures were 275 and 300 °C, respectively. For the separation of the mixture of pesticides the oven temperature was programmed from 180 to 208 °C at 3 °C min^{-1} and then up to 250 °C at a rate of 10 °C min^{-1}. Helium was used as carrier gas and the initial split ratio on the injector was 32:1. In experiments using the nitrogen–phosphorus detector, helium was used as make-up gas at a flow of 30 mL/min and the flow rates of hydrogen and air at the detector were 2.6 and 100 mL/min, respectively. The nitrogen–phosphorus detector was optimized for maximum selectivity (*15*, *16*) and the bead current was kept below maximum sensitivity in order to increase the lifetime of the bead.

GC/MS experiments were conducted on a Kratos MS-50 TCTA mass spectrometer interfaced with a Carlo-Erba Fractovap 4160 gas chromatograph. The DB-1 capillary column was introduced directly into the ion source. In all cases the source temperature was maintained at 220 °C and the electron energy was 70 eV. The gas chromatographic parameters were similar to those described above and the scanning speed was 1 s/decade. Data were acquired by using a Kratos DS-55 data system.

Derivatization. In a typical experiment, 20 μL of a standard solution of the acidic herbicide (1 μg/μL) was put into a 500-μL Reacti-Vial pretreated with dichlorodimethylsilane. Treatment of the glassware is essential to obtain reproducible results (*17*). To the solution, 60 μL of the reagent and 45 μL of ethyl acetate were added to complete the volume at 125 μL. Unless otherwise specified the solution was shaken briefly and within 5 min 1 μL of the reaction mixture injected in the gas chromatograph or GC/MS without prior separation of the reactant and the products. For kinetic studies, triphenylamine was used as an external standard and 2,4-dichlorophenol as an internal standard (*14*). In these experiments various concentrations (total quantities of 20, 10, 5 and 1 μg) of the herbicides and reaction temperatures of 25, 50, and 75 °C were used. Aliquots of 1 μL of the reaction mixture were taken and injected in the gas chromatograph at different time intervals.

RESULTS AND DISCUSSION

The silylation reaction of chlorophenoxy acids and related herbicides with (2-cyanoethyl)dimethyl(diethylamino)silane is examplified below using 2,4-dichlorophenoxyacetic acid. In order to optimize the analytical procedure, the kinetic parameters of the silylating reaction were studied for all the compounds listed in Table I. In these experiments, 20 μg of the compounds were reacted with a molar excess of CEDMSDEA (80:1) at room temperature and the reaction yield was measured as a function of time. The results obtained indicate that for all compounds studied, the reaction is completed within minutes and that the derivatives are stable in the reaction mixture for hours. The samples can be kept for at least 36 h but in some instances losses due to hydrolysis have been noticed after 48 h. The effect of temperature on the reaction yield was also studied for several compounds and no noticeable effects were observed on the overall reaction yield when the reaction temperature was raised to 50 or 75 °C, indicating that the reaction is quantitative as previously observed for carboxylic acids and phenolic compounds (*11*, *14*). The effect of concentration on the reaction kinetics was also studied for NAA, 2,4-DP, and dicamba by using solutions of 20, 10, 5, and 1 μg/μL. In all cases the yields (>98% within experimental error) reached a plateau rapidly and remained constant for hours, indicating no effect of concentration on the total yield. The results obtained from the reaction kinetic studies indicate that CEDMSDEA is an excellent analytical reagent for all the compounds listed in Table I since the reaction is rapid, quantitative, and can be easily performed under very mild conditions.

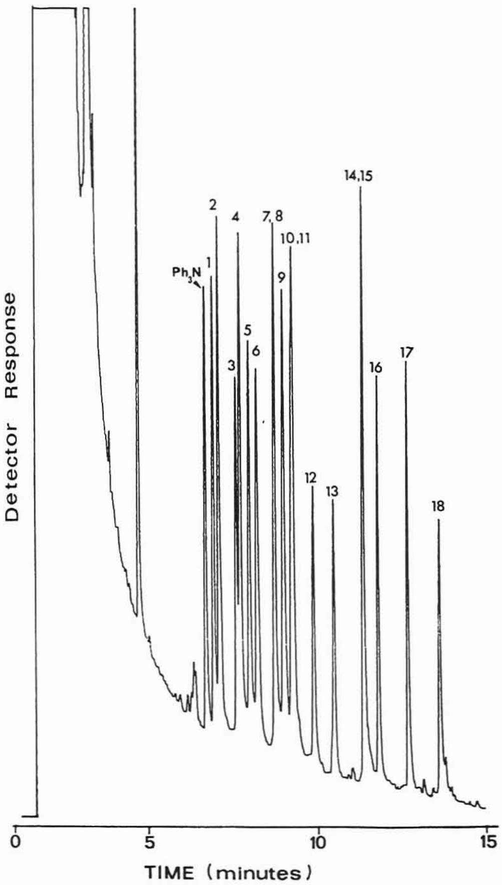

Figure 1. Chromatogram of a mixture of acid herbicides reacted with CEDMSDEA and analyzed by NPD. Numbers refer to Table I.

In order to study the retention behavior and detection properties of the (cyanoethyl)dimethylsilyl derivatives of acidic herbicides, a mixture of the compounds listed in Table I was reacted with the reagent and subsequently analyzed by gas chromatography on a poly(dimethylsiloxane) stationary phase. The elution profile of the mixture as detected by the nitrogen–phosphorus detector is shown in Figure 1. It can be seen from the chromatogram that the peaks corresponding to the herbicide derivatives (numbered 1–18) are well separated from those of the solvent and the reagent. The peak shapes observed are symmetrical and comparable to those of other types of derivatives, but the retention times of the (cyanoethyl)-dimethylsilyl esters were found to be 1.6–2 times those of the corresponding trimethylsilyl and methyl esters under the same experimental conditions. The differences in retention can be attributed to the polar nature of the cyano group on the molecules and can be used to analytical advantage in order to eliminate volatile interferences from the matrix. The chromatographic conditions used to analyze the mixture were chosen as a compromise between resolution and time of

Table II. Relative Retention Times and Relative Molar Response Factors of Herbicide Derivatives

no.	compound	rel retention time[a]	rel response factor
1	MCPP	1.04	1.26
2	dicamba	1.07	1.12
3	2,3,6-TBA	1.16	1.08
4	MCPA	1.18	1.08
5	2,4-DP	1.22	1.26
6	2,6-D	1.26	1.04
7	2,4-D	1.35	1.00
8	2,5-D	1.35	0.92
9	NAA	1.40	1.19
10	2,3-D	1.44	0.94
11	3,4-D	1.44	0.84
12	DCA	1.55	0.88
13	silvex	1.65	0.99
14	chloramben	1.80	1.26
15	2,4,5-T	1.80	0.90
16	MCPB	1.88	1.02
17	benazolin	2.03	1.17
18	2,4-DB	2.18	1.17

[a] Relative to triphenylamine: retention time = 5.93 min.

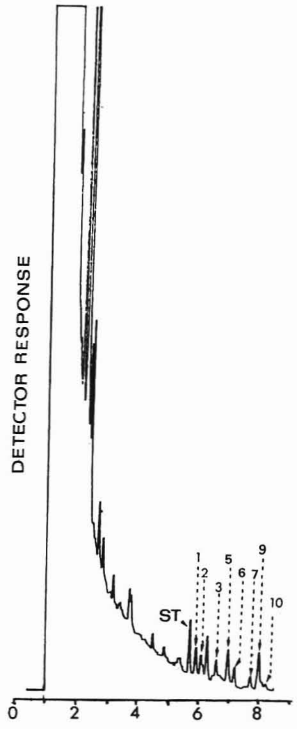

Figure 2. Chromatogram of a water extract treated with CEDMSDEA. Concentration of herbicides in water is 0.1 ppb. Numbers refer to Table I.

analysis and it can be seen that three pairs of compounds (7–8, 10–11, and 14–15) are not resolved. In this instance, efforts were not made to achieve complete separation since the compounds present in this mixture are not usually found together in a single sample.

In order to evaluate the analytical potential of the present approach, pertinent parameters related to the use of the nitrogen–phosphorus detector have been studied. Among the different parameters, sensitivity, selectivity, linearity of response over a wide range of concentrations, relative response factors, and low detection limits are important factors. Standard calibration curves were plotted for all compounds listed in Table I to verify the linearity of response with concentration and to calculate the relative response factors. The response of the nitrogen–phosphorus detector was found to be linear for all compounds from the detection limits up to hundreds of nanograms which were the upper quantities injected on the column. The relative molar response factors of the derivatives were calculated from the slopes of the concentration–response plots and are listed in Table II with the relative retention times. It can be seen that for all compounds studied the factors are close to unity with a mean value of 1.05 ± 0.21, the lowest and highest values being 0.84 and 1.26. It is interesting to note that the relative response factors for chloramben and benazolin are 1.26 and 1.17, respectively, even though these herbicides contain an additional nitrogen atom in their structures. These results reflect the prime importance of the cyano group in the detection mechanism and are of analytical importance since the method has relatively uniform sensitivity for all the compounds, contrary to the electron capture detector. Similar to response factors, the detection limits were measured for all compounds studied and are essentially the same. Under the routine detection conditions used, the lowest quantities detected ($S/N = 5$) were found to be between 50 and 75 pg. These limits can be lowered by increasing the bead current of the detector, but this shortens the lifetime of the bead and can create undesirable noise. Alternatively, the detector can be made more sensitive by changing the H_2/air ratio at the detector (*16*), but this results in a loss of selectivity, which is an important factor in the routine analysis of this type of sample.

It thus appears that the detection properties of the (cyanoethyl)dimethylsilyl derivatives are advantageous for the analysis of acidic herbicides since they offer uniform sensitivity, good linearity, and acceptable detection limits when used with the nitrogen–phosphorus detector. The use of this detector is of further advantage since it is quite insensitive to contamination, is stable, is easy to operate, and offers good selectivity against matrix interferences (*18–20*). In our experiments, the detector selectivity was measured with a mixture of decane and benzonitrile and found to be 2×10^4. However, this value is not entirely representative since the types of impurities present in the samples can vary. To show the effect of selectivity and verify the feasibility of the approach for herbicide analysis, a sample containing eight acidic herbicides (1–3, 5–7, 9, 10 in Table I) at concentrations of 0.1 ppb was prepared by dissolving appropriate amounts of each compound in 1 L of tap water. The solution was extracted using XAD-2 resin and dichloromethane. The extract was evaporated to dryness and reacted with the reagent is described previously. An aliquot of 1 μL of the reaction mixture was injected in the gas chromatograph and the results obtained are shown in Figure 2. It can be seen that all the compounds are detected at this concentration level and that the chromatogram is relatively clean even if an aliquot of the reaction mixture has been injected. This implies that the approach can probably eliminate rigoureous cleanup of the sample which results in a much shorter time of analysis.

Since mass spectrometry is often used in conjunction with gas chromatography to confirm the identity of a peak or to analyze samples at low concentration levels (*20*), the mass spectral behavior of the (cyanoethyl)dimethylsilyl derivatives of the herbicides was also studied. As an example, the mass spectrum of MCPA is shown on Figure 3. Examination of this spectrum and that of the other derivatives reveals that the spectrum contains sufficient information for structure confirmation and that relatively intense diagnostic ions are observed. For most of the compounds, intense molecular ions are present and they appear at odd masses for compounds that do not include nitrogen in their original structure. Fragment ions of varying relative intensities are observed at (M − 15), (M − 54), (M − 82), (M − 98), and (M − 112) and the values of their relative intensities for the compounds studied are given

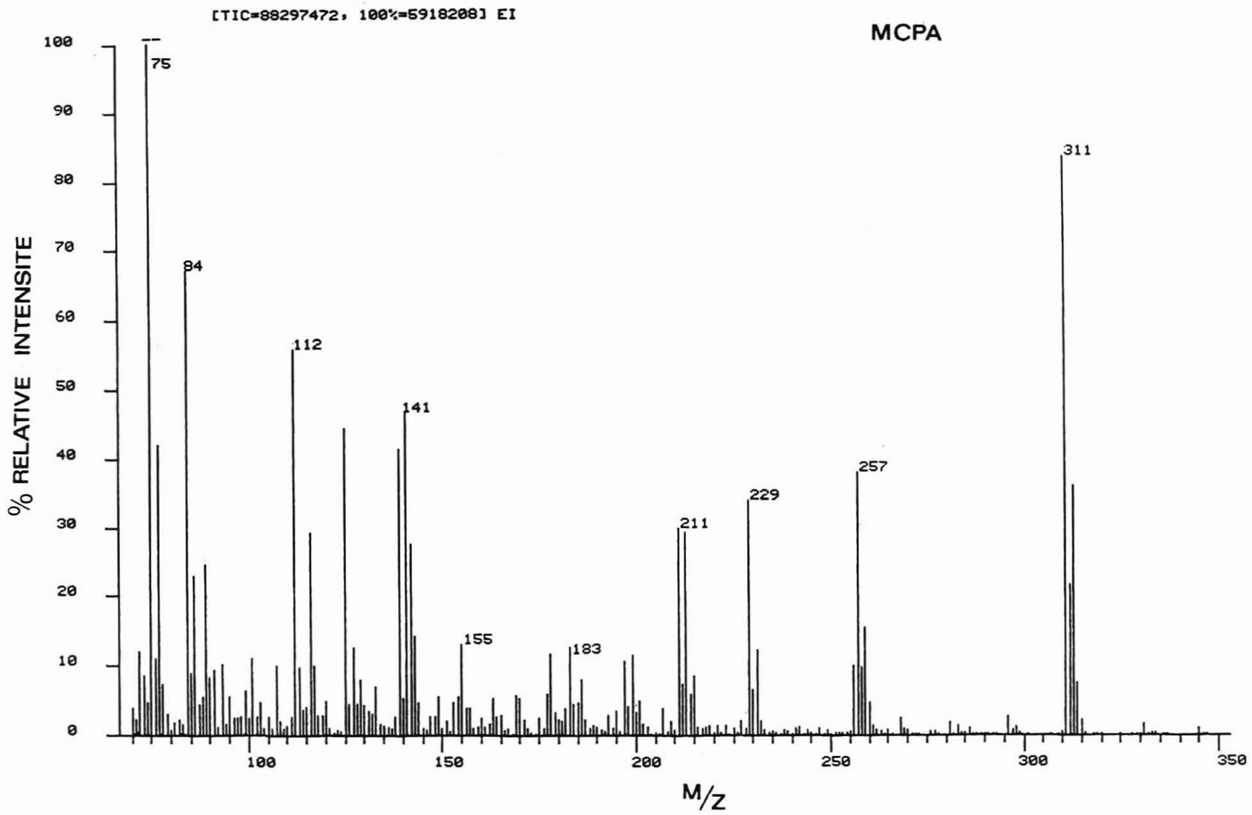

Figure 3. Mass spectrum of the CEDMS derivative of MCPA.

Table III. Relative Intensities of Common Ions in the Mass Spectra of (Cyanoethyl)dimethylsilyl Derivatives of Herbicides

no.	compound	M	M − 15	M − 35	M − 54	M − 82	M − 98	M − 112	other
1	MCPP	62	1		12	8	15*	1	225/37
2	dicamba	17	5	1	87	6	26	6	203/100
3	2,3,6-TBA		8		100		11	1	207/95
4	MCPA	84	4		36	35	30	10	211/30
5	2,4-DP	58	4	5	5	2	24	2	245/22
6	2,6-D	31	2	28	10	39	35	100	
7	2,4-D	55	5	8	10	26	30	41	
8	2,5-D	59	2	7	8	20	25	31	
9	NAA	49	3		100	1	35	3	241/58
10	2,3-D	24	2	20	5	32	18	41	
11	3,4-D	59	1	5	12	25	19	20	
12	DCA	27		9	8	21	14	24	175/27
13	silvex	42	1	3	3	3		3	251/61
14	chloramben	28	3	3	100	2	5	1	244/27
15	2,4,5-T	28	1	5	5	22	18	20	232/16
16	MCPB	3			6				198/100
17	benazolin	28	3	1	100		1	8	170/19
18	2,4-DB	3			3				198/100

in Table III. Ions corresponding to (M − 15), (M − 54), and (M − 112) are generated by fragmentation of the (cyanoethyl)dimethylsilyl group. The loss of the cyanoethyl radical is favored over that of the methyl and it gives rise to a peak at (M − 54) which is highly specific for these derivatives since 54 daltons is a loss quite uncommon in the mass spectra of most organic compounds. The ions observed at (M − 82) and (M − 98) correspond to (M − 54 − CO) and (M − 54 − CO_2) and involve fragmentation with migration of the silicon moiety. This type of rearrangement has already been observed in the mass spectra of the corresponding trimethylsilyl derivatives (*21*).

The relative intensities of the fragment ions given in Table III reflect the structure differences within the various types of acids studied. The spectra of the benzoic acids (2, 3, 14 in Table III) show intense ions at (M − 54), (M − 98), and (M − 28). The phenoxyacetic acids (4, 6–12, 15 in Table III) have (M − 54) ions of relatively weak intensities but those of ions (M − 82), (M − 98), and (M − 112) are relatively strong. The two remaining structures are characterized by the presence of intense M^+ and (M − 100) for the phenoxypropionic acids (1, 3, 13 in Table III) and of weak M^+ and intense ions at m/z 198 for the phenoxybutyric acids (16, 18 in Table III). In the latter cases, the ion at m/z 198 is the base peak in the spectrum and corresponds to the retention of the charge on the aliphatic part of the molecule. In all of the mass spectra, m/z 75 is observed and can be used as a probe for the derivatives. It thus appears that the mass spectral properties of the derivatives are adequate to successfully complement the chromatographic detection features. The mass spectra allow structure confirmation and in most cases several intense ions can be used for selected ion monitoring analysis. The results presented in this study show that the use of CEDMSDEA for the analysis of phenoxy acids is feasible and that its use can provide several analytical advantages over other existing derivatives. The reagent allows the rapid and quantitative derivatization, under very mild conditions, of all the acid herbicides studied and the derivatives formed possess the necessary properties for their selective and specific analysis by gas chromatography, using the nitrogen–phosphorus detector or mass spectrometry.

ACKNOWLEDGMENT

We thank Agriculture Canada for providing us with the analytical standards to herbicides used in this study.

Registry No. **1**, 93-65-2; **1** (CEDMS deriv.), 106864-97-5; **2**, 1918-00-9; **2** (CEDMS deriv.), 106864-98-6; **3**, 50-31-7; **3** (CEDMS deriv.), 106864-99-7; **4**, 94-74-6; **4** (CEDMS deriv.), 106865-00-3; **5**, 120-36-5; **5** (CEDMS deriv.), 106865-01-4; **6**, 575-90-6; **6** (CEDMS deriv.), 106865-02-5; **7**, 94-75-7; **7** (CEDMS deriv.), 106865-03-6; **8**, 582-54-7; **8** (CEDMS deriv.), 106865-04-7; **9**, 86-87-3; **9** (CEDMS deriv.), 106865-05-8; **10**, 2976-74-1; **10** (CEDMS deriv.), 106865-06-9; **11**, 588-22-7; **11** (CEDMS deriv.), 106865-07-0; **12**, 13333-87-4; **12** (CEDMS deriv.), 106865-08-1; **13**, 949-60-0; **13** (CEDMS deriv.), 106865-09-2; **14**, 133-90-4; **14** (CEDMS deriv.), 106865-10-5; **15**, 93-76-5; **15** (CEDMS deriv.), 106865-11-6; **16**, 94-81-5; **16** (CEDMS deriv.), 106865-12-7; **17**, 3813-05-6; **17** (CEDMS deriv.), 106865-13-8; **18**, 94-82-6; **18** (CEDMS deriv.), 106865-14-9.

LITERATURE CITED

(1) Fagan, K; Pollack, J. K. *Res. Rev.* **1984**, *92*, 29–58.
(2) McNeely, R. N.; Neimanis, V. P.; Dewyer, L. *References on Water Quality*; Inland Waters Directorate: Burlington, Ontario, 1980.
(3) Cochrane, W. P. *J. Chromatogr. Sci.* **1975**, *13*, 246–253.
(4) Cochrane, W. P. *J. Chromatogr. Sci.* **1979**, *17*, 124–132.
(5) May, D. S.; Hindin, J. E.; Dernstone, G. H. *Eng. Ext. Ser.* (*Purdue Univ.*) *Eng. Ser.* **1963**, *No. 115*, 321.
(6) Mierzwa, S.; Witek, S. *J. Chromatogr.* **1977**, *136*, 105–111.
(7) Johnson, L. G. *J. Assoc. Off. Anal. Chem.* **1973**, *56*, 1503–1505.
(8) Bache, C. A.; St-John, L. E.; Lisk, D. J. *Anal. Chem.* **1968**, *40*, 1241.
(9) Agemian Heig and Chau, Alfred S. Y. *J. Assoc. Off. Anal. Chem.* **1977**, *60*, 1070–1075.
(10) Sattar, A.; Paasivirta, M. *J. Anal. Chem.* **1979**, *51*, 598.
(11) Bertrand, M. J.; Stefanidis, S.; Sarrasin, B. *J. Chromatogr.* **1986**, *351*, 47–56.
(12) Kolb, B.; Bischoff, J. *J. Chromatogr. Sci.* **1974**, *12*, 625.
(13) Kolb, G.; Auer, M.; Pospicil, P. *J. Chromatogr. Sci.* **1977**, *15*, 53.
(14) Bertrand, M. J.; Stefanidis, S.; Donais, A.; Sarrasin, B. *J. Chromatogr.* **1986**, *354*, 331–340.
(15) Dugal, R.; Masse, R.; Sanchez, G.; Bertrand, M. J. *J. Anal. Toxicol.* **1980**, *4*, 1–12.
(16) Stefanidis, S. M.Sc. Thesis, University of Montreal, 1985.
(17) Kan, J. Y. P.; Mah, T. S.; Wade, N. L. *J. Assoc. Off. Anal. Chem.* **1982**, *65*, 763.
(18) Aue, W. A. *J. Chromatogr. Sci.* **1975**, *13*, 329.
(19) Fairwell, S. O.; Cage, D. R.; Kogel, R. A. *J. Chromatogr. Sci.* **1981**, *19*, 358.
(20) Poole, C. F.; Zlatris, A. *J. Chromatogr. Sci.* **1979**, *17*, 115.
(21) Arjmand, N.; Mumma, R. O. *J. Agric. Food Chem.* **1976**, *24*, 574.

RECEIVED for review July 21, 1986. Resubmitted December 22, 1986. Accepted December 22, 1986. We gratefully acknowledge the National Science and Engineering Council of Canada and the Fonds FCAR, Gouvernement of Quebec, for their financial assistance in this study.

Microgram Scale Determination of Total Lipid Carbon in Valuable Sediments Using a Thin-Layer Chromatography/Flame Ionization Detector Analyzer

Kazuko Ogura,* Masako Ishimura, and Junko Hisatake

Department of Chemistry, Faculty of Science, Tokyo Metropolitan University, Setagaya, Tokyo, Japan 158

Rapid and small size analytical methods of extractable lipid carbon in sediments are presented by applying a thin-layer chromatography/flame ionization detection system (TLC/FID analyzer, Iatroscan TH-10), using silica-coated Chromarod without development. A minimum of 60 samples of total lipid carbon can be analyzed in 10 min. The sample size used averaged 2.5 μg of lipid carbon, with an allowable reproducibility (standard deviation ±10%). The good correlation of total lipid carbon, in a 1400-m core sediment sample of Lake Biwa, is obtained both by this method and by the wet oxidation method. The wet oxidation method has been developed by modifying Menzel and Vaccaro's method, which is the determination of dissolved organic carbon.

A number of studies have appeared concerning lipid compounds in sediments used as biomarkers of paleoenvironments. Some of these are chlorophyll derivatives, hydrocarbons, fatty acids, alcohols, steroids, and triterpenoids. In these studies, lipid compounds have been represented by relative composition in homologous series or as ratios to total organic carbon. Our previous studies have shown that total lipid carbon itself was a good marker of paleoenvironments, such as climate and origins of organic matter in sediments (*1–3*). Further more, it has been suggested that the ratio of the compounds to total lipid carbon may have more advantage than does the compound ratio to total organic carbon. The former reveals a variation or distribution of extractable lipid compounds such as chlorophyll derivatives in sediments (*4*). However a convenient lipid carbon analytical method has not yet been developed, except for CHN analysis and gravimetric analysis. Both the CHN analysis and the gravimetric analysis require a large sample size. Thus we have developed a wet oxidation method to determine trace amounts (microgram level) of total lipid carbon in a small size sample and in many samples for a 200 m long core sediment sample of Lake Biwa (*1*) and a core sample of Lake Haruna (*5*). However, reliable determination of the total lipid carbon by the wet oxidation method required a long time and many replicates.

A thin-layer chromatography/flame ionization detection system (TLC/FID analyzer) has been developed for class analyses of lipids in biological materials and crude oils. Recently, class analyses for lipids in natural samples such as seawater, invertebrates, planktons, and sediments in waters have been studied by use of the Iatroscan (*6–9*). Crane et al. (*10*) has, however, denied the effectiveness of this method for lipid quantification.

The present study was undertaken to provide a more convenient method for rapid determination of the total lipid carbon, in the microgram scale. The determination procedure was created by using the TLC/FID analyzer (Iatroscan TH-10)

0003-2700/87/0359-1306$01.50/0 © 1987 American Chemical Society

without development, compared to the results of the wet oxidation method.

EXPERIMENTAL SECTION

Materials. Geolipids from the surface sediment of Lake Biwa were used to investigate the analytical method. Geolipids of 28 sediment samples in a 1400 m long core from Lake Biwa were taken from the lake in 1982 by Kyoto University. These samples were used for comparison with the wet oxidation method. Eicosane and cholesterol (99% pure) were obtained from Gasukuro Kogyo, Inc., Japan. Organic solvents of special grade were obtained from Wako Pure Chemical Industries, Ltd., and distilled before use. Silica-coated Chromarod (SII), the microdispenser (Drummond), and the Iatroscan TH-10 TLC/FID analyzer were obtained from Iatron Laboratories, Japan. The equipment consisted of the Iatroscan, Shimadzu Chromatopac C-R1A integrator/plotter, and Hitachi recorder 056-1001.

Procedure. *Extraction of the Lipid Fraction from Sediments.* Geolipids were extracted from wet sediments (approximately 3 g in dry mass) by using a 30 mL solvent mixture of chloroform and methanol (2/1) and ultrasonicators. Geolipids were separated from sediments by filtration with glass fiber filters (Whatman GF/C). The lipids were recovered, in the chloroform phase, by washing the filtrate with 30 mL or more of redistilled water. The chloroform phase was separated from the mixtures by centrifugation (10 °C, 3000 rpm), and diluted with chloroform to 25 mL. The major part of the geolipids in the 1400 m long core sample of Lake Biwa was used for analyses of lipid compounds such as chlorophyll derivatives (*4*) and other compounds (*11*).

Spotting Method. Five microliters of the sample and the authentic solution were applied around the SII Chromarods. By use of a microdispenser, the rods were then uniformly rotated manually, creating five or six zones for each rod at 1.5-cm intervals. The rods were scanned a few times just before contaminants removal.

Standard Authentic Sample for Determination of Total Lipids Carbon. For determination, eicosane dissolved in *n*-hexane and cholesterol dissolved in chloroform, chloroform/methanol (2/1), chloroform/methanol (1/1), and acetone were used.

Operating Condition. The flame ionization detector was operated with a hydrogen flow rate of 160 mL min^{-1} and an air flow rate of 2000 mL min^{-1}. Scan setting 4 was used, corresponding to 30 s in each scan.

CHN Analysis. Carbon, hydrogen, and nitrogen of geolipids in chloroform and cholesterol in acetone were analyzed by the CHN analyzer (Perkin-Elmer 240 elemental analyzer). Solvents were evaporated in aluminum boats under an infrared lamp.

Total Lipids Carbon Analysis by Wet Method. Menzel and Vaccaro's analytical method for dissolved organic carbon was modified, as described previously (*1*). In this study, there are some differences in determination, from the analysis described previously. The four different sample sizes, 50, 100, 200, and 400 μL, of the lipid sample in chloroform were put into 10-mL ampules. Three or four ampules were used for each sample size. The solvent was evaporated under reduced vacuum. After evaporation of the solvent, 100 mg of potassium persulfate, 0.2 mL of 3% orthophosphoric acid, and 2 mL of redistilled water were introduced into the ampules. Carbonate carbon in the solutions was removed by introducing nitrogen gas for 3 min. The ampules were then sealed. The organic carbon in the ampules was oxidized in an oven at 110 °C for 1.5 h. Carbon dioxide generated from the lipid was determined by a nondispersive infrared analyzer (Hitachi-Horiba) using glucose as a standard sample. The values of the lipid carbon in the samples were determined by the slopes of the carbon dioxide determined in the four sample sizes.

RESULTS AND DISCUSSION

Most reliable reproducibility of responses on the chromatograms of the standard authentic sample solution was obtained by use of cholesterol dissolved in acetone as seen in Table I. Other standard solutions, i.e., eicosane in *n*-hexane and cholesterol in chloroform, chloroform/methanol (2/1), and chloroform/methanol (1/1), were not suitable for the determination, because broad spots on the rods resulted, causing splitting and/or broad peaks on the chromatograms and reduction of the responses. Broad spots of geolipids in chloroform were scarcely obtained on the rods, compared to that of cholesterol in chloroform. The differences seem to stem mainly from polarities of lipid samples. Geolipids consisted mainly of polar polymerized substances, which were determined by development. Various concentrations of cholesterol in acetone were then used for standard samples. The standard deviation of the values of total lipid carbon in chloroform of surface sediment sample (±10%) was comparable with that of cholesterol in acetone (±10%). Other standard authentic sample solutions, especially eicosane in *n*-hexane (±37%), could not be used for this analysis, as seen in Table I.

Table I. Standard Deviation of Response on the Chromatogram by the TLC/FID Analyzer of Authentic Samples and Geolipid from the Surface Sediment of Lake Biwa

sample	solvent	% std dev
eicosane	hexane	±37 (*n* = 14)
cholesterol	chloroform	±12 (*n* = 6)
	chloroform/methanol (2/1)	±17 (*n* = 6)
	chloroform/methanol (1/1)	±23 (*n* = 6)
	acetone	±10 (*n* = 6)
lipid (sediment)	chloroform	±10 (*n* = 6)

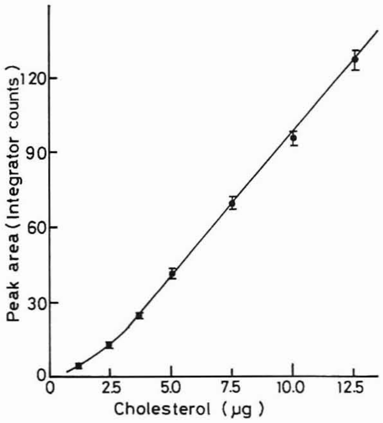

Figure 1. Calibration curve of weight of cholesterol applied on the rods against detector response (integrator counts).

Since the lipid carbon of the second scan was only a small percentage compared to the first, the total lipid carbon of the first scan was used for this study. The one-point spotting method recommended by Iatron Laboratories caused worse reproducibility than the round spotting method of this study. Read (*12*) also recommended the rotation of the rods for applications of samples. The problem of splitting peaks without development has been reported by Parrish and Ackman (*13*). They suggested that the polarity of solvent and lipid compounds caused the splitting and that the development with a slightly polar solvent created sharp splitting peaks. Careful use of the spotting method, using rotating rods, and a varied choice of suitable solvents, enabled the quantitative analysis of lipids without development using the Iatroscan TLC/FID analyzer.

Nonlinearities of responses with concentrations of standard samples have been reported by many authors. In the present study, the linearity of response against various cholesterol concentrations was obtained in normal scale in the range of 2.5–12 μg, as seen in Figure 1. The regression line does not go through the 0 point, which was thought to occur because of lower response detection compared to the concentrations. The concentrated lipid sample of the surface sediment deviated the linearity more than the 5 μg of C (5.95 μg in weight) in cholesterol, calculated by a factor that is 0.84 of the weight of cholesterol, as seen in Figure 2. As the result, the total

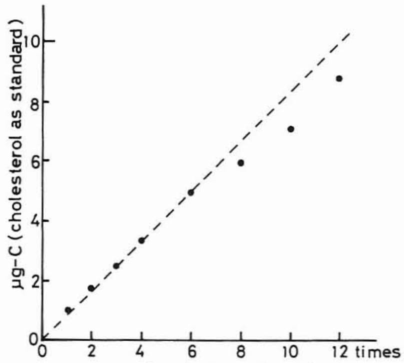

Figure 2. Relationship between the detected total lipid carbon (cholesterol as standard sample) in the geolipid extracted from surface sediment of Lake Biwa and magnification of concentration of the geolipid.

lipid carbon of geolipids was determined in the narrow range of 1–5 μg of C in cholesterol. The lipid in the core sample was concentrated from about 1/10 to 1/40 of the original volume as applied to this analytical method. This was done because the real concentrations of geolipids in 25 mL of chloroform is about 500–2000 μg of C and 0.1–0.4 μg of C, in 5 μL of solvent.

The correlation between the lipid carbon by the wet oxidation method and this method, using the same extracted lipid solution of the 1400 m long core sample of Lake Biwa, was good. The regression curve was obtained as follows:

$$Y = -9.3 + 1.1X \ (r = 0.95,\ n = 28)$$

In the equation, Y is the total lipid carbon determined by the wet oxidation method($\mu g\ g^{-1}$ dry sediment) and X is this method.

The theoretical carbon concentration of cholesterol in acetone was recovered by the CHN analysis. The concentrations of total lipid carbon of the surface sediment of Lake Biwa as determined by the CHN analysis and by this method were 1.34 ± 0.006 mg g^{-1} of dry sediment and 1.05 ± 0.071 mg g^{-1} of dry sediment, respectively. The carbon, hydrogen, and nitrogen in the lipids of the surface sediment were 55.36%, 8.46%, and 1.13%, respectively (56.8:104.4:1 in atomic ratio). The remaining 35% may correspond to oxygen, phosphor, and sulfur. The C/N ratio of the lipids was 49. The recovery of the lipid carbon in the surface sediment by this method was found to be 78% as a result of CHN analysis. The remaining 20% could not be detected by this method, probably due to the difference of response factors between cholesterol and complex mixtures of lipidlike compounds including non-lipid materials. Cholesterol is more sensitive to the Iatroscan flame ionization detector than other lipid compounds such as free fatty acids, hydrocarbons, triglycerides, and phospholipids. In the analysis of total lipid carbon, the extents of differences between CHN analysis and this method may show the differences in kinds of lipids or non-lipid materials, since both of these analyses cannot define the specific compounds.

Though, there are the disadvantages in using standard sample, as mentioned above, the time for determination can be shortened by 1/10, using this method compared to the wet oxidation method. Total lipid carbon in 60 samples can be determined in one operation using 10 rods in maximum, in 10 min, except for the time in application of lipids on the rods. Thus, this method is convenient and useful for determinations of relative total lipid distribution in many samples and small size samples, such as long core sediment samples or horizontal surface sediment samples. In addition, the advantage of using of this method is that attention need not be paid to humidity (deactivation) and vapor phase (equilibrium), necessary to adopt development. It is very important to establish which compound is to be used in a standard sample, as calibration curves vary with each authentic sample in a normal scale. The use of available geolipids as standard samples was considered. However, it was concluded that the use of geolipids was not favorable because of the necessity of frequent CHN analysis due to the effects of storage.

The results of the total lipid carbon in 140 sediment samples, of the 1400 m long core sample of Lake Biwa, were determined by this method, as described previously (*4*). The vertical distribution pattern of the total lipid carbon is consistent with that of total organic carbon, determined by N. Nakai for analysis of carbon isotopic ratios. The total lipid carbon in sediments was only a few percentages of the total organic carbon. A good correlation with the results of the wet oxidation method, as well as a strong correspondence to the distribution pattern of total organic carbon in the sediments, proves that this method is useful for the determination of trace lipid carbon in valuable sediment samples.

In addition to the extractable lipid compounds (unbound), determined in this study, nonextractable lipid compounds (bound) were present in suspended particulate matter, sediments, and sedimentary rocks. These bound lipid compounds, especially fatty acids, can be obtained by hydrolysis, by heating of samples, and also by dissolving silicates. Also reported were significant amounts of tightly bound alkanoic and hydroxy fatty acids in sediments which as indicated by Kawamura and Ishiwatari are obtainable by heating samples (*14–16*). This analytical method also is applicable to those bound lipids, when the organic contaminants in reagents for the treatment, such as hydrolysis, can be removed.

LITERATURE CITED

(1) Ogura, K.; Ishiwatari, R. *Paleolimnol. Lake Biwa Jpn. Pleistocene* **1975**, *3*, 277–284.
(2) Ogura, K. *Proc. Jpn. Acad., Ser. B* **1978**, *54*, 145–150.
(3) Ogura, K.; Takabatake, H.; Ishiwatari, R. *Paleolimnol. Lake Biwa Jpn. Pleistocene* **1982**, *10*, 256–265.
(4) Ogura, K.; Hisatake, J.; Ishimura, M. *Proc. Jpn. Acad., Ser B* **1985**, *61B*, 411–414.
(5) Ishiwatari, R.; Ogura, K.; Horie, S. *Chem. Geol.* **1980**, *29*, 261–280.
(6) Delmas, R. P.; Parrish, C. C.; Ackman, R. G. *Anal. Chem.* **1984**, *56*, 1272–1277.
(7) Gardner, W. S.; Frez, W. A.; Cichocki, E. A.; Parrish, C. C. *Limnol. Oceanogr.* **1985**, *30*, 1099–1105.
(8) Parrish, C. C.; Ackman, R. G. *Lipids* **1985**, *20*, 521–530.
(9) Volkman, J. K.; Everitt, D. A.; Allen, D. I. *J. Chromatogr.* **1986**, *356*, 147–162.
(10) Crane, R. T.; Goheen, S. C.; Larkin, E. C.; Rao, G. A. *Lipids* **1983**, *18*, 74–80.
(11) Ogura, K. *Res. Org. Geochem.* **1986**, *5*, 83–87 (in Japanese).
(12) Read, H. *Lipids* **1985**, *20*, 510–515.
(13) Parrish, C. C.; Ackman, R. G. *Lipids* **1983**, *18*, 563–565.
(14) Kawamura, K.; Ishiwatari, R. *Geochem. J.* **1981**, *15*, 1–8.
(15) Kawamura, K.; Ishiwatari, R. *Nature (London)* **1982**, *297*, 144–145.
(16) Kawamura, K.; Ishiwatari, R. *Org. Geochem.* **1984**, *7*, 121–126.

RECEIVED for review September 24, 1986. Accepted January 15, 1987.

Supercritical Fluid Chromatography/Fourier Transform Mass Spectrometry

Edgar D. Lee and Jack D. Henion*

Drug Testing and Toxicology, New York State College of Veterinary Medicine, Cornell University, 925 Warren Drive, Ithaca, New York 14850

Robert B. Cody* and James A. Kinsinger

Nicolet Analytical Instruments, 5225-1 Verona Road, Madison, Wisconsin 53711

The coupling of supercritical fluid chromatography (SFC) with Fourier transform mass spectrometry (FTMS), or SFC/FTMS, has been accomplished by using standard, commercially available equipment. The feasibility of on-line SFC/FTMS is demonstrated by continuous introduction of supercritical carbon dioxide via a 50 μm i.d. 5 m bonded fused-silica capillary column maintained at 100 °C. The SFC/FTMS separation and identification of a simple synthetic mixture is reported in addition to accurate mass measurement of caffeine to within 0.36 ppm at a resolving power of 8300. Rapid mass spectral scans by SFC/FTMS are shown under electron ionization (EI), self chemical ionization (CI), and CI using isopentane as the reagent gas. Since EI mass spectra and accurate mass measurement are not available from compounds determined by direct liquid introduction (DLI) liquid chromatography/mass spectrometry (LC/MS), these experiments provide a new approach to this structurally important information.

Chromatographers are taking renewed interest in supercritical fluid chromatography (SFC). This technique is well-suited for the separation of components in complex samples that exhibit low volatility or thermal instability (*1*). Supercritical fluids possess properties that are intermediate between those of liquids and gases (*2, 3*). The higher diffusion coefficients and lower viscosities of supercritical fluids as compared with liquids make the analysis time for SFC separations shorter and the chromatographic efficiencies greater than those obtained in HPLC. The higher solvating power of supercritical fluids makes SFC ideal for the separation of higher molecular weight and polyfunctional compounds either not volatile enough or too nonpolar for GC.

The successful combination of HPLC and MS does not provide all the features desired of a truly universal separation/identification system. Most of the various approaches to direct introduction (DLI) LC/MS (*4–7*) produce only chemical ionization (CI) mass spectra of separated compounds because of the excess eluent vapor present in the mass spectrometer ion source. In addition, there are very few instances of LC/MS accurate mass measurements (*8*) or reports of molecular weight detection beyond 1000 daltons (*6*).

The higher volatility of SFC mobile phases makes it an alternative to HPLC for coupling with mass spectrometry. Reports of combined supercritical fluid chromatography/mass spectrometry (SFC/MS) have appeared by using both conventional packed (*9*) and open tubular (*1, 10–12*) HPLC columns. For packed-column applications higher liquid flow volumes are used (*9*) and for capillary SFC/MS (*1*) electron ionization may be achieved because the mass spectrometer vacuum system can more readily maintain the required low pressure for this mode of ionization.

Fourier transfrom mass spectrometry (FTMS) is a technique in which mass analysis is performed by a different means than conventional quadrupole or sector instruments. FTMS has recently graduated from an esoteric specialty to an important potential adjunct of analytical chemistry. Recent work has focussed upon demonstrating that the approach has fewer limitations than conventional mass spectrometers. The latter suffer from restricted mass range, low mass resolution, and slow scanning speeds (*13*) which are not restricted in FTMS. Recent reviews on the subject highlight the potential analytical advantages of FTMS (*14–16*).

FTMS appears to be a unique detector for the characterization of compounds important to areas of biology, biotechnology, and polymer science. Combining it with various sample introduction systems would increase its analytical capability. Combined gas chromatography/Fourier transform mass spectrometry (GC/FTMS) has been reported (*17–19, 23*) and is now commercially available (Nicolet Analytical Instruments, Madison, WI). Because HPLC is more amenable to the separation of polar, higher molecular weight, labile compounds that are not readily amenable to GC separation, HPLC could be a better way of sample introduction.

FTMS achieves its best performance under vacuum conditions that require the maintenance of very low pressures during mass analysis. The direct liquid introduction (DLI) LC/MS technique (*4*) would appear inappropriate to interface with FTMS because of the excessive gas burden to the vacuum system as HPLC effluent is introduced into the FTMS. The direct coupling of capillary SFC to FTMS, however, should be intermediate in difficulty between coupling GC and HPLC to FTMS (*20*).

This report describes the experimental details used to accomplish preliminary SFC/FTMS results with a few simple examples. The focus of this effort was a simple feasibility study to demonstrate that the combination of capillary SFC/FTMS is possible. The emphasis is not on the chromatographic aspect of the system but rather on the instrumental factors relevant to low- and high-resolution mass analysis by the FTMS system. As expected, the main difficulty encountered was maintenance of sufficently low pressure in the FTMS analyzer region. This was achieved, however, by using a commercially available FTMS system employing narrow bore capillary columns for SFC and a differentially pumped tandem cell in the FTMS system. We report here the first published results of SFC/FTMS with emphasis on the experimental criteria necessary for continuous introduction of capillary SFC effluent into the mass spectrometer source/analyzer vacuum region.

EXPERIMENTAL SECTION

Chromatograpy. The chromatographic system (Figure 1) used for these SFC experiments consisted of a microgradient pump

0003-2700/87/0359-1309$01.50/0 © 1987 American Chemical Society

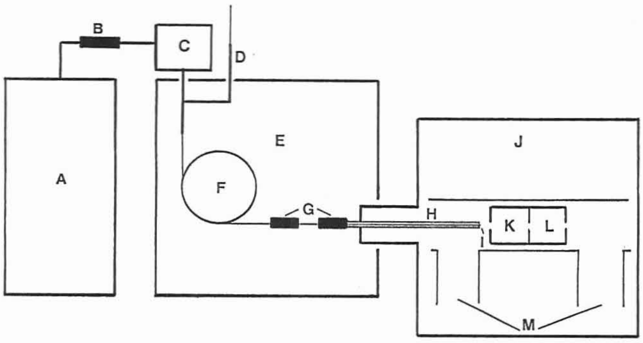

Figure 1. Schematic diagram of the SFC/FTMS system: (A) high-pressure dual-syringe pump; (B) in-line filter; (C) micro injector; (D) splitter; (E) oven, (F) column; (G) mini union; (H) stainless-steel capillary; (I) capillary restrictor; (J) FTMS system; (K) source cell; (L) analyzer cell; (M) high-vacuum pumping.

(Brownlee Labs, Santa Clara, CA) equipped with a Neslab Coolflow Model RTE 4 refrigerator for cooling supercritical carbon dioxide prior to entering the microgradient pump. A Valco micro loop injector (Model A C14W, Valco Instrument CO., Houston, TX) equipped with a digital volt interface (DVI) and a SFC splitter (Scientific Glass Engineering, Austin, TX) was used to inject samples onto the column. The column used was a rather short 0.050 mm i.d. × 5 m fused-silica capillary column that was coated with a 0.25-μm film of polymethylsiloxane (Lee Scientific, Salt Lake City, UT) and was housed in a Hewlett-Packard Model 5890 gas chromatograph maintained at an oven temperature of 100 °C. The injection splitter was operated with an on-column split ratio of approximately 1/100. The linear velocity of an unretained chromatographic peak was measured as 0.6 cm/s at 167 atm of head pressure.

The exit of the column was connected via a SGE mini-union (MVSU/004) to a 1-m fused-silica capillary restrictor. This restrictor was formed by drawing out the end of a deactivated but uncoated 1 m × 50 μm i.d. fused-silica capillary in a microflame to an inside diameter of approximately 1 μm. The resulting fused-silica transfer line/capillary restrictor was snaked through a 0.200 mm i.d. × 1 m stainless-steel capillary (Part No. HTX-27, Small Parts Inc., Miami, FL) which was then passed through a modified GC/MS transfer line of the FTMS used in this work. The standard GC/MS transfer line in this system is a $^{1}/_{16}$-in. stainless-steel tube reaching from the vacuum feed-through to the entrance of the source cell region of the tandem cell positioned between the poles of the electromagnet. The 90° bend in this $^{1}/_{16}$-in. tubing was changed carefully to about 45° to minimize the radius of curvature of the bend. This facilitates passage of the fused-silica capillary restrictor as it is positioned near the entrance of the source cell.

Thus three concentric tubes comprised the transfer line/capillary restrictor: the inner fused-silica tubing housed in the central 0.200 mm i.d. × 1 m stainless-steel capillary which itself was housed inside the normal $^{1}/_{16}$ in. stainless-steel GC transfer line used for GC/FTMS. This entire transfer line assembly was maintained at a nominal temperature of 100 °C by a wrapped resistive heater. It is this region of the SFC/FTMS system that deserves more attention in future work to ensure uniform heating of the fused-silica transfer line/capillary restrictor. In addition, it would be beneficial to selectively heat the terminal restrictor to higher temperatures (250–350 °C) to improve sample volatilization during the fluid decompression process.

As described, uniform heating of the 1-m transfer line/capillary restrictor was maintained between the GC oven and the FTMS source cell. That portion of the transfer line between the GC oven wall and the vacuum feed-through of the FTMS (approximately 30 cm) was wrapped with insulation and maintained at 100 °C by a heating tape controlled by a variable transformer. This region, in particular, needs improved temperature control.

The absolute temperature of the capillary transfer line/restrictor is not critical although it should be maintained carefully with respect to the selected GC oven temperature. Thus uniform heating above the critical temperature of the supercritical fluid is required from the inlet of the fused-silica capillary column to the capillary restrictor. Ideally, additional heating of the capillary restrictor itself is considered beneficial during the course of decompression of the supercritical fluid and dissolved sample inside the FTMS vacuum system. Direct heating of the capillary restrictor in this work was not possible due to the long distance of the restrictor from the GC oven (1 m) and the absence of a heated ion source in this instrument. It is believed that the addition of this heating capability could significantly improve this system's capability of handling higher molecular weight, involatile compounds.

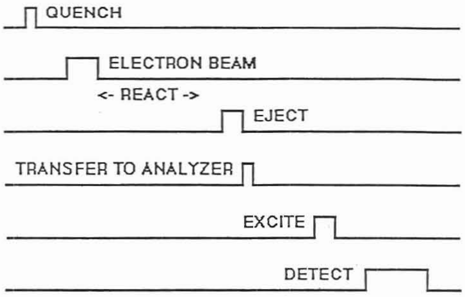

Figure 2. Experimental sequence for SFC/FTMS.

The exit of the restrictor terminated at the entrance of the FTMS cell. All connections of capillary tubing were made within the oven of the GC. Caffeine was used as the standard test compound to monitor whether supercritical conditions were maintained throughout the chromatographic system (*9*). If supercritical conditions are not maintained, this is readily detected by poor chromatographic behavior of caffeine.

Mass Spectrometry. The mass spectrometer employed for these experiments was a Nicolet Analytical Instruments FTMS-2000 Fourier transform mass spectrometer with a differentially pumped, dual-cell geometry (*21–23*) and a superconducting magnet operated at a field strength of 3 T. This instrument incorporates two cubic cells that share a common trapping plate. This common trapping plate also serves as a conductance limit, which divides the vacuum chamber into two separate pressure regions. The ion trapping cell in the higher pressure region (into which the end of the capillary restrictor was introduced) is designated the source cell, and the cell located in the lower pressure region is designated the analyzer cell. If the center trapping plate is grounded, the trapping (z-axis) motion of the ions permits transfer of ions back and forth between the two cells through a small (2-mm diameter) hole in the center of the plate. Once ions have been transferred to the analyzer, they are confined in the analyzer region by restoring the center plate to a trapping potential. The instrument may also be operated in single-cell mode by leaving the center plate at the trapping potential at all times, with detection of ions in the source cell. Two 700 L/s Edwards diffusion pumps permitted a pressure differential between the source and analyzer regions of approximately 100:1 for these experiments.

Initial success was obtained by operating the mass spectrometer in single-cell mode under CI conditions. It was necessary to eject the abundant CO^+ and CO_2^+ ions produced from the ionization of CO_2. This ejection was accomplished by irradiating CO_2^+ at its resonant frequency during the ion formation event and irradiating CO^+ during the CI reaction period. Although adequate CI spectra could be obtained by simply allowing ion–molecule reactions to occur for 150 ms at source pressures in the 1×10^{-5} torr range, it was found that the spectra were improved if a reagent gas (isopentane) was introduced to bring the total source pressure to 5.2×10^{-5} torr. No additional difficulties were associated with the gas load due to the reagent gas.

In the dual-cell mode of operation (Figure 2) ions were formed with a pulsed 5-ms electron beam at a source pressure of 1.4×10^{-5} torr and an analyzer pressure of 1.1×10^{-7} torr. A 3-V trapping potential was employed, with the conductance limit kept at the trapping potential during ion formation. Background CO_2^+ ions were ejected during the ion formation event by irradiation at their resonant frequency. A variable reaction period followed ion formation. For EI spectra, this delay was set to 0, while for CI spectra, a delay of 150 ms was used. After the reaction period, a 5-ms ion ejection event was used to eject the abundant CO^+ ions formed from the CO_2. The conductance limit was then grounded

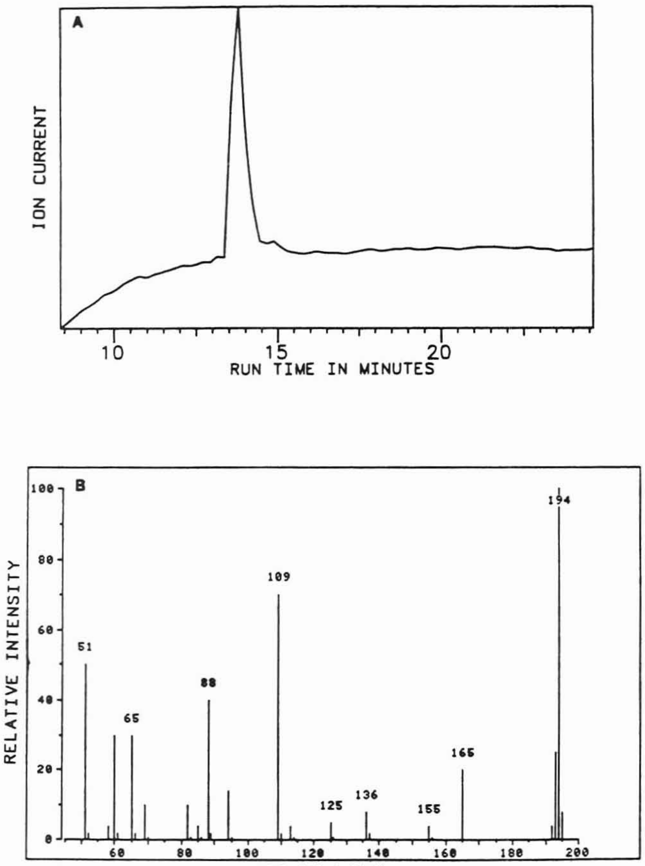

Figure 3. (A) Total ion current profile for 25 ng of caffeine on column. (B) EI mass spectrum of caffeine.

for 100 μs to allow ions to pass from the source to the analyzer cell. Following ion transfer, ions in the analyzer cell were excited into coherent motion. Detection in the analyzer side was performed in direct (broad-band) mode over the mass range 18–3000, with 128K data points collected to provide a detection time of 82 ms/transient. Twenty-five transients were collected per spectrum acquired. Mass calibration was accomplished by using perfluorotributylamine as an internal calibration compound.

RESULTS AND DISCUSSION

The first and most important issue that was addressed in this work was the feasibility of continuous introduction of supercritical carbon dioxide into the high-vacuum region of the FTMS. Even the rather low volume of CO_2 gas that is produced under capillary SFC conditions is a considerable gas burden for the FTMS vacuum system. Ordinarily this system prefers to operate with an indicated pressure of 5×10^{-9} torr although under capillary GC/FTMS conditions elevated pressures 2 orders of magnitude higher may be tolerated. Our goal was to stay within this pressure regime with capillary SFC. This is indeed possible by using the narrow bore capillary, tapered capillary restrictor, and SFC pumping conditions described in this work. It was reasonably straightforward to maintain the following cell pressures under the capillary SFC/FTMS conditions described above: source cell, 1.4×10^{-5} torr; analyzer cell, 1.1×10^{-7} torr. These operating pressures are high for FTMS but typical of those employed for capillary GC/FTMS. Thus it is possible to maintain reasonable FTMS operating parameters with continuous, total SFC effluent introduction. The next area of concern was uniform heating of the 1-m transfer line that housed the capillary restrictor. This uncoated, deactivated extension of the bonded 50-μm capillary column required uniform heating at the GC oven temperature of 100 °C to maintain supercritical conditions throughout the SFC pressure program. In the absence of these conditions, efficient ionization of the separated analytes in the FTMS source cell might not be achieved. Modification of the standard GC transfer line for this instrument resulted in less uniform heating than is needed for the transfer of more involatile analytes. It is for this reason that only rather simple, volatile organic compounds were studied in this work by capillary SFC/FTMS. Thus inherent higher molecular weight capability of FTMS was not utilized in this work due to the difficulty of delivering such involatile compounds to the FTMS under supercritical fluid conditions. This is an important limitation of any chromatography/mass spectrometry combination and must be removed before the technique can be considered routine. Future work must address this important aspect of SFC/FTMS.

Table I. Measured Masses by SFC/FTMS from EI of Caffeine

compositn	mass		diff, ppm
	calcd	measd	
$C_8H_{10}N_4O_2^+$	194.079 827	194.079 833	0.03
$C_8H_9H_4O_2^+$	193.072 002	193.072 128	0.65
$C_4H_6N_2^+$	82.052 549	82.052 666	1.43

Table II. PFTBA Accurate Mass Calibration by SFC/FTMS from Self-CI Used for Mass Measurement of Caffeine

compositn	mass		diff, ppm
	calcd	measd	
$C_3F_5^+$	130.991 48	130.991 51	0.3
$C_4F_9^+$	218.985 10	218.984 62	2.2
$C_5F_{10}N^+$	263.986 58	263.987 13	2.1

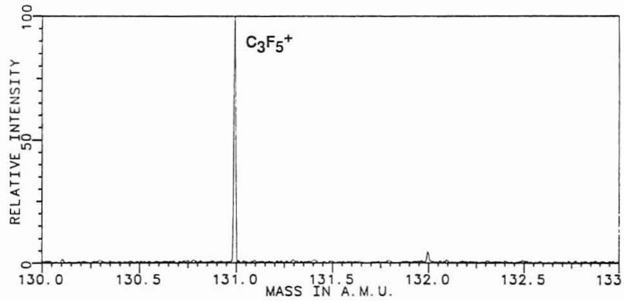

Figure 4. Self-CI mass spectrum of the PFTBA calibrant ion $C_3F_5^+$.

One of the desirable features of FTMS includes accurate mass measurement. This capability was demonstrated under the high-pressure conditions existing in the source side of the tandem cell of the mass spectrometer used in this work. The total ion current (TIC) in Figure 3A was obtained from an on-column injection of caffeine (25 ng). The mass spectrometer was operated in the EI mode. The EI mass spectrum for caffeine (Figure 3B) is comparable to that obtained under conventional GC/MS conditions. Accurate mass measurement of the molecular ion for caffeine at m/z 194 gave a measured exact mass of 194.079 833 which is within 0.036 ppm of the calculated value 194.079 827 (Table I). This demonstrates the feasibility of determining exact mass measurements for this relatively simple compound under EI SFC/FTMS conditions.

One of the unique characteristics of FTMS is that the mode of ionization can be changed from EI to self-CI by increasing the reaction period following ion formation. In addition, we found comparable sensitivity performance between EI and CI modes of SFC/FTMS unlike the considerable loss of sensitivity in the EI mode of quadrupole SFC/MS. The self-CI mass spectrum (Figure 4) of the $C_3F_5^+$ ion from the reference compound, perfluorotributylamine (PFTBA), was

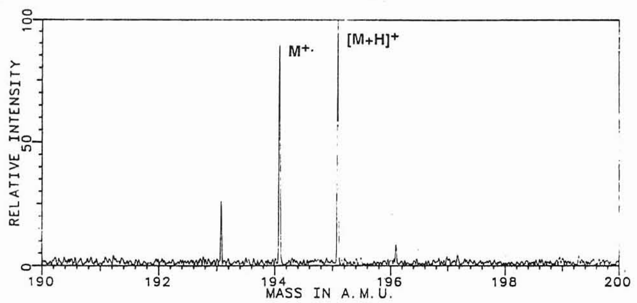

Figure 5. Self-CI mass spectrum of protonated molecular ion region of caffeine.

Table III. Measured Masses by SFC/FTMS from Self-CI of Caffeine

compositn	mass calcd	mass measd	diff, ppm
$C_8H_9O_2N_4^+$	193.072 00	193.071 67	−1.69
$C_8H_{10}O_2N_4^+$	194.079 83	194.079 30	−2.73
$C_8H_{11}O_2N_4^+$	195.087 65	195.086 93	−3.72
$^{11}C_7{}^{13}CH_{11}O_2N_4^+$	196.091 000	196.091 16	+0.76
			av 2.22

measured at a resolution of 12 100 (fwhm). The calibration of *m/z* 131, 219, and 264 ions from the self-CI of PFTBA are listed in Table II. These values were used to calibrate the ions of the protonated molecular ion region from the self-CI SFC/FTMS of 25 ng of caffeine (Figure 5). The average difference for these ions was calculated to be 2.22 ppm (Table III). The resolution obtained under these conditions was 8300.

The separation of methyl stearate and caffeine can be achieved by conventional GC although caffeine often tails badly even with bonded fused-silica capillary columns. Since the mass spectra of both methyl stearate and caffeine are well-characterized and they could be partially separated under the short capillary SFC conditions used in this work, these compounds were chosen for a simple SFC/FTMS separation–detection study. The (TIC) for the SFC/FTMS analysis of a mixture of methyl stearate (20 ng) and caffeine (25 ng) was obtained under CI conditions using isopentane as the reagent. Under these conditions the two compounds were separated to the extent of a 50% valley (not shown). The supercritical fluid, carbon dioxide, was pressure programmed from 170 to 340 atm over 20 min after a 2-min isobaric period at 170 atm with an oven temperature of 100 °C. The mass sepctra of methyl stearate and caffeine obtained from the above separation displayed the abundant protonated molecular ions of the respective compounds at *m/z* 299 and 195 with no fragment ions observed, which is characteristic of the mild ionization conditions expected from isopentane CI.

SUMMARY AND CONCLUSIONS

This work demonstrates that SFC/FTMS can be accomplished on simple compounds with commercially available equipment. The differentially pumped Fourier transform mass spectrometer vacuum system can handle continuous introduction of supercritical carbon dioxide delivered through a 50-μm capillary column. Both chemical ionization and electron ionization mass spectra may be obtained in addition to accurate mass measurement under high-resolution conditions. Analytes may be separated and delivered to the ionization region of the mass spectrometer at chromatographic column temperature well below those possible in GC/MS. This is particularly desirable when thermally labile compounds are of interest.

The high molecular weight capability of FTMS has not been utilized in this work. This capability should be entirely possible by SFC/FTMS with a transfer line optimized for supercritical fluids between the chromatographic oven and the mass spectrometer. Precise temperature control of the transfer line that carries the SFC effluent to the mass spectrometer and the capillary restrictor itself is expected to improve delivery of high molecular weight compounds to the ionization region.

Although the preliminary results presented here do not show capillary SFC/FTMS determinations of complex mixtures, this capability should be entirely feasible. In the present system volatile but thermally labile compounds such as amine oxides, pesticides, and *N*-nitrosoamides should be readily amenable to separation and identification by capillary SFC/FTMS. When appropriate improvements for uniform heating of the transfer line/capillary restrictor have been made, the combined benefits of both capillary SFC and FTMS should be available as a hyphenated analytical technique.

ACKNOWLEDGMENT

E.D.L. and J.D.H. gratefully thank Brownlee Labs for the generous gift of the microgradient pump and Hewlett-Packard for the loan of the 5890 GC oven used in this work.

LITERATURE CITED

(1) Fjeldsted, J. C.; Lee, M. L. *Anal. Chem.* **1984**, *56*, 619A–624A.
(2) Peaden, P. A.; Lee, M. L. *J. Liq. Chromatogr.* **1982**, *5* (Suppl. 2), 179–221.
(3) Fjeldsted, J. C.; Jackson, W. P.; Lee, M. L. *J. Chromatogr. Sci.* **1983**, *21*, 222–225.
(4) Covey, T. R.; Lee, E. D.; Bruins, A. P.; Henion, J. D. *Anal. Chem.* **1986**, *58*, 1451A–1461A.
(5) Eckers, C.; Henion, J. D. *Clin. Chem.* **1982**, *28*, 1882–1886.
(6) Blakely, C. R.; Vestal, M. L. *Anal. Chem.* **1983**, *55*, 750–754.
(7) Yoshida, Y.; Yoshida, H.; Tsuge, S.; Takeuchi, T. *HRC CC, J. High Resolut. Chromatogr. Chromatogr. Commun.* **1980**, *3*, 16–20.
(8) Baty, W. *Anal. Proc.* **1982**, *19*, 251.
(9) Crowther, J. B.; Henion, J. D. *Anal. Chem.* **1985**, *57*, 2711–2716.
(10) Smith, R. D.; Felix, W. D.; Fjeldsted, J. C.; Lee, M. L. *Anal. Chem.* **1982**, *54*, 1883–1885.
(11) Smith, R. D.; Udseth, H. R. *Anal. Chem.* **1983**, *55*, 2266–2272.
(12) Holzer, G.; Deluca, S.; Voorhees, K. J. *HRC CC, J. High Resolut. Chromatogr. Chromatogr. Commun.* **1985**, *8*, 528–531.
(13) Wilkins, C. L.; Gross, M. L. *Anal. Chem.* **1981**, *53*, 1661A–1676A.
(14) Johlaman, C. L.; White, R. L.; Wilkins, C. L. *Mass Spectrom. Rev.* **1983**, *2*, 389–415.
(15) Gross, M. L.; Rempel, D. L. *Science (Washington, D.C.)* **1984**, 261–268.
(16) Marshall, A. G. *Acc. Chem. Res.* **1985**, *18*, 316–322.
(17) White, R. L.; Wilkins, C. L. *Anal. Chem.* **1982**, *54*, 2443–2447.
(18) Sack, T. M.; Gross, M. L. *Anal. Chem.* **1983**, *55*, 2419–2421.
(19) Laude, D. A., Jr.; Brissey, G. M.; Ijames, C. F.; Brown, R. S.; Wilkins, C. L. *Anal. Chem.* **1984**, *56*, 1163–1168.
(20) Brown, R. S.; Shafer, K. F.; Griffiths, P. R.; Wilkins, C. L.; Presented at the Pittsburgh Conference and Exposition on Analytical Chemistry and Applied Spectroscopy, Atlantic City, NJ, March 1984; paper 275.
(21) U.S. Patent Application, Serial No. 610502.
(22) Cody, R. B.; Kinsinger, J. A.; Ghaderi, S.; Amster, I. J.; McLafferty, F. W.; Brown, C. E. *Anal. Chim. Acta* **1985**, *178*, 43–66.
(23) Settine, R. L.; Kinsinger, J. A.; Ghaderi, S. *Eur. Spectrosc. News* **1985**, *58*, 16–17.

RECEIVED for review September 18, 1986. Accepted January 20, 1987.

Anal. Chem. **1987**, *59*, 1313–1319

Isolation of Nonvolatile, Organic Solutes from Natural Waters by Zeotrophic Distillation of Water from *N*,*N*-Dimethylformamide

Jerry A. Leenheer,* Patricia A. Brown, and Eric A. Stiles[1]

U.S. Geological Survey, P.O. Box 25046, Mail Stop 407, Denver Federal Center, Lakewood, Colorado 80225

Nonvolatile, organic solutes that comprise the dissolved organic carbon (DOC) in saline waters were isolated by removal of the water by distillation from a *N*,*N*-dimethylformamide–formic acid–acetonitrile mixture. Salts isolated with the DOC were removed by crystallization of sodium chloride and sodium sulfate from the solvent mixture, removal of silicic acid by acidification and precipitation, removal of boric acid by methylation and volatilization, and removal of phosphate by zinc acetate precipitation. Chemical alteration of the organic solutes was minimized during evaporative concentration steps by careful control of acid concentrations in the solvent mixture and was minimized during drying by conversion of the samples to pyridinium and sodium salts. Recoveries of various hydrophilic organic standards from aqueous salt solutions and recoveries of natural organic solutes from various water samples varied from 60 to 100%. Losses of organic solutes during the isolation procedure were nonselective and related to the number of salt- and precipitate-washing cycles in the procedure.

In 1973, Christman and Hrutfiord (*1*) stated that one of the most critical needs in water quality research was to develop comprehensive analytical schemes for isolation and identification of all classes of organic materials in aquatic environments. Considerable progress has been made toward their goal, but studies that require the isolation of dissolved organic carbon (DOC) from natural waters are usually limited by the selective natures of the isolation procedures chosen for use. Volatile organic solutes can be isolated by various purging, distillation, sorption, and solvent extraction techniques (*2*). Nonvolatile organic solutes with hydrophobic properties can be readily isolated on various reverse-phase sorbents (*3–5*), and separations of nonvolatile hydrophobic solutes from nonvolatile hydrophilic solutes are well-defined in terms of chromatographic theory applied to various organic solute structures (*6–8*). Nonvolatile, hydrophilic, organic solutes usually comprise 30–50% of the DOC of natural waters (*9*) and they are more difficult to isolate for study because of problems in separating these solutes from various salts dissolved in water.

Published procedures for the isolation of nonvolatile hydrophilic organic solutes from water are based upon ion exchange (*6, 10*), reverse osmosis (*11*), or ultrafiltration (*12*) for concentration and gel permeation chromatography (*13*), precipitation (*6, 14*) or selective crystallization (*15*) for desalting. Nonvolatile, hydrophilic organic solutes less than 500 Da are not efficiently desalted by membrane separation techniques and gel permeation chromatography because of their low-resolution separation from salts. Ultrafiltration has been used to isolate approximately half of the DOC from estaurine and seawater (*16, 17*), and the study by Means and Wijayarate (*16*) indicated that much of the DOC isolated by ultrafiltration consists of nonvolatile hydrophilic solutes and colloids. No adequate procedure presently exists for the isolation and desalting from saline waters of most low-molecular-weight organic solutes that are nonvolatile and hydrophilic.

The initial objective of this study was to design a special technique to isolate the DOC from the water of Big Soda Lake, near Fallon, NV, for a ^{14}C-age determination. Big Soda Lake is an alkaline (pH 9.7), chemically stratified lake that contains DOC concentrations as high as 60 mg of carbon/L and a dissolved salt concentration as high as 88 000 mg/L (*18*). For useful ^{14}C-age determinations, the DOC isolated must be representative of all the DOC, rather than isolating a nonrepresentative proportion of the DOC by conventional sorption techniques. A comprehensive approach to DOC isolation, based on reverse-phase sorption and ion-exchange techniques (*6*) failed, because the extremely large salt concentrations saturated the ion-exchange columns before significant concentration of organic solutes occurred.

The principle that forms the basis for the isolation technique involves transfer of the hydrophilic solutes from the aqueous phase, in which inorganic salts are soluble, to an organic phase, in which inorganic salts are insoluble. Solvent extraction is not a suitable phase-transfer technique, because hydrophilic solutes do not partition efficiently into immiscible, low-polarity solents; however, a relatively large number of polar organic solvents are good solvents for natural organic substances (*19, 20*). Hayes (*19*) stated that the best organic solvents for polar organic substances, such as humic acids are good proton acceptors for hydrogen-bonding interactions and that these solvents should be slightly acidified to convert the solute weak-acid groups to the undissociated form. He stated that formamide, *N*-methylformamide, *N*,*N*-dimethylformamide (DMF), anhydrous formic acid, and dimethyl sulfoxide were the best solvents for humic acid. Of these solvents, only DMF and anhydrous formic acid were volatile enough to be removed by vacuum evaporation after extraction, and only DMF had zeotrophic properties (DMF does not form an azeotrope with water) that enabled distillation of water from a water–DMF mixture. Therefore, zeotrophic distillation with DMF rather than solvent partitioning was selected as the phase-transfer mechanism by which hydrophilic solute concentration and isolation might be accomplished.

When the initial study objective (isolation of DOC from Big Soda Lake) was achieved, the objective was expanded to achieve nonselective isolation of DOC from natural waters by the zeotrophic distillation procedure without alteration of the molecular structure of chemically labile substances such as glucose. The procedures developed were especially optimized for recovery of low-molecular-weight hydrophilic organic solutes from saline waters because of the lack of alternative isolation methods for saline waters. Chemical alteration of organic solute standards and detection of procedural con-

---

[1] Present address: McLaughlin Water Engineers Ltd., 2420 Alcott, Denver, CO 80211.

This article not subject to U.S. Copyright. Published 1987 by the American Chemical Society

taminants were assessed by proton NMR spectroscopy. The procedure was also developed for isolation of natural hydrophilic acid solutes (as defined by an operational fractionation procedure (*6*, *21*) from an ion-exchange concentrate which contains large salt concentrations.

EXPERIMENTAL SECTION

Apparatus. A Buchi Rotavapor 150 was used for the large-scale evaporation required in step 2 of Figure 1. This vacuum-rotary evaporator could process volumes of 10 L, and it evaporated water at a rate of 2.4 L/h at a water-bath temperature of 60 °C, when the boiling point of water was 30 °C under reduced pressure. A Buchi Rotavapor was used for evaporating volumes of less than 1 L. An assortment of flask capacities from 1 L to 10 mL were used as required.

A Varian FT-80 A NMR spectrometer was used to determine proton NMR spectra for characterization of standards and samples. Samples were dissolved in deuterium oxide at pH 8, at a concentration of 100 mg/mL. Proton NMR spectra were recorded at 79.5 MHz, using a flip angle of 45°, a pulse width of 3 μs, and a pulse delay of 5 s. Sweep width was 2000 Hz and all spectra were referenced to HDO at 4.63 ppm. These conditions produced quantitative proton NMR spectra for the standards and samples of the study. From 100 to 500 transients were accumulated to generate acceptable NMR spectra. Infrared spectra used for qualitative assays of isolates for reagents, contaminants, and inorganic constitutes were determined on a Perkin-Elmer 580 infrared spectrophotometer. Samples were mounted as cast films on silver chloride windows or in KBr disks.

A rotating-and-reciprocating piston pump (FMI Lab Model RPSY) was used to pump sample concentrates through the 160-mL glass column (2.5 i.d. × 30 cm long), with Teflon end plates purchased from Bethesda Research Laboratories. The column contained MSC-1-H (Dow Chemical, Midland, MI) which was purified and hydrogen-saturated according to published procedures (*6*, *21*). Sample concentrates were freeze-dried in glass-vacuum flasks connected to a Virtis Model 10-141 freeze dryer. Organic-carbon concentrations in water were determined on a Beckman Model 915B total organic carbon analyzer.

Elemental analyses for C, H, O, N, and S, ash, and moisture contents were performed by Huffman Laboratories, Golden, CO. Analytical methods, accuracy, precision, and interlaboratory comparison of the methods used are discussed in detail by Huffman and Stuber (*22*). Briefly, the methods used were as follows: carbon and hydrogen, modified Coulometric; nitrogen, modified Dumas; oxygen, modified Coulometric, Inc., Model 5060 oxygen analyzer; sulfur, Fisher Model 475 sulfur analyzer; ash, residue after combustion in platinum boat; moisture, weight loss upon vacuum drying over P_2O_5. Chloride was determined by a silver nitrate titration of a solution of the isolates in water (*23*) and sodium by titration of a hydrogen-saturated (by ion exchange) solution of the isolates to pH 8.0.

Reagents and Solutions. The solvents acetonitrile, *N*,*N*-dimethylformamide, methanol, methylene chloride, and pyridine were "HPLC grade" quality (J. T. Baker, Phillipsburg, NJ). Formic acid (88% solution in water) was reagent grade (Mallinckrodt, St. Louis, MO). Reagent-grade (98–100%) sodium chloride, sodium sulfate, sodium carbonate, sodium sulfide monohydrate, and dibasic potassium phosphate were obtained from J. T. Baker. Reagent-grade boric acid was obtained from Mallinckrodt; reagent-grade sodium metasilicate monohydrate was obtained from Anachemica, Montreal, Canada. Organic standards used for solute-recovery studies were practical-grade 1,2,4,5-benzenetetracarboxylic acid, 3,4,5-trihydroxybenzoic acid, succinic acid, and tartaric acid obtained from Chemical Service Kit, West Chester, PA. Analytical-grade glucose was obtained from Mallinckrodt; galacturonic acid was obtained from Aldrich Chemical, Milwaukee, WI.

A synthetic solution based on the chemical analyses of the deep-water layer of Big Soda Lake (*18*) was prepared as follows: 45.10 g of sodium chloride, 42.60 g of sodium carbonate, 0.87 g of boric acid, 1.00 g of sodium metasilicate monohydrate, 2.90 g of sodium sulfide monohydrate, and 0.31 g of dibasic potassium phosphate were dissolved in 1 L of reagent water, and the pH was adjusted to 9.9 by titration with 35% hydrochloric acid. For standard-recovery studies, 1,2,4,5-benzenetetracarboxylic acid was dissolved in the synthetic lake water until the concentration of the acid was 100 mg/L, and glucose, 3,4,5-trihydroxybenzoic acid, and galacturonic acid were dissolved until the combined concentrations were 1000 mg/L. Succinic acid, tartaric acid, galacturonic acid, 1,2,4,5-benzenetetracarboxylic acid, and glucose were dissolved in DMF–acetonitrile (1/1) to test for precipitation by dilution with methylene chloride.

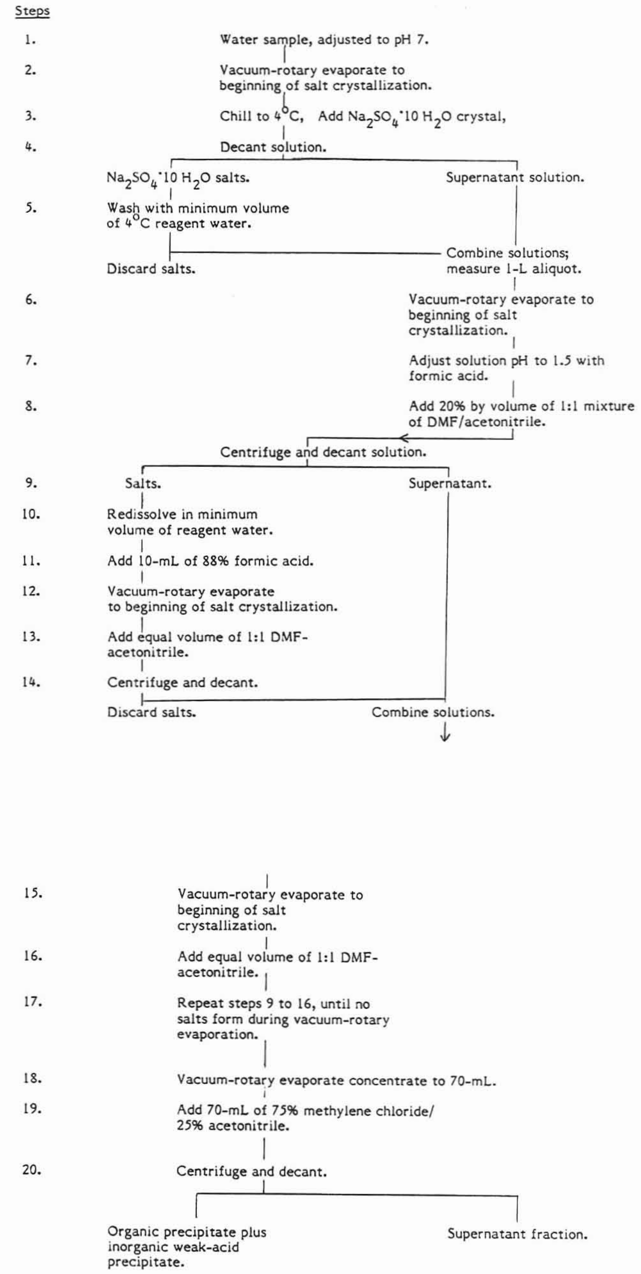
Steps
1. Water sample, adjusted to pH 7.
2. Vacuum-rotary evaporate to beginning of salt crystallization.
3. Chill to 4°C, Add Na2SO4·10 H2O crystal,
4. Decant solution.
Na2SO4·10 H2O salts.
Supernatant solution.
5. Wash with minimum volume of 4°C reagent water.
Discard salts.
Combine solutions; measure 1-L aliquot.
6. Vacuum-rotary evaporate to beginning of salt crystallization.
7. Adjust solution pH to 1.5 with formic acid.
8. Add 20% by volume of 1:1 mixture of DMF/acetonitrile.
Centrifuge and decant solution.
9. Salts.
Supernatant.
10. Redissolve in minimum volume of reagent water.
11. Add 10-mL of 88% formic acid.
12. Vacuum-rotary evaporate to beginning of salt crystallization.
13. Add equal volume of 1:1 DMF-acetonitrile.
14. Centrifuge and decant.
Discard salts.
Combine solutions.
15. Vacuum-rotary evaporate to beginning of salt crystallization.
16. Add equal volume of 1:1 DMF-acetonitrile.
17. Repeat steps 9 to 16, until no salts form during vacuum-rotary evaporation.
18. Vacuum-rotary evaporate concentrate to 70-mL.
19. Add 70-mL of 75% methylene chloride/25% acetonitrile.
20. Centrifuge and decant.
Organic precipitate plus inorganic weak-acid precipitate.
Supernatant fraction.

Figure 1. Flow chart of isolation procedure for organic solutes in water.

Isolation Procedures. Flow charts showing the steps for isolation of organic solutes from water are shown in Figures 1–3. If subfractionation into precipitate and supernatant fractions is not desired, proceed from Figure 1, step 18, to Figure 3, step 3, and complete the procedures. Most natural waters do not contain enough borate and phosphate to warrant their removal in steps 11 to 18 of Figure 2 and steps 13 to 20 of Figure 3; these steps can be deleted, which significantly shortens the procedures. Substances removed or separated and the principles of separation for all the procedures in Figures 1 to 3 are summarized in Table I.

Samples. Big Soda Lake near Fallon, NV, was sampled by the authors at depths of 5 m and 40 m in July 1983, and it was resampled in July 1984. The Okefenokee Swamp near Fargo, GA, was sampled in November 1983; the Sagavanirktok River near Prudhoe Bay, AK, was sampled in August 1984; and Hidden Creek near Soldotna, AK, was sampled by the authors in September

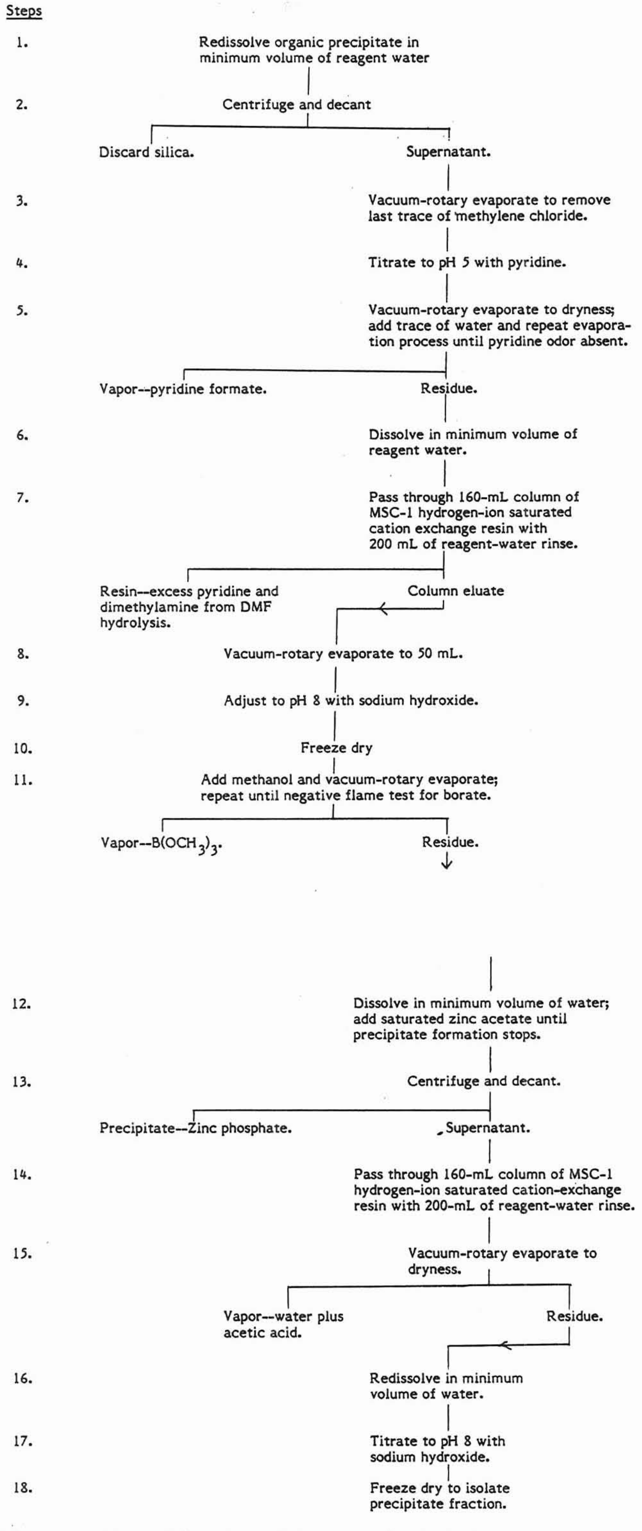
Steps
1. Redissolve organic precipitate in minimum volume of reagent water
2. Centrifuge and decant
Discard silica.
Supernatant.
3. Vacuum-rotary evaporate to remove last trace of methylene chloride.
4. Titrate to pH 5 with pyridine.
5. Vacuum-rotary evaporate to dryness; add trace of water and repeat evaporation process until pyridine odor absent.
Vapor--pyridine formate.
Residue.
6. Dissolve in minimum volume of reagent water.
7. Pass through 160-mL column of MSC-1 hydrogen-ion saturated cation exchange resin with 200 mL of reagent-water rinse.
Resin--excess pyridine and dimethylamine from DMF hydrolysis.
Column eluate
8. Vacuum-rotary evaporate to 50 mL.
9. Adjust to pH 8 with sodium hydroxide.
10. Freeze dry
11. Add methanol and vacuum-rotary evaporate; repeat until negative flame test for borate.
Vapor--B(OCH3)3.
Residue.
12. Dissolve in minimum volume of water; add saturated zinc acetate until precipitate formation stops.
13. Centrifuge and decant.
Precipitate--Zinc phosphate.
Supernatant.
14. Pass through 160-mL column of MSC-1 hydrogen-ion saturated cation-exchange resin with 200-mL of reagent-water rinse.
15. Vacuum-rotary evaporate to dryness.
Vapor--water plus acetic acid.
Residue.
16. Redissolve in minimum volume of water.
17. Titrate to pH 8 with sodium hydroxide.
18. Freeze dry to isolate precipitate fraction.

Figure 2. Flow chart of precipitate fraction isolation procedure.

1984. The Williams Fork Reservoir was sampled near Kremmling, CO, in June 1983, and Spirit lake near Mount St. Helens, WA, was sampled in July 1983. The hydrophilic-acid fraction concentrates from the Okefenokee Swamp, Sagavanirktok River, Hidden Lake Creek, Williams Fork Reservoir, and Spirit Lake samples were obtained by the preparative DOC fractionation procedure (*21*).

RESULTS AND DISCUSSION

Initial attempts to isolate DOC from water samples from Big Soda Lake by zeotrophic distillation of water from acidified DMF were not very successful. Major problems encountered were (1) concentration of acid during evaporation, resulting in DMF hydrolysis and chemical alteration to isolated DOC, (2) loss of DOC with discarded salts, (3) isolation of weak inorganic acids (silicic acid, boric acid, phosphoric acid) with the DOC, and (4) problems with purification of DOC product from DMF and DMF hydrolysis products. A series of experiments were designed to quantitate the DOC loss and to identify the causes of losses, so that procedural modifications could be incorporated that either decreased or eliminated these problems.

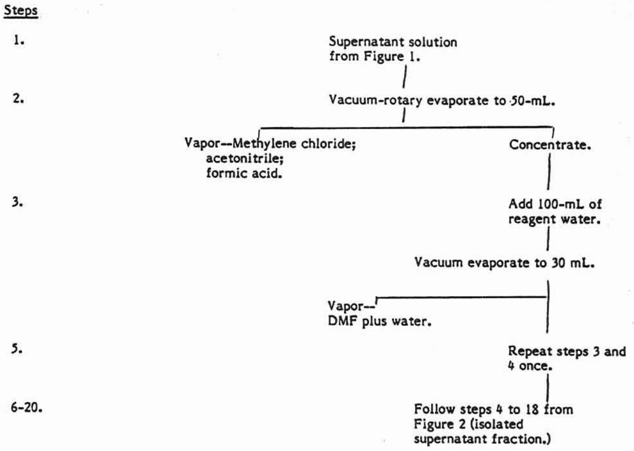
Steps
1. Supernatant solution from Figure 1.
2. Vacuum-rotary evaporate to 50-mL.
Vapor--Methylene chloride; acetonitrile; formic acid.
Concentrate.
3. Add 100-mL of reagent water.
Vacuum evaporate to 30 mL.
Vapor--DMF plus water.
5. Repeat steps 3 and 4 once.
6-20. Follow steps 4 to 18 from Figure 2 (isolated supernatant fraction.)

Figure 3. Flow chart of supernatant fraction isolation procedure.

Removal of Sodium Sulfate by Crystallization. No problems were encountered with the first five steps of the procedure (Figure 1) in which the majority of sodium sulfate was removed. Solubility of sodium sulfate in water varies with temperature from 92.7 g/100 mL at 30 °C to 11.0 g/100 mL at 0 °C (*24*). A seed crystal of sodium sulfate decahydrate was added to prevent supersaturation during cooling of the solution. After crystallization and washing of the crystals, DOC analyses of the supernatant solutions of both samples and standards did not detect any significant loss (less than 5% of DOC) within the crystals. If the sample was a hydrophilic acid concentrate from the DOC fractionation procedure, sulfuric acid and sodium hydroxide were selected for pH adjustment in the DOC fractionation procedure so these reagents could be removed as sodium sulfate after neutralization.

Removal of Sodium Sulfate and Sodium Chloride by Zeotrophic Distillation of Water from DMF. The first problem studied was chemical alteration of the sample and DMF caused by concentration of acid during evaporation. Acids evaluated for use were hydrochloric, trifluoroacetic, acetic, and formic. Glucose dissolved in reagent water without salt, and dissolved in water containing sodium chloride and sodium sulfate at Big Soda Lake concentrations, was used to evaluate chemical alteration to a hydrophilic organic solute.

Loss of DOC occurred with the salts that crystallized during the zeotrophic distillation procedure (steps 12–14 of Figure 1) when the solution pH was greater than 1.5. Certain organic acids, such as benzene hexacarboxylic acid (pK_2 = 1.40) and maleic acid (pK_2 = 1.94), are sufficiently acidic that a pH of 1.5 is necessary to suppress ionization. Hydrochloric and trifluoroacetic acids concentrated during the vacuum rotary evaporation (steps 12 and 15 of Figure 1) and altered the glucose as evidenced by the browning of solution. Acetic acid could not be added in concentrations large enough to decrease the concentrate pH to 1.5. Formic acid was continually lost during vacuum-rotary evaporation, but its periodic addition (step 7, Figure 1) during the salt-washing cycle maintained the concentrate acidity near pH 1.5.

Loss of DOC entrained within salts that crystallized during the zeotrophic distillation procedure was minimized by redissolving (step 10, Figure 1) and recrystallizing the salts (steps 12 and 13, Figure 1), by addition of acetonitrile to DMF (steps

Table I. Summary of Desalting, Separation, and Isolation Procedures for Figures 1, 2, and 3

procedural step	substance removed or separated	principle of separation
1–5 (Fig. 1)	sodium sulfate	crystallization of sodium sulfate decahydrate
5–18 (Fig. 1)	sodium sulfate and sodium chloride	zeotrophic distillation of water from DMF
19–20 (Fig. 1)	precipitate fraction from supernatant fraction	precipitation caused by decrease in solvent polarity
1–2 (Fig. 2)	silicic acid	selective dissolution of organic acids
3–8 (Fig. 2); 1–10 (Fig. 3)	DMF, formic acid, pyridine, dimethylamine	volatilization of DMF and pyridinium formate, adsorption and pyridine and dimethylamine by cation exchange
9–11 (Fig. 2); 11–13 (Fig. 3)	boric acid	volatilization as trimethyl borate
12–13 (Fig. 2); 14–15 (Fig. 3)	phosphoric acid	precipitation as zinc phosphate
14–18 (Fig. 2); 16–20 (Fig 3)	acetic acid, water	volatilization of acetic acid, volatilization of water from sodium salts of hydrophilic acids

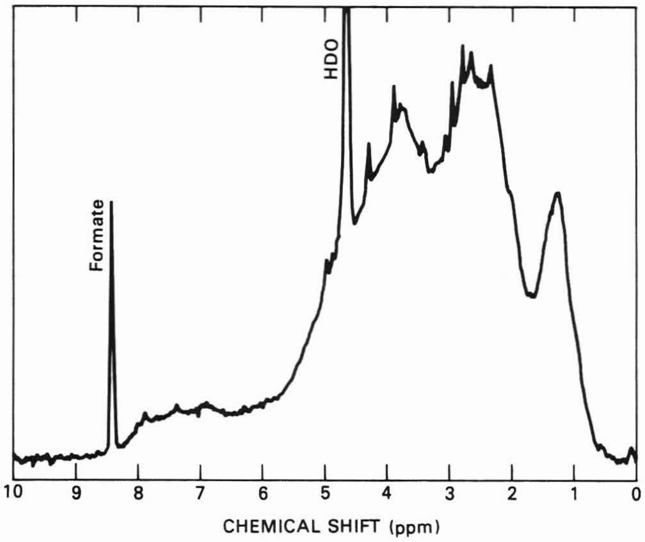

Figure 4. Proton NMR spectrum of precipitate fraction, Sagavanirktok River.

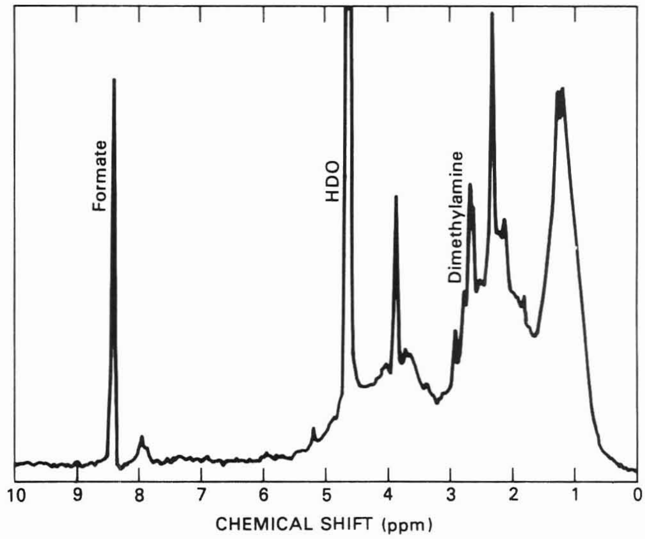

Figure 5. Proton NMR spectrum of supernatant fraction, Sagavanirktok River.

8 and 13, Figure 1) to enhance salt crystallization and increase the volume of solution available to rinse the salts. Only 20% by volume of DMF–acetonitrile (1/1) was added in step 8 (Figure 1), as compared to an equivalent volume of DMF–acetonitrile (1/1) in step 13, to prevent excessive salt crystallization (greater than 25% salt by volume), which is difficult to rinse with insufficient solution volume. This also minimizes DMF addition because DMF is moderately difficult to remove at the end of the procedure. For most samples, a total of three cycles (steps 9 to 16, Figure 1) was required to remove all sodium salts of strong acid anions, primarily sulfate and chloride. By the end of the third cycle, the solvent was DMF and formic acid; water and acetonitrile had been removed by vacuum–rotary evaporation.

Separation of Precipitate Fraction from Supernatant Fraction. The precipitate fraction from step 20 (Figure 1) was operationally defined as the fraction of DOC which precipitated in the DMF, formic acid, acetonitrile, and methylene chloride solvent mixture of step 20. The DOC, which does not precipitate, was defined as the supernatant fraction. The proton NMR spectrum of the precipitate fraction from the hydrophilic acid concentrate of the Sagavanirktok River sample, shown in Figure 4, shows many more protons on carbons attached to oxygen in the 3.5–4.5 ppm region than are present in the supernatant fraction (Figure 5). This difference in fraction composition shown in the proton NMR spectra of Figures 4 and 5 may be related to lower solubility of hydroxy acids (precipitate fraction) than carboxylic acids (supernatant fraction) in the solvent mixture of step 20 (Figure 1). Tartaric acid, galacturonic acid, and glucose were precipitated by the solvent mixture of step 20, whereas succinic acid and 1,2,4,5-benzenetetracarboxylic acid did not precipitate.

The precipitation step (step 20, Figure 1) was instituted to purify the majority of the isolate from reagents and contaminants. Formate (peak at 8.5 ppm, Figure 5) is the only significant reagent contaminant in the hydroxy acid fraction, whereas larger concentrations of formate, protonated dimethylamine (peak at 2.7 ppm, Figure 5), and unknown contaminant peaks at 2.3 and 3.9 ppm were present in the proton NMR spectrum of the supernatant fraction. Silicic acid, boric acid, and phosphoric acid precipitated (or coprecipitated) with the precipitate fraction.

Removal of Silicic Acid, Boric Acid, and Phosphoric Acid. Solvation of silicic acid, boric acid, and phosphoric acid by DMF was expected, because DMF has a substantial affinity for proton-donating solutes; however, the presence of these weak inorganic acids presented purification problems for isolated organic solutes. Recovery studies on 1,2,4,5-benzenetetracarboxylic acid in synthetic Big Soda Lake water indicated that this aromatic polycarboxylic acid was being carried through to the DMF concentrate in step 18 (Figure 1) as determined by measurement of its absorbance at 296 nm. However, vacuum evaporation of the DMF and formic acid yielded a viscous liquid of weak inorganic acids plus the 1,2,4,5-benzenetetracarboxylic acid. Treatment of the DMF concentrate with hydrofluoric acid followed by evaporation successfully removed the silicic acid as volatile silicon tetrafluoride (as determined by the disappearance of the noncrystalline silicate band in the infrared spectrum at 800 cm^{-1}), but acid hydrolysis of the DMF and chemical alteration of glucose were found to be significant problems. Dilution of the DMF concentrate with methylene chloride–acetonitrile (step 19, Figure 1) precipitated the silica along with a portion of the DOC, and redissolution of the DOC (step 1, Figure 2) did not redissolve the silicic acid that was discarded.

Boric acid was removed from the concentrate mixture by conversion to its volatile methyl ester that was then evaporated with methanol (step 11, Figure 2) (*25*). Presence of methyl borate in the vapors can be detected by a green color in a flame test. Organic acids were converted to their sodium salts (step 9, Figure 2) to prevent their methylation during boric acid removal. The removal of boric acid was determined by the disappearance of boric acid bands in the infrared spectrum at 2260 and 548 cm^{-1}.

Phosphate was removed from the residue by precipitation as zinc phosphate by addition of zinc acetate (step 12, Figure 2). The method of Thompson and Markey (*26*) that used barium hydroxide to precipitate barium phosphate from urinary organic acids was attempted, but losses from 45% to 68% of the natural organic solutes were determined with this method. Zinc phosphate precipitation gave variable but smaller losses of natural organic solutes, and a 17% loss was determined for the benzenetetracarboxylic acid standard in synthetic Big Soda Lake water. Much of the organic solute loss with zinc phosphate precipitation may be attributed to simple mechanical loss with precipitate separation, because extensive precipitate-washing steps were not included in the procedure. Acetate added with the zinc was removed as acetic acid by vacuum–rotary evaporation (step 15, Figure 2). Chemical alteration to the organic solutes by acetic acid during drying is minimal, because acetic acid is a weaker acid than formic acid and it has greater volatility with water than does formic acid.

Removal of Solvents and Reagents. After all the inorganic solutes were removed by the separation procedures shown in Figures 1–3, the final freeze-dried residue still contained traces of DMF, dimethylamine, and formic acid (by proton NMR assays) when it was dried in the free-acid form. The residue was a sticky solid that was difficult to remove from the drying flask. Titration of this residue to pH 8 with sodium hydroxide (step 17, Figure 2) eliminated the DMF and dimethylamine during freeze-drying. Apparently DMF volatilizes from the salt form of organic acids but forms a nonvolatile hydrogen-bonded adduct to the free acid form. The neutralized organic acids also formed a flaky organic solid that was easy to remove from the drying flask. Dimethylamine is an acid hydrolysis product of DMF that does not form when the sample is dried at pH 8.

Formic acid can be removed directly by volatilization, but browning of glucose, caused by acid dehydration, was observed when formic acid was removed during drying of the isolate. By titration with pyridine to pH 5 (step 4, Figure 2), formate could be removed as volatile pyridinium formate (step 5, Figure 2), without decreasing the pH.

By use of formic acid and pyridine, glucose recovered from water without salt was unaltered, as evidenced by the proton NMR spectrum of Figure 6a. When pyridine was not used, the proton NMR spectrum (Figure 6b) had altered peak ratios, appearance of additional peaks at 4.9 and 5.3 ppm, and a significant residual peak of formic acid at 8.5 ppm. When glucose was recovered from the sodium sulfate and sodium chloride salt solution, only minimal evidence of chemical alteration was indicated in the proton NMR spectrum of Figure 6c, and no visible browning of the sample occurred.

Occasionally, formic acid was not completely removed as pyridinium formate and it was present to the end of the procedure. An alternative procedure for removing formic acid was to repeatedly vacuum evaporate the sample with acetonitrile after step 16 (Figure 2). Acetonitrile forms a lower-boiling azeotrope with water and minimizes acid hydrolysis as the sample is dried.

Recovery Data and Isolate Characterization. Recovery data for the various standards used in the development of the method are summarized in Table II. Recoveries vary between 80% and 94% except when the salt-washing cycle (steps 9 to 14, Figure 1) was not included for 3,4,5-trihydroxybenzoic acid (59% recovery) or when formic acid was not completely removed from the sample for glucose (121%). High concentrations of the standards (Table II) were used in these studies for convenience to avoid the large-scale vacuum evaporations required by steps 1 to 5 (Figure 1) of the procedure.

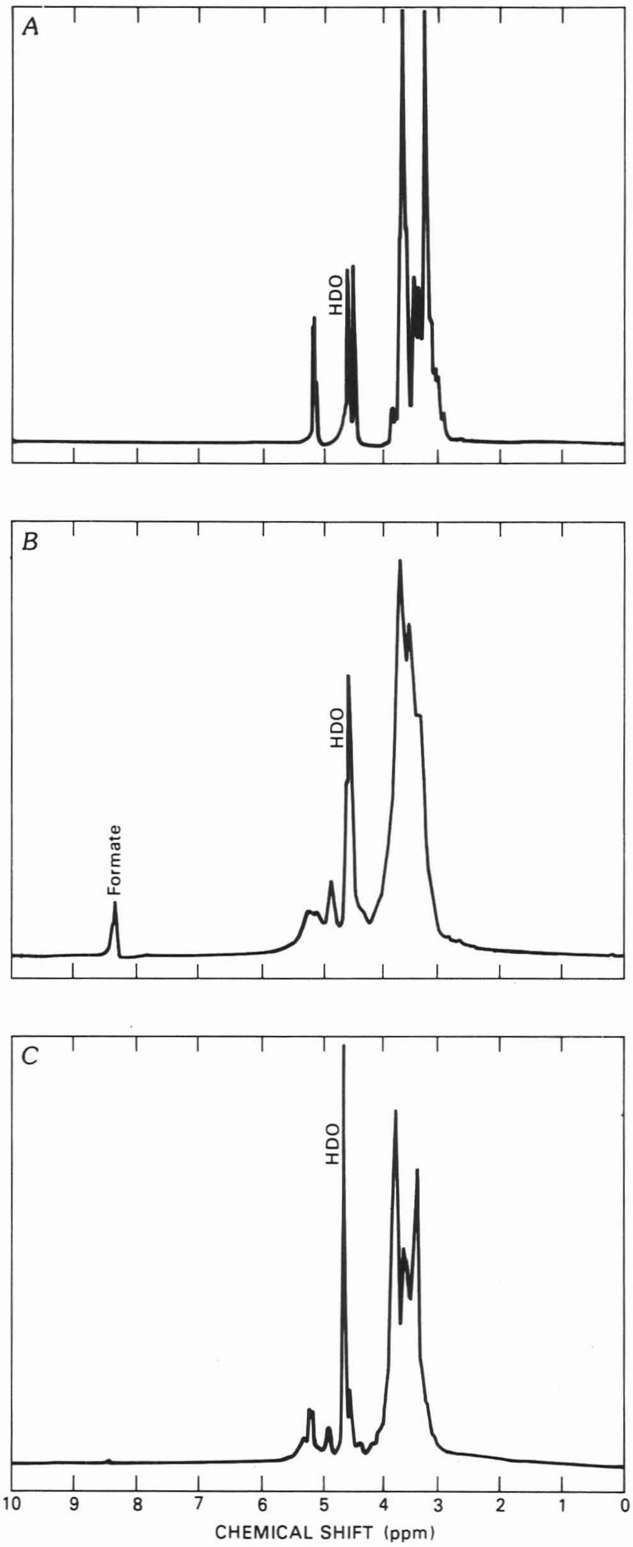

Figure 6. Proton NMR spectra of glucose recovered from: (A) salt-free water, pyridine used during drying; (B) salt-free water, pyridine not used during drying; (C) water containing NaCl and Na_2SO_4, pyridine used during drying.

Recovery data for various water samples and hydrophilic acid concentrates are summarized in Table III. Organic-

Table II. Standard Recoveries

standard	concn, mg/L	salt matrix[a]	% carbon of isolate	% organic carbon recovery	remarks
3,4,5-trihydroxybenzoic acid	1000	NaCl, Na_2SO_4, Na_2SiO_3	35.0	59.1	used HF to remove silicic acid, did not wash salts (steps 9–14, Fig. 1)
galacturonic acid	1000	NaCl, Na_2SO_4, Na_2SiO_3	30.3	80.6	used HF to remove silicic acid
glucose	1000	NaCl, Na_2SO_4, Na_2SiO_3	27.8	87.8	used HF to remove silicic acid; sample acid damaged
glucose	1000	NaCl	29.4	82.2	recovered as precipitate (step 20, Fig. 1)
glucose	40000	none	37.0	94.0	recovered as precipitate (step 20, Fig. 1); used pyridine to prevent acid damage
glucose	6000	NaCl	35.3	121	recovered as precipitate (step 20, Fig. 1); used pyridine to prevent acid damage; formate not completely removed, resulting in recovery of more than 100%
glucose	3000	NaCl, Na_2SO_4	35.9	92.1	recovered as precipitate (step 20, Fig. 1); used pyridine to prevent acid damage

[a] Salt concentrations same as Big Soda Lake water.

Table III. Sample Recoveries

sample	dissolved solids, mg/L	dissolved organic carbon, mg/L	% carbon of isolates	% organic carbon recovery	remarks
Big Soda Lake, sampled at depth of 5 m	25 000	22	supernatant fraction, 9.09; precipitate fraction, 38.7.	61 24	phosphate not removed
Big Soda Lake, sampled at depth of 40 m	87 600	65	supernatant fraction, 9.19; precipitate fraction, 16.8.	43 29	phosphate not removed
Hidden Lake Creek, hydrophilic acid concentrate	ND	185	supernatant fraction, 35.1; precipitate fraction, 38.0.	60 20	phosphate and borate not removed
Okefenokee Swamp, hydrophilic acid concentrate	ND	4,399	supernatant fraction 23.7; precipitate fraction, 40.0	71 16	phosphate and borate not removed
Sagavanirktok River, hydrophilic acid concentrate	ND	101	supernatant fraction, 33.3; precipitate fraction, 25.2	75 14	phosphate and borate not removed
Spirit Lake, hydrophilic acid concentrate	ND	64	supernatant fraction, 34.1; precipitate fraction, 29.3	71 30	phosphate and borate not removed
Williams Fork Reservoir, hydrophilic acid	ND	752	supernatant fraction, 32.7; precipitate fraction, 42.7	56 25	phosphate and borate not removed

carbon recoveries vary between 72% and 101%. Phosphate was not removed from the Big Soda Lake sample, because it did not interfere in proton NMR analysis of the isolate; phosphate and borate were not removed from the remaining samples because phosphate and borate contents were not detected in the isolates by infrared spectral analysis. For every sample, the quantity of organic solutes that precipitated (step 20, Figure 1) was much greater than that which remained in solution in the supernatant fraction.

Examination of the recovery data of Tables II and III, coupled with experience obtained in performing the isolation procedure, indicated that the major source of organic solute loss occurred with the various salts and precipitates. Organic solute recoveries invariably increased when the number of the various salt- and precipitate-washing cycles was increased, which indicates that most of the loss was a nonselective loss of solute. Results presented in Tables II and III represent one salt-washing cycle in steps 5 and 10 of Figure 1.

A proton NMR spectrum for the precipitate fraction isolated from the 5-m level of Big Soda Lake is shown in Figure 7 and a proton NMR spectrum for the supernatant fractions isolated from the 5-m level of Big Soda Lake is shown in Figure 8. The large peak at 2.5 ppm in Figure 8 tentatively has been identified by independent liquid chromatographic analysis as dimethyl sulfoxide. Lake water was injected into a C-18 bonded silica column with a 90/10 water–methanol mobile phase and the detector set at 210 nm; the major peak found in the lake water chromatogram exactly corresponded in retention time to dimethyl sulfoxide standard in a synthetic solution of Big Soda Lake water. Bacteria in the lower anoxic layer in the lake are known to produce methyl sulfide; thus dimethyl sulfoxide may be an oxidation product of methyl sulfide in the upper oxic layer.

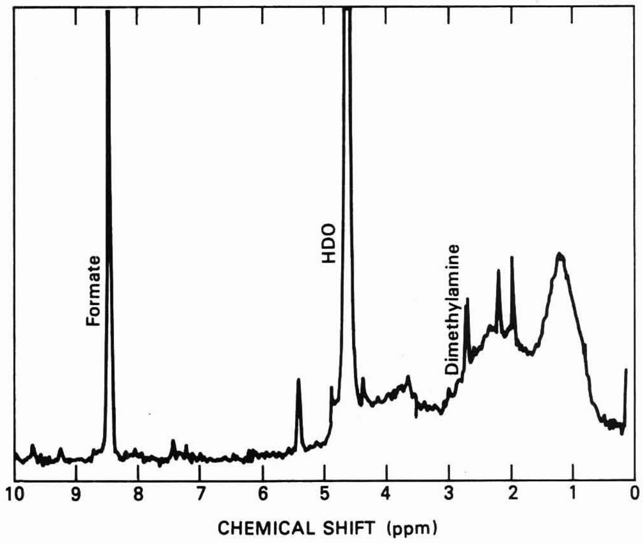

Figure 7. Proton NMR spectrum of precipitate fraction, Big Soda Lake, 5-m depth.

Elemental analyses of the Sagavanirktok River and Hidden Lake Creek samples are summarized in Table IV. Ash values are large in all samples, because elemental analyses were

Table IV. Elemental Analysis (%) of Hydrophilic Acid Isolates

sample	Hidden Lake Creek, supernatant fraction	Sagavanirktok River, supernatant fraction	Hidden Lake Creek, precipitate fraction	Sagavanirktok River, precipitate fraction
carbon	38.03	25.19	35.07	33.33
hydrogen	3.74	2.52	2.74	2.30
oxygen	36.65	44.50	34.17	36.25
nitrogen	2.08	4.05	1.88	1.82
sulfur	0.24	<0.01	0.40	1.28
sodium	15.57	20.51	18.32	19.20
chloride	2.69	2.69	6.34	5.11
ash	28.54	51.30	26.32	35.60
% ash as Na_2O + NaCl	77	58	113	84

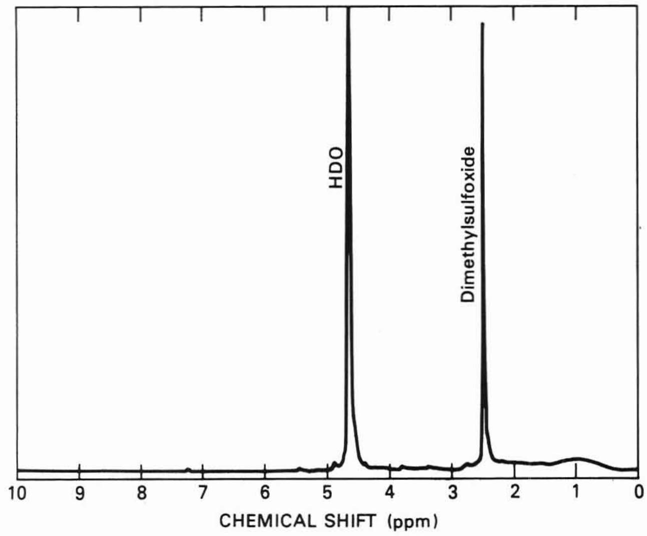

Figure 8. Proton NMR spectrum of supernatant fraction, Big Soda Lake, 5-m depth.

performed on the sodium salt form of the acids. All values sum to greater than 100%, because oxygen also is included in the ash as sodium oxide. The large nitrogen content in the polycarboxylic acid isolate from the Sagavanirktok River supports the evidence from the proton NMR of Figure 5 that this isolate was contaminated with dimethylamine rising from the hydrolysis of DMF. The small content for sulfur indicates that sulfate salts were removed efficiently by the isolation procedure. Sulfate, borate, and phosphate were not detected in the infrared spectra of the isolates, and the nature of the ash not accounted for as sodium oxide or sodium chloride is unknown.

CONCLUSION

Zeotrophic distillation of water from acidified DMF provides a unique method for concentration, desalting, and ultimate isolation of hydrophilic organic solutes from water. This isolation procedure also can be used as a general method for the isolation of nonvolatile DOC in water, and it is not subject to selectivity constraints encountered with isolation procedures based on solvent extraction, adsorption, or precipitation.

The applicability of the method has been demonstrated for a saline alkaline lake and for a variety of organic plus inorganic anion concentrates from a few freshwaters. The limited applications of the method to the few waters presented in this report should caution potential users against blind application of the method without careful assays of isolates for reagent contaminants and inorganic constituents. Potential applications of this isolation method include isolation of organic solutes from seawater concentrates obtainable from desalting plants, isolation of organic solutes from physiological fluids such as urine and blood, and isolation of organic solutes from various wastewaters.

Registry No. DMF, 68-12-2; C, 7440-44-0; H_2O, 7732-18-5; 3,4,5-trihydroxybenzoic acid, 149-91-7; galacturonic acid, 14982-50-4; glucose, 50-99-7.

LITERATURE CITED

(1) Christman, R. F., Hrutfiord, B. F. *Proc.—Water Qual. Conf.* **1973**, *15*, 58–72.
(2) Leenheer, J. A. *Water* Analysis, *Vol. III*; Minear, R. A., Keith, L. H., Eds.; Academic: Orlando, FL, 1984; Chapter 3.
(3) Burnham, A. K.; Calder, G. V.; Fritz, J. S.; Junk, G. A.; Svec, H. J.; Willis, R. *Anal. Chem.* **1972**, *44*, 139–142.
(4) Mantoura, R. F. C.; Riley, J. P. *Anal. Chim. Acta* **1975**, *76*, 97–106.
(5) Thurman, E. M.; Malcolm, R. L. *U.S. Geol. Surv. Water-Supply Pap.* **1979**, *No. 1817-G*, 16 p.
(6) Leenheer, J. A. *Environ. Sci. Technol.* **1981**, *15*, 578–587.
(7) Thurman, E. M.; Malcolm, R. L.; Aiken, G. R. *Anal. Chem.* **1978**, *50*, 775–779.
(8) Pietrzyk, D. J.; Kroeff, E. P.; Rotsch, T. D. *Anal. Chem.* **1978**, *50*, 497–502.
(9) Thurman, E. M. *Organic Geochemistry of Natural Waters*; Nijhoff/Junk Publishers: Boston, MA, 1985; p 105.
(10) Weber, J. H.; Wilson, S. A. *Water Res.* **1975**, *9*, 1079–1084.
(11) Dienzer, M.; Melton, R.; Mitchell, D. *Water Res.* **1975**, *9*, 799–805.
(12) Chian, E. S. K.; De Walle, F. B. *Environ. Sci. Technol.* **1977**, *11*, 158–163.
(13) Gjessing, E. T. *Nature* (*London*) **1965**, *208*, 1091–1092.
(14) Jeffrey, L. M.; Hood, D. W. *J. Mar. Res.* **1958**, *17*, 247–271.
(15) Robinson, T. *The Organic Constituents of Higher Plants*, 4th ed.; Cordus Press: North Amhurst, MA, 1980; pp 46–49.
(16) Means, J. C.; Wijayaratne, R. D. *Bull. Mar. Sci.* **1984**, *35*, 449–461.
(17) Carlson, D. J.; Brann, M. L.; Mague, T. H.; Mayer, L. M. *Mar. Chem.* **1985**, *16*, 155–171.
(18) Kharaka, Y. K.; Robinson, S. W.; Law, L. M.; Carothers, W. W. *Geochim. Cosmochim. Acta* **1984**, *48*, 823–835.
(19) Hayes, M. H. B. *Humic Substances in Soil, Sediment, and Water*; Aiken, G. R., McKnight, D. M., Wershaw, R. L., MacCarthy, P., Eds.; Wiley-Interscience: New York, 1985; Chapter 13.
(20) Porter, L. K. *J. Agric. Food Chem.* **1967**, *15*, 807–811.
(21) Leenheer, J. A.; Noyes, T. I. *U.S. Geol. Surv. Water-Supply Pap.* **1984**, *No. 2230*, 16 p.
(22) Huffman, E. W. D., Jr.; Stuber, H. A. *Humic Substances in Soil, Sediment, and Water*; Aiken, G. R., McKnight, D. M., Wershaw, R. L., MacCarthy, P., Eds.; Wiley-Interscience: New York, 1985; Chapter 17.
(23) *Annu. Book ASTM Stand.* **1977**, Part 31, Method D, 512–67, 286–291.
(24) *Handbook of Chemistry and Physics*, 62nd ed.; Weast, R. C., Astle, M. J., Eds.; CRC Press: Boca Raton, FL, 1981; B-150.
(25) Inscoe, M. N.; King, G. S.; Blau, K. *Handbook of Derivatives for Chromatography*; Blau, K., King, G. S., Eds.; Heyden: London, 1978; Chapter 8, p 330.
(26) Thompson, J. A.; Markey, S. P. *Anal. Chem.* **1975**, *47*, 1313–1320.

RECEIVED for review May 2, 1986. Resubmitted October 24, 1986. Accepted February 9, 1987. The use of trade names is for descriptive purposes and does not constitute endorsement by the U.S. Geological Survey.

Anal. Chem. **1987**, *59*, 1320–1326

Synthesis of Dabsylhydrazine and Its Use in the Chromatographic Determination of Monosaccharides by Thin-Layer and High-Performance Liquid Chromatography

Jen-Kun Lin* and Shan-Shou Wu

Institute of Biochemistry, College of Medicine, National Taiwan University, Taipei, Taiwan, Republic of China

The chromophoric reagent dabsylhydrazine is synthesized from the reaction of dabsyl chloride with hydrazine. Dabsylhydrazine reacts readily with various monosaccharides including glucose, galactose, mannose, xylose, arabinose, ribose, deoxyribose, and glyceraldehyde to form corresponding dabsylhydrazones with strong absorbance at 425 nm. The application of this new reagent in the thin-layer chromatographic and high-performance liquid chromatographic analysis of monosaccharides is described. By use of a Nova-PAK C_{18} reverse-phase column and a concave gradient system of water and acetonitrile as eluent, detection limits in the range of 10 pmol (2 ng) have been reached. The optimum pH for the formation of monosaccharide dabsylhydrazones is around 2–3. The rate of hydrazone formation is different among the monosaccharides investigated. Generally, pentoses reacted more rapidly than hexoses. The present method has been successfully applied for the determination of glucose concentrations in human serum and various fruit juices. The contents of galactose and mannose released from serum glycoprotein on acid hydrolysis have been rapidly determined by the newly developed dabsylhydrazone method.

Monosaccharides are ubiquitous in the biosphere. Qualitative and quantitative analyses of these carbohydrates in biological specimens have become an exciting challenging subject for many biochemists. Recently, several new methods have been developed for the analysis of saccharides. Gas–liquid chromatographic methods have been improved for easier detection and higher sensitivity (*1*). High-performance liquid chromatography (HPLC) on anion-exchange resins (*2, 3*) or bonded-phase silica columns (*4–6*) reduce sample preparation and give great flexibility. However, the sensitivities of refractive index and ultraviolet absorbance monitors are quite low for simple sugars. A previous procedure employed dansylhydrazine to label the reducing end of sugar with a fluorescent tag (*7*) for the determination of these monosaccharides as their dansylhydrazones by HPLC was developed (*8*). The somewhat instability of fluorophore emitted from dansyl derivatives hampered the accuracy and reproducibility of this method. It is apparent that a stable and chromophoric labeling reagent for sugar analysis is urgently needed.

In 1975, dabsyl chloride was first synthesized in this laboratory (*9*). During the last 10 years, in combination with HPLC this newly developed chromophoric reagent has been demonstrated to be very promising for the microdetermination of amino acids (*10–13*), aliphatic amines (*14, 15*), and polyamines (*16, 17*). Recently, dabsylhydrazine was synthesized from the reaction of dabsyl chloride with hydrazine. This new compound reacted readily with monosaccharides and gave corresponding chromophoric dabsylhydrazones. Herein is described a new procedure for the separation and quantitation of monosaccharide dabsylhydrazones by both thin-layer chromatography (TLC) and HPLC procedures.

EXPERIMENTAL SECTION

Instrumentation. Electronic spectra were recorded on a Shimadzu UV-200S double-beam spectrophotometer. IR spectra were measured in a Perkin-Elmer 983 IR spectrophotometer using a pressed pellet consisting of 1 mg of sample and 200 mg of KBr. NMR spectra were taken in a NMR spectrophotometer, JEOL, FX-100, Japan Electronic, ltd., Tokyo, and mass spectra were studied in a Finnigan 4510 quadrupole mass spectrometer, Palo Alto, CA.

HPLC separations were performed on a Waters Associates instrument with a two-pump Model 6000 solvent delivery system, a Model U6K manual injector, a Model 450 absorbance monitor at 425 nm, and a Model 660 solvent programmer. The recorder was a OmniScribe strip chart recorder, Model B 5000 (Houston Instruments, Austin, TX). The HPLC was performed on a Waters Associates Nova-PAK C_{18} (3.9 mm × 15 cm), 4-μm, or μBondapak C_{18} (4 mm × 30 cm), 10-μm, reverse-phase column. A concave gradient elution program (curve 7 or 8) was used: solvent A, water–acetonitrile (78:22 (v/v)); solvent B, acetonitrile (10–85%, 45 min or 15–85%, 45 min). A flow rate of 1.2 mL and an AUFS (absorbance unit at full scale) of 0.02–0.04 were normally employed.

TLC analysis on silica gel plates (E. Merck, Silica Gel 60 F254, catalog no. 5554) was performed in a rectangular or cylindrical glass chamber covered with a glass plate. The inner side of the chamber contained Whatman No. 1 filter paper to prompt and ensure the saturation of solvent vapor in the chamber. The following solvent systems were normally used: A, 1-butanol (water saturated)–triethylamine (30:1 v/v)); B, acetonitrile–1-butanol–hexane (20:2:1 (v/v)); C, acetonitrile–benzene–ethyl acetate (15:15:1 (v/v)); D, acetonitrile–1-butanol–ethyl acetate (20:2:1 (v/v)); and E, benzene–chloroform–ethanol (15:15:10 (v/v)).

Chemicals. D-Glucose, D-galactose, D-mannose, D-fructose, D-arabinose, D-xylose, D-ribose, D-deoxyribose, and D-glycerose (D-glyceraldehyde) were purchased from Sigma Chemical Co. (St. Louis, MO). Hydrazine hydrate, ammonia, hydrochloric acid, tetrahydrofuran, and acetonitrile were purchased from E. Merck Co. (Darmstadt, Germany). Dabsyl chloride (4-[[4-(dimethylamino)phenyl]azo]benzenesulfonyl chloride, mp 186–188 °C) was synthesized by reacting sodium 4-[[4-(dimethylamino)phenyl]azo]benzenesulfonate with phosphorus pentachloride (*9*) or by chlorosulfonation of [[(dimethylamino)phenyl]azo]benzene (*18*).

Synthesis of Dabsylhydrazine (Figure 1). Dabsyl chloride (100 mg) was dissolved in 25 mL of tetrahydrofuran and mixed with 0.2 mL of hydrazine hydrate. The resulted mixture was allowed to stand at room temperature for 30 min. After concentration, orange-yellow crude products (44 mg, yield 44.6%) were obtained. The crude products were further purified by recrystallizing with 30–40 mL of boiling ethanol to give orange crystals (30 mg), mp 163–164 °C. Anal. Calcd for $C_{14}H_{17}N_5O_2S$: C, 51.79; H, 5.07; N, 20.14. Found: C, 51.85; H, 5.06; N, 20.26.

Formation of Monosaccharide Dabsylhydrazones (Figure 1). A 1.0-mL sample containing 1–20 nmol of monosaccharide in ethanol containing 0.1% acetic acid is mixed with 1 mL of 0.1% dabsylhydrazine in ethanol. The mixture is heated at 60 °C for 60 min and then cooled to room temperature. The same procedure can also be performed with smaller samples (5–20 μL) of test solution, keeping the same proportions of reagents as described

0003-2700/87/0359-1320$01.50/0 © 1987 American Chemical Society

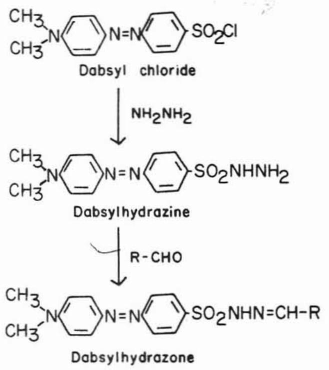

Figure 1. Synthesis of dabsylhydrazine and its reaction with a carbonyl compound.

above. A control tube containing no monosaccharide is used as a reference system to aid in the detection of dabsylhydrazine and its degradation products. The reagents have been stored for weeks in the dark at 4 °C with no loss of potency.

TLC of Monosaccharide Dabsylhydrazones. Samples of the reaction mixture (2–10 μL containing 2–10 pmol of monosaccharides) are applied to starting points of silica gel plates and then developed by the described TLC procedure. The monosaccharide dabsylhydrazones appear as bright yellow spots and dabsylhydrazine also appears as a yellow spot which is usually well separated from the hydrazones. All these yellow compounds appear as bright pink spots when the developed TLC plates were briefly exposed to hydrogen chloride vapor in a closing chamber. The sensitivity of monosaccharide detection was enhanced dramatically after this treatment. The yellow spots may be scraped off the plate into a conical centrifuge tube and the hydrazones are then eluted with ethanol for quantitative analysis.

HPLC of Monosaccharide Dabsylhydrazones. Samples of the reaction mixture obtained as described are passed through a Millipore filter (0.45 μm, HAWP catalog. no. 02500, Millipore Corp., Bedford, MA) and the filtrates (1–10 μL) were used directly for HPLC. For the separation of neutral sugars including glucose, galactose, mannose, xylose, arabinose, ribose, deoxyribose, and glycerose, a concave elution program was employed. The details of the chromatographic conditions are described in the instrumentation section.

HPLC Procedure for the Determination of Glucose in Grape Juice. The original juice of Californian green grapes (seedless, sweet) is obtained by gentle pressing. Four-tenth (0.4)-milliliter aliquots of the clear juice is placed in a vial and lyophilized to dryness. The residue is extracted with 2 mL of warm absolute ethanol (50 °C) and passed through a Millipore filter (0.45 μm). A 1-mL aliquot of the filtrate is taken and reacted with 1 mg of dabsylhydrazine in 1 mL of ethanol at 60 °C for 1 h. The reaction mixture is cooled to room temperature and passed through the Millipore filter. One- to ten-microliter aliquots of the filtrates were used for HPLC. A glucose standard solution (0.1 mg/mL) in ethanol is run simultaneously and used as control.

Other fruit juices such as pineapple, pear, watermelon, banana, and plum were obtained by homogenization and analyzed by the same procedure.

HPLC Procedure for the Determination of Glucose in Human Serum. Human serum (0.2 mL) is deproteinized by homogenizing with 5 mL of absolute ethanol. The mixture is allowed to stand at room temperature for 30 min and then passed through a Millipore filter (0.45 μm). A 1-mL aliquot of the filtrate is mixed with 5 mL of absolute ethanol and again passed through a Millipore filter. A 1-mL aliquot of the filtrate is reacted with 1 mg of dabsylhydrazine in 1 mL of ethanol at 60 °C for 1 h. The reaction is remarkably accelerated when 0.1% of acetic acid is added to the reaction mixture. The reaction mixture is brought to room temperature and passed through a Millipore filter. Finally, 1–5-μL aliquots of the filtrate are taken for HPLC. Authentic glucose (0.1–1 mg/mL) solution in ethanol is reacted with dabsylhydrazine in a similar way and used as standard for HPLC determination.

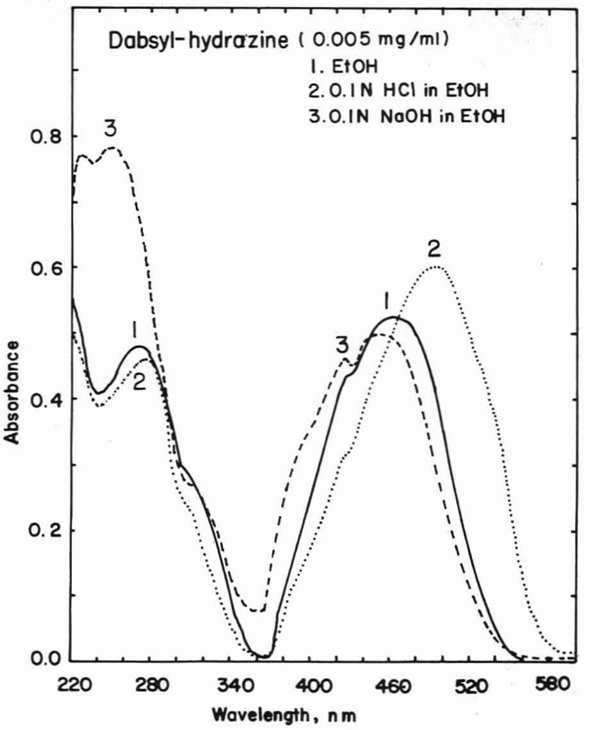

Figure 2. Electronic spectra of dabsylhydrazine.

Table I. Molar Absorptivities of Dabsylhydrazine and Its Glucose Derivative

	dabsylhydrazine		glucosedabsylhydrazone	
solvent	absorption max, nm	molar absorptivity ($\times 10^{-4}$)	absorption max, nm	molar absorptivity ($\times 10^{-4}$)
ethanol	463	3.3	460	5.4
	425	2.7	440	5.3
	272	3.0	422	5.0
	220	3.5		
0.1 N HCl in ethanol	494	3.8	495	5.1
	425	2.9	425	2.7
	275	2.9		
	220	3.0		
0.1 N NaOH in ethanol	452	3.1	445	3.8
	425	2.0	424	3.9
	250	4.9		
	229	4.8		

HPLC Procedure for the Determination of Galactose and Mannose in Serum Glycoprotein. Serum glycoproteins are isolated by the procedure of Mrochek et al. (*2*) with some modifications. Human serum (0.05 mL) is thoroughly mixed with 0.55 mL of 95% ethanol in an Eppendorf tube. After centrifugation at 5000 rpm for 15 min, the precipitate in the bottom of the tube is washed with 0.6 mL of ethanol and dissolved in 0.1 mL of 0.1 N NaOH. The resulting solution is mixed with 0.2 mL of doubly distilled water and 30 μL of concentrated hydrochloric acid (approximately 12 N). The mixture is deaerated with nitrogen for 5 min and sealed tightly with a septum-sealed cap. The hydrolysis is carried out at 100 °C in an electric oven for 4 h; 0.1 mL of the hydrolysate is removed and freeze-dried. The residue is reacted with 1 mg of dabsylhydrazine in 1 mL of ethanol at 60 °C for 1 h. The reaction mixture is brought to room temperature and passed through a Millipore filter (0.45 μm, HAWP). Finally, 1-μL aliquots of the filtrate are taken for HPLC analysis.

RESULTS AND DISCUSSION

Characterization of Dabsylhydrazine. Dabsylhydrazine was synthesized as described in the Experimental Section. The new compound was fully characterized by its elemental analysis, IR, UV, visible (Figure 2), NMR, and mass spectra.

Table II. TLC Data of Dabsylhydrazones Derived from Monosaccharides

monosaccharide	R_f[a]				
	A	B	C	D	E
dabsylhydrazine	0.88	0.92	0.90	0.83	0.80
glucose	0.64	0.52	0.09	0.51	0.59
galactose	0.56	0.42	0.09	0.42	0.50
mannose	0.64	0.39	0.09	0.42	0.52
fructose	0.48	0.77, 0.71	0.19, 0.10	0.81, 0.73	0.70
ribose	0.63	0.80	0.59	0.78	0.75
deoxyribose	0.60	0.80	0.55	0.78	0.75
xylose	0.69	0.75	0.42	0.75	0.72
arabinose	0.50	0.68	0.35	0.68	0.65
glyceraldehyde	0.52	0.92	0.56	0.88	0.47

[a] Solvent systems: A, 1-butanol (water saturated)–triethylamine (30:1 (v/v)); B, acetonitrile–1-butanol–hexane (20:2:1, (v/v)); C, acetonitrile–benzene–ethyl acetate (15:15:1 (v/v)); D, acetonitrile–1-butanol–ethyl acetate (20:2:1 (v/v)); E, benzene–chloroform–ethanol (15:15:10 (v/v)). The R_f values are the averages of three determinations.

The molar absorptivities of dabsylhydrazine and its glucose derivative in neutral, acidic, and alkaline media are given in Table I.

Dabsylhydrazine showed a typical azo dye peak at 463 nm which was shifted to a longer wavelength, 494 nm, in acidic medium. A similar shift was also observed in its glucosehydrazone derivatives. IR spectra (KBr pellet, cm^{-1}): 3350 ($-NH_2$), 3220 ($-SO_2-NH-$), 1602 ($-N{=}N-$), 1515, 1420, 1361, 1334, 1162, 1134 ($-SO_2-NH-$), 849, 821, and 600. NMR spectra ($CdCl_3$, Me_4Si as internal reference, ppm): 3.08 (singlet, ^6H, $-N(CH_3)_2$), 3.62 (doublet, ^2H, $-NH_2$), 5.56 (triplet, ^1H, $-NH-$), 6.72 (quadruplet, ^2H, two aromatic hydrogens ortho to the dimethylamino group), 7.86 (quadruplet, ^2H, two aromatic hydrogens meta to the dimethylamino group), and 7.92 (singlet, ^4H, four aromatic hydrogens on the benzene ring linked to the sulfonamide group). Mass spectra (*m/e*, relative intensity, %): 319 (4, molecular ion, M^+), 304 (0.3, $M - CH_3$), 303 (0.2, $M - NH_2$), 224 (3, $M - SO_2NHNH_2$), 136 (100), and 150 (56).

On the basis of these spectrometric features, the structure of dabsylhydrazine was characterized as 4-[[4-(dimethylamino)phenyl]azo]benzenesulfonylhydrazine as depicted in Figure 1.

Reaction of Dabsylhydrazine with Monosaccharides. Monosaccharides were readily reacted with dabsylhydrazine. Formation of the dabsylhydrazones of individual monosaccharides or their mixtures was found to be proportional to their initial concentrations (Figure 6). The rate of hydrazone formation at less acidic solutions was appreciably slower. Hydrazone formation was found to be complete within less than 60 min when the system was heated up to 60 °C. The sugar dabsylhydrazones were quite stable in the acidic solution and could be chromophorically analyzed by HPLC and TLC.

Many reducing sugars such as glucose, galactose, mannose, arabinose, xylose, ribose, deoxyribose, and glycerose yielded hydrazones with different mobilities on silica gel plates. The rates and yields of hydrazones formed with free hexoses were similar to that observed for glucose. Glycerose and pentoses including xylose, arabinose, ribose, and deoxyribose reacted very rapidly with dabsylhydrazine and yielded high levels of hydrazones under the conditions described. Prolonged heating or even standing at room temperature seemed to increase the yields of hydrazones. It was noted that if hydrazone formation was conducted at pH 4 or higher, ketose (fructose) interacted very slowly with dabsylhydrazine. The reaction of fructose was promoted by lowering the pH to 2 with 0.1 M trichloroacetic acid.

Preparation and Purification of D-Glucosedabsylhydrazone. L-Glucose (0.5 mg) in 1 mL of ethanol was mixed with 0.5 mg of dabsylhydrazine in 1 mL of ethanol and 0.01 mL of acetic acid. The mixture was heated at 60 °C for 1 h. The D-glucosedabsylhydrazone thus formed was isolated by TLC on a silica gel plate (0.2 mm, E. Merck, catalog no. 5554) with a solvent mixture of hexane–1-butanol–acetic acid (50:50:1 (v/v)). Two major spots, $R_f = 0.49$ (hydrazone) and $R_f = 0.60$ (dabsylhydrazine) were obtained. The hydrazone spots were scraped off the plate into a standard conical centrifuge tube and eluted with ethanol. After removal of the solvent, an orange-yellow crystalline powders of D-glucosedabsylhydrazone (mp 308–309 °C) was obtained. The hydrazone gave the following spectrometric properties. IR spectra (KBr pellet, cm^{-1}): 3600–3300 (OH group of sugar), 3000–2900 ($=N-NH-$), 1600–1500 ($-N{=}N-$), and 1415 ($-SO_2-NH-$). Mass spectra did not show up the molecular ion 481 (M^+) but gave a significant peak at 466 $(M - CH_3)^{+}$. The electronic spectra of the product were analyzed and are summarized in Table I. With these spectrometric features, the product was tentatively identified as D-glucosedabsylhydrazone.

TLC Separation of Monosaccharide Dabsylhydrazones. The monosaccharide dabsylhydrazones were prepared from the reaction of individual sugar with dabsylhydrazine as described. A sample of the reaction mixture (2–10 μL containing 0.5–100 nmol of sugar) was applied to starting points on silica gel plates and then developed by the standard TLC procedure as described in the Experimental Section. The R_f values of these monosaccharide dabsylhydrazones are summarized in Table II. The chromophoric properties of these hydrazones provided a reliable marker for rapid detection of these monosaccharides on TLC plate. The lowest limit of visual detection of the chromophoric spot on the plate was found to be in the range of 0.1–1.0 nmol of glucosedabsylhydrazone.

HPLC Separation of Monosaccharide Hydrazones. Monosaccharides were readily labeled with dabsylhydrazine by the described derivation procedure. The monosaccharide dabsylhydrazones were found to be stable for at least 6 days at 4 °C (Table III). The C_{18} reverse-phase column (Nova-PAK C_{18}) with a gradient water–acetonitrile mobile phase (solvent A, water–acetonitrile (78:22 (v/v)); solvent B, acetonitrile, curve 7, 15–85%, 45 min) gave sharp peaks for the neutral monosaccharides commonly found in the biosphere (Figure 3). All peaks were sufficiently resolved to permit quantitative estimation. With organic solvents such as methanol, ethanol, tetrahydrofuran, acetone, and ethyl acetate, either alone or in combination, the selectivity or resolution power was much less than that for acetonitrile alone. The following reverse-phase columns were tested: Nova-PAK C_{18}, 4 μm, 3.9 mm × 15 cm; μBondapak C_{18}, 10 μm, 4 mm × 30 cm; Zorbax ODS, 5 μm, 4.6 mm × 25 cm; MN Nucleosil $_{10}C_{18}$, 10 μm, 4 mm × 25 cm. Better resolution was obtained with

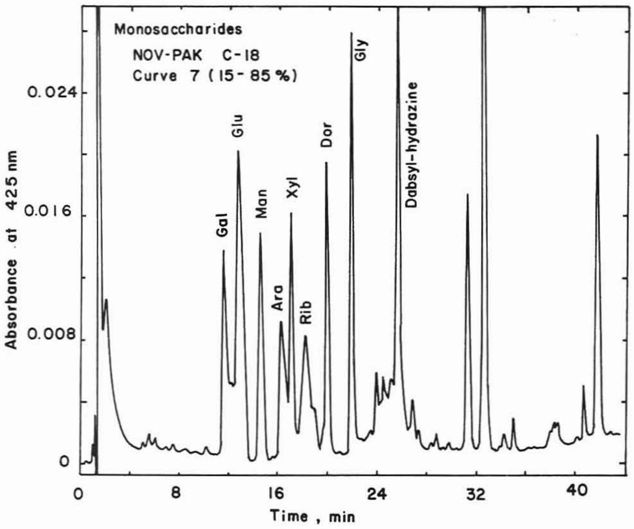

Figure 3. HPLC separation of monosaccharide dabsylhydrazones: chromatographic conditions, Nova-PAK C_{18} reverse-phase column; mobile phase, concave elution program, curve 7, solvent A water–acetonitrile (78:22 (v/v)), solvent B acetonitrile (15–85%, 45 min); flow rate, 1.2 mL/min; AUFS, 0.04. The abbreviations and concentrations (pmol) of monosaccharides are as follows: Glu, glucose (102); Gal, galactose (68); Man, mannose (48); Ara, arabinose (41); Xyl, xylose (33); Rib, ribose (82); Dor, deoxyribose (28) and Gly, glycerose (41).

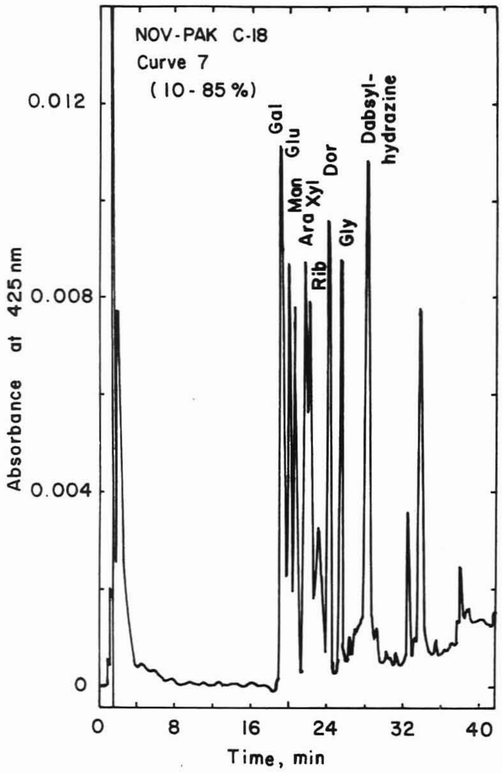

Figure 4. Rapid concave gradient elution of monosaccharide dabsylhydrazones. Chromatographic conditions and abbreviations are as described in Figure 3, except that solvent B is acetonitrile (10–85%, 45 min) and the concentrations of monosaccharides (pmol) are as follows: Glu, 37; Gal, 48; Man, 44; Xyl, 35; Ara, 66; Rib, 66; Dor, 29 and Gly, 12.

Table III. Stability of Dabsylhydrazones Derived from Monosaccharides

storage period, day	absorbance of dabsylhydrazone at 425 nm[a]		
	glucose	galactose	mannose
1	0.0150	0.0128	0.0410
2	0.0144	0.0130	0.0402
3	0.0146	0.0131	0.0420
5	0.0144	0.0128	0.0396
7	0.0141	0.0122	0.0400
8	0.0138	0.0122	0.0380

[a] An ethanolic solution (1 mL) containing 16 nmol of glucose, galactose, or mannose was reacted with 1 mg of dabsylhydrazine in 1 mL of ethanol at 60 °C for 60 min and the resulting hydrazone solutions were incubated at 4 °C for the indicated intervals. At each interval, 20-μL aliquots were removed and the absorbances of dabsylhydrazones at 425 nm were determined by HPLC as described in the Experimental Section.

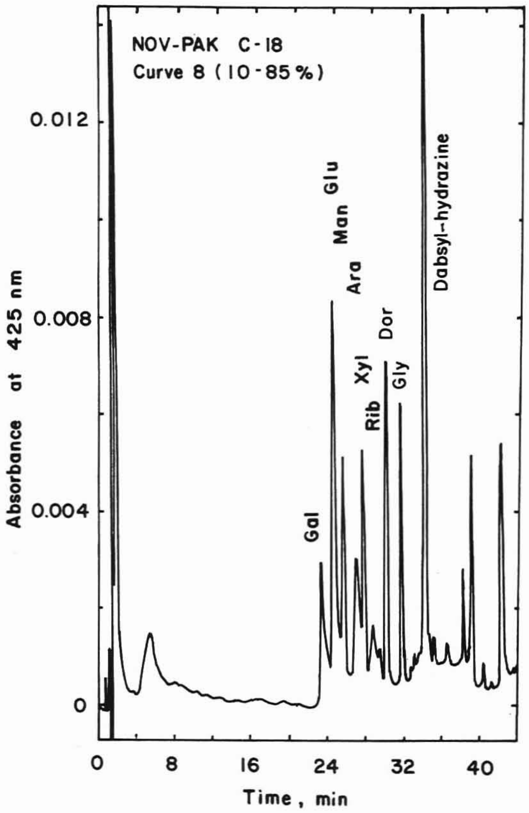

Figure 5. Slow concave gradient elution of monosaccharide dabsylhydrazones. Chromatographic conditions and abbreviations are as described in Figure 3 except that the elution program is set at curve 8, solvent B is acetonitrile (10–85%, 45 min), and the concentrations of monosaccharides (pmol) are as follows: Glu, 50; Gal, 20; Man, 30; Xyl, 35; Ara, 20; Rib, 60; Dor, 20; Gly, 15.

the Nova-PAK C_{18} column under these experimental conditions.

Several isocratic elution systems prepared from various combinations of acetonitrile and water were evaluated; none was good enough to resolve all the monosaccharides tested. Gradient elution systems provided better separation of these sugars. It appeared that a concave gradient program (curve 7 or 8) gave better resolution as compared to the linear gradient program (curve 6). The rate of increment of acetonitrile in the mobile phase has a profound effect on the resolution of hydrazones. If the programmer is set at curve 7, the increment of acetonitrile is rather rapid and the first hydrazone (galactose) comes out earlier at 19 min (Figure 4). The chromatogram in Figure 4 was run with B ranging from 10 to 85%. If the programmer is set at curve 8, then the increment of acetonitrile is rather slow and the first hydrazone comes out later at 24 min (Figure 5). In the latter case, the resolution is remarkably improved.

Linearity and Sensitivity. Visible absorbance detection of monosaccharide dabsylhydrazones provided simplicity and reproducibility with good sensitivity. Mixtures containing various amounts of eight standard sugars were derived with

Table IV. Sensitivities of Recent Published Methods for Sugar Determinations

author	year	method	sensitivity	ref
Mawhinney et al.	1980	GLC, silylation	2 μg	1
Binder	1980	HPLC, UV, and RI	12 μg	6
Vratny et al.	1984	HPLC, UV	18 μg	*a*
Honda et al.	1981	automated analyzer, UV with 2-cyanoacetamide	5 nmol	20
Kesler	1967	anion exchange chromatography	1 μg	3
Mrochek et al.	1975	anion exchange chromatography, cerate oxidimetric	1 nmol	2
Verhaar and Kuster	1981	cation exchange chromatography	1 μg	19
Alpenfels	1981	HPLC with dansylhydrazine, UV 254 nm	1 nmol	8
Grimble et al.	1983	HPLC, postcolumn, cuprammonium	450 ng	*b*
Rabel et al.	1976	HPLC, normal-phase partition, RI	84 μg	5
Mopper and Johnson	1983	HPLC with dansylhydrazine, fluorescence detector	5–15 pmol	*c*
Rosenfelder et al.	1985	HPLC with 4′-(*N*,*N*-dimethylamino)-4-aminoazobenzene	5–80 pmol	22
Hull and Turco	1985	HPLC with dansylhydrazine, fluorescence detector	25–50 pmol	23
Lin and Wu	1986	HPLC, precolumn dabsylhydrazine, 425 nm	2 ng (10 pmol)	*d*

[a] Vratny, P.; Frein, R. W.; Brinkman, U. A. Th; Nielen, M. W. F. *J. Chromatogr.* **1984**, *275*, 355–366. [b] Grimble, G. K.; Barker, H. M.; Taylor, R. H. *Anal. Biochem.* **1983**, *128*, 422–428. [c] Mopper, K.; Johnson, L. *J. Chromatogr.* **1983**, 27–38. [d] Present work.

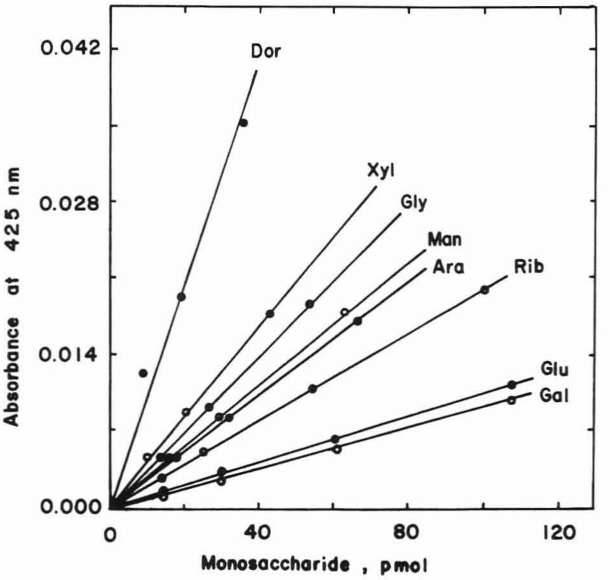

Figure 6. Dose-response curve of monosaccharide dabsylhydrazones. The abbreviations are as described in Figure 3. A mixture containing various concentrations of monosaccharides is reacted with dabsylhydrazine and the resulting hydrazones are determined by HPLC as described in the Experimental Section.

dabsylhydrazine. The HPLC data demonstrated the linear relationships between the absorbances and the concentrations of the individual monosaccharides (Figure 6). The varying responses as illustrated by different slopes of the regression lines may reflect varying equilibrium constants for the derivative reactions for the different sugars. However, the excellent fit and linearity indicate that this procedure is suitable for quantitative determination.

The pH of the reaction mixture was found to affect the rate of hydrazone formation. The optimum pH range for the reaction was around pH 2 as illustrated in Figure 7. It is worthy to note that the formation of glucosedabsylhydrazone at pH 2 is approximately 4 times higher than that at pH 7. The formations of ribose- and arabinosedabsylhydrazones are less affected by pH variation in the 3 to 6 range.

The absolute sensitivity of the method was measured by deriving 100 pmol of monosaccharides by the described procedure. One-tenth of the sample was injected, giving a peak height response within the linear range of dose–response curve and a signal-to-noise ratio of 10. Therefore, the minimum practical detection limit for glucose or other sugars is about 10 pmol (2 ng). This picomole detection limit for any sugar is comparable and even better than gas–liquid chromatographic methods (*1*). A comparison of detection sensitivity among the published methods for reducing sugars is given in Table IV. Several early methods developed before 1980 employed a refractive index (RI) monitor for sugar detection; the limit of detection was in the microgram range (*3, 5, 6, 19*). The sensitivity of detection was significantly improved by using the appropriate labeling reagent and detector (*8, 20–23*).

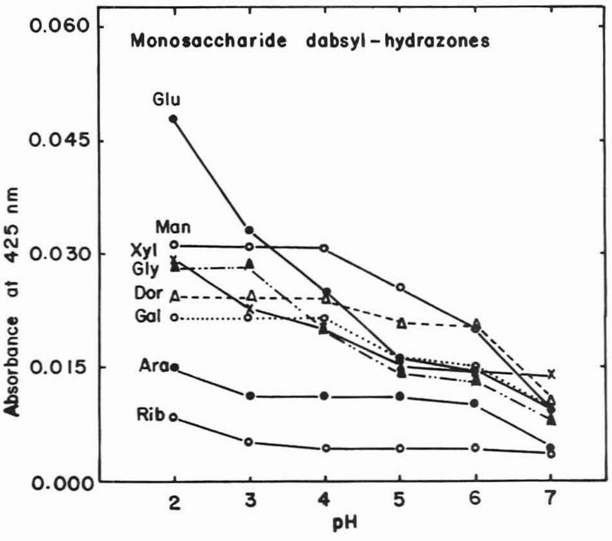

Figure 7. Effect of pH on the formation of monosaccharide dabsylhydrazones.

(Dimethylamino)-4-aminoazobenzene has been used to reductively aminate sugars and provide a chromophoric quantitative method at the 5 pmol level (*22*), but the method including amination and purification steps is rather tedious and time-consuming. In the present study, dabsylhydrazine was found to react readily with monosaccharides to form the highly chromophoric dabsylhydrazones, which were easily monitored spectrophotometrically at 425 nm and provided a straightforward method for sugar detection in the picomole range.

Precision and Recovery. The within-run precision of the assay was measured by processing aliquots of glucosedabsylhydrazone solution through the procedure during a single day. The coefficient of variation (CV) was 4.7% at 100 pmol per injection ($n = 6$). The percentage of analytical recovery of glucose spiked in grape juice samples (20 ng added to 0.2 mL of grape juice) was 97–102% ($n = 7$).

Determination of Glucose Content in Fruits and Human Serum. The aforementioned procedure was applied for the determination of glucose content in various fruit juices. The glucose concentrations of grape, pineapple, banana, pear, plum, and watermelon were found to be 5.7, 10.5, 10.9, 5.5,

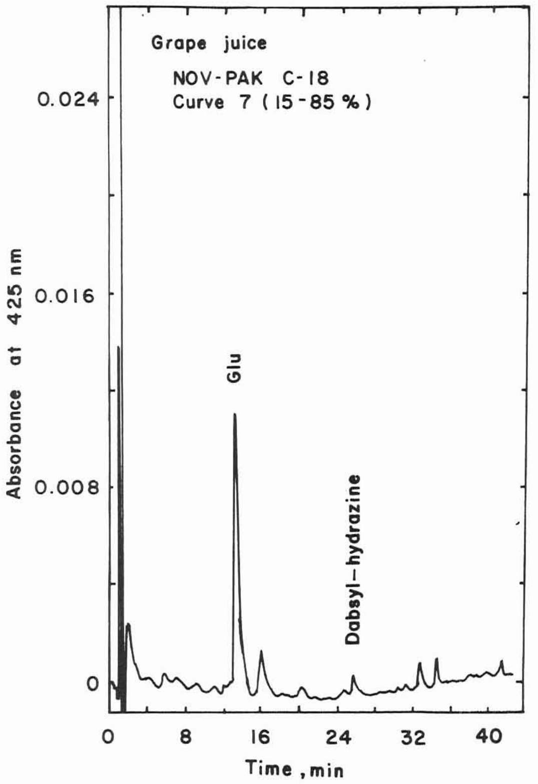

Figure 8. HPLC profile of glucosedabsylhydrazone in grape juice. The chromatographic conditions are as described in Figure 3.

Table V. Comparison of Present Method with Automated Analysis of Serum Glucose

serum sample	automated analysis,[a] mg/dL	present method,[b] mg/dL 1	present method,[b] mg/dL 2
1	94	87	88
2	109	107	106
3	151	141	134
4	256	250	256
5	314	319	315
6	419	407	406
7	343	339	334
8	174	177	166
9	345	321	332

[a] The autoanalysis was performed with Olympus AU-550 based on the glucose oxidase colorimetric method. [b] HPLC–dabsylhydrazine method, the determination was performed twice (1 and 2).

4.3 and 2.9 mg/g, respectively. A representative HPLC profile of grape juice was given in Figure 8. Glucosedabsylhydrazone was resolved as a single sharp peak under the experimental conditions.

The present procedure was also employed for the determination of glucose concentration in human serum. A typical chromatogram of glucose analysis in human serum is illustrated in Figure 9. Glucosedabsylhydrazone was separated completely from other serum components and estimated easily from its peak height. A comparative study on the present method and automated analysis in determining the glucose content of human sera was performed and the results are summarized in Table V. The correlation of the data obtained from these two methods is quite acceptable. It seems that the values obtained from the present method are somewhat lower than those obtained by automated analysis. The autoanalysis of serum glucose was performed with an Olympus AU-550 based on glucose oxidase reaction. It is conceivable that any serum inhibitor or activator of glucose oxidase will certainly affect the accuracy of the routine method. We believe that the present method is a straightforward procedure for glucose determination in various biological samples. The

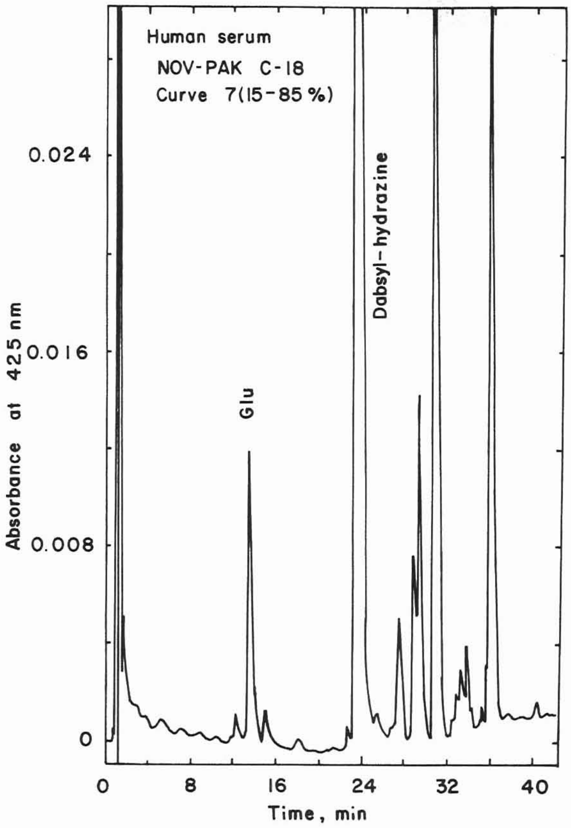

Figure 9. HPLC profile of glucosedabsylhydrazone in human serum. The chromatographic conditions are as described in Figure 3.

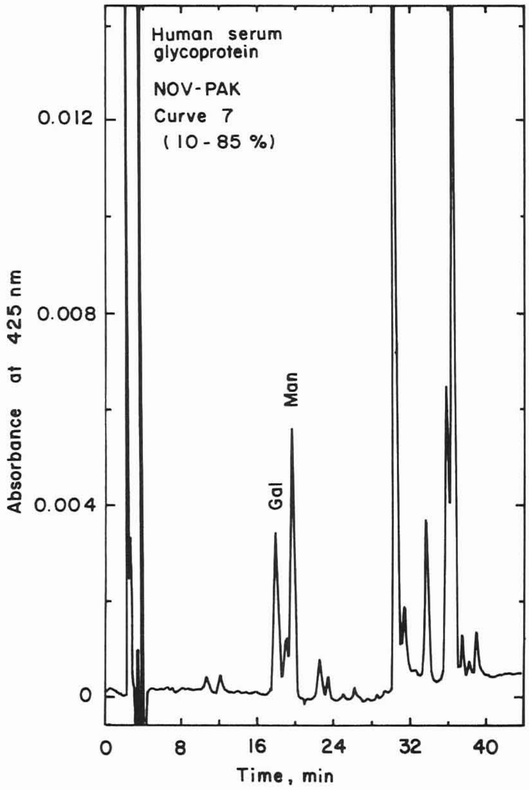

Figure 10. HPLC profiles of galactose- and mannosedabsylhydrazones from human serum glycoprotein. The chromatographic conditions are as described in Figure 4. The experimental procedures for the isolation and hydrolysis of serum glycoprotein are described in the Experimental Section.

HPLC separation and chromophoric detection will stay away from most visible and UV absorbing impurities that preexisted in the samples.

Galactose and Mannose Released from Human Serum Glycoprotein. The present procedure was also applied for the determination of monosaccharides released from serum glycoprotein on acid hydrolysis. A representative HPLC profile of serum glycoprotein hydrolysates is given in Figure 10. The contents of galactose and mannose in the serum glycoprotein were found to be 360 and 260 mg/L, respectively. A previous ion exchange chromatography method gave the values of 414 (range, 302–575) and 392 (range, 345–626) mg/L for galactose and mannose, respectively (*2*). It seems that both methods give the comparable values for the levels of these two monosaccharides in serum glycoprotein. The present HPLC analysis was accomplished in 40 min; whereas the previous method required 18–19 h. Furthermore, the dabsylhydrazone method used far less serum sample (0.05 mL instead of 0.5 mL in the previous method). Theoretically, the volume of serum sample could be reduced down to 0.005 mL if the final aliquot for HPLC analysis were increased from 1 to 10 μL. It is worthy to mention that several unknown peaks appeared on the HPLC chromatogram (Figure 10), further characterization of these unknown sugars derived from serum glycoprotein is in progress.

LITERATURE CITED

(1) Mawhinney, T. P.; Feather, M. S.; Barbero, G. J.; Martinez, J. R. *Anal. Biochem.* **1980**, *101*, 112–117.
(2) Mrochek, J. E.; Dinsmore, S. R.; Waalkes, T. P. *Clin. Chem.* (*Winston-Salem, N.C.*) **1975**, *21*, 1314–1322.
(3) Kesler, R. B. *Anal. Chem.* **1967**, *39*, 1416–1422.
(4) Linden, J. C.; Lawhead, C. L. *J. Chromatogr.* **1975**, *105*, 125–133.
(5) Rabel, F. M.; Caputo, A. G.; Butts, E. T. *J. Chromatogr.* **1976**, *126*, 731–740.
(6) Binder, H. *J. Chromatogr.* **1980**, *189*, 414–420.
(7) Avigad, G. *J. Chromatogr.* **1977**, *139*, 243–247.
(8) Alpenfels, W. F. *Anal. Biochem.* **1981**, *114*, 153–157.
(9) Lin, J. K.; Chang, J. Y. *Anal. Chem.* **1975**, *47*, 1634–1638.
(10) Lin, J. K.; Wang, C. H. *Clin. Chem.* (*Winston-Salem, N.C.*) **1980**, *26*, 579–583.
(11) Lin, J. K.; Liaw, K. Y. *J. Formosan Med. Assoc.* **1982**, *81*, 892–902.
(12) Lin, J. K. Separation of dabsyl amino acids, In *CRC Handbook of the Use of HPLC for the Separation of Amino Acids, Peptides and Proteins*; Hancock, W. S., Ed.; CRC Press: Boca Raton, FL, 1984; Vol. I, pp 359–366.
(13) Lin, J.-K.; Lin-Shiau, S. Y. *J. Chin. Biochem. Assoc.* **1983**, *12*(2), 47–60.
(14) Lin, J.-K.; Lai, C. C. *Anal. Chem.* **1980**, *52*, 630–635.
(15) Lin, J.-K. *Proc. Natl. Sci. Counc. Repub. China, Part B* **1986**, *10*(1), 20–34.
(16) Lin, J.-K.; Lai, C. C. *J. Chromatogr.* **1982**, *227*, 369–377.
(17) Lin, L. I.; Lin, J.-K. *J. Formosan Med. Assoc.* **1985**, *84*(5), 536–545.
(18) Lin, J.-K.; Chen, C. A.; Wang, C. H. *Proc. Natl. Sci. Counc., Repub. China, Part B* **1979**, *3*(2), 158–166.
(19) Verhaar, L. A. Th.; Kuster, B. F. M. *J. Chromatogr.* **1981**, *210*, 279–290.
(20) Honda, S.; Takahashi, M.; Nishimura, Y.; Kakehi, K.; Ganno, S. *Anal. Biochem.* **1981**, *118*, 162–167.
(21) Nordin, P. *Anal. Biochem.* **1983**, *131*, 292–498.
(22) Rosenfelder, G.; Mörgelin, M.; Chang, J. Y.; Schönenberger, C. A.; Braun, D. G.; Towbin, H. *Anal. Biochem.* **1985**, 156–165.
(23) Hull, S. R.; Turco, S. J. *Anal. Biochem.* **1985**, 143–149.

RECEIVED for review July 21, 1986. Resubmitted January 12, 1987. Accepted January 20, 1987. This study was supported by the National Science Council, NSC-75-0412-B002-14, Taipei, Taiwan, ROC, and by the Clinical Medical Research Center, Academia Sinica, ROC. The late stage of this study was also supported by the Department of Health (DOH 76-0402-38), ROC.

Comparison of Extraction Techniques for Munitions Residues in Soil

Thomas F. Jenkins*

U.S. Army Cold Regions Research and Engineering Laboratory, 72 Lyme Road, Hanover, New Hampshire 03755-1290

Clarence L. Grant

Department of Chemistry, University of New Hampshire, Durham, New Hampshire 03824

Extraction of trinitrotoluene (TNT), trinitrobenzene (TNB), hexahydrotrinitrotriazine (RDX), and octahydrotetranitrotetrazocine (HMX) from two soils was studied in terms of process kinetics and recovery. Two solvents, acetonitrile and methanol, and four extraction techniques, Soxhlet, ultrasonic bath, mechanical shaker, and homogenizer–sonicator, were compared. The results were complex in that several interactions were found among analyte, method, and solvent. Acetonitrile was superior to methanol for RDX and HMX from the perspectives of kinetics and recovery, due in part to a much higher solubility. The Soxhlet and ultrasonic bath generally recovered more than the homogenizer or shaker, although a complicating factor was that all techniques were not necessarily at equilibrium. In terms of sample throughput, the ultrasonic bath and shaker offer advantages over the Soxhlet and homogenizer–sonicator. The ultrasonic bath generally approached equilibrium more rapidly than the shaker, so it appears to be the best overall choice. A spike-recovery study using fortified soil and the sonic bath method yielded complete recoveries of TNT and RDX at 1.6 and 2.3 μg/g, respectively.

The Soxhlet extractor is probably the most widely used method for extraction of organic residues from soils and other solids. Solvents used have included methylene chloride (*1–8*), benzene (*1, 3, 6, 7, 9*), toluene (*1, 6*), chloroform (*1, 6, 10*), acetone/hexane (*1, 8, 11*), methanol (*2, 5, 6, 10*), acetone (*6, 12–14*), pyridine (*3, 6*), cyclohexane (*3, 6*), dimethyl sulfoxide (*3, 6*), dimethylformamide (*3, 6*), *N*-methylpyrollidone (*3*), petroleum ether (*13*), acetonitrile (*10, 14*), hexane (*5–7, 14*), diethyl ether (*5, 6*) and various other binary and ternary mixtures (*6, 7, 10, 14*). The Soxhlet procedure has been compared to methods based on equilibration with solvent using either shaking (*1, 10, 13*), an ultrasonic probe (*3, 4, 11, 12*), or an ultrasonic bath (*1, 2*). Depending on the analyte and matrix studied, the preferred solvent or method varies. In general, though, a relatively polar solvent or binary mixture containing a polar solvent is often recommended with either a Soxhlet or ultrasonic method.

Recently two methods were outlined for the determination of six polynitro compounds in soil (*15*) and furnace ash (*16*). The first method involves extraction of the soil with aceto-

0003-2700/87/0359-1326$01.50/0 © 1987 American Chemical Society

nitrile "enhanced by sonication" followed by RP-HPLC analysis of the extract. No further details of the extraction procedure were provided. In the second method, several ash samples were extracted with acetonitrile using a wrist-action shaker followed by RP-HPLC analysis. Both methods exhibited low microgram per gram detection limits and near complete analyte recovery.

It was the objective of our study to compare four different extraction methods and two polar solvents for determination of munitions residues in soil. The two solvents selected were methanol and acetonitrile based on analyte solubility considerations and compatibility with the reversed-phase high-performance liquid chromatographic (RP-HPLC) method used for separation and determination. Soils contaminated in the field over a number of years were selected to examine the kinetics of release of contaminants and to compare the four extraction methods. Sufficient replication was used, where methods and solvents were compared, to permit evaluation by analysis of variance (ANOVA). Fortified soil was used to estimate analyte recovery and detection limits.

EXPERIMENTAL SECTION

Materials. All analytical standards for octahydro-1,3,5,7-tetranitro-1,3,5,7-tetrazocine (HMX), hexahydro-1,3,5-trinitro-1,3,5-triazine (RDX), 2,4,6-trinitrotoluene (TNT), 2,4-dinitrotoluene (2,4-DNT), and 1,3,5-trinitrobenzene (TNB) were prepared from standard analytical reference materials obtained from the U.S. Army Toxic and Hazardous Materials Agency, Aberdeen Proving Ground, MD. Individual compounds were dried to constant weight in a vacuum desiccator in the dark.

Methanol and acetonitrile used as extractants and in the HPLC mobile phase were Baker HPLC grade. Water used in the mobile phase and to dilute extracted samples was type I reagent grade water from a Milli-Q reagent water system (Millipore Corp.). Mobile phase for the primary column was prepared in a volume ratio of 50/38/12 (water, methanol, acetonitrile). Fresh mobile phase was prepared daily and vacuum filtered through a Whatman glass microfiber filter to remove particulate matter and degas the solvent. Mobile phase for the two columns used to confirm analyte identity was 50/50 (v/v) water/methanol, prepared in a like manner.

Two munitions-contaminated soils were collected at the Iowa Army Ammunition Plant in Middletown, IA. Soil 6 was obtained from the surface of an old ordnance burning area that had not been used for several years prior to sampling. Soil 2 was obtained from the dry surface of an old disposal lagoon which had also been out of use for several years. Each soil sample was air-dried to constant weight, ground with a mortar and pestle, and passed through a no. 30 mesh sieve. Both soils were placed in individual bottles and mixed thoroughly on a roller mill to improve homogeneity.

The clay content of soils 6 and 2 was determined to be 52.1 and 60.3%, respectively, using standard hydrometer analysis. The organic carbon content of the soils was determined by combustion analysis after extraction with methanol to remove synthetic organic contaminants. Concentrations of 0.70% and 3.00% were obtained for soils 6 and 2, respectively.

HPLC Analysis. All HPLC measurements were conducted on a modular instrument consisting of a Perkin-Elmer Series 3 pump, a Rheodyne 7125 loop injector, and a Spectra-Physics SP8300 fixed 254-nm UV detector. Peak areas were obtained with an HP 3390A digital integrator.

Separations were performed on a Supelco 25-cm × 4.6-mm LC-8 column (5 μm) using a mobile phase of water/methanol/acetonitrile (50/38/12 (v/v/v)) at a flow rate of 1.5 mL/min (*17*) and either a 100-μL or 20-μL loop. Confirmation of analyte identities was obtained on two additional columns: a Supelco 25-cm × 4.6-mm LC-CN column and a Supelco 25-cm × 4.6-mm LC-18 column, both using a 50/50 water/methanol eluent. The LC-CN was particularly effective as a confirmation column because peak orders were nearly reversed from those for the LC-8 and LC-18 columns.

Extraction Kinetics. Studies were conducted for each extraction method described below to determine the time required to maximize extraction efficiency. Each soil was tested using both methanol and acetonitrile as extraction solvents. Both solvents contained 2,4-DNT as an internal standard because it was not present at measurable concentrations in either soil and it did not sorb to soil particles in the presence of either extracting solvent.

Replication. Six replicates of each soil were extracted by each of the four procedures described below using acetonitrile and methanol as extracting solvents. Soil subsamples were weighed out in random sequence. All analyses for a given extracting solvent were performed on a single day in duplicate and in random order. In view of the DNT internal standard, it was unnecessary to adjust extracts to volume. Mean values were compared by using two-way ANOVA.

Wrist-Action Shaker. For the kinetic study two 2.00-g samples of soil were placed in 2.5-cm × 20-cm screw-cap glass test tubes followed by 50 mL of either methanol or acetonitrile containing a 2,4-DNT internal standard at 545 μg/L. The soil was dispersed with a vortex mixer (Vanlab Model K-55-G) for 1 min and then shaken at maximum speed on a Burrell Model 75 wrist-action shaker for periods ranging from 10 min to 24 h for soil 6 and from 30 min to 48 h for soil 2. Periodically, the tubes were centrifuged at 3500 rpm for 5 min, and 5-mL portions of the supernatant removed, mixed with 5 mL of water, and filtered through a 0.45-μm Gelman Acrodisc CR disposable filter assembly. Soils were redispersed with the vortex mixer and returned to the shaker. For the reproducibility studies, six replicates of both soils were shaken for 24 h, after which samples were collected and processed as described above.

Bath Sonifier. For this procedure 2.00-g subsamples were prepared as described in the previous paragraph and placed in a sonic bath (Cole-Parmer Model 8845-60) for periods ranging from 1 min to 4 h for soil 6 and 15 min to 7 h for soil 2. The bath sonifier operated at 55 000 cycles/s at 200 W. Samples were sonified by the indirect method in which four to six tubes were placed in 1-L beakers suspended in a perforated sample basket. Soil particles were constantly in motion throughout sonication. For the replicate studies, a 4-h equilibration time was used for soil 6 and a 24-h period for soil 2. Samples were processed as described for the wrist-action shaker.

Soil–Plant Homogenizer. Two 1.00-g subsamples were placed in 45-mL Pyrex centrifuge tubes and 25 mL of extracting solvent was added. Each sample was ground in a soil–plant homogenizer (PT 10/35 Brinkmann Homogenizer with PTA 20S generator) at a setting of 4 for periods ranging from 1 to 16 min for soil 6 and 5 to 60 min for soil 2. Although significant solvent evaporation was observed, the internal standard corrected for this. For the replicate studies, grinding times of 10 and 30 min were used for soils 6 and 2, respectively.

Soxhlet Extractor. Two 16.0-g subsamples of soil were placed in Soxhlet extraction thimbles (Whatman, cellulose) and extracted with 400 mL of solvent. Cycle time for the extractors was about 15 min. For the kinetic study samples were withdrawn at periods ranging from 1 to 37 h for soil 6 and from 1 to 48 h for soil 2. For the replicate study, a 24-h extraction period was used for both soils.

Spike-Recovery Study. Recovery efficiency was determined for RDX and TNT using the bath sonifier and a silt loam soil from Lebanon, NH, that contained no RDX or TNT. Each 5-g sample was spiked individually with a 250-μL aliquot of reagent water containing RDX and TNT. Soil samples were spiked in two ways: (a) at a native water content of 10% and (b) after soil was oven-dried at 105 °C overnight. Spike levels were 1.59 and 2.28 μg/g, RDX and TNT on a dry weight of soil basis. Equilibration times (four) varied from 0 to 360 min at room temperature. Two replicates were spiked for each combination of soil dryness and equilibration time. After equilibration, the soil was extracted with acetonitrile containing a DNT internal standard as described for the bath sonifier. Extracts were diluted 1:1 with reagent grade water as usual but were analyzed on an LC-18 column using 50/50 water/methanol eluent.

RESULTS AND DISCUSSION

Munitions Content of Soils. Soil 6, from an ordnance-burning area, contained high levels of extractable components. Four major peaks observed in a methanol extract had reten-

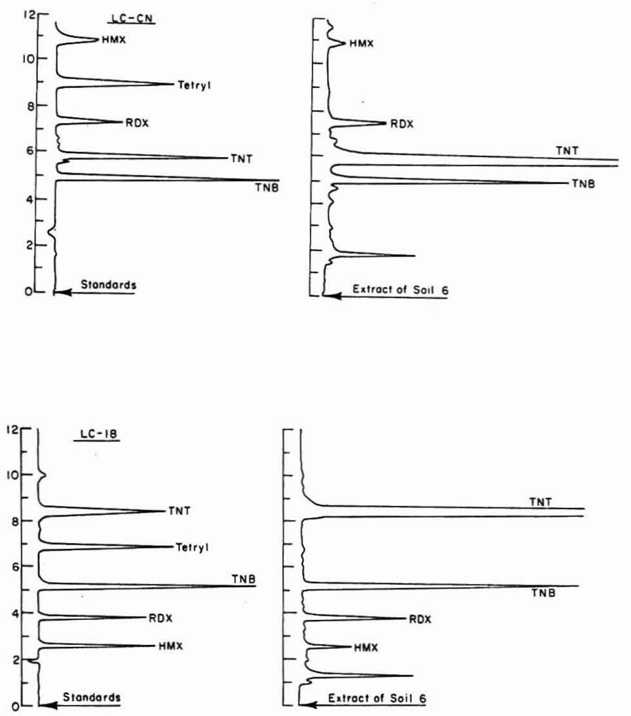

Figure 1. Chromatograms for standards and soil 6 extract on LC-18 (a) and LC-CN (b) using 50/50 water/methanol at 1.5 mL/min.

tion times corresponding to standards of HMX, RDX, TNB, and TNT on a reversed-phase LC-8 column. The identity of these components was confirmed by analysis of this extract on LC-CN and LC-18 columns (Figure 1). The retention order on the LC-18 was very similar to that found for the LC-8 column; however, the retention order for the LC-CN column was almost completely reversed. LC-CN appears to be an extremely useful confirmatory column in conjunction with either LC-8 or LC-18 for these substances.

In contrast, soil 2, from an old disposal lagoon, had much lower, but measurable, concentrations of TNT and traces of TNB, RDX, and HMX. This soil's history is somewhat different from that of soil 6, which came from an ordnance-burning area.

Extraction Kinetics. Kinetic studies were undertaken to determine the time required to approach equilibrium using the three batch extraction techniques and the Soxhlet method, which should approach complete extraction. Acetonitrile and methanol were tested separately. No attempt should be made to compare critically final concentrations with respect to solvent or method, since different subsamples were used without replication and, therefore, sampling error may be substantial. Such a comparison will be made later based on replicated trials. To ensure that emphasis is on the shape of the curves, concentrations have been individually normalized to the highest concentration for that trial. Results for RDX and TNT in soil 6 are presented in Figures 2 and 3. Maximum times were based on practical constraints. For example, the soil–plant homogenizer was studied only up to 16 min, since this is a one-at-a-time method and much longer periods seemed impractical. Furthermore, substantial solvent evaporation occurs during grinding.

Because of the very low concentrations in soil 2, equilibration times were increased from those used for soil 6. In particular, the longest time increments for the Soxhlet and wrist-action shaker were extended to 48 h. The time for the soil–plant homogenizer was extended to 60 min despite our conviction that this would be impractical in routine use. The results of this kinetic study are presented in Figure 4 for TNT. Only trace levels of TNB, RDX, and HMX were observed, and since integrated areas exhibited large uncertainty, no attempt was made to plot these data.

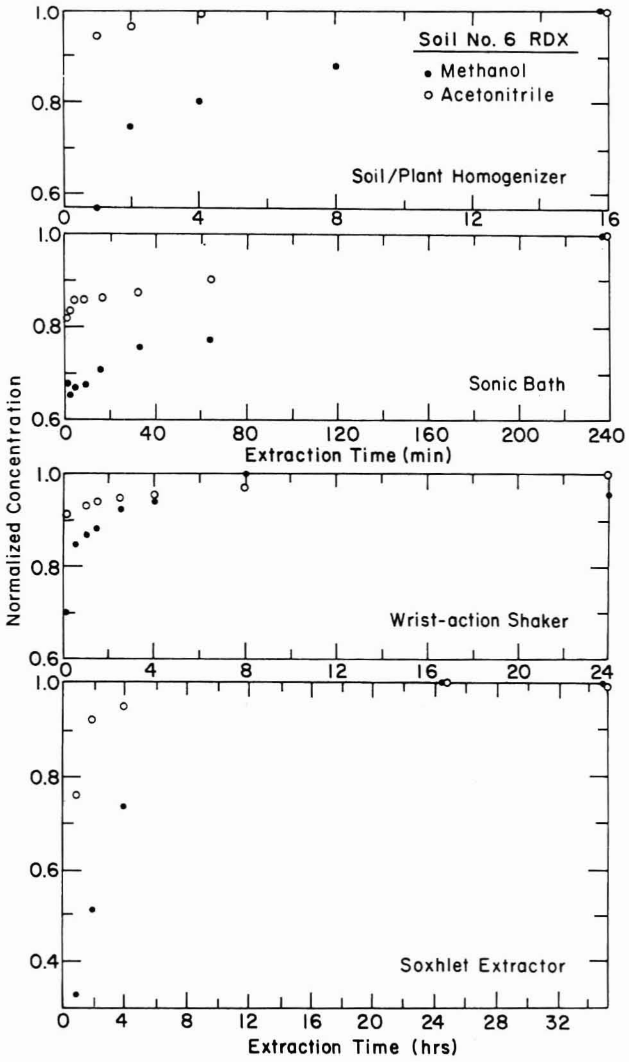

Figure 2. Concentration of extractable RDX as a function of time for various extraction techniques, soil 6.

With the wrist-action shaker, fairly constant values were obtained for soil 6 after about 4 h for all four components (see RDX and TNT in Figures 2 and 3), the amount of increase from the 4-h to the 24-h samples being 5% or less. Results for the bath sonifier indicated a somewhat greater increase in going from a 1-h to a 4-h extraction time, particularly for RDX in methanol. With the soil–plant homogenizer, equilibrium appeared to be reached much more quickly for all four analytes using acetonitrile than with methanol, which had generally not leveled off by 16 min. For the Soxhlet, values very close to the maxima were generally achieved by 4 h for both solvents. One exception was HMX in methanol, where values increased by a factor of 2.5 in going from 4 to 24 h.

TNT levels in soil 2 were about a factor of 100 lower than those found for soil 6, and the kinetics of desorption was slower for all four extraction methods. One possible explanation for this behavior is that the low level of TNT present is preferentially adsorbed to high-energy binding sites. Since the number of these types of sites is limited, the large amount of TNT associated with soil 6 exceeds what can be adsorbed in this fashion, and the bulk of the TNT may, therefore, be less tightly bound. The energy barrier for desorption of this material would be lower, resulting in faster desorption kinetics. Soil 2 also contained over four times as much natural organic matter as did soil 6. This soil fraction is considered by many to be the primary location for adsorption of organic contaminants in soils.

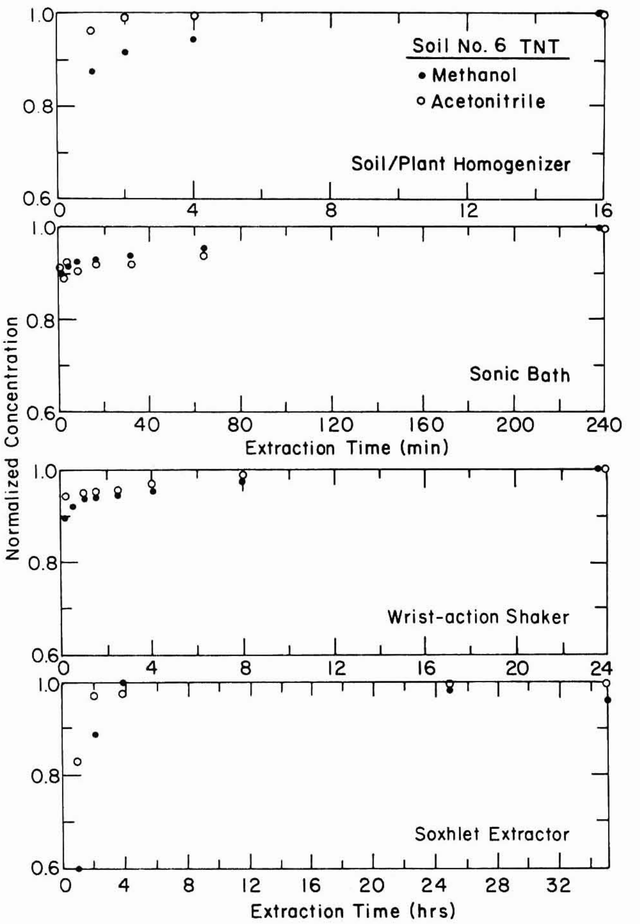

Figure 3. Concentration of extractable TNT as a function of time for various extraction techniques, soil 6.

For soil 2 (Figure 4), it appears that equilibrium was not established during the experiment with either solvent. The Soxhlet and wrist-action shaker appear closer to a terminal value for the times studied than do the soil–plant homogenizer or the sonic bath. Little difference was observed between solvents. Clearly, use of the soil–plant homogenizer for extended periods is impractical since it is a one-sample-at-a-time technique and, in addition, it results in a large degree of solvent evaporation since the tubes are required to be open to the atmosphere during grinding. Use of the sonic bath for longer periods is possible, however. The wrist-action shaker and Soxhlet appear to have come fairly close to final values after 24 h and, from a practical point of view, this is about the maximum time acceptable for soil equilibration–extraction.

Replicate Study. To allow comparison of the four extraction methods and solvents, six subsamples of soil 6 were processed by each method using both methanol and acetonitrile. Equilibration periods were 10 min and 4 h for the soil–plant homogenizer and sonic bath and 24 h for the wrist-action shaker and Soxhlet. A similar comparison was conducted with soil 2 except that the extraction times for the soil–plant homogenizer and the sonic bath were increased from 10 to 30 min and from 4 to 24 h, respectively. Means and standard deviations for each method and solvent are presented in Tables I and II. Statistical significance ($p = 0.95$) of means was established with ANOVA.

On the basis of the relative standard deviations, for both acetonitrile and methanol extraction of soil 6, the analytes fall into two distinct groups. The relative standard deviation for TNT and TNB is generally in the range of 1–3%, indicating very good analytical precision, as well as good analyte homogenization prior to subsampling. The relative standard deviation for RDX and HMX, on the other hand, is generally

Table I. Comparison of Extraction Results for Soil 6

analyte	method	mean concn,[a] μg/g	std dev, μg/g	% RSD
		Acetonitrile Extract		
TNT	shaker	881 a	13	1.4
	sonic bath	883 a	10	1.1
	homogenizer	849 b	13	1.5
	Soxhlet	881 a	8	0.9
TNB	shaker	55 b	1.0	1.9
	sonic bath	56 b	0.6	1.0
	homogenizer	51 c	0.8	1.5
	Soxhlet	62 a	1.1	1.8
RDX	shaker	54 a	10	18
	sonic bath	55 a	13	24
	homogenizer	64 a	56	87
	Soxhlet	65 a	11	16
HMX	shaker	82 a	32	39
	sonic bath	56 a	14	26
	homogenizer	65 a	27	41
	Soxhlet	84 a	12	14
		Methanol Extract		
TNT	shaker	895 a	14	1.6
	sonic bath	840 b	25	3.0
	homogenizer	870 a	39	4.4
	Soxhlet	891 a	5	0.6
TNB	shaker	56 b	0.8	1.4
	sonic bath	53 c	1.5	2.9
	homogenizer	53 c	1.1	2.0
	Soxhlet	58 a	0.6	1.1
RDX	shaker	37 a	12	32
	sonic bath	40 a	8	20
	homogenizer	31 a	17	54
	Soxhlet	48 a	5	11
HMX	shaker	22 a	5	24
	sonic bath	33 a	11	32
	homogenizer	28 a	18	64
	soxhlet	59 a	6	10

[a] Values for given analyte and solvent indicated with the same letter are not significantly different at the 95% confidence level.

Table II. Comparison of Extraction Results for Soil 2

analyte	method	mean concn,[a] μg/g	std dev, μg/g	% RSD
		Acetonitrile Extract		
TNT	shaker	2.46 c	0.12	5.0
	sonic bath	3.54 b	0.22	6.3
	homogenizer	2.10 d	0.11	5.1
	Soxhlet	4.35 a	0.33	7.5
TNB	shaker	0.37 a	0.05	13
	sonic bath	0.45 a	0.11	23
	homogenizer	0.35 a	0.13	37
	Soxhlet	0.33 a	0.05	15
		Methanol Extract		
TNT	shaker	2.76 b	0.25	9.1
	sonic bath	3.91 a	0.19	5.0
	homogenizer	2.23 c	0.08	3.6
	Soxhlet	3.7 a	0.11	2.9
TNB	shaker	0.31 a,b	0.09	28
	sonic bath	0.44 a	0.12	27
	homogenizer	0.27 b	0.08	29
	Soxhlet	0.27 b	0.06	22

[a] Values for given analyte and solvent indicated with the same letter are not statistically different at the 95% confidence level.

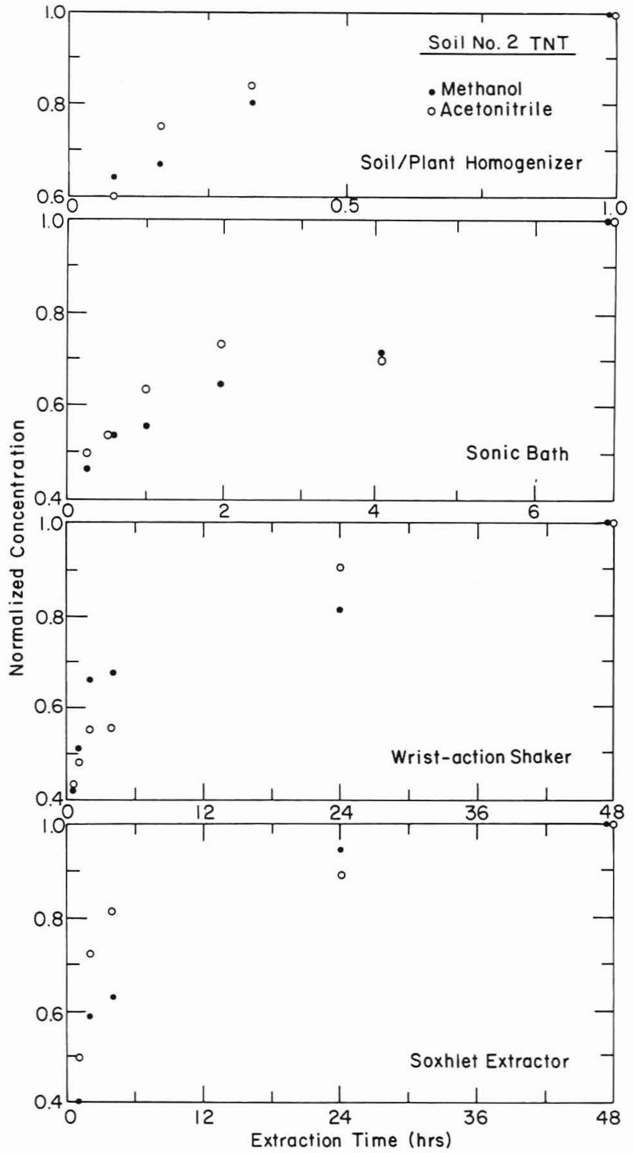

Figure 4. Concentration of extractable TNT as a function of time for various extraction techniques, soil 2.

at or above 20%, and for the homogenizer sometimes over 50%. The mean concentrations for HMX and RDX are about the same as that for TNB, and hence this difference in relative standard deviation is apparently not an analytical problem related to differences in concentration. The most likely explanation is that RDX and HMX are distributed less homogeneously than TNT and TNB in this soil. Because of the much larger sample size for the Soxhlet procedure, relative standard deviations are lower than those for the other methods for HMX and RDX in both solvents. In contrast, relative standard deviation values for the homogenizer, where 1-g subsamples were used, were generally higher than those for the shaker and sonic bath, where 2-g subsamples were used. This behavior is typical for heterogeneously distributed analytes (*18*, *19*). However, we are unable to explain why these two analytes were heterogeneous while TNT and TNB seemed relatively homogeneous in distribution.

Because of the very good precision obtained for TNT, ANOVA indicates a significant difference for the methods at the 95% confidence level. For TNT, the Soxhlet and wrist-action shaker give very similar results with both solvents. The soil–plant homogenizer gives significantly lower values with acetonitrile while the sonic bath is low for methanol. This results in a significant interaction between method and solvent at the 95% confidence level, even though the difference between solvents is not significant overall.

For TNB, excellent precision again enables sensitive comparison of the various extraction procedures and solvents (Table I); method, solvent, and interaction are all significant at the 95% confidence level. With both solvents, the Soxhlet procedure is distinctly superior to the other three methods with respect to the amount extracted, the largest differences being observed with acetonitrile. The reason for this superiority of the Soxhlet for TNB but not for TNT is unclear, particularly in view of the similarity in structure of the two substances. As was observed for TNT, extraction using the sonic bath is better with acetonitrile than with methanol, while the opposite is true for the soil–plant homogenizer.

The sensitivity of ANOVA for RDX and HMX is limited by the large uncertainties for both analytes, which makes it impossible to assign significance to the small differences observed in the various methods. Solvent, on the other hand, was found to be significant for TNB, RDX, and HMX, even with the large random error of the latter two explosives. For RDX and HMX, acetonitrile consistently resulted in higher extraction efficiency. Whether this is a thermodynamic difference attributable to solubility or to an unfavorable partition coefficient is unclear. The solubilities of RDX and HMX, however, were found to be over 20 times higher in acetonitrile than in methanol (*20*); therefore, partitioning is also expected to be more favorable into acetonitrile. Acetonitrile is superior to methanol for RDX and HMX extraction and is as good as methanol for TNT and TNB.

Mean values and standard deviations for TNT and TNB are presented in Table II for soil 2. Experimental precision for TNT averaged about 6% (relative standard deviation), indicating very good analyte homogenization prior to subsampling. This excellent precision for such a low concentration allowed a powerful comparison among methods using ANOVA. Significant differences were found among methods ($P = 0.95$), but as with soil 6, there was no consistent TNT concentration difference between solvents. For acetonitrile, the Soxhlet was significantly better than the other three procedures; the sonic bath was second. These differences were much greater on a percentage basis than those found for the higher level soil 6. For methanol, the sonic bath and the Soxhlet were not significantly different but they extracted significantly higher concentrations than the shaker or homogenizer. There was a significant interaction between method and solvent, indicating that some methods worked better in one solvent while others worked better in the other one.

For TNB, the relative standard deviation was considerably larger than for TNT, averaging over 20%. This is a result of the very low levels of TNB present in this soil (about 0.4 μg/g), which approached the detection limit, estimated to be 0.1 μg/g. Relative standard deviation values typically increase as analyte concentrations approach the detection limit (*21*).

ANOVA for the TNB results revealed a significant difference among methods but not for solvent type or method–solvent interaction. This significant difference in methods was only apparent in methanol, where the sonic bath produced significantly higher results than the Soxhlet or homogenizer. The shaker was not significantly different from any of the other three methods at the 95% confidence level.

Overall, the bath sonifier using acetonitrile seems to be the best compromise. This is based not only on performance with both soils and the four analytes tested but from practical considerations such as apparatus and solvent cost, convenience, and sample size requirements as well.

Spike-Recovery Study. While a comparison of the bath sonifier method to the other three procedures is possible with field contaminated soil, completeness of recovery cannot be adequately evaluated since the total amount of analyte present

Table III. Recovery of RDX and TNT from Spiked Soil Using Acetonitrile and the Bath Sonifier Method

	% recovery			
	RDX[a]		TNT[b]	
equilibrium time, h	wet[c]	dried	wet	dried
0	98	96	105	102
0.25	103	95	102	99
1.5	112	100	106	104
6	99	100	95	100

[a] Soil was spiked at an RDX concentration of 1.59 μg/g on a dry weight basis. RSD was ±5.4%. [b] Soil was spiked at a TNT concentration of 2.28 μg/g on a dry weight basis. RSD was ±4.3%. [c] Wet soil was spiked at a water content of 10%. Dried soil had been oven-dried overnight at 105 °C.

is unknown. To get information on recovery, both wet and dry subsamples of a silt loam soil were spiked with low level aqueous solutions of TNT and RDX, allowed to equilibrate for periods up to 6 h, and extracted with acetonitrile using the bath sonifier method. Results are presented in Table III.

In all cases, recovery of both RDX and TNT was complete. While we were concerned about the effect of contact time prior to extraction, no difference in recovery was observed for equilibration times up to 6 h. The moisture status of the soil prior to spiking also appeared to have little effect. Although these results are encouraging, we must emphasize that natural samples that have aged for months or years may produce lower analyte recoveries.

CONCLUSIONS

No simple explanation adequately describes all of the results from this study. Although methanol and acetonitrile were equally good for extraction of TNT, acetonitrile was superior both kinetically and thermodynamically for RDX and HMX, due in part to a much higher solubility. For TNB, acetonitrile appears to be better only at high concentrations. Overall, acetonitrile is a better choice than methanol.

The sonic bath method is recommended because it can be used to process a number of samples simultaneously. It can also be used in an unattended fashion and is relatively inexpensive. The gentle heating that occurs with the sonic bath ($\approx$39 °C) also seems desirable to increase the rate at which equilibrium is attained. The sonic bath does not suffer from the problem experienced with the Soxhlet device of coextracting significant amounts of interfering substances that have a low solvent–soil partition coefficient. It is also worth noting that thermally labile analytes are often a problem with the Soxhlet.

On the other hand, there are some disadvantages and/or precautions to be noted in conjunction with sonic agitation. Analyte extraction efficiency may depend on the vigor of agitation, which depends on many variables for sonic devices (*22*). It has been observed that the extent of particle disruption varies inversely with solid/solution ratio (*23*); consequently this ratio should be constant in comparison analyses. Solvent variables such as viscosity, vapor pressure, and dissolved air concentration affect acoustic impedance. Not surprisingly, temperature increases allow cavitation bubbles to collapse with less force and, therefore, increased solubility may be offset by reduced agitation. However, as long as conditions are held constant, the sonic bath represents an excellent way to perform such extractions.

ACKNOWLEDGMENT

The authors gratefully acknowledge the technical assistance provided by P. Schumacher of CRREL who conducted a large portion of the experimental work and L. Knapp of CRREL who conducted the spike-recovery study. L. Shahan of Mason Hangar Corp., Iowa Army Ammunition Plant, and J. West of Thiokol, Louisiana Army Ammunition Plant, are acknowledged for their assistance in soil sample collection. The authors also thank J. Cragin and J. Oliphant of CRREL and M. Stutz of USATHAMA for technical review of the report from which much of this information was extracted and C. F. Bauer of UNH for review of this manuscript. A special acknowledgment is due D. C. Leggett of CRREL who, in addition to reviewing the manuscript, contributed useful advice throughout the study and supplied the solubility data.

Registry No. HMX, 2691-41-0; RDX, 121-82-4; TNT, 118-96-7; TNB, 99-35-4; MeOH, 67-56-1; MeCN, 75-05-8.

LITERATURE CITED

(1) Kooke, R. M. M.; Lustenhouwer, J. W. A.; Olie, K.; Hutzinger, O. *Anal. Chem.* **1981**, *53*, 461–463.
(2) Peterson, J. C.; Freeman, D. H. *Int. J. Environ. Anal. Chem.* **1982**, *12*, 277–291.
(3) Junk, G. A.; Richard, J. J. *Anal. Chem.* **1986**, *58*, 962–965.
(4) Sporstol, S.; Gjos, N.; Carlberg, G. E. *Anal. Chim. Acta* **1983**, *151*, 231–235.
(5) Freeman, D. H.; Cheung, L. S. *Science* **1981**, *214*, 790–792.
(6) Grosjean, D. *Anal. Chem.* **1975**, *47*, 797–805.
(7) Harrold, D. E.; Young, J. C. *J. Environ. Eng. Div.* (*Am. Soc. Civ. Eng.*) **1982**, 1211–1227.
(8) USEPA, SW846 Method 3540 Soxhlet Extraction (July 1982).
(9) Haddock, J. D.; Landrum, P. F.; Giesy, J. P. *Anal. Chem.* **1983**, *55*, 1197–1200.
(10) Cotterill, E. G. *Pestic. Sci.* **1980**, *11*, 23–28.
(11) Fowlie, P. J. A.; Bulman, T. L. *Anal. Chem.* **1986**, *58*, 721–723.
(12) Johnson, R. E.; Starr, R. I. *J. Agric. Food Chem.* **1972**, *20*, 48–51.
(13) Wegman, R. C. C.; Hofstee, A. W. M. *Water Res.* **1982**, *16*, 1265–1272.
(14) Miller, H. H.; Crook, M. V.; Spigarelli, J. L. USATHAMA Report DRXTH-TE-CR-82182, 1983.
(15) Bongiovanni, R.; Podolak, G. E.; Clark, L. D.; Scarborough, D. T. *Am. Ind. Hyg. Assoc. J.* **1984**, *45*, 222–226.
(16) Brueggemann, E. E. USAMBRDL Technical Report 8604, 1986.
(17) Jenkins, T. F.; Leggett, D. C.; Grant, C. L.; Bauer, C. F. *Anal. Chem.* **1986**, *58*, 170–175.
(18) Grant, C. L.; Pelton, P. A. In *Advances in X-Ray Analysis*; Grant, C. L., Barrett, C. S., Newkirk, J. B., Rudd, C. O., Eds.; Plenum: New York, Vol. 17, 1973.
(19) Ingamells, C. O.; Switzer, P. *Talanta* **1973**, *20*, 547–568.
(20) Leggett, D. C., personal communication.
(21) Horwitz, W. *Anal. Chem.* **1982**, *54*, 67A–76A.
(22) Alliger, H. *Am. Lab.* (*Fairfield, Conn.*) **1978**, *10* (Sept.), 81–87.
(23) Booth-Britton, K., personal communication.

RECEIVED for review September 30, 1986. Accepted February 9, 1987. This project was funded by the U.S. Army Toxic and Hazardous Materials Agency (USATHAMA) under Order No. A1-5-R0001-XX-A1-48 (R90-Analytical Systems Technology).

1332 *Anal. Chem.* **1987**, *59*, 1332–1339

Properties of an Asymmetrical Flow Field-Flow Fractionation Channel Having One Permeable Wall

Karl-Gustav Wahlund[1] **and J. Calvin Giddings***

Department of Chemistry, University of Utah, Salt Lake City, Utah 84112

We describe here a flow field-flow fractionation channel having only a single permeable wall. This wall, serving as the accumulation wall, consists of a membrane/frit bilayer permeable to the carrier flow but impermeable to the sample. The opposite wall, impermeable to flow, is made of a glass plate, which renders the channel contents visible. In operation the channel has one incoming flowstream and two outgoing streams, one being the diffuse stream permeating the membrane. This design is technically simpler than conventional, more symmetrical designs where the upper wall is also permeable to flow. It is shown that the new design creates both longitudinal and transverse flow velocity gradients but retention, if sufficiently strong, can be interpreted in much the same way as with conventional channels. Theoretical expressions are obtained for velocity gradients, retention, and relaxation and focusing times. A fractionation of a mixture of proteins is shown in order to illustrate the potential for macromolecular separations.

Flow field-flow fractionation, one of the subtechniques in the field-flow fractionation (FFF) family (*1*), is potentially capable of the rapid separation of a wide variety of macromolecular and colloidal materials at high resolution. Previous work in flow FFF was recently summarized (*2*).

The FFF separation unit has typically the geometry of a flat, thin, rectangular channel where the sample is loaded at one end and then transported down the channel with a carrier flow to exit at the other end. While migrating through the channel, the sample is subject to a force (derived from a "field") which causes it to accumulate differentially in the slow moving carrier laminae along one of the channel walls (the accumulation wall). This constitutes the basis of the retention and separation.

In flow FFF the effective force is created by a secondary carrier flow whose direction is perpendicular to the longitudinal flow. This flow arrangement has previously been implemented by using a "symmetrical" configuration of two walls that are both permeable to the carrier flow. The accumulation wall (lower wall) has consisted of a semipermeable membrane, supported on a frit and permeable to the carrier but not to the sample. The upper wall has been made from a frit material (the upper frit). The "field" is induced by pumping carrier into the channel through the upper wall and letting it exit through the accumulation wall.

Performance according to theory requires that this crossflow of carrier be uniform. This puts high technical demands on the construction of the channel, including the requirement that the permeability of the two walls be homogeneous (*3*). However, little is known about the quality of frits and membranes in this respect.

Resolution in flow FFF, unlike that in other FFF subtechniques, has been well below what theory predicts (*4*). This indicates that phenomena causing excessive zone broadening are operative in the channel. These might be associated with distorted flow profiles for axial and transverse flow and/or sample immobilization (e.g., by adsorption) at the accumulation wall. It is essential to develop new methodologies and concepts to help understand and overcome this deficiency.

This paper presents a new design of the flow FFF channel which makes its construction technically simpler. The porous upper wall of the channel is replaced by a solid wall made of a glass plate. Thus the upper wall is impermeable to the carrier flow and the channel is left with only one source of carrier flow. This source is the channel inlet, located at one end of the channel. The carrier will exit the channel as two separate flowstreams, one a thin stream emerging from the outlet at the other channel end, and the other a diffuse stream passing through the accumulation wall.

This new "asymmetrical" design eliminates technical difficulties associated with the possible heterogeneity and uneven permeability of the upper frit and with the machining of that frit to give a uniform planar wall for the channel. Because the upper wall can be made from a glass plate, this channel lends itself to a direct visual observation of sample migration and of flow patterns provided colored or fluorescent samples are used. This is expected to help in the study of channel performance and in the design of improved channels, both of this type and of the symmetrical type.

The presence of the diffuse stream passing out through the accumulation wall, unmatched by an equivalent stream entering through the opposite wall, leads to gradients in the longitudinal and transverse flow velocities. The flow patterns resemble those occurring in tubular channels with porous walls, which can also be used for flow FFF (*5*). Such nonuniform conditions make the theoretical evaluation of the results more complex than in channels with uniform flow. Under certain limiting conditions, however, the theoretical relationships for retention reduce to those valid for uniform channels.

In this paper we present theoretical relationships for the velocity profiles, concentration distribution, retention ratio, void time, and the sample relaxation time. We also formulate guidelines for the experimental use of the channel. We utilize the simplicity of the channel and the visibility of its contents to study the mechanism of flow FFF. The experimental application of the channel is illustrated by the fractionation of a standard protein mixture.

THEORY

Flow Velocity Profiles. Consider the flat thin channel with open ends and one permeable wall as outlined in Figure 1. Flow enters through the inlet end and it exits both through the outlet end and through the permeable accumulation wall. Calculation of the velocity profiles in such a channel can be made as a special case of a general thin-channel theory based on a mass balance approach (*6*). In this theory it is assumed that the transverse flow velocity at any point is much smaller

---

[1] Present address: Department of Analytical Pharmaceutical Chemistry, Biomedical Center, University of Uppsala, Box 574, S-75123 Uppsala, Sweden.

0003-2700/87/0359-1332$01.50/0 © 1987 American Chemical Society

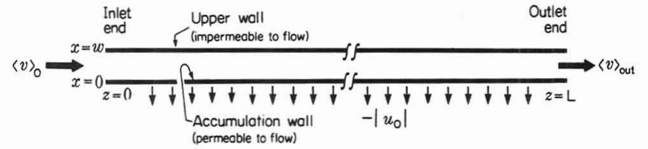
Inlet end
Upper wall (impermeable to flow)
Outlet end
$x=w$
$\langle v \rangle_0$
$\langle v \rangle_{out}$
$x=0$
$z=0$
$z=L$
Accumulation wall (permeable to flow)
$-|u_0|$

Figure 1. Schematic illustration of asymmetrical channel for flow field-flow fractionation. Flow velocities at designated locations are shown as $\langle v \rangle_0$, $\langle v \rangle_{out}$, and u_0 where the first two are the longitudinal flow velocities at the inlet and outlet ends, respectively, and u_0 is the crossflow velocity at the accumulation wall.

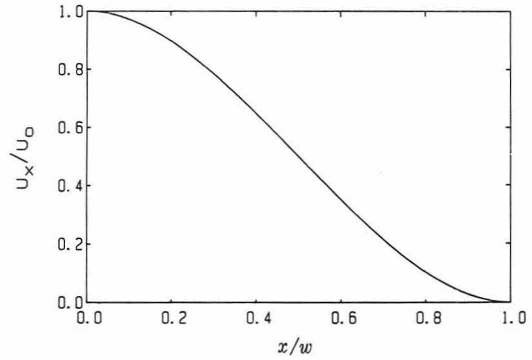

Figure 2. Crossflow velocity profile according to eq 1.

than the average longitudinal flow velocity, resulting in parabolic flow along the channel. Also the pressure drop along the channel is required to be much smaller than that across the accumulation wall in order to ensure a homogeneous permeation of the carrier. The transverse (crossflow) velocity distribution for our system according to this theory is

$$u_x = -|u_0|\left(1 - \frac{3x^2}{w^2} + \frac{2x^3}{w^3}\right) \tag{1}$$

where u_x is the transverse flow velocity at any point x above the accumulation wall, u_0 is the transverse flow velocity at the accumulation wall, and w is the channel thickness, the distance between the accumulation wall and the upper wall. The negative sign accounts for the negative direction of the crossflow along coordinate axis x (Figure 1).

The crossflow velocity given by eq 1 is zero at the upper wall ($x = w$) and increases nonlinearly toward the accumulation wall as illustrated in Figure 2. Close to the accumulation wall, at $x/w < 0.06$, it is nearly constant (to within 1%); i.e., $u_x \simeq u_0$. This suggests that for highly retained samples, which are almost completely contained in this region, the retention can be described by the same relationships as used for the conventional flow FFF channels, in which the crossflow velocity is uniform across the channel. This will be discussed in more detail below in relation to sample retention. As pointed out before (*6*), the crossflow velocity does not vary with position along the longitudinal axis of the channel.

The longitudinal flow velocity at any point z along the channel is given by the linear relationship

$$\langle v \rangle = \langle v \rangle_0 - \frac{|u_0|}{w} z \tag{2}$$

where $\langle v \rangle_0$ is the longitudinal flow velocity at the channel inlet. This shows that $\langle v \rangle$ decreases linearly along the channel at a rate determined by the crossflow velocity u_0 at the accumulation wall (*6*).

Concentration Distribution. As with all forms of FFF the sample is subject to a transverse drift velocity toward the accumulation wall. This is soon balanced by molecular diffusion, leading to a thin steady-state layer of the sample. In flow FFF the drift velocity is created by the crossflow of carrier and therefore equals the crossflow velocity u_x. The present system is unusual because this drift velocity varies across the channel; it is necessary to deduce the concentration profile for this special case. The steady-state profile, based on an earlier formulation of steady-state transport (*7*), is given by

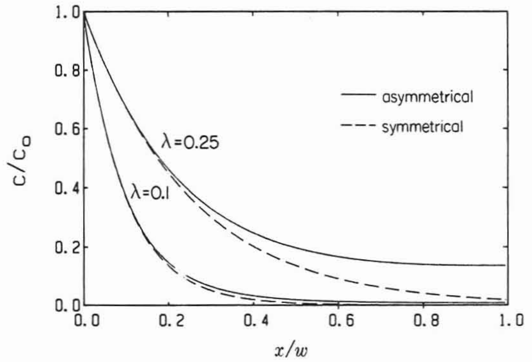

Figure 3. Comparison of concentration distributions created by the nonuniform crossflow velocity of an asymmetrical channel with those of a conventional flow FFF channel having a uniform crossflow velocity. Most practical work is done at λ < 0.1, where the differences between the two curves rapidly disappear.

$$\frac{c}{c_0} = \exp\left(\int_0^x \frac{-|u_x|}{D}\, dx\right) \tag{3}$$

where c is the sample concentration at any point x above the accumulation wall, c_0 is the sample concentration at the accumulation wall, and D is the sample diffusion coefficient. The substitution of eq 1 into eq 3 leads to

$$\frac{c}{c_0} = \exp\left(\frac{-|u_0|}{D} \int_0^x \left(1 - \frac{3x^2}{w^2} + \frac{2x^3}{w^3}\right) dx\right) \tag{4}$$

providing D is a constant independent of x. Integration gives the desired concentration profile

$$\frac{c}{c_0} = \exp\left(\frac{-|u_0|x}{D}\left(1 - \frac{x^2}{w^2} + \frac{x^3}{2w^3}\right)\right) \tag{5}$$

For $x/w < 0.1$, eq 5 can be approximated by

$$\frac{c}{c_0} = \exp\left(\frac{-|u_0|x}{D}\right) = \exp\left[-\frac{x}{l}\right] \tag{6}$$

where the length parameter l is

$$l = D/|u_0| \tag{7}$$

a distance that coincides approximately with that of the center of gravity of the steady-state layer.

Equation 6 has the same mathematical form as that for conventional field-flow fractionation channels with uniform drift velocity throughout. Obviously, for the part of a sample zone contained below the level $x/w = 0.1$, the concentration profile will be the same to within 1% in the two kinds of flow FFF channels. This permits a considerable simplification of the quantitative treatment of retention data in the present system. This will become more obvious when expressions for the retention ratio have been derived.

Figure 3 illustrates the form of the concentration profiles in both kinds of channels for two levels of $\lambda = l/w$. The largest, $l/w = 0.25$, is an unusually large value that illustrates the nature of the difference in the two concentration profiles. The lower value, $l/w = 0.1$, is a more realistic value for sample retention, but still lies at the upper end of the practical retention range. The figure shows that, relative to the symmetrical flow FFF channel in which the crossflow velocity is constant at every point, the sample concentration profile in the asymmetric channel is less compressed against the accumulation wall for equal l/w values.

Retention Ratio. The retention ratio is defined by

$$R = V/\langle v \rangle \tag{8}$$

where V is the migration velocity of the component zone and $\langle v \rangle$ is the average longitudinal carrier velocity. We obtain R from the general expression (*10*)

$$R = \frac{w \int_0^w c(x) v(x)\, \mathrm{d}x}{\int_0^w c(x)\, \mathrm{d}x \int_0^w v(x)\, \mathrm{d}x} \tag{9}$$

When we substitute eq 5 for $c \equiv c(x)$ and utilize the standard parabolic flow expression (*6*) for $v(x)$ we get

$$R = \frac{6}{w} \frac{\int_0^w e^{(-x/l)B(x)} x\, \mathrm{d}x - \frac{1}{w} \int_0^w e^{(-x/l)B(x)} x^2\, \mathrm{d}x}{\int_0^w e^{(-x/l)B(x)}\, \mathrm{d}x} \tag{10}$$

where

$$B(x) = 1 - \frac{x^2}{w^2} + \frac{x^3}{2w^3} \tag{11}$$

Due to the complexity of expression $B(x)$ and its presence in the exponent, the integrals of eq 10 cannot be evaluated in a simple way. However, for $x/w < 0.1$ the value of $B(x)$ approaches unity and eq 10 assumes the form it has in conventional FFF channels. In this form the integrals are easily evaluated, leading to the well-known retention equation (*2*, *3*)

$$R = 6\lambda[\coth(1/2\lambda) - 2\lambda] \tag{12}$$

where (cf. ref 2 and 8)

$$\lambda = \frac{l}{w} = \frac{D}{|u_0| w} = \frac{D V^\circ}{\dot{V}_c w^2} \tag{13}$$

in which V° is the geometric volume (void volume) of the channel and $\dot{V}_c$ is the volumetric flowrate across the accumulation wall, the cross flowrate.

Equation 12 has several useful approximate forms, including

$$R = 6\lambda \tag{14}$$

which is valid to within 2% when $R < 0.06$ and 5% when $R < 0.15$. This means that under conditions of high retention when the major part of the accumulated sample zone is found below the level $x/w = 0.1$, eq 12 and 14, derived for symmetrical channels, can be used for the evaluation of retention data obtained in the asymmetrical channel. This has great practical importance because high retention conditions are preferred in order to get high resolution (*2*). It can thus be concluded that despite the more complex mathematics of flow FFF in the asymmetrical channel, the added complexity largely vanishes under practical conditions. Some calculations of retention ratios in the two kinds of channels will illustrate this in more detail.

Figure 4 shows plots of retention ratio R vs. $1/\lambda$ calculated from eq 10 and 12, which represent the application to asymmetrical and symmetrical channels, respectively. Calculations based on eq 10 were made by numerical integration using a computer. We see that at low retention ratios the two curves nearly coincide. The ratio between the two expressions for R is also plotted in Figure 4. For $1/\lambda > 40$ the difference is less than 1% and eq 12 (or some approximation thereof) can be used instead of eq 10. This corresponds to $R < 0.14$. If a 5% difference can be accepted, we require only that $R < 0.32$. Because one usually wants to work well below $R = 0.3$, it can be concluded that eq 12 can be used in most practical situations to calculate data such as λ values or diffusion coefficients from retention data obtained from the asymmetrical channel. Thus the complexity of eq 10 can be largely avoided, if desired.

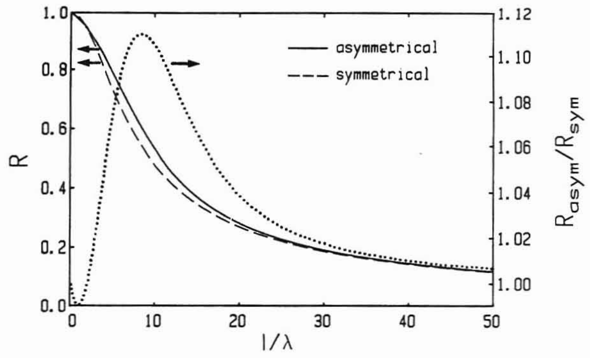

Figure 4. Retention ratios R in symmetrical and asymmetrical channels. The dotted line is the ratio of the two, R(asymmetrical)/R(symmetrical).

Void Time and Retention Time. The retention ratio, given as a ratio of velocities in eq 8, can also be expressed as the ratio of two times

$$R = t^\circ / t_r \tag{15}$$

where t° is the void time and t_r is the retention time of the component of interest. Ideally t° can be obtained as the elution time of an unretained component which travels with the average velocity of the carrier, but in flow FFF such components can be lost through the permeable wall.

Alternatively, t° can be calculated if V° is known. For this, account must be taken of the linear decrease of the longitudinal carrier velocity, eq 2. Integration of $\mathrm{d}t^\circ = \mathrm{d}z/\langle v \rangle$, with the aid of eq 2, gives

$$t^\circ = \int_{z'}^{L} \frac{\mathrm{d}z}{\langle v \rangle} = \int_{z'}^{L} \frac{\mathrm{d}z}{\langle v \rangle_0 - |u_0| z/w} \tag{16}$$

The lower limit, representing the sample starting point, is taken as z' because, as will be discussed below, sample migration will often commence some finite distance z' from the channel inlet end at $z = 0$.

In that experimentally the volumetric flowrates, not the velocities, are measured, we convert the latter to the former using $u_0 = \dot{V}_c/(bL)$ and $\langle v \rangle_0 = \dot{V}_{in}/(bw)$. If we also use $V^\circ = Lbw$, eq 16 transforms to

$$t^\circ = \frac{V^\circ}{\dot{V}_c} \ln \left(\frac{\dot{V}_c(L - z') + \dot{V}_{out} L}{\dot{V}_{out} L} \right) \tag{17}$$

where $\dot{V}_{in}$ is the volumetric inlet flowrate (at $z = 0$) and $\dot{V}_{out}$ is the volumetric outlet flowrate (at $z = L$). The flowrates $\dot{V}_c$ and $\dot{V}_{out}$ can be measured directly and are related to the inlet flowrate through

$$\dot{V}_{in} = \dot{V}_c + \dot{V}_{out} \tag{18}$$

With this expression, eq 17 can be written in terms of $\dot{V}_{in}$ rather than $\dot{V}_{out}$, that is

$$t^\circ = \frac{V^\circ}{\dot{V}_c} \ln \left(\frac{z'/L - \dot{V}_{in}/\dot{V}_c}{1 - \dot{V}_{in}/\dot{V}_c} \right) \tag{19}$$

When sample elution starts at the channel inlet end, in which case the full channel length is used for elution, $z' = 0$ and eq 17 becomes

$$t^\circ = \frac{V^\circ}{\dot{V}_c} \ln \left(1 + \frac{\dot{V}_c}{\dot{V}_{out}} \right) \tag{20}$$

If measurement of the elution time t° of an unretained component can be made at certain flowrates, this expression should yield the void volume V° of the channel.

In general, retention time t_r is calculated from eq 15, namely, $t_r = t^\circ/R$, where we now have theoretical expressions for both t° and R. At high retention levels ($R < 0.15$) the retention time can be approximated by using eq 14 and 13 for R, giving

$$t_r = \frac{t^\circ \dot{V}_c w^2}{6DV^\circ} \tag{21}$$

The replacement of t° by eq 20 and 19 gives, respectively

$$t_r = \frac{w^2}{6D} \ln\left(1 + \frac{\dot{V}_c}{\dot{V}_{out}}\right) \tag{22}$$

and

$$t_r = \frac{w^2}{6D} \ln\left(\frac{z'/L - \dot{V}_{in}/\dot{V}_c}{1 - \dot{V}_{in}/\dot{V}_c}\right) \tag{23}$$

which shows that retention time t_r will be constant for any rate of inflow $\dot{V}_{in}$ as long as all flowrates in the channel are maintained at a fixed proportion to one another.

Diffusion coefficient D can be obtained on the basis of experimentally determined R values (or retention times) by determining λ from eq 14 (or 22 or 23), 12, or 10. The choice depends on the required accuracy in estimating D, which puts restriction on the useful range of experimental retention ratios R. For 1–2% relative error in D, the use of eq 14 requires $R < 0.06$ and eq 12 $R < 0.14$, whereas for a 5% relative error eq 14 requires $R < 0.15$ and eq 12 $R < 0.32$. At retention ratios higher than these limits eq 10 has to be used, in which case λ can be obtained from a plot or table according to Figure 4.

Sample Loading, Relaxation, and Focusing. In symmetrical flow FFF in which a uniform crossflow enters through the upper wall, the sample loading is usually followed by a stopflow period during which the longitudinal flow is halted and only crossflow continues (*3, 9*). This causes the sample to relax toward the accumulation wall where it reaches equilibrium without the disturbance of axial flow. This stopflow procedure requires the passage of one channel void volume of crossflow.

In the present asymmetrical channel, where the crossflow originates at the channel inlet, sample relaxation cannot be induced without longitudinal displacement, even if the channel outlet end is closed. This is because of the ubiquitous longitudinal flow vector, which tends to cause zone broadening during relaxation. To prevent this, a different set of flow conditions must be established such that longitudinal migration is halted at some point down the channel.

The above can be achieved by introducing an inflow of carrier through the outlet end of the channel, which reverses the flow in much of the channel. With continued inflow through the inlet end, the two opposing flowstreams will meet at some point, essentially a focusing point. The sample, no matter where loaded or how widely dispersed, will eventually migrate to and become focused and relaxed as a narrow zone at this point, following which normal FFF is commenced. This procedure, which we designate as "opposing flow relaxation", has been described by Lee et al. (*5*) for tubular ducts.

The coordinate point z' of focusing can be changed by altering the two opposing flowrates according to

$$\frac{z'}{L} = \frac{\dot{V}_{in}'}{\dot{V}_{in}' + \dot{V}_{out}'} \tag{24}$$

where the primes indicate values associated with the relaxation process; $\dot{V}_{out}'$ thus refers to the reverse flowrate through the outlet used for relaxation, as illustrated in Figure 5.

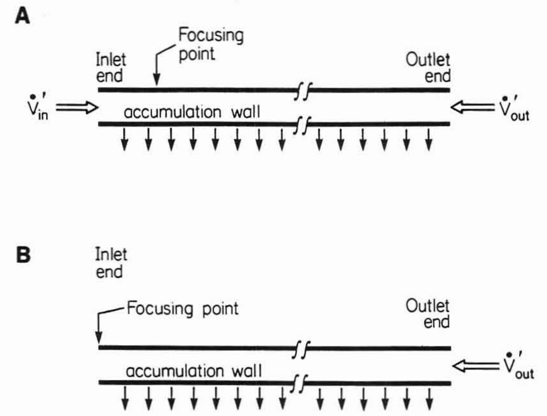

Figure 5. Schematic illustration of flow directions and focusing points for the two sample relaxation procedures. Part A illustrates opposing flow relaxation and B reverse flow relaxation.

The above expression shows that if the two flowrates are equal, the focusing point will be at $z' = L/2$, the midpoint of the channel. The preferred focusing point is somewhere near the channel inlet end where the sample is loaded; for such a point the length of the channel available for elution is maximal.

A special case of the above method (see Figure 5B) is to eliminate the flow through the inlet end of the channel as soon as the sample has been loaded there but to maintain the reverse flow. This approach, termed "reverse flow relaxation", will cause the (somewhat dispersed) sample to migrate backward to focus at the channel inlet end where it becomes relaxed.

The time τ needed for complete sample relaxation is approximately the time required for the transverse displacement of the carrier from the upper wall to the accumulation wall (*10*). We formulate this by examining the time τ_x required to carry sample material from arbitrary coordinate position x to the accumulation wall $x = 0$

$$\tau_x = \int_0^x \frac{dx}{-u_x} = \int_0^x \frac{dx}{|u_0|(1 - 3(x/w)^2 + 2(x/w)^3)} \tag{25}$$

where u_x has been obtained from eq 1. Equation 25 is equivalent to

$$\tau_x = \frac{w}{|u_0|} \int_0^{x/w} \frac{d(x/w)}{2(x/w - 1)^2(x/w + 1/2)} \tag{26}$$

which upon integration and rearrangement yields

$$\tau_x = \frac{V^\circ}{\dot{V}_c}\left(\frac{2}{9}\ln\left(\frac{1 + 2x/w}{1 - x/w}\right) + \frac{x/w}{3(1 - x/w)}\right) \tag{27}$$

When x/w is close to unity, this can be approximated by

$$\tau_x \simeq \frac{V^\circ}{3\dot{V}_c(1 - x/w)} \tag{28}$$

The ratio $V^\circ/\dot{V}_c$ represents the relaxation time for uniform crossflow; the rest of eq 27 and 28 expresses the increase in relaxation time due to the nonuniform crossflow. Clearly $\tau_x \to \infty$ as $x \to w$, which reflects the fact that the crossflow velocity approaches zero at the upper wall. Since there is no crossflow at the upper wall, species near that wall will require excessive times to be swept across the channel. Equation 27 shows that the increase in τ_x relative to $V^\circ/\dot{V}_c$ amounts to a factor of 7.2 if 95% of the sample is relaxed ($x/w = 0.95$) and a factor of 34 for 99% ($x/w = 0.99$). These excessive relaxation times pose one of the most serious obstacles to the asymmetrical system.

To further examine the limitations imposed by the relaxation phenomenon, we examine briefly a mechanism in which diffusion, not crossflow, removes sample material from the thin, virtually stagnant layer of carrier near the upper wall. In some given fraction of the relaxation time τ_x, most of the molecules located between position x and the upper wall at position w will diffuse across plane x providing

$$\tau_x = (w - x)^2/mD \tag{29}$$

where m is a constant of order unity. We assume that components that cross plane x sufficiently early (in a time scaled to τ_x) will then be entrained in the increasing crossflow below x and swept from there to the accumulation wall by the crossflow mechanism. The combination of eq 28 and 29 shows that the approximate time needed for this mechanism to induce relaxation is

$$\tau_x \simeq \left(\frac{V^\circ}{3\dot{V}_c}\right)^{2/3}\left(\frac{w^2}{mD}\right)^{1/3} \tag{30}$$

which for macromolecules will typically be a time of several minutes.

One potential remedy to the relaxation time problem is to increase the crossflow velocity during relaxation to a value many times higher than that used for elution. One possible drawback of this approach is that, with increased crossflow, components will be pushed closer to the accumulation wall than that represented by the equilibrium concentration distribution found in the elution step. A secondary nonequilibrium effect would be induced as the components relaxed from one concentration distribution to another upon changing the crossflow (*11*). However, if operation is properly optimized such that thin clouds of component species are formed during elution, the secondary relaxation from an even thinner layer may take only a few seconds or less, depending on the magnitude of the diffusion coefficient. Thus with proper operation, secondary relaxation might be unimportant even with substantially different crossflow velocities in the two phases of operation.

Another possible difficulty with such an approach is that excessive crossflows might drive the components too vigorously into the membrane where they could be immobilized or lost. We have previously observed the immobilization of components at excessive crossflow rates (*2*). While to some extent the immobilization is reversible, the subject requires considerably more study for clarification.

Another possibility for increasing relaxation speed is the use of a splitter at the inlet end of the channel (*12*). By division of the incoming flow into a thin lamina of sample-containing carrier near the accumulation wall and an overlying lamina of pure carrier, the time-consuming process of evacuating the upper wall region of sample is not required. The relaxation time would thus be much shorter. For example, with a splitter depositing the sample below the level $x/w = 1/3$, the relaxation time would decrease by a factor of 20 as compared to a channel without a splitter (for $x/w = 0.95$ in eq 27) and would be about 1/3 of the relaxation time in a symmetrical channel working without a splitter.

When the reverse flow relaxation method (Figure 5B) is used, the inflow is switched from one channel end to the other. If the crossflow velocity is kept the same during relaxaton and elution, the flowrate for the reversed inflow has to be set equal to the cross flowrate $\dot{V}_c$ for elution. This is less than the inlet flowrate for elution, $\dot{V}_{in}$, as shown by eq 18. Thus an increase in the rate of inflow is required on going from the relaxation procedure to the elution step. A similar increase would be needed for relaxation accomplished with opposing flow relaxation (Figure 5A). The resulting pressure pulse can give a false signal early in the fractogram.

Another time constant also requires attention. This is the focusing time, which is the time necessary to sweep the sample material axially to a position near the focusing point. Focusing times will vary depending upon the starting position of sample molecules. The largest focusing time will be required for molecules beginning their focusing from a position near the accumulation wall at $z = 0$. We will examine the focusing time for this population of molecules in order to avoid underestimating the time required for focusing. We note that the relaxation process described above and focusing (which is another kind of relaxation process) occur simultaneously in the original relaxation period. The duration of that period will be determined by the longest of the two required times.

During focusing the longitudinal carrier velocity goes to zero at the focusing point, that is, $\langle v \rangle \rightarrow 0$ at $z \rightarrow z'$. The linear form required of such flow (*6*), as expressed by eq 2, is now transformed to

$$\langle v \rangle = (|u_0|/w)(z' - z) \tag{31}$$

The "void" time, which is the time required for a hypothetical non-retained component to migrate from the channel inlet to the focusing point, can be obtained by integration of $dt^\circ = dz/\langle v \rangle$ between the limits 0 and fz'. The factor f must be chosen <1 (e.g., 0.99) to avoid the zero velocity region at $z = z'$. We have

$$t^\circ = \int_0^{fz'} \frac{w\ dz}{|u_0|(z' - z)} = \frac{w \ln (1 - f)}{-|u_0|} \tag{32}$$

For components that are retained during the entire focusing process, the focusing time is increased by the factor $1/R$ (see eq 15), giving

$$t_{rf} = \frac{w \ln (1 - f)}{-|u_0|R} = \frac{V^\circ \ln (1 - f)}{-\dot{V}_c'R} \tag{33}$$

where again we have used $u_0 = \dot{V}_c/bL$ and $V^\circ = Lbw$ (see eq 17) to obtain the second expression. For simplicity the discussion is limited to a high retention ratio where eq 14, $R = 6\lambda$, is valid. After the use of this and eq 13 with eq 33, we find

$$t_{rf} \simeq [w^2 \ln (1 - f)]/-6D \tag{34}$$

This expression indicates that the focusing time is independent of any flowrate and, for fixed f, the position of the focusing point. Major factors will be the sample type (as reflected in the diffusion coefficient) and channel thickness w. For high molecular weight samples with low diffusion coefficients run in thick channels, effective focusing may require a time ranging from minutes to hours.

Keeping the focusing point close to the inlet end will contribute to a narrow starting zone because the sample can then, at most, occupy the distance from the inlet end to the focusing point. Under these circumstances only a minimum duration of focusing flow will be needed to adequately sharpen the zone. More quantitatively, if z' is small, then f need not be so close to unity because the zone width is approximated by the product $2z'(1 - f)$. Thus the focusing time expressed in the last equation will decrease at lower z' values for a fixed zone width. Consequently the problem of long focusing times appears to be surmountable.

We note that the focusing zone eventually reaches a steady-state Gaussian profile (*7*) for which the variance can be approximated as that applicable to molecules positioned at the mean elevation $x = l$. We obtain

$$\sigma^2 = w^2/6 \tag{35}$$

which shows that the final zone width is independent of the

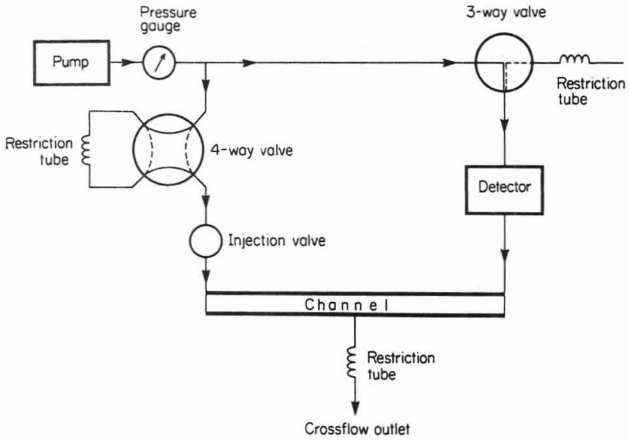

Figure 6. Illustration of flow system. The indicated flow direction and valve positions are for opposing flow relaxation and focusing. Dotted lines indicate valve positions during elution.

component's diffusivity or other properties.

EXPERIMENTAL SECTION

The flow FFF channel was a modification of a channel assembled essentially according to ref 3 and 2. A Lucite block was equipped with a frit of high-density polyethylene having a pore size of about 5 μm. The frit supported a Diaflo ultrafiltration membrane type YM5 obtained from Amicon. This skin membrane consisting of a cellulosic material served as the accumulation wall with a molecular weight cutoff of about 5000. The membrane was stretched lengthwise along the frit by a stretching device in order to even out small creases. The membrane was then covered with a spacer sheet of Teflon of 0.51 mm (0.020 in.) thickness from which a section was cut and removed. The cut, defining the dimensions of the channel, was 43 cm long from tip-to-tip and 2.1 cm (except for the tapered ends) in breadth.

The Teflon spacer was covered by a glass plate to form the upper wall of the channel. Inlet and outlet holes were drilled in the plate to coincide with the two tips of the cutout channel. Teflon tubing of inner diameter 0.5 mm and stainless steel tubing of inner diameter 0.8 mm were fitted into the holes for the outlet and inlet end, respectively. The assembly was clamped together between Lucite blocks, the lower one supporting the frit and membrane. At the conclusion of the experiments the channel was disassembled and the thickness of the spacer measured at 18 points was found to be an average of 0.52 mm. The breadth of the cut in the spacer obtained at eight positions averaged 2.07 cm (except for the tapered ends) as measured by the distance between the imprints made by the spacer's edges along the membrane. These dimensions, together with the tip-to-tip length, give the channel a volume of 4.25 mL.

Sample loading was accomplished by injection through a Rheodyne 7010 sample injection valve equipped with a 20-μL loop. The outlet end of the channel was connected to a Kratos SF 769 Z variable-wavelength UV detector set at 280 nm for the detection of proteins and 645 nm for $CuSO_4$.

Carrier inlet flow was delivered by a Kontron LC pump 410. It was equipped with a Kontron pulse dampener (a coil of approximately 25 mL volume) filled with air. The pulse dampener was followed by a stainless steel restriction tube of 2 m length and 0.25 mm i.d. The restriction tube gave sufficient back pressure for the proper functioning of the pulse dampener and the check valves of the pump. Pulse dampening was necessary in order to reduce detector noise resulting from the flow pulses caused by the reciprocating piston. The flowrates through the outlet end of the channel and the accumulation wall were regulated by the use of flow restrictors made from stainless steel tubing of inner diameter 0.25 mm and inserted into either or both of the effluent lines. Manually operated Hamilton miniature inert valves were used for switching between the sample relaxation and elution steps.

Flowrates were measured with a buret and stopwatch. A pressure gauge was mounted between the pump and the injector.

Soon before or after the sample was loaded, the flow from the pump was divided in two streams, one entering the channel at the inlet end, the other at the outlet end (see Figure 6). The combined flowstreams exited through the accumulation wall. Under the influence of the two opposing flowstreams thus created in the channel, the sample components were allowed to relax to their equilibrium distribution and approach the focusing point. After sufficient time the flowrate setting of the pump was changed and the flow was directed only to the channel inlet end for elution of the sample components.

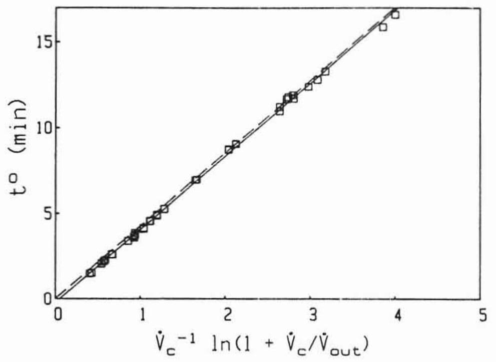

Figure 7. Dependence of void time t°, as measured by a $CuSO_4$ peak, on the flowrate term $\dot{V}_c^{-1}$ ln (1 + $\dot{V}_c/\dot{V}_{out}$). Solid line is least-squares regression of experimental points (slope = 4.27 mL); dashed line is theory using V° = 4.25 mL. Flowrate ranges are as follows: $\dot{V}_c$ = 0.06–2.7 mL/min; $\dot{V}_{out}$ = 0.11–1.7 mL/min; $\dot{V}_c/\dot{V}_{out}$ = 0.13–8.5.

The carrier contained 0.12 M tris(hydroxymethyl)aminomethane (Trizma base, Sigma) and 0.1 M HNO_3, giving a buffer of pH 7.3 and ionic strength 0.1 M. A small amount, 0.02%, of NaN_3 was added to the carrier.

The position of the focusing point was regulated by adjusting the length of the restriction tube in the four-way valve (Figure 6) until a colored sample was focused at the desired position. In some cases a setup of two pumps was used and the focusing point was then regulated by the ratio of the flowrates of the two pumps.

The sample components were proteins purchased from Sigma Chemical Co., including cytochrome *c*, bovine albumin, and thyroglobulin. They were dissolved in the carrier buffer to concentrations around 1% (w/v).

RESULTS AND DISCUSSION

An accurate determination of the retention ratio requires the availability of an accurate value for the void time t° and void volume V°. The void time can in favorable cases be measured experimentally as the elution time of an unretained compound. It can also be obtained from the void volume estimated on the basis of channel dimensions. In the latter case eq 19 or eq 20 can be used.

The validity of eq 20 was tested by measuring the elution time of $CuSO_4$. The diffusion coefficient is sufficiently high to avoid retention under the flow conditions used. The measurement of elution time (to the peak center) was made on the fraction of the sample that does not wash out of the channel through the accumulation wall. The results are summarized in Figure 7 where elution time data are plotted according to eq 20, which predicts zero intercept and a slope equal to the void volume. The dashed line represents the void time calculated by using the geometrically measured volume of 4.25 mL for V°. The good linearity, near-zero intercept, and a slope value close to the known geometrical volume of the channel indicate that good void times/volume measurements are possible in these systems despite partial losses of the test component through the permeable wall. We note that the lowest t° values in Figure 7 fall below the theoretical line. This might be related to the increased tailing of the peak profiles obtained at higher sample velocities. Best accuracy is obviously obtained at lower sample velocities, generally for elution times >5 min. However, even these elution profiles had slight tailing, caused largely by the sample injection technique. Visual observation of the copper sulfate sample

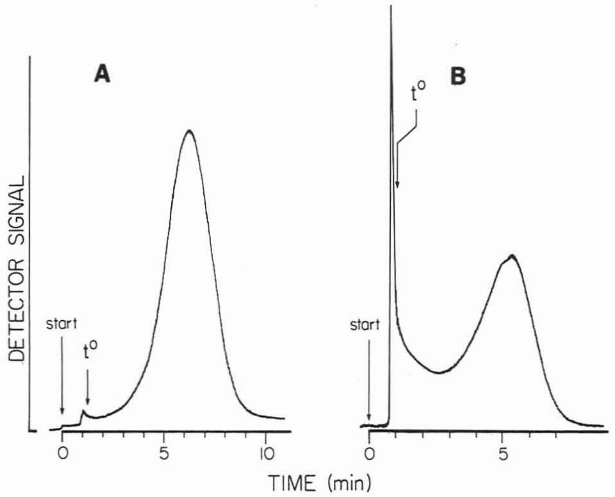

Figure 8. Comparison of cytochrome *c* peaks obtained with two sample relaxation methods. Flowrates during elution are as follows: $\dot{V}_{in}$ = 4.9 mL/min (23 psi); $\dot{V}_c$ = 3.19 mL/min; $\dot{V}_{out}$ = 1.75 mL/min. (A) Opposing flow relaxation with z' = 4.1 cm and cross flowrate ($\dot{V}_{in}'$ + $\dot{V}_{out}'$) = 3.4 mL/min (21 psi); relaxation/focusing time (preceding "start"), 17 min (τ(95%) = 10 min). (B) Reverse flow relaxation using cross flowrate = 4.9 mL/min (36 psi) and relaxation/focusing time = 19 min (τ(95%) = 6 min).

through the upper glass wall revealed a considerable trailing-out of sample as it emerged from the inlet tubing, causing an asymmetric starting profile. When high longitudinal velocity is used, it is therefore preferable to calculate $t°$ from eq 19 or eq 20 using a value for $V°$ obtained from other experiments.

The behavior in the channel of a well-retained component, cytochrome *c*, was investigated. Sample relaxation was performed with both the reverse flow and the opposing flow methods. The reverse flow method did not give effective relaxation as demonstrated in Figure 8. The peak occurring close to the void time appears to come from the incompletely relaxed sample fraction (cf. ref 9). The same figure demonstrates successful sample relaxation using the opposing flow method. Here there is no major response at the void time. On the other hand the peak has a slight "fronting" which points to some deviation from complete relaxation.

The reason for the failure of the reversed flow method may be convective mixing at the very tip of the channel inlet end occurring when the inflow through this end is initiated at the end of the relaxation period. During the reversed flow the sample has been forced into a narrow zone at the inlet end and the part which is closest to the tip of the channel may be susceptible to disturbance by mixing when the elution is started.

With opposing flows a small fraction of the focused zone could be clearly observed (through the glass plate) to move ahead of the main fraction on going from the relaxation period to the elution period, immediately resulting in a "fronting" zone profile. This explains the "fronting" of the recorded peak in Figure 8 and possibly also the minor response occurring close to the void time. The peak profile did not improve upon using longer relaxation times, which indicates that relaxation had reached some terminal stage at the lower relaxation times predicted by eq 27. Several experiments using focusing at different points between the inlet end and the midpoint of the channel did not change the peak profile significantly. Neither did the use of a gradually increasing channel inlet flow just before switching to the elution period.

The focusing of the colored protein cytochrome *c* resulted in a visible equilibrium band of a few millimeters width as shown in Figure 9. The inlet end is to the right. The band, extending across the breadth of the channel, shows no substantial edge effects; only a small amount of incremental band broadening is expected at the edges at equilibrium. However, significant edge effects were observed during migration toward equilibrium.

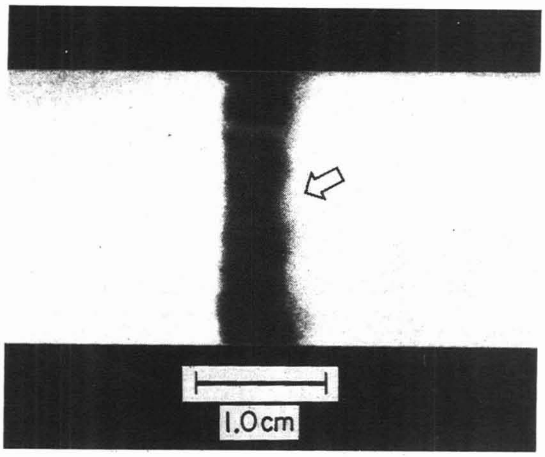

Figure 9. Photograph of focused sample of cytochrome *c* using opposing flow relaxation. The focusing point was at z' = 22.5 cm and the cross flowrate ($\dot{V}_{in}'$ + $\dot{V}_{out}$) was 6.2 mL/min.

The front and back of the zone formed quite sharp boundaries perpendicular to the longitudinal axis of the channel, as shown in the figure. This suggests that the longitudinal flow velocity around the focusing point is quite homogeneous across the breadth of the channel. When focusing closer to the inlet end of the channel, the boundaries were often more uneven. Gross variations of the permeability of the accumulation wall would lead to deviations in the longitudinal flow velocity and therefore the front and back boundaries of the focused sample zone would not form straight lines perpendicular to the longitudinal axis of the channel. Focusing at different points in the channel might therefore be developed as a test of the homogeneity of the permeability of the accumulation wall (the membrane plus the supporting frit).

Various other ways of performing the focusing/relaxation step were tested and gave results not significantly different from those described above. This included keeping the flowrate through the channel inlet end constant while the counterflow was switched on and off. This led to inconveniently high pressures, resulting in leakage, when the focusing point was close to the channel inlet end.

The switch from relaxation/focusing to elution requires a change of the flowrate of the pump and will induce pressure changes in the channel. The largest change of flowrate occurs when the ratio $\dot{V}_c/\dot{V}_{out}$ is low, which often will be the case for samples of low diffusion coefficients.

Because flowrates are adjusted by flow restrictors (Figure 6), the use of detector units giving high resistance to flow should be avoided in order not to reach inconveniently high pressures in the channel, especially at low $\dot{V}_c/\dot{V}_{out}$ ratios.

To demonstrate the ability of the channel to separate macromolecular components, some fractionations of protein mixtures were made. Figure 10 illustrates the separation of three proteins of molecular weights 12384, 68000, and 669000. The flowrates during elution were optimized according to the principles given in ref 2, which require a high cross flowrate, giving a high degree of retention (low *R*), balanced by a high longitudinal flowrate in order to ensure rapid elution. The diffusion coefficients calculated from the observed retention ratios were in good agreement with known values. The resolution appears to be comparable to results from flow FFF with uniform channels (*12*) but the fractionation time is shorter. It is likely that these results could be considerably improved and extended with further work.

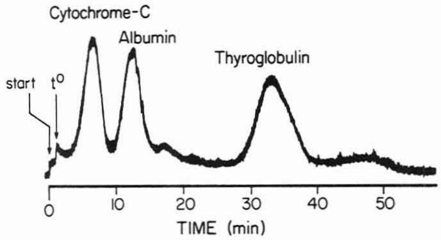

Figure 10. Separation of cytochrome *c*, albumin, and thyroglobulin in an asymmetrical system using opposing flow relaxation with $z' = 4.0$ cm, relaxation/focusing time (preceding "start") = 23 min (τ(95%) = 10 min), and cross flowrate = 3.1 mL/min. Flowrates during elution are $\dot{V}_{out} = 1.69$ mL/min and $\dot{V}_c = 3.24$ mL/min. Retention ratios were 0.20, 0.10, and 0.04, which gave diffusion coefficients of 1.2×10^{-6}, 6.0×10^{-7}, and 2.3×10^{-7} cm²/s, respectively.

ACKNOWLEDGMENT

We are grateful to P. Stephen Williams for assistance with computer calculations and some mathematical derivations.

LITERATURE CITED

(1) Giddings, J. C. *Anal. Chem.* **1981**, *53*, 1170A.
(2) Wahlund, K.-G.; Winegarner, H. S.; Caldwell, K. D.; Giddings, J. C. *Anal. Chem.* **1986**, *58*, 573.
(3) Giddings, J. C.; Myers, M. N.; Caldwell, K. D.; Fisher, S. R. In *Methods of Biochemical Analysis*; Glick, D., Ed.; Wiley: New York, 1980; Vol. 26, p 79.
(4) Giddings, J. C.; Yang, F. J.; Myers, M. N. *Anal. Chem.* **1976**, *48*, 1126.
(5) Lee, H.-L.; Reis, J. F. G.; Dohner, J.; Lightfoot, E. N. *AIChE J.* **1974**, *20*, 776.
(6) Giddings, J. C. *Sep. Sci. Technol.* **1986**, *21*, 831.
(7) Giddings, J. C. In Treatise *on Analytical Chemistry*; Kolthoff, I. M., Elving, P. J., Eds.; Wiley: New York, 1981; Part I, Vol. 5, Chapter 3.
(8) Giddings, J. C.; Yang, F. J.; Myers, M. N. *Science (Washington, D.C.)* **1976**, *193*, 1244.
(9) Yang, F. J.; Myers, M. N.; Giddings, J. C. *Anal. Chem.* **1977**, *49*, 659.
(10) Hovingh, M. E.; Thompson, G. H.; Giddings, J. C. *Anal. Chem.* **1970**, *42*, 195.
(11) Giddings, J. C. *Anal. Chem.* **1986**, *58*, 735.
(12) Giddings, J. C. *Anal. Chem.* **1985**, *57*, 945.
(13) Giddings, J. C.; Yang, F. J.; Myers, M. N. *Anal. Biochem.* **1977**, *81*, 395.

RECEIVED for review November 5, 1986. Accepted January 29, 1987. This work was supported by Grant No. GM10851-29 from the National Institutes of Health and was presented in part at the Tenth International Symposium on Column Liquid Chromatography, San Francisco, CA, May 18–23, 1986.

Retention by Electrical Field-Flow Fractionation of Anions in a New Apparatus with Annular Porous Glass Channels

Joe M. Davis, F.-R. F. Fan, and A. J. Bard*

Department of Chemistry, University of Texas at Austin, Austin, Texas 78712

A new apparatus for electrical field-flow fractionation (EFFF) studies utilizing annular porous Vycor glass (PVG) tubes to define a channel between external carbon and internal platinum electrodes is described. The anions poly(styrenesulfonate) and chromium phthalocyaninetetrasulfonate were retained by EFFF in four annular PVG channels having different channel widths with either high- or low-conductivity aqueous carrier. Experimental retention ratios depart considerably from predictions based on the theoretical EFFF parameter λ, and the departures cannot be explained by channel dead volume, solute relaxation, electroosmotic flow, or screening of the anionic charge by counterions. Results are partially explained by large solute transference numbers and polarization of carrier by the electric field. Experimental plate heights nevertheless agree well with theoretical expectation, when λ is estimated from experimental retention ratios and retention theory. The available PVG tubes are probably too rough to attain retention ratios much smaller than 0.35 and the PVG surface becomes pitted during column use, seriously limiting column lifetime and reproducibility.

Electrical field-flow fractionation (electropolarization chromatography) is a subtechnique of the chromatographic-like separation family, field-flow fractionation (FFF), in which charged species (e.g., ions, proteins, polyelectrolytes, or colloids) are concentrated near the wall of an open channel by an electric field and are differentially transported through the channel by laminar flow. Following sample injection, each species relaxes in the applied field toward one channel wall (the accumulation wall) and forms a quasi-equilibrium concentration distribution (zone) whose characteristic thickness depends (in the simplest case) on temperature and the electrical force on the constituent members of the species. Zones tightly localized near the wall are transported by flow less rapidly than the less localized zones, because the flow is less rapid near the channel walls than in the channel midsection. The fundamental principles of FFF have been detailed elsewhere (*1–4*).

In spite of numerous efforts (*5–12*), the three-component protein separation originally communicated by Caldwell et al. (*5*) and later refined by Kesner et al. (*7*) is the best multicomponent separation by electrical field-flow fractionation (EFFF) reported to date. Given the apparent difficulty in developing a useful EFFF system, further research seems justifiable only if such a system has desirable features lacking in other multicomponent separation methods based on free flow electrophoresis, such as flat fluid band (or fluid curtain or free flow) electrophoresis, continuous flow and density gradient isoelectric focusing, and capillary isotachophoresis and zone electrophoresis. Some minor shortcomings of these methods are noted here to highlight more fully several potential advantages of EFFF. Flat fluid band electrophoresis, although widely used for preparative biological separations, is largely limited by resolution (*13*). Separations based on continuous flow and gradient density isoelectric focusing are relatively slow and frequently require more than 1 day to complete (*14*); they are further complicated by the need to separate the resolved species from the ampholytes that form the pH gradients characteristic of the methods. The small column volumes encountered in capillary isotachophoresis and (especially) zone electrophoresis necessitate the use of so-

0003-2700/87/0359-1339$01.50/0 © 1987 American Chemical Society

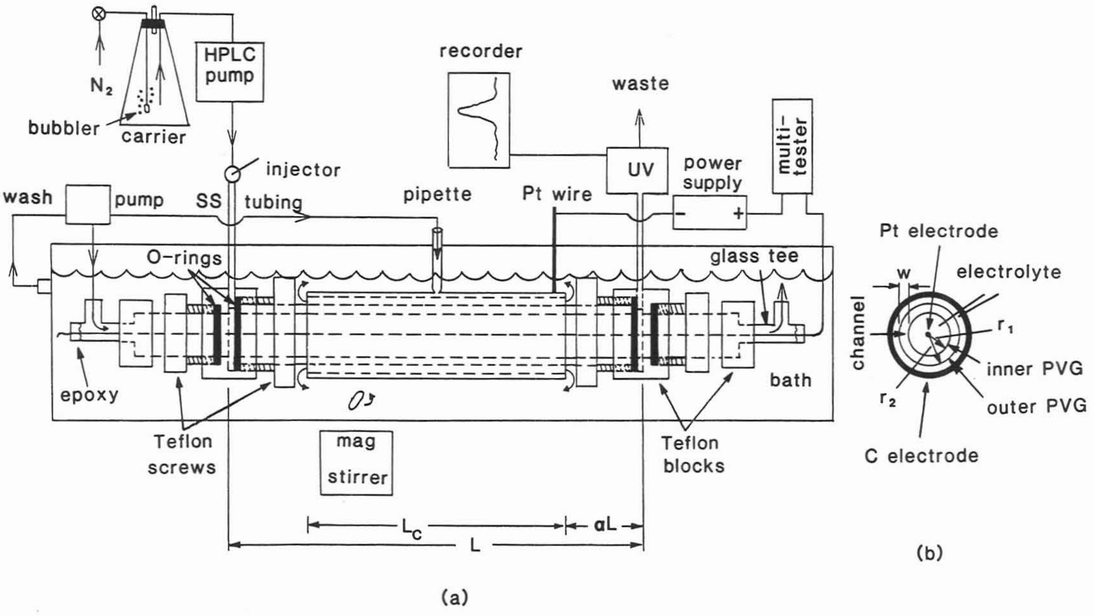

Figure 1. (a) Schematic of EFFF channel constructed from PVG and ancillary apparatus. (b) Cross-sectional side view of channel.

phisticated injection and detection devices (as in capillary LC) and preclude preparative-level separations. Capillary electrophoresis has deservedly attracted much attention because of its high efficiency (*15–18*), but the system's peak capacity is fundamentally limited by the electroosmotic (electroendosmotic) flow that sweeps out the capillary contents.

In contrast, a well-designed EFFF system constructed from inert materials, if one can generalize from more successful FFF methods, should be capable of the rapid high-resolution analytical- or preparative-scale fractionation of mixtures using conventional LC injectors and detectors. High-resolution separations should be attainable in short times by tightly focusing zones at the accumulation wall and rapidly pumping carrier through the channel. Preparative-scale fractionations should be possible with little loss in resolution by increasing the channel cross section while keeping the channel gap small. Furthermore, the peak capacity of EFFF is fundamentally unlimited by the elutive nature of the separation process. In addition, either a steady-state or variable electric field could be used (*19*); the latter would permit separations based on transport parameters as well as charge. These combined features are sufficiently attractive to warrant continued effort to develop a near-ideal system or, failing that, to discover and characterize the fundamental limitations prohibiting its development.

A number of inherent problems must be solved in designing a useful EFFF apparatus. The electrodes that are used to impose the field are in contact with the electrolyte solution and will, of necessity, have faradaic reactions occurring at their surfaces. If the channel walls are defined by these electrode surfaces, gas production at them will disrupt the formation of zones. Moreover corrosion of the electrodes can occur, causing roughening of the surfaces. While it might be possible to minimize such effects by judicious choice of solution–electrode reactions or by forming a suitable layer on the electrode surface (e.g., a conductive polymer with a high electrical capacity), initial experiments in our laboratory with polypyrrole-coated stainless steel electrodes were unsuccessful (*20*). A truly versatile apparatus will probably require that the electrodes be separated from a flow channel defined by a porous separator or an ionically conducting membrane. In previous EFFF apparatus, the channels were defined by dialysis membranes or ultrafiltration fibers (*5–12*). However, for good performance, the channel walls must be very smooth and the separators must be rigid enough to maintain a uniform channel over the full channel length, while permitting sufficient ion flow to yield a significant potential drop across the flowing electrolyte. The separator material should also be chemically inert and not adsorb solution components; the latter would lead to chromatographic effects superimposed on the EFFF process.

We report here the retention by EFFF of the anions poly(styrenesulfonate) (PSS) and chromium phthalocyaninetetrasulfonate (CrPcTS) in annular channels formed from concentric tubes of porous Vycor glass 7930 (PVG), a highly porous glass network of 40-Å-diameter pores (*21*) that permit the transport of small ions. A schematic representation of this EFFF configuration is shown in Figure 1. The study was restricted to anionic species because PVG, a strong cation exchanger (*22, 23*), strongly adsorbed cationic species (e.g., $Ru(bpy)_3^{2+}$, methyl viologen, and Cr^{3+}). The anions were retained in four PVG channels having different gap widths using both buffered and unbuffered aqueous carrier. The results for CrPcTS are the first reported for the retention by EFFF of a species that is not a polyelectrolyte. Overall the results unfortunately fall well short of realizing the potential of EFFF noted above.

THEORY

The simplicity of the mathematical functions for the perpendicular electric field and the velocity profile in EFFF columns has facilitated the derivation of fairly rigorous equations governing zone migration and dispersion. The average velocity ν of a species in any form of FFF is usually measured relative to the average linear velocity $\langle \upsilon \rangle$ of the carrier by retention ratio R (*24*)

$$R = \frac{\nu}{\langle \upsilon \rangle} = \frac{\langle c^* \upsilon \rangle}{\langle c^* \rangle \langle \upsilon \rangle} = \frac{V^\circ}{V_R} = \frac{t^\circ}{t_R} \qquad (1)$$

where c^* is the quasi-equilibrium concentration distribution, υ is the velocity profile of the carrier, V° is the column void volume, t° is the time required to pump one void volume through the channel, V_R is the retention volume, or volume of eluant corresponding to the first moment of the peak generated by the species, and t_R is the time required to elute volume V_R. The broken brackets indicate that c^* and υ are averaged over the channel cross section.

The exact form of R depends on the channel type and electrode configuration, which determine c^* and υ. Equations for R have been derived for an open parallel-plate channel

Table I. Characterization of EFFF Channels

channel	V°(geometric),[a] cm^3	w,[a,b] μm	L_c, cm	L, cm	ρ_1	α	preparation of PVG
A	2.22 ± 0.06	610 ± 20	9.52	15.62	0.85	0.19	acid activated
B	2.33 ± 0.07	610 ± 20	9.52	16.36	0.85	0.21	virgin
C	7.79 ± 0.24	1020 ± 30	13.97	21.59	0.84	0.18	virgin
D	8.05 ± 0.25	1020 ± 30	13.97	22.86	0.84	0.19	virgin

[a] V° and w were calculated from 43 measurements made with dial calipers (±10 μm error) of the outer and inner diameters of the inner and outer tubes. Standard deviations were calculated by propagation of errors. [b] The small-gap (large-gap) channel was constructed from 7 and 10 (10 and 15) mm o.d. PVG.

(OPPC) (*24*) and a cylindrical ultrafiltration fiber (*6*) immersed in a uniform electric field E and for an annular channel immersed in a radial field (*25*). The OPPC R is the simplest and is

$$R = 6\lambda(\coth(2\lambda)^{-1} - 2\lambda) \qquad (2)$$

where

$$\lambda = \frac{D_l}{|U|w} = \frac{D_l}{|\mu E|w} = \frac{l}{w} \qquad (3)$$

In eq 3, D_l, U, and μ are the lateral diffusion coefficient, field-induced velocity, and electrophoretic mobility of a species and are assumed to be constant. Quantity l is the characteristic zone thickness and w is the distance between the two channel walls.

The Nernst–Einstein equation for mobility μ is (*26*)

$$\mu = zeD_l/kT \qquad (4)$$

where e is the electronic charge and z is the signed number of such charges. Thus eq 3 can be also written as

$$\lambda = \frac{kT}{e|zE|w} = \frac{kT}{e|z\Delta V|} \qquad (5)$$

where $\Delta V = Ew$ is the potential difference across gap w. Thus λ can be expressed as the ratio of the thermal energy kT that opposes zone formation to the magnitude of the electrical work $ze\Delta V$ that favors zone formation. Note that, as opposed to electrophoresis, where both molecular parameters z and D_l affect the transport of an ionic species, in EFFF the effect of D_l is absent. (D_l would influence zone transport if the electric field were varied with time (*19*).)

Although the channels used here are annular, the more complicated R derived for them differs by only 6.2% or less from eq 2 (*25*), which is consequently used for simplicity. Gap w for these channels equals $r_2 - r_1 = r_2(1 - \rho_1)$, where r_2 and r_1 are the radii of the larger and smaller tubes and $\rho_1 = r_1/r_2$.

When extracolumn effects (e.g., injector and detector dead volume) are negligible, peak (zone) dispersion in FFF is principally dictated by the differential transport by flow of a zone's constituent members. The dispersion expected in a cylindrical fiber (*27*) and an OPPC (*28*) has been evaluated and can be expressed for the latter geometry as the nonequilibrium contribution H_n to plate height

$$H_n = \frac{\psi(\lambda)l^2\nu}{D_z} = \frac{\psi(\lambda)l^2R\langle v\rangle}{D_z} \qquad (6)$$

where ψ is a mathematically complicated coefficient defined elsewhere (*28*) that approaches the value 4 as λ approaches zero and D_z is the (constant) axial diffusion coefficient. (Equation 6 is strictly the long-time limit for H_n, which must otherwise be evaluated numerically for "short" times (*29*).) H_n is clearly reduced by reducing zone thickness l, i.e., by decreasing R.

Equations 2 and 6 were derived by assuming that distribution c^* describes the zone's lateral concentration along the full channel length. A characteristic time $\tau = w/U = \lambda w^2/D_l$ is required for the zone constituents to relax into the steady-state distribution (*30*). When a zone is transported by flow prior to this relaxation process, the R and H_n expected are greater than the above predictions, because zone species are transported by widely differing velocities during relaxation (*24, 31*). Analytical corrections to R and H_n exist only for the $\lambda \rightarrow 0$ limit (*24*); general corrections must be obtained approximately (*24*) or numerically (*32*).

Relaxation effects can frequently be eliminated by applying the field for a time $>\tau$ after introduction of sample into the channel but prior to the commencement of flow (*30*). For our apparatus shown in Figure 1, however, the channel fraction inside the carrier entrance and exit blocks is virtually insulated from the field, and departure from the above equations is inevitable. An approximate correction to R that is analogous to the R correction for solute relaxation proposed by Hovingh et al. (*24*) is presented here to account for this "dead volume".

If relaxation effects are negligible (and data presented later suggest that they are), to a first approximation a solute will migrate at carrier velocity $\langle v\rangle$ through the entrance block, quickly relax to the velocity ν characteristic of its quasi-equilibrium distribution, and then migrate through the exit block with some characteristic velocity $\bar{v} = \nu + n(\langle v\rangle - \nu)$ between ν and $\langle v\rangle$, where $0 \leq n \leq 1$. If α equals the fractional channel length inside either insulating block, the times, t_1 and t_2, the solute spends inside the entrance and exit blocks are $t_1 = \alpha L/\langle v\rangle$ and $t_2 = \alpha L/\bar{v}$, where L equals the channel length. Similarly, the time t_3 for which solute experiences the field is $(1 - 2\alpha)L/\nu$. The total time t_R that solute is retained is $t_R = t_1 + t_2 + t_3$. Since the time t° corresponding to a void peak is $L/\langle v\rangle$, the experimentally observed retention ratio R^* is related to $R = \nu/\langle v\rangle$ by

$$R^* = \frac{t^\circ}{t_R} = \frac{V^\circ}{V_R} = \frac{R}{1 - \alpha(2 - R - (1 + n(R^{-1} - 1))^{-1})} \qquad (7)$$

An analogous general correction to nonequilibrium plate height H_n is considerably more complicated, even for the $\lambda \rightarrow 0$ limit. Equation 6 necessarily underestimates H_n for this channel because zones are also considerably broadened by flow in the carrier entrance and exit blocks, in which zone thickness l approaches infinity. As is shown below, however, reasonable agreement is nevertheless found between experimental plate heights and eq 6, which is consequently used here as a conservative estimate for H_n.

EXPERIMENTAL SECTION

PVG tubes (7, 10, and 15 mm nominal outside diameters) were obtained from Corning Glass Works (Corning, NY) and were used as received or following surface modification (see below). The characterizing features of the four EFFF channels constructed from these tubes are reported in Table I.

The PVG tubes were held rigidly in an annular configuration by two Teflon blocks, tapped and drilled as shown in Figure 1. The smaller tube passed through both blocks, whereas the ends of the larger tube terminated inside the blocks, adjacent to the $^1/_{16}$-in stainless steel tubing (0.020 in. i.d.) through which carrier entered and exited the channel. Leakage of the channel contents was prevented by rubber O-rings.

The radially symmetric electrodes were isolated from gap w to prevent bubbles formed during electrolysis from disrupting zone formation. The inner electrode (anode) was formed by centering and stretching tautly inside the inner tube a 0.127–0.5 mm Pt wire, which was epoxied to two borosilicate glass tees connected to the inner tube by Teflon blocks (see Figure 1). The outer electrode (cathode) was formed by clamping together around the larger PVG tube two half-cylindrical pieces of graphite, which were made by first drilling out a graphite rod (Ultra Carbon Corp., Sherman, TX) and then halving it. Electrical contact to the graphite was made with a Pt wire. These electrodes form essentially equipotential surfaces; it was estimated that only 1.25 V or so would be dropped over the full Pt wire length under the worst of possible conditions (current, 525 mA; Pt wire diameter, 0.127 mm).

The channel and electrodes were submerged in a stirred bath containing electrolyte (initially) identical in composition with the carrier fluid. The bath was continuously circulated over the electrodes to reduce polarization from gas bubbles.

The conductivities of the column influent and effluent and of the bath were measured with a RC-16B-1 conductivity bridge (Industrial Instruments, Cedar Grove, NJ) operating at 1 kHz. The bath conductivity was found to increase with time (especially for low-conductivity baths), most probably because of slow decomposition of the graphite electrode. (An IR spectrum of a methylene chloride extract of one bath contained sharp bands in the carbon fingerprint region.) A fresh bath was consequently prepared after one to five experiments, depending upon the bath composition. The decomposition of the carbon electrode was greatly accelerated by reversing the electrode polarity (i.e., Pt, −; C, +), which precluded outer-wall retention studies.

Unbuffered solutions of the sodium salts of PSS (ICN Pharmaceuticals, Inc., Plainview, NY; Polysciences, Inc., Washington, PA) and the potassium salts of CrPcTS were prepared from deionized water (MQ) generated by a Milli-Q reagent water system. Solutions buffered at pH 8.0 were prepared from reagent grade KH_2PO_4 and KOH and deionized water. Solute concentrations ranged from 0.8 to 2.5 mg/mL. No more than 25 μL of sample solution was injected at one time.

The carrier was introduced to the column by a Perkin-Elmer LC-65T liquid chromatography pump. Solutes were injected, using a 25-μL Hamilton syringe, onto the column via a 7125 Rheodyne sample injector and were detected by a Perkin-Elmer LC-65T UV–vis detector operating at 240 nm. A constant dc voltage was impressed across the electrodes by a Harrison 6205B dual power supply (Hewlett-Packard, Palo Alto, CA) or a variable power supply (General Radio Co., Cambridge, MA). Currents were measured with a range doubler multitester (Radio Shack, Fort Worth, TX). Fractograms were recorded by an Omnigraphic 3000 recorder (Houston Instruments, Austin, TX) and digitized manually with a Hipad digitizer (Houston Instruments). Peak areas and first and second moments were estimated from these digitized fractograms.

The surface of the PVG was chemically modified to compare the performance characteristics of modified and virgin PVG. First the siloxanes formed during the glass manufacture were hydrolyzed in 1 M HNO_3 (90 °C for 1 h). After being washed repeatedly with deionized water, the PVG was either used directly or further modified by reaction with halosilanes or poly(ethylene glycol) (PEG). The former procedure was carried out by bubbling dry N_2 through liquid triethylbromosilane (Aldrich Chemical Co., Milwaukee, WI) or n-octyldimethylchlorosilane (Petrarch Systems, Bristol, PA) and passing the diluted vapors for 48–120 h through a 160 °C silanized glass tube containing acid-treated PVG previously dried under vacuum ($<10^{-4}$ torr at 160 °C). The latter modification was carried out by bonding a 4000-molecular-weight PEG (Anspec Co., Ann Arbor, MI) to acid-treated PVG via γ-glycidoxypropyltrimethoxysilane (Aldrich), using the procedure reported by Chang et al. (*33*).

The macroscopic surface roughness of PVG was characterized with a JEOL JSM 35C scanning electron microscope and a Sloan Dektak profilometer having a 25-μm-diameter stylus.

PROCEDURES

The ranges of the observable retention ratios R^* of PSS and CrPcTS are reported in Table II as eight data sets. The R^* values were calculated from the first moments V_R of the solutes' elution profiles and eq 7; the appropriate geometrical void volumes V° are reported in Table I. The corrected ratios R were then calculated from these R^* values and eq 7, using the α values reported in Table I. The quantity n in eq 7 was set to zero, so that the resultant R's slightly overestimate the true ones.

To access the agreement between experimental and theoretical R's, the former were plotted against $(\Delta V)^{-1}$, the reciprocal of the estimated potential difference across gap w. This potential difference was not measured (e.g., by inserting electrical probes in the channel) because the voltage so measured would equal ΔV plus two potential drops of unknown magnitude across the double layers at the probe-solution interfaces; ΔV alone cannot be measured. The field (and potential) distribution in the gap is theoretically governed by the current density, carrier conductivity, and geometrical properties of the annulus (exclusive of the few angstroms over which the potential also drops across PVG–solution interfaces), which are known or presumably measurable. Assuming the field distribution was uniform (this assumption will be examined later), ΔV was estimated as

$$\Delta V = IR_{\rm a} = \frac{I}{\sigma}\,\frac{\ln\,(1/\rho_1)}{2\pi L_{\rm c}} \tag{8}$$

where $R_{\rm a}$, σ, and $L_{\rm c}$ are the resistance of a uniform annulus, the average conductivity of the column effluent and the bath, and the carbon electrode length, respectively. (The ranges of I, σ, and ΔV are reported in Table II; $L_{\rm c}$ values are reported in Table I.) The data set $((\Delta V)^{-1}, R)$ was then fit using nonlinear least squares to the following modified form of eq 2

$$R = \frac{6A}{\Delta V}\left(\coth\left(\frac{2A}{\Delta V}\right)^{-1} - \frac{2A}{\Delta V}\right) \tag{9}$$

Examination of eq 2, 3, 5, and 9 shows that A should equal $kT/|z|e = D_1/|\mu|$. The expected and least-squares A values are reported in Table II as the ratio $Y = |z|eA/kT = |\mu|A/D_1$. Y is less than, equal to, or greater than unity when R is less than, equal to, or greater than the prediction of eq 2.

Plate heights H were calculated from the second moment $\sigma_{\rm V}^2$ of the profile about mean $V_{\rm R}$ as (*35*)

$$H = L(\sigma_{\rm V}^2/V_{\rm R}^2) \tag{10}$$

(Column lengths L are reported in Table I.) Henceforth H is identified with the nonequilibrium plate height $H_{\rm n}$. It is also assumed that $D = D_1 = D_z$.

Peak area was found to decrease with increasing field strength. To characterize this decrease, the area of each retained peak was divided by the average area of several peaks generated under zero-field conditions (i.e., void peaks) to obtain a relative peak area, RPA. The data set (ΔV,RPA) was then fit to a straight line using least squares. The slopes (s), intercepts (i), and correlation coefficients (r) of these fits are reported in Table II.

RESULTS AND DISCUSSION

Figure 2 is a plot of the R's of sets A–H vs. −log (ΔV). The curves are the least-squares fits of sets A, C, D, and F–H to eq 9. (For reasons discussed below, the five largest ΔV data were excluded from the least-squares fits.) The following was deduced from this figure and Table II. (a) All R's are larger than those predicted by theory ($Y > 1$), even after first-order corrections for "dead volume". (b) As ΔV is increased, R decreases, levels out at $R \approx 0.35$ over a small ΔV range, and then increases (sets A and F). Peak area nonetheless decreases linearly with increasing ΔV even after R has leveled out. (c) PSS70K (the "70K" designates a number-average molecular

Table II. Experimental Conditions for Data Sets A–H

data set	sample	symbol[a]	column	electrolyte	V^o(moments analysis), cm^3	I, mA	σ, $\Omega^{-1}\cdot$m^{-1}	ΔV, V	R^*	Y	RPA study
A	PSS70K	●	B	MQ	2.69 ± 0.18 (6)[b]	0.085–14.7	$(0.95\text{–}2.2) \times 10^{-4}$	0.023–22.6	0.34–0.80	358[c]	$i = 0.99$; $s = -0.046$; $r = -0.96$
B	PSS70K	△	A	phosphate		185–525	0.42–0.51	0.056–0.17	0.41–0.48		$i = 1.05$; $s = -1.63$; $r = -1.00$[d]
C	PSS16K	◐	C	MQ		6.4–10.8	$(3.0\text{–}6.9) \times 10^{-4}$	2.9–4.3	0.42–0.61	215[c]	
D	PSS70K	○	C	MQ	8.54 ± 0.00 (2)	2.9–12.3	$(3.2\text{–}4.4) \times 10^{-4}$	1.7–6.0	0.31–0.57	147[c]	
E	PSS200K	◪	C	MQ		4.4	4.2×10^{-4}	2.0	0.41		
F	CrPcTS	▼	D	MQ	7.81 ± 0.10 (3)	0.64–26.9	$(1.6\text{–}7.9) \times 10^{-4}$	0.67–15.0	0.39–0.85	51.4	$i = 0.99$; $s = -0.064$; $r = -0.92$
G	CrPcTS	□	D	phosphate	8.04 ± 0.68 (4)	30–150	0.12–0.13	0.046–0.23	0.86–0.91	10.1	$i = 1.13$; $s = -2.26$; $r = -0.99$
H	CrPcTS	■	A	phosphate	2.11 ± 0.08 (7)	185–525	0.44–0.55	0.11–0.30	0.76–0.93	9.8	$i = 0.95$; $s = -0.42$; $r = -0.95$

[a] Symbols represent the indicated data sets in Figure 2. [b] Number of replicates. [c] Based on $D/\mu \approx 1.4 \times 10^{-3}$ V. [d] Based on two data.

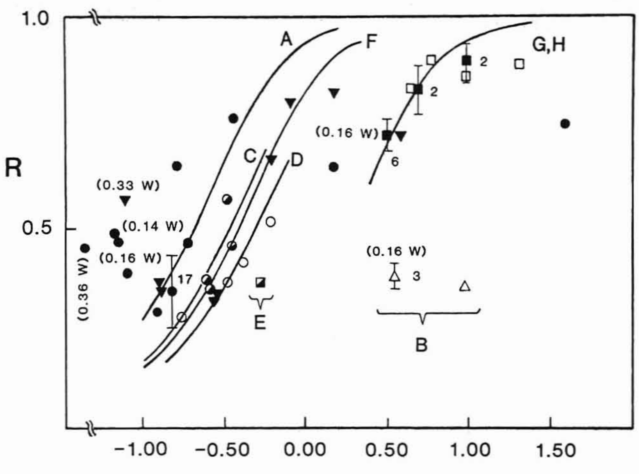

Figure 2. Plot of R vs. $-\log(\Delta V)$ generated from retention of PSS and CrPcTS. The curves are the least-squares fits of eq 9 to data sets detailed in Table II; a single curve depicts the fits to sets G and H. Numbers adjacent to points with error bars and in parentheses indicate the numbers of times experiments were repeated and the estimated powers dissipated within the channel as heat, respectively.

weight equal to 70 000) in MQ (set D) is only retained slightly more than PSS16K in MQ (set C) and is retained more in a large-gap (set D) than in a small-gap (set A) channel. PSS200K in MQ (set E) is retained somewhat more than the other PSSs in MQ (sets A, C, and D). (d) The R's of CrPcTS in MQ (set F) are comparable to those of PSSs in MQ. (e) The R's of PSS70K in MQ (set A) and CrPcTS in MQ (set F) are roughly independent of small ΔV values over the examined ΔV range. (f) The R's of buffered CrPcTS are approximately equal in small-gap (set H) and large-gap (set G) channels and most closely agree with theory.

As is shown further below, theoretical H_n values calculated from eq 6 using λ's estimated from experimental R's and eq 2, and l's from these λ's and eq 3, agree fairly well with experimental H values, even though $Y > 1$. Since H_n depends on λ and l (see eq 6), both parameters must be estimated fairly well to give agreement with experiment. The l's so estimated from the minimum retention ratio in Figure 2, $R \approx 0.35$ ($\lambda \approx 0.067$), are 40 and 68 μm in the small- and large-gap channels, respectively. Evidence nonetheless exists that l values smaller than these were experimentally realized. Assuming that the adsorption sites of PVG were never saturated during an experiment, the finding that peak area decreases with increasing ΔV, even after R has plateaued, indicates that solute is increasingly concentrated at the inner-tube wall. The concentration increases because the zone is more tightly focused at the accumulation wall, i.e., because l decreases. In the plateau region, however, R does not decrease with decreasing l, in contrast to the predictions of eq 2 and 3. An explanation consistent with both observations is that the minimum R value is dictated not by the magnitude of l but by the number of multiple relaxations zone species must undergo near a rough PVG surface (*24*). To support this assertion, it is noted that the l's calculated above are roughly twice the standard deviations of the gap widths reported in Table I and are consequently on the order of the standard deviations of the inner-tube radii. In general, a zone will be repeatedly distorted from its quasi-equilibrium distribution if it is carried by flow over a "roller coaster" of elevations and dips comparable in size to itself. Each distortion results in solute relaxation, which increases R; here, such relaxations are so numerous that they govern the minimum R value.

An alternative explanation for the plateau of R values is the polarization by the field of electrolyte ions, which can cause R to plateau in weakly conducting electrolytes, such as these

(*9, 11*). This is unlikely because the R's of highly buffered PSS70K (set B) are comparable to the R's in the plateau region.

R eventually increases as ΔV is further increased most probably because of ohmic heating and free convection. The electrical power $(\Delta V)^2/R_a$ dissipated within the channel as heat was calculated for each datum in Figure 2 and is largest for the largest ΔV values. (Some large powers are reported in the figure; such data were excluded from least-squares fits to eq 9.) Judging from the data, convection cannot be excessive, since zone formation is only disturbed slightly. A feeling for the amount of convection expected is gained by calculating an upper limit to the free-convective Nusselt number Nu for the experiment corresponding to the largest ΔV datum of set F, following the procedure of Pohl (*34*). From the upper limit ΔT to the temperature change over gap w

$$\Delta T = \sigma(\Delta V)^2/2\kappa \qquad (11)$$

the Prandtl number $\mathrm{Pr} = C_p\mu^*/\kappa$ of water, and the Grashof number Gr of the annular system

$$\mathrm{Gr} = g\beta\Delta T w^3/(\mu^*/\rho)^2 \qquad (12)$$

the Nu = Nu(Pr,Gr) number of the annular system could in principle be determined experimentally. (Symbols are defined in the Glossary.) Rather than do this, the Pr and annular Gr values calculated from the equations above were used to evaluate the Nusselt numbers corresponding to cylinders (Nu = 1.1), plates (Nu = 1.6), and spheres (Nu = 3.3) immersed in a uniform fluid (*36*). The annular Nu is probably comparable. These Nu's, on the order of unity, indicate that convection is minor, in agreement with experimental observation.

The departure of sets G and H from theory is surprising, since these R's are relatively large and should be more free of perturbations from wall effects than other data. This departure cannot solely be attributed to "dead volume" effects because setting parameter n in eq 7 to one (i.e., recalculating R from R^* assuming solute moves through the exit block with velocity $\langle v \rangle$) changes the reported R values by only −18% or less. Nor can the relaxation of solute to the accumulation wall explain the large but almost equal Y values, because relaxation time τ depends on w^2 for fixed λ (or ΔV) and the w's of channels A and D differ by the factor 1.7.

One possible origin of departure is the electroosmotic flow (EOF) that moves through the PVG capillary pores from anode to cathode (at pH 8), a direction opposite to field-induced velocity U. The volumetric flow rate $\dot{V}$ of carrier through the pores is proportional to current I (*37*) and consequently is largest in high-current experiments (such as these). This explanation is unrealistic because, as observed above, the Y values of sets G and H are similar, but the current ranges differ by roughly a factor of 3. In other words, the 3-fold change in $\dot{V}$ does not affect solute migration rate.

Additional evidence that EOF does not disturb zone formation was found experimentally by disconnecting column C from the carrier pump and measuring the rates at which a 0.001 M phosphate buffer (pH 6.05, $\sigma = 0.11\ \Omega^{-1}\cdot\mathrm{m}^{-1}$) flowed out of the column at different currents. (The bath is the origin of the flowing liquid, since the column does not empty.) A linear relationship between $\dot{V}$ and I was found ($r = 0.95$), with slope $\dot{V}/I = 2.2 \times 10^{-9}\ \mathrm{m^3/(A{\cdot}s)}$. This ratio is an underestimation of the potentially zone-disrupting EOF through the inner-tube pores since a fraction of this flow must also exit as EOF through the outer-tube pores. Assuming that this underestimation was minimal (see below), a series of EOF velocities was calculated as $\dot{V}/A'$, where $A' = 2\pi r_1 L_c$ is the inner-tube surface area exposed to field E. These velocities are 13% or less of the U's calculated from the experimental R's of sets G and H, eq 2 and 3, and the estimated D of CrPcTS, $5 \times 10^{-6}\ \mathrm{cm^2/s}$, which was calculated from the Reddy and Doraiswamy equation (*40*). (The above assumption was justified by calculating the ζ potential at the pore/solution interface expected to produce the experimental V/I ratio, using the theories of Rice and Whitehead (*38*) and Morrison and Osterle (*39*). The calculated $\zeta = -89$ mV closely agrees with the ζ potential of vitreous silica in a pH 6, 0.001 M KNO_3 solution, −94 mV (*37*). Thus it appears that most EOF comes from the inner tube and flows out of the channel, which is consistent with the observation of Kesner et al. that flexible OPPCs are expanded by EOF accumulating in the channel (*7*).)

Table III. Data for Sample Calculations of Transference Number t_i

species	μ_j, cm²/(V·s)	z_j	c_j, M	pH
$H_2PO_4^-$	-3.73×10^{-4} (*55*)	−1	3.45×10^{-3} [a]	8.0
			0.0248	4.5
HPO_4^{2-}	-5.91×10^{-4} (*55*)	−2	0.0215[a]	8.0
			4.87×10^{-5}	4.5
K^+	7.62×10^{-4} (*26*)	1	0.0503	8.0
			0.025	4.5
CrPcTS	-7.7×10^{-4}	−4	9.65×10^{-4} [b]	8.0
albumin	1.3×10^{-5} (*8*)	0.57[c]	1.5×10^{-5} [d]	4.5

[a] Total phosphate concentration (i.e., $[H_3PO_4] + [H_2PO_4^-] + [HPO_4^{2-}] + [PO_4^{3-}]$) was 0.025 M. $[PO_4^{3-}]$ is negligible at these pHs. [b] c_s = 1.0 mg/mL; molecular weight = 1036 g/mol. [c] Calculated from eq 4 and $D = 5.9 \times 10^{-7}\ \mathrm{cm^2/s}$ (*8*). [d] c_s = 1.0 mg/mL; molecular weight = 65 000 g/mol.

Sets G and H may furthermore depart from theory because no reduction in the effective CrPcTS charge due to screening of the anion by its counterion atmosphere was considered. The atmosphere thickness is relatively small in these concentrated electrolytes (12.7 Å in a pH 8.0, $\sigma \approx 0.45\ \Omega^{-1}\cdot\mathrm{m}^{-1}$ phosphate buffer), and thus a substantial fraction of the counterion atmosphere will migrate with CrPcTS during its electrophoresis, reducing its charge. This fraction lies principally between the radius of the anion (estimated from its geometrical structure as 9.5 Å) and the radius of hydrodynamic shear (estimated as 5 Å larger than the sphere radius (*26*)). This fraction was evaluated from data comprising set H as 0.17, using a theory describing the spatial distribution of counterions (assumed to be point charges) in the diffuse double layer surrounding a charged sphere (*37*). This approximation suggests that the effective charge on CrPcTS may be only 80% or so of its formal charge ($z = -4$). Furthermore, there is the possibility that CrPcTS forms an ion pair with one of its counterions, which would reduce the formal charge of the anion by one unit. Both these changes in charge are relatively small, however, and can at best only account partially for the departures reported in Table II.

One reason that the R's of sets G and H differ from theory is the surprising nonuniformity of field E that exists because CrPcTS carries a nonnegligible fraction of current I, even in these highly conductive electrolytes. The fractional current carried in solution by CrPcTS, or generally by the ith species, equals its transference number t_i (*36*)

$$t_i = z_i\mu_i c_i / \sum_j z_j\mu_j c_j \qquad (13)$$

where z_j, μ_j, and c_j are the charge, mobility, and concentration of the jth species in solution.

Simple calculations of t_i are given to illustrate this point. The required z_j, μ_j, and c_j values (the latter from set H) are reported in Table III. The concentrations of the various phosphate species and of potassium in the $\sigma \approx 0.45\ \Omega^{-1}\cdot\mathrm{m}^{-1}$ buffer were estimated from multiple equilibria and charge balance equations. The CrPcTS concentration corresponds to that injected, equivalent to 1 mg/mL. The CrPcTS mobility was estimated from $z = -4$, eq 4, and the diffusion coefficient of CrPcTS given earlier.

Based on these data, $t_i = 0.044$ for CrPcTS. In other words, over 4% of current I would be carried by CrPcTS, if the anion were distributed uniformly in solution. The fractional current attributable to CrPcTS migration in the zone vicinity is actually greater, because localization of CrPcTS at the inner-tube wall increases its concentration. A simple mass balance on a solute plug that neglects convective transport relates the inner-wall concentration c_i^* to the concentration c_s injected (*25*)

$$c_i^* = \frac{c_s}{2}\,\frac{(1-\rho_1^{\,2})(a+2)\rho_1^{\,a}}{(1-\rho_1^{\,a+2})} \tag{14}$$

$$a = (\lambda \ln \rho_1)^{-1}$$

and predicts that $c_i^* = 5.9c_s$ for the smallest R of set H, $R = 0.72$ ($\lambda = 0.19$). Other quantities remaining equal, $t_i = 0.21$ for CrPcTS at the inner wall. A similar calculation shows that the uniformly distributed CrPcTS t_i for set G is 0.052, which roughly differs from the set H value by only 10%.

This phenomenon has not been reported previously, most probably because virtually all solutes used in earlier EFFF studies were proteins, for which μ_j and c_j are both relatively small due to the protein's high molecular weight. To justify this assertion, the inner-wall t_i of the protein albumin ($c_s = 1$ mg/mL) in a pH 4.5, $\sigma \approx 0.45\ \Omega^{-1}\cdot\text{m}^{-1}$ phosphate buffer calculated as above using additional data reported in Table III was only 1.4×10^{-4} (or 1500 times smaller than the inner-wall t_i for CrPcTS) for a well-retained albumin zone corresponding to $R = 0.20$.

The principal consequence of a large solute t_i is that the field E is reduced in the zone vicinity, because the current-carrying solute does not migrate through the glass. (No CrPcTS was ever found in the bath, whose UV–vis spectrum was periodically examined.) This phenomenon should be distinguished from the somewhat related field-reducing polarization of electrolyte ions discussed in detail by Lightfoot et al. (*11*), in which E is reduced by the buildup of electrolyte ions at the accumulation walls.

Curves A, C, D, and F in Figure 2 are the least-squares fits to eq 9 of R's generated from PSS and CrPcTS in MQ. It is clear from comparison of these fits and set E to curves G and H and set B that at fixed ΔV R increases as the carrier conductivity decreases, in agreement with earlier studies (*9*), probably because of large solute t_i's (for reasons detailed above) and the polarization of electrolyte at the accumulation wall (*11*). It is difficult to rationalize the apparently similar charges of the PSS and CrPcTS, even though polyelectrolytes immobilize counterions in their strong electrostatic fields (*41*), thus reducing their formal charges.

The PSS R's may in part be similar because the D/μ ratios of the polymers are similar. Although PSS of different molecular weight have been separated by polyacrylamide gel electrophoresis (*42*) (possibly because of sieving effects), their free-solution mobilities, equaling $\sim(2\text{–}4) \times 10^{-4}$ cm^2/(V·s), are largely independent of molecular weight, polymer concentration, and, to a first approximation, an added salt (*41*, *43–45*). Even the PSS mobility at infinite dilution is not much larger, because the equivalent conductivity, Λ, of PSS solutions is almost concentration independent (*46*), in contrast to the sharp increase in Λ that is commonly observed as polyelectrolytes are diluted (which promotes increased dissociation of counterions) (*41*). The diffusion coefficients of PSS also differ by only a factor of 2–3 (assuming equal polymer concentrations) over the molecular-weight-range $(1\text{–}12) \times 10^5$ g/mol (*41*, *44*, *49*) but, unlike the mobilities, depend strongly on polymer concentration (*47–49*) and added salt (*48*). Even though the equations for R and H_n given earlier assume the lateral diffusion coefficient is constant, Hovingh et al. obtained good agreement between these equations and thermal FFF experiments (in which the lateral diffusion coefficient varies with temperature) by assigning to D_l the diffusion coefficient corresponding to the temperature of the zone's center of gravity (*24*). Here, in a similar manner, the value assigned to D_l was the diffusion coefficient corresponding to the concentration c_l of the zone's center of gravity, which is approximately $1/e$ times the inner-wall concentration c_i^* (*24*). The R's considered here are mostly less than 0.6 ($\lambda < 0.14$), and eq 14 predicts for these R's that $c_i^* > 8.2c_s$ or $c_l > 3.0$ mg/mL ($c_s > 1.0$ mg/mL). For polymer concentrations greater than 3–4 mg/mL, the diffusion coefficients of these PSSs in salt-free solutions are fairly independent of polymer concentration, approximately equaling 4.2×10^{-7} cm^2/s (*47*, *49*). Consequently, the ratio $D/\mu \approx 1.4 \times 10^{-3}$ V does not vary much with molecular weight, which is consistent with the observation that the PSS R's are largely independent of molecular weight. (Clearly this does not fully explain the data because the CrPcTS D/μ ratio, 6.5×10^{-3} V, is 4.6 times larger than those for the PSSs but the R's of the two solutes are comparable.)

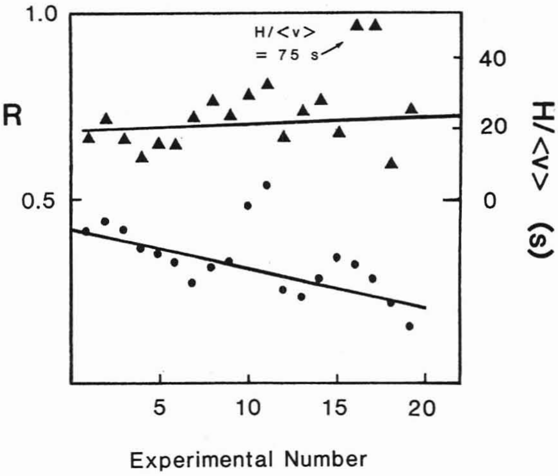

Figure 3. Plots of R and $H/\langle v\rangle$ vs. the experimental number, as generated from PSS70K in MQ. Solid lines are least-squares fits to these data, exclusive of the two largest R's and $H/\langle v\rangle$'s.

Although the expression $\lambda = D/|\mu\Delta V|$ is somewhat consistent with the experimental data, the λ expression derived from the Nernst–Einstein equation (eq 4), $\lambda = kT/e|z\Delta V|$, is clearly inconsistent, since the formal charge z of the PSS increases with molecular weight. (If this latter equation were valid, the PSS could be separated on the basis of molecular weight.) Manning has questioned the significance of calculating the charge of a high-molecular-weight polyelectrolyte from eq 4 because the electrophoretic and diffusive friction coefficients of the polyelectrolyte are not equal, as is assumed in eq 4 (*50*); the former corresponds to a freely draining polymer and the latter to a nondraining one.

The experimental reproducibility of R and H in PVG channels was investigated by retaining PSS70K in MQ (a subset of set A) 19 times over a 2-week period. By and large, the first nine experiments were not contiguous and were staggered among others comprising set A, whereas the latter ten were staggered among void-peak runs only. Figure 3 is the resultant plot of R and $H/\langle v\rangle$ vs. the experimental number (e.g., the abscissa, 12, represents data from the 12th experiment), which is proportional to time or column use. (Quantity $\langle v\rangle$, which spanned a 3.3-fold range, was calculated by dividing the carrier flow rate by the channel cross-section.) R clearly decreases with increasing experimental number but in an apparently cyclical manner, for reasons that are not presently understood. The line of negative slope is a least-squares fit to these data ($r = -0.79$). Furthermore, the R's generated by

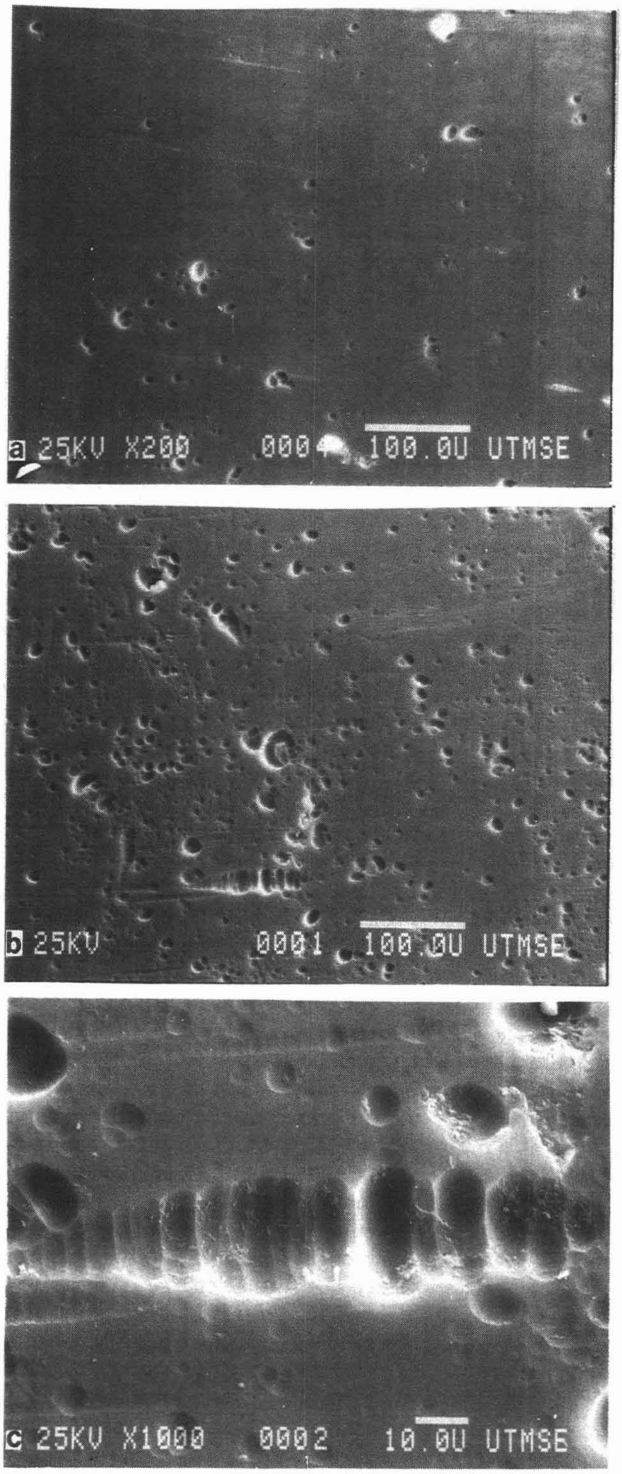

Figure 4. SEM photomicrographs of (a) virgin PVG (140×), (b) the inner tube of column B after 2 weeks of use (140×), and (c) the wormlike pit in the bottom center of Figure 4b, which contains particulate-like deposits (700×).

the final experiments are smaller than the minimum R value (0.35) reported earlier. The ratio $H/\langle v \rangle$ slightly increases uniformly with increasing experimental number.

These systematic changes in R and $H/\langle v \rangle$ can be explained in part by the SEM photomicrographs of the exterior surfaces of a 7-mm-o.d. virgin PVG tube (Figure 4a) and the inner tube from column B (Figure 4b), which was sacrificed after the reproducibility study. The latter surface is much more pitted than the former. A higher magnification of the pitted surface discloses small particulate-like deposits in the pits (Figure 4c), which also were found on the unpitted internal surface of the outer tube from column B but not on virgin PVG. The PVG that was insulated inside the carrier entrance and exit blocks was not as pitted as that exposed to the field, which suggests that pitting was accelerated by the field. Profilometry of the inner-tube surface revealed no extensive structure, indicating that the pit depth was considerably less than 25 μm (the stylus diameter).

All four PVG columns were transparent when assembled but slowly became translucent with increased use, probably due to the refraction and scatter of light from the pitted PVG surface. Since the decrease in transparency was gradual, one can infer that the extent of surface pitting increased with use, which qualitatively explains Figure 3. The R's and H's (or $H/\langle v \rangle$'s) of solutes retained in FFF channels modified by cutting grooves in the accumulation wall are known to be smaller and larger, respectively, than those obtained from unmodified channels (*51*). These R's and H's principally change because quiescent liquid in the grooves acts like a chromatographic stationary phase: solute molecules diffuse into the grooves and remain there until they diffuse out (to a first approximation). Increasing the groove density is analogous to increasing a column's stationary phase loading, which further decreases R and increases H. Here, the "grooving" (pitting) of PVG is not controlled or systematic but the system qualitatively behaves in an analogous way, i.e., R decreases and $H/\langle v \rangle$ increases as the surface becomes more pitted.

Since flat plates (rather than the cylindrical tubes used here) of PVG are commercially available, it should be possible to construct an OPPC channel from such plates, which could be polished with an abrasive grit (the glass is very soft) prior to assembly to reduce the R-limiting roughness of the tubes detailed above. The performance characteristics of such a channel were not explored because, as the study above shows, unmodified PVG does not exhibit the necessary long-term stability and reproducibility required of an ideal column material.

The acid activation of PVG had no apparent effect on R (refer to channels A and D in Table I and sets G and H in Table II), but the chemical derivatization of PVG by halosilane or PEG produced columns inferior in performance to unmodified ones. Both halosilane columns adsorbed much more solute than did virgin PVG, even under zero-field conditions. Even after several days of use, the effluent from the PEG-derivatized column was roughly 100 times more conductive than the MQ influent to the column, and well controlled low-conductivity studies were not possible. The adsorptivity of this column increased with use, and further characterization was stopped when solutes began to adsorb irreversibly.

The magnitudes of the slopes s reported in the final column of Table II indicate that the amount of solute adsorbed on PVG depends on (among other things) the solute type (cf. sets B and H) and the ionic strength (or conductivity) of the carrier (cf. sets F, G, and H; sets A and B). The extent of adsorption increases with ionic strength in part because the double layers around the solute and at the PVG/solution interface are compressed as the salt concentration increases, which reduces the electrostatic repulsion between the solute molecules and PVG (the glass is negatively charged at pH >3.5 (*52*)) and enables the two to approach closely, where short-range attractive forces (e.g., van der Waals) are important (*53*).

The area losses reported here should not be confused with similar ones reported previously (*9–11*) and attributed to electroretention (ER), the apparently "infinite" retention (i.e., $R \rightarrow 0$) of a solute fraction that is observed in an EFFF experiment until the electric field is turned off. Some ER was observed in roughly half of the experiments summarized in Table II, but only rarely did the recovered electroretained fraction exceed 10% of the corresponding void-peak area, whereas the adsorption losses reported in Table II are much greater (as much as 90% of the void-peak area). Because comparable solute masses (e.g., ≈50 μg) were injected onto the PVG columns in this study and the ultrafiltration fibers used to study extensively ER, one wonders if ER depends more on solute concentration than mass, as previously suggested (*11*), since the fraction of material electroretained in the fibers was much greater than that in the PVG channels and the cross-sectional area of even the smaller PVG channel was 29 times greater than that of the fiber (*9*).

Even though experimental R's depart considerably from theoretical expectation, experimental H's agree fairly well with theoretical H_n's (or $H_n/\langle v \rangle$'s) computed from eq 6, λ's estimated from experimental R's and eq 2, and l's estimated from these λ's and eq 3. One particularly close agreement is found between the R's and $H/\langle v \rangle$'s depicted in Figure 3. The average R in the figure ($R = 0.34$) corresponds to $\lambda = 0.056$ and $l = 34$ μm ($w = 610$ μm), as calculated from eq 2 and 3. For this λ, the nonequilibrium coefficient $\psi = \psi(0.056) = 2.67$ (*28*). To calculate the expected ratio $H_n/\langle v \rangle = \psi l^2 R/D$, one further needs the diffusion coefficient of PSS70K in low-conductivity water (e.g., MQ). As stated earlier, the diffusion coefficient of salt-free PSS70K is roughly 4.2×10^{-7} cm^2/s when $R < 0.6$. From this value of D and the above data, the ratio $H_n/\langle v \rangle = 26$ s was calculated from eq 6. This estimate agrees very well with the experimental $H/\langle v \rangle$ values (21 ± 6 s) depicted in Figure 3.

Fair agreement between experimental and theoretical H_n's was also found for the anion CrPcTS in MQ (set F). A series of constant ΔV experiments spanning a 2.6-fold range in $\langle v \rangle$ was carried out, from which a plot of H vs. $\langle v \rangle$ was generated. From the average retention ratio of these data, $R = 0.66$, the parameters $\lambda = 0.16$, $l = 163$ μm ($w = 1020$ μm), and $\psi(0.16) = 1.10$ were estimated as above, and the theoretically expected slope $\psi l^2 R/D$ of the H vs. $\langle v \rangle$ plot was calculated to equal 35 s, using the CrPcTS diffusion coefficient $D = 5 \times 10^{-6}$ cm^2/s given earlier. The slope of the least-squares line fit to the experimental data ($r = 0.78$) was 58 s, or 64% larger than expected. While this error is considerably larger than for the PSS70K case above, it is not atypical of the errors encountered in previous plate-height studies in FFF (*54*).

Thus it appears that experimental results and the predictions of theory are internally consistent provided that the fundamental parameter λ is estimated from experiment and eq 2 instead of eq 2 and 5. The consistency suggests that zone formation, migration, and dispersion are occurring more or less normally but that field-induced velocity U is much smaller than that theoretically expected.

As stated earlier, the relaxation of solute to the accumulation wall had little effect on R in this study. When zone velocity is affected by relaxation, R increases with velocity $\langle v \rangle$. An approximate theory predicts that a plot of $1/R$ vs. $\langle v \rangle$ should be a straight line with a negative slope proportional in magnitude to relaxation time τ (*24*). Such a plot was generated from the CrPcTS data collected for the plate-height study reported above, but the slope of the least-squares line that was fit to these data was positive (i.e., R was actually somewhat larger at slower flow rates). A similar plot was made for the anion PSS70K in MQ, using a subset of set A; the experimental slope was almost zero. Thus relaxation is probably unimportant in these studies.

CONCLUSIONS

The discrepancies between experimental and theoretical R's cannot be explained by relaxation effects, electroosmosis, an electrostatic screening of the anions by their counterion atmospheres, or an incompleteness in addressing channel "dead volume" but are qualitatively explained by a reduction in field strength E due to polarization of electrolyte ions and large solute transference numbers. The semiquantitative treatment given here is inadequate to eliminate the possibility that other effects are also operative. It appears from these data to be primarily the description of E, and thus the theoretical λ, that is erroneous because internal consistency exists between plate-height and retention theories and experimental λ's.

Virgin and chemically modified PVG do not exhibit the inertness, reproducibility, and longevity that are prerequisite to the ideal EFFF column material. It is unlikely that this glass can be readily modified to eliminate these serious shortcomings.

ACKNOWLEDGMENT

The IMSL routine ZXMWD was used for least-squares minimization. The authors thank Michael Schmerling (of the University of Texas at Austin) for the profilometry and SEM studies, Wayne Riley (of Exxon) for the initial EFFF experiments, and Jack Kirkland (of Du Pont) for numerous helpful suggestions.

GLOSSARY

A	coefficient in eq 9
A'	inner-tube surface area exposed to field E
a	$(\lambda \ln \rho_1)^{-1}$
C_p	constant-pressure heat capacity of water
c^*	quasi-equilibrium concentration
c_{i}^*	inner-wall concentration
c_j	concentration of jth species in solution
c_{l}	center-of-gravity concentration
c_{s}	concentration of solute injected onto column
D	general diffusion coefficient
D_{l}	lateral diffusion coefficient
D_{z}	axial diffusion coefficient
E	constant field strength
e	elementary charge
Gr	Grashof number
g	acceleration due to gravity
H	experimental plate height
H_{n}	nonequilibrium plate height
I	current
i	intercept
k	Boltzmann's constant
L	channel length
L_{c}	carbon electrode length
l	characteristic zone thickness
Nu	Nusselt number
Pr	Prandtl number
R	retention ratio
R^*	experimentally observed retention ratio
R_{a}	macroscopic resistance of uniform annulus
r_1	inner-PVG-tube radius
r_2	outer-PVG-tube radius
r	correlation coefficient
s	slope
T	temperature
ΔT	maximum temperature drop across annulus
t°	void time
t_i	transference number
t_{R}	retention time
U	field-induced velocity
V°	void volume
V_{R}	retention volume
$\dot{V}$	volumetric flow rate due to EOF
v	velocity profile of carrier
$\langle v \rangle$	average linear velocity of carrier
$\bar{v}$	characteristic velocity of solute in exit block
ΔV	potential difference across annulus
w	channel width or gap
Y	$\lvert \mu \rvert A/D$
z	signed number of fundamental charges
α	fractional channel length inside insulating block
β	coefficient of volume expansion of water
ζ	zeta potential
κ	thermal conductivity of water

Λ	equivalent conductivity
λ	$D/\lvert u\Delta V\rvert$
μ	electrophoretic mobility
μ^*	viscosity of water
ν	zone velocity
ρ	density of water
ρ_1	r_1/r_2
σ	average conductivity of column effluent and bath
σ_v^2	second moment of peak about mean V_R
τ	relaxation time
ψ	nonequilibrium coefficient

ACRONYMS

CrPcTS	chromium phthalocyaninetetrasulfonate
EFFF	electrical field-flow fractionation
EOF	electroosmotic flow
ER	electroretention
FFF	field-flow fractionation
MQ	low-conductivity water from Milli-Q system
OPPC	open parallel-plate column
PEG	poly(ethylene glycol)
PVG	porous Vycor glass
PSS	poly(styrenesulfonate)
RPA	relative peak area
SEM	scanning electron microscope

LITERATURE CITED

(1) Giddings, J. C. *Sep. Sci. Technol.* **1984**, *19*, 831.
(2) Giddings, J. C.; Myers, M. N.; Caldwell, K. D. *Sep. Sci. Technol.* **1981**, *16*, 549.
(3) Giddings, J. C. *Anal. Chem.* **1981**, *53*, 1170A.
(4) Lightfoot, E. N.; Chiang, A. S.; Noble, P. T. *Annu. Rev. Fluid Mech.* **1981**, *13*, 351.
(5) Caldwell, K. D.; Kesner, L. F.; Myers, M. N.; Giddings, J. C. *Science* **1972**, *176*, 296.
(6) Reis, J. F. G.; Lightfoot, E. N. *AIChE J.* **1976**, *22*, 779.
(7) Kesner, L. F.; Caldwell, K. D.; Myers, M. N.; Giddings, J. C. *Anal. Chem.* **1976**, *48*, 1834.
(8) Giddings, J. C.; Lin, G.-C.; Myers, M. N. *Sep. Sci.* **1976**, *11*, 553.
(9) Chiang, A. S.; Kmiotek, E. H.; Langan, S. M.; Noble, P. T.; Reis, J. F. G.; Lightfoot, E. N. *Sep. Sci. Technol.* **1979**, *14*, 453.
(10) Shah, A. B.; Reis, J. F. G.; Lightfoot, E. N.; Moore, R. E. *Sep. Sci. Technol.* **1979**, *14*, 475.
(11) Lightfoot, E. N.; Noble, P. T.; Chiang, A. S.; Ugulini, T. A. *Sep. Sci. Technol.* **1981**, *16*, 619.
(12) Alam, T. M.; Russell, D. 37th Pittsburgh Conference and Exposition on Analytical Chemistry and Applied Spectroscopy, Atlantic City, NJ, March 1986; No. 734.
(13) Andrews, A. T. *Electrophoresis: Theory, Techniques, and Biochemical and Clinical Applications*; Clarendon Press: Oxford, 1981.
(14) Bours, J. In *Isoelectric Focusing*; Catsimpoolas, N., Ed.; Academic: New York, 1976; Chapter 8.
(15) Jorgenson, J. W.; Lukacs, K. D. *Science* **1983**, *222*, 266.
(16) Gassman, E.; Kuo, J. E.; Zare, R. N. *Science* **1985**, *230*, 813.
(17) Lauer, H. H.; McManigill, D. *Anal. Chem.* **1986**, *58*, 166.
(18) Walbroehl, Y.; Jorgenson, J. W. *Anal. Chem.* **1986**, *58*, 479.
(19) Giddings, J. C.; Caldwell, K. D. *Anal. Chem.* **1984**, *56*, 2093.
(20) Fan, F.-R. F.; Riley, W.; Bard, A. J., unpublished experiments, The University of Texas at Austin, 1984.
(21) Corning Glass Works, brochure on Porous Vycor Glass 7930, 1985.
(22) Wolfgang, S.; Gafney, H. D. *J. Phys. Chem.* **1983**, *87*, 5395.
(23) Wei, S.; Gafney, H. D.; Clark, J. B.; Perettie, D. J. *Chem. Phys. Lett.* **1983**, *99*, 253.
(24) Hovingh, M. E.; Thompson, G. H.; Giddings, J. C. *Anal. Chem.* **1970**, *42*, 195.
(25) Davis, J. M.; Giddings, J. C. *J. Phys. Chem.* **1985**, *89*, 3398.
(26) Bard, A. J.; Faulkner, L. R. *Electrochemical Methods: Fundamentals and Applications*; Wiley: New York, 1980; pp 67, 135.
(27) Reis, J. F. G.; Ramkrishna, D.; Lightfoot, E. N. *AIChE J.* **1978**, *24*, 679.
(28) Giddings, J. C.; Yoon, Y. H.; Caldwell, K. D.; Myers, M. N.; Hovingh, M. E. *Sep. Sci.* **1975**, *10*, 447.
(29) Krishnamurthy, S.; Subramanian, R. S. *Sep. Sci.* **1977**, *12*, 347.
(30) Giddings, J. C. *Anal. Chem.* **1985**, *57*, 945.
(31) Yang, F. J.; Myers, M. N.; Giddings, J. C. *Anal. Chem.* **1977**, *49*, 659.
(32) Jayaraj, K.; Subramanian, R. S. *Sep. Sci. Technol.* **1978**, *13*, 791.
(33) Chang, S. H.; Gooding, K. M.; Regnier, F. E. *J. Chromatogr.* **1976**, *120*, 321.
(34) Pohl, H. A. *Dielectrophoresis*; Cambridge University Press: Cambridge, 1978.
(35) Giddings, J. C. In *Treatise of Analytical Chemistry: Part I*, 2nd ed.; Kolthoff, I. M., Elving, P. J., Eds.; Wiley: New York, 1982; Vol. 5.
(36) Bird, R. B.; Stewart, W. E.; Lightfoot, E. N. *Transport Phenomena*; Wiley: New York, 1960.
(37) Hunter, R. J. *Zeta Potential in Colloid Science: Principles and Applications*; Academic: London, 1981.
(38) Rice, C. L.; Whitehead, R. *J. Phys. Chem.* **1965**, *69*, 4017.
(39) Morrison, F. A., Jr.; Osterle, J. F. *J. Chem. Phys.* **1965**, *43*, 2111.
(40) Sherwood, T. K.; Pigford, R. L.; Wilke, C. R. *Mass Transfer*; McGraw-Hill: New York, 1975.
(41) Armstrong, R. W.; Strauss, U. P. *Encycl. Polym. Sci. Technol.* **1969**, *10*, 781.
(42) Chen, J.-L.; Morawetz, H. *Macromolecules* **1982**, *15*, 1185.
(43) Nagasawa, M.; Noda, I.; Takahashi, T.; Shimamoto, N. *J. Phys. Chem.* **1972**, *76*, 2286.
(44) Meullenet, J.; Schmitt, A.; Drifford, M. *J. Phys. Chem.* **1979**, *83*, 1924.
(45) Nagasawa, M.; Soda, A.; Kagawa, I. *J. Polym. Sci.* **1958**, *31*, 139.
(46) Vink, H. *Makromol. Chem.* **1982**, *183*, 2273.
(47) Gruner, F.; Lehmann, W. P.; Fahlbusch, H.; Weber, R. *J. Phys. A: Math. Gen.* **1981**, *14*, L307.
(48) Koene, R. S.; Mandel, M. *Macromolecules* **1983**, *16*, 220.
(49) Koene, R. S.; Mandel, M. *Macromolecules* **1983**, *16*, 973.
(50) Manning, G. S. *J. Phys. Chem.* **1980**, *84*, 1059.
(51) Giddings, J. C.; Smith, L. K.; Myers, M. N. *Sep. Sci. Technol.* **1978**, *13*, 367.
(52) Bolt, G. H. *J. Phys. Chem.* **1957**, *61*, 1166.
(53) Marra, J.; van der Schee, H. A.; Fleer, G. J.; Lyklema, J. In *Adsorption from Solution*; Ottewill, R. H., Rochester, C. H., Smith, A. L., Eds.; Academic: London, 1983.
(54) Davis, J. M.; Giddings, J. C. *Sep. Sci. Technol.* **1985**, *20*, 699.
(55) Mason, C. M.; Culvern, J. B. *J. Am. Chem. Soc.* **1949**, *71*, 2387.

RECEIVED for review November 6, 1986. Accepted January 27, 1987. This work was supported by the Separations Research Program of the University of Texas at Austin.

Anal. Chem. 1987, 59, 1349–1351 1349

Direct Determination of β-Lactam Antibiotics by Circular Dichroism

Neil Purdie* and Kathy A. Swallows

Department of Chemistry, Oklahoma State University, Stillwater, Oklahoma 74078-0447

Circular dichroism spectra have been characterized for nine penicillins and three cephalosporins dissolved in aqueous pH 5.4 buffer solutions. Discriminations among either the penicillin or the cephalosporin homologues are not possible from these spectral data, but the distinction between the two groups is easy. Direct determinations of penicillin V present in prepared laboratory mixtures with lactose, starch, caffeine, and cephalothin and in pharmaceutical preparations were accomplished after a simple extraction into aliquots of the buffer. Correspondence between the experimental and theoretical results was better than 1% for the prepared samples and within a few percent for the pharmaceutical preparations.

The analytical determinaton of the penicillins is important for a number of reasons and has been the object of a very large number as well as a wide variety of studies. These have been conveniently reviewed in recent publications (*1–3*). In a summary of the methods it is appropriate to point out that a direct method of analysis has not been described. Determinations have usually required that some kind of prior chemical reaction or derivatization step be performed, and the products of these processes were used in the detection step. In this way a certain degree of selectivity is introduced by the exclusion of interfering compounds. Among the methods employed are titrimetry, colorimetry, polarography, and chromatography. Where speed in performing repetitive analyses was an important priority, such as in quality control applications, automatic and kinetic methods of analysis have been developed.

Circular dichroism (CD) spectropolarimetry has emerged as an analytical detector with considerable selectivity which is based upon the fact that two prerequisites must be satisfied before an analyte is CD active, namely, optical activity and absorption. The degree of selectivity has been sufficient in a number of cases to determine an analyte without any chromatographic separation of the sample, or any other kind of workup, except a simple extraction into a recommended solvent system. Examples of single analytes successfully analyzed in this way are (−)-cocaine (*4*), heroin (*5*), and (+)-LSD (*6*). More complex systems containing more than one CD-active analyte have also been successfully determined, the most impressive among these being plant extracts (*7*). Pharmaceutical products have also been investigated, for example, demerol for meperidine (*8*) and seconal for secobarbital (*9*). The β-lactam drugs are known to be CD-active (*10–12*) and as such are potential candidates for their direct determination by CD. Accordingly we have characterized the CD spectra of 12 analogues in a variety of solvents and have chosen a slightly acid medium as the optimum solution for extraction and analysis.

EXPERIMENTAL SECTION

The substances obtained for this study were amoxicillin, ampicillin, cloxacillin, dicloxacillin, methicillin, nafcillin, oxacillin (Bristol Meyers), cephalexin, cephalothin, and cephapirin (Bristol Meyers and Sigma Chemical Co.) or their sodium salts, and the potassium salts of penicillin G and penicillin V (Sigma Chemical Co.). All were used without further purification. Pen-V tablets (250 mg) (Parke-Davis) were obtained from a local pharmacy. A sample of filtered and arbitrarily diluted penicillin (Pen-V) fermentation broth was provided to us by Eli-Lilly, Inc. Lactose, starch, and caffeine hydrobromide, used in the preparation of laboratory mixtures, were obtained from Fischer, Mallinckrodt, and Matheson Coleman and Bell, respectively. These are typical of the additives commonly encountered in pharmaceutical preparations. Their special interest in this case is that lactose and starch are both chiral but nonabsorbing, while caffeine absorbs radiation but is not chiral. None should interfere with the CD measurement but their presence might affect the signal quality. Starch was also included because it is insoluble in the buffer system chosen for the study. Centrifugation was required to separate any undissolved matter in the workup of the commercial preparations. As a test to see if any of the analyte is retained by adsorption, starch was added to stimulate this condition for the laboratory samples.

The penicillin content in the laboratory samples was varied from approximately 7% to 70% by weight. These were thoroughly mixed. To sample the pellets, the entire pill was first ground and then finely powdered by shaking in a Wig-L-Bug for approximately 2 min. Several samples of approximately 20 mg were chosen at random from each of the solid mixtures, extracted into 25-mL aliquots of the buffer solution, and centrifuged where necessary and the spectrum was measured. For the sample of fermentation broth 50-μL aliquots were diluted with 10 mL of buffer and the spectrum was run directly. Limited solubilities eliminated a number of potential organic solvents as the extracting medium. Aqueous solutions worked very well but strong acid and strong basic media were avoided to minimize hydrolysis problems. The signal quality was best for the solutes dissolved in a 5.4 buffer solution, spectra at pH 7.6 and 9.2 showing considerably more noise.

CD measurements were made as before with a JASCO-500A/DP-500N automatic spectropolarimeter/data processor combination (*7*). Instrument parameters were arranged to give the optimum signal-to-noise (S/N) ratio. The instrument was calibrated daily with a standard solution of androsterone in dioxane as recommended.

RESULTS AND DISCUSSION

The basic structures of the penicillin and the cephalosporin homologues are given in Figure 1, the fundamental differences being associated with the identities of the R and R_1 substituents which are listed in Table I for reference.

All the analytes absorb in the UV range of the spectrum, Figure 2, which is the typical range for an aromatic chromophore, so the CD spectra were measured from 320 to 220 nm, Figure 3. Considerably more use can be made of CD for analytical purposes based on the comparative appearances of the UV vs. CD spectra. CD spectra for the penicillins are qualitatively indistinguishable from one another showing a strong positive Cotton band maximizing at 230 ± 2 nm, Figure 3a. A similar spectral correspondence is observed for the three cephalosporins which show two maxima. The first band is positive with a maximum around 260 ± 2 nm, associated with the ring unsaturation, and is separated from a second negative band with a maximum at 230 ± 2 nm by a cross over point of zero ellipticity at approximately 243 nm, Figure 3b. Discrimination between the groups is easy because of these

0003-2700/87/0359-1349$01.50/0 © 1987 American Chemical Society

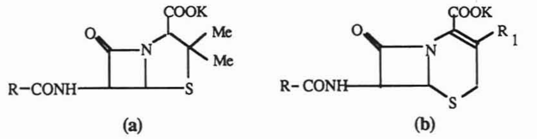

Figure 1. Molecular structures of (a) the penicillins and (b) the cephalosporins.

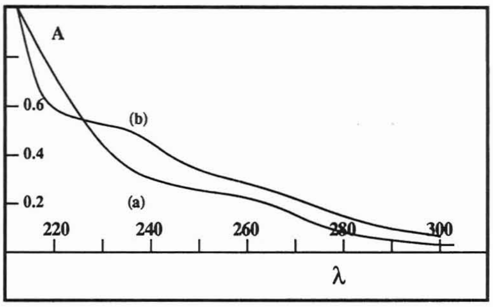

Figure 2. UV absorption curves for (a) Pen-V and (b) cephalothin in pH 5.4 buffer.

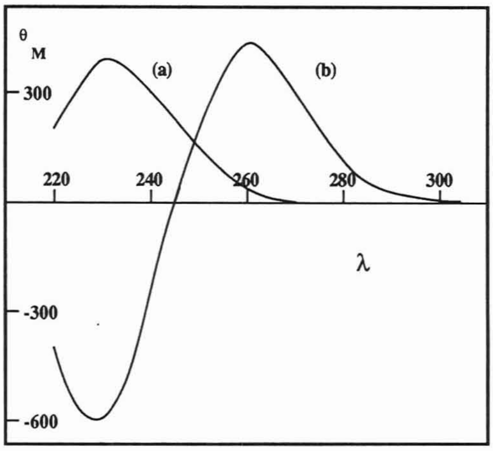

Figure 3. CD spectra for (a) Pen-V and (b) cephalothin in pH 5.4 buffer.

Table I. Molecular Structures and Molar Ellipticities for Penicillins and Cephalosporins

name	R^a	R1	θ_M (nm)
amoxicillin	2-amino(*p*-hydroxyphenyl)-		+398 (230)
ampicillin	2-amino-2-phenyl-		+431 (230)
cloxacillin	3-(*o*-chlorophenyl)-Z-		+333 (230)
dicloxacillin	3-(2,6-dichlorophenyl)-Z-		+323 (230)
methicillin	2,6-dimethoxyphenyl-		+265 (230)
nafcillin	2-ethoxynaphthalenyl-		+237 (230)
oxacillin	3-phenyl-Z-		+482 (230)
Pen-G	benzyl-		+394 (230)
Pen-V	benzoxy-		+363 (230)
cephalexin	2-amino-2-phenyl-	$-CH_3$	+395 (260) −632 (230)
cephalothin	2-(2-thienyl)-	$-CH_2OCOCH_3$	+452 (260) −600 (230)
cephapirin	2-(4-pyridylthio)-	$-CH_2OCOCH_3-$	+501 (260) −674 (230)

[a] The symbol Z is used to represent 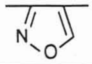

Table II. Determinations of In-House and Commercial Lactam Mixtures

mixture	lactam	additive	prepared, %	measd, %
S1	Pen-V	lactose	23.9	23.6
S2	Pen-V	lactose	40.5	39.5
S3	Pen-V	caffeine	72.3	72.2
S4	Pen-V	starch	7.1	6.3
S5	Pen-V	starch	29.6	28.2
S6	Pen-V	starch	63.5	63.8
PC1	Pen-V	lactose	1.28	1.53
	cephalothin		0.63	0.65
PC2	Pen-V	lactose	2.22	2.53
	cephalothin		4.79	4.74
PC3	Pen-V	caffeine	6.47	7.19
	cephalothin		5.58	5.46
PC4	Pen-V	lactose	3.50	4.11
	cephalothin		1.80	1.68
T1	Pen-V	?	(250 mg)	63.3 ± 0.9
broth	Pen-V	see text	(7.94 + 0.1 mg)	8.07 ± 0.12

spectral dissimilarities. The same basic features are observed in alcoholic solvents and as a function of pH for aqueous solutions. The spectra in Figure 3 are for the drugs dissolved in an aqueous solution of pH 5.4, the condition that produced the best S/N ratio. The spectra are not quantitatively identical however, and a calibration curve would be a necessary prerequisite before any specific analyte could be determined. Curves were obtained for ampicillin, amoxicillin, Pen-V, and cephalothin. For the others, values for the molar ellipticity, θ_M at the maxima were calculated for only one concentration in order to obtain a rough idea of the relative intensities, Table I. θ_M is defined in this work as the ellipticity of a *one molar* solution and values reported are 100 times smaller than *molecular* ellipticities contained in earlier work (*11, 12*).

θ_M is the CD equivalent of the molar absorption coefficient in absorption spectrophotometry, and the Beer–Lambert law applies equally well to CD data. In the simplest case, where interference is not a serious problem, determinations can be made from data taken at a single wavelength and as such the CD method can be automated for rapid repetitive analyses. The selectivity inherent to the method is the single important advantage of CD over potentially competitive methods. Obviously the groups of β-lactams could theoretically be distinguished by measuring the optical rotation at 230 nm, where the signs of the rotations are of opposite sense. One would have to be certain however that *all* possible optically active interferences had been successfully separated prior to making the measurement. One could just as easily presume that the distinction and determination could be done from absorption measurements, Figure 2, but once again the total separation of the lactam from other absorbing species would have to be confirmed. Neither of these restrictions alone is limiting to the determination of a CD-active analyte. This is apparent from the spectra we have obtained, Figure 3, and the determinations we have performed on several laboratory in-house blinds, S1–S6, PC1–PC4, and the samples of penicillin V in the commercially available products, T1, and broth, Table II.

The presence of the strongly absorbing caffeine in the mixtures affects the spectra only in the reduction of the S/N ratio. Whenever the nondrug residual material is completely soluble, the correspondence between the calculated and experimental results is uniformly excellent. Some indication of possible adsorption on undissolved starch is evident from the decrease in the correspondence with the increasing percentage of the insoluble material in the mixture. Reproducibility is excellent for the in-house mixtures. As might be expected it is poorer for the Pen-V tablets which are presumably prepared from aliquots taken from a much larger and less uniform sample. In fact considerable variation was observed in the total weights of the tablets. If the Pen-V content is reported as a percentage of the total weight, rather than compared with the nominal 250-mg prescription amount, then the correspondence between samples is much better (±0.9%).

A similar correspondence was observed for the determination of Pen-V in the fermentation broth. The composition

Anal. Chem. 1987, 59, 1351–1356

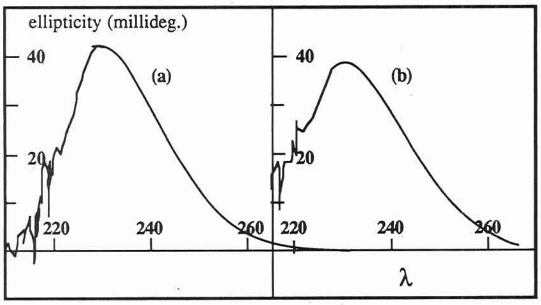

Figure 4. CD spectra for (a) the Pen-V fermentation broth and (b) the Pen-V standard at a similar concentration in pH 5.4 buffer.

of the broth reported by Lilly was 7.94 mg/mL Pen-V and <0.1 mg/mL *p*-hydroxy-Pen-V (as the potassium salts), 1.01 mg/mL phenoxyacetic acid and 0.12 mg/mL *p*-phenoxyacetic acid (as the sodium salts), inorganic salts of alkali and alkaline-earth metals plus ammonium and trace heavy metal cations, and various unknown organic compounds typically found in fermentation broths. The organism and several large proteins were removed in the filtration step. Of these ingredients the only known CD-active molecules were the penicillins, and the extent of the matrix distortion in the CD spectrum of the standard is a slight asymmetry on the low wavelength end of the band with little loss in S/N quality, Figure 4. Since we are unable to distinguish between the penicillins, our value of 8.07 mg/mL is representative of the *total* penicillin calculated as if it were all Pen-V, which assumes that θ_M is the same for both, and within 1% it appears to be an acceptable assumption.

In-house mixtures of Pen-V and cephalothin, PC1–PC4, Table II, were determined without a separation step. The spectral analysis is relatively straightforward when cephalosporin is in large excess since it is essentially the only contributor to the positive band whose maximum is at 260 nm. For the other mixtures however the determinations were done by using a simple curve fitting program in which weighted contributions from the standard curves were added in order to simulate the experimental curve (*7*). Once again the agreement between the prepared and calculated data is excellent.

In summary therefore the present work is a further endorsement of the analytical capabilities of CD in the direct determination of pharmaceutically important substances. Assuming that every method employed for the determination of a lactam would involve the same extraction procedure, the relative time taken for detection by CD is very short, i.e., a matter of minutes, which can be improved by automation. In addition there is no cause for modifying the analyte by derivatization or for the addition of an internal standard.

ACKNOWLEDGMENT

We wish to thank Anthony J. Tietz of Eli Lilly, Inc., Indianapolis, IN, for providing us with the sample of penicillin broth.

Registry No. Amoxicillin, 26787-78-0; ampicillin, 69-53-4; cloxacillin, 61-72-3; dicloxacillin, 3116-76-5; methicillin, 61-32-5; nafcillin, 147-52-4; oxacillin, 66-79-5; cephalexin, 15686-71-2; cephalothin, 153-61-7; cephapirin, 21593-23-7; penicillin G, 61-33-6; penicillin V, 87-08-1; penicillin, 1406-05-9; cephalosporin, 11111-12-9.

LITERATURE CITED

(1) Hamilton Miller, J. M. T.; Smith, J. T.; Knox, R. *J. Pharm. Pharmacol.* **1963**, *15*, 81.
(2) Hughes, D. W.; Vilim, A.; Wilson, W. L. *Can. J. Pharm. Sci.* **1976**, *11*, 97.
(3) Fairbrother, J. E. *Pharm. J.* **1977**, *218*, 509.
(4) Bowen, J. M.; Purdie, N. *Anal. Chem.* **1981**, *53*, 2237.
(5) Bowen, J. M.; Crone, T. A.; Kennedy, R. K.; Purdie, N. *Anal. Chem.* **1982**, *54*, 66.
(6) Bowen, J. M.; McMorrow, H. A.; Purdie, N. *J. Forensic Sci.* **1982**, *27*, 822.
(7) Han, S. M.; Purdie, N. *Anal. Chem.* **1986**, *58*, 113.
(8) Han, S. M.; Purdie, N. *Anal. Chem.* **1984**, *56*, 2822.
(9) Han, S. M.; Purdie, N. *Anal. Chem.* **1984**, *56*, 2825.
(10) Nagarajan, R. In *Cephalosporins and Penicillins: Chemistry and Biology*; Flynn, E. H., Ed.; Academic: New York, 1972; Chapter 15.
(11) Richardson, F. S.; Yeh, C.-Y.; Troxell, T. C.; Boyd, D. B. *Tetrahedron* **1977**, *33*, 711.
(12) Busson, R.; Roets, E.; Vanderhaeghe, H. *J. Org. Chem.* **1978**, *43*, 434.

RECEIVED for review November 12, 1986. Accepted January 30, 1987.

Do Optical Sensors Really Measure pH?

Jiří Janata

Center for Sensor Technology, University of Utah, Salt Lake City, Utah 84112

The problems that are inherent in the optical determination of pH and of other ion activities are present also in the optrodes. Furthermore, because of the complicated relationship between the bulk and the surface pH, these problems are amplified in optical sensors. While neither optrodes nor pH electrodes can measure pH, the thermodynamic compromises that have to be made in electrochemical estimation of pH are less severe then those that have to be made when using optical sensors. Furthermore, the flexibility in design of the liquid junction suitable for any practical measuring situation makes electrochemical sensors preferable to optical ones.

A large number of papers dealing with optical sensors has been published recently, among them articles describing various optical pH probes (optrodes or optodes) figure prominently (*1–6*). The main reasons cited for development of optical sensors are the lack of necessity of a reference electrode and electrical safety. Because it is the most ubiquitous species encountered in chemical reactions, hydrogen ion occupies a very special place in chemistry and biology. From the analytical point of view it is also special because it is almost always quantified in terms of pH—the negative logarithm of its *activity*:

$$\mathrm{pH} = -\log a_{\mathrm{H}^+} \tag{1}$$

It is a well-known and accepted fact that for thermodynamic reasons single ion activities cannot be measured (e.g. ref 7) and that all experimental techniques used for measurement of pH and other "ion activities" always contain some thermodynamic compromises. This issue has been long recognized

0003-2700/87/0359-1351$01.50/0 © 1987 American Chemical Society

by the electrochemists, and various practical ways of dealing with it have been extensively discussed (e.g. ref 8–10). Any weaknesses in the fundamental operating principles should be a matter of concern in the development of a new sensor because such devices are likely to encounter some practical problems sooner or later. The purpose of this article is to evaluate critically the thermodynamic compromises that have been made for various pH optrodes and to compare them with those that have to be made in electrometric estimation of pH.

Optical sensors constructed in different laboratories show different degrees of sophistication but the basic concept is the same (e.g. ref 1): The incident beam of light is passed through a light guide to the active end of the sensor where it interacts with the chemical indicator, which alters the beam's intensity, usually by absorption or by fluorescence. The modified optical signal is guided to the detector. The indicator is usually confined to the surface of the optical sensor or immobilized in an adjacent layer. The dissociation constant of the acid–base indicator is defined by the following equations:

$$HA + H_2O = H^+ + A^- \tag{2}$$

$$K = \frac{a_{H^+}C_{A^-}}{a_{H_2O}C_{HA}}\,\frac{f_{A^-}}{f_{HA}} = K_a\,\frac{f_{A^-}}{f_{HA}f_{H_2O}} \tag{3}$$

In logarithmic form it is the Henderson–Hasselbalch equation

$$\mathrm{pH} = \mathrm{p}K + \log\,(C_{A^-}/C_{HA}) + \log\,(f_{A^-}/f_{HA}) - \log\,a_{H_2O} \tag{4}$$

where C_{A^-} and C_{HA} are the *concentrations* of the indicator conjugate base and conjugate acid, respectively, and K is defined in terms of activities.

It is in the nature of the interaction between the electromagnetic radiation with atoms, molecules, and ions that it results in counting their numbers, i.e. their concentration. The solute–solvent and solute–solute interactions, which determine the value of the activity, show up only as a second-order effect, such as shifts of the absorption maxima, etc. Thus, most optical measurements deal only with the second term in the eq 4. What can be done about the third and the fourth term? Most optrode papers ignore them. This omission can be tolerated for very dilute aqueous solutions where the activity coefficients tend to unity and their ratio converges even faster with dilution. Unfortunately, conditions in most real measuring situations are such that these terms can rarely be ignored. Various ways of dealing with this problem have been suggested.

Electrochemical measurements face similar problems: They are done in cells with or without liquid junction, which separates the inner reference electrode compartment from the measured solution and contributes liquid junction potential, E_j, to the cell voltage. A liquid junction separating two dissimilar solutions is a nonequilibrium element in this measuring circuit. Therefore, any measurements done in the cells with liquid junctions are not equilibrium measurements, by definition. A schematic representation of the cell with liquid junction (||) is

indicator electrode|sample||reference solution|
reference electrode

for which the cell voltage E_{cell} is

$$E_{cell} = E_{indicator} - E_{ref} + E_j \tag{5}$$

Another alternative is to use cells without liquid junction in which case the activity of another ion, which determines the potential of the reference electrode, is included in the overall measurement (*11*). For example

glass electrode/sample + F^-/LaF_3 electrode

For most practical applications the problem of the liquid junction potential is mitigated by calibration. The *operational definition* of pH (X) of unknown solution measured potentiometrically is then:

$$\mathrm{pH\ (X)} = \mathrm{pH\ (S)} + (E_{glass,X} - E_{glass,S})\,F/2.303RT + (E_{j,X} - E_{j,S})F/2.303RT \tag{6}$$

where subscript S belongs to the standard solution and subscript X to the sample, respectively. It is normally *assumed* that the two liquid junction potentials ($E_{j,X} - E_{j,S}$) are the same, i.e. that they have been calibrated out. It is this *assumption of the invariability* of the liquid junction potential that represents the most serious flaw in the practical electrochemical determination of pH. Fortunately, it is almost always possible to design a liquid junction in such a manner that it is suitable for the given application and that the error due to the change of E_j is minimal. In any case, the pH electrode itself *does respond to activity* of hydrated hydrogen ion. The third alternative (*12–15*) is to use another type of cell without liquid junction in which the reference potential is provided by a pH-independent, fast redox electrode reaction such as oxidation/reduction of unsubstituted metallocenes (*12–15*). The inevitable nonthermodynamic assumption in that case is the lack of the effect of the medium on the *ratio* of activity coefficients of the oxidized/reduced form of the metallocene (*15, 16*). This is the same assumption that has to be made for optical indicators except that the metallocene/metallocenium couples are known to have minimal solute–solvent interactions (*16*). With this procedure an electrochemical determination of hydrogen ion activity from pH −10 to +26 has been made by using a cell containing

glass electrode/sample +
metallocene/mercury electrode

The operational definition of pH for this type of measurement is

$$\mathrm{pH\ (X)} = \mathrm{pH(S)} + (E_{glass,X} - E_{glass,S})\,F/2.303RT + \log\,(f_{M^+}/f_M)_S(f_M/f_{M^+})_X \tag{7}$$

in which the assumption about the invariability of the ratio of the activity coefficient of the metallocene/metallocenium couple (f_{M^+}/f_M) has to be made. Although this procedure works well in different pure media it is not practical for measurements in which other redox species are present at high concentrations or for direct measurement of pH in real samples.

Because single ion activities are not experimentally accessible in principle, the title question needs to be rephrased as "Do optrodes measure pH better than pH electrodes?" In other words, are the compromises that have to be made in either case more or less damaging in the case of optical sensors? There is no simple answer to these questions because each application has to be treated on its own merit. Although a good glass electrode responds to activity of hydrogen ions under most circumstances, the performance of a liquid junction in the cell depends on the experimental conditions.

The errors associated with optical measurements of pH have been thoroughly discussed decades ago (*7, 10, 17, 18*). One reason why so many pages have been devoted to this subject is that no definitive thermodynamic statement can be made about these questions because they lie outside the realm of thermodynamics. Therefore the arguments brought forward are of mostly casuistic nature. The reality of the situation is that electrometric measurement of pH is the generally accepted practice, perhaps with the exception of acidity functions in nonaqueous and mixed solvents. The arguments for and against the use of optical measurements of pH discussed on so many pages many years ago for bulk optical measurements remain valid and are directly applicable to the

Table I. Examples of Errors due to Variations of Ionic Strength for Electrometric and Optical Determination of pH

ionic strength	electrochemical[a]		optical[b]		
	HCl	KCl	Br-phenol Blue	Br,Cl-phenol Blue	Cl-cresol Purple
1.0	0.24	0.003	0.26	0.33	0.29
0.5	0.22	0.005	0.22	0.28	0.22
0.2	0.14	0.008	0.12	0.16	0.16
0.005		0.025[c]	−0.25	−0.14	−0.09

[a] Extrapolated from ref 35. [b] From ref 17, p 183, Table 30. The standard values of pH have been based on electrochemical measurements with a 3.5 M KCl Henderson junction. [c] From ref 19. Electrochemical measurements with a 3.5 M KCl Henderson junction.

optrodes. The important difference is the fact that the indicator is confined to the surface or to the interphase of the optical sensor, which complicates the issue even further. In the following paragraphs the effects of ionic strength, the presence of polyelectrolytes, mixed solvents, and adsorption are discussed in the context of these two types of sensors.

EFFECTS OF IONIC STRENGTH AND OF POLYELECTROLYTES

A liquid junction exists between two electrolyte compartments 1 and 2 of different chemical composition. These can contain different solvents, different electrolytes, or both. If all the charge-carrying species move with equal ease through the junction (i.e. the charge transference numbers, t_i, are approximately equal), the junction is nonselective and E_j approaches zero. The performance of a liquid junction in a practical measuring situation can be further improved by using a so-called salt bridge, which is a double-junction filled with electrolyte consisting of ions of equal transference numbers, for example potassium chloride. It is usually present in the highest convenient concentration (often saturated) in which case it dominates the charge transport through the junction. The exact equation describing the liquid junction potential is

$$E_j = \pm \frac{RT}{F} \int_1^2 \Sigma_i \frac{t_i}{Z_i}\, d(\ln C_i f_i) \qquad (8)$$

Only when some approximations are made can eq 8 be integrated; the main ones are the constancy of the activity coefficients and the linear concentration gradients of the charge transporting species throughout the junction. The latter can be also implemented in the actual physical design of so-called Henderson junction for which the E_j can be calculated. A detailed design of such practical junction has been recently published (*19*). The values of pH error caused by the residual liquid junction potential in the least (HCl) and the most (KCl) optimal sample are shown in Table I.

The effect of polyelectrolytes, specifically of proteins, on electrometric pH measurement is twofold: the physical blockage or obstruction of the junction and/or deposition of heavy coating on the glass electrode. If the polyelectrolyte layer is continuous and sufficiently thick, it may acts as a membrane in its own right and contribute its own interfacial potentials to the overall signal. Such deposits may occur in some biological fluids where the protein concentrations may be high. Otherwise, a thin adsorbed layer of polyelectrolytes at the surface of the glass electrode should have no effect on the final potential except that the time response may be longer. That this is the case has been demonstrated by Buck in 1965 when he made a Ca^{2+} sensor by covering a glass pH electrode with a Ca^{2+}-selective membrane (*20*). In the same context, ion selective field effect transistors with added ion-selective membrane are another example of complex potentiometric sensors of this type (*21*).

The effect of ionic strength on the dissociation equilibrium of the indicator is through the ratio of the activity coefficients of its two forms (eq 4). The nonspecific electrostatic effects can be derived from the classical Debye–Huckel theory. This approach works well for a uni-univalent electrolyte up to ionic strength $I < 0.1$ M (*7, 10*). For higher ionic strengths and/or multivalent ions the specific interation theory must be used (*22–25*). According to this theory the overall effect on activity coefficient is

$$\log f_i = -z_j^2 D + \Sigma_k \epsilon(j,k,I)\, m_k \qquad (9)$$

where, at 25 °C

$$D = 0.51\,(I^{1/2})/[1 + a(I^{1/2})] \qquad (10)$$

Thus, the nonspecific interactions are expressed by the first term in eq 9 while the specific interactions are expressed by the second. Parameter "a" in eq 10 is related to the ionic size and for most ions is taken to be 1.5. The value of the specific interaction term, $\Sigma_k \epsilon(j,k,I)\, m_k$, depends on the type of the indicator used (both chemical- and charge-type) and on the kind of ions j, k present in the medium. It has been shown recently (*25*) that agreement between the theoretical and experimental values of the dissociation constants for neutral, azo-, triphenylmethane-, and sulfonate-type indicators in solutions of ionic strength $0.1 < I < 3.5$ M can be obtained but the specific interactions must be included. The specific interaction term for indicator anion A^- is given by (*23*)

$$\epsilon(A^-,k,I) = (\log f^\circ_{k,A^-} + D z_k z_{A^-})(z_k + z_{A^-})^2/4I \qquad (11)$$

The term f°_{k,A^-} is the mean activity coefficient of the pure indicator salt solution (i.e. A^-k) at ionic strength I. For solutions containing high concentrations of indifferent electrolyte kj (e.g. KCl, NaCl, etc.) and a neutral indicator HA, eq 9–11 and eq 4 can be combined to yield

$$\log K_a = \log K + \log a_{H_2O} + 2D - [\epsilon(H^+,j,I) + \epsilon(A^-,k,I) - B_{HA}(k,j)]m_{k,j} \qquad (12)$$

where $B_{HA}(k,j)$ represents the ionic strength effects on the neutral form of the indicator species. Analogous equations describing other indicator charge-types (e.g. HA^-, H_2A, etc) can be derived. A simple form of eq 12, which neglected the nonspecific interactions, was used recently (*3*) for the design of optical sensors for measurement of ionic strength. However, because of that approximation such sensors can operate only up to $I < 0.1$ M. Experimentally determined pH errors for several types of bulk indicators are shown in Table I for comparison with the errors due to the liquid junction potentials. These data show that even in the worst possible case (HCl) the pH errors caused by the liquid junction are smaller than those caused by the effect of ionic strength on the indicators.

The effect of proteins on the dissociation constant of indicators, so-called "protein error", has been known to exist for a long time (*17*). It is defined as the difference between the colorimetrically determined values of pH in the presence and in the absence of the proteins in solution whose pH has been adjusted (electrochemically) to its original value. Again,

Table II. Protein Error of Color Indicators[a]

protein concn (wt %)	Neutral Red		Phenol Red	
	IgG	albumin	IgG	albumin
0.1	0.00	0.10	0.00	−0.03
0.5	−0.03	0.34		
1.0	−0.10	0.44		
2.0	−0.22	0.56	0.00	
4.0	−0.45		0.02	
6.0	−0.62		0.02	
8.0	−0.73		0.03	
10.0	−0.80		0.03	

[a] Extrapolated from ref 17, p 186, Table 34.

it has its origin in the specific interactions. Several values illustrating the magnitude of this effect are given in Table II. It has been shown recently (*25*) that the specific interaction theory may be extended to cover the interaction of polyelectrolytes with acid–base interactions. *The* prerequisite for such treatment is that the individual ionic sites on the polyelectrolyte molecule behave independently of each other. There are many proteins that fit this requirement within the physiological range of pH. However, it remains to be seen if such an approach is generally applicable.

PRACTICAL SOLUTIONS

It follows from the above discussion that the relative contribution of the terms in eq 4 to the observed value of pH depends on both specific and nonspecific interactions as expressed in eq 12. That contribution, in turn, depends on the type of the indicator used and on the type and concentrations of all ions in the sample. Optical sensors for determination of pH *and* ionic strength (*3, 4*) depend on these relative differences. Thus, in one approach (*3*) two different charge-type indicators have been used and measured at two different wavelengths: hydroxypyrenetrisulfonic acid and β-methylumbelliferone. Because both specific and nonspecific interaction terms for these two indicators are very different, their dependence on the ionic strength is also sufficiently different to yield the two sets of equations that are necessary to solve for both pH and ionic strength. The problem is that those interaction terms are valid only for one specific type of ion (both charge and chemical type). Another difficulty is that both relationships are highly nonlinear, which makes linear regression analysis impossible. Another approach (*4*) has been to place the indicator in a highly charged environment by surrounding it with charged groups in hope of making any variations in the ionic strength of the sample negligible. This, however, creates another problem, which will be discussed later.

SOLVENT EFFECTS

So far, we have ignored the last term in eq 4, the logarithm of activity of water. This is legitimate in aqueous solutions in which the ionic strength does not exceed approximately 4 M. However, in mixed solvents or in concentrated electrolyte solutions this term becomes dominant. This fact is used for preparation of extremely acidic and extremely basic solutions. For example, solutions as basic as pH 26 (and perhaps higher) can be prepared by changing the concentration ratio of a water–dimethyl sulfoxide (Me_2SO) mixture while keeping the concentration of the base relatively low *and constant* (*14*). This phenomenon is common, to a varying degree, for all water–organic solvent mixtures, and it is due to the fact that the activity term of free, uncoordinated water (eq 4) decreases as the concentration of the organic solvent increases. Because solvation equilibria are interdependent for all species and for interphases present in the system, it is not surprising that the activities of all species are affected in a most profound way by the presence of organic solvents (*24*). The degree to which individual ions, including the indicators, are affected by the medium depends very much on their structure, which gives rise to a multiplicity of acidity functions obtained with different types of indicators (Figure 1). To illustrate this point, four typical acidity functions established with different indicator types are compared with pH determined in a liquid-junction-free electrochemical cell. In this procedure the potential of a glass electrode is measured against the half-wave potential of ferrocene/ferricinium (H_{GF}) or against cobaltocene/cobalticinium (H_{GC}) at a dropping mercury electrode (Figure 1) (*12–15*). The two electrochemical acidity scales are based on the usual aqueous pH standards. Even a cursory examination of this figure shows that color indicators are useless for determination of absolute value of acidity under conditions of high basicity and high acidity. Thus, for example, the difference in the absolute value of pH measured with triphenylcarbinol indicators (H_R) and aromatic amine indicators (H_0) (*26*) would be approximately 4 pH units at a pH value of −5 (i.e. in aqueous 6.5 M H_2SO_4). The error of 2 pH units at pH 17 is between an acidity scale based on primary amines (H_-) and on substituted aminobenzoic acids (H_{2-}) (*27*). It must be understood that these errors are independent of the reference procedure (here electrochemical). Arguably, those are rather unusual conditions, but so is the magnitude of the error which illustrates the seriousness of this problem!

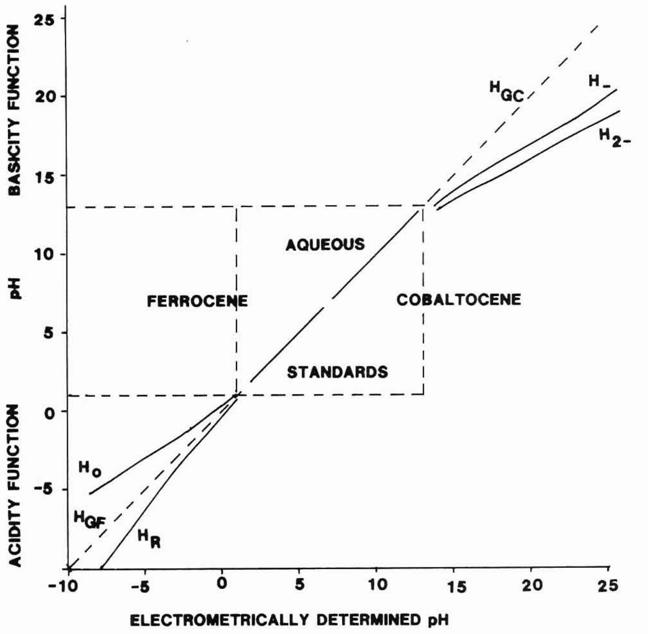

Figure 1. Comparison of optically and electrometrically determined acidity (basicity) functions. The acidic solutions were aqueous solutions of sulfuric acid (0.25 M to 11.0 M). The basic solutions were aqueous solutions of Me_2SO that were 0.011 M tetramethylammonium hydroxide (see text for description of individual acidity functions).

Electrometric measurements in mixed solvents using liquid junctions suffer from equally difficult problems. Let us imagine an aqueous liquid junction that is placed in a water-miscible organic solvent. In such a case a steep gradient of activity of water will develop along the junction. Furthermore, salts that are insoluble in one or the other medium will precipitate inside the junction. It is not surprising to find that such junctions may exhibit very large (up to hundreds of millivolts) and unstable potentials. Fortunately, there is a simple practical solution (*28*); a stable and reproducible reference system can be realized by placing the same solvent, as the sample, inside the reference electrode compartment. In such case the thermodynamical uncertainity lies only in determining the standard state (*10*) of the reference electrode, which is not critical for most practical applications.

SURFACE EFFECTS

The most fundamental difference between the optical and the electrochemical pH sensors is that in the latter the signal originates from the bulk–bulk interactions whereas in optical sensors the signal originates from the bulk–surface interaction. Specifically, in a glass electrode the potential difference between the bulk of the hydrated glass layer and the bulk of the sample is determined only by the equality of the electrochemical potential of the hydrated hydrogen ion in the two phases (*7*). In principle, there are no potentials affecting the measurement that are due to the adsorbed species. In practice, heavy adsorbed layers may behave as an interposed membrane and contribute a relatively small potential to the cell voltage as has been mentioned above. Also, the kinetics of the response are affected in the presence of adsorbed layers.

In contrast, the color indicator is confined to the surface of the optrode or to the adjacent layer of the optical fiber and the measured species must equilibrate between the bulk of the sample and this surface region. Thus the eq 4 must be written in the form:

$$\mathrm{pH_{surf}} = \mathrm{p}K_{\mathrm{surf}} + \log\,(C_{\mathrm{A^-}}/C_{\mathrm{HA}})_{\mathrm{surf}} + \log\,(f_{\mathrm{A^-}}/f_{\mathrm{HA}})_{\mathrm{surf}} - \log\,(a_{\mathrm{H_2O}})_{\mathrm{surf}} \quad (13)$$

In other words, the signal is obtained based on the conditions as they exist at the sensor interphase and the above discussion including the ionic strength, polyelectrolyte, and solvent effects must be interposed on the interphasial conditions. For example, most proteins will be present at the interphase in concentrations that far exceed their bulk value; the activity of water will be determined by the hydrophobicity of the interphase; ions will specifically adsorb, etc. It is a well-known fact that upon covalent immobilization at the surface the dissociation constant of the acid–base indicator changes by as much as 3 pK units (e.g. ref 4). This alone would not be a problem because the immobilized dye can be treated as a "new indicator" with different pK_a. Nevertheless this shift clearly illustrates the dramatic effect that the interphase has on ionization equilibria. It is perhaps the most serious problem with optical sensors that the surface activity of any species is related to its corresponding bulk value through an adsorption isotherm, which, with the exception of Henry's law, is a highly nonlinear relationship. It is further known (*10, 29*) that the surface pH is different from the bulk value due to the electrostatic repulsion

$$\mathrm{pH_{surf}} = \mathrm{pH_{bulk}} + \frac{Ne\psi}{2.3RT} \quad (14)$$

The surface potential ψ depends on the concentration profiles of all ionic species present at the interphase, i.e. diffuse layer, specifically adsorbed, species and on the surface ionizable groups. Thus the surface itself possesses acid–base properties that are reflected in the $\mathrm{pH_{surf}}$.

The density of the surface ionizable groups depends on the chemical composition and on the morphology of the surface (Table III) (*30, 31*). Changes of $\mathrm{pH_{surf}}$ spanning over 6 pH units have been reported for γ-aluminas with various amounts of impurities (*31*). An optical sensor with a high concentration of surface ionizable groups (quarternary ammonium groups) has been mentioned above (*4*). The purpose of this modification was to make small variations in the ambient ionic strength negligible as compared to the artificially elevated ionic strength at the sensor surface. As expected the pH response of this sensor was significantly different from the one in which no ionizable groups were added. Because both fixed and diffuse changes contribute to the potential profile, any ionic species in the solution will affect it along with the $\mathrm{pH_{surf}}$ value.

Table III. Surface pH at γ-Aluminas[a] and Silicates[b]

material	surface pH
Al_2O_3(γ-alumina)	3.61[a]
Al_2O_3; SiO_2 (0.05%); Na_2O (0.7%)	5.60[a]
Al_2O_3; Na_2O (0.7%)	9.90[a]
SiO_2 (precipitated)	5.8[b]
SiO_2 (quartz)	6.9[b]
SiO_2 (pyrogenic)	7.8[b]

[a] Measured at potential of zero charge at the surface (*31*). [b] Measured at the surface charge $\sigma = -10\ \mu\mathrm{C\ cm^{-2}}$ (*30*).

This complicated situation is even worse for sensors in which the indicator is confined within a surface layer (*1, 2, 32*). Such a layer has its own buffer capacity and constitutes a concentrated solution with all attendant problems discussed above. If the layer is enclosed inside a dialysis membrane (*2, 31*), a separate electrochemical equilibrium (Donnan potential) is set up at its interface, which controls the partitioning of all species. Unfortunately, partitioning equilibria are usually neglected in discussion of sensors containing gel layers (*32*), such as enzyme sensors. This omission is treated at length in a forthcoming publication (*36*).

CONCLUSIONS

It can be stated unequivocally that for thermodynamic reasons neither optical nor electrochemical sensors can measure pH precisely. The fundamental difference between these two types of sensors lies in the nonthermodynamic assumptions that are built-in to their modes of operation. In the optical sensors these are the solute–solvent interactions of the immobilized indicator and the relationship between the surface and the bulk value of pH and of all other involved species. These problems do not exist in electrochemical measurements. On the other hand the electrochemical sensors can provide thermodynamically correct values only of the activity of the whole electrolyte or a thermodynamically contaminated value of a single ion activity. The contamination comes from the undefined error due to the liquid junction of the reference electrode, or due to the uncertain value of the activity coefficient ratio of the reference redox couple. However, because these errors can be minimized by the design over a wide range of experimental conditions, in my opinion, the electrochemical measurements of ion activities are superior to the optical sensors. It is evident that the recent enthusiasm for optical sensor measurements of pH ignores the problems that are associated with the optical measurement of pH and that have been known for over half a century. The likely explanation of this situation can be the fact that in most papers that report on development of the optrodes the sample matrix has been kept invariant. In such case the errors of whatever origin tend to cancel out. It is a mandatory practice to test a new sensor in as wide range of conditions as is practically possible in order to be able to assess objectively its true performance.

It is important to realize that this critique does not apply fully to the sensors that depend on measurements of concentrations rather than activities, such as optical sensors for electrically neutral species (e.g. O_2, CO_2, etc.) and enzyme- and immunochemical-based optical sensors. In those sensors the effects of activity coefficient variations are much less serious than in ionic sensors. However, the issue of the relationship between the bulk and surface concentration of the analyte is a difficult, complicating factor in any sensors whose response depends entirely on bulk–surface interactions, such as optical sensors.

ACKNOWLEDGMENT

The author wishes to express thanks to his colleagues at the UK Atomic Energy Authority, Harwell Laboratory, for

providing the stimulating environment in which this work was done.

LITERATURE CITED

(1) Peterson, J. I.; Vurek, G. G. *Science* **1984**, *224*, 123–127.
(2) Peterson, J. I.; Goldstein, S. R.; Fitzgerald, R. V.; Buckhold, D. K. *Anal. Chem.* **1980**, *52*, 864–869.
(3) Opitz, N.; Lubbers, D. W. *Sens. Actuators* **1983**, *4*, 473–479.
(4) Wolfbeis, O.; Offenbacher, H. *Sens. Actuators* **1986**, *9*, 85–91.
(5) Munkholm, C.; Walt, D. R.; Milanovich, F. P.; Klainer, S. M. *Anal. Chem.* **1986**, *58*, 1427–1430.
(6) Seitz, W. R. *Anal. Chem.* **1984**, *56*, 16A–34A.
(7) Kortum, G. *Treatise on Electrochemistry*; Elsevier: New York, 1965.
(8) Mattock, G.; Band, D. M. In *Glass Electrodes for Hydrogen and Other Cations*; Eisenman, G., Ed.; Marcel Dekker: New York, 1967.
(9) Band, D. M.; Treasure, T. In *Ion Selective Electrode Methodology*; Covington, A. K., Ed.; CRC Press: Boca Raton, FL, 1979.
(10) Bates, R. G. *Determination of pH*; Wiley: New York, 1973.
(11) Mohan, M. S.; Bates, R. G. *NBS Spec. Publ.* **1977**, *No. 450*.
(12) Janata, J.; Jansen, G. J. *Chem. Soc. Faraday Trans. 1* **1972**, *68*, 1656–1665.
(13) Janata, J.; Holtby-Brown, R. D. *J. Electroanal. Chem. Interfacial Electrochem.* **1973**, *44*, 137–143.
(14) Janata, J.; Holtby-Brown, R. D. *Chem. Soc. Perkin Trans. 2* **1973**, *99*, 991–994.
(15) Modro, T. A.; Yates, K. Janata, J. *J. Am. Chem. Soc.* **1975**, *97*, 1492–1495.
(16) Strehlow, H.; Wendt, H. *Z. Phys. Chem. (Munich)* **1961**, *30*, 141–144.
(17) Clark, W. M. *The Determination of Hydrogen Ions*, 3rd ed.; Williams & Williams: Baltimore, MD, 1928.
(18) Mattock, G.; Taylor, G. R. *pH Measurement and Titration*; Heywood: London, 1961.
(19) Dohner, R. E.; Wegmann, D.; Morf, W. E.; Simon, W. *Anal. Chem.* **1986**, *58*, 2585–2589.
(20) R. P. Buck Beckman Instruments Co., 1965, unpublished results.
(21) J. Janata, In *Solid State Chemical Sensors*; Janata, J., Huber, R. J., Eds.; Academic: Orlando, FL, 1985.
(22) Scatchard, G. *Chem. Rev.* **1936**, *19*, 309–331.
(23) Guggenheim, E. A. *Aplications of Statistical Mechanics*, Claredon Press: Oxford, U.K., 1966.
(24) Harned, H. S.; Owen, B. B. *The Physical Chemistry of Electrolytic Solutions*; Reinhold: New York, 1958.
(25) Salvatore, F.; Ferri, D.; Palombari, R. *J. Solution. Chem.* **1986**, *15*, 423–431.
(26) Boyd, R. H., In *Solute-Solvent Interactions*; Coetzee, J. F., Ritchie, C. D., Eds.; Marcel Dekker: New York, 1969; Vol. 1.
(27) Bowden, K.; Buckley, A.; Stewart, R. *J. Am. Chem. Soc.* **1966**, *88*, 947–954.
(28) Bruckenstein, S.; Kolthoff, I. M. *J. Am. Chem. Soc.* **1956**, *78*, 2974–2979.
(29) Davies, J. T.; Rideal, E. K. *Interfacial Phenomena*; Academic: Orlando, FL, 1963; Chapter 2.
(30) Furlong, D. N.; Yates, D. E., Healey, T. W. In *Electrodes of Conductive Metallic Oxides*, Part B; Trasatti, S., Ed.; Elsevier: New York, 1981.
(31) Vordonis, L. Koutsoukos, P. G. Lycourghiotis, A. *Langmuir* **1986**, *2*, 281–283.
(32) Zhujun, Z.; Mullin, J. L.; Seitz, W. R. *Anal. Chim. Acta* **1986**, *184*, 251–258.
(33) Offenbacher, H.; Wolfbeis, O. S.; Furlinger, E. *Sens. Actuators* **1986**, *9*, 73–84.
(34) Caras, S. D.; Petelenz, D.; Janata, J. *Anal. Chem.* **1985**, *57*, 1920–1924.
(35) Milazzo, G. *Elektrochemie*; Springer-Verlag: Vienna, 1952; p 98.
(36) Buck, R. P. *J. Electroanal. Chem. Interfacial Electrochem.* **1987**, in press.

RECEIVED for review November 19, 1986. Accepted February 2, 1987. This material is based upon work supported by the National Science Foundation Grant No. INT-8606514.

CORRESPONDENCE

Tubular Microporous Membrane Entrapped Enzyme Reactors for Flow Injection Analysis

Sir: In his first decennial reevaluation of the status of immobilized biocatalysts in analytical chemistry, Bowers (*1*) has concluded that immobilized-enzyme technology will only achieve the success envisioned in 1976 when it provides economical and unique solutions to analytical problems of the 1980s. A principal focus of our research is the determination of trace atmospheric gases. In recent years, hydrogen peroxide, photochemically produced and ubiquitous in the atmosphere, has been of particular interest because of its important role in the phenomenology of acid precipitation. We are committed to a fluorometric determination method, originally developed by Guilbault et al. (*2*), in which nonfluorescent *p*-hydroxyphenylacetic aicd (PHPA) is oxidized to a fluorescent dimer by hydrogen peroxide, mediated by the enzyme peroxidase (donor: hydrogen peroxide oxidoreductase, EC 1.11.1.7). Major atmospheric research groups are in accord that the PHPA procedure is the one of choice for the determination of trace quantities of H_2O_2 (*3–6*). We concur and in our hands, the method has evolved both configurationally and in chemical details (*7–9*).

Even though peroxidase is one of the less expensive commercially available enzymes, having invested a small fortune over the last few years into this biocatalyst, we have been, of necessity, interested in more affordable alternatives. Although we have not attempted to use the recently introduced wall-embedded open tubular reactor concept (*10*), we successfully attached the enzyme to spherical macroporous polymeric beads (*11*) and used the same in the single bead string reactor configuration (*12*) with a greater enzymatic activity per unit reactor volume than that attainable with etched glass or silica spheres.

However, for small volume reactors desirable in our application, the attainable activity was insufficient.

Thus, we looked for alternatives and, because of the considerable involvement of this laboratory with various types of membranes, looked particularly into membrane-based devices for a solution to the problem.

EXPERIMENTAL SECTION

Reagents. *p*-Hydroxyphenylacetic acid (PHPA) (Eastman Kodak, Rochester, NY) was purified by recrystallization from hot water and decolorization with activated carbon treatment. Peroxidase (type II, Sigma Chemical, St. Louis, MO) and glucose oxidase (type, X, Sigma Chemical) exhibited activities of 200 and 114 Sigma units/mg, respectively. Manganese dioxide (analytical reagent grade granules, Mallinckrodt), hydrogen peroxide (30%, without added stabilizers, Fisher Scientific), and D-glucose (analytical reagent grade, Mallinckrodt) were obtained as indicated. An iodometric method was used to standardize hydrogen peroxide (*8*); glucose solutions were prepared by weight and used fresh.

The fluorescence derivatization reagent was prepared by dissolving 2 g of purified PHPA and 0.156 g of Na_2EDTA in 1 L of water followed by adjusting the pH to 5.5 with NaOH. Blood plasma samples were obtained from the Department of Anesthesiology, Texas Tech University Health Sciences Center, Lubbock, TX.

Equipment. A fluorescence detector (Fluoromonitor III,

0003-2700/87/0359-1356$01.50/0 © 1987 American Chemical Society

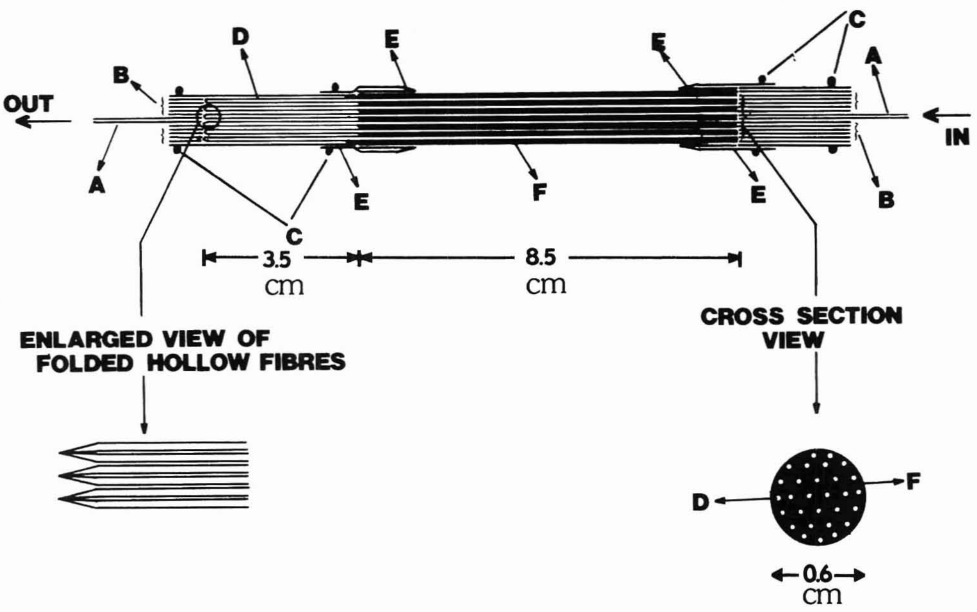

Figure 1. Design of the membrane entrapped enzyme reactor: (A) inlet/outlet tubes; (B) nested PTFE tubes; (C) wire crimp; (D) Celgard fibers; (E) PVC tube; (F) epoxy adhesive.

Laboratory Data Control, Riviera Beach, FL) equipped with a Cd-lamp source, a 30-μL quartz flow-through cell, a 326-nm interference filter for excitation, and a 370-nm high-pass emission filter was used for all work. The maximum fluorescence of the fluorophore occurs at 329 and 412 mm respectively for excitation and emission (*7*).

Preparation of Enzyme Reactors. Figure 1 schematically shows the typical enzyme reactor used in this work. Microporous hollow fibers (Celgard X-20, 400-μm i.d., 25-μm wall, 0.02-μm mean pore size, average molecular weight cut off 100 000 daltons, 40% surface porosity, Celanese Corporation, Charlotte, NC) were taken as a 15–18 fiber bundle, 23–25 cm in length. The bundle was folded in half to form a U, resulting in a new bundle with twice the number of fibers, one end of the bundle being closed. Note that the fibers fold into sharp bends as shown in the enlarged view, not smooth bends invoked by the description "U"-shape. Starting from the open end, 70–75% in length of the exterior of the fiber bundle was next liberally coated with clear epoxy adhesive (Duro E-Pox-E, Loctite Corp., Cleveland, OH) to prevent any effusion from the walls. After the adhesive was cured, 2-cm lengths of PVC tubing, into which the coated fiber bundle fits snugly, were introduced at each bundle end and affixed to the coated bundle with further adhesive. After curing, inlet and outlet connections were made to the reactor with 0.8-mm i.d., poly(tetrafluoroethylene) (PTFE) tubing with the help of a series of tightly nested PTFE tubes of increasing diameter and secured with a nichrome wire crimp to prevent leakage. Methanol was injected from the open end of the fiber bundle. Methanol wets the membrane and penetrates through the pores on the folded side. Once the liquid connection is established, liquids with higher surface tension can penetrate the pores. Thus, water is next injected in copious quantities to flush all of the methanol out. (Note: failure to remove the methanol will denature most enzymes.) Next, 0.5 mL of a prefiltered solution of the desired enzyme (peroxidase, glucose oxidase), typically at a concentration of 4 mg/mL in pH 7 phosphate buffer, is injected into the lumen of the fiber. (Note that flow in the reactor is always unidirectional, from the open to the folded end.) The reactor is then connected to a pump and a generous amount of phosphate buffer (≥50 mL) is pumped through to ensure that whatever amount of the enzyme is unretained will be washed out. During this time, the reactor effluent is collected; it contains significant amounts of the enzyme. The reactor is now ready for use. When not in use, the inlet and outlet are connected to each other to form a closed system.

Analytical System. Figure 2 shows the schematic flow diagram in the fluorometric flow injection analysis system.

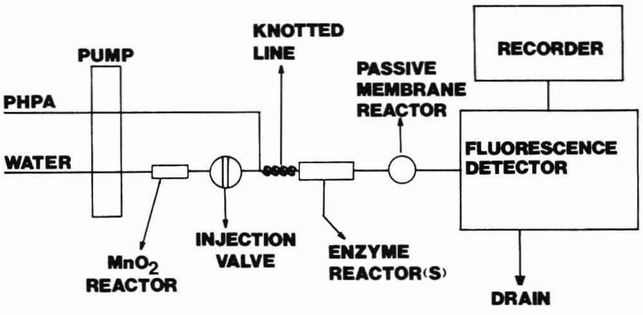

Figure 2. Analytical system schematic.

The fluorescence derivatization reagent was pumped into one channel of a Minipuls 2 slow speed peristaltic pump (Gilson Medical Electronics, Middleton, WI) at 0.52 mL/min (pump setting 999, 1.0-mm id. PVC tubing) while water was pumped as the carrier solution through the second channel at 2.0 mL/min (3.16-mm i.d. PVC tubing). A MnO_2-packed tubing (6-cm long, 4.5-mm i.d., PTFE tube) was placed in the second line between the pump and the injection valve to remove any residual peroxide in the water. After the injection valve (PTFE, Rheodyne type 50 with a 0.8-mm connecting passages, Cotati, CA; equipped with a 90-μL loop), the flow streams were mixed at a tee and were made to flow through a knotted mixing line (25-cm length, 0.8-mm i.d.) to achieve uniform mixing. Then, the flow stream went through the reactor(s) containing the entrapped enzyme as a catalyst. The reaction product passed through the passive membrane reactor, comprised of a filament-filled perfluorosulfonate cation exchange membrane tubing immersed in concentrated NH_4OH (see ref 9 for further details of the reactor) which increased the pH to permit optimal fluorescence of the product.

For the determination of H_2O_2, only the peroxidase reactor was present in the system and the system calibrated with H_2O_2 standards. Thawed snow samples were injected through a membrane filter as test unknowns. For the determination of plasma glucose, a glucose oxidase reactor preceded the peroxidase reactor and the system was calibrated with glucose standards. Centrifuged plasma samples were injected into the systems as test unknowns, directly, diluted with 0.9% NaCl, diluted and spiked with known amounts of glucose (standard addition).

RESULTS AND DISCUSSION

The use of membranes for immobilizing enzymes is not novel. However, this has been limited to covalently bonding the enzyme to the membrane, for example, heterogeneous ultrafiltration membranes (*13*, *14*) or more conventional dialysis membranes (*15*). In both cases, available surface area sets the upper limit to the amount of enzymatic activity attainable in a given system. Immobilization in the membrane matrix itself, e.g., in a membrane cast from collagen and the enzyme, has also been carried out (*16*). While considerable efforts have been made to study the kinetics and to model the combined mass-transfer–kinetic effects in both of the above systems (*17*, *18*), these systems offer little attraction except for cases where separation of matrix components through transmembrane transport is a key desired ingredient.

Because all proteins carry a net charge except at the isoelectric point, initially we attempted to find if peroxidase can be retained at any convenient pH by strongly acidic cation exchange or strongly basic anion exchange membrane filters; this quest proved to be unfruitful. Next we attempted to use reactors made from cellulose-based hollow fiber bundles used for dialysis, in a reactor design similar in essence to that described in the experimental section. However, desirable transmembrane flow rates could not be attained at low enough pressures to permit continued operation without membrane rupture or other pressure-induced device failure.

Encouraged by the microporous hollow fiber membrane devices recently introduced for cell harvesting (*19*), we considered the use of such devices. Even though peroxidase is a protein of 40 000 daltons while the stated molecular cutoff for Celgard X-20 is 100 000 daltons, and despite literature reports that peroxidase has been introduced into reaction systems via a Celgard membrane (*20*), we examined retention of peroxidase in earlier versions of the reactor desdribed in the experimental section. These reactors involved a single fiber of longer length which was tied shut at one end and was not adhesive coated. They were not particularly effective in catalyzing the desired analyte → product conversion. For obvious reasons, most of the influent stream immediately effused through the fiber walls upon entering the fiber, rather than traveling down the lumen. However, it was possible to make two important observations. First, when the enzyme was initially introduced into the lumen, portions of it were deposited on the fiber walls, as evidenced from the discoloration of the wall. Second, this deposit did not perceptibly alter upon reasonably prolonged washing. Peroxidase is a highly water-soluble hydrophilic globular protein and this deposition is not due to chemisorption on the hydrophobic membrane. When most of the exterior of the enzyme-filled fiber, beginning from the entrance, was covered with a tightly fitting PVC jacket from which there was no exit, the efflux through the initial portion of the fiber walls was eliminated. When use as a reactor was reattempted, excellent analyte → product conversion was observed, indicative of high resident enzyme activity within the lumen. Aside from exterior physical observation, destructive dissections indicate that the enzyme is not principally located as a bed or a plug at the closed end of the reactor but significant amounts of it are deposited, seemingly uniformly, on the walls. It appears that some of the protein is simply deposited in the pores on the fiber wall and is not easily removed. The multiple fiber design evolved out of the necessity to obtain larger flow rates at a lower pressure and coating the exterior surface of the fibers was a simpler alternative in this design than individual closely fitting jackets for each fiber.

Although more detailed experiments were carried out with the multiple-fiber reactors to elucidate the nature of retention of the enzyme, the exact mechanism could not be unequivocally established. When ~2.25 mg of (Sigma Type II) peroxidase is put into the reactor, the reactor is flushed and the total amount of peroxidase in the efflux determined by a kinetic version of the fluorescence assay used here with an excess of substrate, the typical washout pattern is shown in Figure 3. Approximately a fourth of the enzyme remains in the reactor or, at worst, is washed out at a rate not easily detectable. Spectrophotometric measurements of the effluent at 210 nm led to essentially the same conclusions as the kinetic assay, albeit the poor absorptivity of peroxidase and the finite background absorbance of the wash buffer led to a much greater scatter in the data. When the retention experiment is repeated in the same reactor using a second aliquot of the enzyme, essentially the same fraction is retained once again. Depending on the dimension (and thus the available internal surface area and volume of the reactor; for the dimensions stated in the experimental section, the internal volume is ~200 μL), this experiment can be repeated more times with the same fractional retention. We believe therefore that the retention mechanism does not involve pseudofiltration or a layering effect which would have been expected to increase fractional retention with continued injections. Admittedly, the pores in Celgard are highly assymmetric with high (≥10) length/width aspect ratios, characteristic of the thermal stretching process used to fabricate this material. There may be thus some confusion as to how one may relate the stated "mean pore size" to the retention probability of a spherical marcomolecule. Nevertheless, the stated molecular weight cutoff values (*21*) have been determined with spherical hydrophilic polymers [poly(styrenesulfonate)] and a difference in molecular shape cannot be invoked to explain the retention.

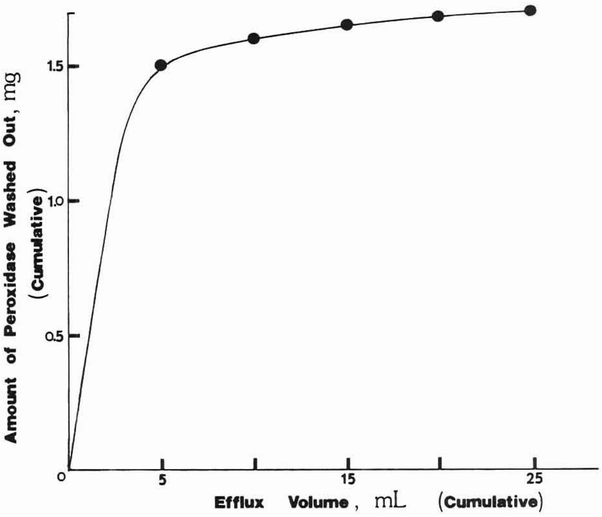

Figure 3. Cumulative washout profile of the unretained enzyme in the reactor. Initially 2.25 mg of enzyme was put in the lumen.

We believe that the most plausible solution to the dilemma about the retention mechanism is that the membrane is in fact retaining protein that is considerably larger than 40 000 daltons, indeed probably significantly over its stated molecular weight cutoff. Although we have no categorical proof that the particular enzyme preparation used in our work contains significant amounts of enzymatically active material of higher molecular weight, it has long been known that commercial enzyme preparations, especially lyophilized preparations, often contain very significant amounts of polymeric aggregates which are nevertheless enzymatically active and display the requisite specificity (*22*). Indeed, if this hypothesis is correct, less pure enzyme preparations available at lower cost may be successfully used in many cases. An unequivocal solution is difficult with peroxidase; peroxidase isolated from horseradish is by no means a single compound (*23*). In any case, the majority of biocatalysts of interest have a molecular weight significantly above 100 000 daltons and should be effectively retained. Glucose oxidase (β-D-glucose–oxygen 1-oxidoreductase, EC 1.1.3.4), an enzyme with a reported MW of 150 000 daltons, is indeed efficiently retained by the described reactors. Smaller molecular weight cutoff polysulfone hollow fibers are commercially available (A/G Technology, Needham, MA) and may be worthy of investigation to attain better

Table I. Plasma Glucose Determination Results

sample	nominal value, mg/dL (commerical clinical analyzer)	this work, mg/dL
1	86.5	80.5 ± 2.1[a] 85.1 ± 1.5[b] 87.0 ± 1.3[c]
2	141	149 ± 1[b]
3	249	273 ± 1[b]
4	248	257 ± 1[b]

[a] Neat plasma. [b] Plasma diluted 10–20-fold with isotonic saline. [c] Result from two-step standard addition to sample *b*, from linear extrapolation.

retention of macromolecules with an MW below 100 000 daltons.

For the determination of hydrogen peroxide, the response was found to be linear from essentially the limit of detection to over 1 mg/L H_2O_2. This linear range compares favorably with any previously reported method. On the basis of a 3 times blank noise criterion, the limit of detection was 600 ng/L H_2O_2, within a factor of 2 of the best limit of detection attainable in the carefully optimized system reported earlier (*9*). A number of peroxidase reactors were reexamined after 1 month of storage in refrigerated condition and at laboratory temperature (~22 °C). The reactors from either storage regime showed no detectable loss of activity as evidenced from their performance in the analytical system; however, this may not be an acceptable measurement for determining the exact amount of activity. This is because the initial enzyme content of these reactors is significantly in excess of the amount necessary to achieve near-stoichiometric conversion of the analyte to the desired product. Thus, only drastic changes may be noticeable by this test. The high enzymatic activity retainable in the present reactors is used to advantage; it should be noted that the residence time of the injected sample in the enzyme reactor is under 5 s compared to ≥15 s for the system described in ref 9. A number of precipitation samples (snow) from late 1985 and early 1986 in Lubbock, TX, were assayed for H_2O_2 by this technique immediately following collection. The values ranged from a low of 30 to 450 µg/L and in each case were in excellent agreement with independent measurements by a method employing the enzyme in solution (*9*).

Parallel to our experience with peroxidase chemically bonded to a porous polymeric support (*11*), severe loss of activity was immediately apparent after methyl hydroperoxide was injected into the system. A single 90-µL injection of 1 mM CH_3HO_2 reduced the enzyme activity of the reactor toward H_2O_2 by 48%. While this unfortunately precludes the use of such reactors for the analysis of organic hydroperoxides (*8*), there appears to be enough evidence in the literature that inactivation of peroxidase by hydroxymethyl hydroperoxide (*24*) or methyl hydroperoxide (*25*) due to irreversible or very slowly reversible enzyme–substrate adduct formation is intrinsic to the behavior of the enzyme itself and cannot be attributed to the specific nature of immobilization of the enzyme (i.e., physical entrapment vs. covalent binding).

The dispersion induced by the present enzyme reactor is twice as large as that induced by a single bead string reactor (70-cm-long, 0.8-mm-i.d. PTFE tube, filled with 0.5-mm-diameter glass beads) of same residence volume. For a 90-µL sample and carrier flow rate of 2.5 mL/min, the dispersion coefficient at peak maximum (*26*) was found to be 8.3 for the string reactor and 16 for the membrane-entrapped enzyme reactor.

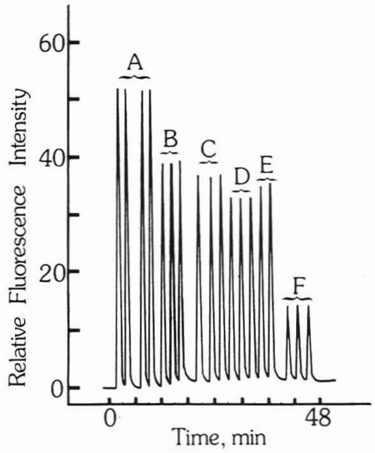

Figure 4. System output: (A, C, F) glucose standards, 1100, 777, and 333 µM, respectively; (B, D, E) plasma samples diluted with isotonic saline.

For the glucose determination system, the response was found to be linear from essentially the limit of detection (13 µg/L) to 2.5 g/L, spanning well over 5 orders of magnitude. These results come from the sequential two-enzyme reactor system described. When both enzymes were put in the same reactor, the response was significantly worse and such a system was not therefore pursued further. Plasma samples, when injected directly, tended to produce glucose values ~7% lower compared to injection of identical samples prediluted an order of magnitude or more with isotonic saline (results corrected for dilution). This is most likely due to matrix interferences in the undiluted samples. Because our primary purpose was not to accurately measure plasma glucose per se but to investigate the utility of the enzyme reactors, these details were not studied. Prediluted samples were injected for the most part and in-system dilution using a smaller injection volume was not investigated either. Some representative data are shown in Table I, along with nominal clinical values determined with a commercial clinical analyzer. Precision of our repeated measurements was excellent, a typical chart output is shown in Figure 4. Our results were also consistent with data obtained by standard addition of glucose to the same samples. While efforts to determine the stability of glucose oxidase in the reactor were not as extensive as for peroxidase, no change in analytical calibration and performance was apparent over use and storage at room temperature for 2 weeks.

The method described here can attain much higher enzymatic activity per unit reactor volume compared to other immobilization approaches. Because no chemical attachments are involved, the specificity and stability characteristics of the enzyme are expected to be the same as those in concentrated aqueous solution.

ACKNOWLEDGMENT

We are grateful to Joan M. Slep (Celanese Corp., Charlotte, NC) for the generous gift of various types of Celgard membranes, to Marita A. Mercurio-Cason (Texas Tech University Health Sciences Center) for the plasma samples, and to our colleague Robert W. Shaw for valuable discussion.

Registry No. H_2O, 7732-18-5; H_2O_2, 7722-84-1; Celgard, 9003-07-0; glucose, 50-99-7; glucose oxidase, 9001-37-0; peroxidase, 9003-99-0.

LITERATURE CITED

(1) Bowers, L. D. *Anal. Chem.* **1986**, *58*, 513A–530A.
(2) Guilbault, G. G.; Brignac, P. J., Jr.; Juneau, M. *Anal. Chem.* **1968**, *40*, 1256–1263.
(3) Lazrus, A. L.; Kok, G. L.; Gitlin, S. N.; Lind, J. A.; McLaren, S. E. *Anal. Chem.* **1985**, *57*, 917–922.
(4) Lazrus, A. L.; Kok, G. L.; Lind, J. A.; Gitlin, S. N.; Heikes, B. G.; Shetter, R. E. *Anal. Chem.* **1986**, *58*, 594–597.
(5) Kok, G. L.; Thompson, K.; Lazrus, A. L.; McLaren, S. E. *Anal. Chem.* **1986**, *58*, 1192–1194.
(6) Tanner, R. L.; Markovits, G. Y.; Ferreri, E. M.; Kelly, T. J. *Anal. Chem.* **1986**, *58*, 1857–1865.

(7) Hwang, H.; Dasgupta, P. K. *Anal. Chim. Acta* **1985**, *170*, 347–352.
(8) Dasgupta, P. K.; Hwang, H. *Anal. Chem.* **1985**, *57*, 1009–1012.
(9) Hwang, H.; Dasgupta, P. K. *Anal. Chem.* **1986**, *58*, 1521–1524.
(10) Gosnell, M. C.; Snelling, R. E.; Mottola, H. A. *Anal. Chem.* **1986**, *58*, 1585–1587.
(11) Hwang, H.; Dasgupta, P. K. *Mikrochim. Acta* (*Wien*) **1985**, *III*, 77–87.
(12) Gnanasekaran, R.; Mottola, H. A. *Anal. Chem.* **1985**, *57*, 1005–1009.
(13) Staude, E.; Jorisch, W. *Angew. Makromol. Chem.* **1986**, *96*, 21–36.
(14) Staude, E.; Jorisch, W.; Ansorge, W. *J. Memb. Sci.* **1982**, *11*, 289–296.
(15) Ciucu, A.; Magearu, V.; Luca, C. *Anal Lett.* **1985**, *18*, 299–313.
(16) Ikariyama, Y.; Aizawa, M.; Suzuki, S. *J. Solid-Phase Biochem.* **1980**, *5*, 223–233.
(17) Ansorge, W.; Staude, E. *J. Membr. Sci.* **1985**, *22*, 283–295.
(18) Hsieh, F.; Davidson, B.; Vieth, W. R. *J. Appl. Chem. Biotechnol.* **1976**, *26*, 631–644.
(19) Lasky, M.; Grant, G. *Am. Biotechnol. Lab.* **1985**, *1* (6), 16–21.
(20) Pilosof, D.; Nieman, T. A. *Anal. Chem.* **1982**, *54*, 1698–1701.
(21) "Celgard Microporous Hollow Fibers: Technical Information, Fabrication and Handling Bulletin", Celanese Corporation, Charlotte, NC, May 1983.
(22) Margoliash, E.; Schejeter, A. *Adv. Protein Chem.* **1966**, *21*, 113–286.
(23) Marklund, S; Ohlsson, P.-I.; Opara, A.; Paul, K.-G. *Biochim. Biophys. Acta* **1974**, *350*, 304–313.
(24) Marklund, S. *Arch. Biochem. Biophys.* **1973**, *154*, 614–622.
(25) Chance, B. *Arch. Biochem.* **1949**, *22*, 224–252.
(26) Ruzicka, J.; Hansen, E. H. *Flow Injection Analysis*; Wiley: New York, 1981.

Hoon Hwang
Purnendu K. Dasgupta*
Department of Chemistry and Biochemistry
Texas Tech University
Lubbock, Texas 79409-4260

RECEIVED for review September 8, 1986. Accepted December 19, 1986. The research in synthetic membrane technology is supported by the State of Texas Advanced Technology Research Program; the research on determination of hydrogen peroxide is supported by the U.S. Environmental Protection Agency through cooperative agreement no. CR-812366-01-0. However, this manuscript has not been subjected to review by the Environmental Protection Agency and no endorsements should be inferred.

Field Desorption Mass Spectrometry with Suppression of the High Field

Sir: Field desorption (FD) has proven to be a useful ionization technique for mass spectrometric analysis of many types of samples including synthetic polymers (*1*). More generally, FD complements (*2*) other ionization techniques such as laser desorption (*3*) or kiloelectronvolt atom bombardment (*4*). The mass spectra obtained by using FD typically exhibit molecular ions $[M]^{\bullet+}$ and/or so-called pseudomolecular ions, such as $[M + H]^+$ and $[M + Na]^+$, and fragment ions some of which, it has been proposed (*5*), are formed by field dissociation (*6*). An advantage of FD, compared to ionization techniques such as kiloelectronvolt atom bombardment, is that FD mass spectra are relatively clean and simple. Even so, interpretation of FD mass spectra is not always straightforward, particularly if judged by the standards set by electron impact mass spectra of gaseous samples. The theory of ion formation in FD has been developed in recent years (*7, 8*), but it can still be difficult to predict the peaks expected in the FD mass spectrum of a new compound. Another disadvantage of FD has been poor transmission due to ion losses at the counter electrode, i.e. most ions leaving the wire emitter do not pass through the slit in the counter electrode (*9*). We report here the introduction of a shield to the wire emitter type of FD source, which affords possibilities for raising the efficiency of ion transmission and significantly simplifying the mass spectra. The use of shielding to suppress high fields is well documented in other areas of field emission (*10, 11*).

EXPERIMENTAL SECTION

All measurements were made with a large double-focusing mass spectrometer, which has been described (*12, 13*). The emitters were produced from 10-μm tungsten wire by using a standard conditioning procedure (*14*). The microneedles on the emitters were 20–30 μm in length. The emitter heating currents employed for polypropylene glycol were in the range 10–11 mA. The slit in the counter electrode was 2 mm in width. Emitter potential was typically approximately 8 kV, and the separation from the normally grounded counter electrode was approximately 2 mm. Shields were fabricated by machining cylindrical grooves of various diameters (typically 1 mm) in brass electrodes, which were then attached to conditioned FD emitters.

RESULTS

Figure 1 shows calculated ion trajectories in the region between an unshielded wire emitter and counter electrode in the FD source. The wire emitter has been represented as a smooth wire of diameter 60 μm, corresponding to the average diameter of tungsten wire plus microneedles. The potential distribution in the region has been calculated (*14, 15*) by using a finite difference method (*16*). Repeated magnifications of the region around the emitter were used to achieve the spatial resolution required. Calculated field strengths for the unshielded emitter were similar to those obtained by using a simple analytical expression for an indefinitely long wire (*17*). It is evident from Figure 1 that the proportion of the total emitted ions passing through the slit in the counter electrode is low. The ion trajectories (Figure 1) begin at points around the circumference of the wire over the range from +90° to −90°. Adjacent points are separated from each other by 5°. Ions initially have zero kinetic energy. Trajectories within 20° of the central axis pass through the slit. Figure 2 shows the calculated ion trajectories in the case of an identical wire emitter with a shield in place. The diameter of the groove in the shield is 1 mm. The shield is at the same electric potential as the wire emitter. It is clear from Figure 2, that a much larger proportion of the ions pass through the slit in the counter electrode when the shield is in place. According to these calculations, trajectories within 70° of the central axis pass through the slit.

The calculated electric fields at ±90°, ±45°, and 0° on the surface of the wire are 5.8, 8.1, and 9.2 MV m^{-1}, respectively, with the shield in place (Figure 2) and 48.6, 49.5, and 49.9 MV m^{-1}, respectively, without the shield (Figure 1). These fields refer to a smooth circular wire of diameter 60 μm. Carbonaceous microneedles on the 10-μm wires used in the experiments below would considerably enhance the electric fields above these calculated values (*18*). The calculations show that the shield affects the electric field close to the wire emitter in two significant ways. The electric fields are generally

0003-2700/87/0359-1360$01.50/0 © 1987 American Chemical Society

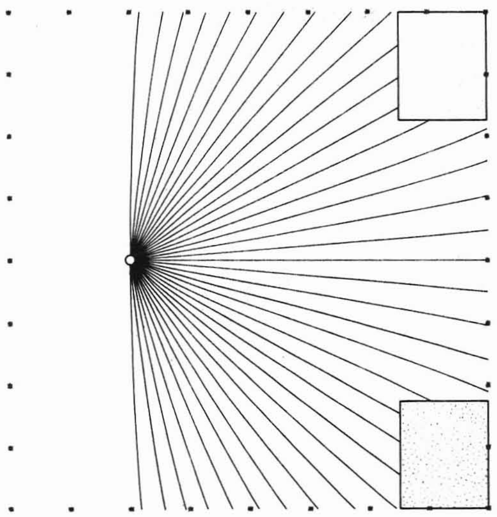

Figure 1. Calculated ion trajectories between wire emitter and counter electrode in a standard FD source.

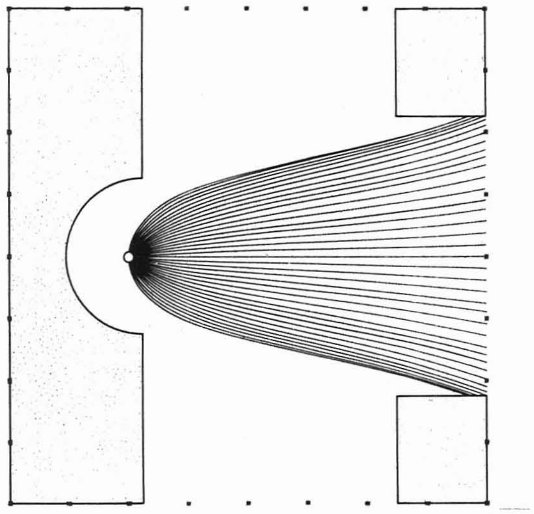

Figure 2. Calculated ion trajectories between wire emitter and counter electrode with shield around the wire.

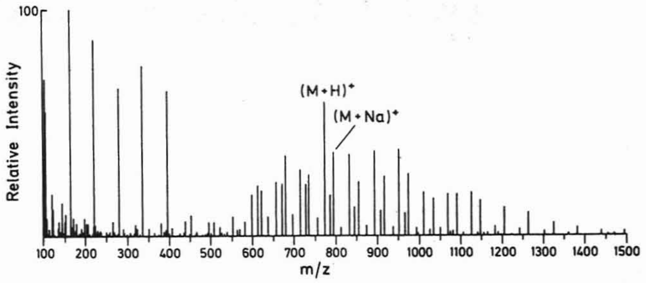

Figure 3. FD mass spectrum of poly(propylene glycol) obtained by using a standard FD source. ^{13}C isotope peaks have been omitted.

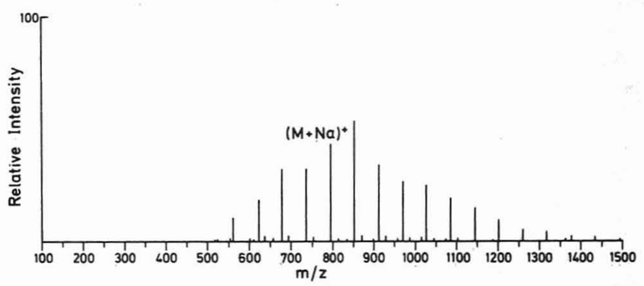

Figure 4. FD mass spectrum of poly(propylene glycol) obtained by using a shield around the wire emitter. ^{13}C isotope peaks have been omitted.

lowered. The field at the central front surface (i.e. 0°) with the shield in place is lower by a factor of 5, compared to the field at the same point without the shield. The second effect is to alter the distribution of fields over the surface of the wire. Without the shield, the fields at the sides of the wire (±90°) are almost as high (0.97 lower) as that at the front (0°). With the shield, the fields at the sides of the wire are lower by a factor of 0.63, compared to that at the front.

An FD mass spectrum of a sample of poly(propylene glycol) measured by using a wire emitter *without* a shield is shown in Figure 3. There are peaks due to $[M + H]^+$, $[M + Na]^+$, and various fragment ions (*19*). The intense fragment ion peaks at low m/z are attributed to field dissociation (*5*). An FD mass spectrum of the same sample measured with identical instrumental settings by using the same wire emitter *with* a shield is shown in Figure 4. Running the spectrum with the shield before that without the shield did not affect the results. With the shield, the major peaks are due to $[M + Na]^+$ ions. There are smaller peaks due to $[M + K]^+$ ions. It is to be noted that the absolute intensities of the peaks for $[M + Na]^+$ ions obtained when using the shield (Figure 4) were the same within a factor of 2 as those obtained without the shield (Figure 3). At the same time, the total ion current as indicated by the ion current measured at the counter electrode was 2 orders of magnitude *lower* for the shielded emitter, as compared to the unshielded or normal case. With the shield, both the total ion current and the mass-resolved ion currents appeared to be steadier than is normally the case in FD. The ion emission was at least as long-lived as is normally the case. We have observed this same general behavior with other compounds, including peptides. Spectra of poly(propylene glycol) essentially similar to that obtained when using the shielded emitter (Figure 4) were obtained by using a bare-wire emitter (10 μm W) and by using an unshielded conditioned emitter with a low potential difference (3 kV) between emitter and counter electrode. With the bare wire, signals were weak, fluctuating, and short-lived. With the ordinary emitter at low potential difference, $[M + Na]^+$ had not wholly replaced $[M + H]^+$ and the signals were very weak.

DISCUSSION

The calculations indicate that the shield should improve focusing characteristics between wire emitter and counter electrode and should substantially lower the electric field at the wire emitter. The measurements are consistent with these theoretical predictions. With the shield in place, the mass spectrum (Figure 4) exhibits only $[M + Na]^+$ ions, and the formation of $[M + Na]^+$ is generally considered to be a relatively low-field process (*20*). The absence of $[M + H]^+$ is seen as a consequence of the fields being too low. It has been shown (*5*) that the intensities of the fragment ion peaks at low masses depend strongly on the magnitude of the electric field, so that their disappearance on introducing the shield is to be expected given that that shield lowers the electric field. With the shield in place it was not possible to obtain field ionization signals, indicating that the electric field strength is indeed lowered. The extent to which the field is lowered by the shield can be estimated from the results of the experiments with unshielded conditioned emitters at lower potential difference. When the potential difference was reduced (by raising the cathode potential), the intensities of $[M + H]^+$ peaks fell at a greater rate than those of the corresponding $[M + Na]^+$ peaks and the intensities of the low mass fragments fell at a greater rate than those of the $[M + H]^+$ peaks. Reducing the potential difference by a factor of 3 removed all low-mass fragment peaks but did not cause $[M + Na]^+$ to wholly replace $[M + H]^+$. On the basis of this observed field dependence of the mass spectrum of poly(propylene glycol), it is estimated that the shield lowers the field strength by at least a factor of 3 (compared with a factor of 5 on the basis of the calculations).

The mass-resolved $[M + Na]^+$ ion currents were not significantly lowered on introducing the shield; however, total ion currents as measured at the counter electrode were drastically reduced. This is consistent with improved focusing between wire emitter and counter electrode together with lower total emission due to suppression of many of the ionic species present without the shield. There is a second possible effect contributing to the increased transmission through the slit in the counter electrode. The presence of the shield causes the electric field on the central axis of the wire emitter to exceed that at the sides of the wire, thus ion formation is expected to occur preferentially on the front central surfaces of the wire. Thus the shield can be considered both to increase the acceptance angle within which ions are transmitted through the slit and to encourage ion formation at the central parts of the wire from which ions are most easily collected.

Calculations with different sized grooves in the shield show that reducing the size of the groove increases the above-mentioned effects leading to increased focussing, decreased field strengths, and a greater percentage drop in field strength from the front to the sides of the emitter. The optimum sized groove would involve a balance between enhanced transmission of the ion beam and reduction in the field strength (necessary for the ionization process) and for the latter reason would therefore be sample dependent.

The analytical protocol suggested by the results is to use shields on wire emitters. The lower electric fields would bring practical side benefits through reducing the risk of sparks and breakage of emitters. The sample should be doped with an alkali halide salt. Sodium iodide at the 0.01 M level would usually be appropriate. Molecular ion peaks in the mass spectrum would be assignable with some confidence to $[M + Na]^+$ species. The sensitivity in terms of mass of sample consumed relative to mass-resolved ion current would be higher than with standard FD sources by something like 2 orders of magnitude, depending on the loading of the emitter and the exact positioning of shield and wire emitter. If a sample were appropriately loaded on the front of an emitter (*21*), it would be possible by using a shield to transmit 100% of the ions through the slit in the counter electrode. Finally, the shielded emitter provides a practical way of studying the effects of lowering the electric field on ionization and evaporation of ions in FD (*7*).

ACKNOWLEDGMENT

Preliminary measurements were made by Muljadji Agma. The contribution of Colin E. Allison to initial discussions concerning shaping of fields around emitters is acknowledged.

Registry No. Poly(propylene glycol), 25322-69-4.

LITERATURE CITED

(1) Latimer, R. P.; Harmon, D. J.; Hansen, G. C. *Anal. Chem.* **1980**, *52*, 1808–1811.
(2) Burlingame, A. L.; Baillie, T. A.; Derrick, P. J. *Anal. Chem.* **1986**, *58*, 165R–210R.
(3) Cotter, R. J. *Anal. Chem.* **1984**, *56*, 485A–504A.
(4) Barber, M.; Bordoli, R. S.; Sedgwick, R. D.; Tyler, A. N. *J. Chem. Soc., Chem. Commun.* **1981**, 325–327.
(5) McCrae, C. E.; Derrick, P. J. *Org. Mass Spectrom.* **1983**, *18*, 321.
(6) Beckey, H. D. *Z. Naturforsch., A: Astrophys., Phys. Chem.* **1964**, *19A*, 71–83.
(7) Derrick, P. J. *Fresenius Z. Anal. Chem.* **1986**, *324*, 486–491.
(8) Rollgen, F. W. *Ion Formation from Organic Solids*; Benninghoven, A., Ed.; Springer-Verlag: Berlin, F.R.C., 1983; p 2–13.
(9) Derrick, P. J. *Mass Spectrom.* **1977**, *4*, 132–145.
(10) Muller, E. W.; Nishikawa, O. *Rev. Sci. Instrum.* **1965**, *36*, 556.
(11) Orloff, J.; Swanson, L. W. *J. Vac. Sci. Technol.* **1981**, *19*, 1149–52.
(12) Darcy, M. G.; Rogers, D. E.; Derrick, P. J. *Int. J. Mass Spectrom. Ion Phys.* **1978**, *27*, 335–347.
(13) Cullis, P. G.; Neumann, G. M.; Rogers, D. E.; Derrick, P. J. *Adv. Mass Spectrom.* **1980**, *8b*, 1729–1738.
(14) Neumann, G. M.; Rogers, D. E.; Derrick, P. J.; Paterson, P. J. K. *J. Phys. D* **1980**, *13*, 485–494.
(15) Davis, S. C., unpublished work, Sydney, Australia, 1985.
(16) Lawrenson, P. J.; Binns, K. J. *Analysis and Computation of Electric and Magnetic Field Problems*; Pergamon: London, 1963.
(17) Migahed, M. D.; Beckey, H. D. *Int. J. Mass Spectrom. Ion Phys.* **1971**, *7*, 1–18.
(18) Beckey, H. D. *Principles of Field Ionization and Field Desorption Mass Spectrometry*, Pergamon: London, 1977.
(19) Neumann, G. M.; Cullis, P. G.; Derrick, P. J. *Z. Naturforsch., A: Phys., Phys. Chem., Kosmophys.* **1980**, *35A*, 1090–1097.
(20) Heinen, H. J.; Giessmann, U.; Rollgen, F. W. *Org. Mass Spectrom.* **1977**, *12*, 710–715.
(21) Linden, H. B.; Winkler, H. U.; Beckey, H. D. *J. Phys. E* **1977**, *10*, 657–660.

Stephen C. Davis
Gregory M. Neumann
Peter J. Derrick*

School of Chemistry
University of New South Wales
P.O. Box 1
Kensington, 2033 NSW, Australia

RECEIVED for review July 3, 1986. Resubmitted December 29, 1986. Accepted January 16, 1987.

Positive-Signal Indirect Fluorometric Detection in Ion Chromatography

Sir: Indirect detection in ion chromatography has been shown to be a useful and viable approach, especially as used in the "single-column" or "nonsuppressed" mode (*1*). The terminology of indirect and direct detection is sometimes confusing and provides no information as to the directionality of the analyte signal. Regardless of the "directness" of the chromatographic detection method, it is obvious that the detection must depend on a difference in some property of the analyte ion compared to an equivalent amount of the eluent ion. By and large, the method is considered indirect if the property being monitored (absorbance, fluorescence, conductance) is much larger for the eluent ion (after whatever type of postcolumn manipulation, including suppression) than for the analyte ion. This concept of directness of detection is not without problems. Pinschmidt's method (*2*) for the measurement of weak acid anions uses a "suppression" technique and indirect conductance detection. Should it instead be considered direct resistivity detection, as the author originally termed it? Second, single-column conductimetric anion chromatography with an hydroxide eluent clearly depends on indirect detection because hydroxide has the highest equivalent conductance of all anions. However, the more commonly used phthalate eluent leads to an ambiguous situation. While the majority of anions have greater equivalent conductances than phthalate, some organic anions do have lower equivalent conductances.

It is important to note that the directness of the detection method may or may not have much to do with the attainable limits of detection. Two of the most widely used determination modes in all of analytical chemistry involve measurements of optical absorption and electron capture detection. At the transducer level, both of these involve the measurement of a small change of current in a large standing current. Fluorimetry is considered one of the most sensitive analytical techniques. Mho and Yeung (*3*) have described a highly sensitive ion chromatographic method utilizing indirect

0003-2700/87/0359-1362$01.50/0 © 1987 American Chemical Society

double-beam laser fluorometric detection. Of all common properties monitored in chromatographic detection, fluorescence is perhaps the only one that is not a monotonic function of concentration. If indirect detection is defined as a technique which monitors deficiencies in eluent constituents rather than the emergence of sample components per se, a unique potential exists for indirect fluorimetric detection. Thus, the purpose of this paper is to report that with the eluent ion concentration in the strongly self-quenched region, indirect but positive signal fluorometric detection is a possibility worthy of consideration.

EXPERIMENTAL SECTION

A Perkin-Elmer Tri-Det HPLC system equipped with a 75-μL loop was used for all experiments. The system uses a trifunctional detector that accomplishes fixed-wavelength (254 nm) UV detection and uses the same source light for fluorescence excitation; the emitted light is monitored by a photodiode and conductance detection is achieved in the same cell by utilizing the steel connecting tubes to the cell as electrodes (*4*). While any of the individual functions offer far from the utmost in performance; the low-cost system was deemed ideal for exploratory studies. Relatively inefficient first-generation agglomerated anion exchanger columns from Dionex Corp. (3 × 150 mm precolumn + 3 × 500 mm analytical column) with an eluent flow rates of 2.0 mL/min were used in this work. Sample ions were prepared from analytical reagent grade potassium or sodium salts. 4-amino-1-naphthalenesulfonic acid (Aldrich) used as eluent was recrystallized from large volumes of hot water. The other eluent, sodium 6,7-dihydroxy-2-naphthalenesulfonate (Aldrich), was used without further purification. Because both eluents tend to undergo oxidative degradation (especially at high pH, readily apparent from discoloration), eluent solutions were prepared in water freed from oxygen by prolonged boiling and purging with O_2-free N_2 (passed through alkaline pyrogallate) while hot. Eluent fluorescence measurements were conducted on a Perkin-Elmer Model LS-5 spectrofluorometer.

RESULTS AND DISCUSSION

Our experiments were initially targeted toward selecting suitable eluents for single-column ion chromatography which takes advantage of the fact that all three outputs (conductance, UV, and fluorescence) are simultaneously accessible from the Tri-Det system, so as to derive maximum pedagogic benefits. Strong UV absorption at 254 nm and reasonable fluorescence quantum efficiency when excited at this wavelength (the instrument employs a photoiode for fluorescence detection, this is not especially sensitive) were desired criteria and limited the choice to large organic ions. Such ions automatically display the third desired chracteristic, low specific conductance. Hydroxy- or amino-substituted aromatic sulfonic acids were deemed suitable candidates. 6,7-Dihydroxy-2-naphthalenesulfonic acid, aniline-2-sulfonic acid, and 4-amino-1-naphthalenesulfonic acid were found to be good candidates; their molar absorptivity at 254 nm and fluorescence intensity increase in the order listed. The eluent strength of each of these ions was checked by injections of the individual ions as samples with 20 mM K_2SO_4 as eluent on a 3 × 150 nm column. The capacity factors of the three compounds were determined to be ~30, 1.5, and 6, respectively. Because it was found necessary to operate with these eluents at fairly low concentrations (≤1 mM), aniline-2-sulfonic acid was not further studied.

When 4-amino-1-naphthalenesulfonic acid was used as eluent in the concentration range 10^{-4}–10^{-3} M, the conductivity and UV response from typical sample anions were largely as expected (positive and negative, respectively) but fluorescence detection unexpectedly resulted in positive peaks. A typical separation of fluoride, chloride, and bromide is shown in Figure 1A. (Note that the small response due to fluoride is due to poor ionization at low pH, the pH of the 10^{-3} M eluent is 2.85. The eluent probably exists as a zwitterion under this condition, resulting in limited eluting power. The response and eluent strength may be increased by adjusting eluent pH to higher values, but oxidative degradation problems are exacerbated.) When 6,7-dihydroxy-2-naphthalenesulfonate was used as the eluent at a concentration of 10^{-3} M, once again conductivity and UV responses were as expected, while positive signals were observed in the fluorescence mode. This eluent was also considerably more powerful in eluent strength, as may be predicted from the initial retention study of the eluent ion itself, and allowed separation of much more strongly held sample ions under otherwise identical conditions. A typical chromatogram is shown in Figure 1B. While the relative response of fluoride is higher (eluent pH is 5.5), the absolute sensitivity attainable for other anions with this eluent is more than an order of magnitude lower.

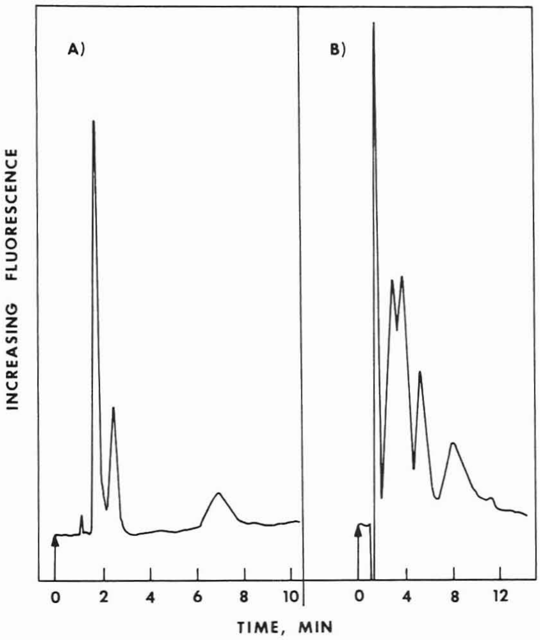

Figure 1. (A) Eluent: 10^{-3} M 4-amino-1-naphthalenesulfonic acid (pH 2.85), 2 mL/min. Peaks from left to right: Fluoride, system peak, chloride, bromide. The halide concentrations are 10^{-4} M. (B) Eluent: 10^{-3} M 6,7-dihydroxy-2-naphthalenesulfonic acid, sodium salt (pH 5.5), 2 mL/min. Peaks from left to right: fluoride, bromide, iodide, thiocyanate, sulfate (and perchlorate appearing as a shoulder). The injected sample ion concentrations are 10^{-3} M; the detector sensitivity is 4 times that in chromatogram A.

With both eluent systems, the retention order of sample ions was found to be similar to those reported earlier by Dasgupta (*5*) and Gjerde et al. (*6*). Response, as measured in terms of peak heights, was linearly related to sample concentration within the range 7.5–75 nmol.

The initially puzzling behavior of the system in the fluorescence detection mode became clear when the fluorescence of the eluents was studied as a function of concentration. The results, depicted in Figure 2, clearly show that at the concentrations used, the eluent fluorescence is in the strongly self-quenched region and therefore increases with dilution. This property may be useful in applications where one may tailor the eluent strength to operate at a relatively low background fluorescence, without severely sacrificing the sensitivity. Note that as shown in Figure 2, the maximum slope of the fluorescence intensity vs. concentration plot for 4-amino-1-naphthalenesulfonic acid in the quenched region is ~12% of the slope in the linearly increasing, low-concentration range. Considering that the inherent fluorescence efficiency of this compound is excellent (detectability is lower than 0.1 μM), this potential sensitivity is respectable. Although it has not been possible with the presently used column and detection system to demonstrate the exploitation of the

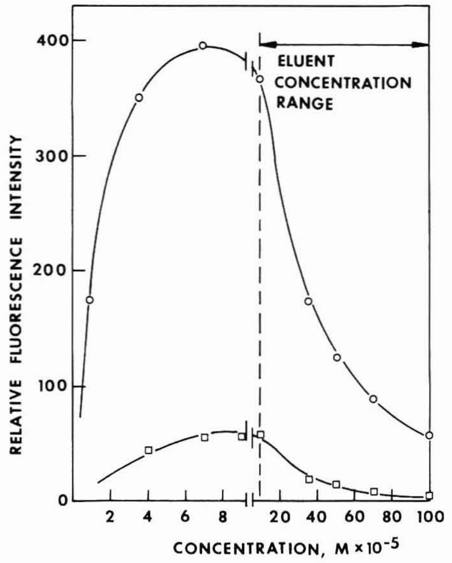

Figure 2. Fluorescence of 4-amino-1-naphthalenesulfonic acid (circles) and sodium 6,7-dihydroxy-2-naphthalenesulfonate (squares) as a function of concentration. Excitation wavelength 254 nm; emission wavelength 420 nm.

self-quenched eluent indirect fluorescence detection method at its optimum, the potential is evident.

ACKNOWLEDGMENT

We thank R. Quin Bligh for the initial screening of potential eluent substances.

Registry No. 4-Amino-1-naphthalenesulfonic acid, 84-86-6; sodium 6,7-dihydroxy-2-naphthalenesulfonate, 135-53-5; fluoride, 16984-48-8; chloride, 16887-00-6; bromide, 24959-67-9; thiocyanate, 302-04-5; sulfate, 14808-79-8; perchlorate, 14797-73-0; iodide, 20461-54-5.

LITERATURE CITED

(1) Fritz, J. S.; Gjerde, D. T.; Pohlandt, C. *Ion Chromatography*; Huthig: New York, 1982.
(2) Pinschmidt, R. K. In *Ion Chromatographic Analysis of Environmental Pollutants*; Mulik, J. D., Sawicki, E., Eds.; Ann Arbor Science: Ann Arbor, MI, 1979; Vol. 2, pp 41–50.
(3) Mho, S.-I.; Yeung, E. S. *Anal. Chem.* **1985**, *57*, 2253–2256.
(4) Gant, J. R.; Perone, P. A. *Am. Lab.* (*Fairfield, Conn.*) **1985**, *17*, 104–111.
(5) Dasgupta, P. K. *Anal. Chem.* **1984**, *56*, 769–775.
(6) Gjerde, D. T.; Schmuckler, G.; Fritz, J. S. *J. Chromatogr.* **1980**, *187*, 35–45.

Kazimierz Jurkiewicz[1]
Purnendu K. Dasgupta*
Department of Chemistry and Biochemistry
Texas Tech University
Lubbock, Texas 79409-4260

RECEIVED for review September 22, 1986. Accepted December 23, 1986. This work was supported by the Office of the Basic Energy Sciences of the U.S. Department of Energy through Grant DE-FG-05-84ER-13281. However, this manuscript was not subject to review by the agency and no endorsement should be inferred.

---

[1] Permanent address: Department of Physical Chemistry, Marie Curie Sklodowska University, 20031 Lubin, Poland.

AIDS FOR ANALYTICAL CHEMISTS

Generation of Excess Low Frequency Noise on an Optical Source

Edward Voigtman[1] **and James D. Winefordner***
Chemistry Department, University of Florida, Gainesville, Florida 32611

Just as the concept of an ideal signal source facilitates the analysis of a physical system model, so too does the concept of an ideal noise source. Such a source would provide noise power of arbitrary intensity, in arbitrary domain (i.e., electrical, acoustic, mechanical, and so on), and of arbitrary power spectral density (equivalently, arbitrary autocorrelation or autocovariance function). Such a noise source does not exist and would probably be too versatile and expensive anyway.

In this paper, we address the problem of impressing an excess low frequency (ELF) noise on an optical source. We do not much care what the noise intensity is, in what domain the noise is originally generated, or precisely what the noise power spectral density is, so long as the noise is ELF noise, i.e., noise that is predominantly low frequency in character. Clearly, this task is easiest when the optical source is readily electrically modulatable, as is the case for continuous wave (CW) lasers, LEDs, and hollow cathode lamps. The task is much more difficult when constraints are added. Thus, if the ELF noise power spectral density is required to monotonically decrease with increasing frequency or if the ELF noise is expected to fit a $1/f^{\alpha}$ power spectrum, then the problem may be all but intractable.

We consider the easy case, first assuming that direct modulation of the optical source is easy, then assuming direct modulation is infeasible. In particular, in the latter case, we consider a He–Ne laser without modulation input and having "resin-dipped" circuitry. This situation arose in connection with an experiment involving the multiplex disadvantage in UV–vis Fourier transform spectroscopy. It was desired to produce a strong, flickering "interferent" spectral line and use it to degrade the detection of a weak, stable "analyte" spectral line. The question is: does interferent flicker noise uniformly spread throughout the spectrum or is it worse in the vicinity of the interferent line? The answer is given elsewhere (*1*). Here, we will demonstrate several simple ways to generate ELF noise on several optical sources. Note that we have used the term "flicker" to describe the ELF noise above. More, properly, flicker noise is ELF noise with $1/f$ power spectrum. The term will be used in its more rigorous sense below.

ELECTRICAL ELF NOISE

When it is desired to generate noise in the electrical domain, the available noise generation techniques are very good and provide an adequate approximation of ideal behavior. White noise may be generated merely by using a noise diode (from, e.g., Microwave Diode Corp., West Stewartstown, NH) or, in the digital domain, by using a noise generator integrated

---

[1] Present address: Chemistry Department, University of Massachusetts, Amherst, MA 01003.

0003-2700/87/0359-1364$01.50/0 © 1987 American Chemical Society

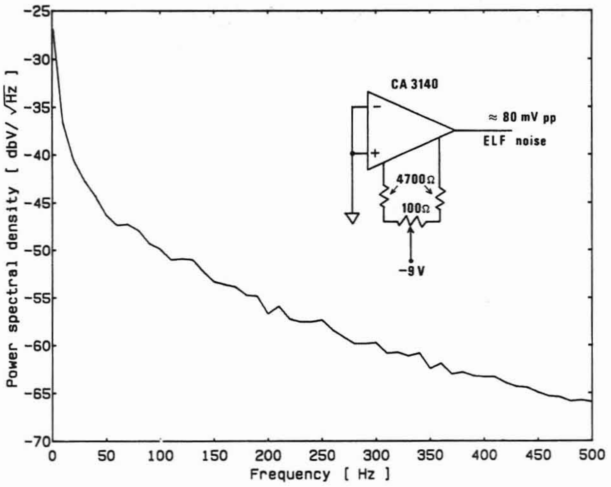

Figure 1. Analog ELF noise generator circuit and its noise power spectral density out to 500 Hz.

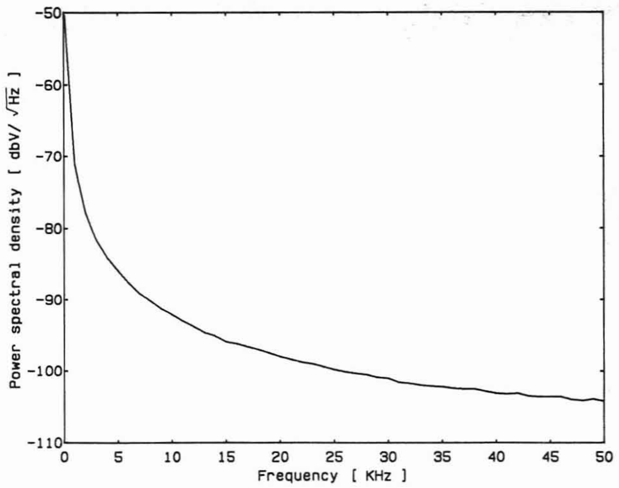

Figure 2. Noise power spectral density, to 50 kHz, for the circuit in Figure 1.

circuit (essentially just an appropriately tapped shift register and clock) such as the MM5837. With appropriate filtering, nonwhite noise is produced. As an example, Horowitz and Hill (*2*), among others, describe a "pink" (1/*f*) noise generator using the MM5837 and a filter with approximately 1/*f* power transfer function over the range of 10 Hz to 40 kHz. This range, an octave above and below the defined human hearing range, makes the circuit useful in equalizing stereo speaker systems.

Unfortunately, it is impractical to scale the filter components to produce a more useful 1/*f* noise range of, e.g., 0.01 to 40 Hz. Another drawback of the circuit is that the -3 dB/octave (1/*f*) filter needed to produce pink noise from white noise can only be constructed in an approximate manner because true 1/*f* noise behavior seems to require a continuum of time constants for its generation. The filter used by Horowitz and Hill (and others) uses four time constants in lieu of the continuum and is accurate within ±0.25 dB over the stated frequency range. The MM5837 is also unsuitable for low-frequency applications because it produces no frequency components below about 1 Hz (*2*).

Laeven et al. (*3*), in a well-written paper, describe a much more sophisticated noise generation scheme involving a suitably fast microcomputer or minicomputer with analog-to-digital (A/D) and digital-to-analog (D/A) capabilities. This system, which comes close to the ideal noise generator in the electrical domain, is not quite capable of real-time operation, although a previously generated noise data set may be "read-out" at high speed, giving a simulacrum of real-time performance. The main disadvantage of computer-generated noise is the relative expense of the method. Overall, a simple hardware technique would be preferable in many instances.

Given the mature state of semiconductor physics and device technology, it should be relatively easy to fabricate a flicker noise diode and much easier to fabricate an ELF noise diode. Lacking these useful devices, a simple active circuit may be devised which produces ELF noise and has the advantage of buffered output. This circuit is shown in Figure 1 together with the noise power spectrum, out to 500 Hz, measured with a Wavetek 5820B cross-channel spectrum analyzer. Figure 2 shows the noise power spectrum out to 50 kHz.

The extreme simplicity of the circuit derives from the observation that the RCA CA3140 op amp has a 1/*f* noise power spectral density, for the equivalent input voltage noise, over the entire published frequency range of 10 Hz to 100 kHz (*4*). Horowitz and Hill (*2*) extend the range down to 0.1 Hz, so the op amp has no noise corner frequency. Thus, the circuit shown in Figure 1 is simply designed to eliminate all noise sources other than the equivalent input voltage noise. Alternatively, it may be considered as a simplified version of the low frequency noise test circuit used by op amp manufacturers, e.g., Precision Monolithics (*5*). The output trimming is necessary because both the equivalent input voltage noise and the input offset voltage are amplified by the (frequency dependent) open loop gain of the op amp. The frequency dependence of the gain causes the observed noise power spectrum to be different than 1/*f* but, nevertheless, quite usable in many cases. At frequencies below about 10 Hz, the observed noise power spectrum approaches 1/*f* behavior.

We have used this circuit, which requires 5–10 min warm-up time, to modulate an LED output, using a voltage-to-current converter (transadmittance amplifier). Using a photodiode to convert the noisy LED output to current and then a current-to-voltage converter (transimpedance amplifier) gives an output which may be processed by the spectrum analyzer. The noise power spectra (direct and transimpedance amplifier output) are identical, as are the voltage waveforms, which may be compared by using an oscilloscope in differential mode and adjusting the gain of one channel suitably.

With an appropriate high-voltage transistor or op amp, it is straightforward to modulate a neon bulb (the incoherent version of a He–Ne laser) to produce atomic spectral lines with ELF noise spectra. With a suitable interference filter, a spectrally clean, atomic spectral line ELF noise source is obtained. Alternatively, hollow cathode lamps may be directly modulated since their power requirements are modest (several hundred volts and a few milliamperes) and the modulation is inherently at low frequency.

NONELECTRICAL ELF NOISE

For domains other than the electrical domain, it may be possible to convert from the preferred electrical domain, as with a speaker, motor, or modulator, or it may be possible to directly generate noise with the requisite properties without bothering with the electrical domain. Unfortunatley, these alternatives are usually not as satisfactory as might be hoped, but an exception occurs in the case where the noise is only mildly constrained, i.e., when the noise merely needs to be ELF noise.

For the case where a He–Ne laser must be modulated by nonelectrical means, one obvious method is to use a chopper wheel with the wheel replaced by a noise disk. The noise disk is simply a transparency sprayed (sputtered) with black paint. A disk was cut from such a transparency, the edge was darkened to simulate a five sector disk (because the chopper wheel driver uses an opto-coupler to sense and control the wheel speed), and the resultant noise transparency was rotated at 11 rpm. The He–Ne laser beam passing through the ro-

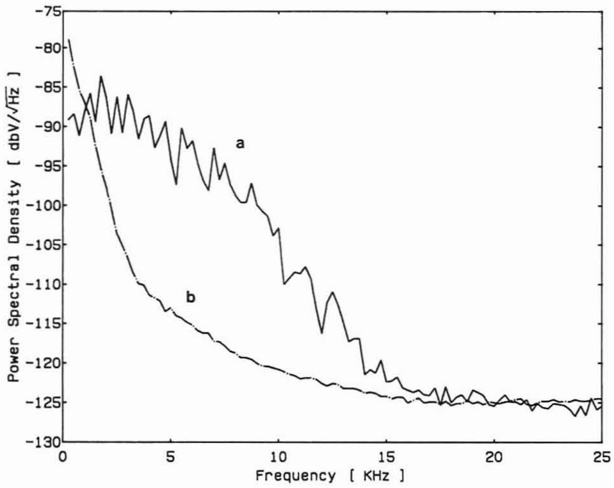

Figure 3. (a) ELF noise power spectrum generated by a rotating noise disk. (b) ELF noise power spectrum generated by a "sandfall".

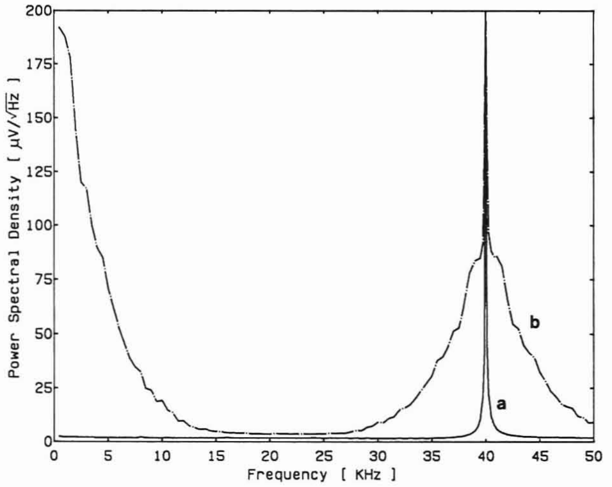

Figure 4. (a) Modulated, noiseless He-Ne laser power spectrum. (b) Modulated, noisy (rotating noise disk) He-Ne laser power spectrum.

tating transparency was attenuated and then converted to an electrical signal by a large area photodiode and transimpedance amplifier. The resulting noise power spectrum is shown in Figure 3a. As in the case of white or pink noise generated by the tapped shift register technique, the noise is periodic and the power spectrum is really a series of closely spaced discrete frequencies, but this is usually not detrimental. Varying the disk rotation rate varies the spectral width of the noise power spectrum in a convenient manner. Figure 3b is discussed later.

The utility of this noise power spectrum may be seen in Figure 4. Figure 4a shows the fundamental frequency component obtained when a He–Ne laser is square-wave modulated at 40 kHz using an acoustooptic modulator. The dc laser component is suppressed by ac coupling and the spectrum analyzer resolution element, for this frequency span, of 125 Hz. Figure 4b shows the case where the rotating noise disk is placed between the laser and the acoustooptic modulator. Both the dc component of the He–Ne laser beam and the fundamental component at 40 kHz are seen to be spectrally "tagged" with the distinctive noise disk power spectrum.

Another easily constructed noise source is suggested by a statement in Horowitz and Hill to the effect that the fall of sand in an hourglass is characterized by flicker noise (*2*). Presumably, this means that the weight of a running hourglass, i.e., one with freely falling sand grains, is noisy and the noise is $1/f$ noise. If a He–Ne laser beam is directed through such a "sandfall", from a funnel, the resultant noise power spectrum is shown in Figure 3b. This spectrum is significantly different from the rotating noise disk spectrum; e.g., they have different "curvature", and the spectrum is truly random. Neither ELF spectrum is adequately described by a $1/f^{\alpha}$ curve fit, so neither technique produces true flicker ($1/f$) noise, but, as seen above, this is not always of prime importance. The two demonstrated ELF noise generation schemes, having the advantages of extreme simplicity, inexpensiveness, and robustness, will suggest themselves to the reader.

LITERATURE CITED

(1) Voigtman, E.; Winefordner, J. D., submitted for publication in *Appl. Spectrosc.*
(2) Horowitz, P.; Hill, W. *The Art of Electronics*; Cambridge University Press: New York, 1980.
(3) Laeven, J. M.; Smit, H. C.; Lankelma, J. V. *Anal. Chim. Acta* **1984**, *157*, 273–290.
(4) RCA Solid State "Linear Integrated Circuits and MOS/FET's"; Report SSD-240B, RCA, 1982; p 162.
(5) *Linear and Conversion Products*; 1986/1987 Data Book; Precision Monolithics Inc.: Santa Clara, CA, 1986; pp 5–135.

RECEIVED for review September 16, 1986. Accepted January 12, 1987. The authors gratefully acknowledge support from DOE–AS05–780R06022.

Photolysis and Photo Cyclic Voltammetry as Mechanistic Tools

William R. LaCourse, Carl M. Selavka, and Ira S. Krull*

Barnett Institute and Department of Chemistry, 341 Mugar Building,
Northeastern University, Boston, Massachusetts 02115

Although high-performance liquid chromatography (LC) methods and instrumentation have become quite sophisticated and powerful, it is clear that there will always be analytical problems that cannot be solved solely on the basis of chromatographic resolution. For this reason, there has been substantial effort to produce selective detection approaches for LC. In addition, the desire to quantitate analytes of interest at ultratrace levels has been a driving force for a great deal of research to improve the sensitivity of LC detectors. Electrochemical (EC) detection in LC (LCEC) is an inexpensive method which has been demonstrated to offer a sensitive and selective alternative to UV absorbance and fluorescence detection. However, there remain several analytically important classes of compounds that are not amenable to these conventional detection methods, for which derivatization has been utilized to improve detectability (*1*).

Many pre- and postcolumn, on- and off-line derivatizations have been devised specifically for LCEC (*2*). Our work has centered around the use of UV light as a "derivatization reagent" for improved EC detectability and has generated two distinct analytical methods. In the first of these, known as LC–photolysis–EC (LC–$h\nu$–EC) detection, the eluent from the analytical column is irradiated in a continuous, on-line manner as it flows through a knitted open tubular (KOT) photolysis

0003-2700/87/0359-1366$01.50/0 © 1987 American Chemical Society

chamber constructed from Teflon tubing. Following this postcolumn UV irradiation, the eluate is directed to a conventional amperometric detector, which is operated at oxidative potentials. In this way, analytes that either exhibit no inherent electroactivity or may only be electrochemically reduced are photolytically converted to relatively stable species, which are amenable to oxidative EC detection. To date, LC–*hν*–EC detection has been successfully applied for the trace determination of explosives and related nitro compounds in postblast residues (*3, 4*), organothiophosphate pesticides in grain extracts (*5*), β-lactam antibiotics in commercial formulations (*6*), barbiturates and benzodiazepines in biological fluids (*7*), cocaine in illicit preparations (*8*), and organoiodides in pharmaceuticals (*9*).

A second derivatization-detection device, known as the photoelectrochemical detector (PED), has also been described recently. In LC–PED, the eluate from the analytical column passes through a thin-layer, amperometric cell that has been modified such that the working electrode can be continuously irradiated with high-intensity UV light. In this manner, nonelectroactive analyte molecules are able to absorb photoenergy, which is directly converted to electrochemical energy via a photoreduction reaction. As the photochemical reactions ensue, the PED monitors the electroactivity of transients, intermediates, and/or photoproducts generated in excited-state processes. Since the photochemical "derivatization" takes place in the immediate vicinity of the working-electrode surface, the lifetimes of detected species are on the order of microseconds. This complements LC–*hν*–EC detection, where relatively long-lived ions, intermediates, and/or solvolysis products are generated and detected. Since the introduction of PED in 1984, this detector has been optimized and characterized and has been found to be generally selective and sensitive for carbonyl-containing compounds, as well as several analytes containing other functional groups (*10–12*). PED has been successfully applied to the determination of benzaldehyde in various foodstuffs (*13*).

For both LC–*hν*–EC detection and LC–PED, it was essential to define the mechanisms of detection. One of the most important aspects of these mechanistic studies was the identification of the species formed during the photochemical processes that were responsible for the electrochemical responses. In LC–*hν*–EC detection, since the species involved are relatively stable, it was possible to perform product analysis following bulk photolysis of an analyte of interest through the use of ion-, gas-, or liquid-chromatographic methods, and appropriate standards of the possible photohydrolysis products. However, these chromatographic methods did not provide information regarding the electrochemical properties of product(s) in the photolyzed solutions. It was, therefore, desirable to produce a method that would allow for rapid study of the convoluted electrochemical behavior of the photogenerated species. Cyclic voltammetry (CV), coupled to a bulk photolysis arrangement, appeared to offer a simple, rapid, and inexpensive means for studying the EC properties of irradiated compounds. It was also envisioned that such an experimental design would provide for rapid screening of analytes, to determine their amenability to LC–*hν*–EC detection and to study the relationships between EC response and pH, supporting electrolyte composition, dissolved oxygen content, and irradiation time. A similar, yet less entailed, experiment has been reported in a technical publication (*14*), in which the CV behavior of flavin mononucleotide was examined after exposure to room light for 0, 10, and 20 min.

The criteria for an electrochemical probe for PED mechanism elucidation were substantially different than those for *hν*–EC detection. Due to the short lifetimes of the electrochemically active species formed in the PED process, it was envisioned that proper EC sampling would have to be rapid and would have to occur at the site of irradiation. Some early detailed examinations of the behavior of transients formed during flash photolyses, in static solutions, incorporated polarographic detection (*15–19*). More recently, Johnson et al. employed a modified rotating ring–disk electrode (RRDE), which was altered in such a way that continuous irradiation of the solution directly adjacent to the electrode could be performed (*20, 21*). The RRDE added hydrodynamic control to the system, in that photochemically generated species were swept toward the working-electrode surfaces, while the detected species were transported away from the electrode area. This method has also been used by other workers to study photochemically generated semiquinone intermediates (*22*). "Reconstructed" cyclic voltammograms were produced on a point-by-point basis, but the emphasis of these techniques was to provide temporal resolutions of sequentially produced, short-lived, photointermediates.

For the PED work, a technique was needed in which the net photocurrent of a multiplicity of species could be obtained, as a function of the applied potential, in a rapid and efficient manner. Again, CV appeared to offer advantages over other possible approaches, as long as the sampling cell could be modified to allow for direct irradiation of the electrode surface. This photo-CV method would also be useful in rapidly ascertaining the PED activity of untested compounds, optimizing LC–PED conditions, and observing and studying ensuing photochemical reactions.

On the basis of potential advantages offered in the use of CV for mechanism elucidation, methods optimization, and related studies in both LC–*hν*–EC detection and LC–PED, approaches for performing photolysis-CV and photo-CV (summarily termed PCV) were devised. The utility of PCV was tested using an organoiodide for photolysis-CV, while benzophenone and anthraquinonedisulfonate (AQDS) were examined in photo-CV studies.

EXPERIMENTAL SECTION

Apparatus. Both of the PCV designs incorporated commercially available CV equipment, including a 3-mm-diameter glassy-carbon working electrode, an Ag/AgCl/3 M NaCl reference electrode (RE-1), and a platinum-wire auxiliary electrode (Bioanalytical Systems, Inc. (BAS), West Lafayette, IN). Voltammograms were produced using a Model CV-1B cyclic voltammograph (BAS), and data were collected on a Hewlett-Packard Model 7004B X-Y recorder. Light sources and associated equipment, as well as the cell designs for PCV, were different for the two related techniques, and thus require individual explanation.

Photolysis-CV. Construction of the photolysis-CV system required two modifications of the basic CV apparatus. As shown in Figure 1, the first modification involved the use of a 25-mL glass Luer-lok syringe (Becton, Dickinson and Co., Rutherford, NJ) to load liquid samples into the photolysis chamber for batch irradiation. The photolysis apparatus incorporated in these experiments was the Photronix Model 816 UV batch irradiator (Photronix Corp., Medway, MA) with a knitted open tubular (KOT) reactor made of Teflon. The KOT was composed of 9.144 m (30 ft) of 0.5-mm-i.d. × 1.6-mm-o.d. tubing, having a volume of about 1.8 mL. The irradiator was composed of a low-pressure Hg lamp, having principle output at 254 nm and minor bands at 314, 365, 404, and 435 nm, a quartz finger to isolate the lamp from the cooling bath, and a stainless steel bucket, used to contain the cooling ice-water bath in which the quartz finger and lamp assembly were immersed. These particular components were chosen because they are used in the LC–*hν*–EC experiments (*4, 6–9*). Thus, their inclusion in PCV experiments would provide data that would be useful for the formulation of answers to the mechanistic questions under study.

The second modification involved the reduction of the sample cell volume for PCV. The commercially available CV apparatus

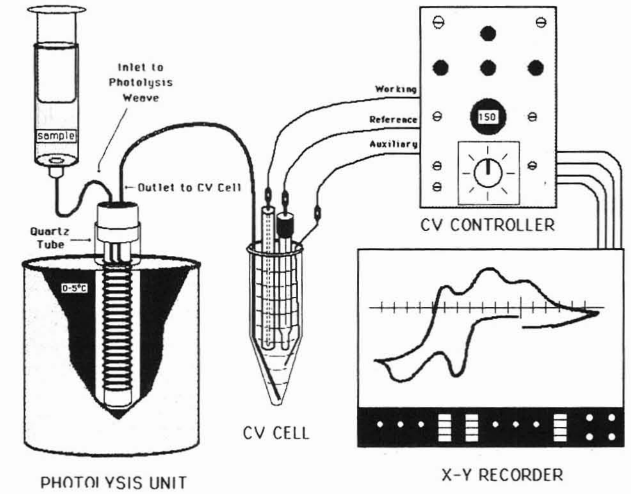

Figure 1. Schematic representation of the photolysis-CV apparatus.

normally used in this laboratory (part number MF 1052, BAS) requires approximately 10 mL of sample, which is substantially greater than the 1.8-mL volume delivered by the KOT used in the PCV design. To reduce this requisite volume to the appropriate level, the three electrodes (working, auxiliary, and reference) were fastened together with Teflon tape and were positioned as deep as possible in a 10-mL conical test tube. In order to facilitate this positioning, the conical tube was scored and broken at the middle of its length, and the edges of the break were fire-polished. Additionally, a short piece of Teflon tubing was positioned in the tube to allow for rapid purging and cleaning of the cell between experiments, as well as for the removal of aliquots of photolyzed solutions for chromatographic analysis. In use, this modified "micro-CV" cell readily allowed for CV analysis of solution volumes between 1 and 3 mL.

Photo-CV. In addition to the basic CV instrumentation, photo-CV required a modified voltammetry cell and a Model USSH-102D 100-W high-pressure Hg lamp with an LPS-200 power supply (Photon Technology International, Princeton, NJ). The modified voltammetry cell is illustrated in Figure 2. For its construction, an RC-2A reference electrode compartment (BAS), with the cell inlet port machined to enlarge the existing cavity to a diameter of 1.2 cm, was placed in an inverted position. A 7-mm-diameter hole was drilled in the side of the cell, at a 30° angle, to accommodate a tight-fitting 4.5-cm length of Teflon tubing. Two 1.6-mm holes were also drilled through the body of the cell, near the bottom of the cavity; through one, a 1.6-mm-diameter platinum wire (auxiliary electrode) was positioned, and in the other was placed a 3-cm length of 1.6-mm diameter Teflon tubing. This tube was fitted with a three-way single key valve (Anspec Co., Ann Arbor, MI), which allowed the tubing to act both as a drain and a helium purge port. All tube/cell wall interfaces were sealed with Duro brand epoxy cement (Loctite Corp., Cleveland, OH).

As with photolysis-CV, an Ag/AgCl reference electrode and a glassy-carbon working electrode (BAS) were incorporated and were arranged as shown in Figure 2. A flat mirror was used to focus the converging light from the Hg lamp onto the working electrode surface. The entire system was surrounded by a grounded, flat-black-painted, aluminum box in order to reduce UV-light hazards to laboratory personnel and to act as a Faraday cage.

Reagents. All organic and inorganic reagents were obtained in the highest available purity from Aldrich Chemical Co. (Milwaukee, WI), except HCl and NaOH, which were purchased from J. T. Baker (Phillipsburg, NJ). Solvents used were the Omnisolv-grade, from EM Science (Cherry Hill, NJ).

Procedure. Warning! UV radiation can cause eye injuries. The use of protective goggles is recommended, and bare skin should not be exposed to the radiation source. Researchers should take appropriate precautions to minimize the escape of UV light from the apparatus.

Photolysis-CV. Typically, photolysis-CV was performed by first loading the solution to be analyzed in the sample syringe and then pushing the solution into the KOT. After irradiating the sample for the desired amount of time, the lamp was switched off and the irradiated solution was forced into the micro-CV cell. Separation of the irradiated solution from the bulk, unphotolyzed solution in the syringe was achieved by introducing air bubbles into the stream (by tilting the syringe). The initial potential was chosen such that no oxidative or reductive current was apparent (0.0 V). Recording the CV involved a forward scan to the positive switching potential followed by a reverse scan to the negative switching potential. The potential range was rescanned through two more cycles before the experiment was terminated. With the exception of the studies designed to test the scan rate dependence of the current responses, the scan rate used was 150 mV/s. In each of the specific experiments described below, PCV of the supporting electrolyte was performed as part of the procedure, using the same experimental parameters as those used for solutions containing the analyte of interest, to ascertain the presence or absence of a PCV response endogenous to the supporting solution. Unless otherwise noted, the supporting electrolyte was the mobile phase commonly used in feasibility studies in LC–$h\nu$–EC, viz. 50/50 (v/v) MeOH/0.2 M NaCl.

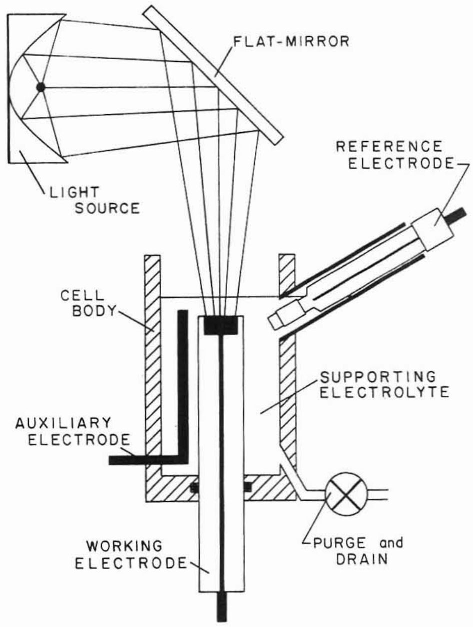

Figure 2. Schematic diagram of the photo-CV apparatus.

Several experiments were performed to test the design utility of the apparatus for mechanistic studies of organoiodides. First, it was important to understand the fate of any I^- that might be formed, photolytically, from appropriate organoiodide precursors, especially with respect to the possibility of recombination with dissolved oxygen in the supporting electrolyte, leading to formation of oxygenated anions of iodide. In order to study the endogeneous and photolytically induced electroactivity of such species, 1 part per thousand (1 ppt, 1 mg/mL) solutions of I^-, IO_3^-, and IO_4^- were prepared in supporting electrolyte and subjected to CV and PCV analysis, using periods of irradiation between 1 and 6 min, at 1-min increments. Positive and negative switching potentials of +1.2 and −0.4 V, respectively, were used. Also, PCV was performed on 1 ppt solutions of I^- that had been sparged of dissolved oxygen by bubbling with N_2 before irradiation or had been bubbled with oxygen for 1 min, to determine the effect of the presence of dissolved oxygen on the generation of IO_3^- and IO_4^-. Study of the coupling of oxidative and reductive waves in the voltammogram for I^- was facilitated by manipulating the initial potential, the anodic switching potential, and the direction of the scan.

Once the CV and PCV behavior of iodide and its oxygenated species had been ascertained, PCV experiments were attempted on solutions of 1-iodopentane (IP). These experiments were designed to study the temporal behavior of the photogeneration process, as well as the pH dependence of limiting current values and peak potentials for oxidative and reductive waves evidenced in the voltammograms. In this set of tests, a stock solution of the analyte was prepared at 25 ppt in MeOH. Then, 1-mL aliquots

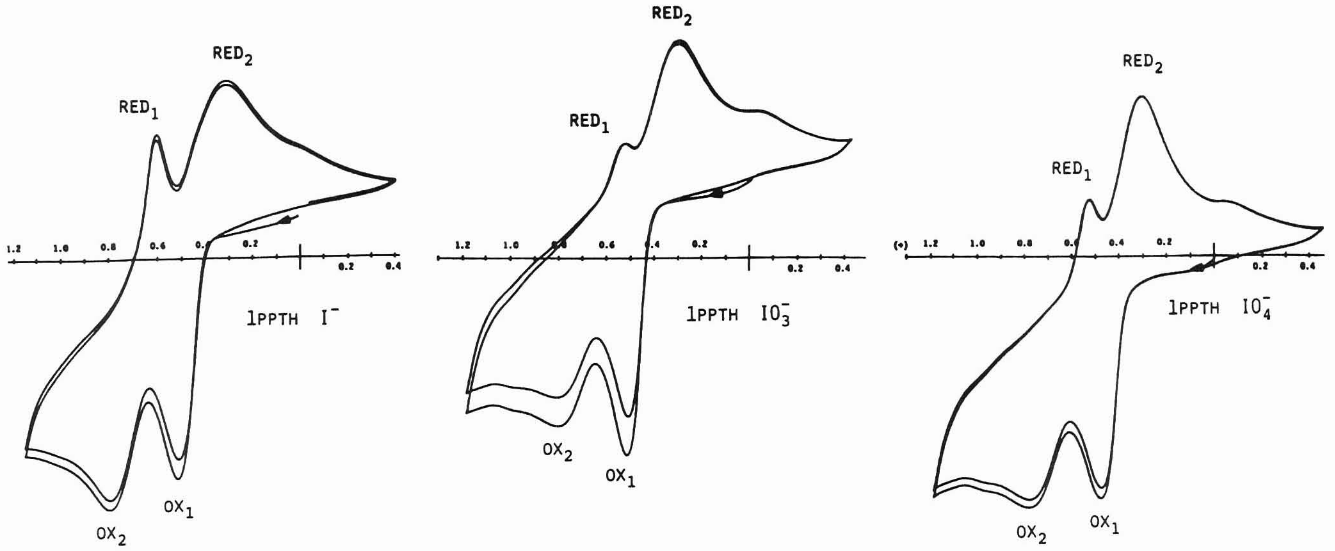

Figure 3. Photolysis-cyclic voltammograms of 1 ppth I^-, IO_3^-, and IO_4^- solutions in 50:50 MeOH:0.2 M NaCl, after 6-min irradiations.

of this stock solution were diluted to 25 mL with 50/50 MeOH/0.2 M NaCl, which had been adjusted to the desired pH (between 3 and 10) using HCl or NaOH. PCV of these 1 ppt solutions was performed using the same regimen of irradiation periods (1 to 6 min at 1-min increments) as those for inorganic iodide.

Photo-CV. In order to simulate the experimental conditions of the PED, all sample solutions and blanks were filtered and purged of dissolved oxygen. Approximately 5 mL of solution was degassed for 3 min by helium sparging. The solutions were then passed through a 10-mL plastic syringe, which was packed with ca. 2-mL of 400-mesh granular Zn (Fisher Scientific, Pittsburgh, PA) and fitted with a 0.45-μm LS025 disposable filter (Millipore Corp., Bedford, MA), into the modified CV cell (*23*). A continuous flow of helium was introduced into the cell, except during the time analysis. This system of deoxygenation allowed for determination of the relative photoactivity of PED-active compounds. The cell could be modified with a sealed quartz window and valved vent to produce a completely air-free environment. The working electrode was positioned such that only a thin layer of solution was between the electrode and the liquid's surface. This served to minimize the effective irradiated volume above the working electrode. With the exclusion of the time during which irradiated CV sampling was performed, the light from the lamp was blocked with a shutter.

An initial potential of 0.0 V was chosen for all PCVs because the oxidative and reductive currents at this point were generally minimal. The forward scan proceeded to a negative switching potential of −1.0 V, and the reverse scan encountered a positive switching potential of +0.4 V. The first cycle of each run was recorded, but the second cycle was also monitored to confirm the validity of the first. Most PCVs were obtained using a scan rate of 200 mV/s, and, unless otherwise noted, the supporting electrolyte for photo-CV experiments consisted of various compositions of isopropyl alcohol and water with an overall NaCl concentration of 0.1 M. This supporting electrolyte composition mimicked the mobile phase that allowed for optimum response on the PED. Analyte solutions were prepared at ca. 100 ppm in supporting electrolyte.

PCV response of the blank supporting electrolyte was first ascertained under experimental conditions identical with those used for test analytes. Nonirradiated and irradiated scans of the supporting electrolyte were similar, except for a slight overall decrease in background currents as a result of irradiation. Any waves or photocurrents in the analyte sample were assigned only after comparison of PCVs and CVs of supporting electrolyte and analyte samples. The nonirradiated CVs were collected in the usual manner. For an irradiated CV, the first cycle was run with the shutter closed; as the second cycle began the shutter was opened, and the PCV was recorded. Since the electrode could become passivated by absorption of photogenerated radicals and intermediates during an irradiated trial, the working electrode was examined between runs. If a cloudy film was observed, the electrode was disassembled and cleaned. Cleaning of the working electrode was also necessitated by the evidence of nonreproducible data.

RESULTS AND DISCUSSION

Photolysis-CV. Two well-defined oxidative and two reductive waves were present in the CV of iodide, while iodate and periodate did not exhibit endogenous electroactivity within the scan limits chosen. However, all species exhibited similar electrochemical activity following UV irradiation (Figure 3). Identical behavior was observed in the PCV for IO_3^- and IO_4^- both when the supporting electrolyte had been degassed, and when it had not. These findings clearly illuminated the power of PCV as a tool in methods optimization, in that the 30-min investment in these experiments saved the large expenditure of time that would have been required to generate an on-line, deoxygenator to test the same relationship between response and the presence of dissolved oxygen. On-line degassing would be difficult because the KOT is constructed of Teflon, through which oxygen easily permeates. Fortunately, as the PCV aptly demonstrated, deoxygenation was not important for the photolytic electrochemical detection of iodide.

Manipulation of the switching potentials and the direction of scan allowed for the evaluation of coupling of the oxidative and reductive electrochemical processes. For I^-, and identically for photolyzed solutions of iodate and periodate, two coupled redox processes were identified: the oxidative wave at ≈515 mV (OX_1 in Figure 3) with the reductive wave at ≈300 mV (RED_2), and OX_2 at ≈810 mV with RED_1 at ≈580 mV. The reductive wave at ≈0.0 V was a component of the residual response for photolyzed blank supporting electrolyte. Additionally, it was determined that the position of the peak potentials for the first redox couple (OX_1–RED_2) was not affected by pH, while increasing pH shifted the peak potential for OX_2 to a lower anodic potential. All of these findings are in general accord with previous reports (*24–26*), in which the first redox couple was attributed to the reversible process

$$2I^- \leftrightarrow I_2 + 2e^- \qquad (1)$$

The second process was attributed to the oxidation of iodine, formed in the original oxidation of iodide, to a transient species

$$I_2 + 2H_2O \leftrightarrow 2HIO + 2H^+ + 2e^- \qquad (2)$$

The pH studies, and the coupling of the oxidative and reductive processes, supporting this electrochemical mechanism. The inverse relationship between the OX_2 peak potential and

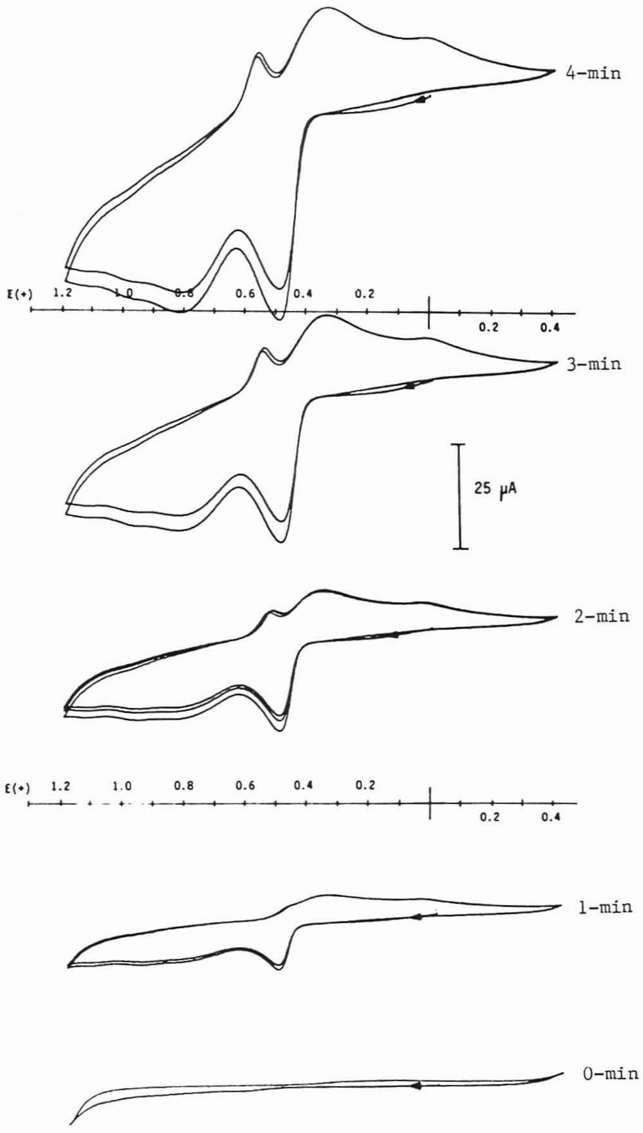

Figure 4. Temporal PCV study of 1 ppth IP in 50:50 MeOH:0.2 M NaCl, showing generation of electrochemical response as a function of increasing irradiation time.

solution pH is understandable if eq 2 adequately describes the oxidation of iodine to hypoiodite (*27*). It has also been suggested that HIO can react with I^- in the diffusion layer to form I_2 (*25, 26, 28*). In Figure 3, the broad shape of OX_2 and the diminished peak current for RED_1 with respect to RED_2 may be interpreted as electrochemical effects of this chemical reaction.

One of the more important facets of these data was that it indicated that the electrochemical behavior of iodide could be used to advantage in a dual, series EC detection approach in LC–*hν*–EC detection.

Iodopentane (IP) did not display native electrochemical activity within the scan limits of +1.2 and −0.4 V. However, PCV temporal analysis evidenced the generation of voltammograms that were very similar in appearance to that for iodide. As shown in Figure 4, when IP was subjected to increasing periods of photolysis, the two sets of redox couples gradually surfaced in the voltammetric trace, and this rapid and facile experiment provided data that were quite suggestive of the generation of iodide from the organoiodide precursor. It was also determined that the OX_1 and RED_2 peak currents for IP were inversely proportional to the pH of the supporting electrolyte (correlation coefficient = 0.812), wherein at lower pHs the peak currents were greater. Since it had already been ascertained that the peak currents for OX_1 and RED_2 of I^- were not pH dependent, the inverse relationship between peak currents and pH for photolyzed IP must be coupled to the pH dependence of I^- photogeneration from the organoiodide. These findings were directly applicable to the development of LC–*hν*–EC detection for a number of organoiodides; specifically, PCV obviated the need to determine the pH dependence of peak currents under LC–*hν*–EC conditions, which would have required significantly greater expenditure of time. These findings led to incorporation of a mobile-phase pH of 3 in LC–*hν*–EC experiments (*9*). PCV also provided very strong evidence for the photolytic formation of iodide from IP. When this information was coupled to data from ion- and gas-chromatographic analyses, it provided strong support for a proposed mechanism for the LC–*hν*–EC detection of IP and, by analogy, of other iodinated aliphatic compounds. Results of the full mechanistic study have been reported elsewhere (*9*).

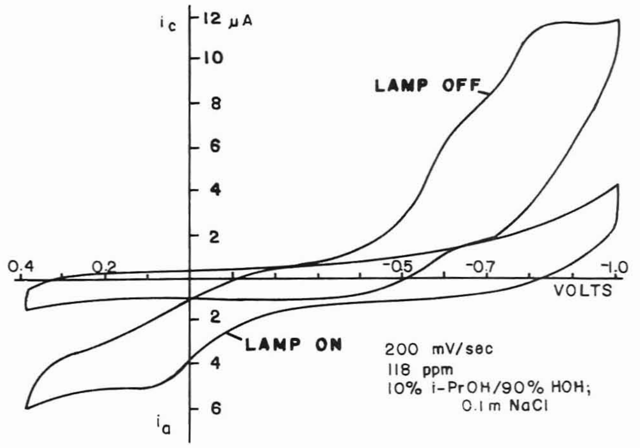

Figure 5. Photo cyclic voltammograms of benzophenone with and without irradiation.

Photo-CV. One class of compounds which are PED active are those that undergo photoreduction by the radical intermediate mechanism, as follows:

$$\mathrm{RRCO} \rightarrow (\mathrm{RRCO})^{*1} \rightarrow (\mathrm{RRCO})^{*3} \quad (3)$$

$$(\mathrm{RRCO})^{*3} + \mathrm{R'R'CHOH} \rightarrow \mathrm{RR\dot{C}OH} + \mathrm{R'R'\dot{C}OH} \quad (4)$$

$$\mathrm{R'R'\dot{C}OH} + \mathrm{RRCO} \rightarrow \mathrm{R'R'CO} + \mathrm{RR\dot{C}OH} \quad (5)$$

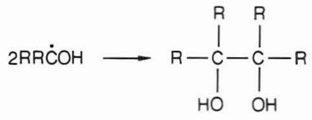

$$2\mathrm{RR\dot{C}OH} \longrightarrow \mathrm{R{-}C(R)(OH){-}C(R)(OH){-}R} \quad (6)$$

where R and R′ are any combination of H, alkyl, or aryl groups (*29*). It has been experimentally established that the triplet-state plays an intermediate role. Alternate experiments indicated that radical intermediates may be responsible for PED response. A paper describing in detail the mechanism of detection in the PED will be published at a later date (*30*).

Benzophenone behaves as a typical aromatic carbonyl compound, as this compound is known to undergo photoreduction in protic solvents. Since ground-state benzophenone is reduced at potentials cathodic of −1.4 V, reduction current for nonirradiated benzophenone was not observed under the CV conditions used in these experiments. In Figure 5, the current observed at cathodic potentials without irradiation was attributed to the reduction of residual oxygen and/or impurities in the supporting electrolyte. A "blank" scan of the supporting electrolyte without irradiation was identical with that of the nonirradiated analyte CV. Upon irradiation, an oxidative photocurrent was observed from −1.0 to 0.4 V. The photocurrent can be attributed to the unresolved oxidation current of the ketyl radical and ketyl radical anion,

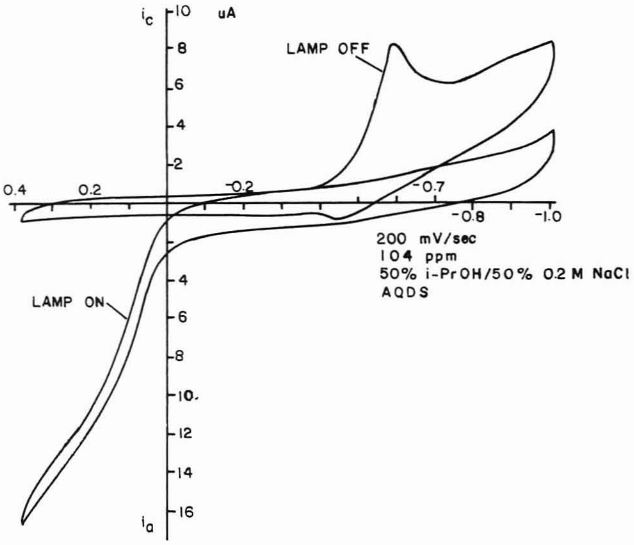

Figure 6. Detection of photogenerated semiquinone intermediates by PCV.

occurring at potentials more positive than −1.2 V, in combination with the anodic wave of benzopinacol starting at ca. −0.2 V. The radical/radical anion oxidation wave did not reach a maximum, because the heterogeneous electron-transfer rate is slow and because the species are continuously formed in the double-layer and (catalytically) at the electrode surface. These results agree well with those described in the introduction (*15–21*) and are observed within the ranges of the published redox potentials for these species, determined using alternate techniques (*29, 31*). PCV results confirmed previous photochemical and electrochemical experiments and were supportive of the roles of radicals and photoproducts in PED detection. PCV findings also were useful in selecting LC–PED instrumental parameters, in that an applied voltage of +0.3 V was used in the LC–PED analysis of similar compounds.

Another advantage of PCV is that it could be used to rapidly scout the PED activity of a compound. Figure 6 demonstrates the CV and PCV results for 9,10-anthraquinone-2,6-disulfonate (AQDS). The prominent reductive peak at −0.6 V without irradiation was produced by the reduction of the quinone functionality to the hydroquinone. A CV of the supporting electrolyte without irradiation resembled the lamp-off scan in Figure 5, wherein the wave at −0.6 V was not apparent. Upon irradiation, an intense anodic peak was observed at potentials positive of ca. 0.0 V due to the detection of the photogenerated semiquinone radical intermediates. However, the cathodic peak at −0.6 V in the nonirradiated scan was diminished to zero in the irradiated scan. In other words, the electrode was incapable of discriminating between ground-state AQDS and the photoproduct/semiquinone radical. Under these conditions, the photochemically generated flux of semiquinone radicals and photoproducts to the transport-limited region of the electrode produced a drop in the flux of AQDS. These results were in agreement with the work of Albery (*22*). Again, one must keep in mind that many effects and processes are occurring simultaneously and that the thrust of this work was to predict photoelectrochemical activity. It could be predicted from these data that AQDS should be PED active at +0.2 V in LC–PED, and, as shown in Figure 7, this prediction was borne out in flow injection analysis PED determination of AQDS with the lamp "on" and lamp "off". Therefore, PCV demonstrated excellent utility in the prediction of PED activity.

Although the PCV is a qualitative tool and has limited quantitative applicability, due to the complex nature of the voltammetric traces produced, it was found to be well-suited for screening compounds for photoelectrochemical activity, optimizing LC–PED, and studying photochemical reactions. In addition, as pointed out by one reviewer, the PCV could be easily modified with a monochromator to obtain electrochemical spectra ($i_{h\nu}$ vs. λ). This would greatly facilitate prediction of the relative electroactivity of species contributing to UV absorption in a spectrum.

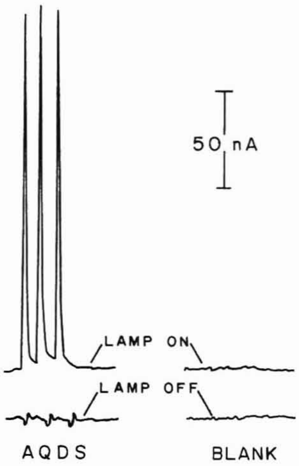

Figure 7. FIA-PED trace for anthraquinone disulfonate. Sample solution was 9.3 ppm AQDS diluted in mobile phase. Conditions: 50:50 *i*-PrOH:HOH; 0.1 M NaCl at *F* = 1 mL/min. Glassy-carbon working electrode set at +0.2 V vs. Ag/AgCl.

CONCLUSION

PCV is clearly a powerful method for those involved with the development and understanding of techniques coupling photochemistry and electrochemistry. The method is information rich, in that a minimum amount of time is required to set up and perform experiments, yet the results are useful for a number of facets of methods development and mechanistic study. Photolysis-CV provides empirical results that are complementary to the chromatographic methods commonly utilized for photochemical product analysis, and thus fills a void in the study of the mechanisms operative in LC–*hν*–EC detection. On the other hand, photo-CV is a standalone technique that offers the rapid, in situ probe needed for the electrochemical study of photogenerated transient species. The results of photo-CV experiments are useful for the elucidation of complex photoelectrochemical behavior and provide for straightforward transfer of knowledge for improved LC–PED analyses. Both of these approaches require a minimum of instrumentation and may be applicable for the resolution of a diverse number of analytical problems. The designs incorporated here are only examples of those possible, and the techniques could easily be modified, as required, to more closely mimic the experimental approaches used by other workers.

ACKNOWLEDGMENT

The authors gratefully acknowledge the continued interest and technical support of P. T. Kissinger and R. E. Shoup at Bioanalytical Systems, Inc., as well as T. R. Gilbert at Northeastern University for his helpful discussions and support.

Registry No. IP, 628-17-1; AQDS, 84-50-4; I^-, 20461-54-5; IO_3^-, 15454-31-6; IO_4^-, 15056-35-6; benzophenone, 119-61-9.

LITERATURE CITED

(1) *Reaction Detection in Liquid Chromatography*; Krull, I. S., Ed.; Marcel Dekker: New York, 1986.
(2) Krull, I. S.; Selavka, C. M.; Duda, C.; Jacobs, W. *J. Liq. Chromatogr.* **1985**, *8*, 2845.
(3) Krull, I. S.; Ding, X.-D.; Selavka, C. M., Bratin, K.; Forcier, G. *J. Forensic Sci.* **1984**, *29*, 449.
(4) Selavka, C. M.; Krull, I. S. *J. Energ. Mater.* **1986**, in press.
(5) Ding, X.-D.; Krull, I. S. *J. Agric. Food Chem.* **1984**, *32*, 622.

(6) Selavka, C. M.; Krull, I. S.; Bratin, K. *J. Pharm. Biomed. Anal.* **1986**, *4*, 83.
(7) Selavka, C. M.; Krull, I. S. *J. Chromatogr. Sci.* **1985**, *23*, 499.
(8) Selavka, C. M.; Krull, I. S.; Lurie, I. S. *Forensic Sci. Int.* **1986**, *31*, 301.
(9) Selavka, C. M.; Krull, I. S., submitted for publication in *Anal. Chem.*
(10) LaCourse, W. R.; Krull, I. S. *TrAC Trends Anal. Chem.* (*Pers. Ed.*) **1985**, *4*, 118.
(11) LaCourse, W. R.; Krull, I. S. *Anal. Chem.* **1985**, *57*, 1810.
(12) LaCourse, W. R.; Krull, I. S. *Proc. Electrochem. Soc.* **1987**, *86*(14), 181.
(13) LaCourse, W. R.; Krull, I. S. *Anal. Chem.* **1987**, *59*, 49–53.
(14) Sanderson, S. *CV Note on Flavin Mononucleotide*; Bioanalytical Systems, Inc.: West Lafayette, IN.
(15) Perone, S. P.; Birk, J. R. *Anal. Chem.* **1966**, *38*, 1589.
(16) Birk, J. R.; Perone, S. P. *Anal. Chem.* **1968**, *40*, 498.
(17) Kirschener, G. L.; Perone, S. P. *Anal. Chem.* **1972**, *44*, 443.
(18) Jamisson, E. A.; Perone, S. P. *J. Phys. Chem.* **1972**, *76*, 830.
(19) Patterson, J. I. M.; Perone, S. P. *J. Phys. Chem.* **1973**, *77*, 2437.
(20) Johnson, D. C.; Resnick, E. W. *Anal. Chem.* **1972**, *44*, 637.
(21) Lubbers, J. R.; Resnick, E. W.; Gaines, P. R.; Johnson, D. C. *Anal. Chem.* **1974**, *46*, 865.
(22) Albery, W. J.; Archer, M. D.; Field, N. J.; Turner, A. D. *Faraday Discuss. Chem. Soc.* **1974**, *56*, 28.
(23) MacCrehan, W. A.; May, W. E. *Anal. Chem.* **1984**, *56*, 625.
(24) Miller, F. J.; Zittel, H. E. *J. Electroanal. Chem.* **1966**, *11*, 85.
(25) Zittel, H. E.; Miller, F. L. *J. Electroanal. Chem. Interfacial Electrochem.* **1967**, *13*, 193.
(26) Dryhurst, G.; Elving, P. J. *Anal. Chem.* **1967**, *39*, 606.
(27) Geissler, W.; Nitzsche, R.; Landsberg, R. *Electrochim. Acta* **1966**, *11*, 389.
(28) Beran, P.; Bruckenstein, S. *Anal. Chem.* **1968**, *40*, 1044.
(29) Bansai, K. M.; Gratzel, M.; Henglein, A.; Janata, E. *J. Phys. Chem.* **1973**, *77*, 16.
(30) LaCourse, W. R.; Krull, I. S., submitted for publication in *J. Am. Chem. Soc.*
(31) Rao, P. S.; Hayon, E. *J. Am. Chem. Soc.* **1974**, *96*, 1295.

RECEIVED for review October 8, 1986. Accepted December 29, 1986. The photo-CV work was supported by an ACS Analytical Division Fellowship, sponsored by the Society of Analytical Chemists of Pittsburgh, a Gustel Giessen Advanced Research Award, an award from the Research and Scholarship Development Fund from Northeastern University, a Barnett Institute Innovative Research Award, and by a grant from the Analytical Research Department of Pfizer & Co., Inc., Groton, CT, to Northeastern University. Funding for the photolysis-CV work was provided by an NIH Biomedical Research Grant No. RR07143 to Northeastern University, as well as an NIH-Small Business Innovation Research Grant, 1R43ES04057-01 (in cooperation with Cambridge Analytical Associates, Boston, MA). Support for C.M.S. was provided by a National Institute of Justice, U.S. Department of Justice, Graduate Research Fellowship (86-IJ-CX-0058). Points of view or opinions stated in this document are those of the authors and do not necessarily represent the official position or policies of the U.S. Department of Justice. This is contribution number 308 from the Barnett Institute of Chemical Analysis and Materials Science at Northeastern University.

Mass Spectral Analysis of Isotopically Labeled Compounds: Average Mass Approach

Karl Blom,[1] **Cecil Dybowski, and Burnaby Munson***

Department of Chemistry, University of Delaware, Newark, Delaware 19716

Bruce Gates and Lori Hasselbring

Department of Chemical Engineering, University of Delaware, Newark, Delaware 19716

Stable isotope labels are used in many areas of chemistry, geology, biology, and pharmacology. Their roles as probes into the mechanisms of organic reactions (*1–3*) and metabolic pathways (*4*), as environmental (*5, 6*) and process tracers (*7*), and in the quantitation of trace components in mixtures (*8*) are well documented. Mass spectrometry is the most commonly used method of analyzing the isotopic content of labeled compounds. For relatively simple compounds containing predominantly monoisotopic elements (e.g., C, N, O, etc.) the degree of labeling is easily calculated from the ratio of the intensities of the relevant peaks in the mass spectrum (*9*). However, for larger molecules or compounds containing polyisotopic elements (e.g., inorganic or organometallic compounds containing Mo, Sn, Pt, Hg, etc.), the complexity of the isotopic cluster often makes direct analysis of the isotopic content difficult. Sophisticated computational procedures have been reported for estimating the isotopic enrichment of these compounds (*10–12*). In general, these approaches attempt to "fit" the experimentally determined isotopic pattern to a pattern calculated for an estimated isotopic composition. These approaches have some drawbacks since the results will depend upon the particular method used to calculate the difference between the experimental and calculated patterns and upon the criterion used to determine a match. All of the methods for determining isotopic content reported in the literature require mass spectral data with unit resolution.

The average mass or "centroid" of complex isotope clusters can be measured very precisely even at high mass (*13*) or when unit mass resolution is not available (*14–16*). It has been proposed that the most useful mass for characterizing compounds with high molecular weights is the average mass, which can be combined with the shape of the isotopic cluster (e.g., full width at half height) to verify the elemental composition of the ion (*11–14*). This approach should also be applicable to lower molecular weight compounds, particularly those which contain polyisotopic elements. The purpose of this communication is to present a simple method for calculating the total isotopic content of a sample directly from its mass spectrometrically determined average mass.

EXPERIMENTAL SECTION

The CH_4 chemical ionization mass spectra were obtained for "natural" 2,5-dichlorophenyl azide, double ^{13}C enriched 2,5-dichlorophenyl azide, a mixture of the natural and labeled azides, and an osmium carbonyl, $H_4Os_4(CO)_{12}$, partially enriched with ^{13}C. The data were acquired oscillographically with a Du Pont 21-492B mass spectrometer operated at unit mass resolution. The masses of the peaks were determined to the nearest 1 amu (nominal mass precision). Peaks less than 0.5% of the base peak were not included in the analysis. Triplicate determinations were made for each sample. The estimated average uncertainty in the intensity measurements (one standard deviation) was about 2%. The average mass for a cluster was calculated with

$$M_a = \sum_{i=1}^{n} I_i M_i \Big/ \sum_{i=1}^{n} I_i \qquad (1)$$

where n is the number of peaks in the cluster and I_i and M_i are

---

[1] Present address: E. I. du Pont de Nemours & Company, Medical Products Department, Experimental Station, Wilmington, DE 19898.

0003-2700/87/0359-1372$01.50/0 © 1987 American Chemical Society

the intensity and mass for peak i, respectively.

The $(M + H)^+$ cluster was used for the analysis of the osmium carbonyl. The $(M + C_2H_5)^+$ adduct ion was used for the analysis of the 2,5-dichlorophenyl azide samples because the $(M + H)^+$ cluster was distorted by the presence of a significant M^+ ion.

THEORY

Consider the cluster of peaks corresponding to a "pure" molecular ion in the mass spectrum of a sample compound in which one element has been enriched in the heavy isotopic form of that element. The average mass, M_a, for this cluster can be expressed as the sum of the average masses of the elements in the enriched compound

$$M_a = \sum_j N_j M_j + N X_H M_H + N(1 - X_H) M_L \qquad (2)$$

where N_j and M_j are the number of occurrences and average masses for those elements not involved in the isotopic enrichment, N is the number of sites within the ion which contain the enriched population of the label element, M_L and M_H are the nuclidic masses for the light and heavy isotopic forms of the label element, and X_H is the mole fraction of the heavy isotope in the enriched population. The product, NX_H, is the fraction of label sites within the ion which contain the heavy isotope label, averaged over the entire sample. Thus, the term NX_HM_H represents the average mass of the heavy isotope label in the ion. Similarly, the term $N(1 - X_H)M_L$ represents the average mass of the light isotope in the ion, and the sum of N_jM_j's in eq 2 represents the average mass for the remainder of the ion, i.e., the average mass for the atoms not involved in the isotopic enrichment.

Replacing the summation in eq 2 with M_0 and solving for the mole fraction of the heavy isotope gives

$$X_H = (M_a - M_0 - NM_L)/N(M_H - M_L) \qquad (3)$$

The average mass for the nonenriched portion of the ion, M_0, is easily calculated from standard tables of the average masses of the elements (see Table I) and N, M_L, and M_H are usually known a priori. Thus, the mole fraction of the heavier isotope in the enriched population can be calculated directly from the experimentally determined average mass of the ionic cluster using eq 3.

The "exact" average mass for a distribution of peaks or isotopic forms can be expressed as the sum of a "nominal" average mass which is the average of the nominal masses of the species in the distribution and a "defect" average mass which results from the mass defects of the species. Thus, if the masses of the peaks in the mass spectral analysis are measured with nominal mass precision (integral masses), then the average mass which is calculated with eq 1 will be the "nominal" average mass of the ionic cluster. Mathematically, the "nominal" and "defect" average masses have the same properties as the "exact" average mass. Consequently, the "nominal" average mass of an ionic species can be expressed as the sum of the "nominal" masses of its component elements, as in eq 2; and eq 3, which describes the isotopic content of an enriched sample in terms of its average mass, is valid even if the masses of the peaks in the cluster are only measured with unit precision. However, if the "nominal" average mass is used, then all of the quantities in eq 3 must be expressed in terms of their nominal masses; i.e., M_H and M_L must be the nominal masses of the light and heavy isotopic forms of the label element and M_0 must be calculated from the "nominal" average masses of the elements. Table I shows the "exact" and "nominal" average masses for a few common elements as calculated with

$$M_j = \sum_{i=1}^{n} P_{ji} M_{ji} \qquad (4)$$

where P_{ji} and M_{ji} are the normalized abundance and mass (either exact or nominal) for isotopic form i of element j.

Table I. Average Masses of Several Elements[a]

element	calcd av masses[b] for the following mass precisions: 1 amu	0.0001 amu
H	1.000 15	1.007 97
C	12.011 10	12.011 14
N	14.003 70	14.006 76
O	16.004 45	15.999 37
F	19.000 0	18.998 40
Si	28.108 80	28.085 61
P	31.000 0	30.993 76
S	32.090 64	32.062 53
Cl	35.489 4	35.453
Br	79.989 2	79.906 5
I	127.000	126.900 4
Os	190.278	190.237

[a] Data from ref 17. [b] Calculated with eq 4, in amu.

The uncertainty in the isotopic content calculated from eq 3 results primarily from the uncertainty associated with the measured average mass

$$\Delta X_H = \Delta M_a / N(M_H - M_L) \qquad (5)$$

The major source of uncertainty in the experimental determination of an average mass lies in the measurement of the ionic intensities. Propagating the error through eq 1 gives the uncertainty in M_a as

$$\Delta M_a = \{(\Delta I/n)^2[\sum(M_i^2) - 2M_a\sum M_i + nM_a^2]\}^{1/2} \qquad (6)$$

where ΔI is the average relative uncertainty in the intensities of the peaks, n is the number of peaks in the cluster, and M_i is the mass of peak i. The most obvious implication of eq 5 and 6 is that the uncertainty in the calculated isotopic content is inversely related to the number of peaks in the cluster; i.e., the precision is better for larger clusters. The term in the brackets in eq 6 is related to the symmetry of the cluster; the precision of the average mass analysis increases with increasing symmetry of the cluster.

RESULTS AND DISCUSSION

As a simple test of the average mass approach, the isotopic contents of several ^{13}C-enriched samples were calculated by using eq 3 and using standard ratio and pattern matching methods. The results are summarized in Table II. These results represent the average for three determinations ±1 standard deviation. The isotopic contents calculated by using the average masses of the clusters and eq 3 are the same as those calculated by the standard methods within experimental error. The agreement establishes the validity of eq 3.

The accuracy and precision of the results in Table II are reflective of the small data sets used in these calculations and should not be interpreted as indicative of the ultimate obtainable by either procedure. However, one may note that, for these data, the uncertainties for the average mass results are approximately the same or slightly better than those for the ion ratio results. A simple analysis of the likely errors indicates that this improvement is due to the larger number of peaks used in the average mass analysis and should be general.

The advantage of an average mass approach is illustrated by the osmium carbonyl example, $H_4Os_4(CO)_{12}$. Figure 1 shows the $(M + H)^+$ cluster for the natural and ^{13}C-enriched materials. The clusters for these species are very complex. The most intense peak containing a manageable number of isotopic forms is m/z 1085 (predominantly $^1H_5{}^{186}Os_4(^{12}C^{16}O)_{12}{}^+$). However, this peak is <0.1% of the base peak.

Table II. Comparison of Average Mass and Conventional Methods

sample	labels	no. of peaks in cluster[a]	mole fraction of ^{13}C[b] av mass method	mole fraction of ^{13}C[b] conventional method
$C_{12}H_8N_2Cl_2$	"natural"	6	0.013 ± 0.001	0.012 ± 0.001
$C_{12}H_8N_2Cl_2$	double ^{13}C	7	0.984 ± 0.007	0.983 ± 0.015[c]
$C_{12}H_8N_2Cl_2$	mixture	7	0.565 ± 0.007	0.556 ± 0.011[c]
$H_4Os_4(CO)_{12}$	^{13}C enriched	24	0.390 ± 0.002	0.388[d]

[a] Number of peaks with intensities ≥0.5% of base peak. [b] Average of three determinations ±1 standard deviation. [c] Calculated from $X_H = [I_{280} + 2(I_{281} - RI_{279})]/[2I_{279} + 2I_{280} + 2(I_{281} - RI_{279})]$, where I represents the measured intensity for the indicated mass in the $(M + C_2H_5)^+$ cluster and R is the naturally occurring abundance of ^{37}Cl for two chlorines. [d] Estimated by systematically varying the ^{13}C abundance, calculating the resulting isotope pattern (assuming statistical distribution of ^{13}C), comparing calculated and measured patterns, and determining the ^{13}C abundance which produces the "best fit"; i.e., when $\Delta F = \sum|(I_{\mathrm{obsd},i}/\sum I_{\mathrm{obsd},i}) - (I_{\mathrm{calcd},i}/\sum I_{\mathrm{calcd},i})|$ is a minimum. ΔF for the best fit was 6.8%.

Table III. Partial Listing of Isotopic Forms Present at m/z 1104 for $(H_4Os_4(CO)_{12} + H)^+$

$^{1}H_5{}^{187}Os_1{}^{192}Os_3{}^{12}C_{12}{}^{16}O_{12}$
$^{1}H_5{}^{189}Os_1{}^{190}Os_1{}^{192}Os_2{}^{12}C_{12}{}^{16}O_{12}$
$^{1}H_5{}^{186}Os_1{}^{192}Os_3{}^{12}C_{11}{}^{13}C_1{}^{16}O_{12}$
$^{1}H_5{}^{189}Os_2{}^{192}Os_2{}^{12}C_{11}{}^{13}C_1{}^{16}O_{12}$
$^{1}H_5{}^{188}Os_1{}^{190}Os_1{}^{192}Os_2{}^{12}C_{11}{}^{13}C_1{}^{16}O_{12}$
$^{1}H_5{}^{190}Os_3{}^{192}Os_1{}^{12}C_{11}{}^{13}C_1{}^{18}O_{12}$
$^{1}H_5{}^{187}Os_1{}^{190}Os_1{}^{192}Os_2{}^{12}C_{10}{}^{13}C_2{}^{16}O_{12}$
$^{1}H_5{}^{188}Os_1{}^{189}Os_1{}^{192}Os_2{}^{12}C_{10}{}^{13}C_2{}^{16}O_{12}$
$^{1}H_5{}^{189}Os_2{}^{190}Os_1{}^{192}Os_1{}^{12}C_9{}^{13}C_3{}^{16}O_{12}$
etc.

Every peak of reasonable intensity is composed of an enormous number of isotopic forms. Table III gives a partial listing of the significant forms that are found in the ^{13}C-enriched species at a nominal mass of 1104 amu. Obviously, it will be very difficult to solve this system directly to obtain any reasonable estimate of the isotopic content from a ratio of ionic intensities. The isotopic content could be approximated by a pattern matching or least-squares approach. However, all of these methods either are difficult to apply or involve approximations which could lead to large errors (*18*). The average mass method, on the other hand, avoids most of these approximations and is easy to apply. For the clusters shown in Figure 1, M_0 is the average mass for $H_5Os_4O_{12}$ and is easily calculated from Table I (M_0 = 958.166 amu for nominal mass precision); N is 12; and M_L and M_H are 12 and 13 amu (again, for nominal mass precision), respectively. Inserting these values into eq 3, along with the average masses given in Figure 1, we immediately obtain ^{13}C abundances of 0.2% and 39.0% for the natural and enriched samples, respectively.

CONCLUSIONS

The average mass approach to isotopic analysis is valid for both partially enriched materials which contain a statistical distribution of isotopic labels (such as the osmium carbonyl) and specific mixtures of labeled and unlabeled compounds (such as the azide mixture). The calculation is simple even for compounds that produce very complex clusters of peaks.

For relatively simple systems (like the 2,5-dichlorophenyl azide examples) the standard ionic ratio methods are easy to use and work well. However, an average mass approach might find wide application in the isotopic analysis of inorganic, organometallic, and higher molecular weight samples which produce complex clusters. An average mass approach should also be applicable in those cases in which the mass analyzer cannot provide unit mass resolution.

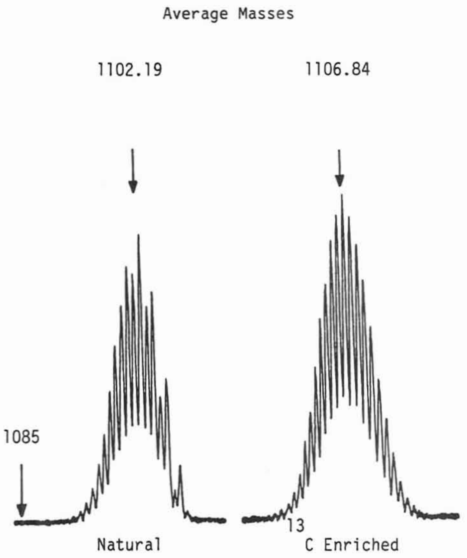

Figure 1. $(M + H)^+$ clusters for $H_4Os_4(CO)_{12}$.

ACKNOWLEDGMENT

The authors thank Henry J. Shine, Texas Tech University, for supplying the natural and double ^{13}C labeled 2,5-dichlorophenyl azide and Henry Lamb, University of Delaware, for supplying the ^{13}C-enriched $H_4Os_4(CO)_{12}$.

Registry No. ^{13}C, 14762-74-4; $H_4Os_4(CO)_{12}$, 12375-04-1; 2,5-dichlorophenyl azide, 75458-15-0.

LITERATURE CITED

(1) Knapp, D. R.; Gaffney, T. E.; Compson, K. R. *Advances in Biochemical Psychopharmacology*; Costa, E., Holmstedt, B., Eds.; Raven: New York, 1973; Vol. 7, pp 83–94.
(2) Bencivengo, D. J.; San Filippo, J., Jr. *Organometallics* **1983**, *2*, 1907–1909.
(3) Kwart, H.; Stanulonis, J. *J. Am. Chem. Soc.* **1978**, *98*, 4009.
(4) Shine, H. J.; Hobdas, J.; Kwart, H.; Brechbiel, M.; Gaffney, A.; San Filippo, J., Jr. *J. Am. Chem. Soc.* **1983**, *105*, 2823–2827.
(5) Halverson, J. E. *Energy Res. Abstr.* **1982**, *7*, Abstr. No. 4820.
(6) Rokop, D.; Alei, M.; Cappis, J.; Mroz, E.; Mason, A.; Norris, T.; Paths, J.; Guthals, P.; Bryant, E.; Cowan, G.; Dye, S.; Goldblatt, M.; Jefferies, R.; Mills, T. Presented at the 33rd Annual Conference on Mass Spectrometry and Allied Topics; San Diego, CA; May 26–31, 1985.
(7) Maurer, O. A.; Parent, G.; Laporte, R. Presented at the 33rd Annual Conference on Mass Spectrometry and Allied Topics; San Diego, CA; May 26–31, 1985.
(8) Horning, E. C.; Thenot, J. P.; Horning, M. G. *Quantitative Mass Spectrometry in Life Sciences*; De Leenheer, A. P., Roncucci, R. R., Eds.; Elsevier: New York, 1977; pp 1–14.
(9) Biemann, K. *Mass Spectrometry: Organic Chemical Applications*; McGraw-Hill: New York, 1962; Chapter 5.
(10) Sukharev, Y. N.; Nekrasov, Y. S. *Org. Mass Spectrom.* **1976**, *11*, 1239–1241.
(11) Lee, W. N. P.; Whiting, J. S.; Fymat, A. L.; Boettger, H. G. *Biomed. Mass Spectrom.* **1983**, *10*, 641–645.
(12) Benz, W. *Anal. Chem.* **1980**, *52*, 248–252.
(13) Yergey, J.; Heller, D.; Hansen, G.; Cotter, R. J.; Fenselau, C. *Anal. Chem.* **1983**, *55*, 353–356.
(14) Hakansson, P.; Kamensky, I.; Sundqvist, B.; Fohlman, J.; Peterson, P.; McNeal, C. J.; MacFarlane, R. D. *J. Am. Chem. Soc.* **1982**, *104*, 2948–2949.
(15) McNeal, C. J.; Ogilvie, K. K.; Theriault, N. Y.; Nemer, M. J. *J. Am. Chem. Soc.* **1982**, *104*, 976–980.
(16) Ens, W.; Standing, K. G.; Westmore, J. B.; Ogilvie, K. K.; Nemer, M. J. *Anal. Chem.* **1982**, *54*, 960–966.
(17) *Handbook of Chemistry and Physics*, 54th ed.; Weast, R. C., Ed.; CRC Press: Cleveland, OH, 1974.
(18) Jonckheere, J. A.; De Leenheer, A. P.; Steyaert, H. L. *Anal. Chem.* **1983**, *55*, 153–155.

RECEIVED for review July 21, 1986. Accepted February 10, 1986. Bruce Gates and Cecil Dybowski acknowledge the support of the National Science Foundation under Grant CPE82-17890.

Anal. Chem. **1987**, *59*, 1375–1376

Microdetermination of Chlorine in Noble Metal Organic Compounds and Determination of Palladium by Atomic Absorption Spectrometry

Virendra G. Shah and Suresh Y. Kulkarni*

Division of Organic Chemistry, National Chemical Laboratory, Pune 411008, India

The microdetermination of halogens in organic and organometallic compounds is carried out by various methods (*1–5*). The samples containing platinum group metals, however, present difficulties due to formation of sparingly soluble metal–halogen complexes, which interfere in the titrimetric or gravimetric determination of halogens. A few methods have been reported in which such interference is avoided by masking the metal with ethylenediaminetetraacetic acid (EDTA) (*6, 7*), reducing the metal ions to elemental form by magnesium (*8*), mixing the sample with ammonium fluoride during oxygen flask combustion (*9*), etc. Our efforts to solve this problem by modifying the micro-Carius combustion, which normally involves heating of the sample with concentrated nitric acid and silver nitrate (followed by gravimetric determination of the halogen) led not only to a very simple and accurate method for the microdetermination of chlorine in organopalladium, –rhodium, and –rhuthenium compounds but also to the determination of chlorine (by gravimetry) and palladium (by atomic absorption spectrometry (AAS)) in organopalladium compounds. The possibility of incomplete oxidation in the oxygen flask method (*10*) is avoided by using the very reliable Carius method (*10, 11*). Also the procedure for the determination of chlorine and palladium on the same sample reported here is very simple as compared to the one described by earlier workers (*7*) which involves fusion with Na_2O_2 followed by titrimetric determination of chlorine (or bromine), after masking palladium with EDTA, and photometric determination of palladium. This factor becomes particularly important when samples are to be analyzed on a routine basis.

EXPERIMENTAL SECTION

Reagents. Palladous chloride was from Johnson Matthey (U.K.). Silver nitrate was A.R. grade from B.D.H. (U.K.).

Apparatus. A micro-Carius Furnace from the Arthur H. Thomas Co. (Philadelphia, PA) and a Pye-Unican, Model SP-1900, double-beam, with air–acetylene flame, atomic absorption spectrometer were used.

Procedure. About 5–8 mg of the sample was weighed accurately in a micro-Carius tube and was digested in concentrated nitric acid–sulfuric acid (0.3 mL each) mixture containing ~20 mg of silver nitrate at 280 °C for 4 h. After cooling, the contents of the tube were diluted with distilled water to about 15 mL and heated by placing the tube in a beaker of hot water (~85 °C) for 5 min. The silver chloride precipitate was filtered, washed, dried, and weighed and the chlorine content calculated as usual (*12*).

To determine palladium, the filtrate, after removal of silver chloride precipitate, was quantitatively transferred to a volumetric flask and was diluted to an appropriate volume which contained ~2–20 ppm of Pd. Absorbance was measured at 247.64 nm by AAS.

RESULTS AND DISCUSSION

Determination of Chlorine. In the microdetermination of halogen in noble metal organic compounds, the usual Carius oxidation with concentrated nitric acid alone forms colored, insoluble salts, which interfere in the gravimetric determination of the halide. Alternatively, oxidation with concentrated sulfuric acid alone is slow and needs either high temperature or a catalyst (*13*).

Table I. Microdetermination of Chlorine in Compounds Containing Pd, Rh, and Ru[a]

		% Cl		
no.	compound	theory	found	difference
1	$Pd(Py)_2Cl_2$	21.1	21.4	+0.3
2	$Pd(PyCOP)_2Cl_2$	13.1	12.9	–0.2
3	$Pd(PyC_2H_5)_2Cl_2$	18.1	17.8	–0.3
4	$Pd(CD)Cl_2$	24.9	24.5	–0.4
5	$Pd(TPP)_2Cl_2$	10.1	9.8	–0.3
6	$Pd(TPPO)_2Cl_2$	8.9	8.5	–0.4
7	$Rh\ COCl(TPP)_2$	5.1	5.3	+0.2
8	$Rh\ (TPP)_3Cl$	3.8	3.4	–0.4
9	$Rh\ (Py)_3Cl_3$	23.9	23.3	–0.6
10	$Ru\ (COCl)_2(TPP)_2$	9.4	8.9	–0.5
11	$Ru\ H\ COCl(TPP)_3$	3.7	3.8	+0.1
12	$Ru\ (TPP)_3Cl_2$	7.4	7.0	–0.4
13	$Ru\ COCl(TPP)_2BA$	4.2	4.4	+0.2
14	K_2PdCl_6	43.4	43.8	+0.4
15	$PdCl_2$	40.0	39.9	–0.1

[a] Py, pyridine; TPP, triphenylphosphine; P, phenyl; TPPO, triphenyl phosphite; CD, cyclooctadiene; BA, benzoylacetone. Note: All analyses were done in duplicate.

It was therefore decided to use concentrated nitric acid–sulfuric acid mixture, which is known to be a versatile oxidizing mixture for organic and organometallic compounds (*13*).

When the organopalladium, –rhuthenium, and –rhodium samples were oxidized in sealed Carius tubes by using concentrated HNO_3–H_2SO_4 (1:1) in the presence of silver nitrate, only a white precipitate of silver chloride was obtained, indicating formation of soluble metal salts. A very small amount of silver sulfate precipitate was also formed as detected on running blank determinations. This was dissolved by heating the solution for a while. The resultant silver chloride was weighed. The results for a number of such samples are presented in Table I. It can be seen that the results are within 0.5% of the theoretical values, and the interference from Pd, Rh, and Ru is completely removed. The procedure is equally applicable to inorganic salts as seen from the results of compounds 14 and 15 in Table I.

Determination of Chlorine and Palladium. After the oxidation of the sample with modified oxidation mixture, chlorine was determined as above. The filtrate, after removal of silver chloride, contained metal salts, silver sulfate, silver nitrate, and acidic components. Use of ethanol, which is normally employed during filtration of silver halide precipitate, was avoided since this would interfere with the determination of metal by AAS.

On dilution of the filtrate to desired levels (~2–20 ppm of the metal) as required in the AAS measurements, absorbance was measured at 247.64 nm for Pd. Concentration of the metal was determined from a calibration graph, concentration (ppm) vs. absorbance. $PdCl_2$ was treated in the same way as described above and absorbance was measured for five different concentrations (2–20 μg of Pd mL^{-1}) to obtain a calibration graph of absorbance vs. concentration.

Table II gives the results obtained in the determination of chlorine and palladium. The error is within ±0.5% for chlorine and for palladium, indicating the suitability of the approach.

0003-2700/87/0359-1375$01.50/0 © 1987 American Chemical Society

Table II. Results of Microdetermination of Chlorine and Palladium in Organopalladium Compounds

no.	compound	% Cl theory	% Cl found	% Pd theory	% Pd found
1	$PdCl_2$	40.0	39.9		
2	$Pd(Py)_2Cl_2$	21.1	21.2	31.7	31.6
3	$Pd(PyCOP)_2Cl_2$	13.1	13.5	19.6	20.0
4	$Pd(PyC_2H_5)_2Cl_2$	18.1	17.7	27.2	27.3
5	$Pd(CD)Cl_2$	24.9	24.5	37.3	37.2
6	$Pd(TPP)_2Cl_2$	10.1	9.7	15.2	15.3
7	$Pd(TPPO)_2Cl_2$	8.9	9.1	13.3	13.9

ACKNOWLEDGMENT

We thank V. S. Pansare for helpful discussions and S. S. Tamhankar for AAS measurements.

Registry No. **1**, 14872-20-9; **2**, 107134-60-1; **3**, 107134-61-2; **4**, 12107-56-1; **5**, 13965-03-2; **6**, 29891-44-9; **7**, 13938-94-8; **8**, 14694-95-2; **9**, 15617-30-8; **10**, 14564-35-3; **11**, 16971-33-8; **12**, 15529-49-4; **13**, 66683-03-2; **14**, 16919-73-6; **15**, 7647-10-1; Pd, 7440-05-3; chlorine, 7782-50-5.

LITERATURE CITED

(1) MacDonald, A. M. G. In *Comprehensive Analytical Chemistry*; Wilson, C. L., Wilson, D. W., Eds.; Elsevier: Amsterdam, 1960; Vol IB, Chapter VIII-3d.
(2) Celon, E.; Volponi, L.; Bresadola, S. *Gazz. Chim. Ital.* **1969**, 514–520. *Anal. Abstr.* **1971**, *21*, 1162.
(3) Volodina, M. A.; Khamed, M. D. *Zh. Anal. Khim.* **1972**, *27*, 1828–1833. *Anal. Abstr.* **1974**, *26*, 2101.
(4) Obtemperanskaya, S. I.; Khoi, F. T.; Karandi, I. V. *Anal. Abstr.* **1972**, *23*, 2514.
(5) Sakla, A. B.; Rashid, M.; Karim, O.; Barsoum, B. N. *Anal. Chim. Acta* **1978**, *98*, 121–126.
(6) Strukova, M. P.; Kashiricheva, I. I.; Abdulina, R. G.; Kalashnikova, L. K. *Zh. Anal. Khim.* **1970**, *25*, 1198–1201. *Anal. Abstr.* **1971**, *21*, 3447.
(7) Strukova, M. P.; Kashiricheva, I. I.; Kalashnikova, L. K. *Zh. Anal. Khim.* **1973**, *28*, 819–821. *Anal. Abstr.* **1974**, *26*, 904.
(8) Horáček, J.; Sir, Z. *Collect. Czech. Chem. Commun.* **1976**, *41*, 2015–2019.
(9) Borda, P. *Microchem. J.* **1980**, *25*, 72–74.
(10) Olson, Edward In *Treatise on Analytical Chemistry*, Kolthoff, I. M., Elving, P. J., Ed., Wiley-Interscience: New York, 1971; Part II, Vol. 14, pp 4 and 7.
(11) Tiedcke, C. *Microchem. J.* **1965**, *9*, 334–339.
(12) Steyermark, Al *Quantitative Organic Microanalysis*, 2nd ed.; Academic: New York, 1961; p 316.
(13) Bock, Rudolf *A Handbook of Decomposition Methods in Analytical Chemistry*; Wiley: New York, 1972; pp 211 and 215.

RECEIVED for review September 4, 1986. Accepted January 5, 1987. NCL Communication No. 4141.

CORRECTION

Automated Sample Deoxygenation for Improved Luminescence Measurements

M. E. Rollie, Gabor Patonay, and I. M. Warner (*Anal. Chem.* **1987**, *59*, 180–184).

On p 180, eq 1 and 2 should read:

$$I_0/I_{O_2} = K_{SV}[O_2] + 1 = k_{O_2}\tau_0[O_2] + 1 \qquad (1)$$

$$EF = I_{max}/I_{O_2} = k_{O_2}\tau_0[O_2] + 1 \qquad (2)$$

CHEMICAL & ENGINEERING
NEWS
Chemical firms plan modest
R&D funding increase this year
Page 25

People who make the news, read the News.

When you're sitting at the top, you need to get to the bottom of news that affects your business. That's why senior executives throughout industry read Chemical & Engineering News each week.

It's the only weekly chemical magazine that covers the news from three angles. Not just science. Not just technology. Not just business. But all three. So you not only know what's happening in chemistry, you know how it's going to affect your business.

Read the weekly the newsmakers read. Read Chemical & Engineering News.

Call 800-424-6747

American Chemical Society, 1155 Sixteenth Street, N.W., Washington, D.C. 20036.

CHEMICAL&ENGINEERING
NEWS

BUSINESS
SCIENCE
TECHNOLOGY

WHAT ARE YOU REALLY BUYING WHEN YOU BUY FROM LECO® ?

The quality, performance and speed of LECO® instrumentation are internationally recognized. However, when considering the purchase of instrumentation, consider the support for the instrument once it is in your laboratory. Every LECO® instrument is backed by a full service support system.

The support system provides knowledgeable sales engineers to aid in selecting the preferred instrument for any application, and an experienced field service group, which includes field engineers stationed throughout the world, that installs your new instrument and conducts initial operator training for the most efficient use of the instrument within your laboratory.

LECO®'s entire staff is devoted to keeping your system operating efficiently. The LECO® Applications Laboratory can help you achieve maximum efficiency in testing procedures by assisting in developing or refining testing procedures pertinent to your application.

The service support system also includes high quality accessories and supplies, each of which is subject to a rigorous quality assurance program to insure you only receive the best. Telephone services assistance, parts replacement assistance, computerized warehousing and same day shipping are also provided. Just a few reasons why LECO® service support is second to none.

LECO®'S COMMITMENT TO YOU DOES NOT STOP WHEN THE INSTRUMENT IS PURCHASED, IT BEGINS!

CIRCLE 90 ON READER SERVICE CARD

The Carl E. Schultz Technical Center is where the vital research and development functions are performed which will provide LECO® with innovative products throughout the years to come.

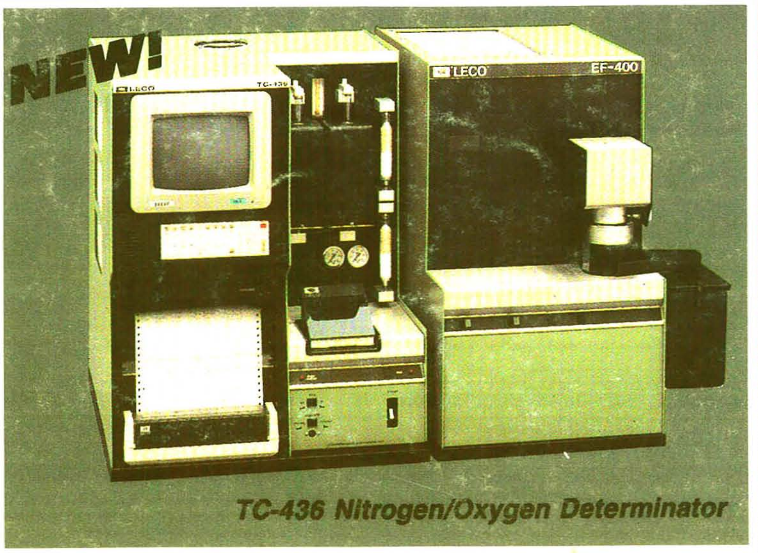

TC-436 Nitrogen/Oxygen Determinator